FINITE ELEMENT ANALYSIS OF WELDED TUBULAR CONNECTIONS

Thesis submitted to University of Nottingham for the Degree of Doctor of Philosophy

by

Peter Crockett. BEng.

Department of Civil Engineering
University of Nottingham
July 1994

Some text bound close to the spine.

ABSTRACT

This thesis presents a nonlinear Finite Element analysis of welded tubular connections, addressing several areas of recent interest in the field.

A comprehensive study of multiplanar axially loaded T-DT joints in both CHS and RHS was undertaken to add to the available knowledge and interest/activity in the field of multiplanar connections. Sections of this study are supported by earlier experimental work undertaken at Nottingham (not by the author) and from a combination of these and FE results, a series of design rules to supplement the current IIW planar design formulae developed.

Analysis of the effect of brace angle on the difference between axially loaded T and Y joints was undertaken to resolve differences between current codes of practice.

Finally an analysis of a family of partial overlapped RHS K joints was undertaken to ascertain the effects of boundary conditions, brace angle, β ratio, reversal of loading and hidden weld on the ultimate capacity and performance of such joints.

All of the FE work was undertaken using ABAQUS, including both geometric and material non-linearity. Recommendations for further work are made.

ACKNOWLEDGEMENTS

The author wishes to acknowledge his sincere gratitude to the following:-

Professor S.F.Brown and Professor D.A.Nethercot, Heads of Department for making available department facilities.

Dr.G.Davies and Professor D.A.Nethercot for acting as supervisors to this work, all their help, guidance, criticism and encouragement.

Mr.G.Watson and other staff of the Cripps Computing Centre at Nottingham for their patience and efforts.

Mr.L.Williams and the staff of the SERC regional computing facilities at Manchester for their patience, time and efforts under sometimes difficult circumstances.

Miss.G.Lowe for her help and expertise in word processing, formatting and preparation of both published papers and this thesis.

SERC for their financial support for this project.

BOMEL (formerly Billington Osborne Moss Engineering Limited) for their financial support and the use of their computing facilities for the colour plots and work contained in Chapter 8.

CONTENTS

Title	Page No
Abstract	
Acknowledgements	
List of Tables	(xi)
List of Symbols	(xiv)

CHAPTER 1

Introduction

1.1 Introduction: Tubular Sections - a Brief History of Research	1
1.2 Factors Governing Design of Tubular Structures	2
1.2.1 Static Strength Design of Tubular Connections	3
1.2.1.1 Static Design of Joints in CHS	3
1.2.1.2 Static Design of Joints in RHS	4
1.2.2 Fatigue Design of Tubular Connections	5
1.3 Modes of Loading and Failure in Tubular Connections	6
1.3.1 Modes of Failure in RHS Connections	6
1.3.2 Modes of Failure in CHS Connections	8
1.4 Finite Element Methods	9
1.4.1 Non-linear Structural Analysis	9
1.4.2 Finite Element Theory	10
1.4.3 Steps in Creating and Analysing an FE Model	14
1.4.3.1 Constructing the Model Geometry	14

1.4.3.2 Additional Data for the Analysis 15

1.4.3.3 Mesh Generation 16

1.4.4 Main Elements in Use 18

1.4.4.1 Solid Elements 18

1.4.4.2 Beam Elements 19

1.4.4.3 Shell Elements 19

1.5 Conclusions 20

CHAPTER 2

A Review of the Literature

2.1 Introduction 26

2.2 Tubular Connections : Development of Design Guidance 26

2.2.1 Circular Connections - Development of Design Guidance 27

2.2.1.1 A Brief History of CHS Joint Design Codes 27

2.2.1.2 Circular Hollow Section Joints - Development of Codes 28

2.2.1.3 On-going Problems and Concerns Over the Codes 31

2.2.2 Rectangular Hollow Section - Joint Design Guidance 32

2.2.2.1 A Brief History of Research 32

2.2.2.2 RHS Joints - Development of Codes 32

2.2.2.3 On-going Problems Over RHS Codes 33

2.3 Non-linear FE Validation for Ultimate Static Strength 35

2.4 Developments in Multiplanar Connections 36

2.4.1 Introduction 36

2.4.2 Classification and Notation of Multiplanar Connections 37

2.4.3 Review of the Literature on Multiplanar CHS Connections 38

2.4.4 Review of the Literature on Multiplanar RHS Connections 40

CHAPTER 3

Modelling Welds and Corner Radii in Tubular Connections

3.1 Introduction 42

3.2 Experimental Database 43

3.3 FE Modelling of the Experimental Test Series 46

3.4 FE Modelling of the Fillet Weld 47

3.4.1 Basic Review of Weld Modelling 47

3.4.2 Weld Models Considered Using Four Noded Shell Elements to Model the Brace and Chord 49

3.4.2.1 Weld Model Case (a) 49

3.4.2.2 Weld Model Case (b) 50

3.4.2.3 Weld Model Case (c) 51

3.4.2.4 Weld Model Case (d) 52

3.4.2.5 Weld Material Properties 52

3.4.3 Weld Models Considered Using Eight Noded Shell Elements to Model the Brace and Chord 53

3.4.3.1 Weld Model Case (e) 53

3.4.3.2 Weld Model Case (f) 54

3.4.3.3 Weld Model Case (g) 54

3.4.3.4 Weld Model Case (h) 55

3.5 Discussion 55

3.5.1 Limitations of the Weld Models Considered 55

3.5.2 Discussion and Analysis of the Results 57

3.6 Conclusions 62

CHAPTER 4

Finite Element Modelling of the E.C.S.C Joint Series

4.1 Introduction 76

4.2 Representation of the Experiments 77

4.3 Mesh Convergence 78

4.4 Calibration of the FE analyses with the Experimental Results 79

4.4.1 Models Using 4 Noded Shells for the Brace and Chord Elements 80

4.4.2 Models Using 8 Noded Shells for the Brace and Chord Elements 80

4.4.3 Definition of Ultimate Capacity and Differences 81

4.4.4 Sidewall and Strain Calibrations 83

4.5 Discussion 85

4.6 Yield Line Theory 88

4.7 Conclusions 90

CHAPTER 5

Slenderness, Imperfections and Chord Length Effects on Rectangular Hollow Section Joints

5.1 Introduction and General Comments 106

5.2 Chord Length Effects in $\beta = 0.6$ Joints 107

5.3 Chord Slenderness Investigation $\beta = 0.6$ Joints 109

5.4 Chord Slenderness Investigation $\beta = 1.0$ Joints 110

5.4.1 Aspects of the Modelling of $\beta = 1.0$ Joints 110

5.4.2 The Australian Tests on Axially Loaded Full Width Joints ($\beta = 1.0$) 112

5.4.3 The FE Analysis on $\beta = 1.0$ Joints 113

5.4.4 Imperfection Investigations on Planar Full Width T Joints 115

5.4.4.1 Initial Imperfection Investigation 115

5.4.4.2 Second Imperfection Investigation 116

5.5 Discussion 117

5.5.1 Chord Length Effects 117

5.5.2 $\beta = 0.6$ Joint Chord Slenderness Investigation 117

5.5.3 $\beta = 1.0$ Joint Chord Slenderness Investigation 119

5.5.4 Imperfections Within $\beta = 1.0$ Joints 122

5.6 Conclusions 124

CHAPTER 6

RHS T-DT Joints: An Interaction Diagram and Three Dimensional Effects

6.1 Introduction 140

6.2 Finite Element Modelling of the $\beta = 0.6$ Joint Series 141

6.2.1 Determination of the Ultimate Capacities in the Joint Series 141

6.2.2 FE Analyses of the $\beta = 0.6$ Joint Series 142

6.3 Finite Element Modelling of the $\beta = 0.25$ Joint Series 145

6.4 FE Modelling of the $\beta = 1.0$ Joint Series 147

6.5 Discussion 148

6.5.1 $\beta = 0.6$ Joints 148

6.5.2 $\beta = 0.25$ Joints 151

6.5.3 β = 1.0 Joints 152

6.6 Conclusions 153

CHAPTER 7

Multiplanar CHS T-DT Joints

7.1 Introduction 165

7.2 Joint Geometry and Load Effects on β = 0.6 Joints 166

7.3 FE Modelling of the β = 0.6 Joint Series 167

7.3.1 Model Arrangement and Boundary Conditions 167

7.3.2 Modelling of the Weld and Initial Chord Boundary Condition Effects 168

7.3.3 Check of Meshes to HSE (1990) Design Guidance and Existing Databases 169

7.4 Analysis of β = 0.6 Joint Series 171

7.4.1 Main Multiplanar Analysis Series 171

7.4.2 Effect of OPB Boundary Conditions on the Behaviour of T-DT Joints 173

7.5 Analysis and Modelling of β = 0.25 Joint Series 174

7.5.1 Modelling and Geometry of β = 0.25 Joints 174

7.5.2 Basic Calibration to Codes of Practice, β = 0.25 175

7.5.3 Analysis of the Multiplanar Joint Series 176

7.6 Discussion 178

7.6.1 Check of the FE Model to Planar Design Guidance and Weld Considerations 178

7.6.2 Multiplanar Interaction Diagram for T-DT Joints β = 0.6 179

7.6.2.1 Out-of-Plane Braces (DT) Free to Rotate 179

7.6.2.2 Out-of-Plane Braces (DT) Constrained to Remain Parallel 180

7.6.2.3 Boundary Condition Effects in the Compression- Compression Quadrant of the Interaction Diagram in Figure 7.8 182

7.6.3 Discussion Multiplanar Interaction Diagram $\beta = 0.25$ Joints 183

7.7 Conclusions 184

CHAPTER 8

Influence of Brace Angle and Intersection Length on CHS T,X and K Joint Capacity

8.1 Introduction 195

8.2 History of the Adoption of the Effective Length Factor K_a 195

8.3 Original Motivation for the Analyses 198

8.4 FE Modelling and Joint Properties T and Y Joints 199

8.4.1 FE Analyses Undertaken at BOMEL 199

8.4.2 FE Analyses Undertaken at Nottingham 201

8.5 DT and X Joints 202

8.6 Discussion 203

8.6.1 T and Y Joints 203

8.6.2 DT and X Joints 207

8.6.3 K Joint Implications 208

8.7 Conclusions 208

CHAPTER 9

Influence of Brace Angle and Intersection Length on RHS Joint Capacity

9.1 Introduction 223

9.2 Yield Line Theory Verification for T and Y Joints 224

9.3 Finite Element Modelling 225

9.3.1 T and Y Joints 225

9.3.2 DT and X Joints 227

9.4 Discussion 228

9.4.1 T and Y Joints 228

9.4.2 DT and X Joints 229

9.5 Conclusions 230

CHAPTER 10

Partial Overlap RHS K Joints - Boundary Condition Effects

10.1 Introduction 235

10.2 Modes of Failure of Overlappped and Partially Overlapped K Joints 236

10.3 Finite Element Modelling of K Joints 237

10.4 Boundary Condition Study, $\beta = 0.6$ 238

10.4.1 Boundary Condition Matrix 238

10.4.2 Determination of Failure in K Joints 239

10.4.3 Analysis and Results for $\beta = 0.6$ Joints 239

10.5 K Joint Boundary Condition Study, $\beta = 1.0$ 241

10.6 Discussion 242

10.6.1 β = 0.6 K Joints 242

10.6.2 β = 1.0 K Joints 244

10.7 Conclusions 245

CHAPTER 11

Effect of Hidden Weld and Brace Thickness on Partial Overlap RHS K Joint Capacity

11.1 Introduction 256

11.2 Joints and Load Cases 259

11.2.1 Dimensions and Load Cases for Initial θ = 60° β = 0.6 K Joints 259

11.2.2 Finite Element Modelling 260

11.2.3 Weld Modelling 261

11.3 Analysis and Results 262

11.3.1 Analysis of the Initial Warren K Joints, 60°, β = 0.6 and Ov = 58.8% 262

11.3.2 Analysis of θ = 60° ,β = 1.0 K Joints 263

11.3.3 Analysis of θ = 30°, β = 0.6 K Joints, Ov= 58.1% 265

11.3.4 Effect of Brace Thickness on Ultimate Capacity 267

11.4 Discussion 268

11.4.1 Hidden Weld Effects on β = 0.6 K Joints 269

11.4.2 Hidden Weld Effects for the β = 1.0, 60° K Joints 274

11.4.3 Effect of Brace Thickness on Ultimate Capacity 275

11.5 Conclusions 277

CHAPTER 12

Conclusions and Recommendations for Further Work

12.1 Introduction 291

12.2 Conclusions 291

12.3 Recommendations for Further Work 296

References 299

LIST OF TABLES

Table	Title	Page No
	CHAPTER 2	
Table 2.1	Classification Multiplanar Tubular Joints	38
	CHAPTER 3	
Table 3.1	Joint Material Properties and Dimensions	44
Table 3.2	Details of the Weld Material Properties	45
Table 3.3	Summary of Weld Cases in Initial Investigation	56
	CHAPTER 4	
Table 4.1	Comparisons of the FE and Yield Line Theory	83
	CHAPTER 5	
Table 5.1	Ultimate Capacities for $\beta = 0.6$ Joints with Slenderness Varied	110
Table 5.2	Zhao's (1992) C22B2 Material Properties for $\beta = 1.0$ Joint	113
Table 5.3	Ultimate Capacities for $\beta = 1.0$ Joints	114
Table 5.4	Comparisons of the Planar $\beta = 1.0$ Joint Capacities with the IIW (1989) Design Recommendations	120
	CHAPTER 6	
Table 6.1	Ultimate Capacities for $\beta = 0.6$ Joints with Arms Restrained Horizontal and Basic Yield Line Theory	144
Table 6.2	Ultimate Capacities for $\beta = 0.6$ Joints with Arms Free	145

Table 6.3 Ultimate Capacities for β = 0.25 Joints 146

Table 6.4 Ultimate Capacities for β = 1.0 Joints 147

CHAPTER 7

Table 7.1 Comparison of Planar FE Results with Code Capacities for the β = 0.6 Joints 170

Table 7.2 Joints Series (β = 0.6) for T-DT Joints Under Combined Axial Loading 172

Table 7.3 Comparison of Planar FE Results with Code Capacities for the β = 0.25 Joints 175

Table 7.4 β = 0.25 Joint Series Peak Capacities 177

Table 7.5 Delft and Nottingham Multiplanar and Planar Capacities (β = 0.6) 181

CHAPTER 8

Table 8.1 Effect of K_a on Ultimate Strength of T/Y Joints for Various Brace Angles θ 197

Table 8.2 Comparisons of T and Y Joint Analyses undertaken at BOMEL 200

Table 8.3 Comparisons of Nottingham T and Y Joint Analyses with HSE the Guidance 202

Table 8.4 Results of the DT and X Joint Analyses Undertaken at BOMEL 203

CHAPTER 9

Table 9.1 Variation of Packer Capacity with Brace Angle,θ for β < 0.85 225

Table 9.2 T and Y FE/Packer comparisons at β = 0.6 226

Table 9.3 T and Y FE/Packer comparisons at β = 0.2 227

Table 9.4 T and Y FE/Packer comparisons at β = 1.0 227

Table 9.5 DT and X FE/Packer comparisons at β = 0. 228

CHAPTER 10

Table 10.1 Material Properties and Dimensions for K Joints 238

Table 10.2 Tabulated Capacities of the β = 0.6 Boundary Condition Matrix 240

Table 10.3 Tabulated Capacities of the β = 1.0 Boundary Condition Matrix 242

CHAPTER 11

Table 11.1 β = 0.6, θ = 60° K Joint Test Parameters and Material Properties 259

Table 11.2 FE Capacities for Various Hidden Weld Assumptions β = 0.6, θ = 60° K Joints 263

Table 11.3 Test Parameters and Material Properties for β = 1.0, θ = 60° K Joints 264

Table 11.4 FE Capacities β = 1.0, θ = 60° K Joints 265

Table 11.5 β = 0.6, θ = 30° K Joint Test Parameters and Material Properties 266

Table 11.6 β = 0.6, θ = 30° K Joint FE Capacities 267

Table 11.7 FE Peak Loads for β = 0.6 60° K Joints with Varying Brace Thickness 268

Table 11.8 Direct Stresses for Elements 163 to 168 (Chord Top Face) 272

Nomenclature

Symbol	Title
E	Modulus of elasticity (kN/mm^2)
p_y, f_y	Yield strength of material (N/mm^2)
p_u	Ultimate tensile strength of material (N/mm^2)
a	Fillet weld throat thickness (mm)
b_e	Effective bracing width (bracing onto chord) $\frac{10.0}{b_o/t_o} \cdot \frac{p_{yo} \cdot t_o}{p_{yi} \cdot t_i} \cdot b_i$
b_{ep}	Effective bracing width (for punching shear) $\frac{10.0}{b_o/t_o} \cdot b_i$
$b_{e(ov)}$	Effective bracing width (bracing i onto bracing j) $\frac{10.0}{b_j/t_j} \cdot \frac{p_{yj} \cdot t_j}{p_{yi} \cdot t_i} \cdot b_i$
b_o	Width or breadth of chord member for RHS (out of the joint plane)
b_i,b_j	Width or breadth of bracing member i or j (out of the joint plane)
d_o	Diameter of CHS chord
e	Joint eccentricity
f_k	Chord sidewall buckling strength (N/mm^2)
h_o	Width of chord in the plane of the joint (mm)
h_i,h_j	Width of bracing member i or j (in the plane of the joint)
t_o,t_i	Thickness of chord and brace member i respectively
β	brace to chord width ratio $\frac{b_i}{b_o}$
γ	Chord width or diameter to thickness parameter $\frac{b_o}{2t_o}$
θ_i	Angle between chord and brace member i

Q_g	Gap parameter (=1.0 for T joints)
K_a	Brace effective area term = $\frac{1+\frac{1}{\sin\theta}}{2}$
Q_β	$\frac{0.3}{\beta(1-0.833\beta)}$
Q_β'	Q_β for $\beta > 0.6$ or = 1.0 for $\beta \leqslant 0.6$
q	Projected area distance of overlap in K joints
Ov	Percentage overlap = $\frac{q\sin\theta_i}{h_i}$
α	Chord Length Parameter = $2L/d_o$
BOMEL	Billington Osbourne Moss Engineering Limited
ECSC	European Coal and Steel Community - Research Agreement 7210/SA/830
el-pl	Elastic-plastic intersection technique
f_y	Yield stress from stub column tests (N/mm^2)
i	Imperfection
M-planar	Multiplanar

CHAPTER 1

INTRODUCTION

1.1 Introduction - Tubular Sections - A Brief History of Research.

The popularity of structural hollow sections has increased considerably world wide in recent years due to their increased availability and structural advantages. Their particular advantages are their high strength weight ratio upon subjection to axial load, their aesthetic advantages from an architectural point of view, ease of maintenance (smaller surface area to paint) and less surfaces for ponding of water and hence corrosion possibilities and their relatively high second moment of area, I in all directions which gives good resistance to axial buckling.

There are several problems however associated with the relatively thin walls which are susceptible to collision damage and in particular to the difficulties of formation of the joints between the members. Such arrangements can cause high local axial or flexural stresses at various points in the member walls. In the case of circular hollow sections (CHS) profiling of interconnecting members is often essential.

This had been a major problem with CHS but with the development of square and rectangular hollow sections (RHS) the practical difficulties in the fabrication and profiling of the joints

have been largely overcome with a consequent reduction in connection cost. This has led to a substantial increase in the use of RHS in off and on-shore situations. CHS however remains the main form for constructing offshore oil and gas platforms due to their better resistance to the wind and ocean loading. CHS's also possess the same radius of gyration and second moment of area in all directions giving them greater stability against buckling when acting as struts or columns. This is particularly valuable for structures where environmental loadings are of paramount importance.

Both CHS and RHS connections have therefore been the subject of considerable research effort in the past 30 years using experimental testing. Significant theoretical work based on yield line theory has been used for RHS joints. More recently non-linear FE analysis has come into its own as a research tool. Dissemination of the results of this research has been aided in the last ten years by a series of International Symposia on Tubular Structures.

1.2 Factors Governing the Design of Tubular Structures

The design rules governing the behaviour of tubular steel structures cover two main areas. The first of these is the ultimate static strength of the structure, that is to say the loading magnitude that will cause total or partial collapse of the structure. Naturally this is of paramount importance to the designer and determines the geometry and material properties of the structural members selected. The second major factor is that of the fatigue life of the structure. This is particularly important in offshore situations where structures are subjected to a large amount of cyclic loading

through wave and wind action. This generally leads to crack propagation around the weld toes in the joints, leading to loss of structural integrity. The main problem for the designer is therefore to predict how long it will be for a crack to emerge and then when will the joint be no longer fit to fulfil its purpose and repairs become necessary. Fatigue design is not such a major concern in most of the on-shore situations since significant dynamic loading is not usually so common.

1.2.1 Static Strength Design of Tubular Connections

Design of structural members is well understood both in practice and in theory; however, this is not the case for joints and connections. However several design guides have been compiled using combinations of experimental test results, backed up where possible by yield line theory. A review of the current guides available is undertaken here, this being split into two sections, the first dealing with CHS and the second with RHS.

1.2.1.1 Static Design of Joints in CHS

Static strength recommendations for CHS joints are entirely based on statistical analysis of test databases. Several codes of practice are in existence the three major ones being :-

1) HSE (Health and Safety Executive -formerly Department of Energy): Background to new Static Strength Guidance for Tubular Joints in Steel Offshore Structures (1991).

2) API (American Petroleum Institute): Recommended Practice for Planning, Designing and Constructing Fixed Offshore Platforms. API RP2A, 19th Edition (1991).

3) IIW Document XV-701-89: Design Recommendations for Hollow Section Joints - Predominantly Statically Loaded (1989).

The first two were created primarily as offshore design guides while the IIW recommendations were developed for conventional rolled hollow section for use in on-shore situations. These recommendations have been adopted for use in the Eurocode EC3 (1991) rules for tubular joint design presented in Annex K.

Perhaps the most useful of these is the HSE document (1990), as it provides an understanding of the approaches used for CHS code derivations. Here, joints are considered as belonging to a particular family, as shown in Figure 1.1. A review of the available experimental joint data is provided, accompanied by a certain amount of screening for data where doubts exist about its validity, or the information is incomplete. Various scatter plots are then established in order to quantify the effects of the parameters on joint capacity. Addition of constants after the creation of lines of best fit through the data and statistical adjustments to ensure conservatism results in the formulation of the design capacities for the joints. Similar techniques are used for the other design codes.

1.2.1.2 Static Strength Design for Joints in RHS

Design for RHS joints is covered in only one of the three guides formulated, that of the IIW. As for the CHS guide many recommendations have been based on experimental work, but a significant number of the design recommendations have been

backed up using the yield line theory approach, for example Davies and Roper (1975), on gap RHS K joints.

Experimental testing is time consuming and expensive and recently there has been a growth in the use and popularity of non-linear FE analysis for assessing joint ultimate behaviour. Difficulties and differences in modelling approaches adopted have as yet restricted the application of its results for use with the experimental databases. It remains however a useful technique for analysing trends in results due to the fact that models can be analysed rapidly and relatively inexpensively. The growth in popularity is easily illustrated in the increase in the number of papers using FE analysis in the series of Proceedings emanating from the International Symposia on Tubular Structures (1990, 1991 and 1993).

The content of this thesis is concerned with the ultimate static strength of both CHS and RHS joints using the FE method as the main tool for the investigation. However before going on to review here the main classifications of joint types, their particular characteristics and modes of failure, a brief summary of the basis used for fatigue design guidance is given.

1.2.2 Fatigue Design of Tubular Connections

Fatigue design of tubular joints is generally based on the evaluation of Stress Concentration Factors (SCF's) at the member intersections. These SCF's are usually expressed as the ratio of the peak stress (at some point in front of the weld toe on the chord) to the nominal brace stress under service loads. The fluctuating stress range undergone is obtained by multiplying this SCF by the nominal brace stress in the worst loading cases. This stress range is

then checked using an appropriate S-N curve (Stress to No.of cycles to failure) in order to estimate the fatigue life of the structure. Several sets of equations have been used to present the SCF's as these vary with joint configuration, and are generally derived from acrylic model tests, steel model tests or linear elastic FE analyses. Among the most frequently used equations are those proposed by Efthymiou (1988) and Smedley and Fisher (1991). A review of many of these equations including the benchmarking and calibrating of these (to test results not used in deriving the equations) was undertaken by BOMEL (1993) as part of their joint industry tubular joints group activity.

1.3 Modes of Loading and Failure in Tubular Connections

In practice joints are subject to three different main loading conditions. These are illustrated in Figure 1.2. For most truss structures the main loads are axial and these form the basis of the failure mode descriptions.

1.3.1 Modes of Failure in RHS Connections

For RHS joints with branch to chord width ratios (β) < 0.85 (that are not overlapped K joints) the mode of failure in compression is generally associated with a local punching-in of the brace into the chord connecting face. Tensile failure is often associated with the opposite mode, i.e with the outward deformation of the local chord face. Ultimate tensile load is often reached when wall tearing occurs at the weld toe. This failure mode and typical load vs indentation plots can be seen and are described more

fully in Chapter 4, where FE modelling of $\beta = 0.6$ ratio joints is considered. This kind of failure involving one of the chord faces lends itself to the application of yield line theory for T, X and gap K joints used by several researchers (Davies and Roper (1975), Davies and Morita (1991)). For joints where $\beta > 0.85$ compression failure of the joint is more often associated with the instability of the chord side wall as the punching-in becomes impossible for $\beta = 1.0$ (i.e braces and chord are the same width). In these cases the chord sidewall can act in a similar manner to a strut where axial loading is applied. This is illustrated in Figure 1.3. For overlapped and partially overlapped K joints failure modes are more difficult to determine and combinations of different modes of failure are often seen. These are discussed in more detail in later chapters but punching-in/pulling-out of the 'through' brace (Figure 10.2) is often observed along with failure of the braces in the region of the overlap. Tearing of the weld around the toe of the tension brace may occur depending on the loading pattern while failure of the chord beneath the heel of the tension brace has also been observed (Bensalem 1989). In the failure modes of overlapped RHS K joints discussed briefly here it has been assumed that the two braces comprising the joint are of the same width. Should one of the braces support a lower width section then other modes of failure such as punching-in between these members may occur. Details of the basic modes of failure for the fully overlapped K joints are discussed by Roodbaraky et al (1990) and Bensalem (1989). These are restated for the case considered in this thesis of partially overlapped as opposed to fully overlapped K joints.

1.3.2 Modes of Failure in CHS Connections

Failure modes for CHS joints are generally more complicated than those for RHS joints as they do not possess the flat faces. They show much more global 'ovalisation' at failure for medium β ratios (0.4 to 0.8). At very small β ratios (<0.4) where the footprints of the braces are almost flat a local 'punching-in' or 'pulling-out' similar to that associated with RHS joints can occur. These two modes of failure are illustrated in Figure 1.4 for T/Y, X and gap K joints. For larger β (i.e β > 0.8) ratios the problem becomes more complex and failure can be heavily dependant upon the degree of cut-back in evidence on the joint. The cut-back is caused by the curtailment of the brace member before it reaches its wall theoretical intersection point with the chord. The difference between theory and practice on cut-back is illustrated for the full width DT or X joint in Figure 1.5. Here the failure is likely to occur with the small section of the chord PP acting as a strut in compression, deformations being a local flattening of this. For gap K joints of large β ratio failure is likely to occur by a shearing across the gap combined with a tearing of the chord at the weld toe of the tension brace. This is illustrated in Figure 1.6. These failure modes for high β ratio joints are illustrated clearly in the test program undertaken by Billington Osborne Moss Engineering Limited (on-going and confidential) under the 'Joint Industry Tubular Frames Project'. For overlap and partial overlap K joints in CHS failure modes are much more difficult to identify and are often a combination of several of the types described for RHS.

The main content of this thesis concentrates on a series of investigations on various joint configurations. The motivation for examining these joints is recorded in Chapter 2 but a more

thorough analysis of the techniques used to assess and resolve these problems is presented here. The Finite Element Analysis (FE) method has been an accepted method of analysis for a number of years now. It has in particular been used in determining stress concentration factors (SCFs) in tubular joints for application to fatigue life calculations, a review of much of the available data being undertaken in BOMEL (1993). Such analyses are linear elastic a common assumption in many engineering problems. However with the rapid development of computers in terms of space and speed and the emergence of non-linear FE analysis packages, for example ANSYS (1992) and ABAQUS (1991), ultimate strength analyses involving both material and geometric non-linearities can be undertaken.

1.4 Finite Element Methods

1.4.1. Non-linear Structural Analysis

Many engineering problems are assumed to be linear;that is to say that the displacements of the whole FE model are assumed to be infinitesimally small and the material is linearly elastic. However if ultimate behaviour of steel tubular joints is to be examined then the displacements will clearly not be infinitesimally small and the material behaviour will not be linearly elastic. The most general case which should give correct solutions is where the material and model is assumed to be subject to large displacements and large strains, the material properties here also being non-linear (i.e plasticity can occur). The use of a more restrictive formulation can be applicable in certain situations (i.e linear elastic analysis with

small displacements in determination of SCF's for fatigue life analysis) with the advantage of much reduced computing time and disk space and still give reliable results.

For the subject of this thesis - an examination of the ultimate static strength of tubular joints, combined material and geometric non-linearity must be considered. Material non-linearity arises from an elastic-plastic stress-strain relationship while geometric non-linearity arises from changes in the original geometry. Generally the mathematical techniques that can be used to analyse one of these types of non-linearity are applicable to others. The method of arriving at a solution involves trial and error. A trial solution is selected and then used to calculate stresses and forces, equilibrium is checked and the procedure repeated (iteration) until a specified accuracy (or convergence) is reached.

1.4.2 Finite Element Theory

The aim of this section is not to provide a detailed description of FE theory which can be found in many textbooks (Zienkiewicz (1977) and Stasa (1985)) but to give a brief outline of the basic principles involved to enable the reader with little or no knowledge of the FE method to have some appreciation of the method in relation to simple problems and the procedure by which more complex FE models are constructed and analysed. Brief characteristics of the elements used within the work in this thesis will also be discussed.

To simplify the explanation of the theory a two-dimensional truss problem will be considered, taking one element from that. It

can be appreciated that for larger problems, the formulation can be simply built up by repetition.

Consider the following truss problem in Figure 1.7. Taking element e and labelling the ends in the general notation i and j the possible forces and displacements at the nodes are shown in Figure 1.8. Here x′ and y′ is the local axis system for the member, U_j', V_j', U_i' and V_i' are the respective member end forces and u_i', v_i', u_j' and v_j' are the respective displacements at the member ends. Using $P = k\delta$ where k is defined as the stiffness (AE/L in the linear elastic case) we can establish the member end forces in terms of deflections or vice versa. e.g

$$U_i' = AE\,(u_i' - u_j')/L \quad \text{and} \quad U_j' = AE\,(u_j' - u_j')/L$$

These can be assembled into matrix format as here

$$\frac{AE}{L}\begin{bmatrix} 1 & 0 & -1 & 0 \\ 0 & 0 & 0 & 0 \\ -1 & 0 & 1 & 0 \\ 0 & 0 & 0 & 0 \end{bmatrix}\begin{bmatrix} u_i' \\ v_i' \\ u_j' \\ v_j' \end{bmatrix} = \begin{bmatrix} U_i' \\ V_i' \\ U_j' \\ V_j' \end{bmatrix}$$

which can be written as $[\,K^{e\prime}\,][\,a^{e\prime}\,] = [\,f^{e\prime}\,]$ [1.1]

and $K^{e\prime}$ can be expressed as

$$\begin{bmatrix} K^{e\prime}i.i & K^{e\prime}i.j \\ K^{e\prime}j.i & K^{e\prime}j.j \end{bmatrix} \qquad [1.2]$$

This can be performed for each element or component of the structure and each must be converted to the global co-ordinate system to enable all the elements to be compiled together in the whole model.

Let $a^{e'} = Ra^e$ where $a^{e'}$ is as before, a^e is the displacement vector in terms of the global co-ordinate system and R is the direction cosine matrix that can be used to convert from the global to local co-ordinate systems and vice-versa. It is not felt worthwhile to detail the mechanics behind the establishment of R here but derivations of it for particular problems can be found in many textbooks, for example Stasa (1985) and Rockey et al (1983).

Similarly $f^{e'} = Rf^e$ where f^e is the force matrix in the global coordinates.

Using [1.1] $K^{e'}Ra^e = Rf^e$

$$R^TK^{e'}Ra^e = f^e$$

Allow $K_e = R^TK^{e'}R$ then $K^ea^e = f^e$

Once this is completed for each element the whole structure or body being analysed is re-assembled from the elements comprising it. The whole essence of this step is that it is based on compatibility, i.e displacements at a node on an element must equal those at the same node on a different element. The equation system can then be solved using any of the usual techniques. Obviously as problems become large and three-dimensional these equations become impossible to solve manually and hence the requirement for computers with large capacity. This has until fairly recently been the main factor in restraining the use of FE for structural analysis up to ultimate loads.

As an example of the reconstructing of the problem, the simple truss in Figure 1.7 is considered and the nodes and structural

elements are labelled as in Figure 1.9 then we have three elements each having a corresponding stiffness matrix K^e of :-

$$\begin{bmatrix} K^{(1)}_{1.1} & K^{(1)}_{1.2} \\ K^{(1)}_{2.1} & K^{(1)}_{2.2} \end{bmatrix}$$ Element 1

$$\begin{bmatrix} K^{(2)}_{2.2} & K^{(2)}_{2.3} \\ K^{(2)}_{3.2} & K^{(2)}_{3.3} \end{bmatrix}$$ Element 2

$$\begin{bmatrix} K^{(3)}_{1.1} & K^{(3)}_{1.3} \\ K^{(3)}_{3.1} & K^{(3)}_{3.3} \end{bmatrix}$$ Element 3

The structure stiffness matrix, K^a is then assembled as follows

$$\begin{bmatrix} K^{(a)}_{1.1} & K^{(a)}_{1.2} & .. & K^{(a)}_{1.N} \\ K^{(a)}_{2.1} & K^{(a)}_{2.2} & & \\ \vdots & & & \\ K^{(a)}_{N.1} & & & K^{(a)}_{N.N} \end{bmatrix}$$

where N is the number of nodes

In the above example the structure stiffness matrix terms become:

$$\begin{bmatrix} K^{(1)}_{1.1} + K^{(3)}_{1.1} & K^{(1)}_{1.2} & K^{(3)}_{1.3} \\ K^{(1)}_{2.1} & K^{(1)}_{2.2} + K^{(2)}_{2.2} & K^{(2)}_{2.3} \\ K^{(3)}_{3.1} & K^{(2)}_{3.2} & K^{(2)}_{3.3} + K^{(3)}_{3.3} \end{bmatrix}$$

The above procedures have not considered how to apply the necessary loading, provide for boundary conditions to the structure or, how these are taken into account. As for the compiling of the stiffness assemblage matrix the applied nodal forces matrix can be assembled. Forces must be resolved into their global axis components. For example for the truss in Figure 1.8

$$f_a = \begin{bmatrix} 0 & F_x \\ 0 & F_y \\ 0 & F_x \\ -100 & F_y \\ 0 & F_x \\ 0 & F_y \end{bmatrix}$$

In a similar fashion boundary conditions can be applied to nodes. Several procedures can be used to do this, two of which are covered in Stasa (1985). Basically the systems of equations within the matrix are modified to ensure the displacements of the node at which the boundary condition is required (in the original problem formation/stiffness matrix calculation an unknown) is given the specified value. Frequently for many problems this is zero. For example at node 3 in our truss (Figure 1.8) ux = 0 and at node 1 ux = uy = 0.

1.4.3 Steps in Creating and Analysing a Finite Element Model

The aim of this section is to give the reader some idea of the time and effort and alternative methods of establishing a Finite Element model of a tubular joint/connection. Particular reference will be made to the ABAQUS FE package as this is the one used for all the analyses described within the thesis, but similar techniques apply to other packages.

1.4.3.1 Constructing the Model Geometry

Originally, models had to be generated by keying in the coordinates of principal nodes and using commands available to generate nodes between these. Elements are constructed from nodes and again with pre-planning, work can be kept to a

minimum by generating elements in a regular fashion. This method is cumbersome but for regular shapes involving largely straight (i.e RHS) sides it is reasonably efficient. For CHS however regular layout of nodes and elements becomes much more difficult to achieve at the planning stage, especially if the mesh is to be graded (i.e made finer around the tubular intersection). Many hand calculations would also be necessary to define the intersections between chord and brace members.

These difficulties have been overcome by the introduction of geometric modelling and mesh generating packages such as FEMGEN (Femview Limited 1990) and SDRC-IDEAS (1990). These packages can be used to generate meshes onto a system of geometry. The user inputs key geometric points which are then connected via lines and arcs, which are in turn used to generate surfaces. Special facilities allow surfaces to be intersected automatically making light work of problems such as the intersection between members described above. The user can then select certain surfaces or parts of surfaces and generate elements onto them. Control of the mesh density is exercised by specifying any number of parameters, a common one being the number of elements per line/side of the region. These packages have the ability to transfer the node co-ordinates etc and elements to the input deck of any of the major FE suites (e.g ABAQUS 1991).

1.4.3.2 Additional Data for the Analysis

After the initial construction of the model the remaining data and information required to enable the model to be analysed must

be added. This information falls into four main categories and each one will be taken in turn.

(i) Material Properties: The definition of the relevant material properties must be performed. For an ultimate static strength analysis these include the elastic (Young's modulus and Poisson's ratio) and plastic yield strengths and definitions of any further strain hardening properties that the user wishes the material to possess. Elements must also be labelled to a particular material type.

(ii) Boundary Conditions: Establishment of symmetry restraints on various nodes or nodesets as required as well as pins, directional restraints etc must be done.

(iii) Loads: Loads, their type (dynamic, static), their form (udl, point, line etc), their method of application (ramp/step) and the parameters that define when the analysis is to terminate (at a certain load magnitude, at a certain displacement , at a certain convergence etc) need to be added.

(iv) Output: The data output in terms of hard copy, file output, displaced shape and mesh plots must be defined.

Options exist within generating programs such as IDEAS to define these items there. As each of these requires at largest 15-20 lines of input however they do not consume significant amounts of time in model preparation and can be easily added to the input deck after it has been written in ABAQUS format.

1.4.3.3 Mesh Generation

Having mentioned methods of mesh generation it is perhaps apt here to touch on a few items concerning the actual size of the mesh. There is no hard and fast rule for determining the number of

elements and refinement but there are a few aides and accepted procedures for good meshing in order to obtain credible results.

It is accepted practice for each problem encountered to undertake a mesh convergence study. Meshes of different densities are tried and the results are compared. Beyond a certain refinement (i.e a Nº of elements) it is often found that increasing the number of elements no longer has any effect on the accuracy of the solution. Two convergence studies are undertaken on the main models in this thesis but other well documented examples can be found in the literature and many of the Delft reports (de Koning et al 1992, Vegte van der et al 1991) on joint testing and finite element modelling contracts.

In tubular joints problems where high stress gradients occur in the brace-chord intersection regions it is necessary to grade the mesh. A fine mesh is maintained in the intersection area where failure occurs and accuracy is most critical, but a reduced number of elements is used in the outer regions of the brace and chord where stresses are more uniform and accuracy less critical. This is not strictly necessary but if 50 % of the elements can be saved cpu time can be reduced by 60 to 75% with very little loss in accuracy providing care is taken. The reader need only look at any mesh contained within the finite element papers in the 'Tubular Structures' conference proceedings (1990, 1991 and 1992) to observe examples of this grading.

It is also accepted as good FE practice to keep the aspect ratios (for a shell element length to width ratio) of the elements as low as possible (ideally one to one) . This is to say that long thin elements should be avoided where at all possible. Where practicable this is adhered to in this thesis, although in certain cases this has proved

difficult, other researchers also having the same problem. This will be discussed in more detail as it arises.

Due to the large computing capacity required for the operation of finite element packages a workstation such as a SUN SPARCII or a mainframe computer (if there are likely to be several parallel users) is necessary. At Nottingham computing capacity is met by an ICL VAX mainframe, although capacity for jobs is artificially limited to ensure fairness and equality between the users of ABAQUS.

1.4.4 Main Elements in Use

Generally in Finite Element analysis there are three main types of stress displacement elements, solid, shell and beam as described briefly below.

1.4.4.1 Solid Elements

These are the basic volume elements available within the program and consist of linear and second order (quadratic) elements. There are three basic forms available within ABAQUS: truss elements (can transmit axial forces only with three displacement degrees of freedom), plane stress and strain elements (with two planar degrees of freedom) and three dimensional solid elements of either tetrahedral, triangular prism or brick formats, these element nodes having three displacement degrees of freedom. These solid elements (triangular) are used to model the weld in several cases in this thesis.

1.4.4.2 Beam Elements

These elements allow for bending and stretching and are most useful in modelling of whole structure such as offshore jackets. They are available within ABAQUS in two different formats, in-plane (two displacement degrees of freedom and one in-plane rotational degree of freedom) and three dimensional where all six degrees of freedom are active.

1.4.4.3 Shell Elements

These elements generally have five degrees of freedom per node, with rotation in the plane of the shell element not considered although some, including the shell section elements used in the analyses contained within this thesis contain six degrees of freedom per node. As shell elements are the main elements used in this investigation and for tubular joint analysis generally it is intended here to briefly describe their development, advantages and reasoning behind these.

For problems involving the analysis of curved shell-like structures (pipes and tubes etc) it would appear that the use of solid elements with a reduced thickness would be appropriate. However numerical problems as noted in Zienkiewicz (1977) may occur and more importantly the use of several nodes across a shell thickness is uneconomic and ignores the fact that for thin shells the normals to the middle surface remain practically straight after deformation. This carries severe penalties in the computing time required to analyse such problems. These constraints led to the development of the shell element where the element is divided into several

through thickness layers and only one node is required through the thickness, an example shell element being shown in Figure 1.10. Several types of shell element are available within the ABAQUS suite including both four and eight noded quadrilateral elements and various forms of triangular elements. These are all available as thick (6 dof) or thin (5 dof) shells. It is the thick shell type of element that is used exclusively to model the main brace and chord members in this thesis. The two elements used in this thesis are the four noded and eight noded thick shells, these being illustrated in Figure 1.11. The integration points number one in the four noded shell and four in the eight noded shell. The number of layers within the shells can be determined by the user, the default being five, the ABAQUS manual (1991) recommending that this is suitable for simple non-linear problems such as the limit load analysis considered here.

1.5 Conclusions.

This chapter has briefly summarised tubular joint development, modes of failure and approaches used to derive design guidance for both static and where appropriate fatigue strength. It has also given the reader unfamiliar with finite element techniques a brief introduction to the finite element method and how it is used in practice to analyse problems. The main elements in use within the work contained in this thesis have also been described.

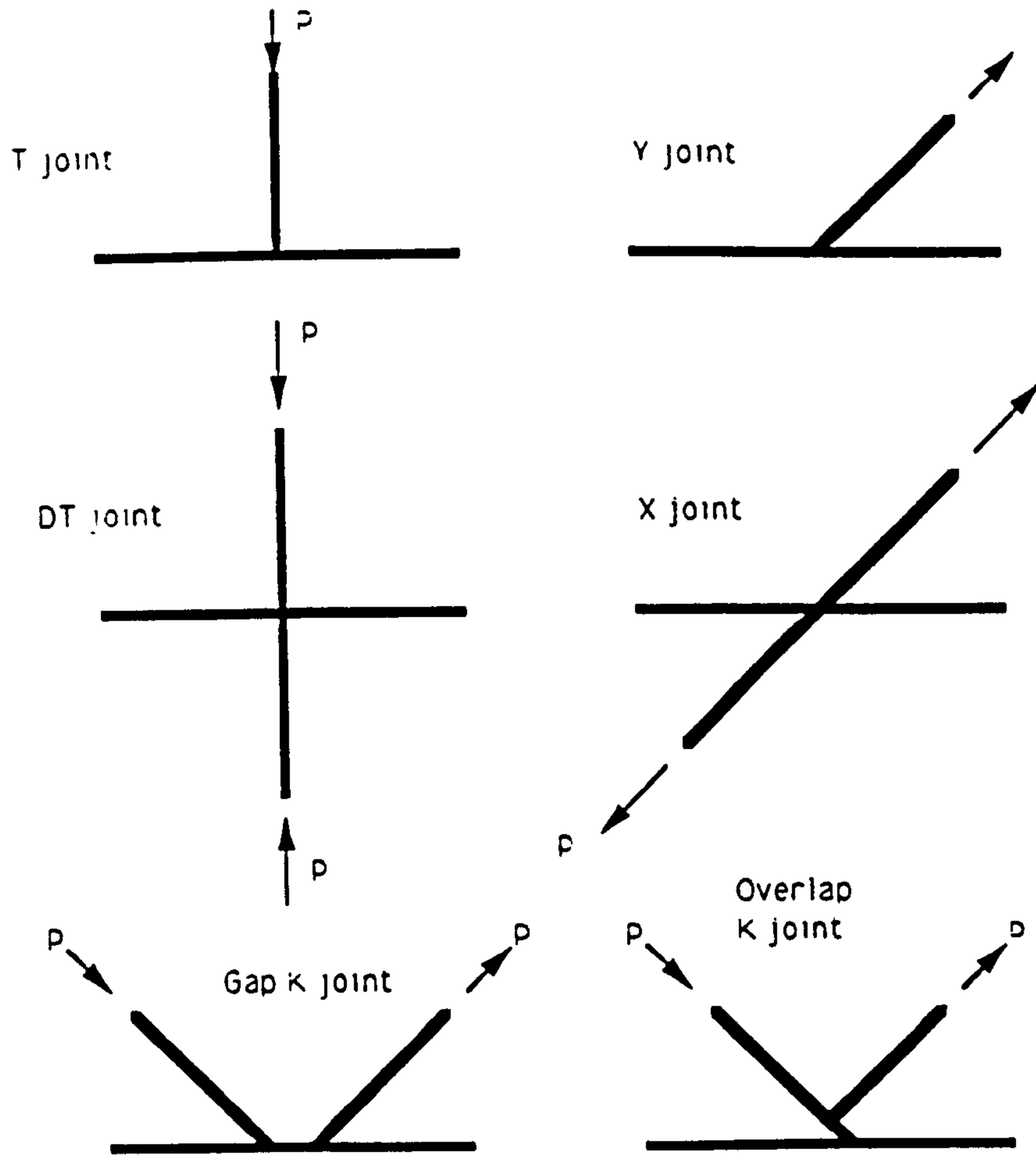

Figure 1.1 Typical Joint Configurations and Classifications

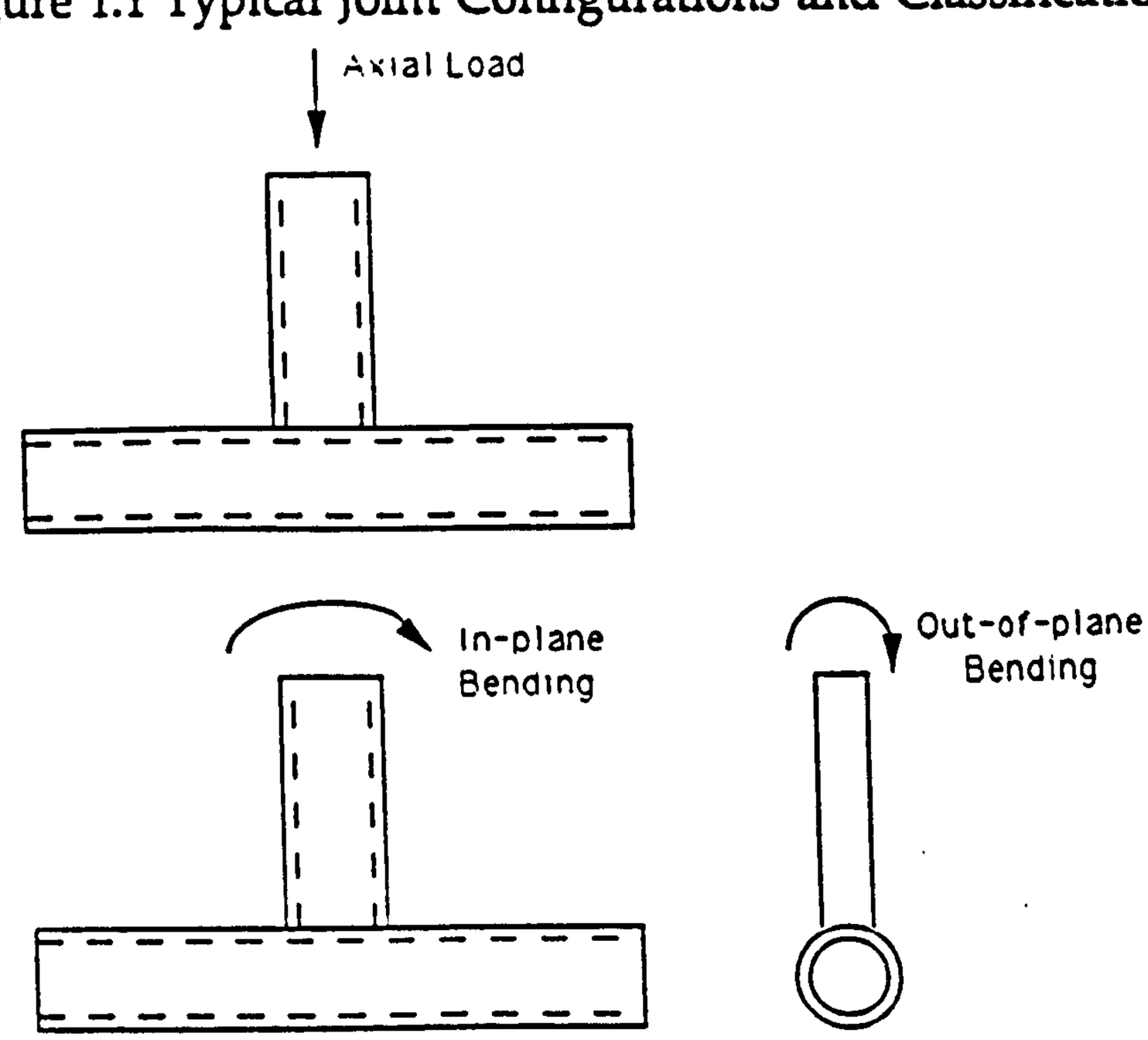

Figure 1.2 A Typical T Joint and Loading Modes

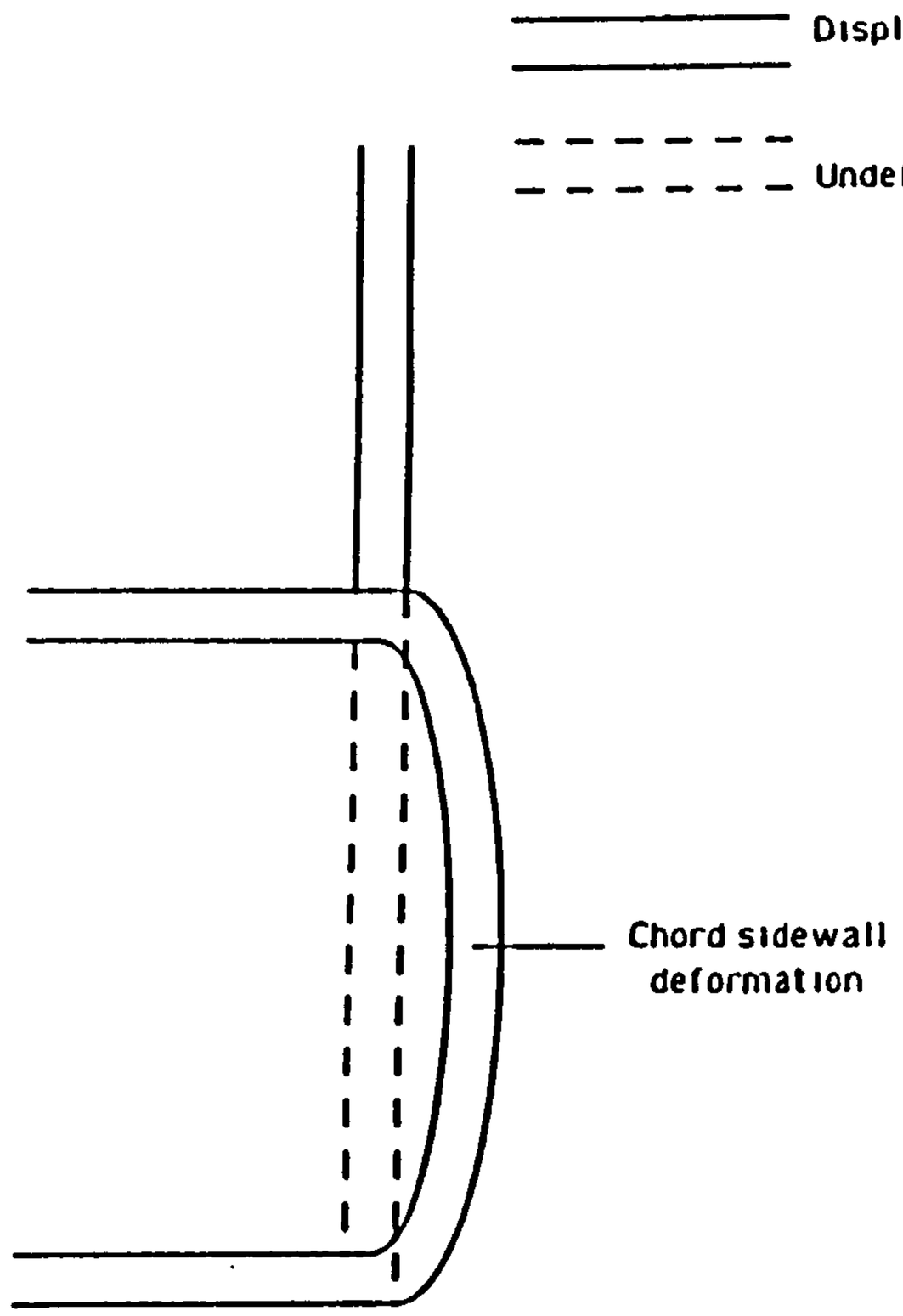

Figure 1.3 $\beta = 1.0$ RHS T Joint - an illustration of side wall 'strut' buckling

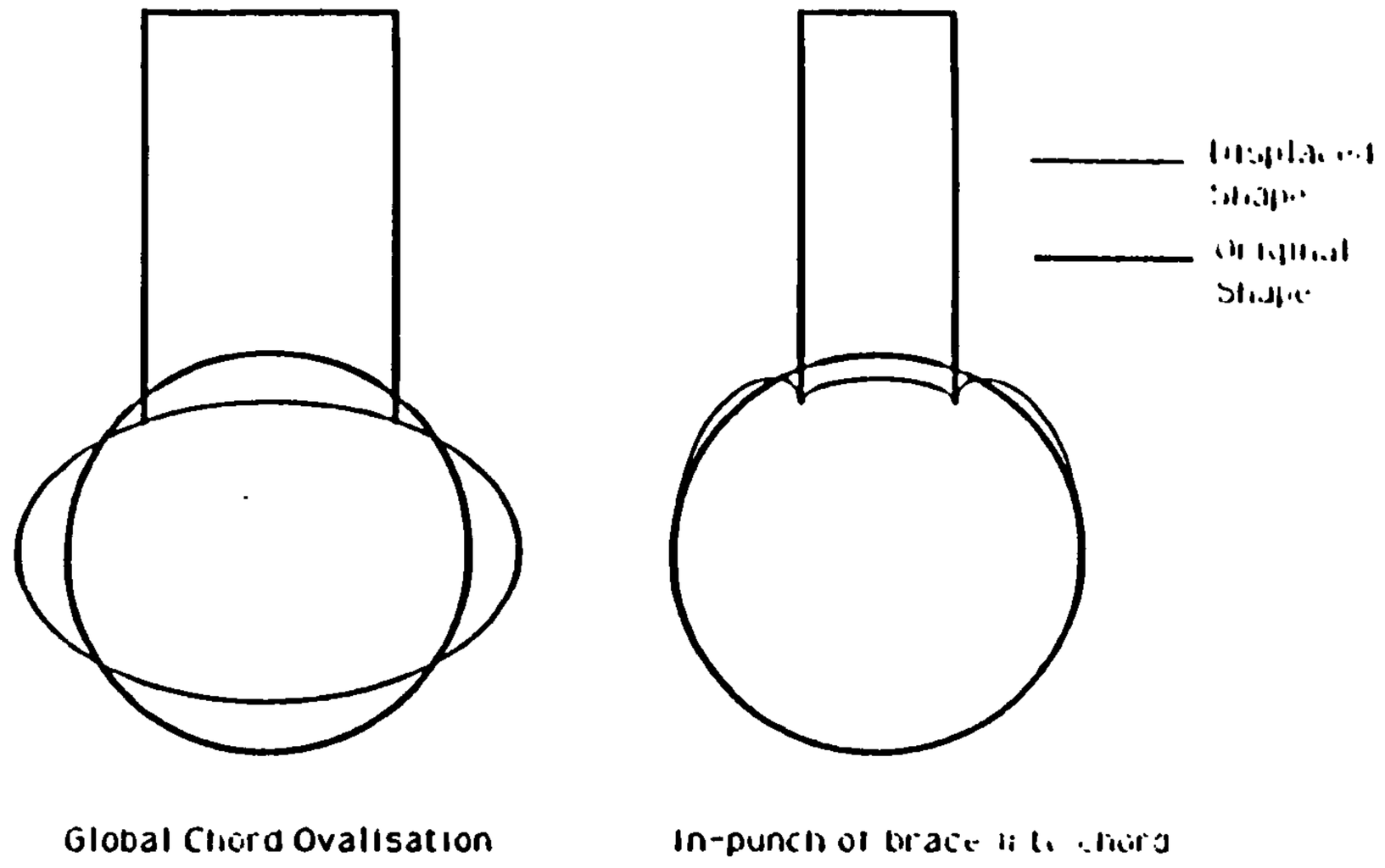

Figure 1.4 Typical CHS Failure Modes

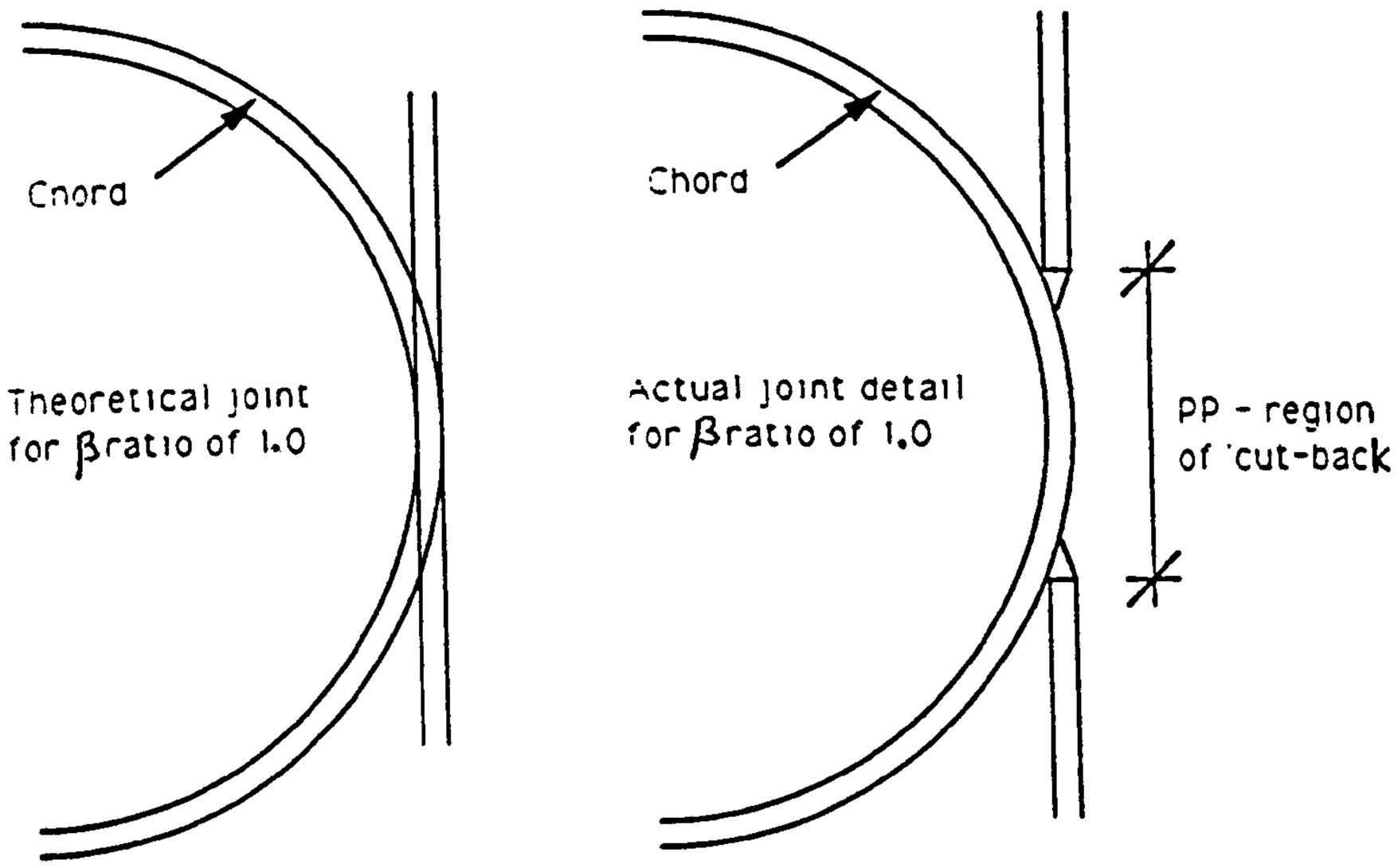

Figure 1.5 Weld cut back on CHS β = 1.0 Joints

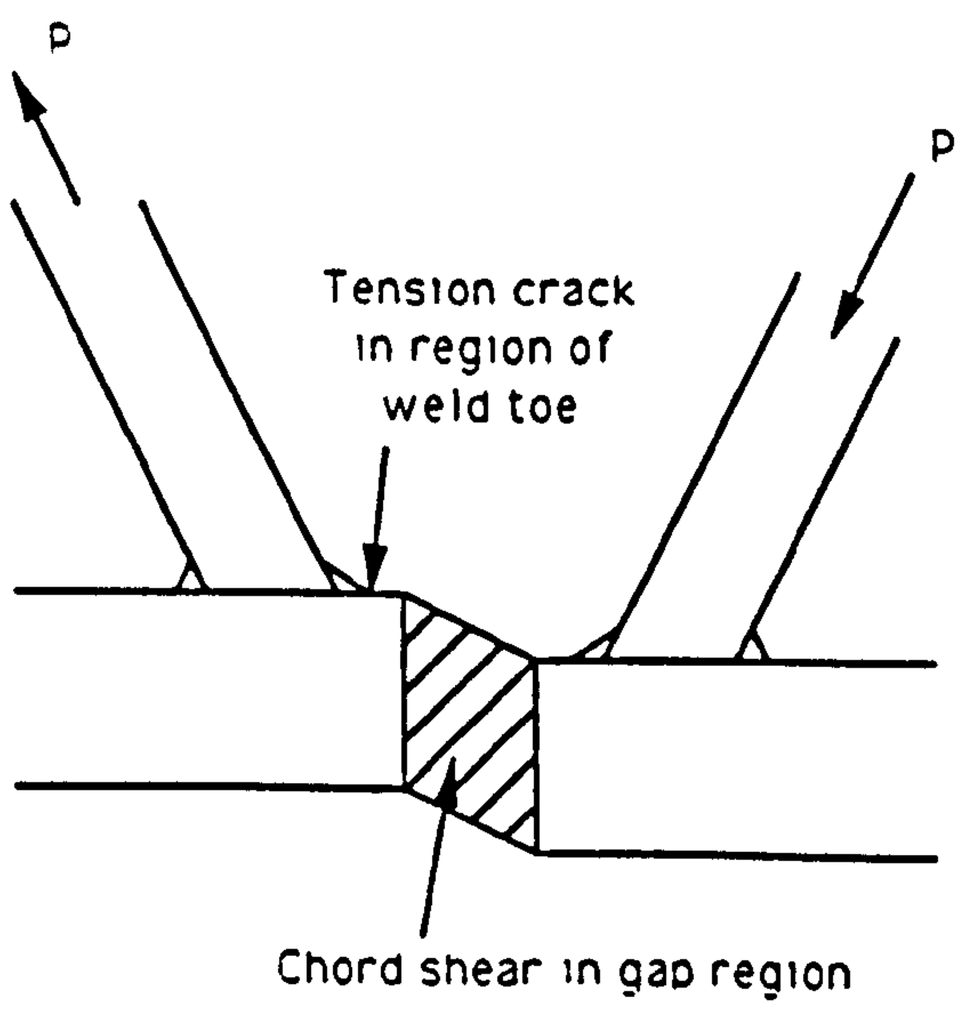

Figure 1.6 Gap K joint with $0.85 < \beta < 1.0$

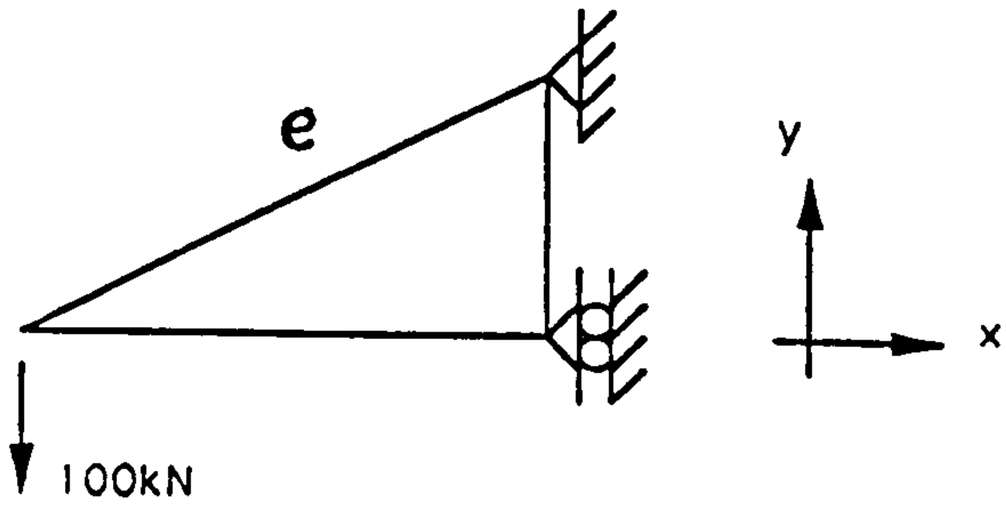

Figure 1.7 A Simple Truss Problem for Finite Element Analysis

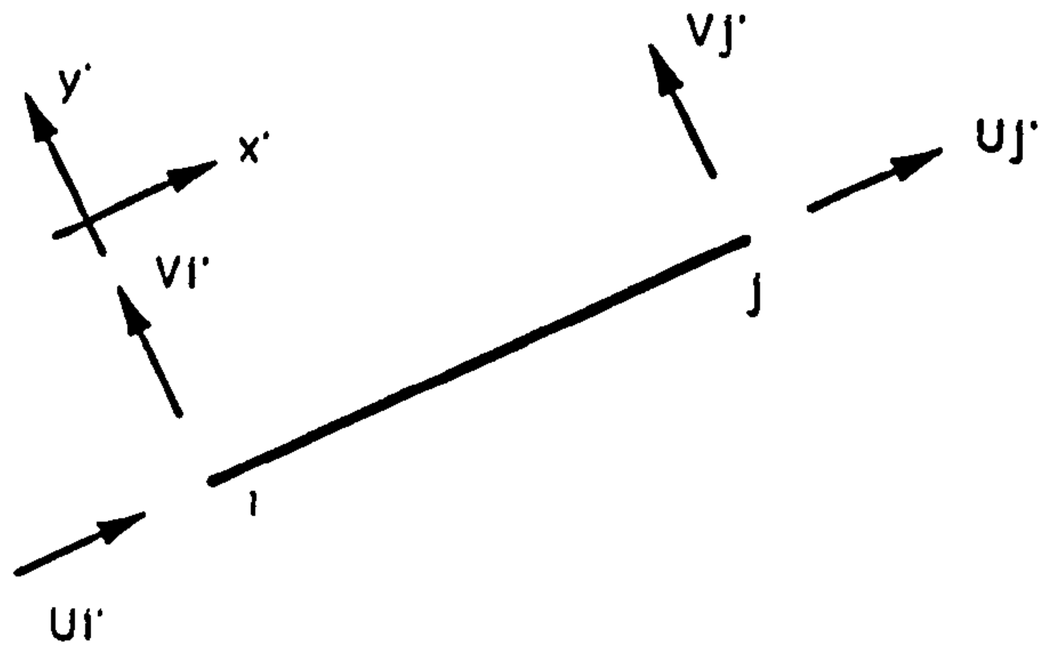

Figure 1.8 Element 'e' forces and displacements at nodes i and j in the local axis coordinate system x'y'.

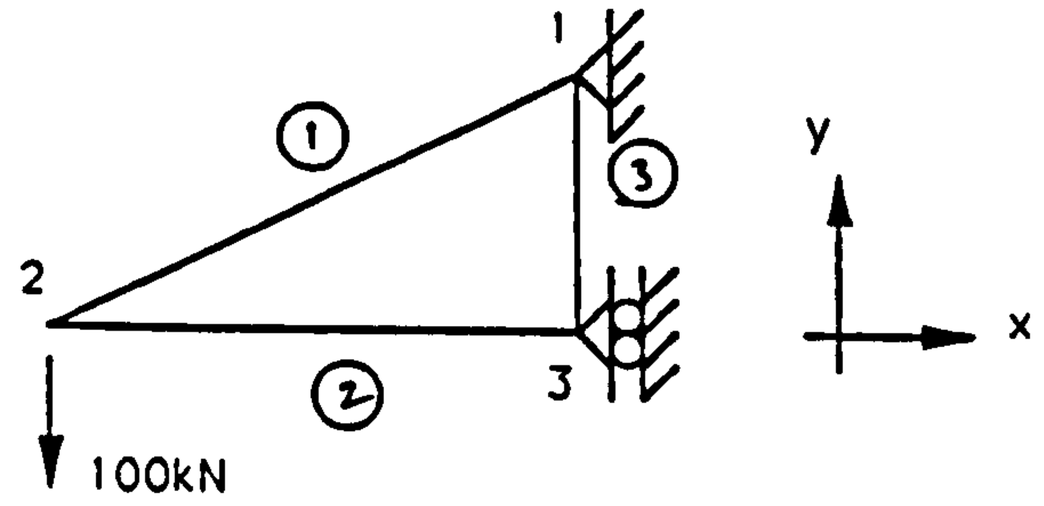

Figure 1.9 Node and Element Numbering System for the Truss

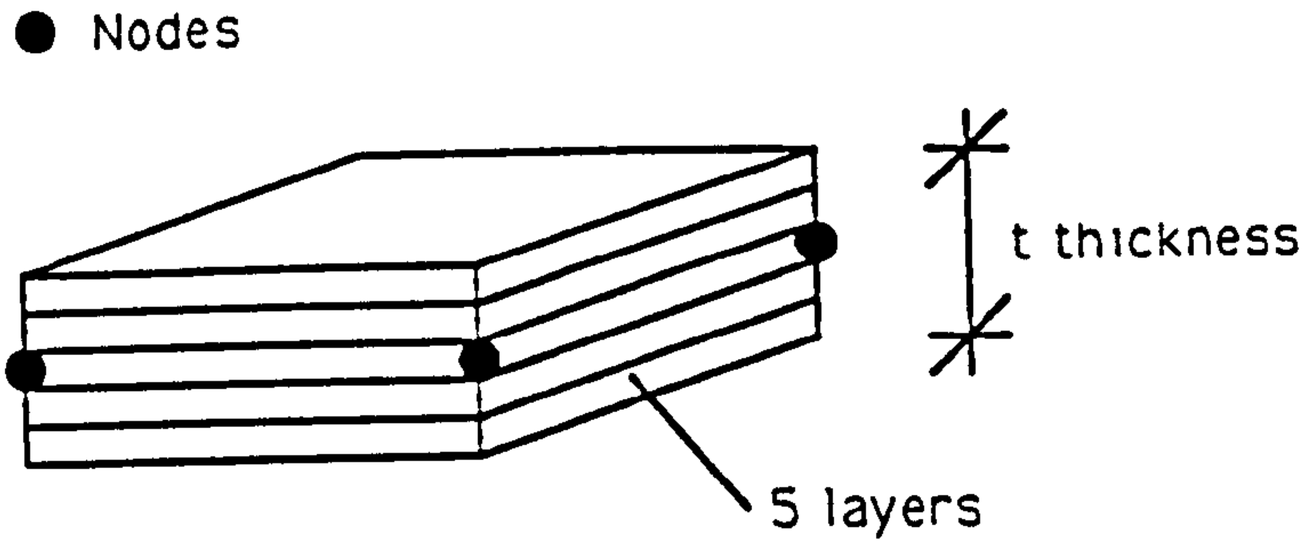

Figure 1.10 Structure of a Typical Shell Finite Element.

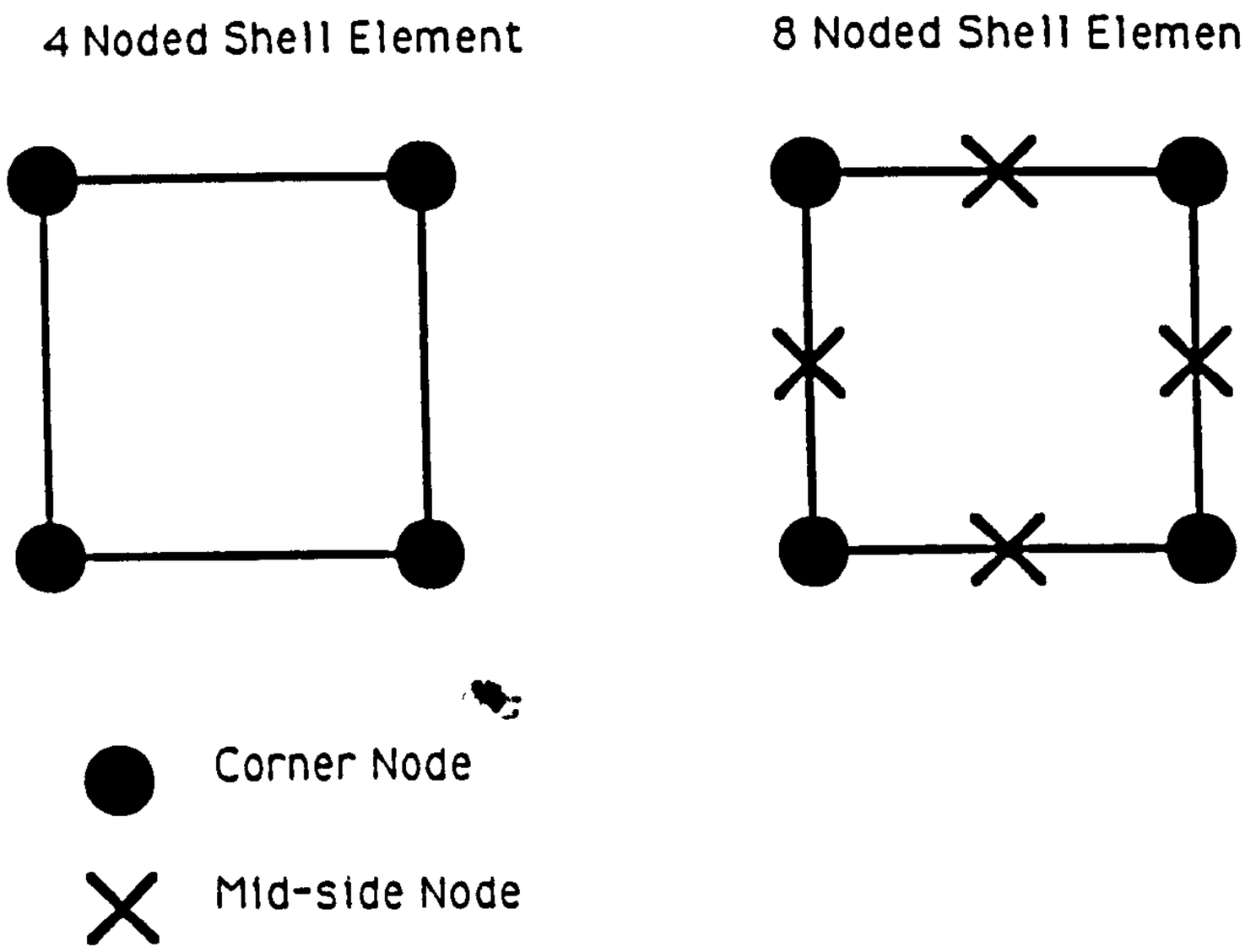

Figure 1.11 Configuration of Four and Eight Noded Shell Elements

CHAPTER 2

A REVIEW OF THE LITERATURE.

2.1 Introduction

The aim of this literature review is to outline the progress of research and development work in tubular joint behaviour over the years. This includes the development of engineering codes of practice and the emergence of non-linear finite element analysis for determining the ultimate static strength of joints. It also includes a review of the existing literature on the development of the behaviour of multiplanar CHS and RHS connections. A considerable amount of this work, particularly on the RHS has only entered the literature during the duration of this thesis; nevertheless it is still felt appropriate to discuss it here in order to establish a 'state of the art' review. Brief outlines on the motivation for the other work undertaken on existing problems within planar connections will also be given here but will be discussed in more detail in the relevant chapters.

2.2 Tubular Connections and Development of Joint Design Guidance

Welded tubular steel sections are used extensively in the

construction of lattice on-shore frameworks and offshore jacket structures. Their efficiency in compression, good dynamic response characteristics and ease of maintenance all contribute to their increasing popularity. Originally these connections were difficult to fabricate for CHS but this has been largely overcome by improvements in technology and the development of RHS sections. This has led to the increasing use of RHS on-shore while CHS remain popular offshore due to their superior dynamic behaviour which is a critical factor in off-shore situations. In open sections connections are made via gusset plates, members being bolted or welded to these. In hollow sections the gusset plate requirement is no longer necessary.

Since 1963 and the formation of CIDECT, many design recommendations have been produced for both CHS and RHS joints, for example the IIW (1989) recommendations. CIDECT has also acted to coordinate research internationally enabling dissemination of results and avoiding wasteful duplication of effort. A comprehensive review of CIDECT initiated work and resulting reports and recommendations is given by Yeomans (1991)

2.2.1 Circular Connections- Development of Design Guidance

2.2.1.1 A Brief History of the CHS Joint Design Codes

Around the time of the formation of CIDECT an American engineer, Johnston (1963) undertook a review of available CHS data and organised a joint industry attack on the problem of CHS connections for oil companies operating in the Mexican Gulf. The

ensuing research effort resulted in the first U.S design guides covering the problem but with most the emphasis being on theory. Marshall, in his book (1992) also noted that a large body of work undertaken in Japan was brought to the attention of the Americans. Due to the interest of the offshore industry many large testing programs have been undertaken over the years and these have resulted in several codes emerging, some aimed at general design, for example the AWS (1988) and IIW (1989) recommendations and some aimed specifically at the offshore situation, for example the HSE (1990) and API (1991) guidance.

2.2.1.2 Circular Hollow Section Joints - Development of Codes

In the field of circular hollow sections design codes are largely based on analysis of experimental test databases, the HSE (1990) background document being a good example of this. This document contains a full description of the procedure and data used in deriving the ultimate static strength formula. Assumptions and reasoning/validation for each of these are detailed within the document; however a brief description of the document to give an idea how the formula were arrived at is given here.

This document was updated in 1990 to include the full range of CHS experimental results performed up to 1985, previous D.En sponsored design guides having been limited to a report from Kurobane et al (1976). A brief review of other existing codes including earlier versions of the API (1991) document is also undertaken and the introduction also covers the transition from permissible stress to a

limit state approach in the design of tubular joints. The main advantage of the limit state design is that the safety factors relating to the material properties and design loads etc are treated separately ensuring that the differing degrees of uncertainty with regard to each one can be properly identified and quantified. In the permissible stress approach the global factor of safety is assumed to cover all aspects with regard to material properties and loads.

The general strategy adopted within the document is as follows:-

(i) a reliable database is established and screened (suspect or incomplete data is removed according to various quality criteria).

(ii) the effect of each parameter known to govern strength is established for different joint configurations and loading modes. In this code these take the form of scatter graphs. Constants, mean lines and characteristic lines can then be developed. Examples of these scatter graphs and datasets can be seen later in Chapter 8.

(iii) formulae developed

(iv) ranges of application for the formulae are then given so as to exclude their use outside the ranges of experimental results available.

(v) design strength equations are defined from statistical analysis of the data to obtain the mean and a measure of the spread of the results.

Some 200 references were used in establishing the expressions for the static strength of tubular joints. These ranged from individual tests, to much larger test programs such as the Society of Steel Construction of Japan program (1982) and the program undertaken by Kanatani (1966). These were screened to eliminate various dubious data according to the following criteria:-

1) Results where the chord diameter was less than 125mm. This was due to concern over actual scale effects. Where only nominal yield strengths (unmeasured) were given, results were discounted due to lack of evidence on unconservative safety margins.

2) Where failure did not occur at the joint (ie brace yield) results were discounted.

3) Where the tests were carried out with short chords ($\alpha < 5.0$ where α is 2L/D) the results have been discounted. This is due to concerns about the chord end conditions affecting the capacity of the joint. An illustration of this is shown in Chapter 8 when discussing the CHS T/Y joint problem.

4) Ultimate loads taken in the dataset are the maximum loads reached during the experimental tests.

The remaining screened data is then classified according to joint and loading type and the main factors affecting the strength of joints analysed. Basic expressions for the three main loading modes are then identified and the influence of the factors quantified on scatter plots. Before dealing with each category in turn several basic assumptions and considerations are discussed including the effect of chord length, the brace angle inclination (appears as the $\sin\theta$ term in design codes) and K_a (brace area of projection onto the chord) which are common to all joint configurations.

Design guides such as this therefore provide comprehensive reviews of the main experimental results in existing literature, these being the major basis of CHS design guidance compilation to date.

2.2.1.3 On-going Problems and Concerns over the Codes

Study of guides such as the HSE (1990) reveals several areas in which knowledge is lacking. For the databases of planar T/Y joints and DT/X joints under axial loads there is very little Y joint data and no X joint data (i.e $\theta < 90^o$). This creates problems in the validation of the formulae for these joints, particularly for factors such as K_a (K_a = 1.0 for the T joints), this being discussed later in Chapter 8. Observing other data such as the K joints under axial loads, a large spread of experimental results exists within the data with differences up to 70% where the gap parameter, g/D is small (0.05). Several explanations may be given including the effects of the size of the weld on the gap size (reducing the nominal gap) and the effects of different boundary conditions on the joint test capacity. An illustration of this is provided in the paper by Seyed Kebari et al (1992). There is a general absence of data concerning joints under combined in-plane and out-of-plane moment loading within the databases in this code. No recommendations are made with respect to multiplanar connections, guidance only being given for planar joints. This is common to all design guides except the AWS (1990) which has some recommendations based on elastic considerations. However the recent CIDECT publication "Design Guidance for CHS Joints Under Predominantly Static Loading" (1991) contains some guidance for certain joint configurations based on the work undertaken in the last ten years by various researchers. This work will be discussed later in 2.4.3.

2.2.2.Rectangular Hollow Section Joint Design Guidance

2.2.2.1 A Brief History of Research.

Most of the research undertaken on RHS has been coordinated by CIDECT. RHS have only been available in a mass produced form since about 1960. Initial planned research was undertaken at Sheffield in the 1960's largely on several series of N type joints (Eastwood et al 1967, 1970) with RHS chords and both RHS and CHS braces. Separate tests within the program involved both ultimate static and fatigue loading.

2.2.2.2 Rectangular Hollow Section Joints - Development of Codes

As for CHS, RHS codes are largely based on statistical analysis of the experimental test database. The CIDECT monograph 6 is the background document for the IIW (1989) design recommendations on RHS joint capacity. These CIDECT design guidelines are currently being adopted as the basis for the tubular joint design guidance in Eurocode EC3 Annex K (1991). The monograph contains several sections and takes a slightly different approach to that of the previously described HSE (1990) design guidance for CHS. Initially a review of available experimental literature is undertaken and the joint types and loading modes tabulated according to the joint configuration and loading mode. This is followed by a brief review of the major experimental programs giving more detail of these. Failure modes observed are then discussed and on the basis of this ultimate design capacity equations are formulated. There is however an important difference in the

formulation of the design capacities within the CIDECT RHS code when compared to the CHS design guidance in the HSE (1990) background document. In sections (i.e where formulae are evaluated for T and X joints where $\beta < 0.85$) where the mode of failure involves predominantly deformation of the connected chord face, the formula is initially derived from yield line theory and then it is checked against the experimental data to ensure it is realistic and conservative.

Thus for significant proportions of the RHS design guidance, yield line theory is the main tool used in the analysis, this being validated by application of the experimental results.

2.2.2.3 On Going Problems Over RHS Codes.

As for CHS there exist gaps in knowledge and assumptions made within the codes for RHS. These assumptions are less suspect than those to which CHS are subjected due to the considerable amount of validation given by the experiments to the theory. Observation of the experimental literature on which the tests are based reveals similar problems to that of the CHS. There is an absence of data for planar Y and X joints for which the brace angle is not 90°, i.e they are not DT or T connections. The yield line theory is adjusted for these using the projected area of the brace onto the chord (as similar to K_a for CHS), although this is perhaps less suspect than for CHS due to the usefulness and reliability of the yield line methods in determining T and DT joint capacity equations. However no traces of any examination using experimental or numerical (FE) techniques could be found in the literature, hence the reason for the study in Chapter 9 comparing Y/T

and DT/X joints in RHS at various β ratios. Again as for CHS, gaps in the literature exist for K joints and considerable spread within the data exists. Details of the restraint conditions for joints are not considered and there has been increasing interest in CHS about frame behaviour effecting capacity when compared to isolated joint tests, this being addressed currently in the on-going Joint Industry Static Strength Project administered by Billington Osborne Moss Engineering Limited. This has been covered in part within the CIDECT document by some of the data for K joints in RHS being obtained from a series of full scale Warren girder tests at Nottingham (Dasgupta 1970). However there could still be significant scatter in isolated joint tests due to boundary conditions. Also no recommendations are given within the literature as to which brace in overlap and partial overlap joints (the overlapping or through brace) is better to load in tension. For a range of boundary conditions this has been investigated within this thesis. Recommendations are also absent from the guidance regarding the effect of the hidden weld on the strength of partial overlapped K joints. This area has received some attention in CHS using the finite element method by Exxon but as yet the results are still subject to confidentiality restrictions and are hence unavailable. Again no information could be traced addressing the problem in RHS.

As for CHS there is an absence of design guidance for multiplanar joints, some of the issues being addressed by a CIDECT led ECSC sponsored investigation into the multiplanar behaviour of K-K, DT-DT and T-DT joints consisting of both experimental and numerical work to back up the experimental findings. The application of yield line theory by Davies and Morita (1991) indicated that the increase in strength

observed by certain joint configurations in CHS would not occur in similar RHS configurations.

2.3 Non-linear Finite Element Validation for Ultimate Static Strength

The growth in non-linear finite element analysis as a technique for validating experimental results is evident in the papers dealing with the subject in the series of Proceedings from the Symposia on Tubular Structures (1984, 1986, 1990, 1991 and 1993). As yet the technique is still at its early stages and results are not accepted for inclusion into databases and the development of formulae for ultimate joint static strength. The reasons for its current lack of acceptance concern the problems associated with the modelling techniques (elements and meshes), boundary conditions and the ability to model the weld area accurately. The finite element method is however accepted as a powerful tool for examining the effects of changing parameters (i.e t_o, t_b etc) as the model, once verified can be rapidly re-analysed. A good example of this is presented by Healy et al (1993) where $\gamma\,(D/2t_o)$ is varied by changing t_o to establish trends in the in-plane bending strength of CHS T and Y joints and establish whether the various design guides are correctly picking up the trends.

Currently there is a strong emphasis on using the finite element technique to model test results accurately. This enables the basic mesh modelling/support condition modelling to be validated. It is then possible to investigate with a reasonable degree of confidence changes in parameters such as slenderness and loads to establish a much more comprehensive database than would be obtained through experimental

tests with savings in cost also. Examples of this in the literature include O'Connor (1993), Crockett and Davies (1993) and the reports issued by Delft on the multiplanar CHS (Vegte et al 1991) and RHS (de Koning et al 1992) connections. In the absence of experimental results, finite element results may be calibrated to design guidance for simple joints. Care must be taken in interpretation of the results however as design formulae are sometimes based on data which is not comprehensive and on certain assumptions (for example K_a) as discussed earlier. Design equations also do not represent the mean of the data on which they are based but an adjusted statistical basis which will depend not only on the mean but on the scatter of the data about the mean.

2.4 Developments in Multiplanar Connections

2.4.1 Introduction

Whilst most major design codes give guidelines for planar connections and assume design on a plane by plane basis, in reality most joints are multiplanar, especially in offshore structures. In the last ten years there has been an increase in the consideration of the multiplanar effects of both out-of-plane loads and their associated forces. The main concern centres around certain cases where the planes may interact and cause capacity to be below that of the planar case, this clearly being unconservative from a designer's point of view. As was mentioned earlier in 2.2.1.3 only the AWS (1990) code gives any recommendation regarding multiplanar connections, the basis and limitations of these (largely due to lack of test results) being discussed

by Lalani and Bolt (1990). This lack of information has led to a steady increase in research effort throughout the 1980's in the Netherlands (Paul et al 1990) and Japan (Makino et al (1984), Paul et al (1990)) on CHS multiplanar joints and a recent ECSC funded project undertaken at Delft (de Koning et al (1991) and Yu et al (1993)), Nottingham (Davies et al (1993)), the Steel Construction Institute (O'Connor (1993)) and British Steel (Yeomans (1993)) on a variety of multiplanar RHS connections.

Before going on to review the contents of these in more detail it is perhaps appropriate to review the methods of classification of multiplanar connections.

2.4.2 Classification and Notation of Multiplanar Connections

Marshall's book (1992) outlines a complex binary code obtained from a table to classify joints. However for the review of the literature here a more simple system is proposed. Joints analysed and referred to in the literature will be classified according to Table 2.1.

The assumptions made in the following table are:-

1) Multiplanar joints consist of only two planes located at 90º to each other unless otherwise stated.

2) Each plane is classified according to the simple joint nomenclature described in Chapter 1.

3) Plane 1 is referred to as in-plane (i.e in-plane braces) and plane 2 the out-plane (i.e out-of-plane braces /axial loads etc).

Plane 2

Plane 1	K	KT	N	T	Y	DT	X	Angle
K	K-K	K-KT	K-N	K-T	K-Y	K-DT	K-X	
KT	KT-K	KT-KT	KT-N	KT-T	KT-Y	KT-DT	KT-X	
N	N-K	N-KT	N-N	N-T	N-Y	N-DT	N-X	
T	T-K	T-KT	T-N	T-T	T-Y	T-DT	T-X	
Y	Y-K	Y-KT	Y-N	Y-T	Y-Y	Y-DT	Y-X	
DT	DT-K	DT-KT	DT-N	DT-T	DT-Y	DT-DT	DT-X	
X	X-K	X-KT	X-N	X-T	X-Y	X-DT	X-X	

Table 2.1 Classification for multiplanar tubular joints

2.4.3 Review of the Literature on CHS Multiplanar Connections

The first experiments carried out on multiplanar CHS joints were undertaken at Kumamoto by Makino et al (1984). These concern ultimate static strength experiments on K-K 60º joints. The paper notes that a small decrease in strength occurs as the gap between the in-plane and out-of-plane braces widens (the braces reduce in width or the angle between the two planes increases) but that insufficient data on this variation is available to formulate any design rules.

In the late 1980's a program was undertaken by Delft University involving experimental testing on DT-DT joints (Vegte van der et al (1991)) including a series of non-linear finite element analyses to validate the test results. Compression loading was applied in plane 1, with a variation of zero, compressive and tensile axial loads being

applied in the plane 2 braces. The study concluded that both the presence of the plane 2 braces and axial loads had significant effects on the plane 1 capacity which was not reflected in the codes. In the case of $\beta = 0.6$ equal compressive forces in the two planes increased strength by a factor of three over a planar joint.

In 1991 Paul et al reported on a series of tests on T-T joints with variations in β, g/D and the angle between the planes. Both braces were loaded in axial compression. The paper discusses the various failure modes that can occur and concludes that in all cases tested the multiplanar T-T's give capacities greater than those observed for the planar T joints. The paper compares the results with the AWS (1990) multiplanar formula and concludes that for this type of joint this formula is not reflecting the real effects of the multiplanar braces on capacity. The authors did not investigate the effect of axial compression in one plane with axial tension in the other which may lead to a reduction in capacity over a planar joint. This will be discussed later.

Rondal and Mouty (1992) reported on a series of experimental tests conducted on 94 K-K specimens in CHS at Liege. However, capacities were significantly lower than those obtained by Makino et al (1984). Finite element work undertaken at Swansea by Wilmhurst and Lee (1993) on K-K joints from both sets of tests (Makino and Rondal) have verified the former but have cast doubts about the appropriateness of the testing arrangement and the methods of loading and therefore on these test results. The IIW (1993) have since discounted them.

In 1992, Paul undertook a range of 18 tests on K-K 44.4° and K-K 70.5° joints under axial loading to supplement earlier work

undertaken. Two main failure modes are identified by Paul and the effects on the gaps (in-plane) and between planes are quantified. The paper concludes that existing formulae proposed for CHS K-K joints do not adequately reflect the variation in capacities observed and the AWS multiplanar prediction is inadequate in reflecting behaviour but the capacities predicted by it do fall on the conservative side.

As a result of all this work the latest CIDECT publication 'Design Guide for Circular Hollow Section Joints Under Predominantly Static Loading' (1991) contains limited design rules for the types of 3D joint described above (K-K, DT-DT and T-T) under axial loads. These new design rules take the form of modification factors to be applied to the existing design guidance for planar joints. However this information is limited and in certain cases (DT-DT) it is based on only one β ratio. This can give cause for concern as shown later in this thesis where the β ratio can have a considerable effect on the multiplanar capacity.

2.4.4 Review of the Literature on RHS Multiplanar Joints.

Interest in the development of understanding of multiplanar effects for RHS connections has been considerably less than for CHS, but recently the European Coal and Steel Community (ECSC) has sponsored a large experimental and numerical research project on the K-K, DT-DT and T-DT configurations which with one exception were concerned with in-plane and out-of-plane axial loads. Results of these investigations have only reached the literature recently in the form of conference papers and reports. Several of these, concerning the T-DT configuration were issued from Nottingham and will be dealt with

later in Chapter 4. The others concerning the DT-DT configuration (Delft) and K-K configuration (SCI and BS Swinden) will be briefly reviewed here, reference being made to an earlier paper concerned with ring models by Davies and Morita (1991) which provided some of the stimulus for this work on the three-dimensional effects in RHS.

de Koning et al (1992) undertook a series of eight experimental tests, two on planar (DT) and six on multiplanar (DT-DT) joints. Four joints (including one planar one) were subject to in-plane axial compression with the three multiplanar joints subject to a variety of zero, compressive and tensile axial loads in the out-of-plane braces, the other series was subjected to in-plane bending with similar axial loads to those above applied to the out-of-plane braces. The results of this series of experiments and the numerical modelling also undertaken by Delft will be discussed more fully at the end of Chapter 6 but it is worthwhile to note here that the out-of-plane loads and braces were observed to have significant effects on the ultimate capacity when compared to the planar joints.

Yeomans (1993) describes a set of nine experimental tests undertaken on RHS K-K joints at three different β ratios. This study concluded that for all cases except for $\beta = 0.4$ capacities of the joints exceed the planar mean values. These joints have also been modelled using the finite element method by O'Connor (1993) as part of the same project, this work and comparisons to planar joints being on-going at the time of writing.

CHAPTER 3

MODELLING WELDS AND CORNER RADII IN TUBULAR CONNECTIONS.

3.1 Introduction

Traditionally analysis of multiplanar connections has been undertaken on a plane by plane basis, so that in analysing one plane, the effects of out-of-plane braces (OPBs) and their associated forces are ignored. Recent work undertaken by Vegte et al (1991) on CHS multiplanar DT-DT joints has shown that the presence of OPBs can significantly enhance capacity and the existence of forces in these can either enhance or reduce the capacity further. While this is the case for CHS joints it is unlikely to be so for joints with RHS members. Davies and Morita (1991) using yield line theory have shown that OPBs and their associated forces are unlikely to have similar enhancing effects upon the capacities of RHS joints. Hence the justification for a coordinated program of experimental tests.

In 1992 Davies, Coutie and Bettison undertook a series of experimental tests on RHS multiplanar T-DT joints (i.e T in-plane, DT out-of-plane) under axial loading to ascertain the effect of the presence of the OPBs and their relevant restraints and forces on the stiffness and ultimate capacity of the joints. This was part of a larger European Coal and Steel Community (ECSC) sponsored project into

the behaviour of three dimensional joints in RHS and administered by the Steel Construction Institute (SCI). Experimental and numerical investigations into multiplanar RHS DT-DT joints by de Koning et al (1992) and multiplanar K-K joint experiments at BS Swinden laboratories (Yeomans (1993)), and the numerical analysis by the Steel Construction Institute (O'Connor (1993)) were also included in this project.

The numerical modelling of the 3D T-DT joints experimentally tested at Nottingham was formally undertaken by Delft under contract, but the ready availability of the Nottingham test results with which to calibrate the finite element modelling was an ideal opportunity for gaining experience and developing the complex techniques required to model tubular joint connections. These results form the basis of the FE investigation for examining the effect of modelling the weld for such connections, and with care would allow an investigation of the other parameters not varied in the experimental work. It also allowed comparisons to be made with the Yu et al (1993) investigation using a different FE suite, and the value of constructive criticism of both the FE and experimental work. The remainder of this Chapter deals solely with the establishment of reliable FE weld models. Comparisons of different mesh grades and the use of four or eight noded shells in the modelling of the chord and brace will be dealt with in Chapter 4 alongside the main experimental and FE comparisons for the joint series.

3.2 Experimental Database

The series of T-DT joints experimentally tested are shown in

Figure 3.1. Joint MPJT1 is a planar T joint while joints MPJT2 to MPJT4 are multiplanar and have the OPBs constrained to remain parallel during the test, while joints MPJT5 to MPJT7 replicate joints MPJT2 to MPJT4 apart from the fact that they have their OPBs free to rotate during the tests. The aim of these differences was to attempt to simulate the different restraint or 'frame' conditions that would exist in practical situations. More detailed descriptions of the tests are given in the two reports by Davies, Coutie and Bettison (1992). As can be seen in Figure 3.1 (a), all joints were loaded with compression in the in-plane T brace (IPB), joints 2 and 5 unloaded out-of-plane, joints 3 and 6 being loaded in tension out-of-plane and joints 4 and 7 being loaded in compression out-of-plane. The measured material properties of the joints are shown in Table 3.1 and the measured and idealised (FE) stress-strain relationship is shown in Figure 3.2.

	CHORD		BRACE	
	Nominal	Actual	Nominal	Actual
b_i mm	150.0	150.0	90.0	90.5
h_i mm	150.0	149.5	90.0	89.5
t_i mm	6.3	6.2	6.3	6.2
A mm^2	3600	3505	2090	2062
f_y N/mm^2	355	420	355	423
f_u N/mm^2	490	546	490	530
Weld a mm			6.3	6.9
f_s N/mm^2		392		422

Table 3.1 Joint Material Properties and Dimensions

Strain ε	Stress (p_y) (N/mm^2)	p_y + 10%	p_y + 20%
0.0020	420	462	504
0.0100	420	462	504
0.0405	510	510	612
0.1005	540	540	648

Table 3.2 Details of the weld material properties.

For joints of β ratio = 0.6 the main mode of failure was punching-in of the IPB into the chord top face, although several joints within the experimental series experienced some indentations in the out-of-plane braces alongside the main failure mode, this depending on the sign and magnitude of the out-of-plane loads applied. It is on the basis of the load vs punching-in of the IPBs that the finite element model is predominantly calibrated, although some other comparisons based on chord side-wall deflections and strains in the chord and brace members have been carried out and are shown later in the Chapter 4. It should be noted at this point that the aim of this work is not to duplicate exactly the work undertaken under contract by Yu et al (1993), but rather to use the experimental results to develop and validate finite element techniques that can be used to investigate other joint configurations and to undertake further studies and parameter variations on this particular joint configuration. The remainder of this chapter is concerned solely with the establishment of reliable FE models and the development of appropriate techniques to model the corner radii and welds in order to replicate the test results as closely as possible.

3.3 Finite Element Modelling of the Joint Test Series

Finite Element modelling was undertaken using the ABAQUS package (1991) which includes facilities for both geometric and material non-linearity. Both of these were used in all models. Advantage was taken of the symmetry within the joints to model only one quarter of the joint, enabling savings to be made in CPU time. Details of the boundary conditions required to do this are given in Figure 3.3. Due to their time and capacity saving advantages initial models used four noded thick shell elements to model the chord and brace, no weld modelling being undertaken. Later however eight noded shells were used when more computing capacity became available, comparisons between these two alongside a discussion of the advantages and disadvantages of both being undertaken later in Chapter 4.

The initial finite element results are compared to the experimental ones in Figure 3.4 (a) and (b) with regard to punching-in of the IPB vs applied compressive load. This punching-in is measured between a point on the IPB and the underside corner of the chord as illustrated in Figure 3.5. It is clear from these that the lack of accounting for the weld in these models gives very conservative and unrealistic finite element results. Thus it can be said that if realistic results are to be obtained from the FE analysis the weld must be taken into account in some form in the model. Past research on the weld modelling has been undertaken by Reimer et al (1979), Bhuyan (1986), Vegte (1991) and de Koning (1992) but none of these contain a comprehensive study of the weld modelling and it was therefore felt that a further and more

comprehensive investigation was justified. Thus a wide ranging investigation of the weld modelling was undertaken at Nottingham the results of which, alongside considerations about the corner radius present in RHS members form the remaining content of this chapter.

3.4 Finite Element Modelling of the Fillet Weld

3.4.1 Basic Review of Weld Modelling

Although modelling of the weld is obviously an important issue in joint modelling, there exists no clear or universal consensus on this and very little published material where weld modelling has been undertaken. Reimer et al (1979) used 2-dimensional shell elements to model the weld on a selection of joint types. This was part of a joint industry sponsored project to develop a FE package for the analysis of tubular joints in order to determine SCF's for fatigue analysis. Bhuyan et al (1986) used eight noded (solid) brick elements to model the main joint while using six noded solids in the weld region. It was commented that this method was very time consuming and unjustified as the through thickness stress variation in thin walled structures is often negligible. de Koning et al at Delft (1992) and Vegte et al (1991) have undertaken finite element studies using eight noded quadrilateral shell elements for the weld as well as for the brace and chord. These studies concern the modelling of both RHS and CHS multiplanar DT-DT joints. There are several difficulties within these two pieces of work. The first of these is what thickness to make the weld shell elements (throat thickness (Figure 3.6(a)) or equivalent area (Figure

3.6 (b))) and the dimensions and distances from the brace chord intersection of the points of attachment (x and y in Figure 3.6 (b)). The modelled area may also contain an 'air gap' which is not present in actual joints, this also being shown in Figure 3.6 (b). Ideally whole joints should be modelled with solid brick elements which would make the problem of modelling the weld much simpler. However such a method would be very impractical as large numbers of nodes would be required, especially if several analyses were desired as it would require extensive CPU time and disk space, then unavailable at Nottingham. However, all these studies have not considered a large range of models and most have been aimed at a linear elastic type analysis in order to evaluate SCF's for fatigue design. Hence an investigation using several element types and connectivity variations for the weld and the widely accepted shell elements for the brace and chord was undertaken. This would establish which models were most reliable and accurate for ultimate static strength analysis.

During the study two separate elements have been used to model the brace and chord sections of the joint, the four noded thick shell element and the eight noded thick shell element. Although it is acknowledged by researchers that the four noded element is less accurate than the eight noded shell, due to it having only one integration point compared to four for the eight noded shell, it does have the advantage of a reduced analysis time and in certain situations as shown in the series of analyses in Chapter 4, may offer results of comparable quality with the advantage of a substantially reduced analysis time. This can be beneficial especially if many analyses are required.

The results of this investigation are now considered in two sections, the first dealing with the FE weld models using the four noded shell to model the brace and chord, the second using the eight noded shells. The FE model series using four noded shells was established on joint MPJT1 (planar) while that using the eight noded shell was, for reasons discussed later, established on joint MPJT3. Comparisons between the best weld model from both the four and eight noded joint series are undertaken on the whole series of seven experimentally tested joints in Chapter 4.

3.4.2 Weld Models Considered with Four Noded Linear Shell Elements used to Model the Brace and Chord

This investigation was undertaken on the model of the planar joint, MPJT1 shown in Figure 3.1. Four basic model cases are considered and the brace and chord elements are modelled using four noded thick shell elements. In these four models, unless otherwise indicated, the stress-strain relationship of the weld material is taken to be that of the parent metal, i.e Grade 50 steel (see Figure 3.2). Welds are modelled using both four noded shells and six noded solid elements with different layouts and methods of fixity. Each weld model will now be considered in turn.

3.4.2.1 Weld Model Case (a)

In the first instance the weld is modelled as shown in case (a) in Figure 3.7, using six noded solid elements for the weld material, where the nodes of the weld elements are shared with the nodes of brace and chord elements. In Figure 3.8 a comparison of the FE

results for case (a)(i) with the FE result with no weld and the experimental results with regard to the brace indentation described earlier is presented. It is clear from these two cases that a significant difference exists and that the physical presence of the weld has an important effect in re-defining the effective brace to chord width ratio β and hence joint strength. The general shape of the load vs indentation curve for the FE analysis can be seen however, to be relatively unchanged. Further modifications of this model illustrated in Figure 3.9 extend the weld around the corner of the brace, either as a right angle (case (a)(ii)) or using a tetrahedral four noded solid element (case (a)(iii)). As expected the orthogonal arrangement case (a)(ii) gives the greatest increase in strength over the base case (a)(i). It can be seen that there is growing divergence between FE and experimental results for large deflections. It is also worth noting that weld model (a)(ii) gives the best agreement in the elastic and early elasto-plastic regime, while both case (a)(i) and (a)(iii) give better results for intermediate plastic regime - but all of the models fail to predict the small reduction apparent in the experimental result for large deflections.

3.4.2.2 Weld Model Case (b)

The second weld model, case (b) in Figure 3.7 uses an offset six noded solid weld model, the weld nodes being physically offset from those of the brace and chord by a distance of $t_o/2$. It can also be seen that a small gap exists between the brace and the chord. This represents the practical situation where the brace is only connected to the chord via the fillet weld. The weld nodes are connected to the adjacent brace and chord nodes by fixing their displacements in all

three directions to be equal utilising the multi-point constraint (MPC) available within ABAQUS (1991). The multipoint constraint option enables the analyst to establish a relationship between specific displacements or rotations (selected by the user) between two or more nodal points in the FE model. Figure 3.10 shows the results of this series of models with respect to the experimental load vs indentation curve. Case (b)(i) is the first model in the series which does not include the corner weld (see case (i) in Figure 3.9), case (b)(ii) includes the corner weld as a right angle (see case (ii) in Figure 3.9). Case (b)(ii)-r is the same weld model as case (b)(ii) but with the corner radii of the chord introduced into the model. There are problems in simulating the corner radius, since the use of shell elements inevitably entails the use of very long narrow elements unless an excessive number of elements are used to keep aspect ratios low. This is undesireable from a computing time point of view. This problem has also been encountered by Yu et al (1993) in their study of these joints and O'Connor (1993) in a similar study on RHS K-K joints.

3.4.2.3. Weld Model Case (c)

The effect of using six noded solid weld model case (c)(i) (in Figure 3.7) is illustrated in Figure 3.11 when compared to the basic form of previously described cases (a)(i) and (b)(i) without the corner weld element in place. Case (c)(i) differs from case (b)(i) by the slight adjustment of the position of the chord nodes constrained to the weld. These have been moved from being directly under the brace centre line to being under the edges of the weld as shown in Figure 3.7. Case (c)(i) can be seen to give good agreement in the

elastic and early elasto-plastic zone, but gives a considerable over estimate when compared to the experimental curves for large indentations.

3.4.2.4 Weld Model Case (d)

The remaining case of weld modelling using four noded shell elements for the weld as well as for the brace and chord is shown as case (d)(i) in Figure 3.7. The results of this are illustrated in Figure 3.12, case (d)(i) not including the corner weld (see case (i) Figure 3.9) while case (d)(ii) includes the corner weld as a right angle (see case (ii) Figure 3.9) using two three noded triangular shell elements in the corner location.

3.4.2.5 Weld Material Properties

As stated earlier all the weld material properties in the analyses up to this point have been assumed to be the same as those of the Grade 50 steel used in the brace and chord. Welds are usually specified to have strength properties greater than that of steel in order to prevent failure occurring in the weld. As tensile tests were not possible on the weld material two additional analyses were undertaken increasing the weld material yield and ultimate stresses by 10% and 20% respectively. These stress-strain relationships are tabulated in Table 3.2 alongside those of the base material used in the other analyses in this chapter that were shown graphically in Figure 3.2. These analyses were undertaken on weld model case (b)(ii)-r on multiplanar joint MPJT2 and the effect of the two increases are shown in Figure 3.13 with respect to the original FE

analysis of this joint. It is clear from this that the difference in joint capacity caused by a significant change in the properties of the weld material is negligible.

3.4.3 Weld Models with Eight Noded Shells used to Model the Brace and Chord

The investigation using the eight noded shell to model the brace and chord was undertaken on joint MPJT3 (see Figure 3.1), one of the multiplanar tension loaded joints, that Delft investigators had found problems in obtaining reasonable correlation with the Nottingham experimental results. Use of the eight noded quadrilateral shell element for the chord and brace allows accurate modelling of the corner radii, as the boundaries of the eight noded shell element can initially be curved, a property which the four noded linear shell element does not possess. This is illustrated in Figure 3.14. Due to this property the effects of differences in modelling the corner radius as a curve or a right angle were not investigated and it was included in the chord as shown in Figure 3.14 (a) in all four cases considered. The series of weld models investigated in this half of the investigation is shown in Figure 3.15.

3.4.3.1 Weld Model Case (e)

This model used six noded solid elements to model the weld. The general layout and attachment being shown in Figure 3.15 case (e) . As can be seen nodes 1,2 & 3 are common to both brace, chord and weld elements and are thus an automatic means of connecting

the weld elements to the rest of the structure. Nodes 4 and 5 are mid-side nodes of the brace and chord shell elements. These are not attached to the weld in any way. The weld is included as a full corner weld (refer to Figure 3.9 case (ii)) and the results of this model plotted against those of the experimental results are shown in Figure 3.16.

3.4.3.2 Weld Model Case (f)

This model also uses the six noded solid element to model the weld. These elements are offset from the chord and brace by half of the chord thickness, this being illustrated in Figure 3.15. The chord and brace are connected together via the weld and a series of multi-point constraints (see 3.4.2.2) ensuring the three displacement components remain equal, mid-side nodes of the brace and chord elements being excluded. Nodes 1-6 are so connected, as are 3-9, 2-8 and 8-7. These are illustrated in Figure 3.15. As before a full corner weld was utilised and the results of this analysis is compared to that of the experimental results in Figure 3.17.

3.4.3.3 Weld Model Case (g)

This model uses the same layout and format as that of model case (e) described earlier. However 15 noded solid elements replace the six noded elements as the weld elements. These elements possess more nodes and integration points than the six noded solid, hence the weld element is more flexible. However with reference to the Figure 3.15, the mid-side nodes 4 and 5 are also common nodes and therefore points of connection between the chord and brace.

Results of this analysis are compared to those of the experiment in Figure 3.18.

3.4.3.4 Weld Model Case (h)

This model used eight noded shells to model the weld, the method of attachment being shown in Figure 3.15. This is similar to the model used by Vegte et al (1991) in their modelling of the multi-planar CHS DT-DT joints. The main problem is in the determination of an appropriate weld shell element thickness t_w. A common approach is to make t_w equal to the throat thickness of the weld and this was the method adopted here. Further investigation of this model and differing methods of determining the weld element thickness are discussed in the work undertaken by Yu et al (1993). The results of this analysis are compared with those of the experimental results in Figure 3.19. Again to ensure compatibility with the other three analyses in this section a full corner weld was used (see case (ii) Figure 3.9).

3.5 Discussion

3.5.1 Limitations of the Weld Models Considered.

Ideally the whole joint should be modelled with solid three dimensional brick and tetrahedral elements throughout but due to the much greater CPU times required it will be much more expensive, prohibitive and currently impossible at Nottingham. Such analyses are only necessary if a rigourous analysis of stresses and strains throughout the whole joint or the region in and around

the weld are required. Therefore for most practical purposes the inclusion of any of the described weld simulation models yields much more realistic results than not including the weld at all.

However all these models have assumptions, compromises and limitations. It is possible that the numerical incompatibility of the solid and shell elements in certain cases is likely to lead to poor calibration with any measured experimental strains in and around the weld area. This numerical incompatibility could be avoided if shell elements were used for the weld. However these too are unlikely to produce stresses and strains in and around the weld region that bear any relation to experimental ones. This will be partly due to the 'air gap' (see Figure 3.6(b)) which does not exist in real joints and partly due to the fact that shell elements can only analyse stress and strain in the two planar directions, whereas in reality the weld area is a complex three dimensional solid region.

Weld Case	Brace/Chord Elements	Weld Elements	Comments & Description
(a)	4N shells	6N solid	Share nodes
(b)	4N shells	6N solid	Offset nodes and MPCs
(c)	4N shells	6N solid	Offset nodes and MPCs
(d)	4N shells	4N shell	Share nodes
(e)	8N shells	6N solid	Share nodes
(f)	8N shells	6N solid	Offset nodes and MPCs
(g)	8N shells	15N solid	Share nodes
(h)	8N shells	8N shell	Share nodes

Table 3.3 Summary of Weld Cases in Initial Investigation.

The nature of the shell elements could also lead to much greater flexibility in the weld area with the possibility of buckling of the weld element. This would not occur in reality due to the solid nature of the weld. Buckling of the weld element is impossible when the solid elements are used in the modelling of the weld. The use of solid elements for the weld also disposes of the problem of determining the dimensions of the weld elements as they can simply be the same physical size as that of the weld on the real joint being analysed. For the remainder of this discussion the reader may find it helpful to refer to Table 3.3 which summarises details of the weld cases described above to aid reading the remainder of this discussion.

3.5.2 Discussion and Analyses of the Results

From models using four noded shell elements for the brace and chord, it is clear that all weld models investigated give a much closer correlation to the experimental results than the model without a weld. This can be seen by comparing the relevant curves in Figure 3.4 (a) and 3.11. However considerable differences exist between each of the weld models.

The first three cases (a)(i), (b)(i) and (c)(i) have been compared in Figure 3.11, all of these using the six noded solid elements for the weld. All models appear to overestimate the capacity in the ultimate plastic region while cases (a)(i) and (b)(i) under-shoot the experimental results in the early plastic portion of the curve. These models all omit the inclusion of a full corner weld at this stage and this is likely to cause increases in the finite element capacities on inclusion. The results for the model using the four noded shell

elements for the weld are shown in Figure 3.12 and as can be seen they considerably overestimate capacity (by 25%) whether corner welds are included (d)(ii) or not (d)(i). This model case is not considered worthy of further investigation.

The other three weld model cases (a)(i), (b)(i) and (c)(i) as can be seen from Figure 3.11 give much better correlation with the experimental results than (d)(i) and it is cases (a)(i) and (b)(i) that were selected for further investigation. These were selected as the possible alterations would generally be expected to raise the finite element capacities. These alterations included the absence in the original cases (a)(i) and (b)(i) of the corner portion of the weld (see Figure 3.9) which, on inclusion would be expected to stiffen the region around the brace and chord intersection and the actual properties of the weld material itself which would be expected to be slightly greater than those of the steel. In all weld analyses so far these properties were assumed to be the same as those of the parent hollow section steel, shown in Table 3.2 and Figure 3.2. These steel properties were obtained from tensile tests on coupons extracted from the joint fabrication steel. BS639 (1978) gives a nominal tensile strength for a Grade E51 electrode, the type used in the fabrication of the experimental specimens, of 510-650 N/mm^2 and a yield strength of 360 N/mm^2. This would seem to indicate that the strength of the weld material is significantly greater than that of steel whose nominal yield strength was 355N/mm^2. However, with the lack of knowledge of accurate properties of the weld material within the joints assumptions must be made as to the properties of the material.

Two other items may come into play regarding the correlation of FE and experimental results. The first of these, involving

modelling of the corner radii in the chord and the relative increase in thickness of the material around the radius have been investigated for the case (b)(i), offset solid weld model. The second item is the residual stresses induced into both the chord and brace material during the welding process. These are almost impossible to measure and account for in the analysis and have been ignored here.

As was stated in the last paragraph cases (a)(i) and (b)(i) have no corner weld in place and adjustments to install this as a full corner weld are shown in Figure 3.9. The results are shown in Figure 3.8 (cases (a)(ii) and (a)(iii)) and Figure 3.10 (case (b)(ii)). As would be expected inclusion of the full corner weld (case (a)(ii) and (b)(ii)) have the most beneficial effect, significantly improving the calibration in the late elastic-early plastic region of the indentation curve. Observation of the actual test specimens would suggest that this full corner weld is the nearest approximation to the welds that exist on the specimen. The analysis still overshoots in the latter plastic regions of the curve but this is common to the other analyses undertaken so far as well. Case (b)(ii)-r in Figure 3.10 has the corner radius added to the model. Due to the nature of shell elements, this causes some problems. If it is to be avoided using a wasteful number of elements in the outer regions of the chord where the mesh density can be less fine then some large aspect ratios (length to width) within the elements in this area becomes unavoidable. This problem is clearly visible in the meshes used in the main analyses in the next chapter. The reasons for trying to avoid too many elements, especially in less critical regions such as the outer chord area in this analysis, is that it is wasteful, time consuming and beyond a certain refinement does not improve results any further.

The presence of the corner radii (case (b)(ii)-r in Figure 3.10) appears to reduce the capacity in the upper plastic regions of the load vs indentation curve, while having a negligible effect on the elastic and early plastic parts of this curve. Both the addition of the weld and the chord corner radius raise capacity of the FE model. This would appear to agree with the yield line theory developed by Davies et al (1991), this theory accounting for the effects of the weld and corner radius on the locations of the formation of the plastic hinges and effective β ratio. This is shown in Figure 3.20 and discussed in further detail in the Chapter 4.

The sensitivity of the results to variations in weld strength is illustrated in Figure 3.13 using the three sets of material properties detailed in Table 3.2. This investigation is actually undertaken on the first multiplanar joint MPJT2. It can be seen that this has very little impact on the results, the increase being around 4% in the ultimate joint capacity for a 20% increase in weld strength both for f_y and f_u.

The second set of models using eight noded quadratic shell elements for the brace and chord were run on joint MPJT3, this being a multiplanar joint with a tensile force present in the OPBs, as shown in Figure 3.1(a). The reason for selecting this joint was to provide assistance to Delft (1993) who, at the time were having difficulty in the analysis of the joints, this particular joint being their worst calibration. Another reason for selecting a multiplanar joint for the second part of the investigation was that as most of the joints in the experimental series were multiplanar it was felt important to test several weld models on one of these. This would establish if the differences in capacities exhibited by the variation of the weld model on the planar joint were also present on the

multiplanar joint. Modelling with the eight noded shell as mentioned earlier allows the modelling of the corner radius to be undertaken accurately (Figure 3.14 (a)) as these elements by their definition can have curved boundaries. The corner radii on the chord was therefore included in all models here. All welds in cases (e) to (h) were full corner welds (refer to Figure 3.9 case (ii)), as this from the earlier work in section 3.4.2.2 on the planar joint using the four noded shells for the chord and brace appeared to be the closest to the experimental result (Figure 3.10 case (b)(i) to (b)(ii)). From observations of the weld pattern on the experimentally tested joints this full corner weld format also appears justified and therefore the effect of not including this corner weld was not investigated for this series of analyses.

The results of this series of models are shown in Figures 3.16 to 3.19. The first, Figure 3.16 illustrates the results for the weld case (e) which uses a solid six node weld model sharing nodes with the shells of the brace and chord. It can be seen that this model under predicts the ultimate capacity by around 12.5%, this being significantly low. Moving the solid weld to an offset position and tying the nodes with MPCs as in case (f) significantly improves the correlation with the experimental results. This is illustrated in Figure 3.17, the FE results under-predicting the experimental results by around 8% in the large displacement region of the load vs indentation curve.

The results for the model using 15 noded solid elements under predict the experimental capacity by some 20% as illustrated in Figure 3.18. This is likely to be caused by the 15 noded solid element being much more flexible than the six noded solid element due to it possessing larger numbers of integration points and hence

lowering capacity. It would therefore be anticipated that the 15 noded elements should be more accurate than the six noded solids for the weld, but several reasons may account for it not giving as close a representation to the experiments. Among these may be the method of connectivity. If the elements were offset as opposed to sharing common nodes with the chord and brace as here, then FE capacity is likely to increase, evidence from the earlier four noded shell models supporting this.

The results for the eight noded shell model case (h) are shown in Figure 3.19. These under predict the experimental capacity by approximately 10% in the upper plastic region of the load vs indentation curve giving overall correlation similar to that of case (f), the offset six noded solid model. The advantages and limitations of these two models were discussed earlier in the text in 3.4.1.

For the analysis work in this thesis the aim is to develop an understanding of the joint behaviour overall and in particular the ultimate static strength of joints. The techniques developed above for the weld modelling, whilst not obtaining mathematically correct solutions, have been shown to give reasonable and generally slightly conservative ultimate static strength predictions compared with the test results and thus can be used with due care to investigate other joint configurations and problems within this thesis with a reasonable level of confidence in the results.

3.6 Conclusions

1) Inclusion of the weld is vital if realistic results are to be achieved for FE analysis of the ultimate static strength of tubular

joints. This is clearly illustrated in Figures 3.4(a) and 3.4(b) for both planar and multiplanar models.

2) It would appear that the full corner weld model, case (ii) in Figure 3.7 gives the best results and is most appropriate when compared to the weld profile on the experimental specimens.

3) The models using offset solid elements give the most consistent results despite the numerical incompatibility problems associated with the elements. These incompatibilities can be tolerated when observing overall joint behaviour and looking for engineering solutions.

4) Different models are suited to different joint types. This is discussed in Chapter 7 where models are selected for different joint configurations.

5) Most models considered here, and those that are taken forward and utilised on joints where experimental results are not available, have given slightly conservative results when applied to the experimental results here. For the purpose of FE analysis this is not considered a disadvantage.

6) For the practical reasons discussed, the modelling of the weld in order to observe overall joint behaviour has to be a compromise unless the excessive computing capacity and time required to model the whole joint using solid elements throughout can be justified.

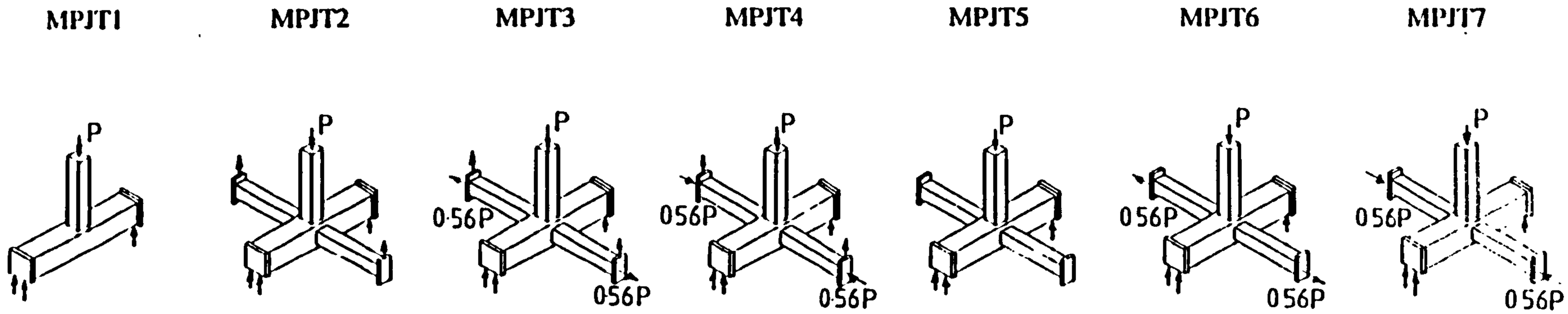

(a) The Experimental Joint Test Series

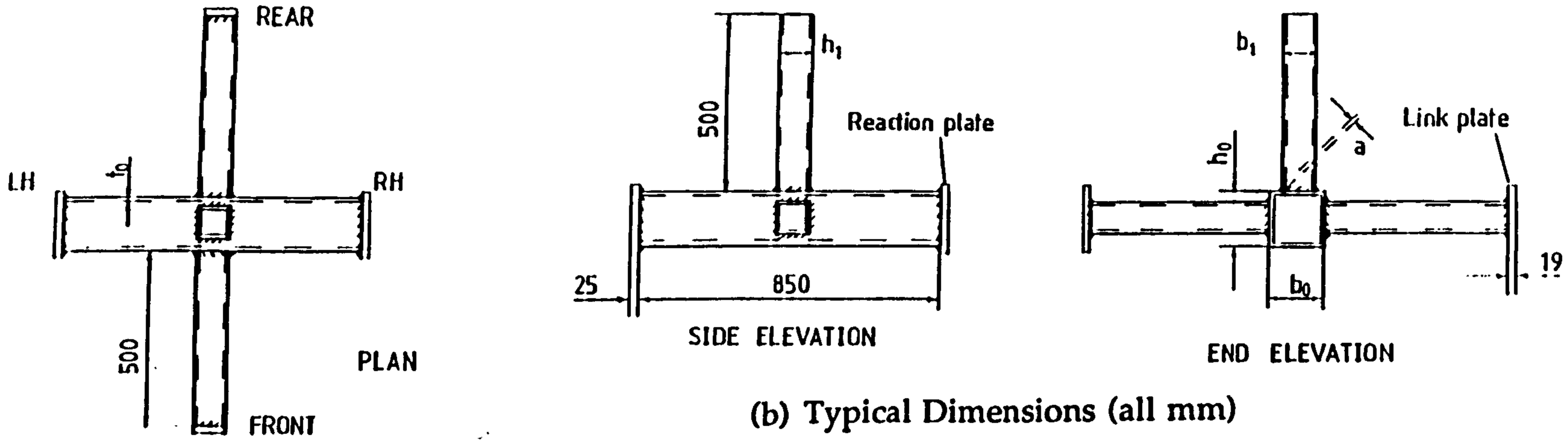

(b) Typical Dimensions (all mm)

Figure 3.1 The Experimental Series and Typical Dimensions

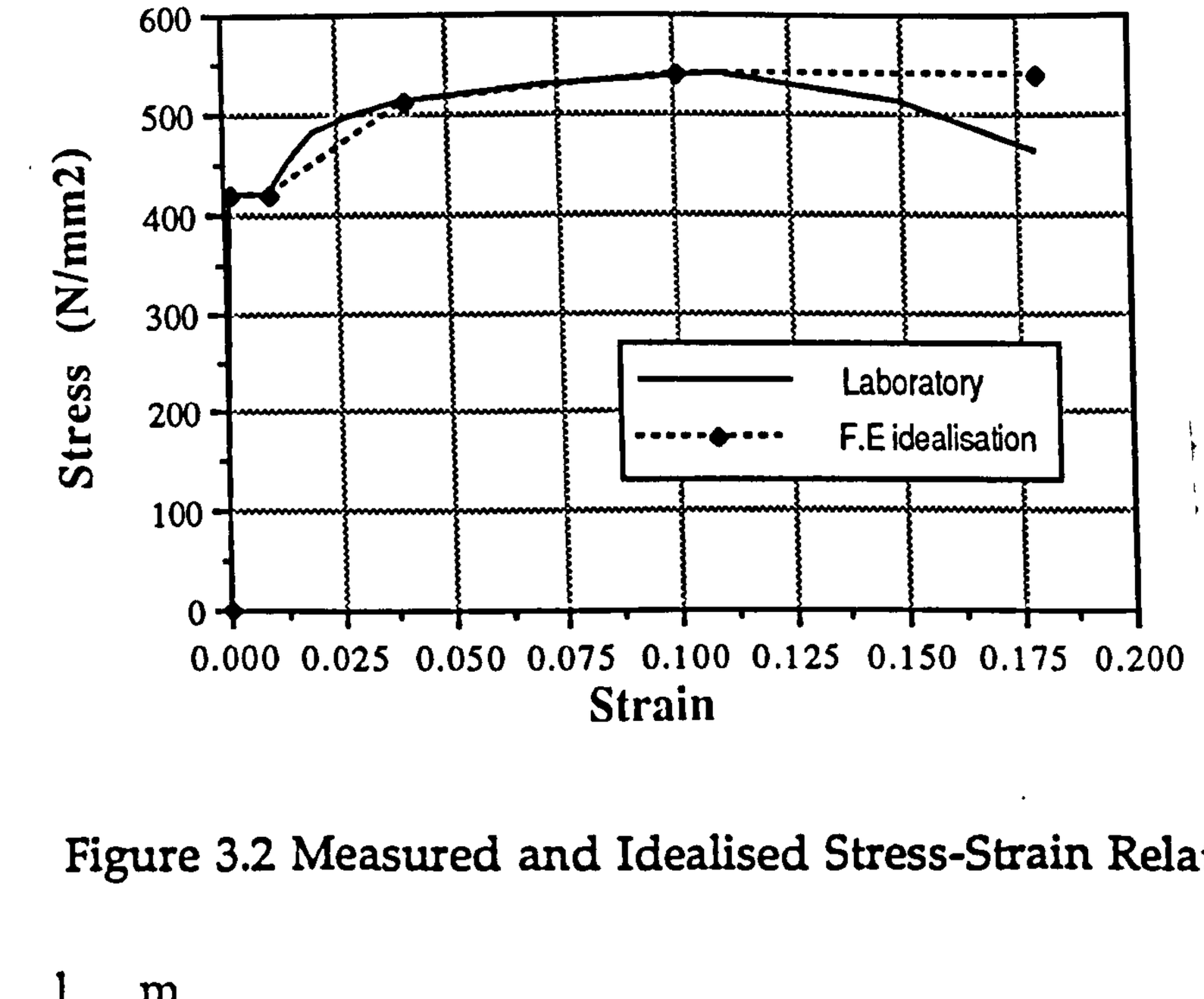

Figure 3.2 Measured and Idealised Stress-Strain Relationships

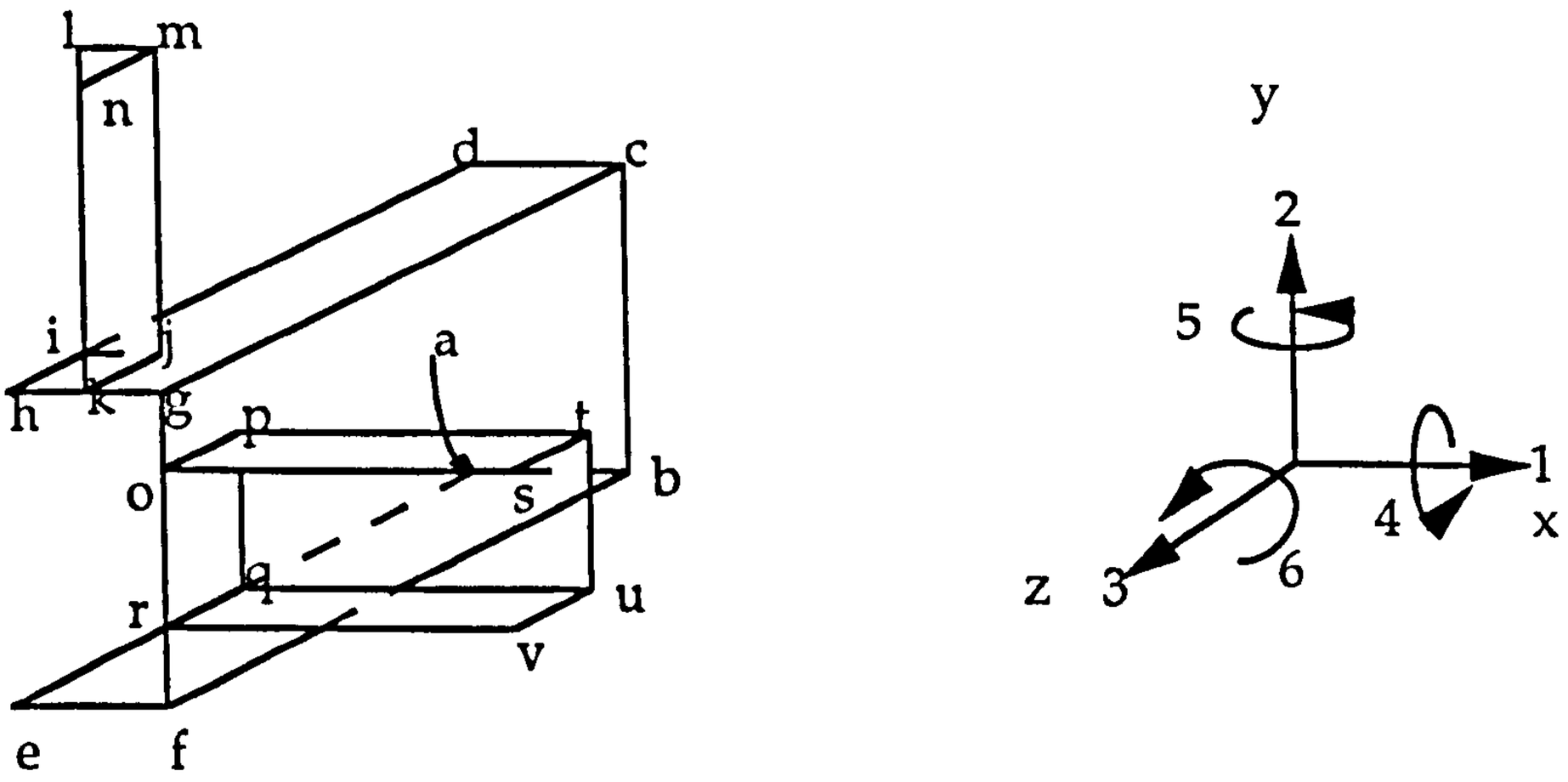

Boundary	Directions of zero displacement/rotation	Reason
ab	1, 2	Support Condition
ae, dh, il	1, 5, 6	Symmetry Requirement
ef, fg, gh, os, rv, kn	3, 4, 5	Symmetry Requirement
lm, mn	1, 3	Support Condition

Figure 3.3 Boundary Conditions and Symmetry Restraints Implemented to Model Half of the Joint

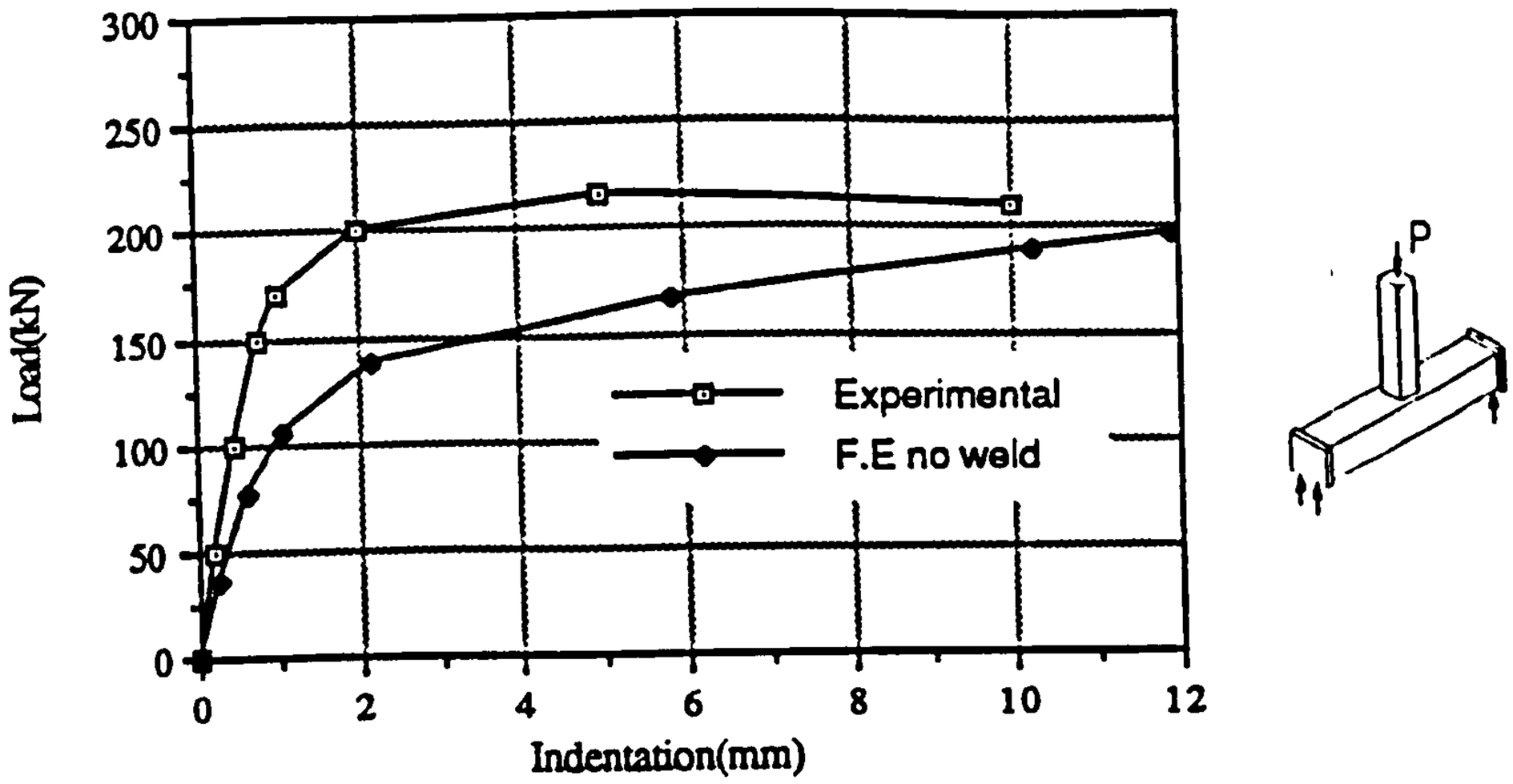

Figure 3.4 (a) Initial Finite Element Indentation compared with Experimental Indentation for Planar Joint MPJT1 .

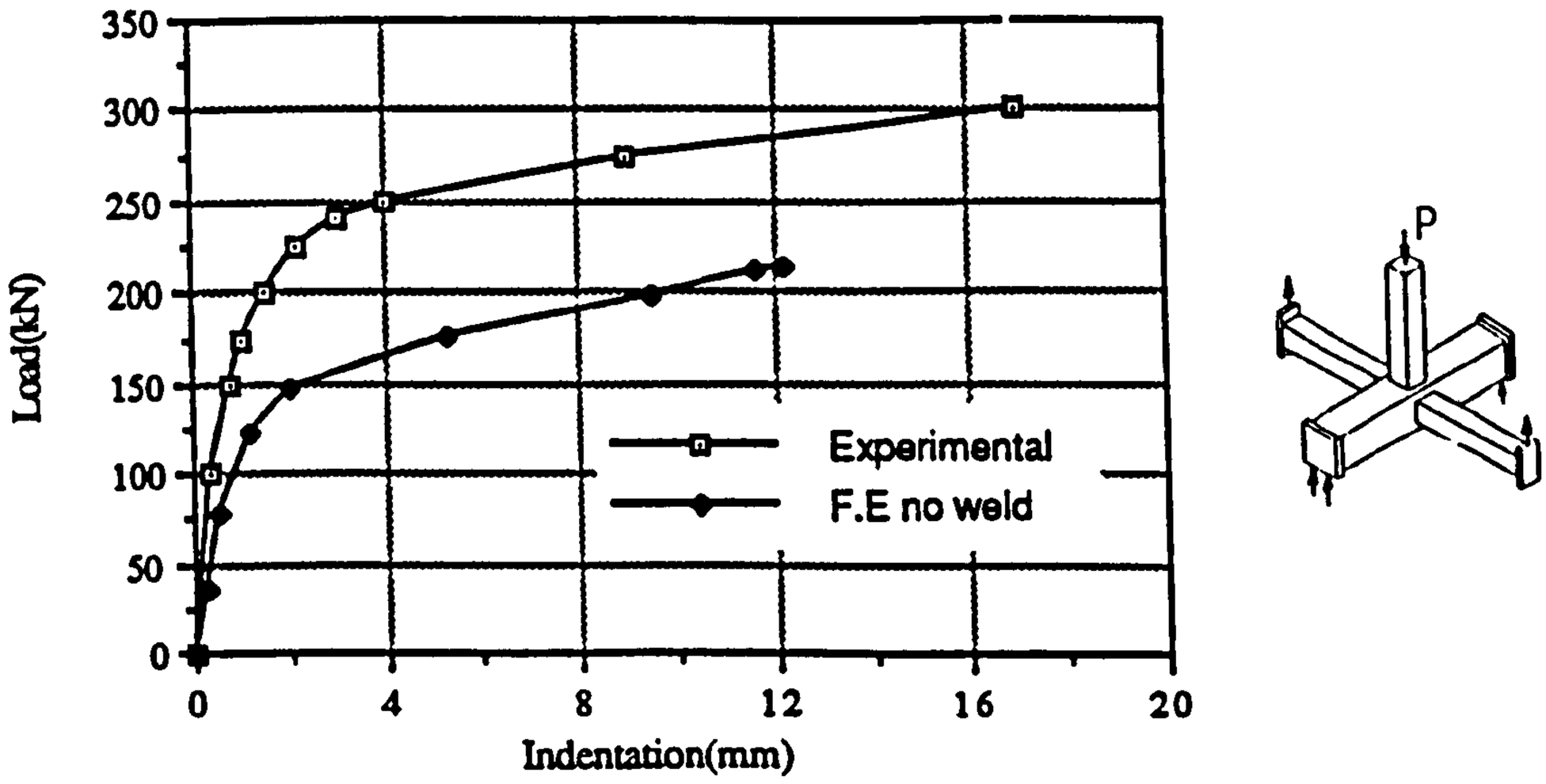

Figure 3.4 (b) Initial Finite Element Indentation compared with Experimental Indentation for Multiplanar Joint MPJT2.

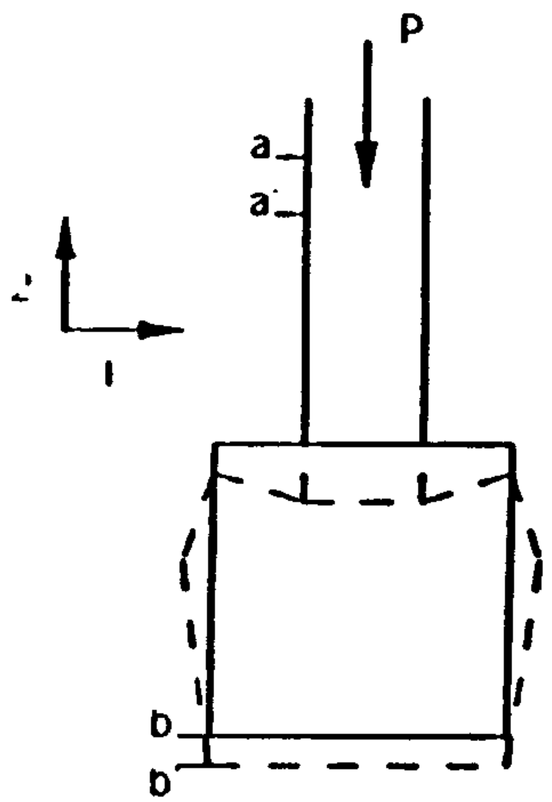

Displaced Shape

Original Shape

Indentation = (a'-a) - (b'-b)
in direction 2

Figure 3.5 Method of Measuring Brace Indentation.

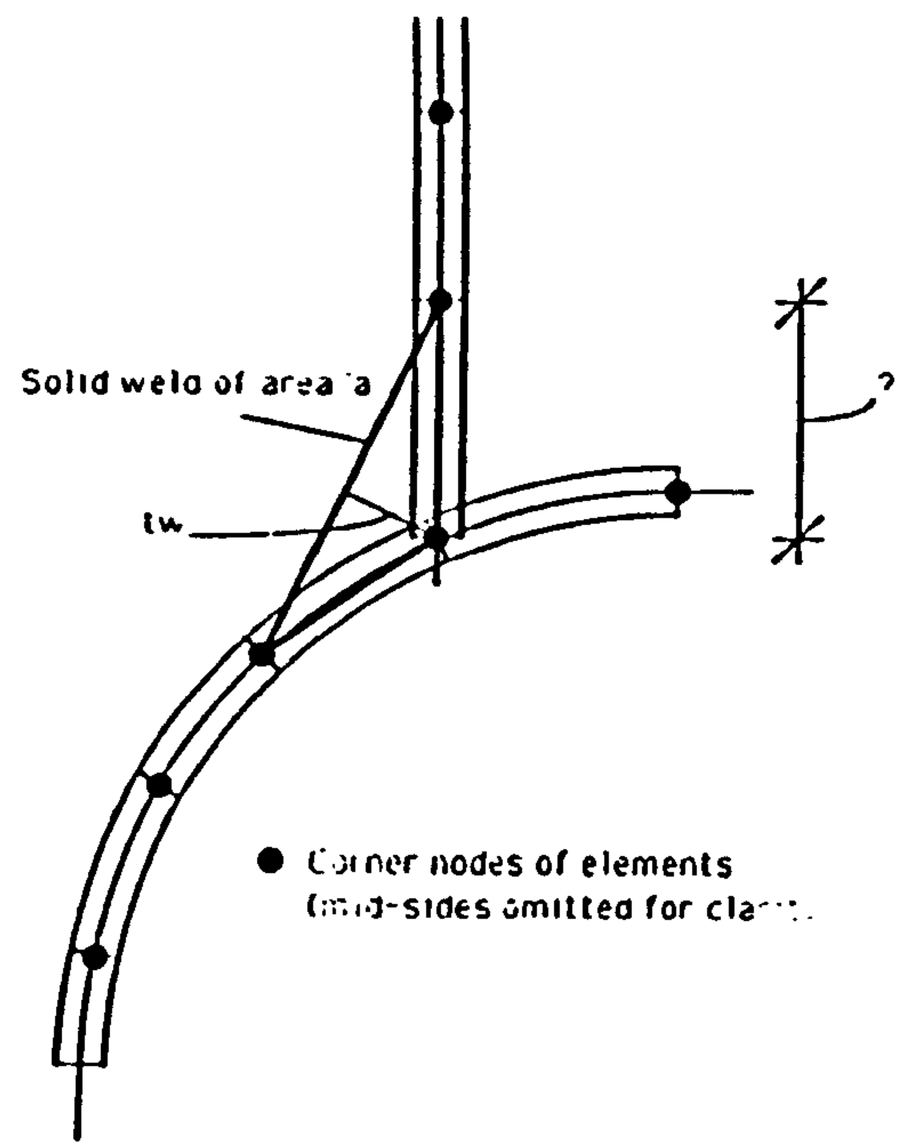

(a) Detail of a typical fillet weld area showing throat thickness (tw) and weld material area 'a'.

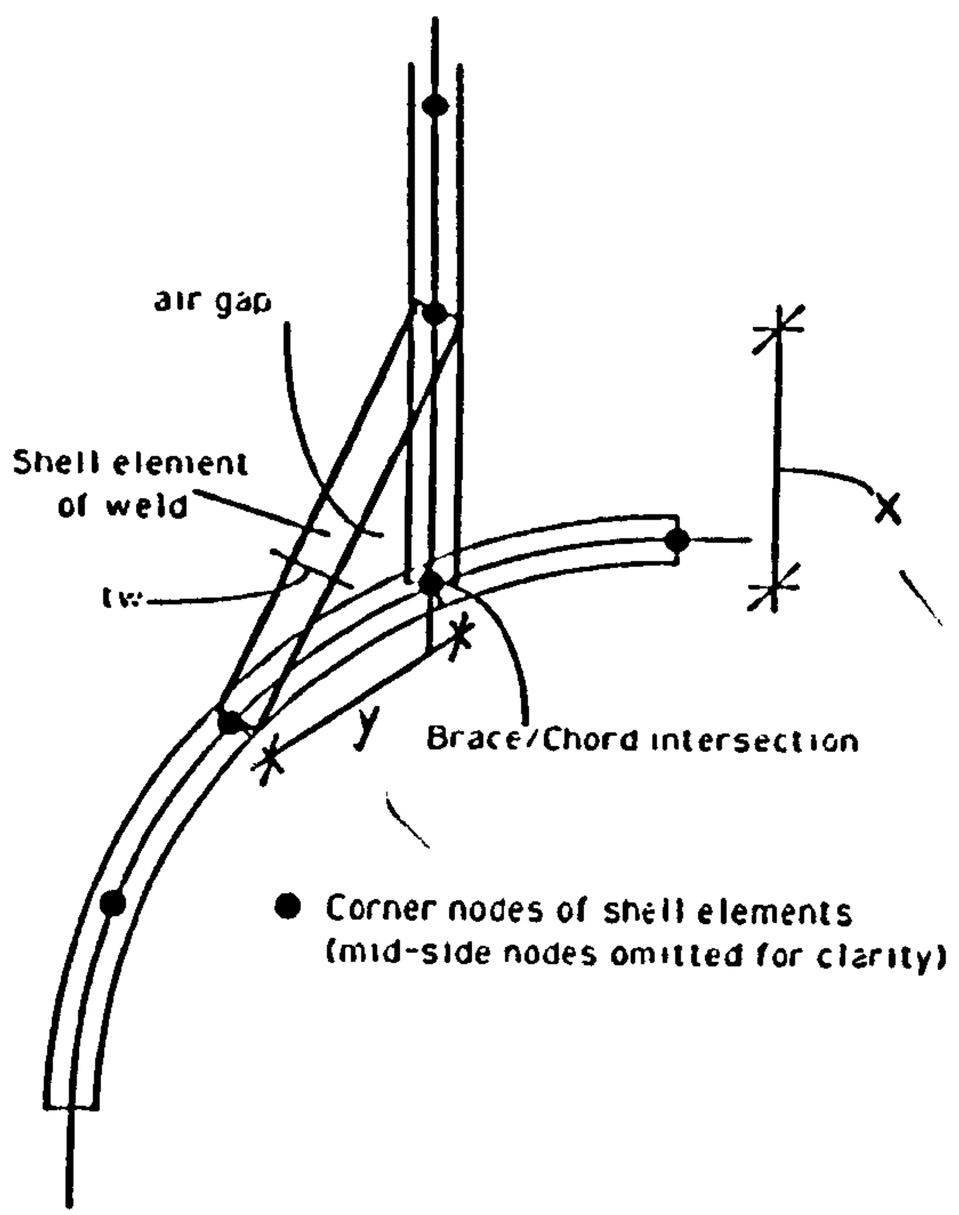

(b) Problems associated with points of attachment of the weld shell elements to the brace and chord.

Figure 3.6 Problems associated with dimensions of the weld.

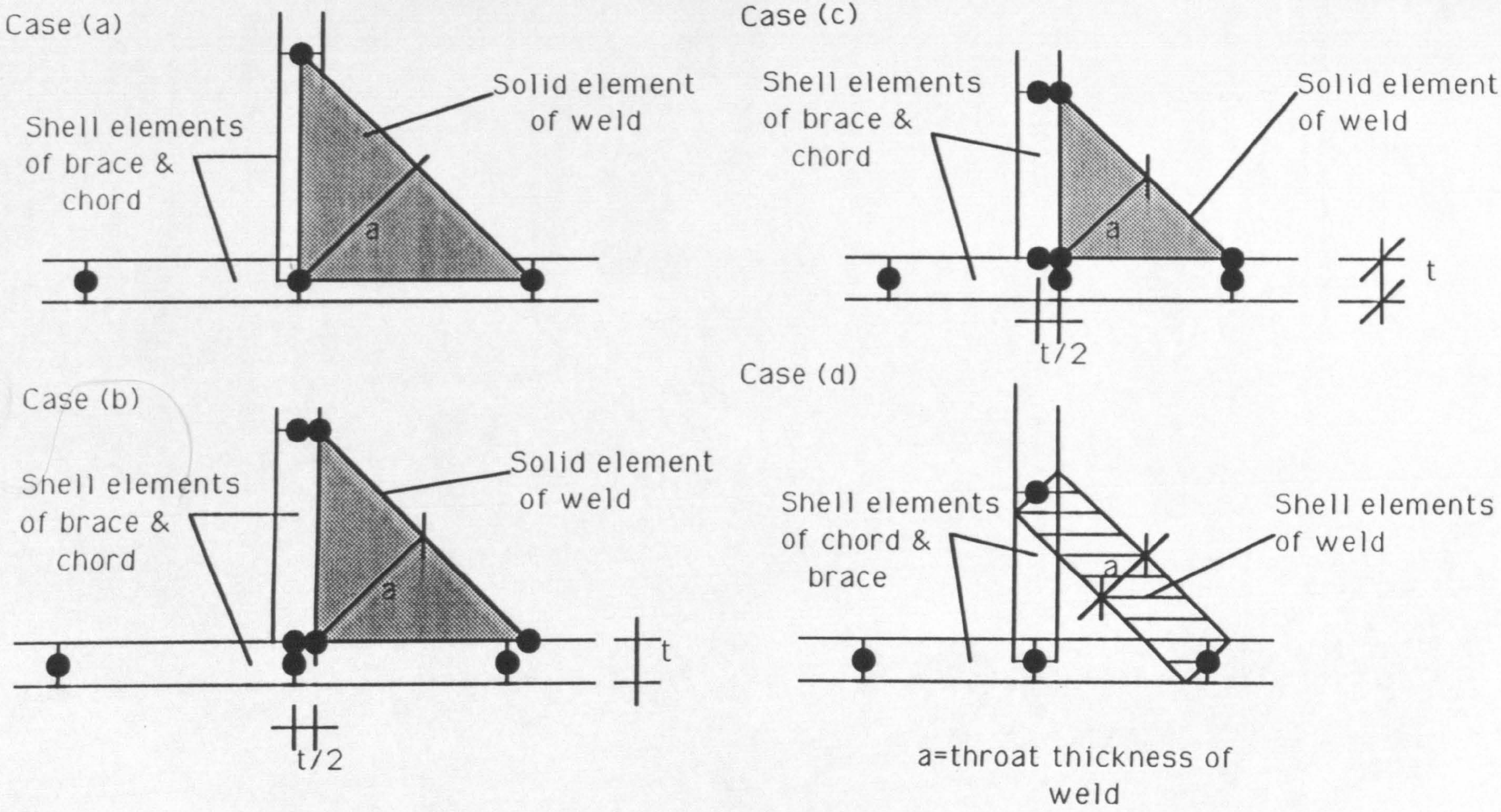

Figure 3.7 Initial Four Weld Models considered in the weld investigation

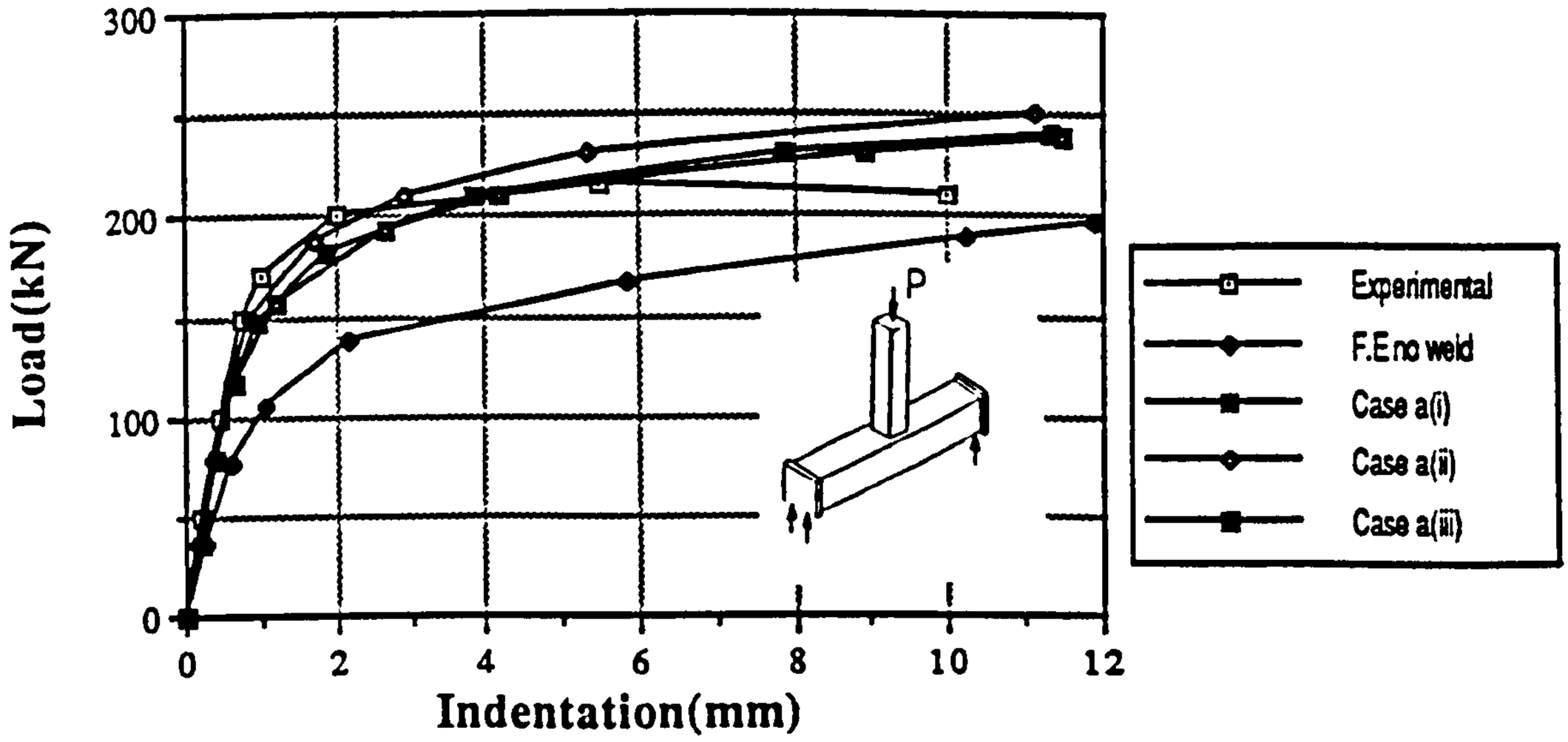

Figure 3.8 Load vs Indentation Curves for Weld Case (a) Series undertaken on Planar Joint MPJT1.

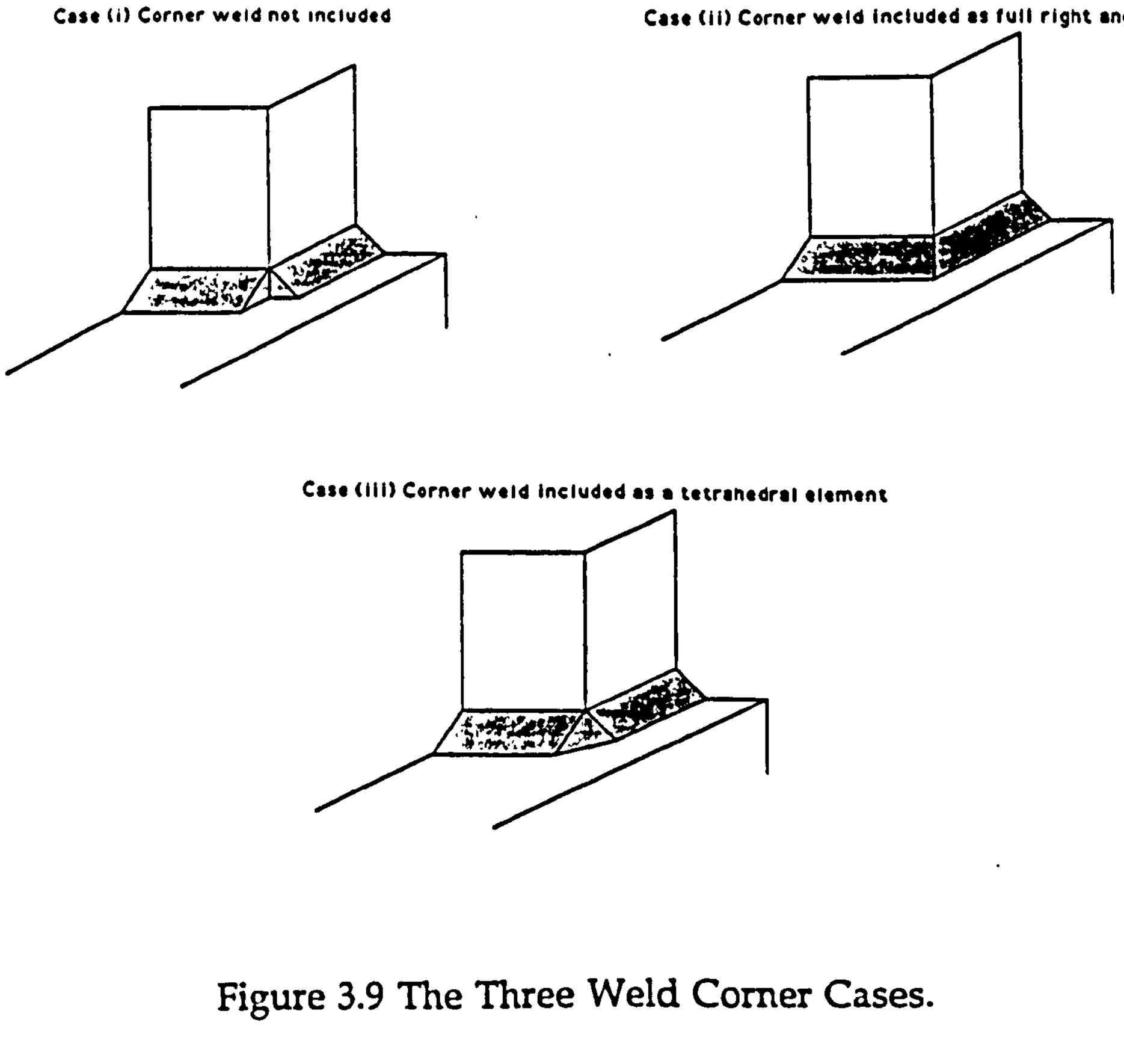

Figure 3.9 The Three Weld Corner Cases.

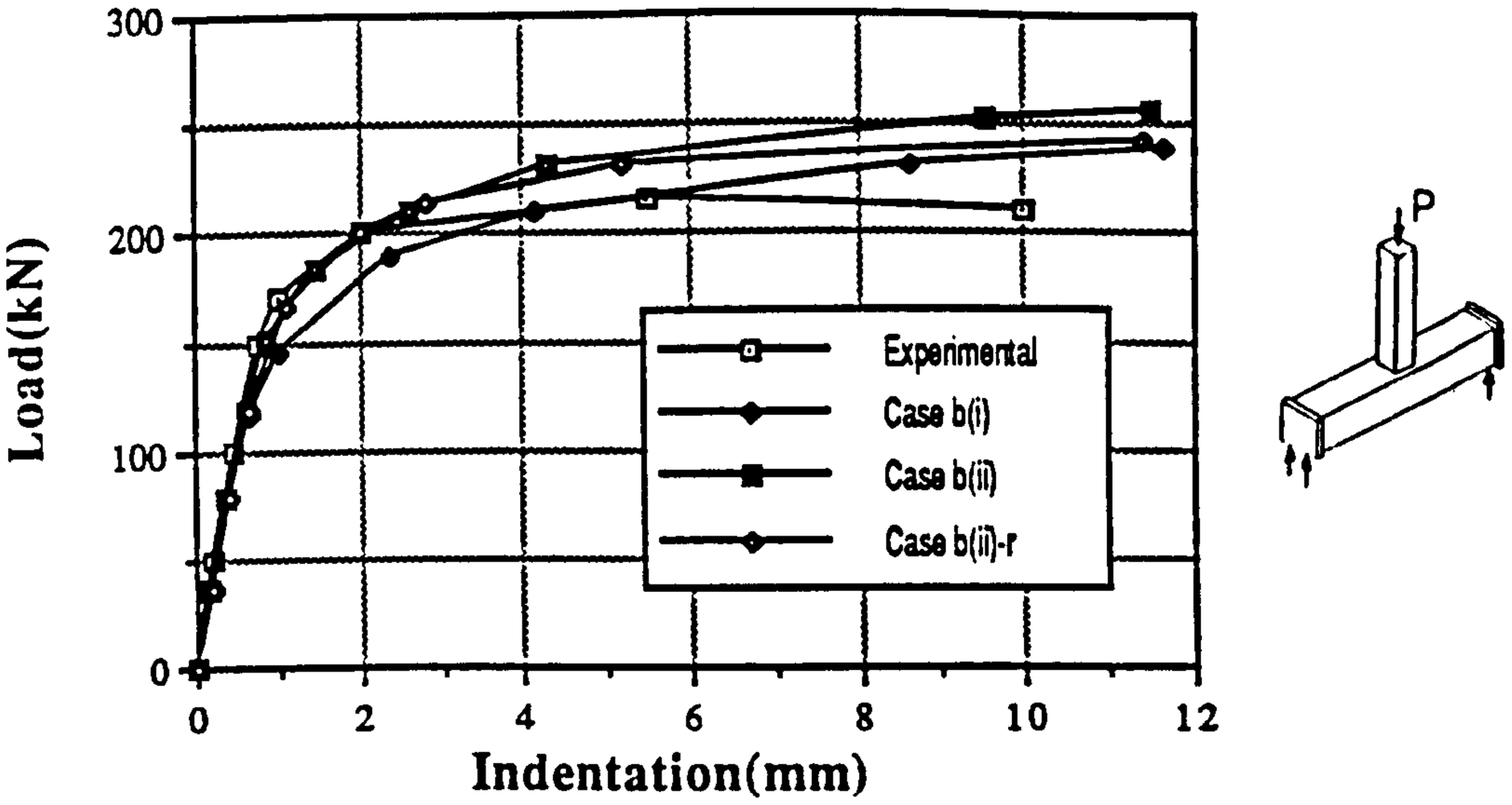

Figure 3.10 Load vs Indentation Curves for Solid Weld Case (b) undertaken on Planar Joint MPJT1.

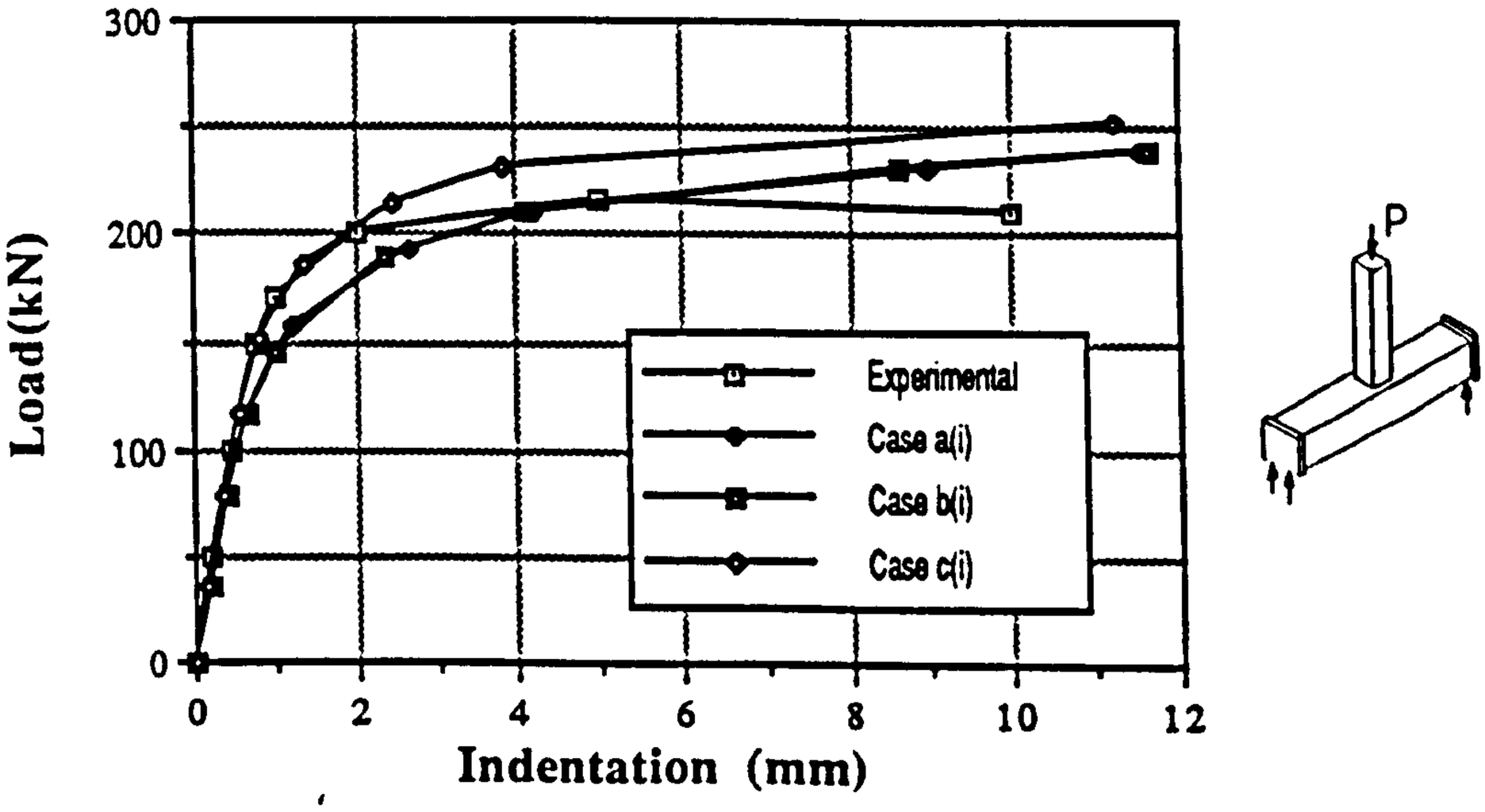

Figure 3.11 Solid Weld Model Cases (a)(i), (b)(i) and (c)(i) on Planar Joint MPJT1.

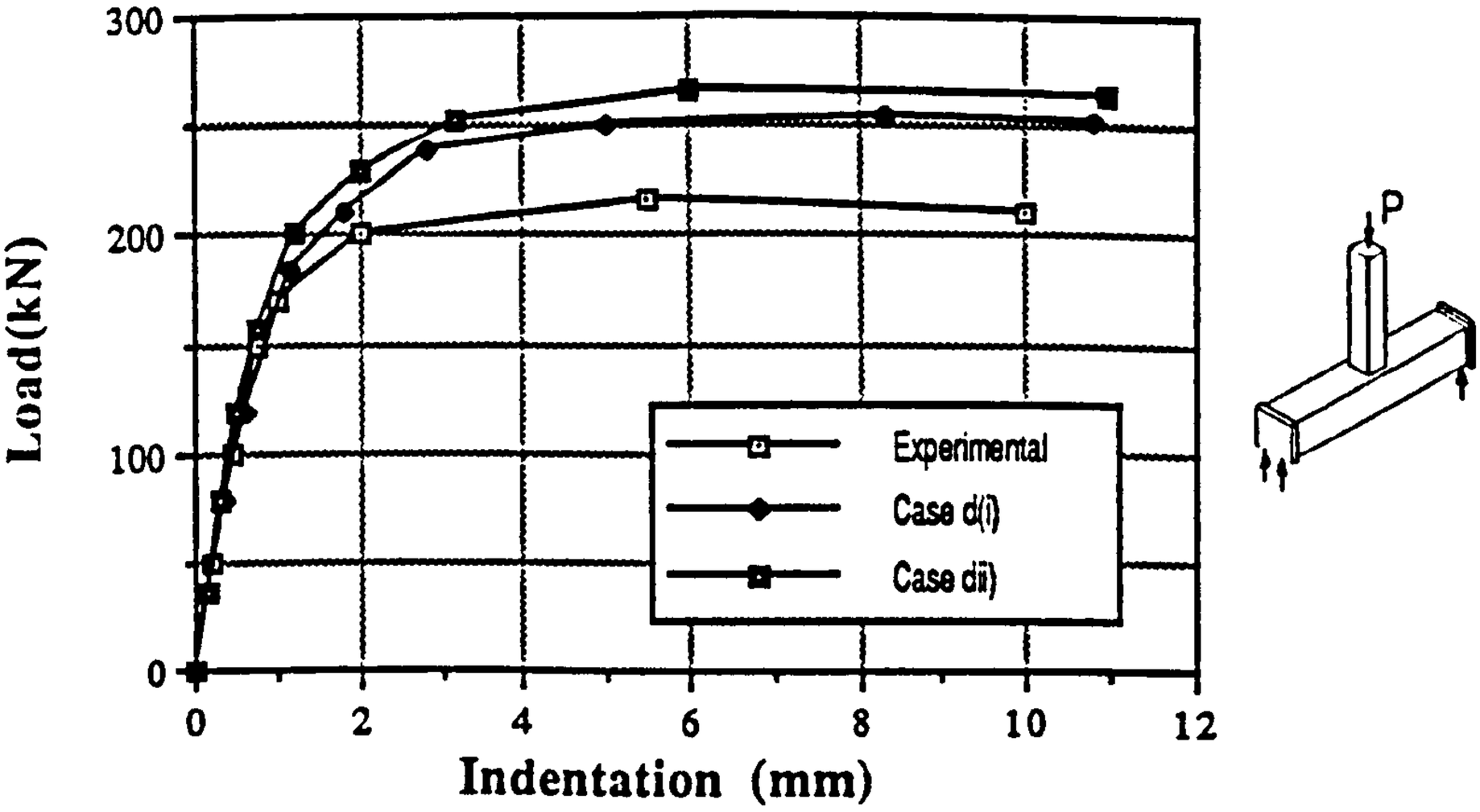

Figure 3.12 Load vs Indentation Curves for Weld Case (d).

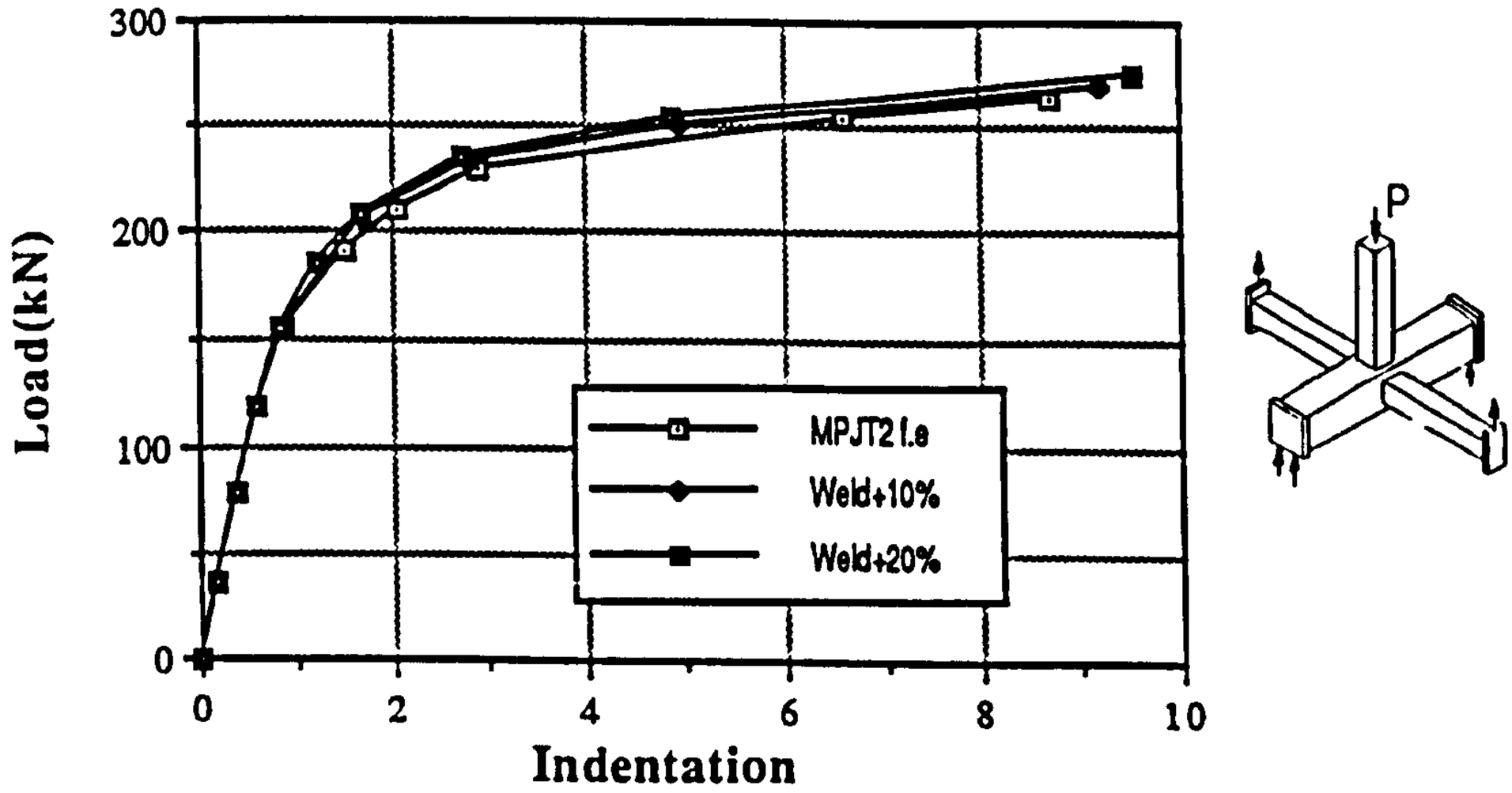

Figure 3.13 Effect of Variation of Weld Material Properties on MPJT2.

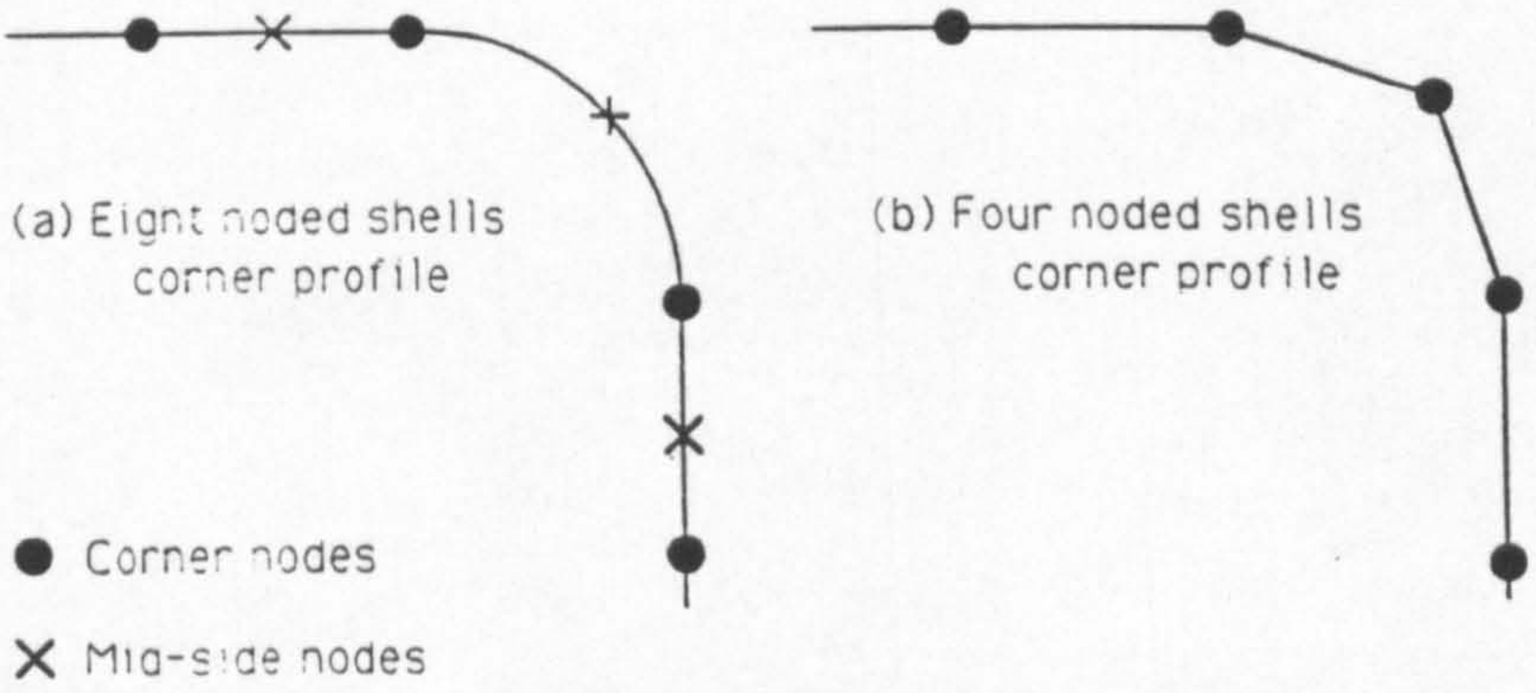

Figure 3.14 Modelling of Corner radii using
Four and Eight Noded Shells

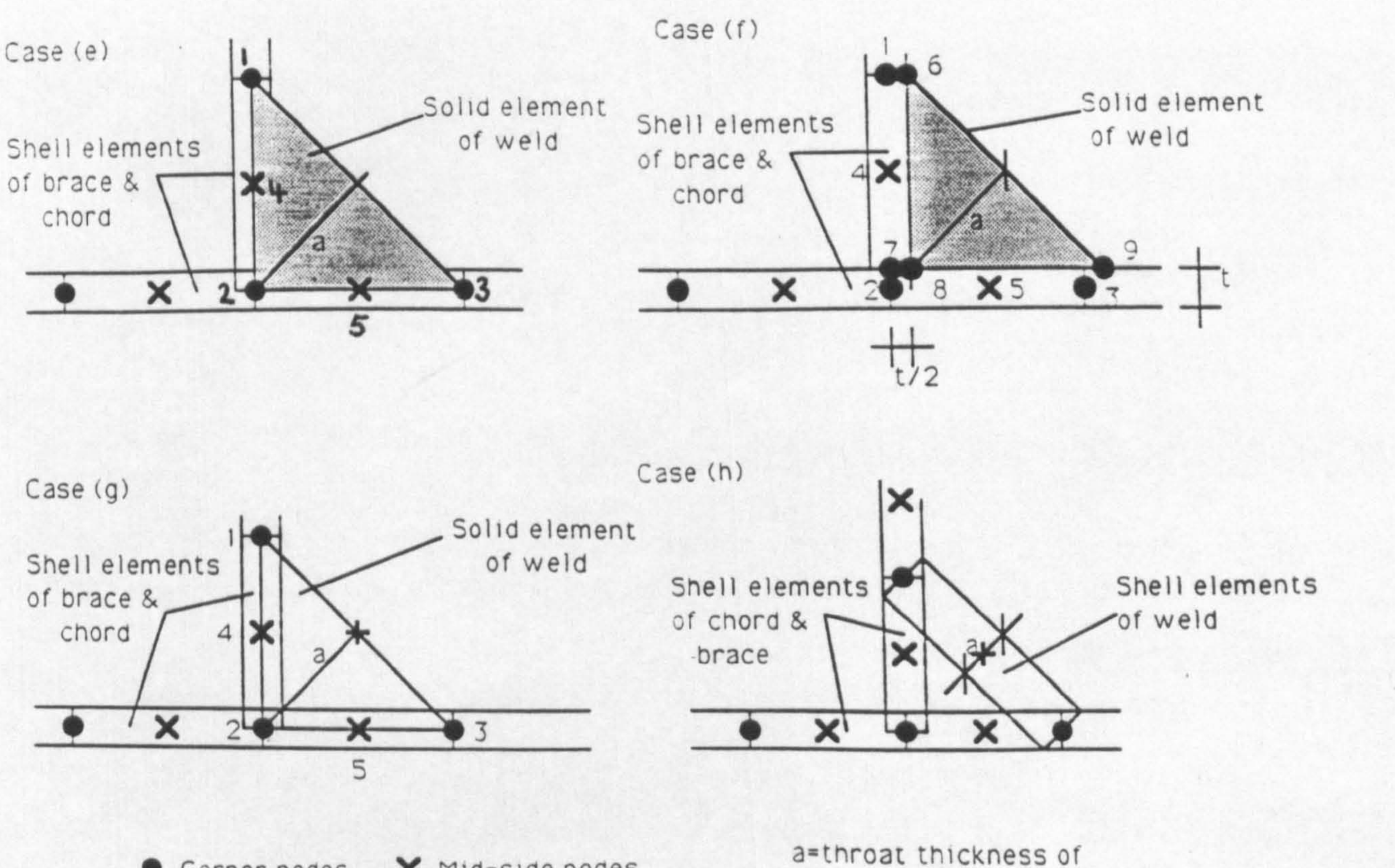

Figure 3.15 Four Weld Cases Considered for Models where Chord and Brace are modelled using Eight Noded Shells.

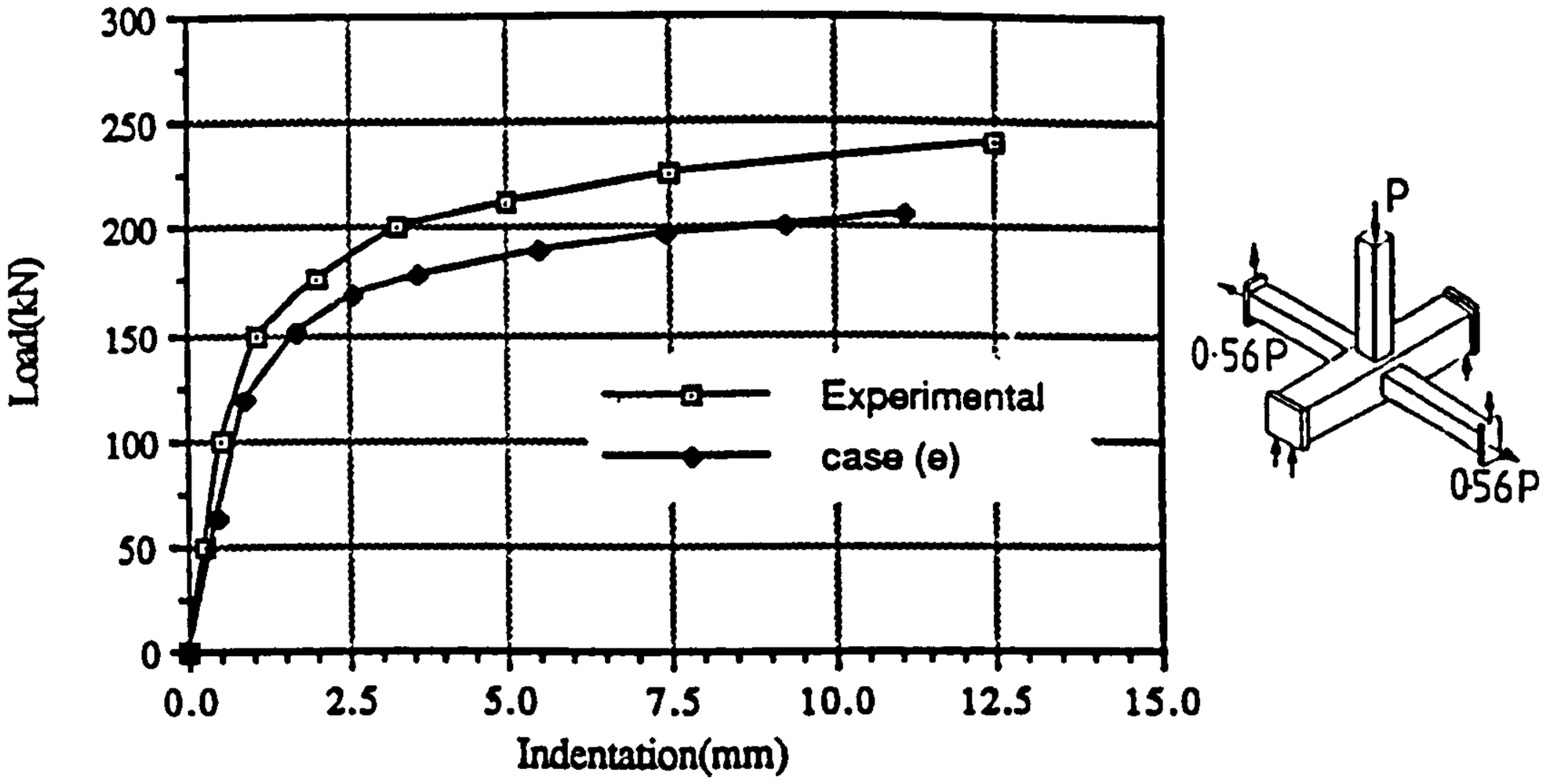

Figure 3.16 Comparison of FE Model Case (e) with Experimental Indentation on MPJT3.

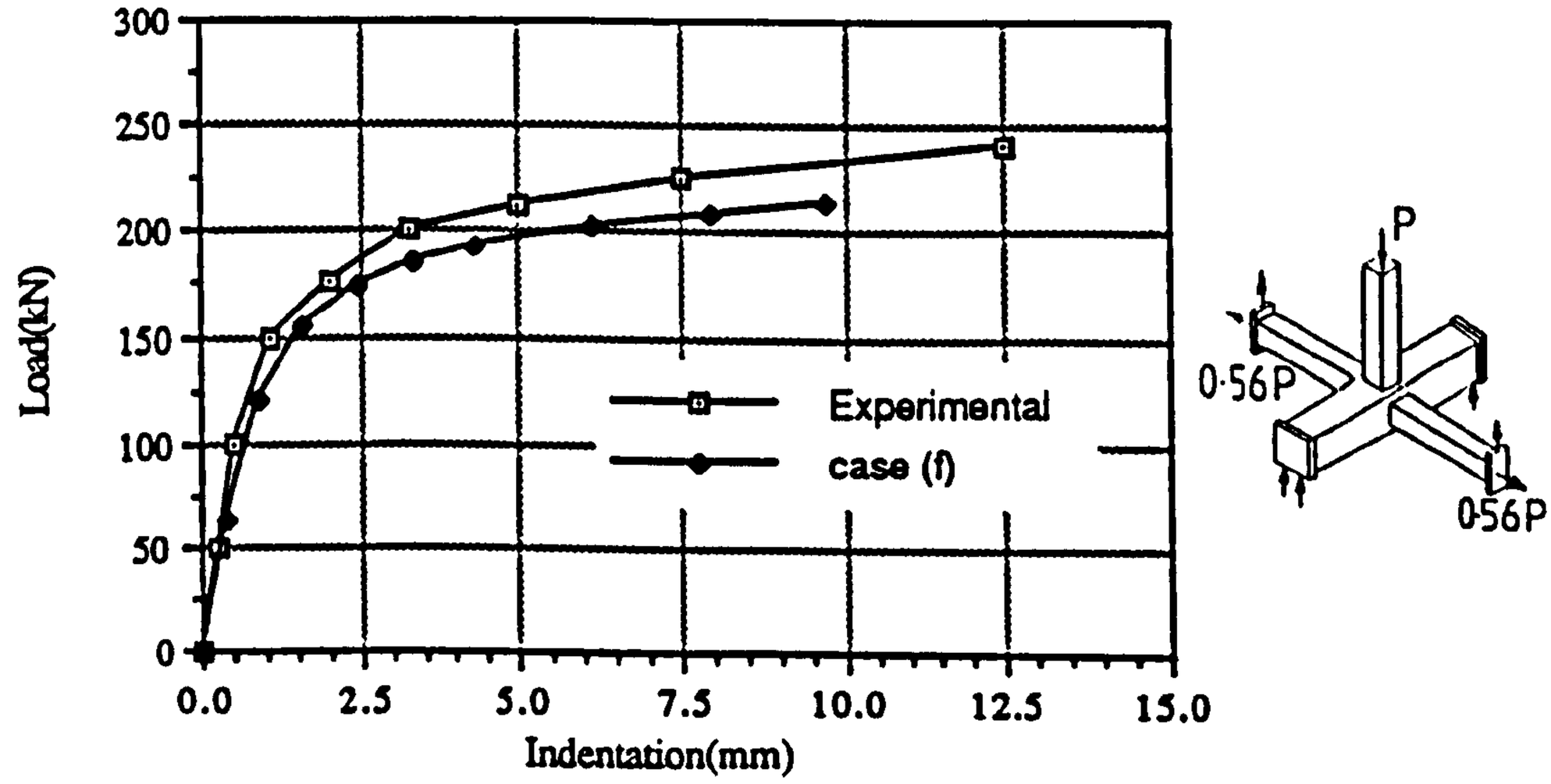

Figure 3.17 Comparison of FE Model Case (f) with Experimental Indentation on MPJT3.

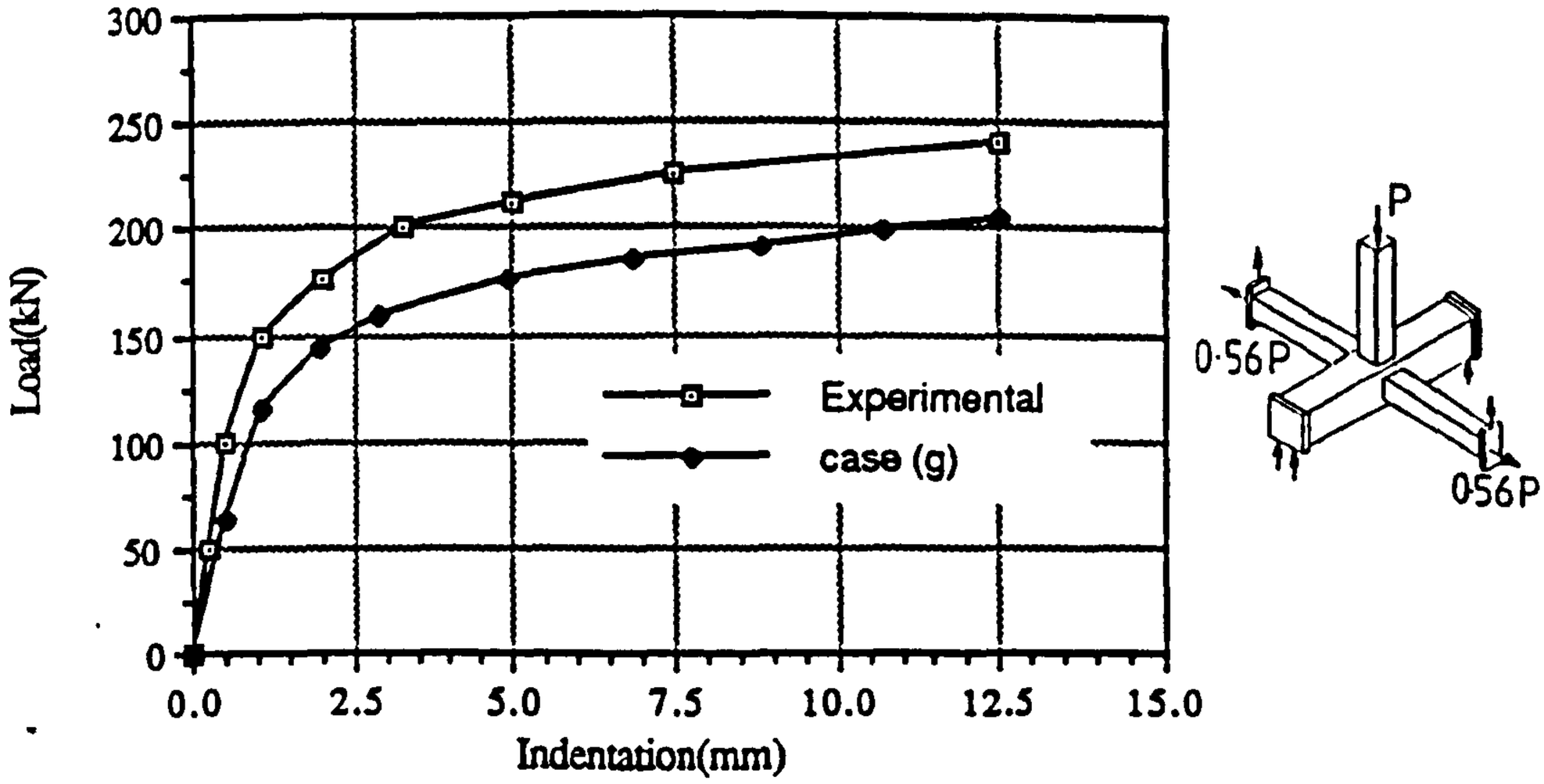

Figure 3.18 Comparison of FE Model Case (g) with Experimental Indentation on MPJT3.

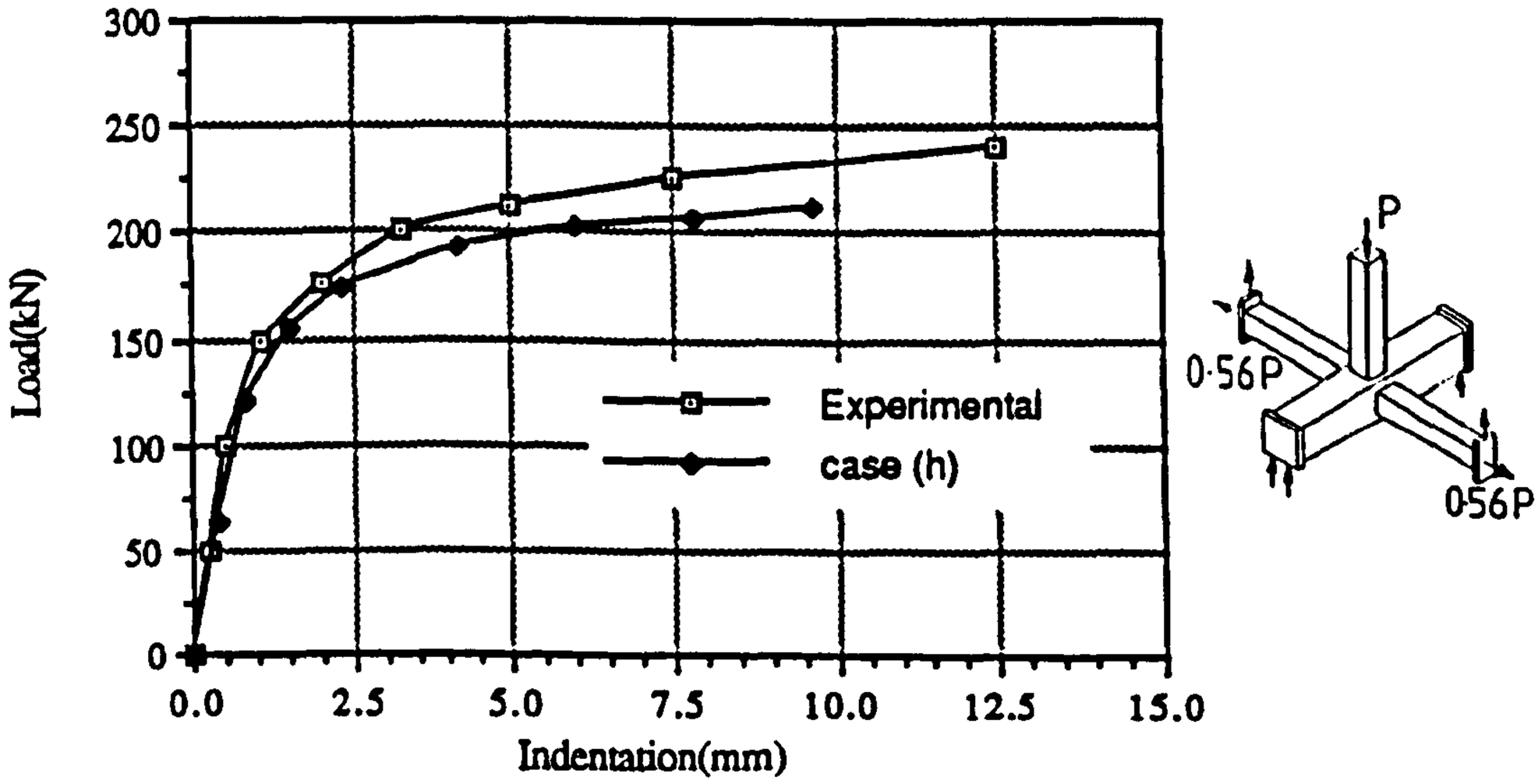

Figure 3.19 Comparison of FE Model Case (h) with Experimental Indentation on MPJT3.

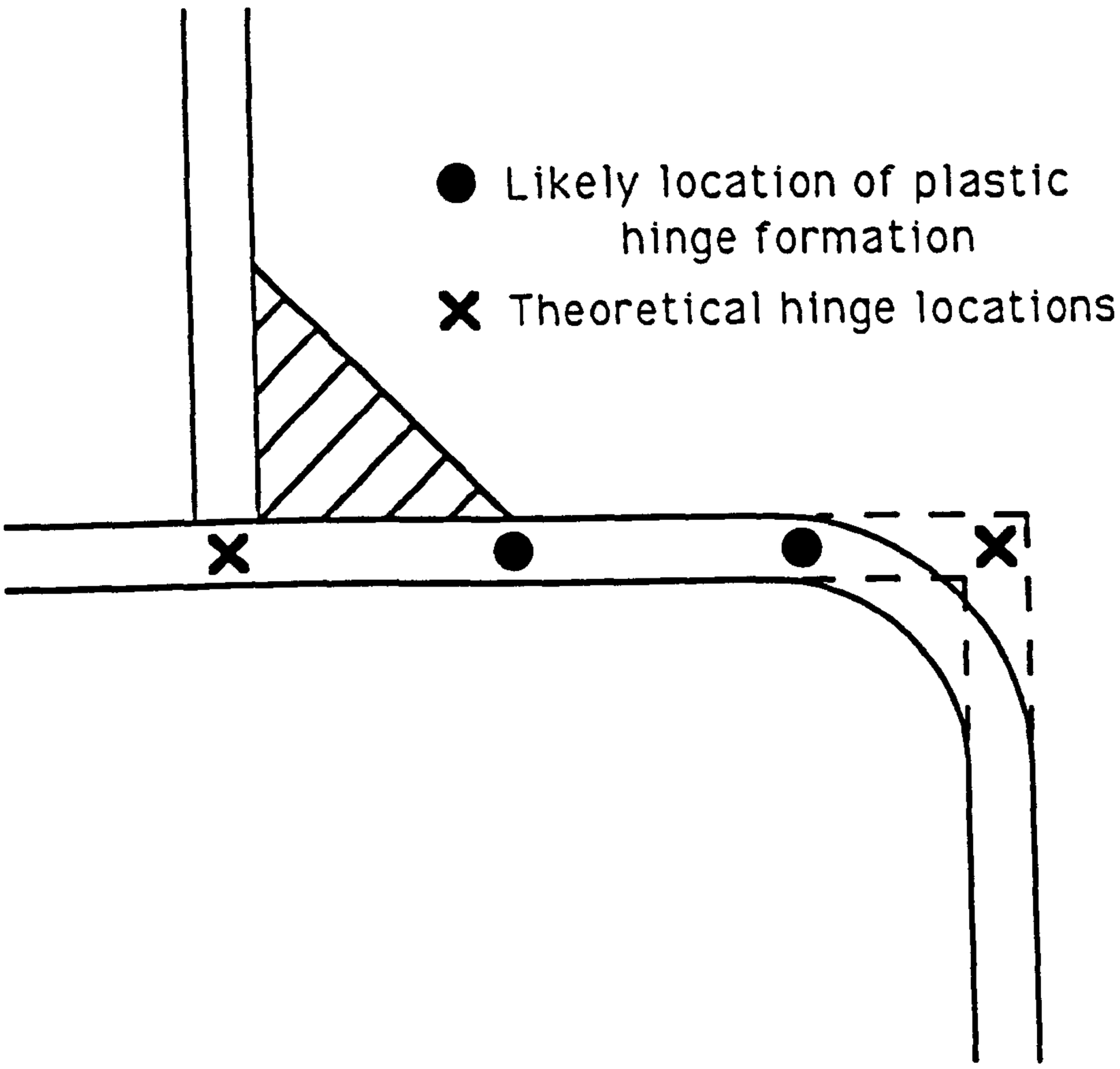

Figure 3.20 Likely Positions of Formation of Plastic Hinges compared to Yield Line Theory

CHAPTER 4

FINITE ELEMENT MODELLING OF THE E.C.S.C JOINT SERIES

4.1 Introduction.

This chapter presents the results of the finite element analysis of the full series of experimental test specimens using the two weld models developed in Chapter 3. It also contains details of the mesh convergence study used in arriving at the mesh density used in Chapter 3.

Having dealt with the details of the weld modelling in Chapter 3, this chapter describes the actual modelling of the ECSC test joint series, as shown in Figure 3.1. Two models were selected from Chapter 3, these being model case (b) (with four noded shells for the brace and chord as in Figure 3.7) and model case (f) (with eight noded shells for the brace and chord as in Figure 3.14), these two being judged to be the best correlating methods accordingly. Using these two models also enables a comparison to be made between eight noded and four noded shell elements for the main brace and chord while the weld modelling is identical. It also demonstrates that in this particular case, four noded shells gave reasonable calibration with the test results. Four noded shells, although accepted to be less accurate than eight noded shells possess

the advantage of needing less CPU time, this being beneficial where large numbers of analyses need to be run.

4.2 Representation of the Experiments

In order to achieve good correlation with the experimental results, it is necessary to set up the finite element analysis to represent the experimental procedure used in the laboratory as closely as possible. A centreline sketch of a symmetrical specimen showing the points of chord support and symmetry restraints is shown in Figure 3.3. The effective simple support at the chord ends is straightforward to reproduce by installing boundary conditions on the nodes on the end of the lower face of the chord (ab in Figure 3.3) which prevents movement in the 2 (in-plane) direction. The other restraint conditions necessary to ensure that symmetry requirements are met are shown in Figure 3.3. It will be noted that these conditions include some nodes that are restrained from movement in directions 1 & 3, this also being necessary to maintain symmetry, ensuring that the model does not move as a rigid body in any direction.

It can also be seen in Figure 4.1 that in the experiments the actual specimen had end plates in place to stiffen the ends of the chords and thus simulate the presence of further chord material. This can be modelled several ways, including using more elements with appropriate thickness and material properties.

The method used here is to tie all nodes at the end of the chord (abcd in Figure 3.3) to have exactly the same magnitude in the three rotation components as the node a in Figure 3.3. This ensures

that the whole end remains in a plane during the analysis, closely resembling the test conditions with a rigid plate.

The final detail to ensure the model was a reasonable representation of the tests was the method of restraining the ends of the out-of-plane braces in the joints MPJT2 to MPJT4. This was undertaken in the experiments by adjusting the shear force in the chord as the external loads were applied until the two dial gauges positioned upon the top faces of the out-of-plane braces (1 and 2 in Figure 4.1) gave the same reading. This was done at each load increment, but allows a small curvature to form in the brace as indicated in Figure 4.2.

Two alternative methods are available using either the *EQUATION option or *MPC (multi-point constraint) option within the ABAQUS suite. Using either of these, the two nodes (positioned in the locations of the dial gauges indicated in Figure 4.1) were tied in a direction 2 (in-plane) to displace by exactly the same amount.

4.3 Mesh Convergence.

The mesh convergence study was undertaken with joint MPJT1, the planar joint. In order to simplify the mesh convergence study, welds were not included in these analyses. The three meshes (fine, medium, coarse) are shown in Figure 4.3, the medium mesh corresponding in intensity to those used in Chapter 3 for the joint series analysis. All these meshes used four noded shell elements. As in the experimental joint, the loading was axial compression in the brace with failure being by 'in-punch' of this brace into the top face of the chord. The results of this investigation with respect to 'in-

punch' of the brace are shown in Figure 4.4. Thus it can be seen that the medium mesh is adequate for our analysis of the joint series as differences between it and the fine mesh are negligible. Further justification of the 'medium' mesh will be undertaken later in this chapter when strain comparisons are undertaken. The corresponding medium mesh using eight noded shells is also shown in Figure 4.4. The results from this can be seen to be slightly lower than those of the corresponding four noded medium mesh.

4.4 Calibration of the Finite Element Analyses with the Experimental Results

During the experiments several measurements were made as each joint was loaded. The principal one used to determine joint failure is that of in-punch of the compression loaded brace into the chord top face. This 'in-punch' is measured in the direction of the in-plane brace as was shown in Figure 3.5. Other measurements compared include that of the mean chord sidewall horizontal deformation at a distance of 58mm from the brace centreline (see Figure 4.1) and the output of electrical resistance strain gauges at several locations on the chord and braces. The positions are shown in Figure 4.5. Correlation of these latter two measurements, horizontal deformation and strains has been undertaken only on one joint. This was done to check the accuracy of the modelling once, but not repeated. More detailed calibrations across the whole joint series have been undertaken by Yu et al (1993). The aim of this thesis is not to repeat this work but use the availability of experimental results to develop reliable and realistic modelling techniques that could then be applied to other joint configurations

and to generate further results for this configuration. Once developed the multiplanar T-DT joint model could then be easily modified to investigate other aspects of this configuration such as various load conditions and differences in material properties.

4.4.1 Models using 4 Noded Shells for Brace and Chord Elements

The model selected to analyse the joint series was chosen to be that of case (b)(ii)-r in 3.4.2.2. This weld model is shown again in detail in Figure 4.6. It contains an offset solid weld with corner radii on the chord and full corner weld in place. This was chosen as it appeared to give the best results on joint MPJT1 in the previous chapter. The results of the set of analyses for the joints are shown in Figures 4.7 (MPJT1), Figure 4.8 (MPJT2 to MPJT4) and Figure 4.9 (MPJT5 to MPJT7). These analyses use a mesh similar in grading to the medium mesh shown in Figure 4.3, the actual mesh being shown later in Figure 4.21.

4.4.2 Models using 8 Noded Shells for Brace and Chord Elements.

The model selected here was that of case (f) as described in 3.4.3.2 as this gave the closest fit to the experimental results in the plastic region of the indentation plots, this model also being shown in Figure 4.6. Again this model used the six noded offset solid element in order to model the weld. This was shown in Figure 3.14. The results of this set of seven analyses are shown in Figures 4.10 (MPJT1), Figure 4.11 (MPJT2 to MPJT4) and Figure 4.12 (MPJT5 to MPJT7).

4.4.3 Definition of Ultimate Capacity and Differences.

Several methods of determining ultimate capacities have been used for tubular joints. One widely accepted method is that proposed by Yura et al (1980). This measures failure at the point when the deformation reaches a value given by :-

$\delta = 4f_yL/E$ where δ = deflection at a certain point

f_y = yield strength of the material

L = 30 times brace width

E = Young's modulus for the material

Another similar limit is used by de Koning et al (1992) to enable comparison between test results and this is where the measured deformation reaches 2% of b_o where b_o is the width of the chord.

It is apparent that ultimate capacities determined from both of these will depend on the locations at which the deformations or deflections are measured as the defined 2% of b_o is a constant and the actual indentation or deformation will vary depending on where it is measured. The capacities so measured bear little relationship with actual theoretical results obtained from yield line theory.

The method adopted for determining both the finite element and experimental ultimate capacities in this study is described below. For this particular series of joints the behaviour after plasticity has occurred is characterised by relatively large increases in deflection for small increases in load. In general no fall off in capacity was observed in this region except for the planar joint test MPJT1 and where joint instability occurred. Where reductions in capacity were observed, they were due to cracking overcoming the

'in-punching'. This mode of failure occurs very late on into the plastic region and involves very complex and undeveloped numerical modelling techniques. The method chosen to determine the capacity is described as follows. The point used to define ultimate capacity is the point of intersection of the linear elastic part of the load vs indentation graph and the 'straight' part of the plastic region of this graph. This is illustrated in Figure 4.13. This point will relate closely to the theoretical yield point in the rigid plastic yield line theory proposed by Davies and Morita (1992). The method also has the advantage over the two methods described above in that regardless of where the indentation is measured exactly (indentation is in-punch of the compression loaded IPB with respect to a point on the base of the chord) it should give equivalent ultimate capacities. The method does however possess some disadvantages, the major one being the determination of the two linear parts of the graph and the start and finish of the 'straight' parts of these. The lines themselves are rarely exactly straight and errors in fitting these by eye may occur. An illustration is given in Figure 4.14. As can be seen the major difficulty occurs in the fitting of a straight line to the 'plastic' section of the curve, in the example in Figure 4.14, two possible lines drawn giving a difference of up to 7% in the determined ultimate capacity. However the error in the ultimate capacity so determined, due to the actual curves is likely to be small. In some cases, particularly for CHS of low β ratio, the tendency is for a peak load to occur in the analysis. Where this occurs ultimate capacity is taken as the maximum load as shown in Figure 4.13. Ultimate capacity results for all joints using this elastic-plastic intersection technique are shown in Table 4.1 alongside experimental capacities determined in the same way.

Joint	Experimental Elastic-Plastic Intersection (kN)	F.E 4 Node (kN)	F.E 8 Node (kN)	Eqn [1] (kN) Section 4.6	Eqn [2] (kN) 4.6
MPJT1	200	210	210	197.5*/155.4	
MPJT2	240	235	215	197.5	
MPJT3	190	190	185	197.5	213
MPJT4	240	225	220	197.5	
MPJT5	210	220	210	197.5	
MPJT6	175	185	165	197.5	213
MPJT7	225	225	215	197.5	

Table 4.1 Comparison of Finite Element and Yield Line Theory.

*Weld and wall thickness taken account of.

4.4.4. Side Wall and Strain Calibrations

All the comparisons so far have been based on the 'in-punching', however as mentioned in Section 4.4 other considerations were also undertaken on MPJT2. This involved comparing both the strains and the side wall deformation of the model with those of the experiments. This was undertaken on the multiplanar model MPJT2 using the 'coarse' mesh shown in Figure 4.15, with the four noded shell element mesh used to obtain the load vs indentation results in Figure 4.8 (a). The results for the side wall deflections of this model are compared with those of the experimental result in Figure 4.16 and the various strain gauge comparisons in Figures 4.17, 4.18, 4.19 and 4.20. The positions of

these gauges were shown in Figure 4.5. As can be seen the side wall deformation and in-plane and out-of-plane brace strain gauge calibrations give reasonable agreement with the experimental results despite the large aspect ratios present in the elements in the outer regions of these members, while those for the chord strain gauges differ significantly in places. It can be noted that this is particularly so on the chord side wall where, upon considering the chord as a beam the transition between compression and tension of the top and bottom faces of the chord material will occur. A re-run of the model was undertaken with twice as many elements in the chord in order to see if this gave improved strain results. In addition to this the eight noded shell element model was also analysed to obtain the strains on the chord. The results of these are also shown in Figures 4.17 and 4.18 alongside those of the fine and coarse four noded meshes and the experimental results. This modified mesh is shown in Figure 4.21. The results of this for the chord strain gauges are shown in Figure 4.17 and 4.18 alongside those of the experimental results and the original 'high aspect' ratio mesh. As can be seen, use of an eight noded shell element mesh or the finer four noded chord mesh in Figure 4.21 has improved the results considerably on these strains, particularly on gauges 11 and 16 (see Figure 4.5) around the chord mid-height where calibration was previously very poor. It can therefore be seen that to improve experimental and numerical strain agreement, an increase in the number of elements is necessary. This is particularly so where changes in strain magnitudes are rapid, such as the chord mid-height 'beam bending' situation here, where a transition from compression in the top face to tension in the underface of the chord occurs. It can also be concluded that the high aspect ratio 'coarse'

mesh used for the original strain comparisons and also for the joint series modelling is giving good correlation with the experimental results for ultimate capacity predictions and thus confidence can be placed in its ability to predict ultimate response of this type of joint. The limitation is the loss of accuracy at the micro-strain level in certain regions for example, the chord mid-height. This however, is unlikely to be important since the critical strains and stresses occur around the weld toes and brace to chord intersection area. Strains here for the reasons and limitations of the weld models described in 3.5.1 are all but impossible to obtain accurately, particularly when the additional problem of residual stresses present due to the welding process in this region is considered.

4.5 Discussion.

As can be seen from the test Figures 4.7 to 4.12 the finite element results verify the experimental results. The models using the four noded shell elements appear to give better calibration than those of the eight noded shells. This can be seen by comparing Figures 4.7/4.10, 4.8/4.11 and 4.9/4.12. This is somewhat surprising considering the eight noded shell is more flexible and is widely accepted as being more accurate for reasons discussed in Chapter 3. The four noded shell mesh used originally contains some rather large aspect ratios in the outer chord regions (Figure 4.15), but this is also true of the eight noded shell meshes used. This is a problem related to the modelling of the corner radii which Yu et al (1993) have also been unable to overcome without resorting to the use of excessive numbers of elements. However the model has been verified under seven load cases with the worst ultimate capacity

discrepancy using the elastic/plastic intersection technique described before of 8% (see Table 4.1). Having been verified on these load cases which include both tension and compression, this model is suitable for further investigations for this actual β ratio and the multiplanar T-DT joint configuration. The eight noded shell models can be seen to give conservative predictions of joint strength, this being especially so for joints MPJT2, MPJT3 and MPJT4. Whether this is a coincidence or is caused by factors associated with the restraining of the out-of-plane braces to remain horizontal has not been resolved even after several attempts. The eight noded shells do give better agreement on the planar joint MPJT1. The eight noded shell model series (Figures 4.10 to 4.12) give closer correlation in the elastic region of the load vs indentation curves when compared to the four noded shell series (Figures 4.8 to 4.10). The one disadvantage of both these models over some of the others discussed in Chapter 3, is that a considerable amount of extra inputting time is required to define the extra offset nodes for the weld elements and the multi-point constraints to attach these to the adjacent brace and chord nodes. While the joints are made of RHS such as is the case here, this is not too much of a problem, especially if several analyses on the same mesh are to be undertaken. This is because the calculations of the co-ordinates involved for one offset node can be used for many other nodes, whereas for CHS each node requires three individual co-ordinate calculations. When models become more complex, for example involving circular hollow sections, K joints or non right angle configurations the calculations involved with this arrangement will become very complex.

Figure 4.22 presents the FE results for the whole joint series with four noded shells and it can be seen that the joints loaded in

out-of-plane tension possess much lower stiffness in the elastic region than that of the planar and other joints, although ultimately their load carrying capacity is similar to that of the planar joint. This Figure also shows the clear increase in elastic stiffness obtained by loading the out-of-plane braces in compression. Figure 4.23 shows the difference the presence of the OPB's have upon the behaviour of the joint and also the effect of the two restraint conditions, namely free OPB's and OPB's constrained to remain horizontal during loading. It can be seen that adding the braces to the original planar joint has very little effect on either the elastic stiffness or the ultimate capacity of the joint. This is illustrated in Figure 4.23 by the difference between, the planar joint MPJT1 and the multiplanar joint MPJT5 with unloaded out-of-plane braces free to rotate. Only a small pick up in capacity after an indentation of 5mm can be observed due to the presence of these unloaded braces. The effect of restraining these braces to remain horizontal can be observed in the change from MPJT5 to MPJT2 in Figure 4.23. A detectable pick up of stiffness in the upper elastic region of the curve and an increase in ultimate capacity of approximately 10% can be observed. The effect of restraining the branches to be almost horizontal is to severely restrict the deflection of the chord sidewalls when compared to the joints where the out-of-plane braces are free to rotate and the planar joint. Figure 4.24 shows the results for the series of identically restrained joints MPJT2 to MPJT4, the purpose of this being to illustrate the effects of the different loading conditions in the out-of-plane braces on the joints elastic and ultimate response. The joint with tension present in the out-of-plane braces (MPJT3 in Figure 4.24) can clearly be seen to be less stiff and have a lower ultimate capacity than the joint with unloaded out-of-plane braces (MPJT2 in

Figure 4.24). The joint with compression in the out-of-plane braces (MPJT4 in Figure 4.24) has a very significant stiffening effect upon the elastic and early elasto-plastic sections of the load vs indentation curve. Figure 4.25 illustrates similar trends for the series of joints with out-of-plane braces free to rotate. Again the tension presence in the out-of-plane brace (MPJT6 in Figure 4.25) can be seen to lower the elastic stiffness and ultimate capacity when compared to the other joints while the addition of compression in the out-of-plane braces enhances the elastic stiffness and in this case the ultimate capacity slightly when compared to MPJT5 the joint with unloaded out-of-plane braces.

4.6 Yield Line Theory

Various mechanisms of collapse may occur on the T-DT joint and a selection of these are presented by Davies, Coutie, Bettison and Morita (1992) and are shown again for convenience in Figure 4.26. Mechanism 1 is appropriate to the planar joint MPJT1 and to all the other joints if failure occurs on one of the four individual chord faces. However for the cases where tension is present in the out-of-plane braces, mechanism 2 (MPJT3 and MPJT6) and mechanisms 4 and 5 (MPJT6) may become the critical cases and give a lower capacity than mechanism 1 depending upon the magnitude of the out-of-plane (DT) force. The formulae proposed by Davies et al (1992) for mechanisms 1 and 2 are stated below.

Mechanism 1

$$P_y = \frac{f_y t_o^2}{(1-\beta)} \left\{ \frac{2h_1}{b_o} + 4(1-\beta)^{.5} \right\} \qquad [1]$$

Mechanism 2

$$P_y = \frac{4f_y t_o^2}{(1-\beta)}\left\{\frac{h_1}{b_o} + (6(1-\beta))^{.5}\right\} \qquad [2]$$

The capacities according to these equations are compared with those of the experimental results and finite element predictions in Table 4.1. As can be seen all finite element and experimental results exceed yield line calculated capacities except for the cases of MPJT3 and MPJT6 where all experimental and numerical results are below those of the yield line theory. The reason for this is likely to be the much greater elastic deformation/flexibility exhibited by the joints MPJT3 and MPJT6 (see Figures 4.24 and 4.25) where tension is present in the OPB's (DT braces). This increased flexibility/elastic deformation makes the joint capacities less likely to agree with the yield line capacities due to the yield line theory assuming perfectly plastic (no elastic deformation) behaviour. However it can be seen that the yield line theory generally gives good and conservative results for this type of joint.

In selecting the effective β ratio for use in the yield line formulae the effects of the weld and wall thickness are taken into account to improve the accuracy of the answer. Differing interpretations as to where the plastic hinges may occur were shown in Figure 3.20 in Chapter 3 and formulae for these developed by Davies et al (1992). It can thus be seen that the theory is open to some interpretation regarding where the plastic hinges actually form which in turn will have a significant impact on calculated capacities.

4.7 Conclusions.

1) The presence of forces of the opposite sense in the out-of-plane (DT) braces clearly reduces both the elastic stiffness and the ultimate capacity. This will be investigated further in Chapter 6.

2) The medium mesh shown in Figure 4.15 is adequate for the joint ultimate capacity predictions. Some refinement is required in the chord if strains are to compare realistically with those of the experiments.

3) The eight noded shell model gives conservative but realistic predictions of ultimate capacity. This is of benefit when going on to investigate other joint configurations for which experimental results are unavailable as conservatism is safe.

4) For this particular joint configuration four noded shells give adequate results compared to eight noded with the benefit of reduced CPU time. Care must be taken of the fact that these elements are less accurate than eight noded shells when examining other joint configurations.

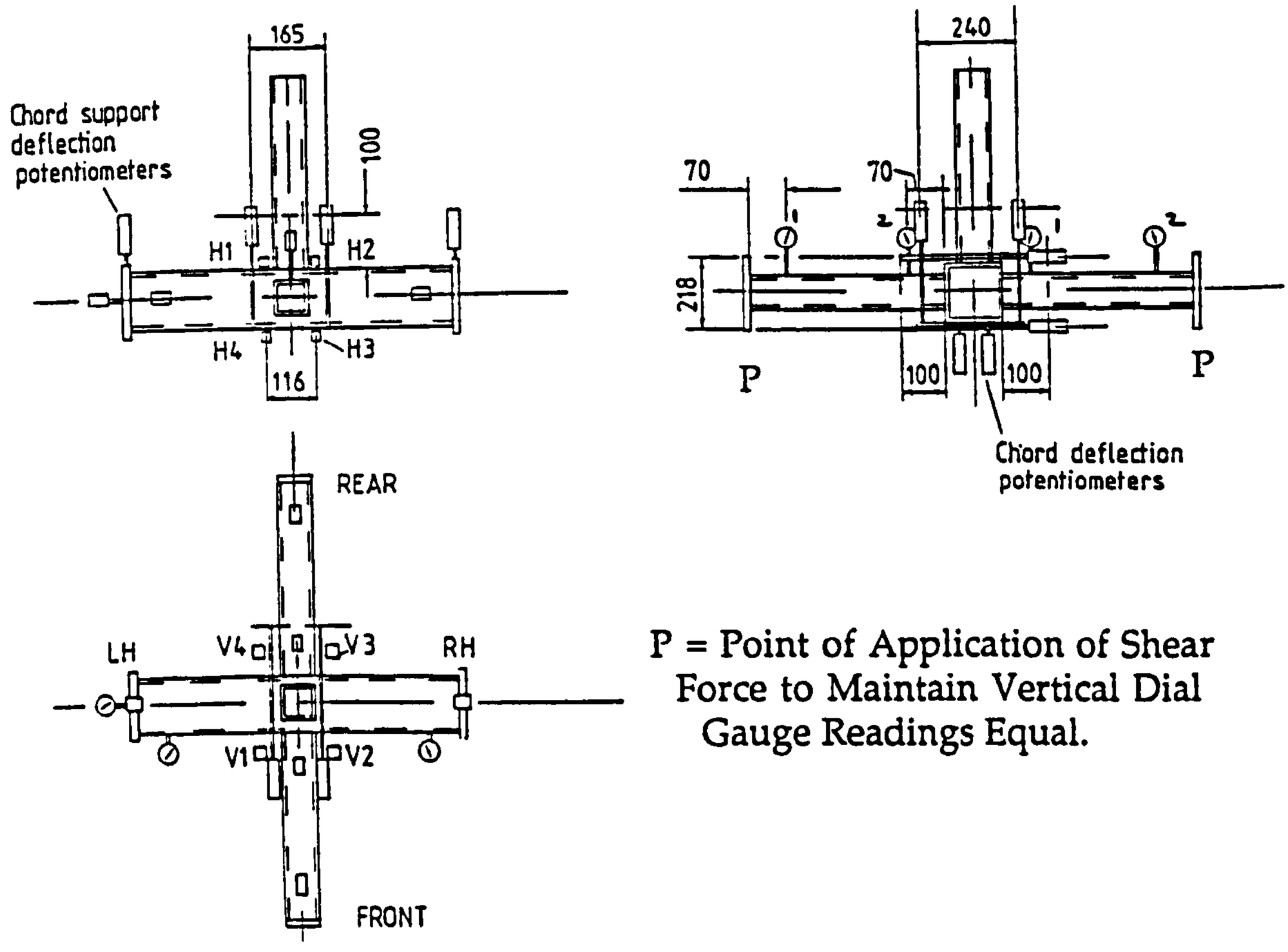

Figure 4.1 Positions of Dial Gauges and Potentiometers for measuring the horizontal displacements on the Experimental Joints.

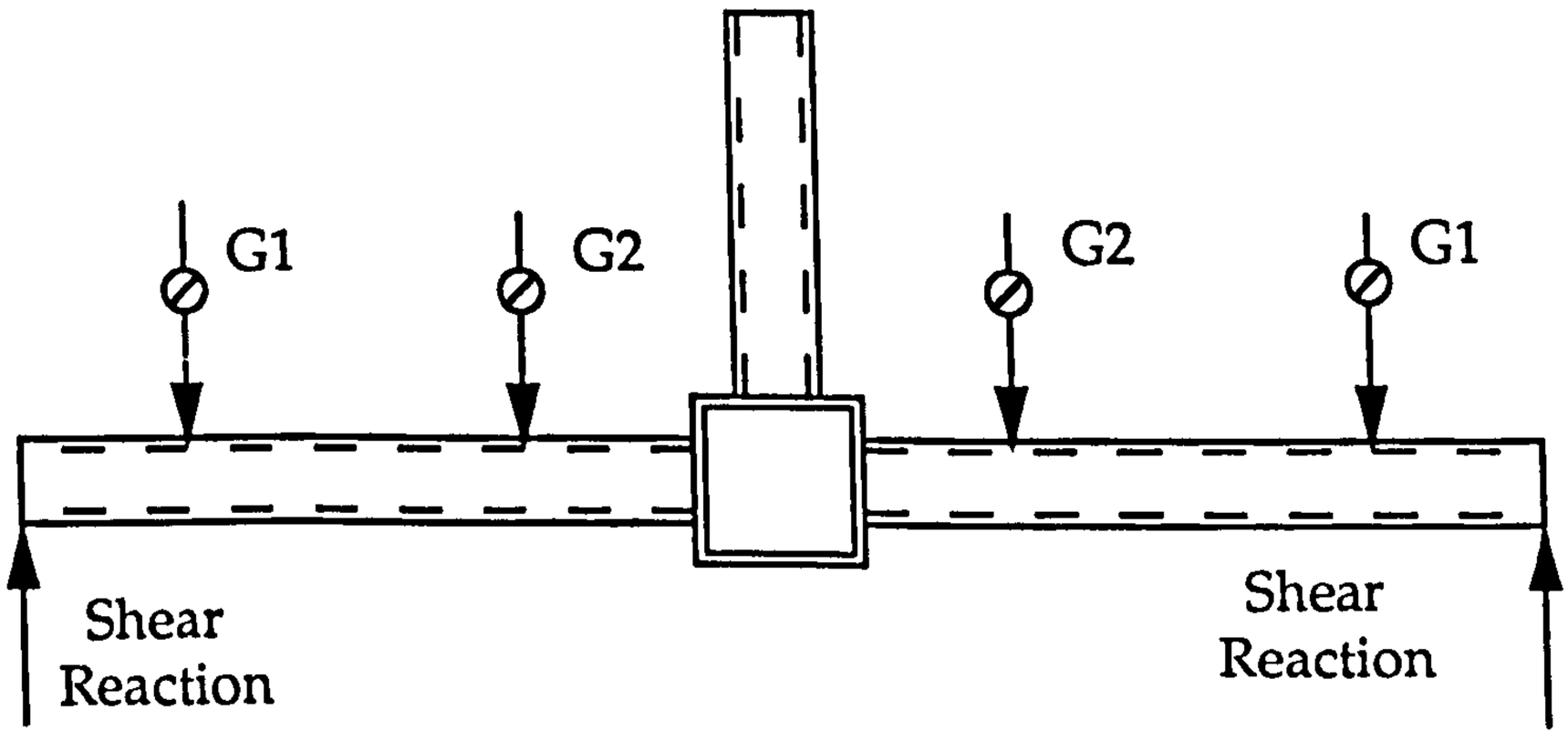

Deflection G1 = Deflection G2

Figure 4.2 Possible curvature that may occur on the out-of-plane braces due to the shear force applied to maintain these horizontal.

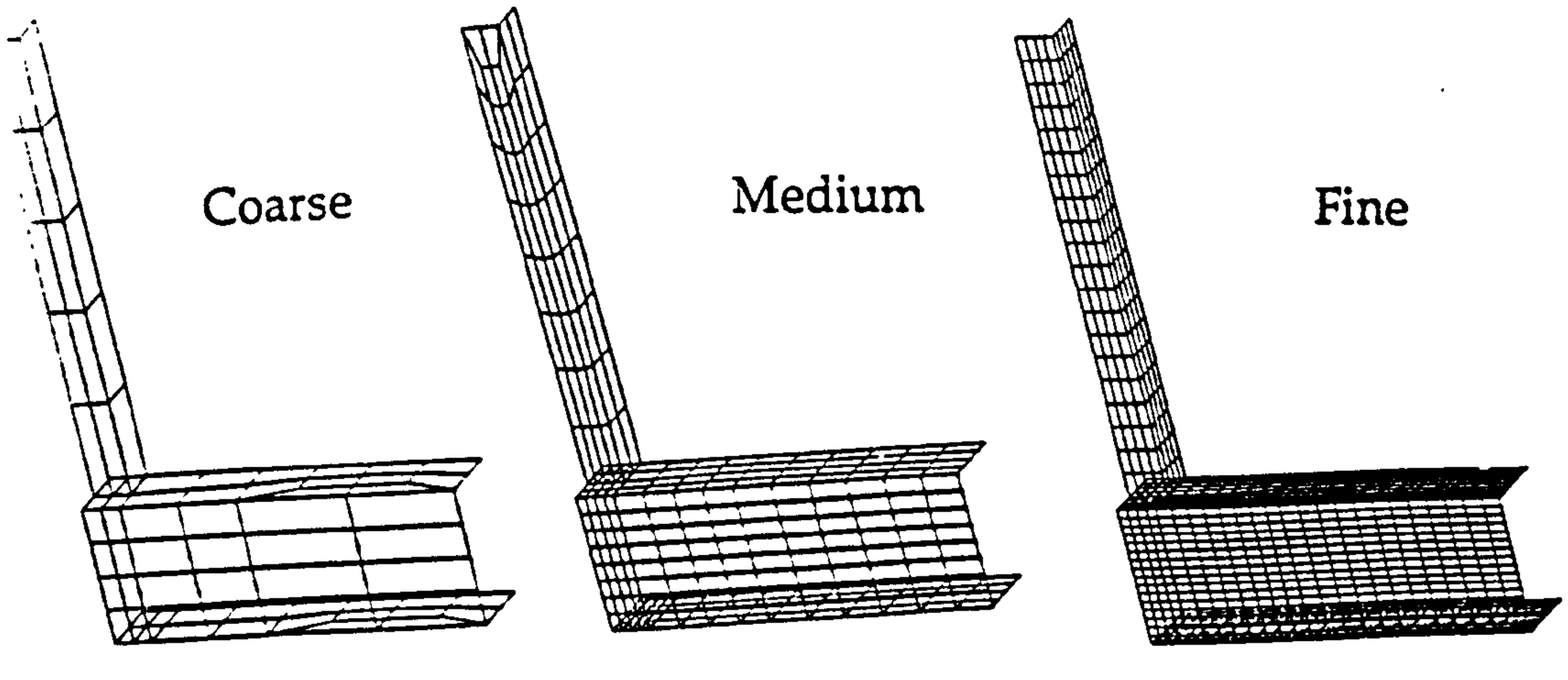

Total Elements = 75 Total Elements = 274 Total Elements = 928

Figure 4.3 The three meshes using four noded shells used in the mesh convergence study (weld modelling ignored).

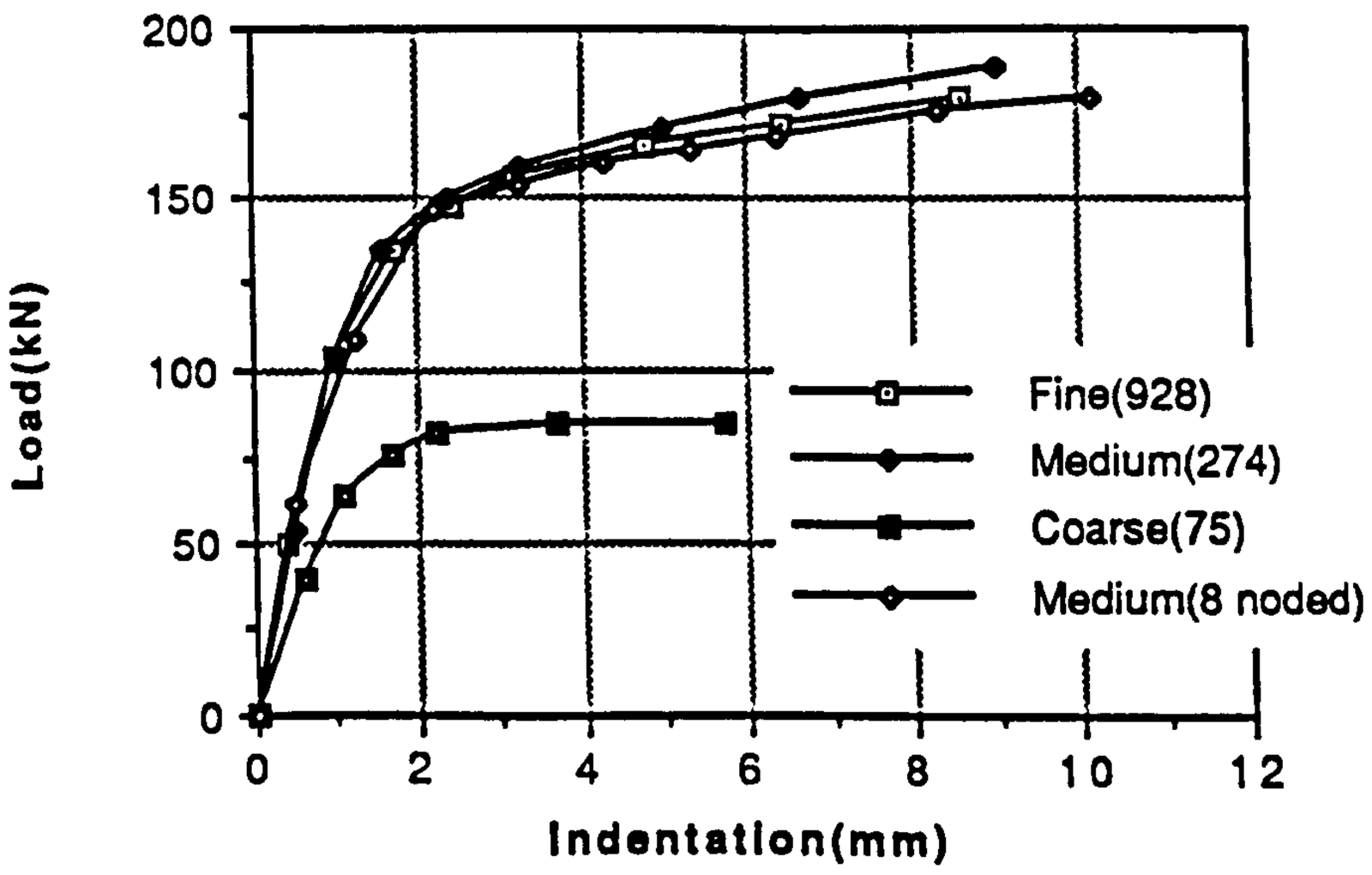

Figure 4.4 Load vs Indentation Plots for the Three Four Node Meshes in Figure 4.3 and Eight Node Medium (274 Elements) Mesh.

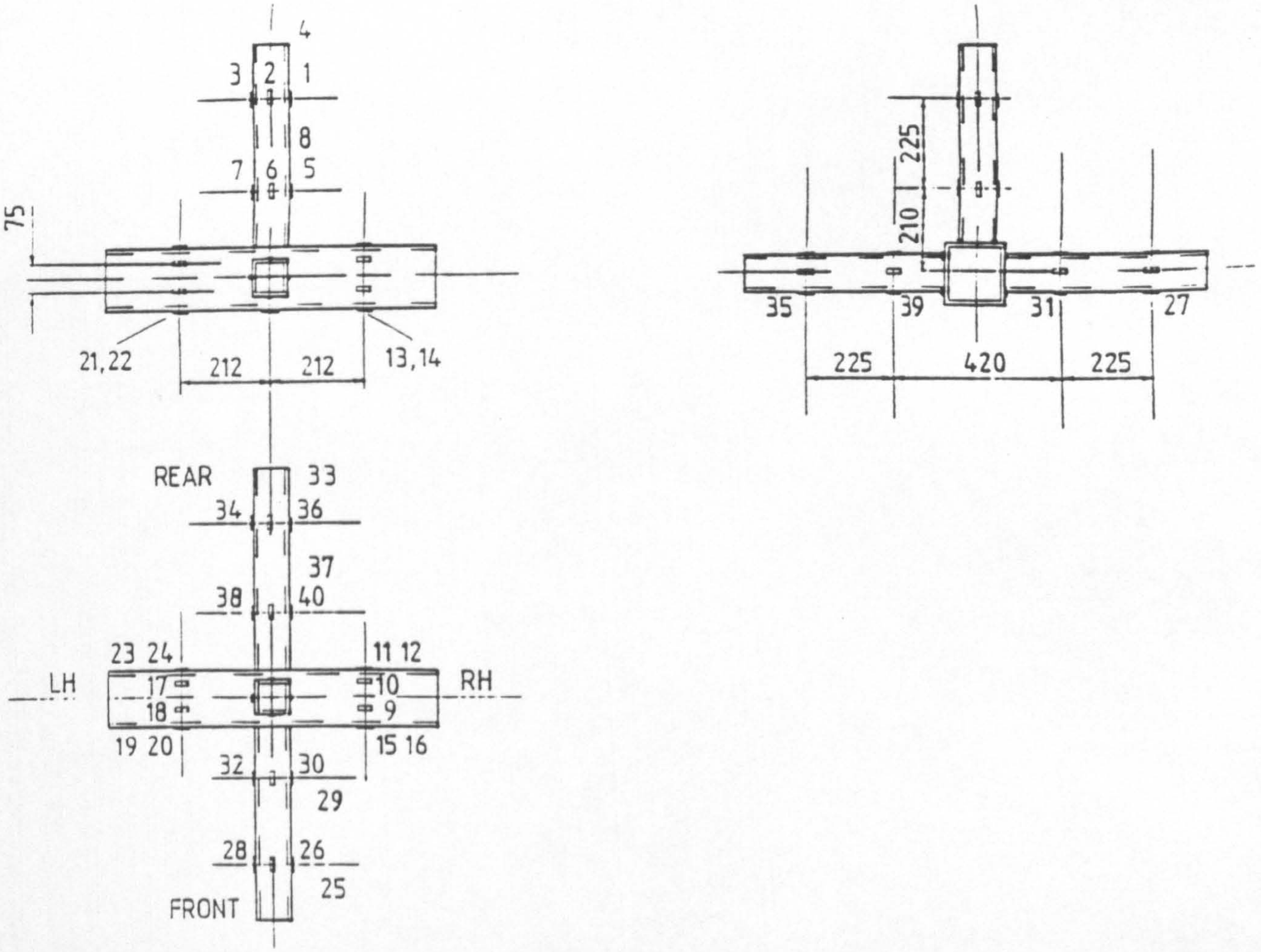

Figure 4.5 Strain Gauge Positions for the Multiplanar Joints (MPJT2 to MPJT7).

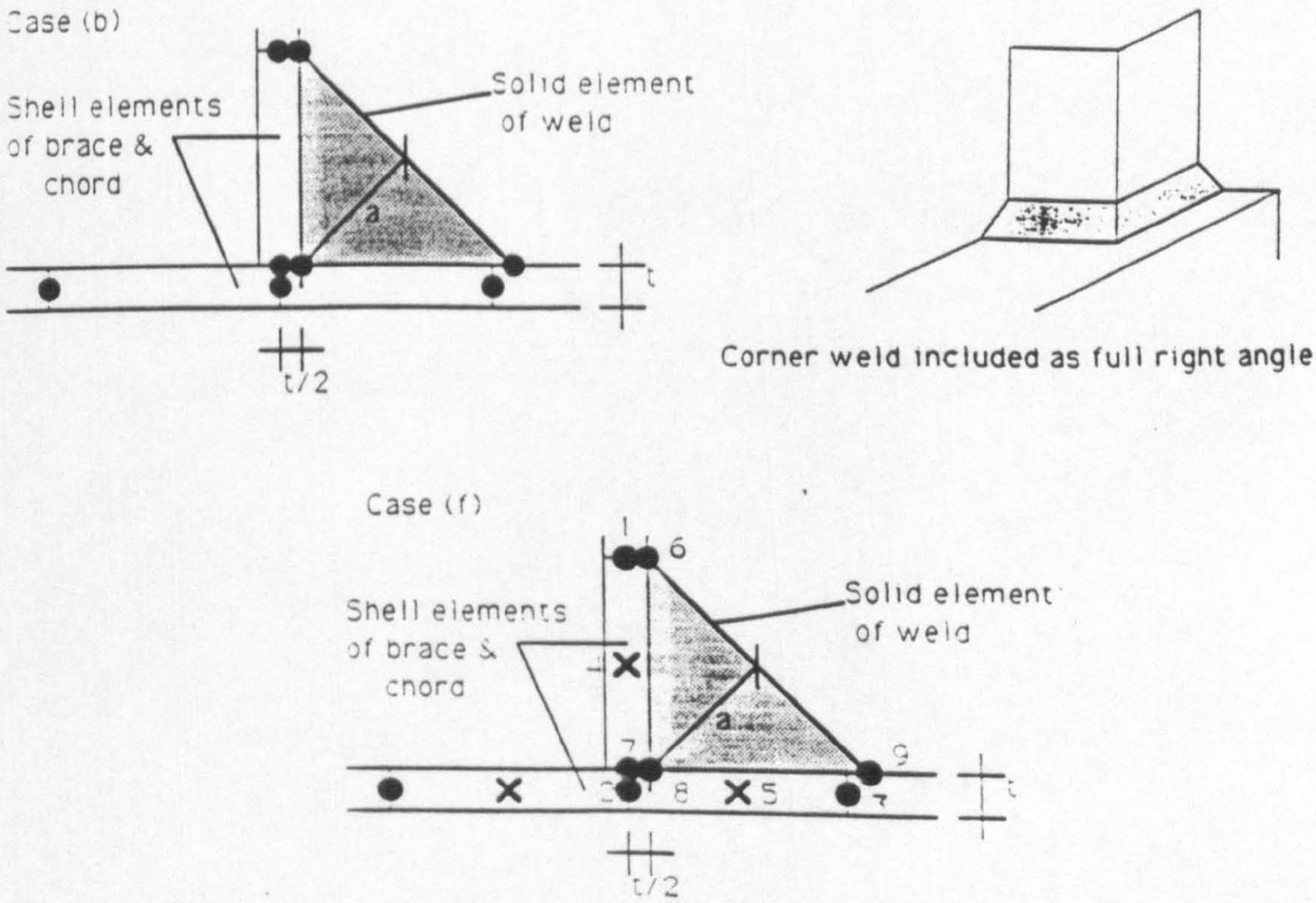

Figure 4.6 Weld Model Cases (b)and (f) from Chapter 3

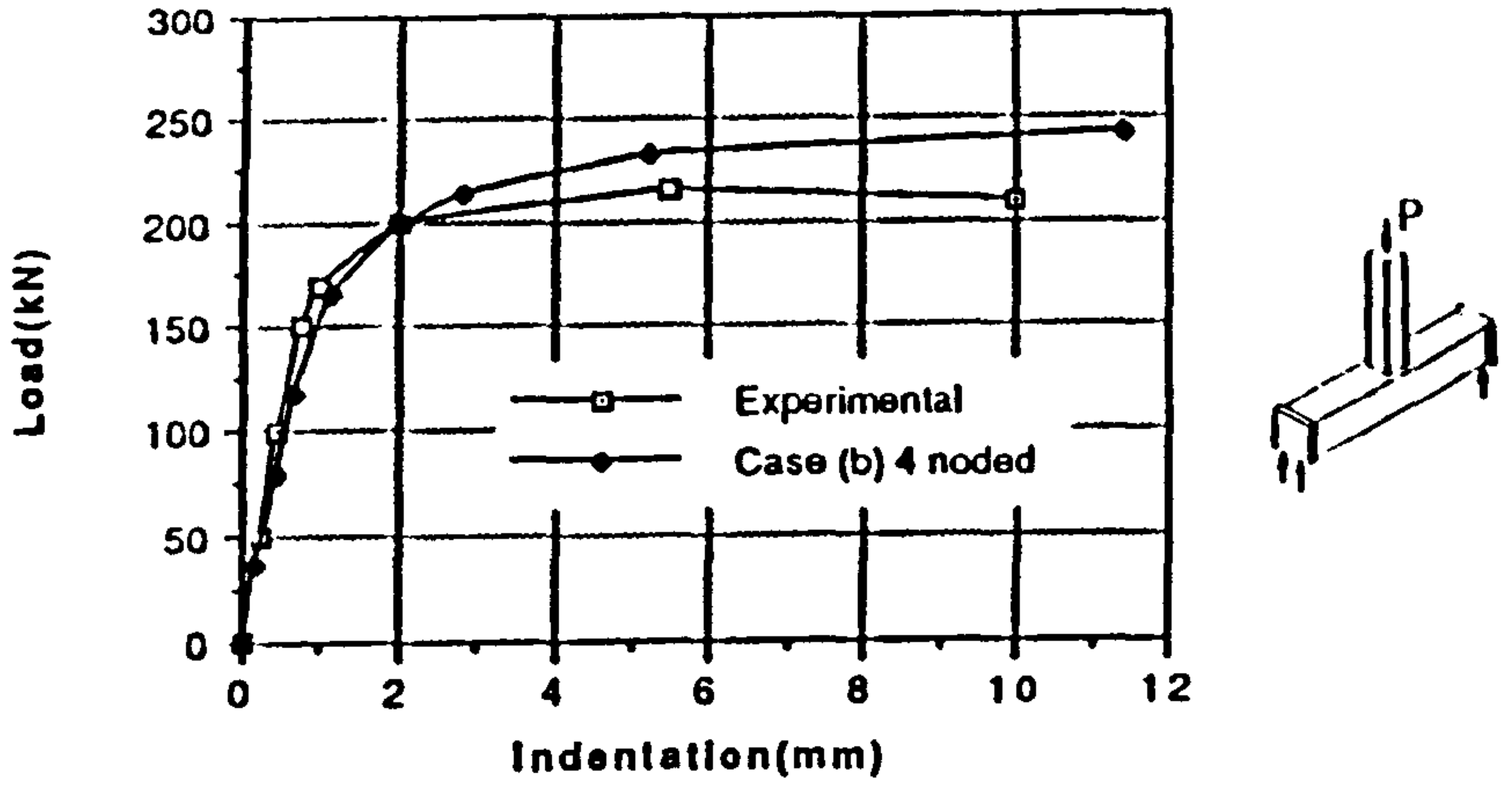

Figure 4.7 Experimental and Four noded FE results compared for MPJT1 (Mesh as in Figure 4.15).

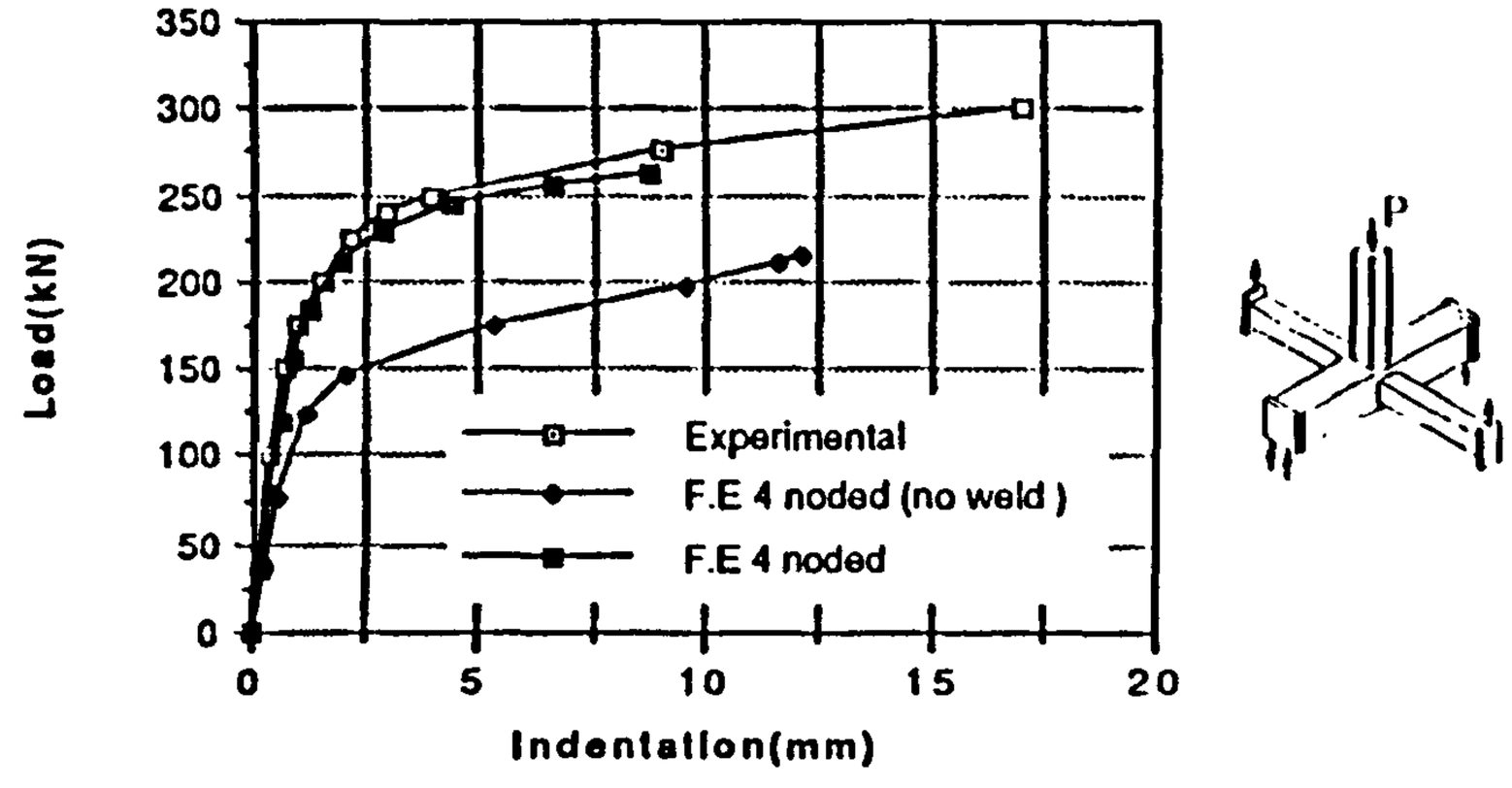

Figure 4.8 (a) Experimental and Four noded FE results compared for MPJT2 (Mesh as in Figure 4.15).

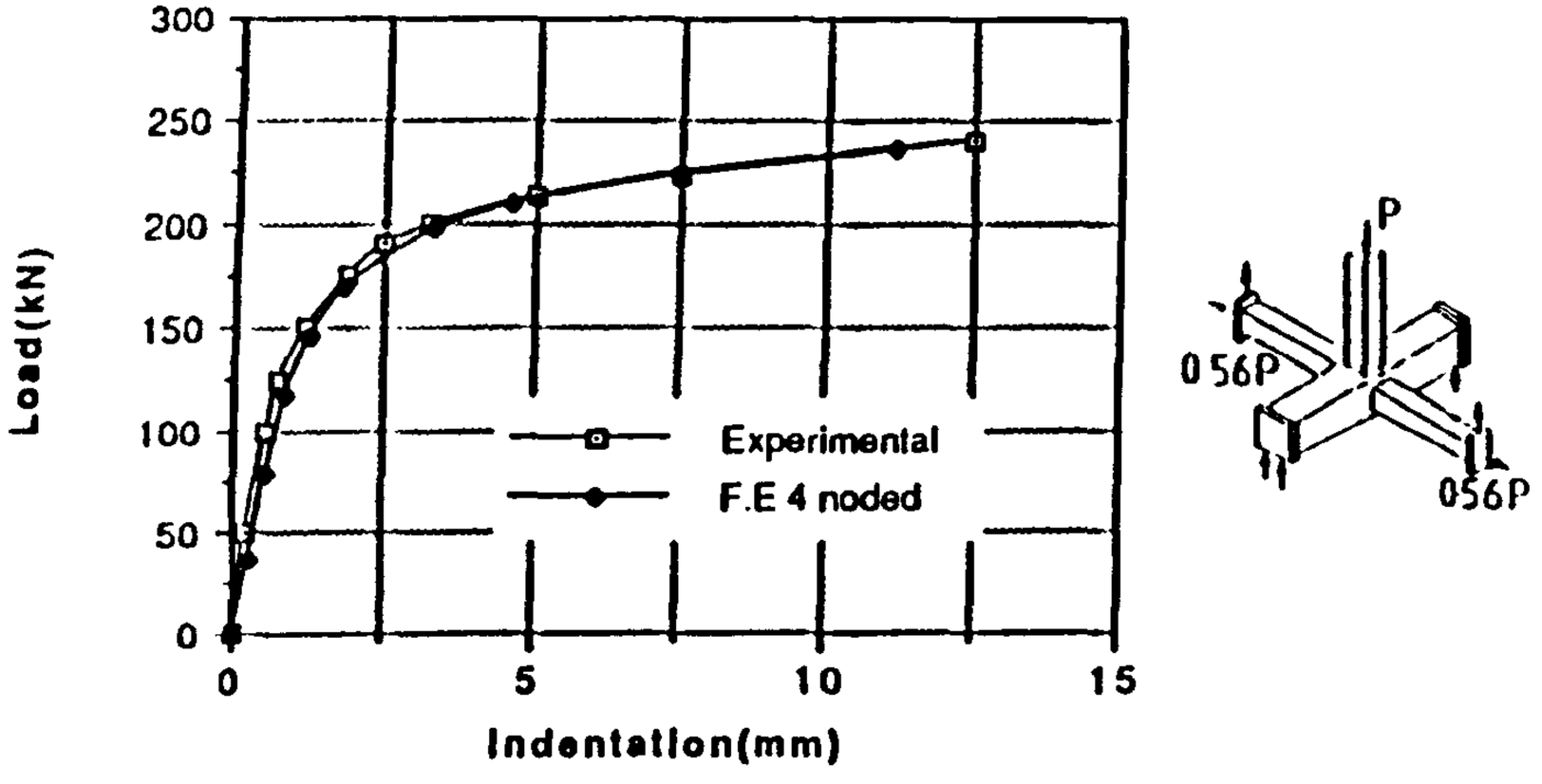

Figure 4.8 (b) Experimental and Four noded FE results compared for MPJT3 (Mesh as in Figure 4.15).

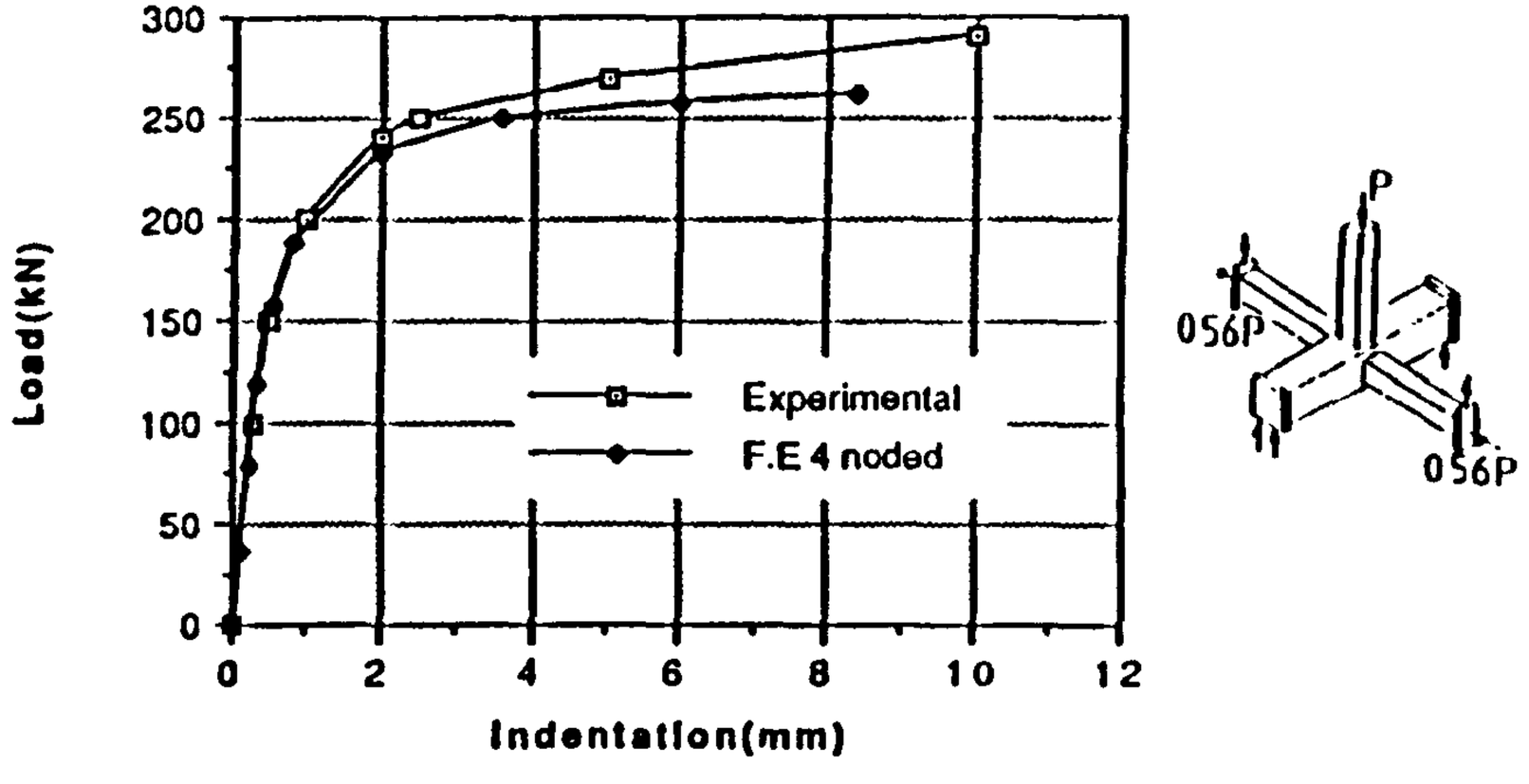

Figure 4.8 (c) Experimental and Four noded FE results compared for MPJT4 (Mesh as in Figure 4.15).

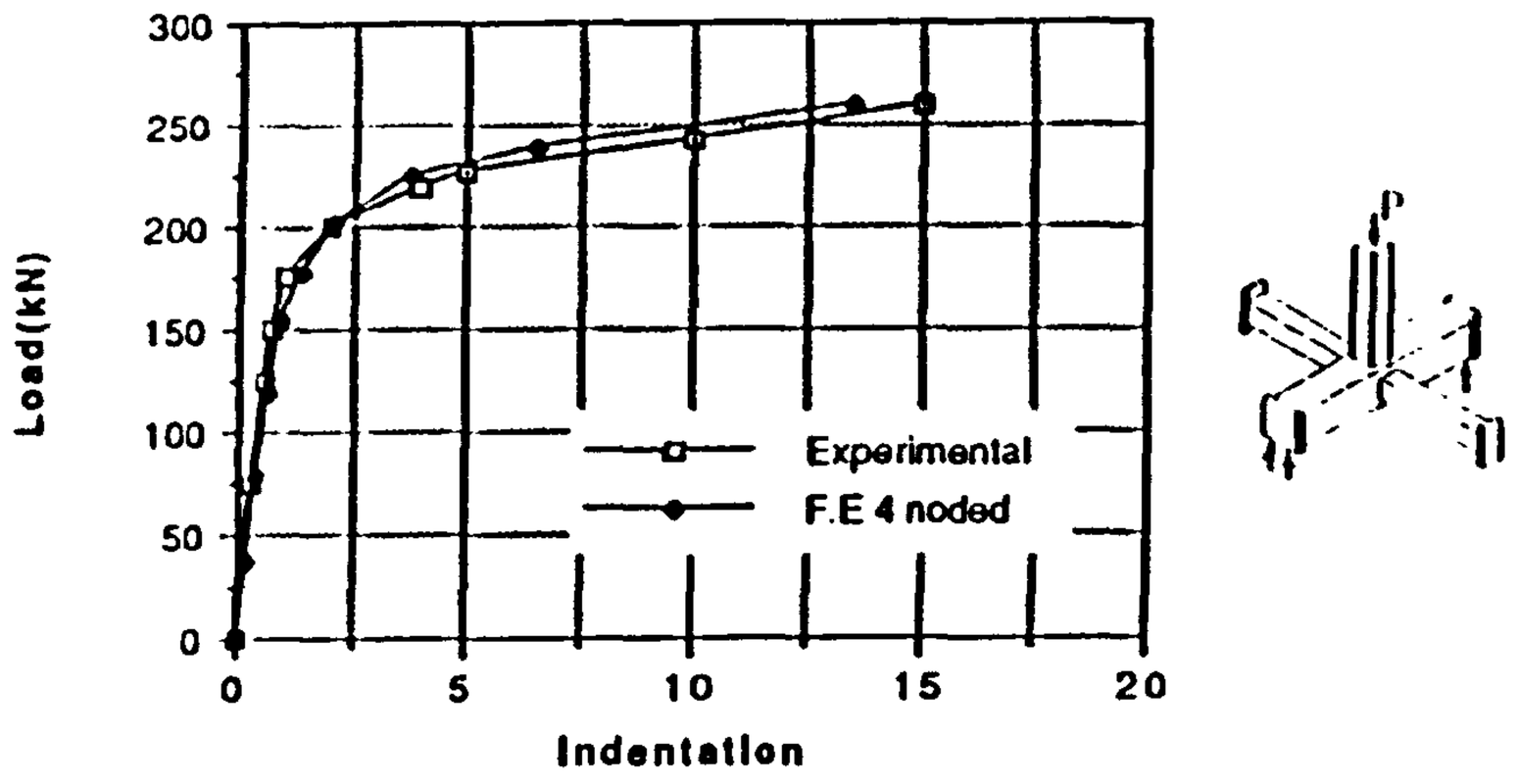

Figure 4.9 (a) Experimental and Four noded FE results compared for MPJT5 (Mesh as in Figure 4.15).

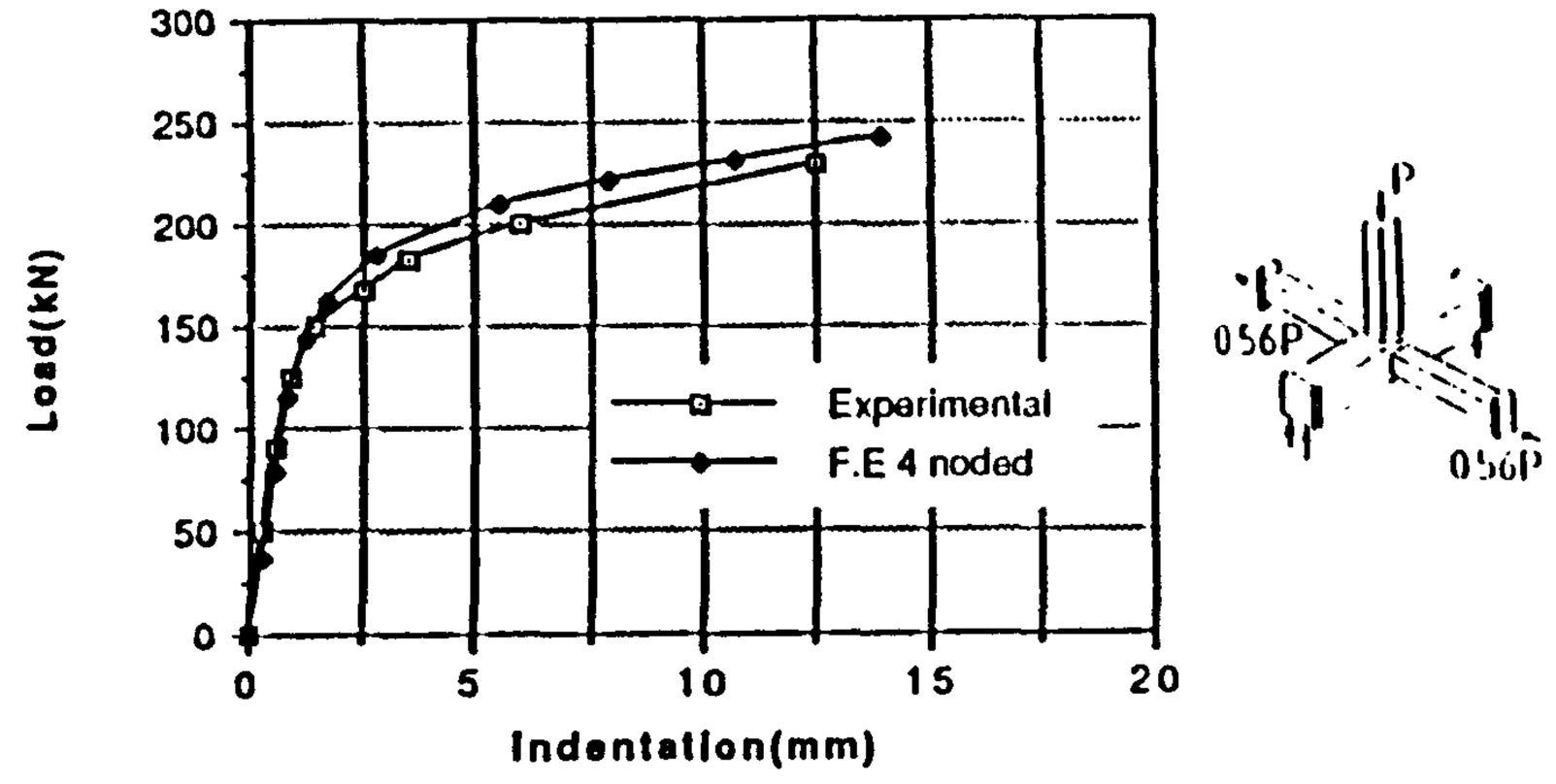

Figure 4.9 (b) Experimental and Four noded FE results compared for MPJT6 (Mesh as in Figure 4.15).

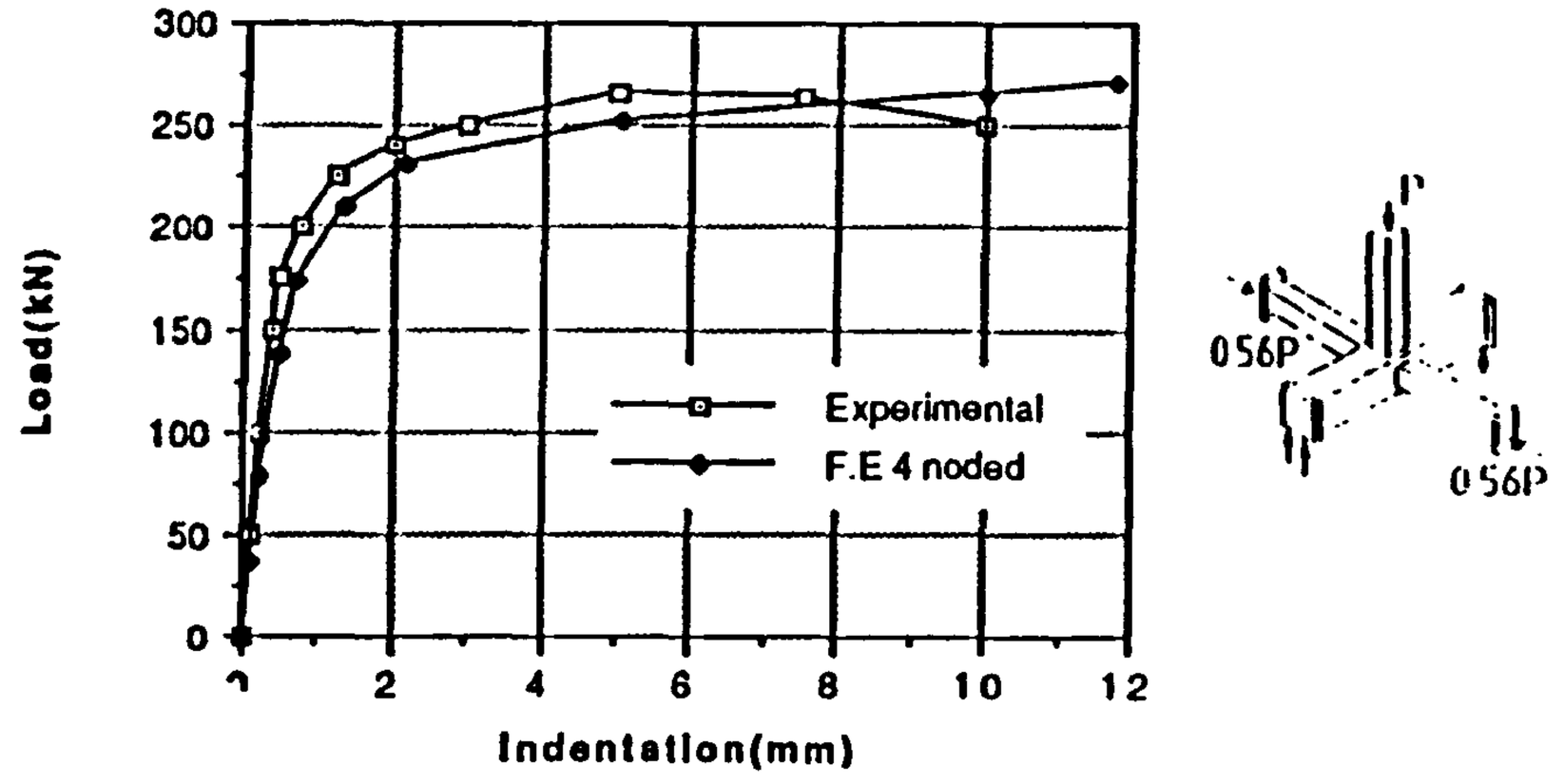

Figure 4.9 (c) Experimental and Four noded FE results compared for MPJT7 (Mesh as in Figure 4.15).

Figure 4.9 Experimental and FE Comparisons for MPJT5 to MPJT7.

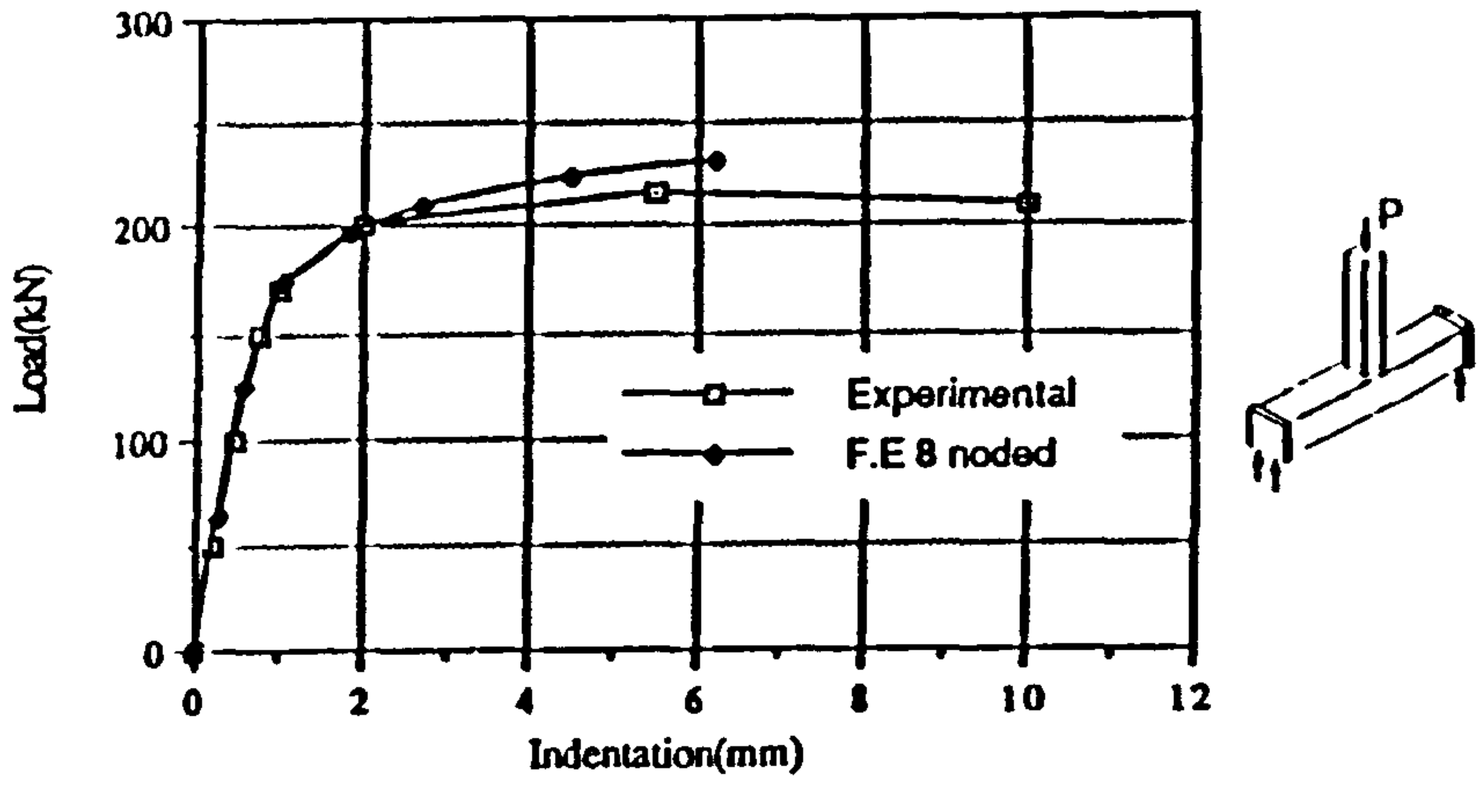

Figure 4.10 Experimental and Eight noded FE results compared for MPJT1 (Mesh as in Figure 4.15).

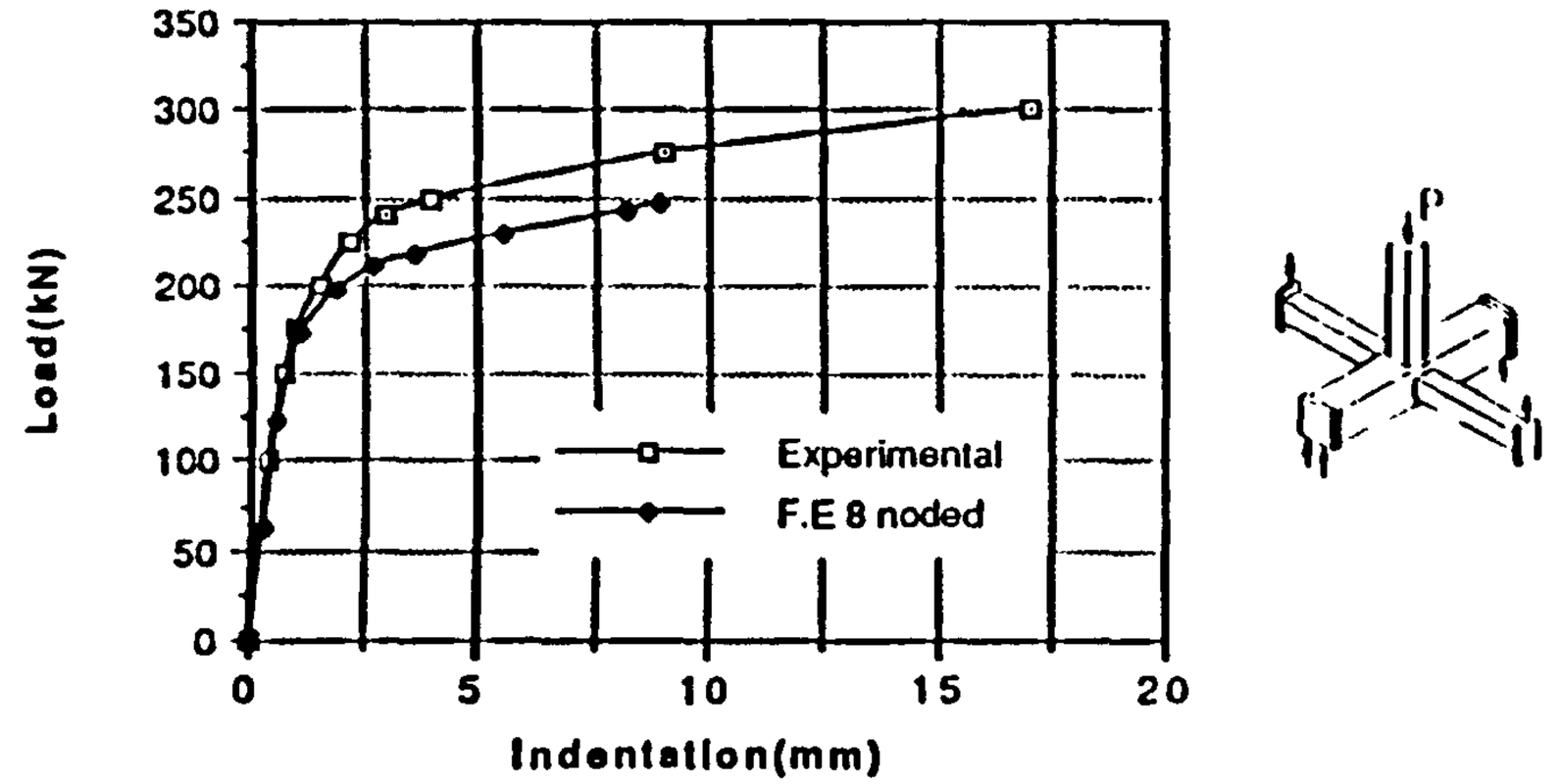

Figure 4.11 (a) Experimental and Eight noded FE results compared for MPJT2 (Mesh as in Figure 4.15).

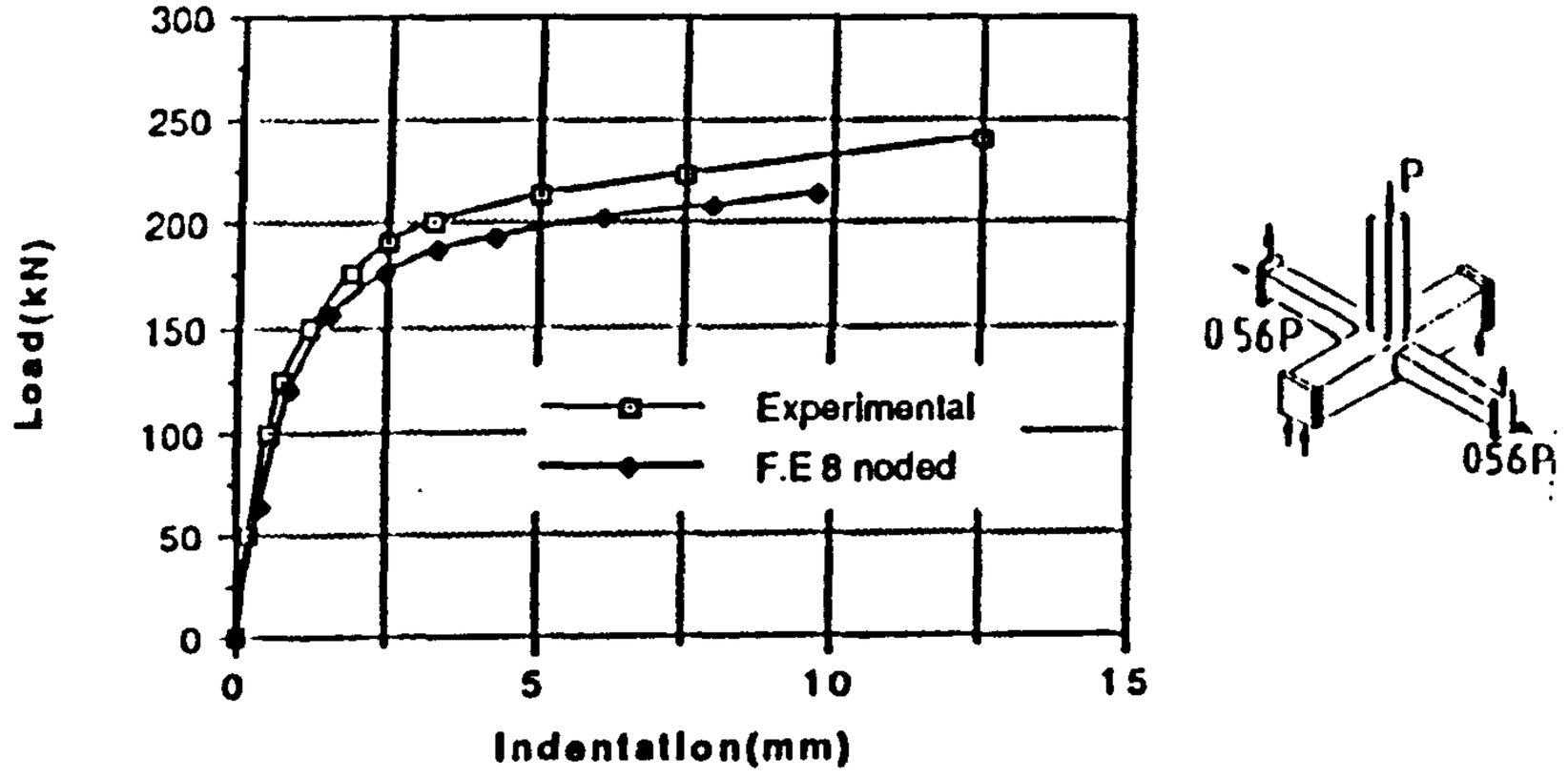

Figure 4.11 (b) Experimental and Eight noded FE results compared for MPJT3 (Mesh as in Figure 4.15).

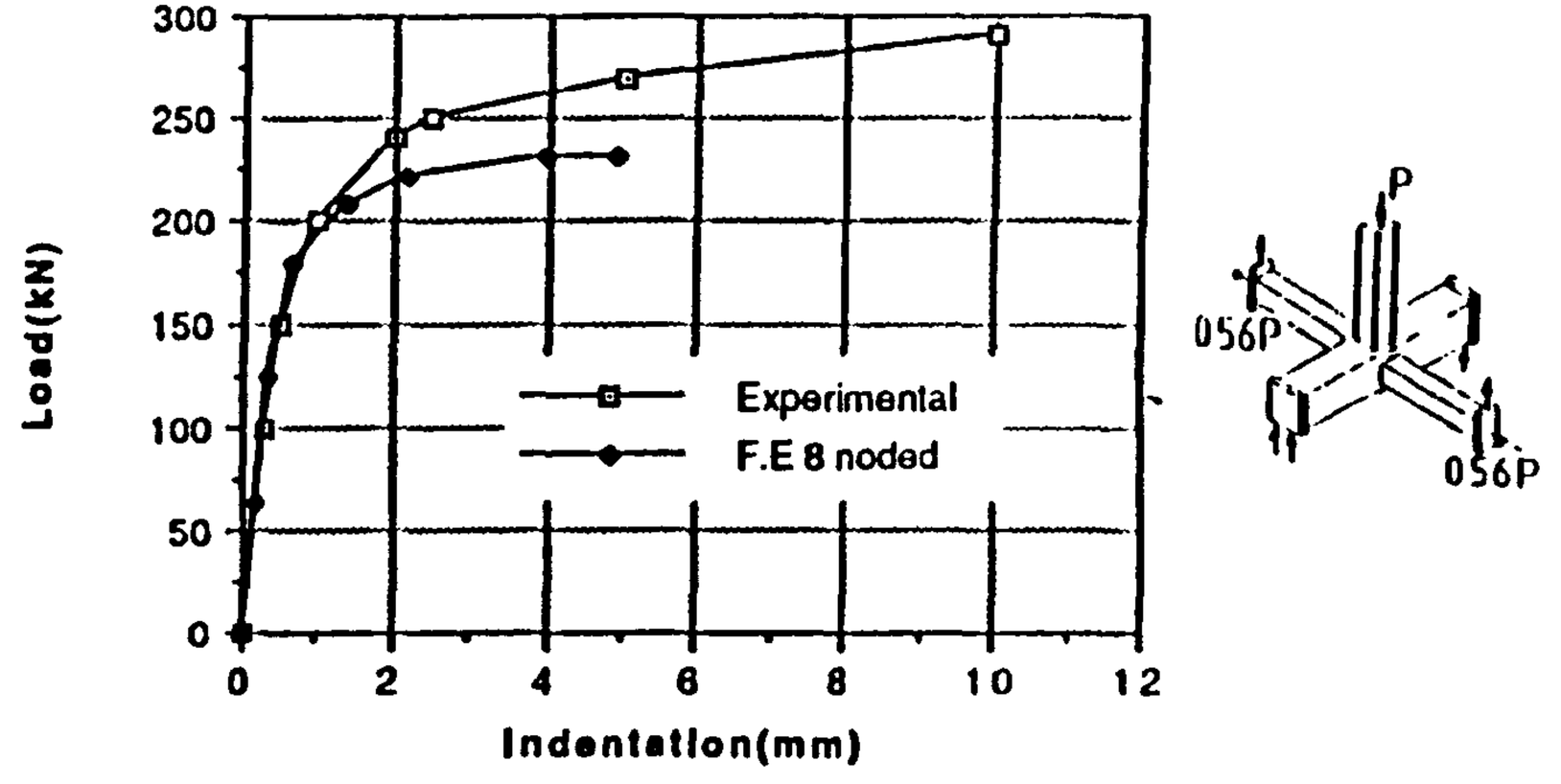

Figure 4.11 (c) Experimental and Eight noded FE results compared for MPJT4 (Mesh as in Figure 4.15).

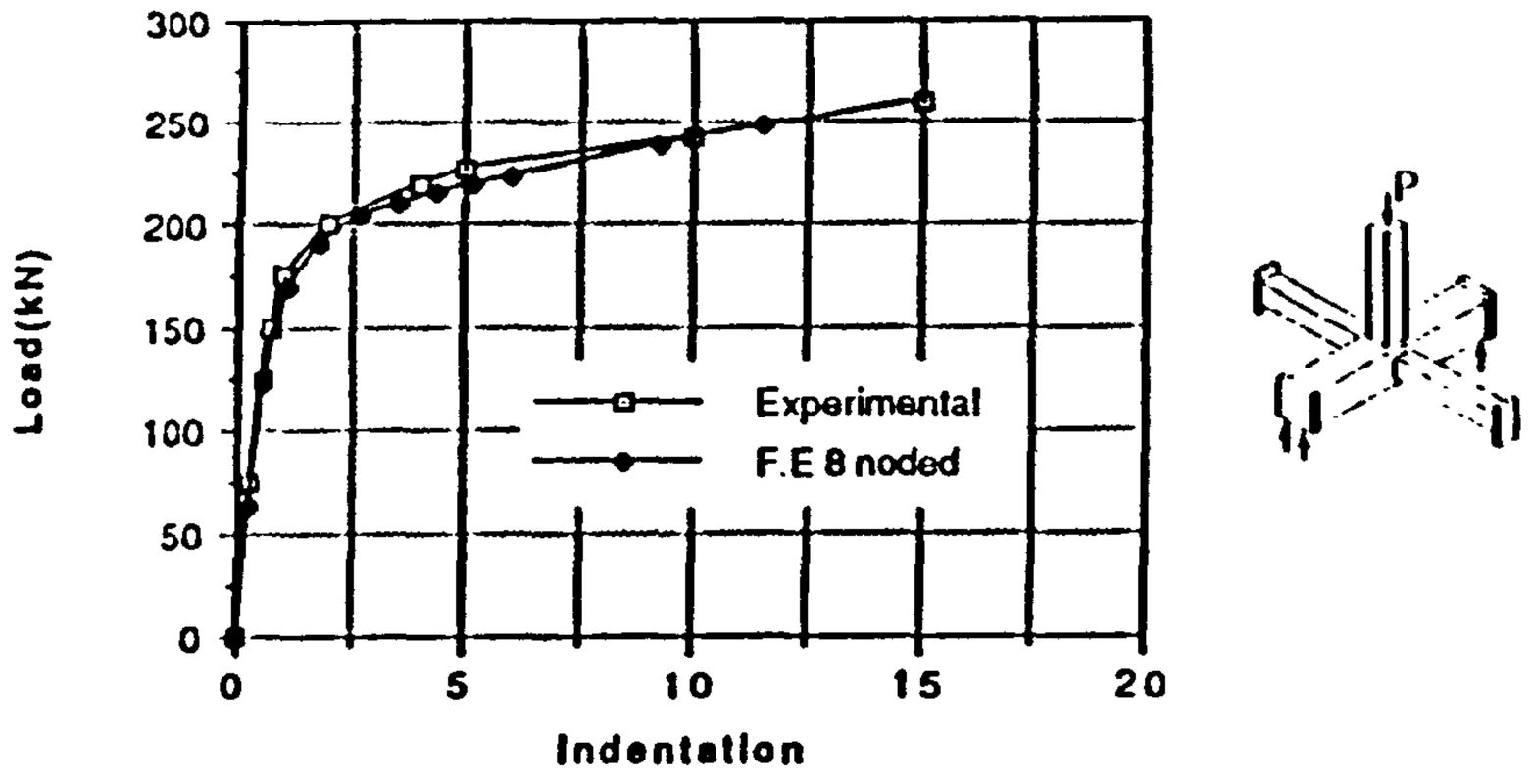

Figure 4.12 (a) Experimental and Eight noded FE results compared for MPJT5 (Mesh as in Figure 4.15).

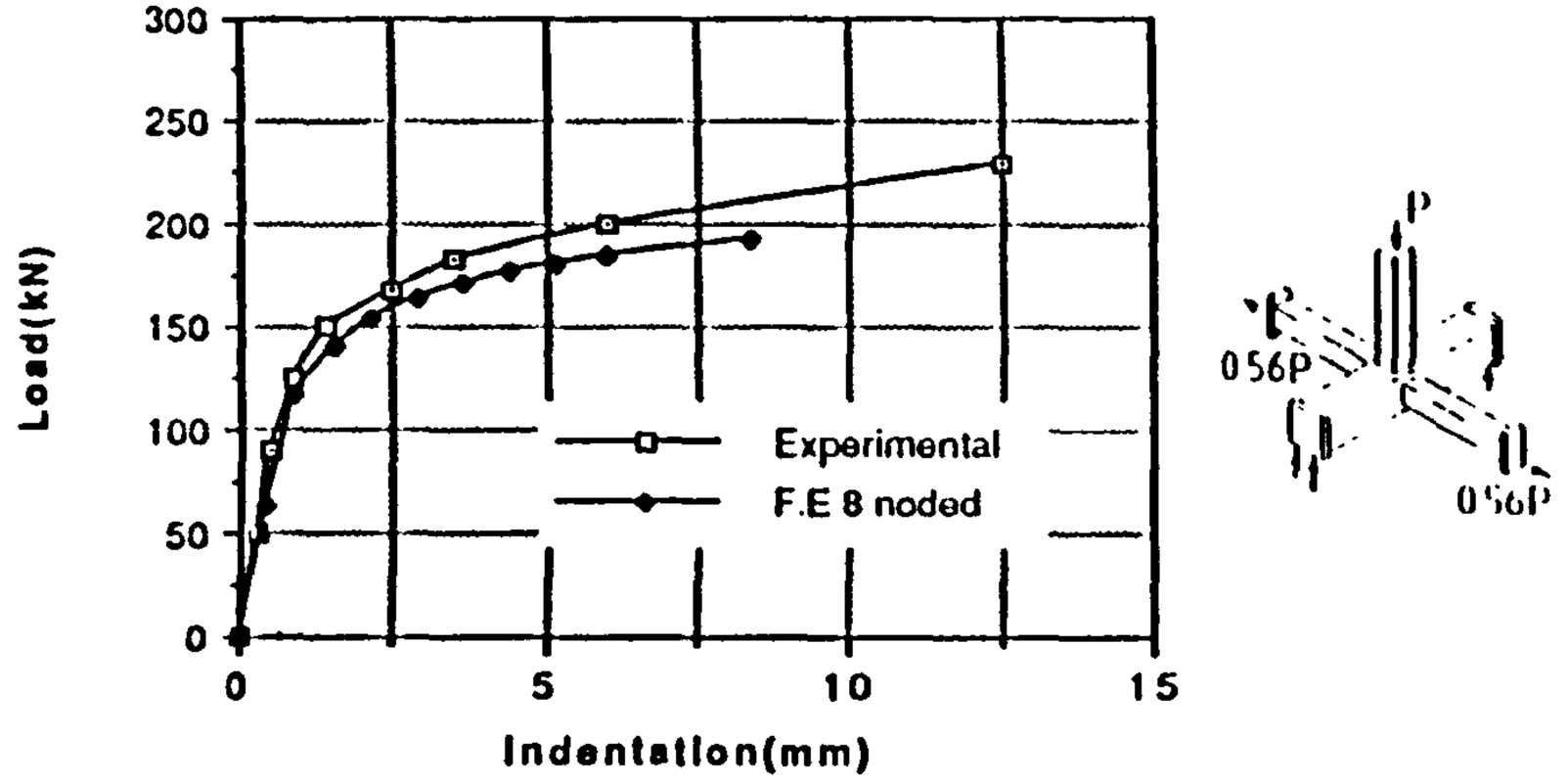

Figure 4.12 (b) Experimental and Eight noded FE results compared for MPJT6 (Mesh as in Figure 4.15).

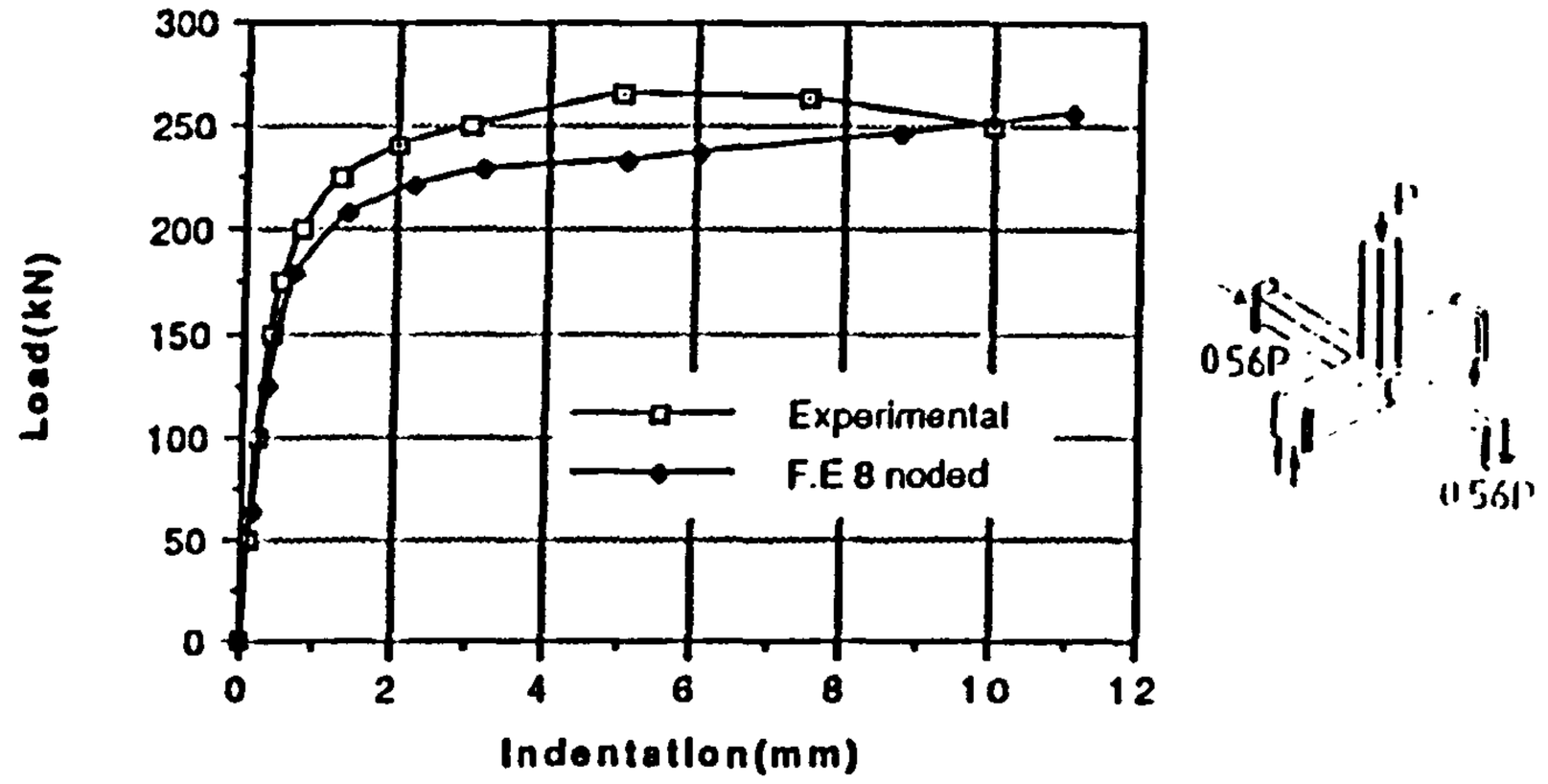

Figure 4.12 (c) Experimental and Eight noded FE results compared for MPJT7 (Mesh as in Figure 4.15).

Figure 4.12 Experimental and FE Comparisons for MPJT5 to MPJT7.

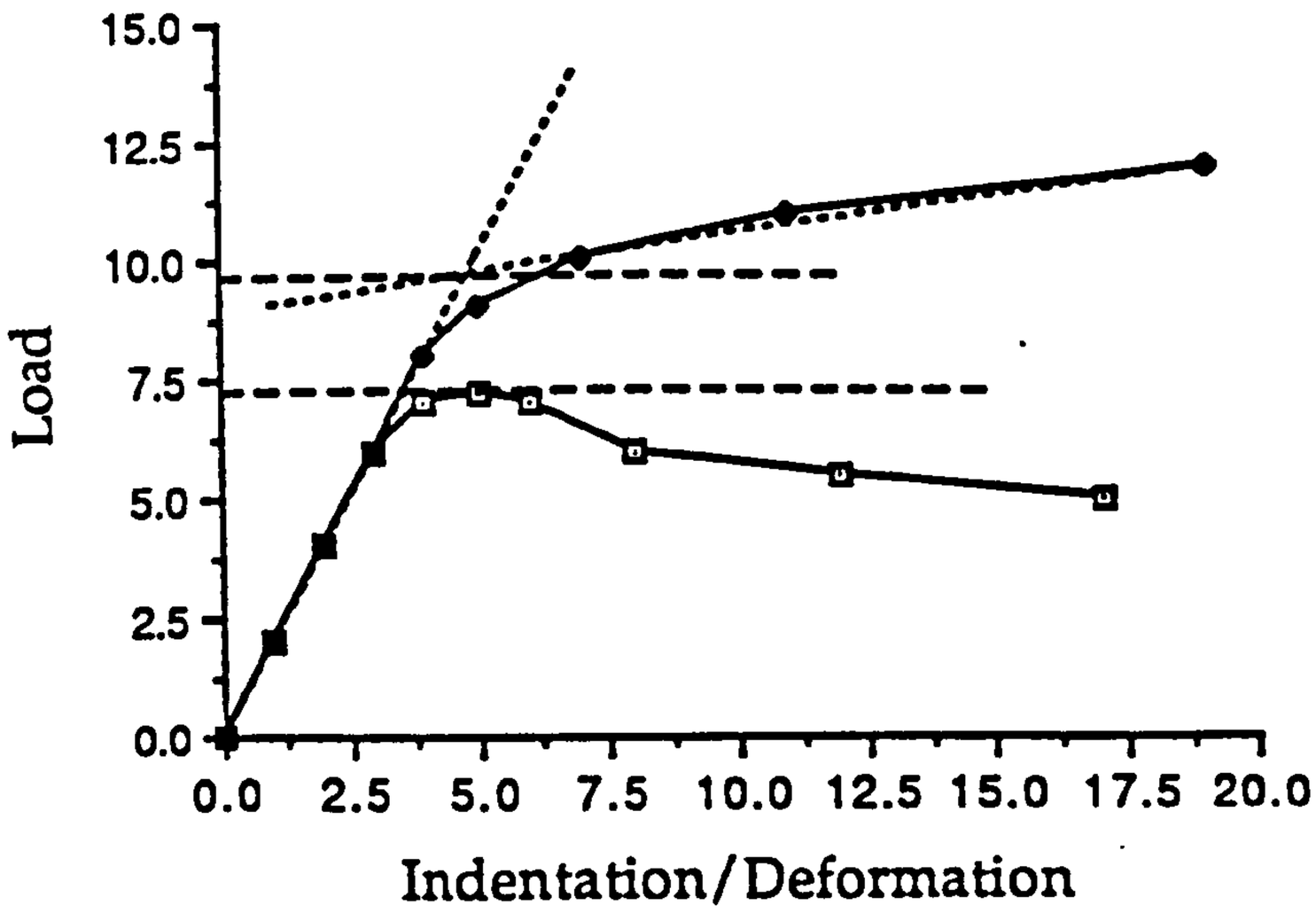

Figure 4.13 Methods of determining ultimate capacities of joints.

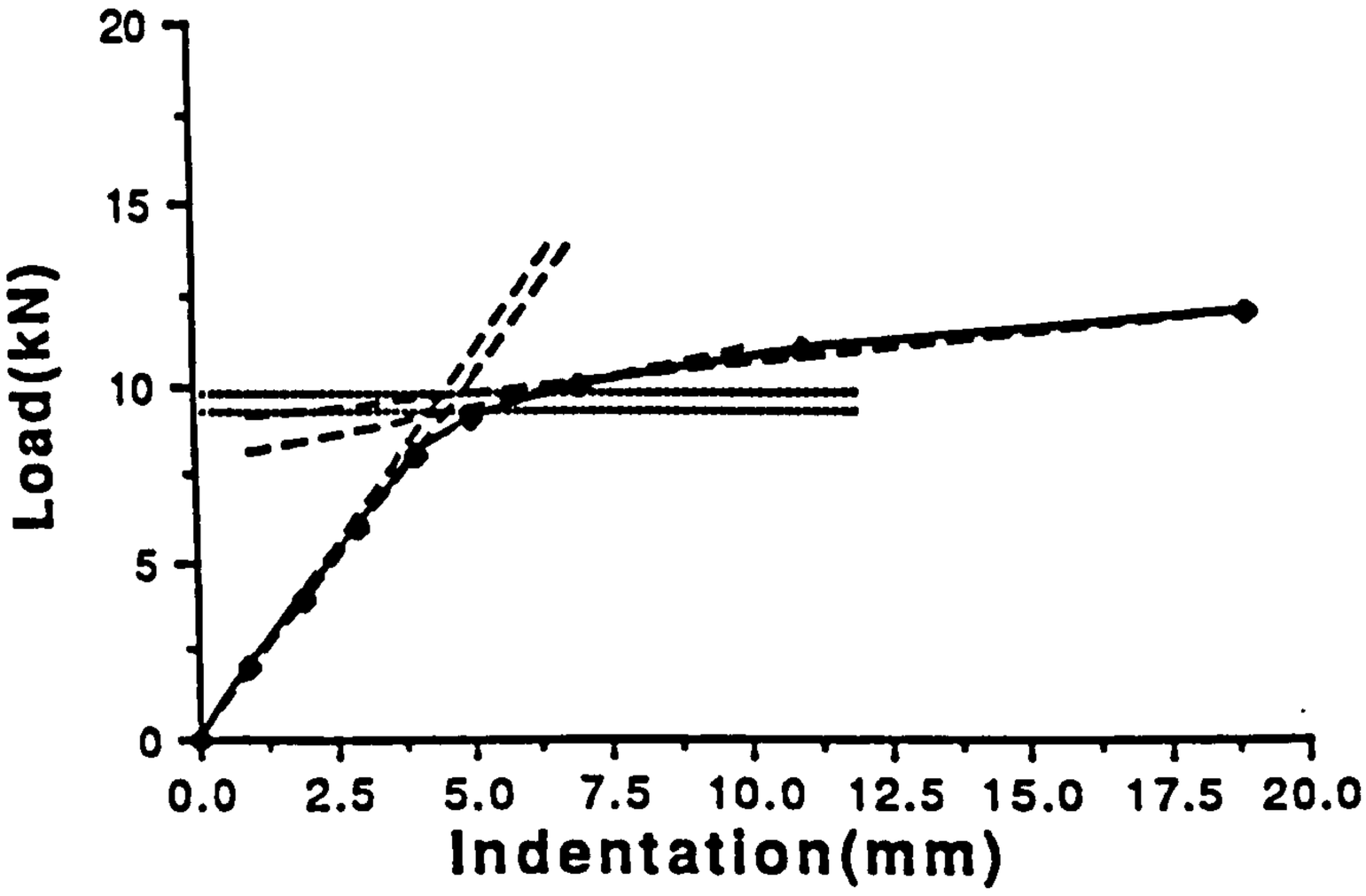

Figure 4.14 Possible discrepancies in fitting by eye the 'straight' elastic and plastic lines.

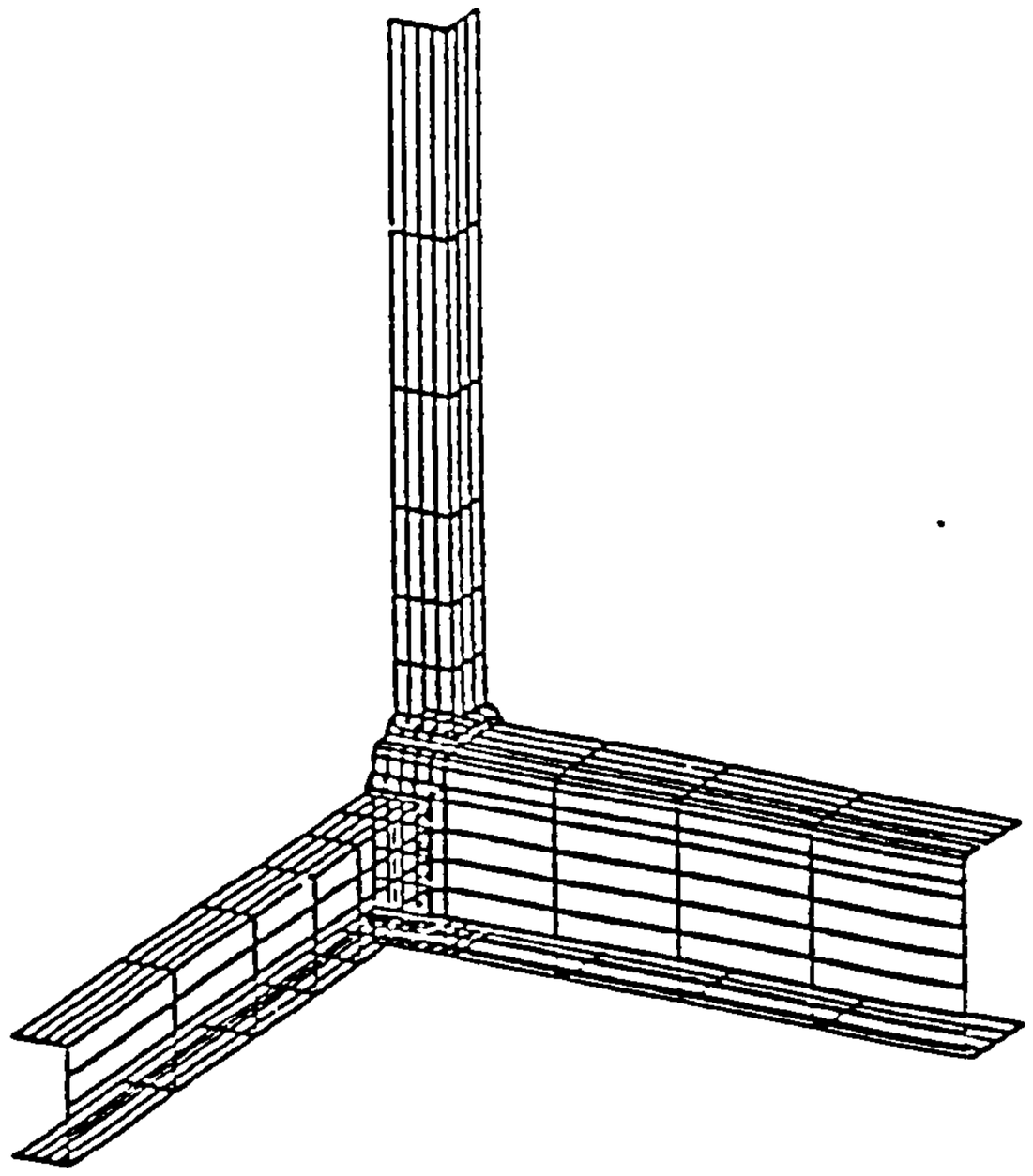

Figure 4.15 The Finite Element Mesh used to model MPJT2 to MPJT7. (Planar Joint MPJT1 Equivalent with OPBs Removed).

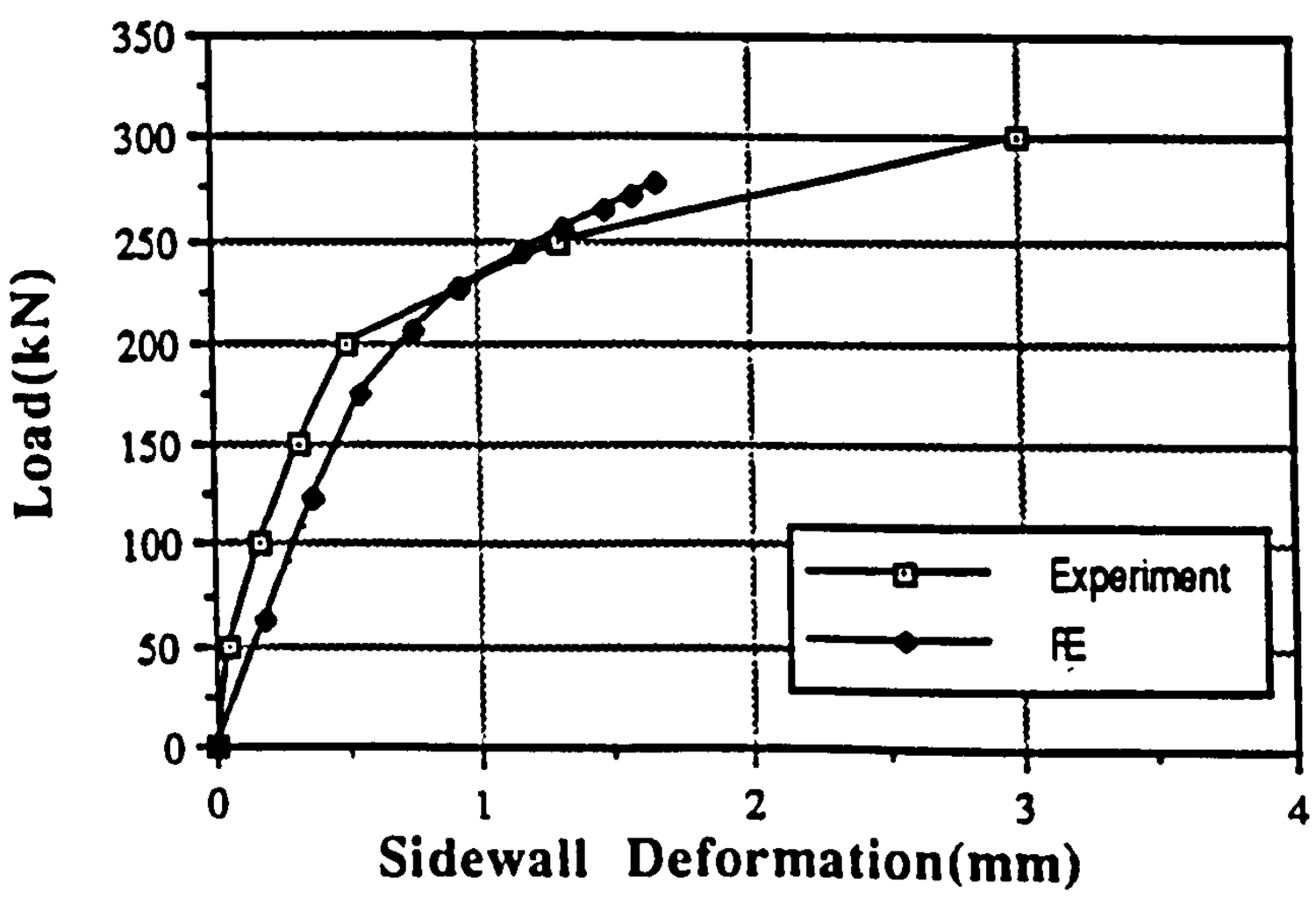

Figure 4.16 Comparison of Experimental and FE Chord Sidewall Deformations in MPJT2.

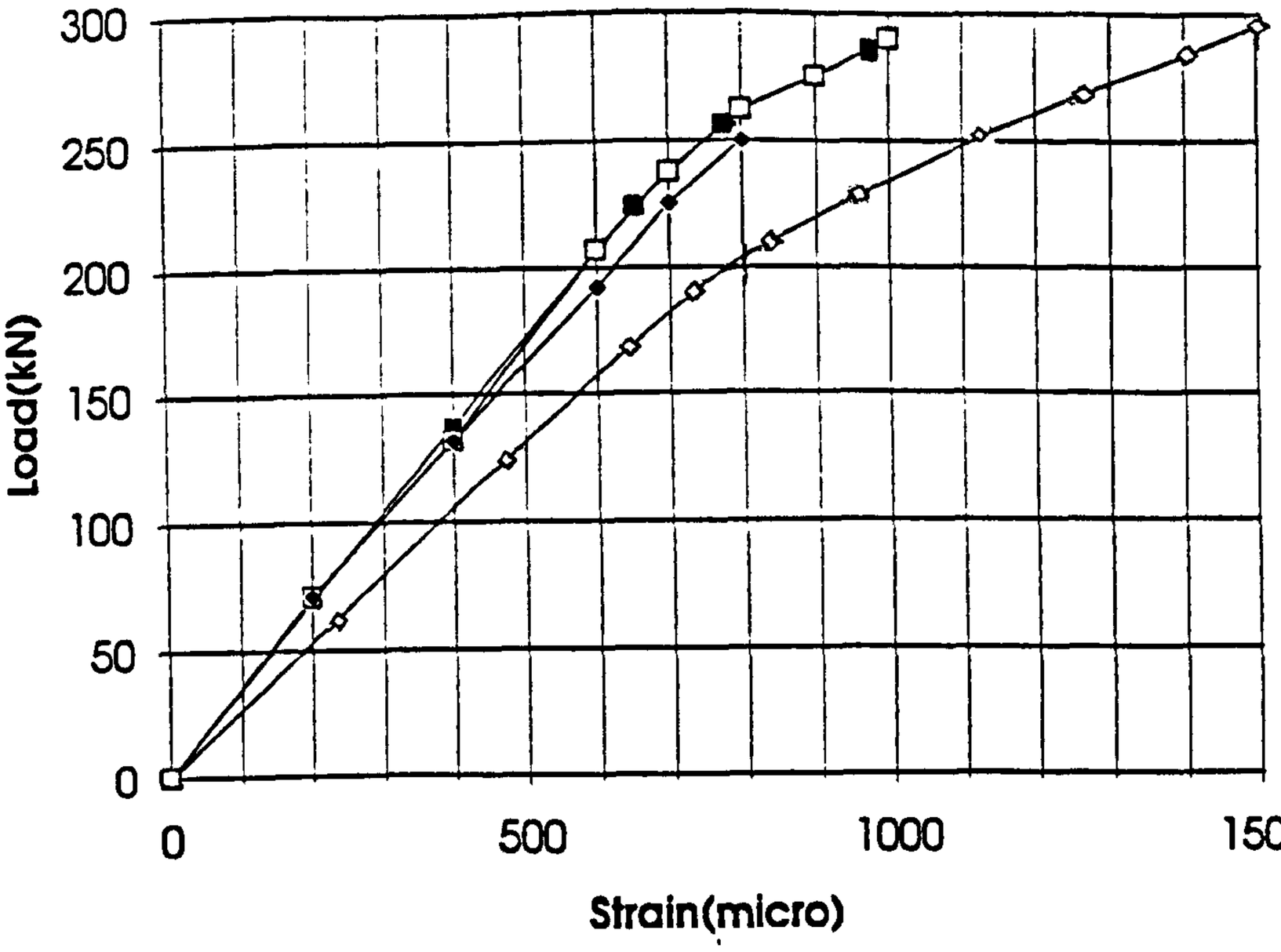

(a) Strain Gauges 13/14/19/24 in Figure 4.5 - Chord Underface

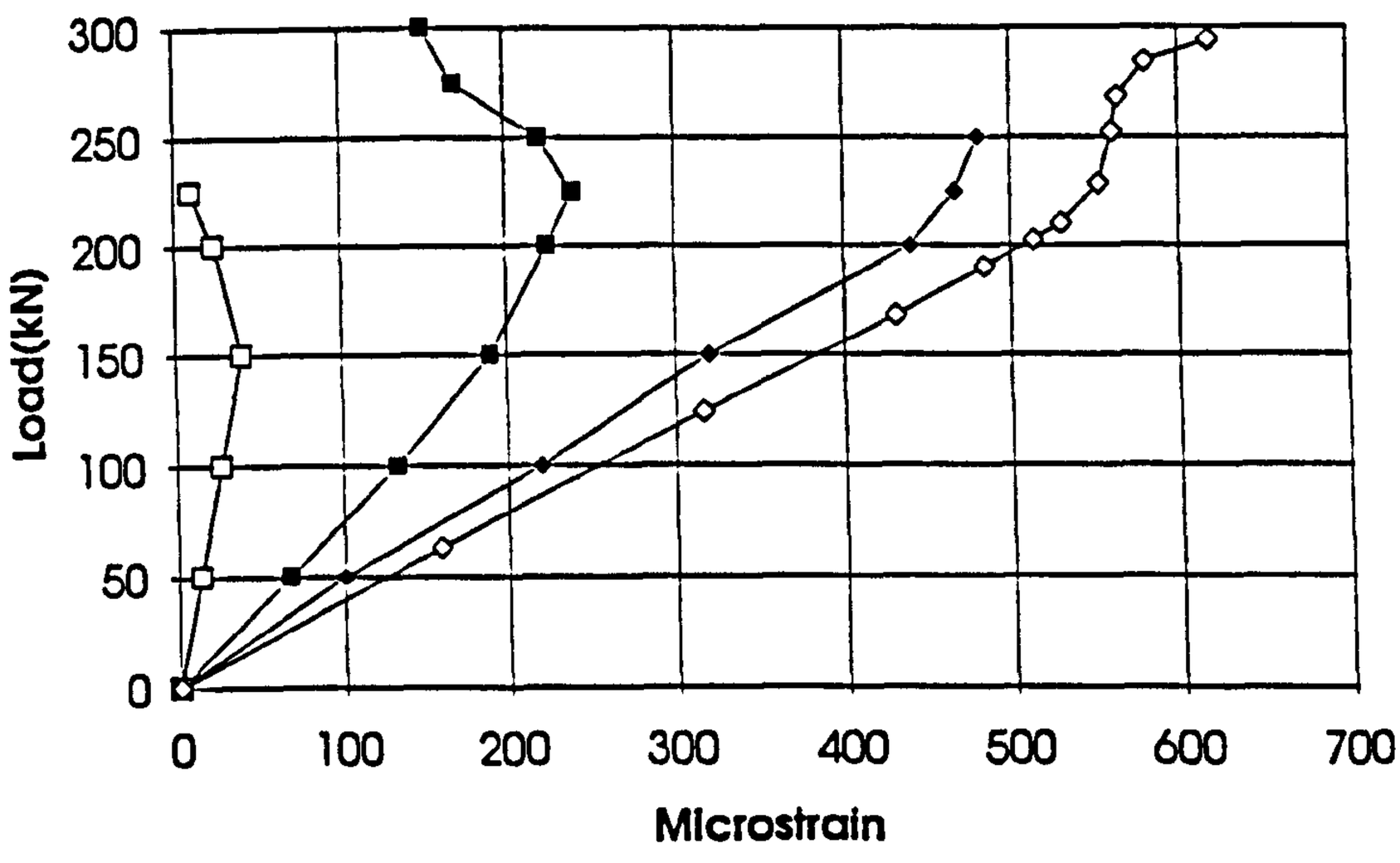

(b) Strain Gauges 12/15/20/23 in Figure 4.5 - Chord Sidewall Lower

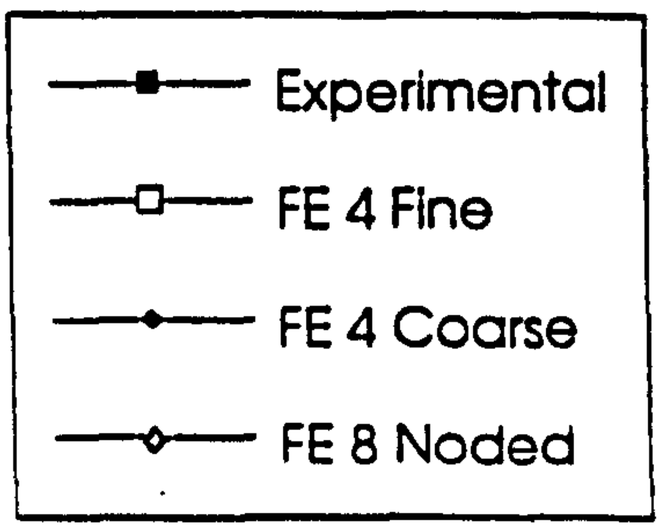

Figure 4.17 Experimental and FE Strains Compared (Chord Underside and Chord Sidewall Lower).

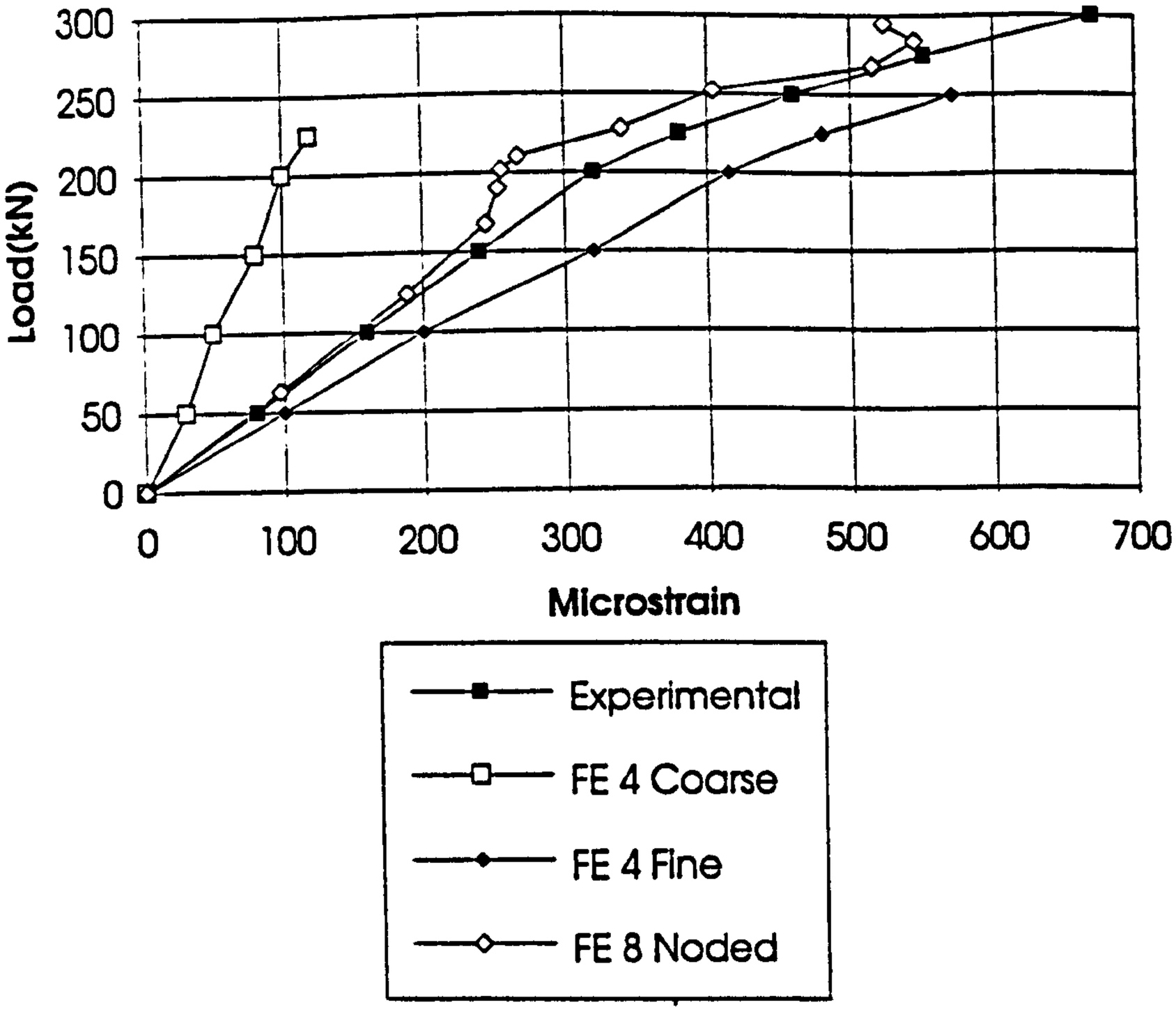

(a) Strain Gauges 11/16/21/22 in Figure 4.5 - Chord Sidewall Upper

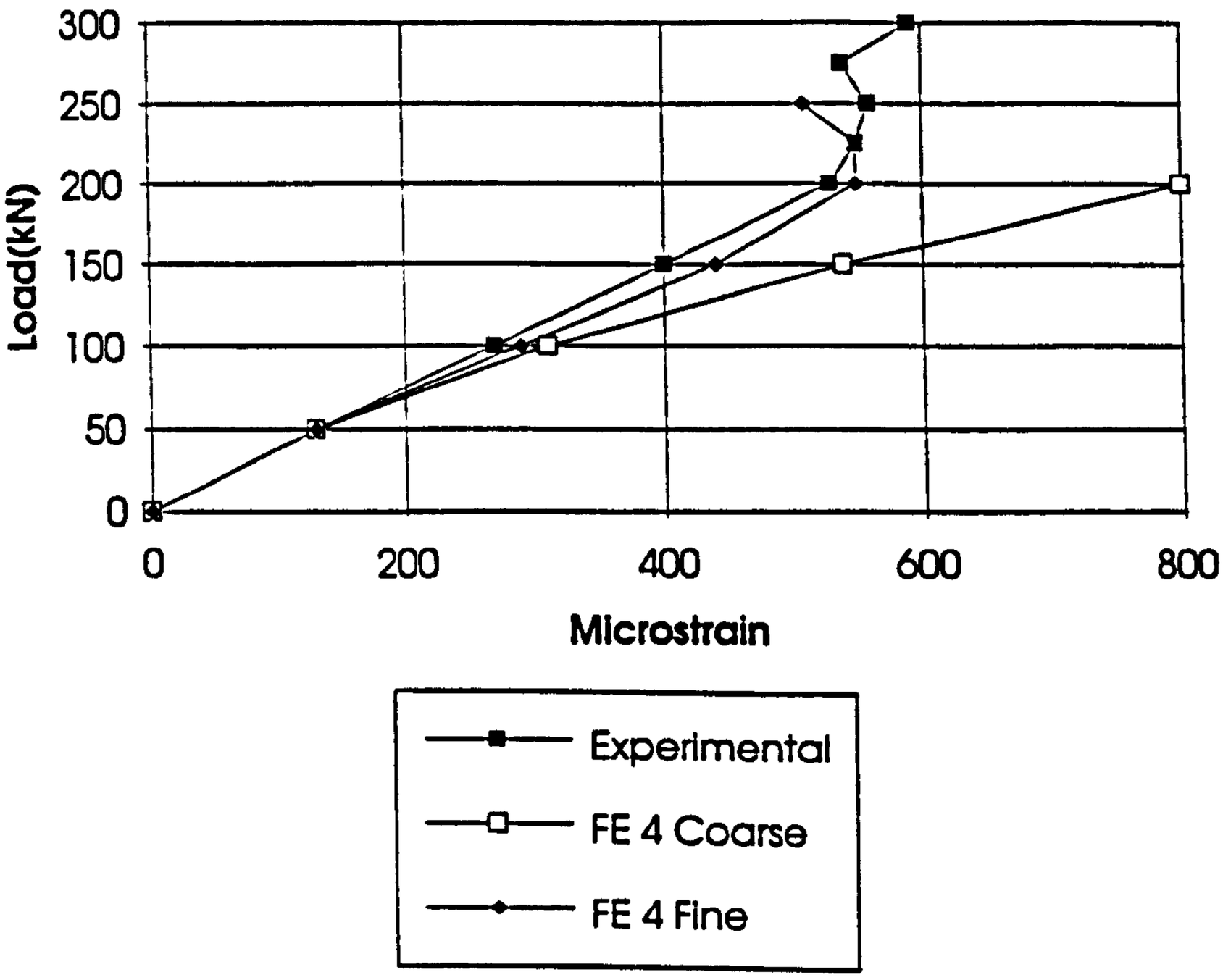

(b) Strain Gauges 9/10/17/18 in Figure 4.5 - Chord Topface

Figure 4.18 Experimental and FE Strains Compared (Chord Top Face and Chord Sidewall Upper).

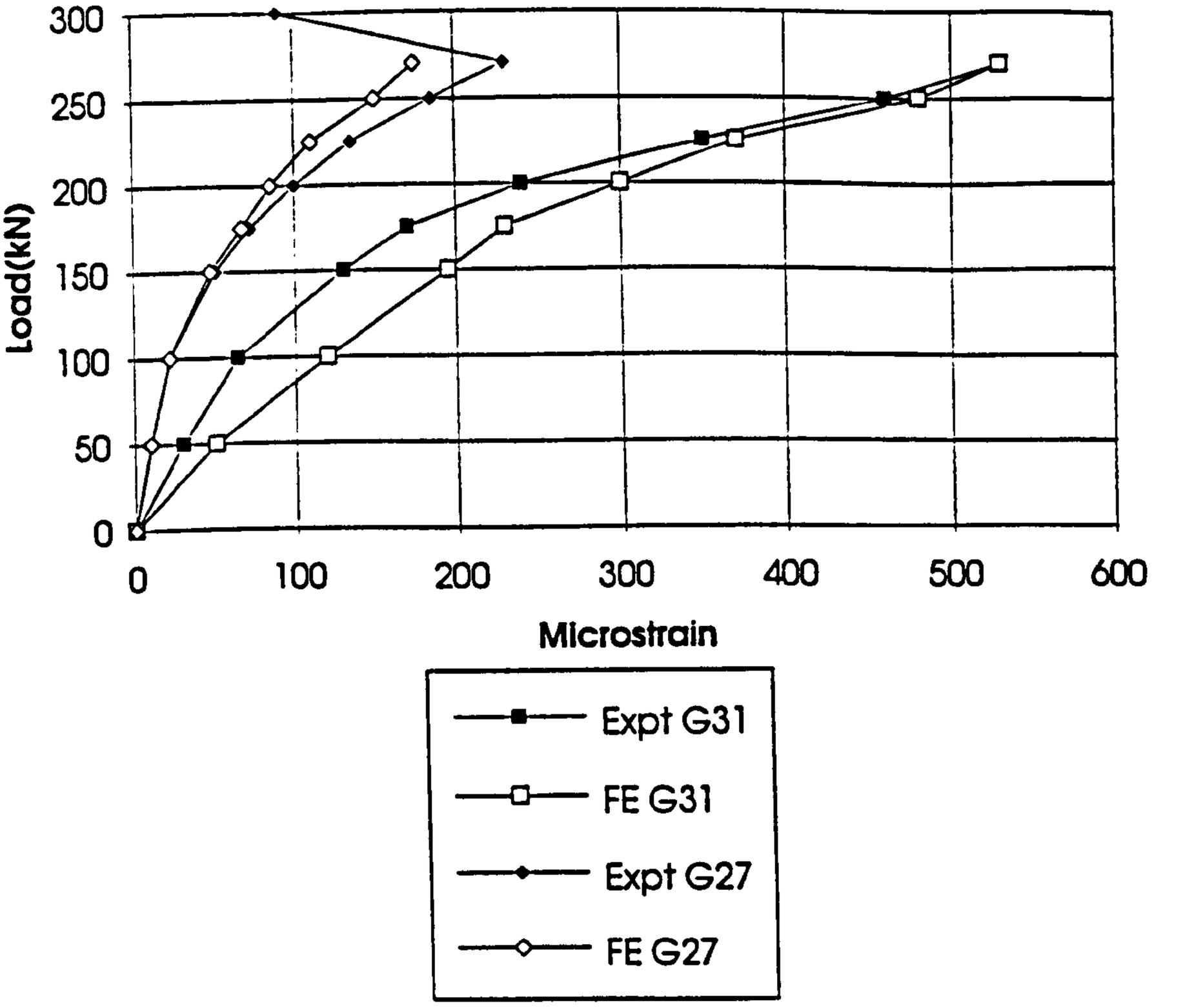

Figure 4.19 Experimental and FE Strains Compared (Out-of-plane Braces Gauges 27 and 31).

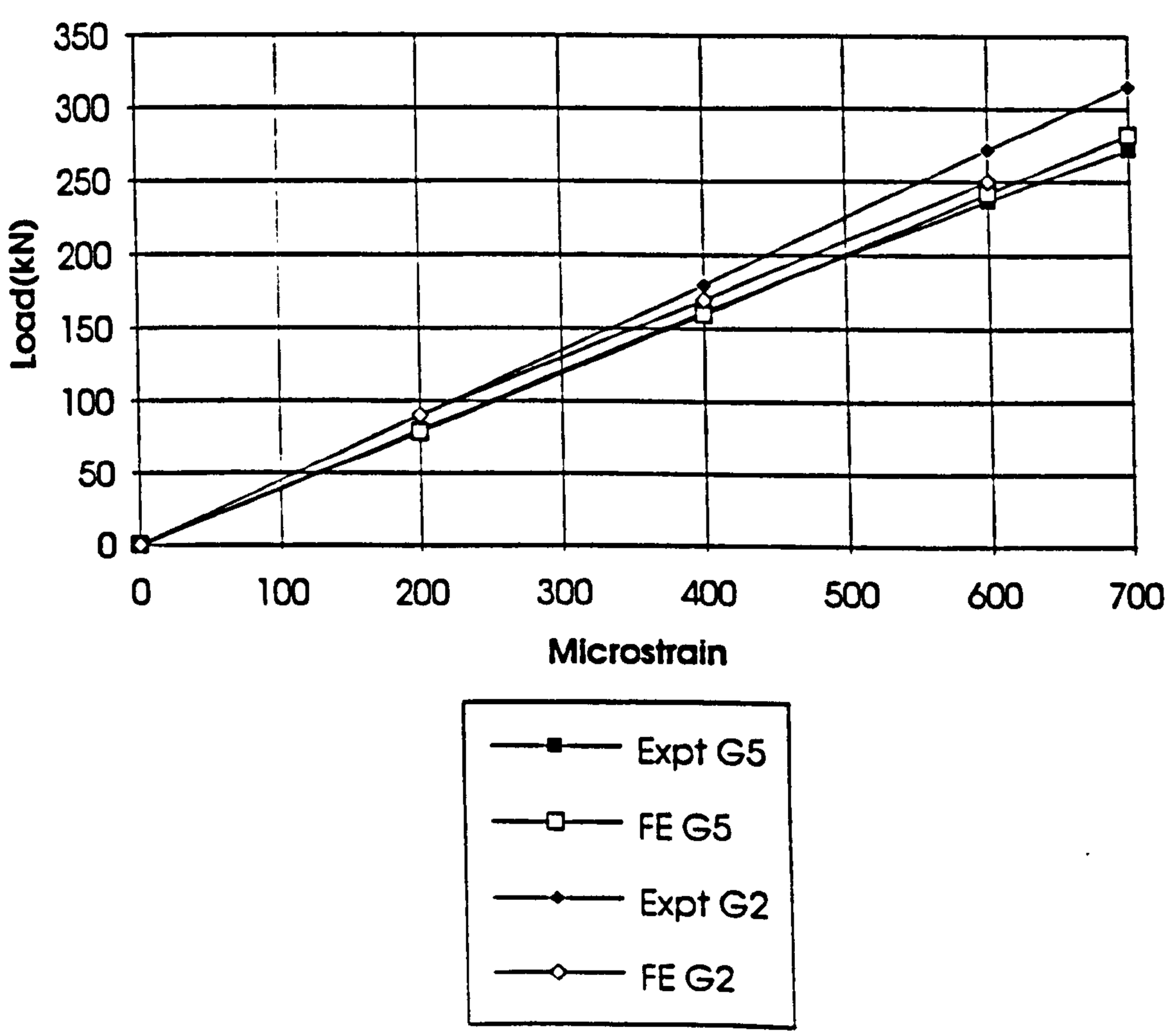

Figure 4.20 Experimental and FE Strains Compared (In-plane Brace Gauges 2 and 5).

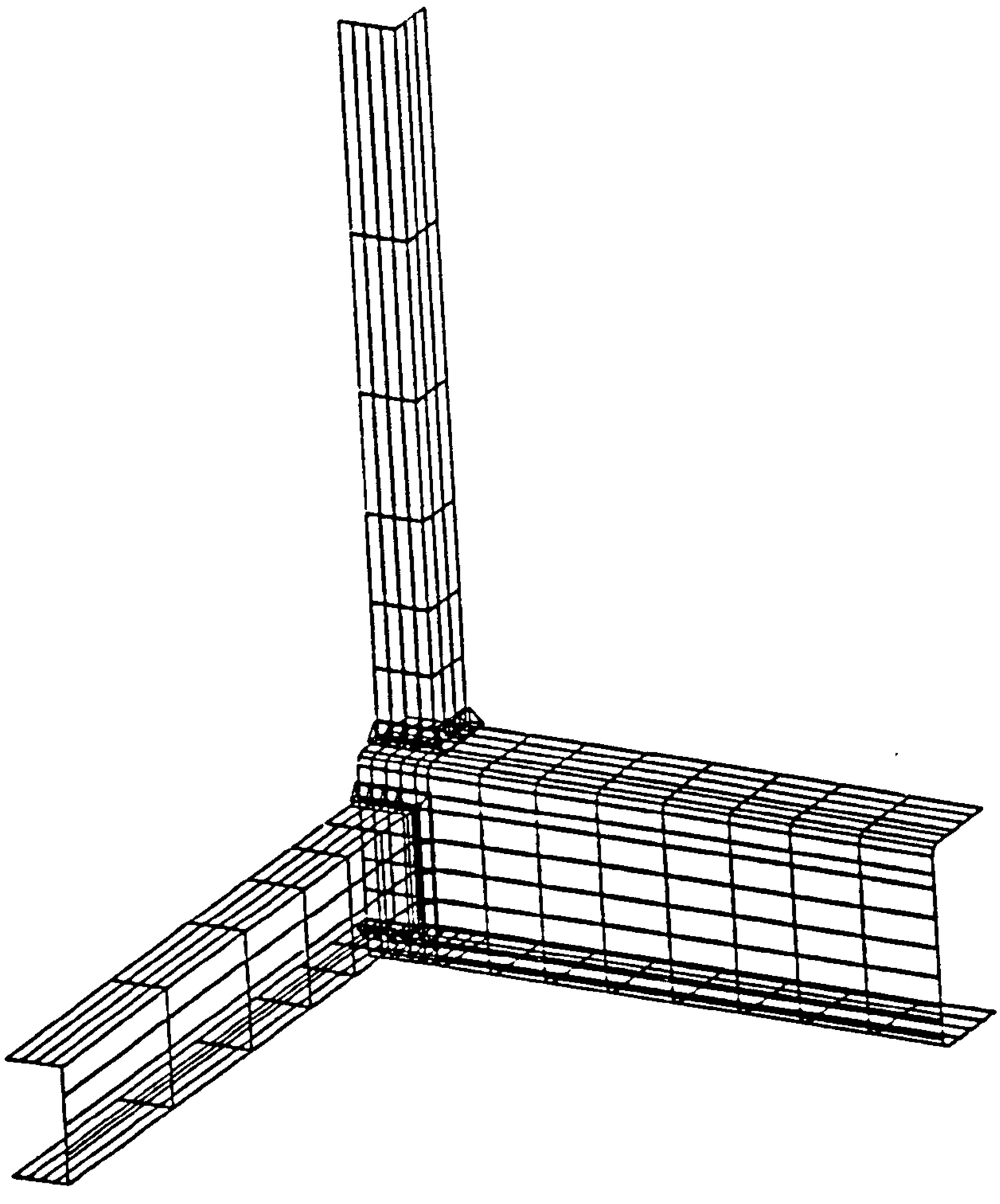

Figure 4.21 Modified Mesh with an Increased Number of Elements in the Chord.

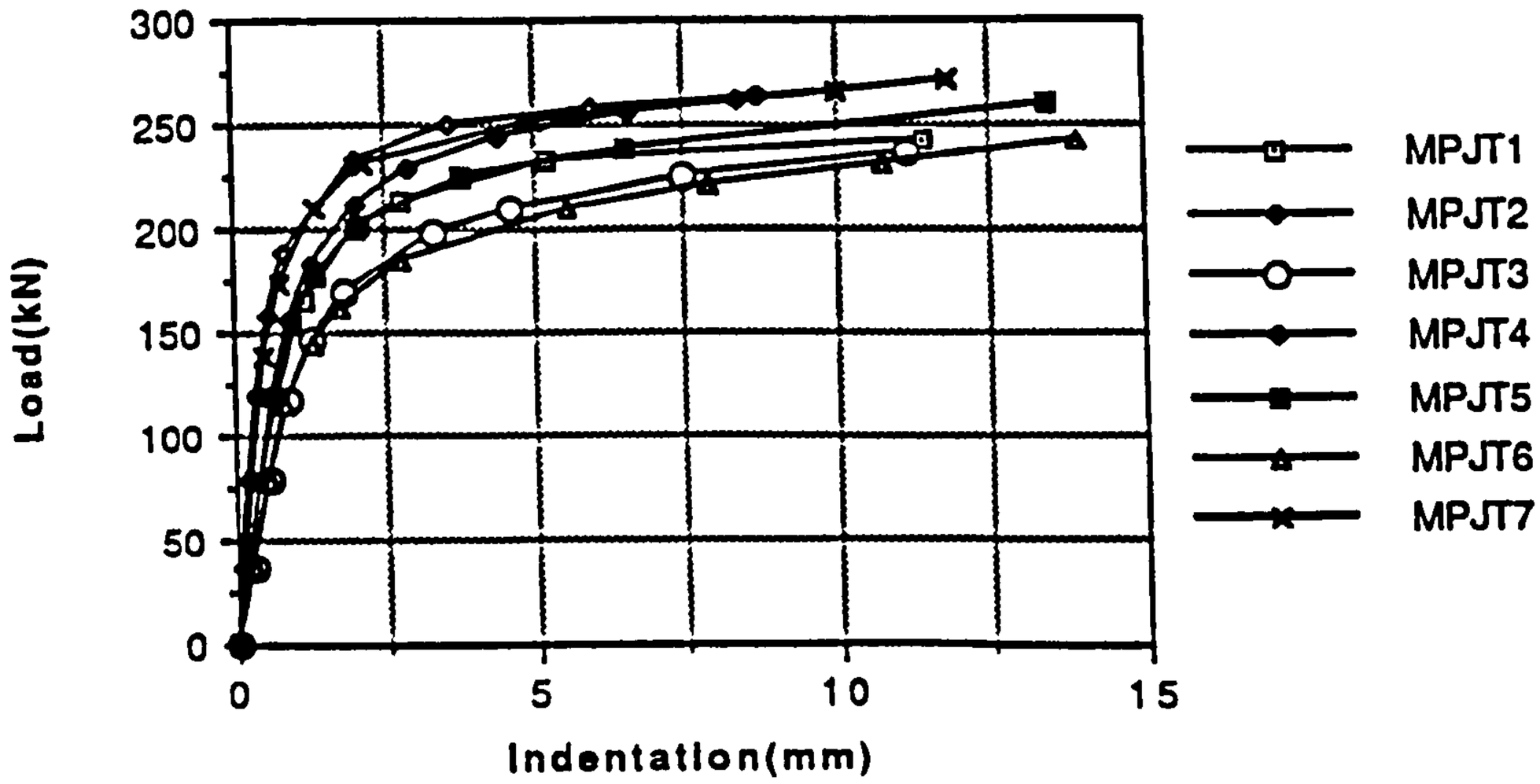

Figure 4.22 FE Load vs Indentation Plots for the Seven Joints (four noded shells for the brace and chord).

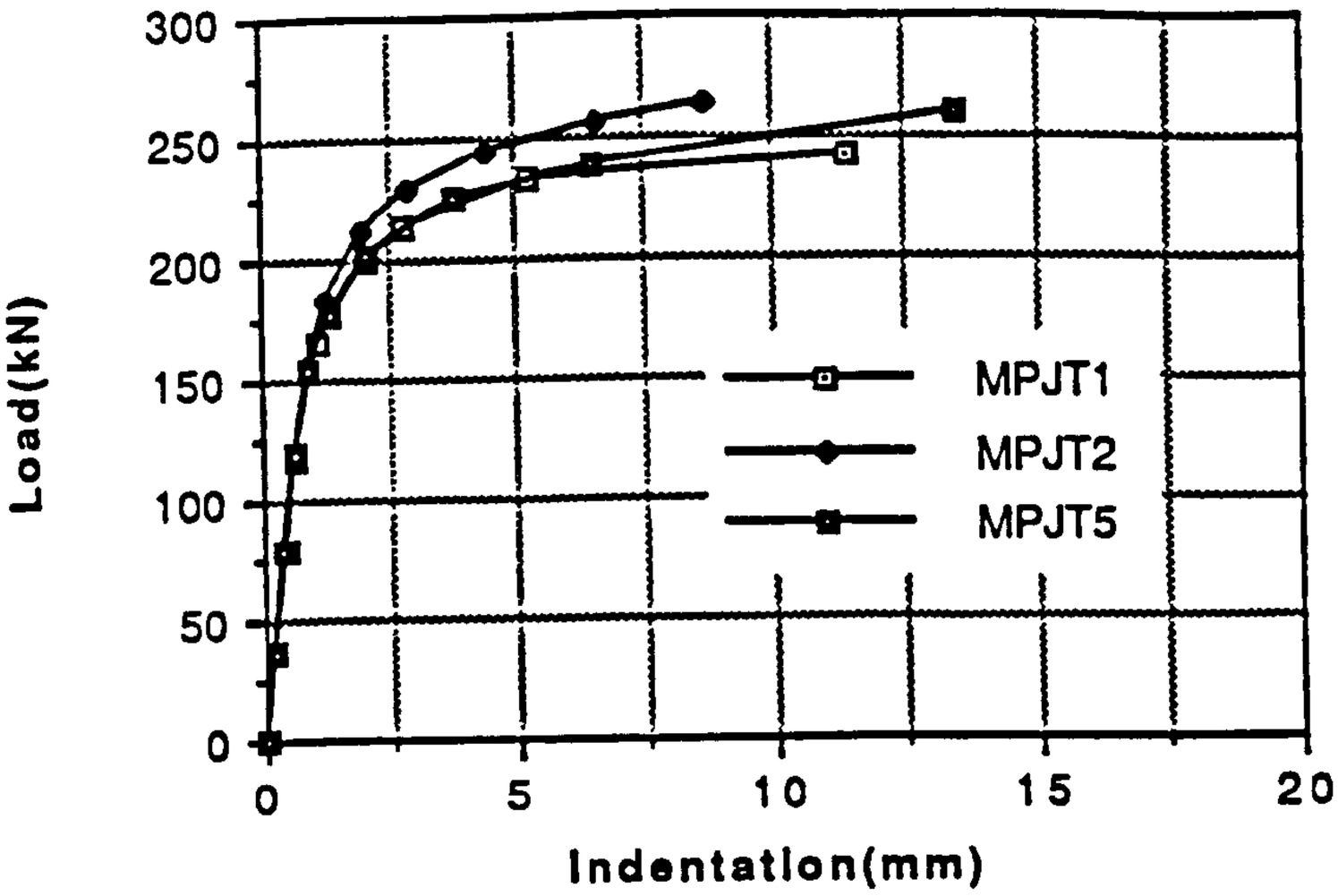

Figure 4.23 FE Load vs Indentation Plots for Joints MPJT1/2 and 5.

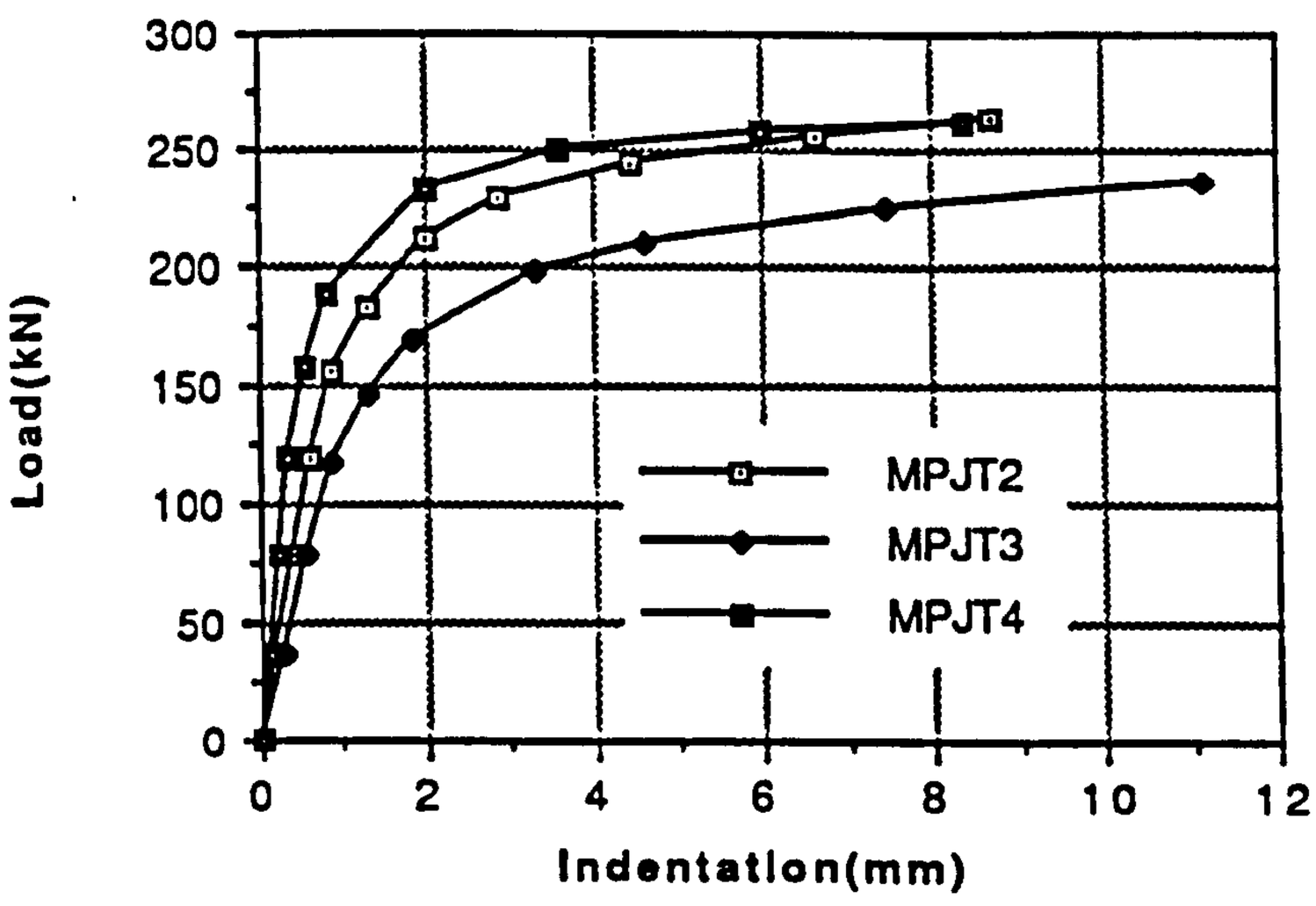

Figure 4.24 FE Load vs Indentation Plots for Joints MPJT2/3 and 4.

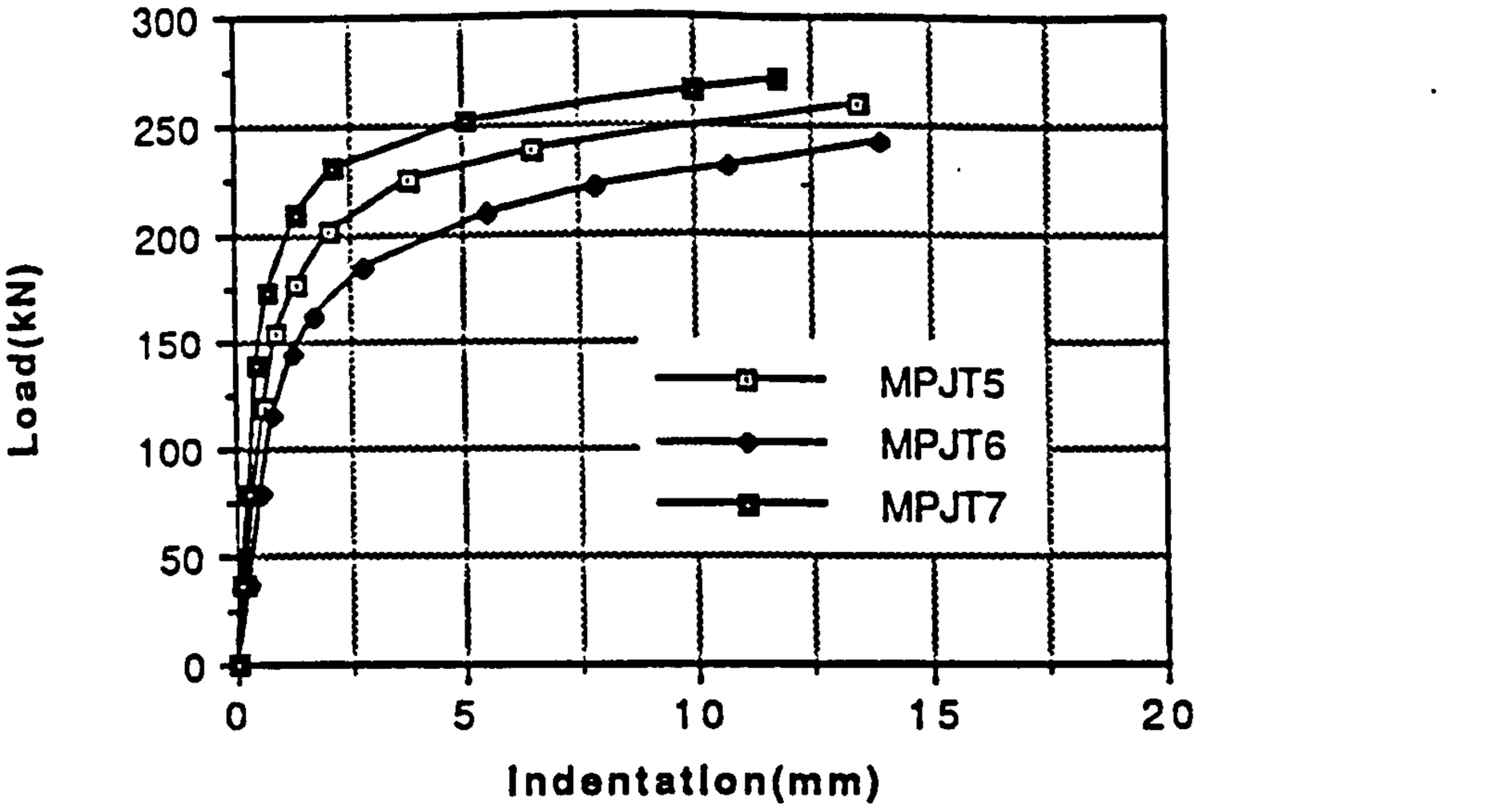

Figure 4.25 FE Load vs Indentation Plots for Joints MPJT5/6 and 7.

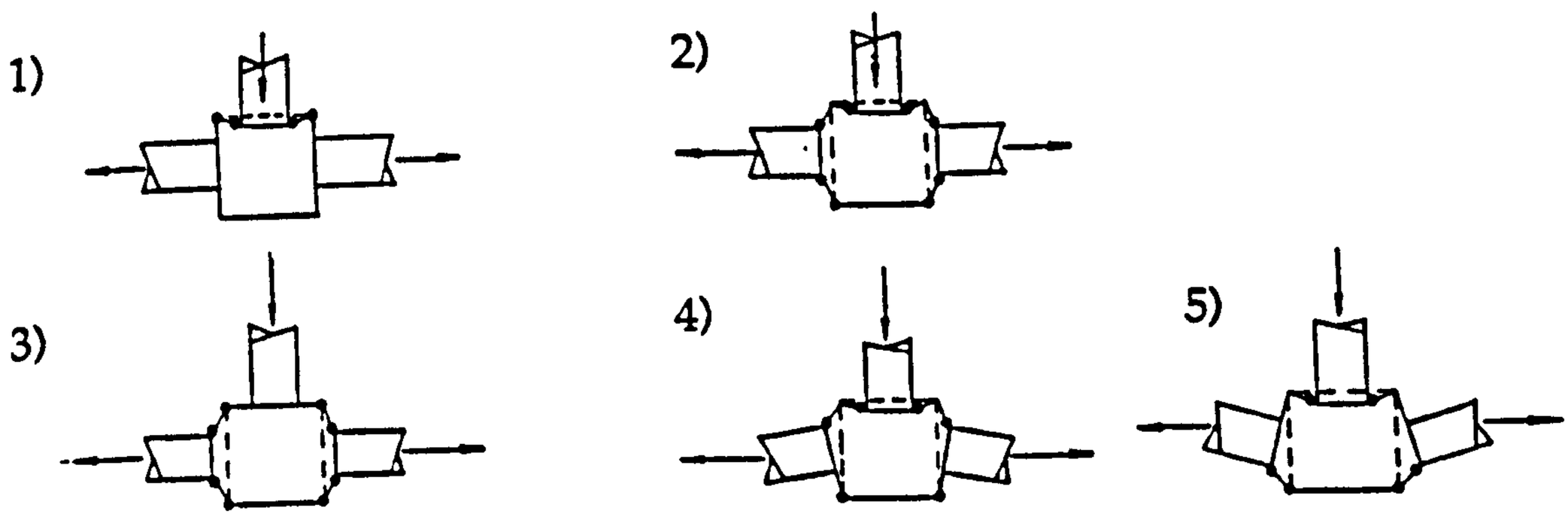

Figure 4.26 Yield Line Mechanisms Possible in the T-DT ring.

CHAPTER 5

CHORD WALL SLENDERNESS, IMPERFECTIONS AND CHORD LENGTH EFFECTS ON RECTANGULAR HOLLOW SECTION T JOINTS.

5.1 Introduction and General Comments

This chapter deals with chord length and chord wall slenderness effects upon the ultimate and elastic behaviour of rectangular hollow section T joints under axial load. Two T joints are considered, a planar and a multiplanar joint with unloaded out-of-plane braces. In addition to the $\beta = 0.6$ ratio joints, for which the previously developed model can be used, similar techniques are also developed to analyse a full width $\beta = 1.0$ T joint. Both planar and multiplanar joints will be considered. The failure mode for RHS T and X joints for β ratios up to 0.85 is generally local deflection 'in-punching' of the brace into the chord connecting face. Other modes of failure begin to predominate for greater values of β often involving buckling of the chord side-walls as shown in Figure 5.1. This is likely to be the case for X and DT joints but T joints may also fail in chord bending (beam failure) involving yielding or buckling of the chord connecting faces if the chord is simply supported. This is obviously dependent on restraints used at the chord ends and the chord length, these being the two factors

affecting the magnitude of the bending moment along the chord. Simple calculations of the bending moment values for various chord lengths are shown in Figure 5.2. To prevent chord bending failure, in $\beta = 1.0$ joints the actual length of the chord needs to be reduced as β increases and other research by Efthymiou (1986) has indicated that short chord effects may significantly increase joint capacity. A way to avoid this interfering short chord effect and to ensure joint as opposed to beam failure in the $\beta = 1.0$ joints was to install a simple support to restrict vertical deflection along two strip lengths of the chord base as illustrated in Figure 5.3. This prevents beam bending failure and ensures that an adequate length of chord can be utilised to prevent enhancements in strength due to short chord effects.

5.2 Chord Length Effects in $\beta = 0.6$ Joints.

To attempt to distinguish where beam action begins to influence joint failure for $\beta = 0.6$ joints, an investigation varying the chord length of the FE model was undertaken. For the reasons discussed above, an investigation into the transition between joint and beam failure of $\beta = 1.0$ joints was impractical (due to the level of support necessary to ensure joint as opposed to beam failure) even for short chords, therefore this investigation was only undertaken for $\beta = 0.6$. For the $\beta = 0.6$ planar joint considered in Chapter 3 with the properties as detailed in Figure 3.1 and Table 3.1:-

RHS 150 x 150 x 6.3 mm:-

$S_x = 194\ cm^3$

$Z_x = 165\ cm^3$

$p_y = 420\ N/mm^2$

BS5950 (1990) - Clause 4.6 $M_{cx} = p_y S_x \not> 1.2 p_y Z_x$

Capacity for 150 x150 x 6.3 RHS beam - Mcx = 81.5 kN-m.

For a simply supported joint with a point load applied at the centre, the maximum bending moment is given by WL/4. For a chord of length 1.25m, a load of 250 kN in the in-plane brace will give a bending moment close to the chord maximum of 81.5kN-m. Thus as the chord length approaches and exceeds this a transition in failure from in-punching of the brace to chord yield in bending will occur. The mesh displayed in Figure 4.15 (L = 850mm) is the basis for the analysis, extra elements being added to increase the chord length as and when necessary. As used previously for the $\beta = 0.6$ models, 4 noded shell elements were used for the brace and chord members, with the welds being modelled with offset 6 noded solid elements connected to the main structure by MPC's, i.e weld case (b) in Chapter 3.4.2.2. This is shown again in Figure 5.4. Material properties are as those used in the analysis Table 3.1. Load vs indentation plots for the series of multiplanar joints considered are given in Figure 5.5 for the MPJT2 multiplanar (Figure 3.1) joint with the overall chord length varied from 450mm to 1250mm. The indentation is measured as previously recorded in Section 3.3. Figure 5.6 illustrates the variation in deflection of the centre point of the chord underside.

5.3 Chord Slenderness Investigation for $\beta = 0.6$

Utilising existing models of MPJT1 and MPJT2 from the previous chapter, the chord wall slenderness was varied over a slenderness range (b_o/t_o) of 15.6 to 41.7 by altering the chord material thickness. All of these were undertaken upon an overall chord length of 850mm (the actual symmetrical model using a half length of 425mm). The modelling techniques used for these analyses were discussed in 3.4.2.2 and 5.2. Four noded shells were used for the brace and chord with six noded solids (weld case(b) in 3.4.2.2) being used for the weld elements as shown in Figure 5.4. All material properties are given in Table 3.1. The load vs indentation results for these are shown in Figure 5.7 (planar T joint) and Figure 5.8 (multiplanar T joint). Comparisons of planar joints vs multiplanar joints for slenderness ratios of 41.7 (Figure 5.9) and 23.6 (Figure 5.10) are also given. These results are tabulated alongside the IIW (1989) design recommendations in Table 5.1. The IIW design equation based on yield line theory (for $\beta < 0.85$) is given by:-

$$P = p_y t_o^2 \left\{ \frac{2h_1}{b_o \sin\theta} + 4\sqrt{1-\beta} \right\} \frac{1}{1-\beta} \frac{1}{\sin\theta} \qquad \text{Eqn [5.1]}$$

where the symbols are as defined at the beginning of this thesis.

Displaced shape plots for the planar and multiplanar joints at a slenderness ratio of 23.8 are shown in Figure 5.11.

b_o/t_o	Planar FE (kN) (a)	Multi-planar FE (kN) (b)	FE ratio $\frac{(b)}{(a)}$	Yield Line Theory and IIW (kN) Eqn [5.1]	$\frac{FE}{IIW}$ (planar)
41.7	90	100	1.11	51	1.71
30.0	150	160	1.07	98	1.53
23.8	220 *	240 *	1.09	155	1.42
15.6	420	450	1.07	361	1.16

Table 5.1 Ultimate Capacities for β = 0.6 Joints with Slenderness Varied. * Corresponds to experimentally tested joints.

5.4 Chord Slenderness Investigation for β = 1.0

5.4.1 Aspects of the Modelling of β = 1.0 Joints

As discussed in the Chapter 4, although the four noded shells gave better results for the β = 0.6 joint case, eight noded shells are accepted as being more accurate. The joint was initially modelled using both elements to compare the differences. To maintain consistency with the β = 0.6 joints, the material and overall dimensions were kept the same, these being shown in Table 3.1. Support conditions were shown in Figure 3.3. Initially the joint was simply supported with end plates attached via the multipoint constraints as described in section 4.2. This however induced failure at the chord underside adjacent to the end plate and calculations of the joint capacity according to the IIW (1989) design recommendations and the chord capacity as a beam according to BS5950 (1990) revealed failure would occur by chord bending rather

than joint sidewall failure, although failure in the FE analysis was local buckling of the chord adjacent to the end plate simulation. In order to prevent this and chord beam failure, two strip lengths of the chord underside, directly below the chord sidewall were placed on a simple support to restrict vertical deflection along this strip, this being shown in Figure 5.3. This method has been used in experimental tests by Zhao (1992) to ensure joint as opposed to beam failure. Due to the lack of identical test results the finite element results for these planar joints are compared to the existing IIW (1989) recommendations. Once these restraints had been installed both eight and four noded shell element models were re-run but the four noded linear shell elements were still drastically underestimating capacity when compared to the IIW (1989) design recommendations. This appears to reflect their poor ability to pick up the sidewall buckling behaviour adequately. The four noded shell model was therefore abandoned at this stage and the remainder of the investigation proceeded with the eight noded quadrilateral shell model. The weld directly above the chord sidewall is by nature a butt weld and was included as shell elements with a thickness equal to that of the brace material, this being illustrated in Figure 5.12. The transverse fillet weld spanning the top of the chord sidewall was thought unlikely to affect the overall results for this β case. However in order to check this an analysis was undertaken for the planar joint of chord slenderness 23.8 both with and without this transverse weld in place. The weld was modelled using six noded solid elements sharing nodes of the chord and brace. This corresponded with the model case (e) in Section 3.4.3.1, which although accepted as not being the best model, will still give an indication as to the effect of this weld on the joint

ultimate strength. It also possesses the advantage of being simple and rapid to install into the existing model. Results for the side wall deflection of these two models are given in Figure 5.13, where midheight sidewall deflection is shown as δ in Figure 5.1.

5.4.2 The Australian Tests on Axially Loaded Full Width Joints (β = 1.0)

During the course of this work test results undertaken by Zhao (1992) became available for square hollow sections using the same method of support for the chord. These were for the same β ratio of 1.0 but a different chord size of 100 x 100 x 6.3mm. Two models of different mesh gradings were established using the same techniques as before in order to evaluate the reliability of the finite element strategy for the β = 1.0 joints. A comparison of these results with the experimental one is shown in Figure 5.14 with regard to the vertical displacement on the brace. More details of these tests are available in Chapter 4 of the thesis by Zhao (1992). The joint material properties for joint C22B2 in this case are given in Table 5.2. The meshes used to investigate the effects of mesh refinement and to establish if the first mesh was too coarse to pick up the buckling effects in the sidewall are illustrated in Figure 5.15. From Figure 5.14 it can be seen that the less dense mesh is fine enough for the analysis and the quadrupling of the number of elements to achieve the fine mesh results in very little increase in accuracy. It can be seen that both results overestimate the ultimate capacity by 8%, although picking up the shape and mode of failure. Capacity of this joint calculated according to the IIW recommendations is 462kN.

External Dimensions (mm)	100 x 100
Material Thickness (Chord and Brace mm)	6.3
Yield Strength p_y (N/mm^2)	412
Ultimate Strength p_u (N/mm^2)	455

Table 5.2 Zhao's (1992) C22B2 Material Properties for $\beta = 1.0$ Joint

5.4.3 The Finite Element Analyses on $\beta = 1.0$ Joints

Using the mesh illustrated in Figure 5.16 a series of chord slenderness ratios between 15.6 and 41.7 were analysed for both planar and multiplanar joints. The multiplanar joints had the out-of-plane braces free to rotate and deflect at their ends - the amount of rotation due to the nature of the sidewall buckling being almost negligible. The results with respect to the sidewall deformation as shown as 'δ' in Figure 5.1 are given in Figures 5.17 (planar) and 5.18 (multiplanar). Comparisons between the planar and multiplanar joints of the same slenderness are given for a slenderness of 23.8 (Figure 5.19) and 41.7 (Figure 5.20) to give an indication of the effects of the physical presence of the unloaded out-of-plane braces on the joint capacity. Ultimate loads for the $\beta = 1.0$ joints are taken to be the peak loads achieved during the analysis as was shown in Figure 4.13. The ultimate loads achieved are compared to the IIW (1989) design recommendations in Table 5.3 (planar and multiplanar FE) and Figure 5.21. The IIW equation for the design capacity of full width T joints is:-

$$P = f_k t_o \left\{ \frac{2h_1}{\sin\theta} + 10t_o \right\} \frac{1}{\sin\theta} \qquad \text{Eqn [5.2]}$$

where $f_k = p$ and p is obtained from Table 27(a) BS5950 for an $\frac{l}{r}$ value of $3.46(\frac{h_o}{t_o}-2)\sqrt{\frac{1}{\sin\theta}}$

Displaced shape plots for the $\beta = 1.0$ series joint are shown in Figure 5.22 at a slenderness of 23.8. As can be observed from the results and the comparisons with the existing Zhao (1992) test results in 5.4.2 the finite element method is over-predicting ultimate strengths considerably with respect to the design recommendations and experimental results. This is expected when comparing the results with the design recommendations, as design recommendations generally represent a lower bound. However, it was not the case for the $\beta = 0.6$ series of joints when comparing the FE with the experimental results in Chapter 4. In this case a scatter of slightly higher and lower ultimate capacities was observed over the joint experimental results. This difference in FE to code comparison is likely to be explained by differing modes of failure in the $\beta = 1.0$ joints. Full width joints fail due to side wall buckling as

b_o/t_o b_o=150mm	FE (kN) Planar (a)	FE (kN) Multiplanar (b)	Ratio $\frac{(a)}{(b)}$	IIW (kN) Eqn [5.2]	Planar IIW
41.7	462	690	1.49	121	3.82
30.0	747	1013	1.36	326	2.29
23.8	985	1320	1.34	629	1.57
15.6	1789	1997	1.12	1418	1.26

Table 5.3 Ultimate Capacities for $\beta = 1.0$ Joints.

opposed to vertical 'in-punch' of the in-plane brace into the chord top face. Buckling is a much more sensitive form of failure to material and geometric imperfections than the in-punching present in $\beta = 0.6$ joints.

5.4.4 Imperfection Investigations on Planar Full Width T Joints

The finite element model assumes that all the material is perfectly homogeneous and the dimensions are perfect, whereas in reality this is rarely the case. The finite element technique offers a good opportunity to accurately model imperfections of various forms and re-analyse them in order to quantify their effect on joint behaviour. The size and nature of the imperfections can be input accurately so as to observe and quantify their effects. An investigation of this type is impossible to perform experimentally due to the random nature of imperfections created within the manufacturing process. A series of FE models for the planar full width T joint were analysed to investigate the effects of geometric imperfections in the chord sidewalls, this being the critical region in the buckling mode of failure.

5.4.4.1 Initial Imperfection Investigation

The first imperfection was installed as a point imperfection at mid-height of the chord side wall directly beneath the centre line of the brace on the planar $\beta = 1.0$ joint of slenderness = 23.6, this being shown in Figure 5.23. Due to the nature of generating the mesh from key nodes several other nodes generated between the key nodes have also been displaced. The extent of this is shown in

Figure 5.23 with regard to position of the brace and other chord nodes, P_1 being the point (node) at which the imperfection was installed. The displacement of this node was varied from 0 to 1.5mm in increments of 0.3mm, 1.5mm (1% of b_o). 1% of b_o is the maximum tolerance permissible in rolling for British Steel Sections (1992). The results of this series are plotted in terms of load vs side wall deformation (as defined 'δ' in Figure 5.1) in Figure 5.24. The displacement of this is relevant to the unloaded position.

A follow-on investigation for a full width planar joint with a chordwall slenderness ratio of 41.7, but using only eccentricities of 0.75mm and 1.5mm on the chord was also undertaken. The results of this analysis are shown in Figure 5.25.

5.4.4.2 Second Imperfection Investigation.

A further investigation was undertaken with chord slenderness ratios of 23.6 and 41.7 using t_o = 3.6mm and 6.3 mm respectively in order to determine whether the nature (extent) of the imperfection had an effect on the results. The form of this imperfection analysis was a development of the previous one. A keynode 71.85mm ($b_1/2$) to the side of the existing altered keynode (P_1) was moved to an eccentricity equal to that of the node in the above analysis. This node is indicated as P_2 in Figure 5.26. This ensures a larger length of imperfection than previously analysed. The results are shown alongside those of the original (no imperfections) joint in Figures 5.27 and 5.28.

5.5 Discussion

5.5.1 Chord Length Effects

As can be seen in Figures 5.5 and 5.6 increasing the chord length reduces the ultimate capacity of the $\beta = 0.6$ T joint . This capacity at larger spans (i.e 1.25m or greater) tends towards the beam capacity of the chord under simply supported conditions and a central point load. However the main mode of failure observed for the range of chord length investigated is still 'in-punch' of the brace into the top face of the chord. The fact that as span increases the ultimate capacity decreases suggests that beam failure is having an impact on the response. This can be observed in Figure 5.5 in the plateauing out of longer spanning joints ultimate response, those with the shorter spans achieving a defineable pick-up of load after plastification. It is expected that the longer spans, after initial in-punch, begin to yield on the underface of the chord allowing increased bending, thus preventing the pick up of membrane strength on the top face. These findings indicate that chord length has a significant effect upon the ultimate response of RHS T joints although effects will vary with the β ratio, chord slenderness and chord end fixity.

5.5.2 $\beta = 0.6$ Joint Chord Slenderness Investigation

It can be seen from the Figures 5.7 and 5.8 and Table 5.1 that increasing chord wall thickness (decreasing slenderness) results in increasing capacity. Comparisons of the ratios of finite element to the IIW (1989) design recommendations reveal that the ratios of FE

to IIW/yield line theory decrease as slenderness decreases. However all FE capacities are greater than the design equations for $\beta = 0.6$ in the IIW recommendations indicating that these are conservative and realistic. The yield line theory in Table 5.1, upon which the IIW guidelines are based can be seen to give rapid and conservative results. The yield line calculations in Table 5.1 are made on the basis of :-

$$P_u = p_y t_o^2 \left\{ \frac{2h_1}{\sin\theta b_e} + 4\sqrt{1-\beta} \right\} \frac{1}{1-\beta} \frac{1}{\sin\theta} \qquad \text{Eqn [5.1]}$$

The effect of the physical presence of the out-of-plane braces for the joint alone enhances capacity by around 8% compared to the equivalent planar case when these out-of-plane braces are restrained to move in a parallel fashion during the analysis, as discussed in Chapter 4. As can be seen from the displaced shape plots in Figure 5.11 these out-of-plane braces and their method of restraint (held parallel) hold the sidewall of the chord in its original plane, thus restricting the deformation in the joint to the top face of the chord. This as can be seen in Figures 5.9 and 5.10 leads to an initial stiffening in the elastic region of the load vs indentation graph when the response of the multiplanar joint is compared to the planar joint. Yield line theory, being based on perfect plastic assumptions is inappropriate to explain the sidewall deflection in planar joints. However actual addition of the multiplanar braces has little effect on the overall response, save for small increases in capacity.

5.5.3 β=1.0 Joint Chord Slenderness Investigation

Joint ultimate capacities are given in Table 5.3. As no equivalent experimental results were available the capacities have been compared directly to those of the IIW (1989) design recommendations. Figure 5.13 shows the effect of adding the transverse fillet weld across the top face of the chord. Although some discernable increase in capacity was observed due to the addition of the weld, it does not effect the ultimate response significantly in this case where both the chord and brace are the same width and square.

The Zhao (1992) test result modelled to check FE procedures is shown in Figure 5.14 while the two finite element models (fine and medium meshes) used to analyse it are shown in Figure 5.15. It can be seen that the finite element idealisation over predicts the experimental strength of the joints by approximately 8% when compared to the experimental results. This is an important benchmark to be used when comparing the finite element results of the main analyses series with those of the IIW (1989) design recommendations.

It can be seen from Table 5.3 and Figure 5.21 that the FE results for planar joints considerably over predict the IIW (1989) recommendations. Bearing in mind the Australian result above, where experimental capacity was 8 % lower than that of the finite element capacity but 40% greater than the IIW calculated capacity of 462kN, these still indicate a large discrepancy between experimental/FE capacities and the IIW (1989) design guidance predictions. It is understood design strength equations are conservative in this case to allow for variations in experimental

capacity in almost identical joints due to the nature of failure being unstable and concern over the accuracy of quoted qualities of some manufactured steel and the method of fabrication. This is of particular importance in high β ratio joints (β = 0.85) where side wall buckling is the dominant mode of failure as can be seen from Figure 5.14, where a significant fall of capacity is observed after peak loads. The main areas of concern with steel are yield strength and material and geometric imperfections. These are all factors that are affected by the measure of quality control. Comparisons of the β = 1.0 planar joints at various slenderness ratios can be seen in Figure 5.17 with respect to chord sidewall deformation and the ratios of these ultimate capacities with respect to the IIW (1989) design guidance are shown in Table 5.3. The planar joint capacities are presented again in Table 5.4 alongside the IIW (1989) design formula for β = 1.0 T joints. It can be seen that the FE peak capacity to IIW ratio falls as slenderness decreases due to the concerns of geometric properties noted above.

b_o/t_o	t_o (mm)	Capacity FE (kN)	$\frac{FE}{IIW}$
41.7	3.6	462	3.82
30.0	5.0	747	2.29
23.8	6.3	985	1.57
15.6	9.6	1789	1.26

Table 5.4 Comparisons of Planar β =1.0 Joint Capacities with IIW Design Recommendations (1989).

Comparisons of sidewall deflection vs load curves for the multiplanar joints for are shown in Figure 5.18. Again increasing capacity with decreasing slenderness is illustrated. Comparisons between results of planar joints and multiplanar joints are shown in Figures 5.19 ($b_o/t_o = 23.6$) and Figure 5.20 ($b_o/t_o = 41.7$). Difficulties arise in interpreting the comparison due to the nature of the sidewall buckling and this is best explained by referring to the displaced shape plots in Figure 5.22. It can be seen from these that the addition of the out-of-plane braces has a significant effect on the nature and position of the sidewall buckling, moving it towards the top of the chord sidewall. The buckling is seen to be much more localised than that exhibited in the planar joint. This creates difficulty in the direct comparison of the results. The position selected to compare results was that of the mid-height of the chord as shown in Figure 5.1, the apparent small deformations of the multiplanar joints in Figures 5.19 and 5.20 when compared to the planar results being explained by this point of measurement. Deflections in the upperside of the chord in the multiplanar joints can clearly be seen to be much greater than those at mid-height in the displaced shape plot in Figure 5.22. This will have no effect on the magnitude of the capacities. The main effect of the addition of the out-of-plane braces is to increase capacity over the planar joints by an average of approximately 30%, this reducing slightly at the lowest slenderness ratio. The addition of the braces also has an effect on the post peak behaviour of the joints. It can be observed from Figures 5.19 and 5.20 that the planar joints exhibit a reduction in capacity after the peak load has been achieved, this decrease not being observed for the multiplanar joints, although no noticeable increase in capacity occurs. The increase in strength observed due to

the addition of out-of-plane braces is much more pronounced for the $\beta = 1.0$ joints than for the $\beta = 0.6$ joints. This is to be expected as the connection of the two side walls of the full width out-of-plane braces limits the boundary of the buckling displacement severely. These strips effectively provide lateral restraint on the whole chord sidewall producing an effect similar to that of internal ring stiffeners in the chord. In $\beta = 0.6$ joints these strips only provide restraint for part of the sidewall depth thus allowing considerable flexibility above and below the connection points. The flexibility allowed by this is illustrated in the yield line sketches in Figure 4.26. For both β ratios the largest enhancement in ultimate capacity occurs at the highest slenderness ratios.

5.5.4 Imperfections Within $\beta = 1.0$ Joints

The sidewall deformation results of the initial imperfection at mid-height of the chord sidewall are shown in Figure 5.24 for $b_o/t_o = 23.8$. A full description of the imperfection was given in 5.4.4.1. The presence of the imperfection only reduces the planar joint capacity from 990kN to 930kN in Figure 5.24, post peak plots tending towards the same value. The maximum eccentricity of 1.5mm was taken from the British Steel Sections (1992) as the maximum manufactured tolerance. A similar analysis was carried out for a slenderness of 41.7 and the results are shown in Figure 5.25. Here a much more significant reduction in peak load occurs (460 to 380) although again post peak behaviour tends towards the same curve. In both groups of analyses the imperfection also reduces the elastic stiffness of the joint considerably (in the lower load region of the analysis). The second, larger imperfection

analysed, described in 5.4.4.2 has its sidewall deformation results shown in Figure 5.27 for a slenderness of 23.8. Again the reduction in capacity is clearly visible and the tendency for post-peak load deflection behaviour to be the same is apparent. This analysis was also conducted for a slenderness ratio of 41.7, the results being shown in Figure 5.28. It can be again seen that results all lead to the same post peak behaviour but the presence of the imperfection reduces the peak load by the order of 25% for the largest imperfection (1.5mm) and removes the sudden instability apparent within the upper region of the curve for the joint with a zero imperfection. Comparing Figures 5.27 and 5.28 it can be seen that the imperfection has a more significant effect on the reduction in the peak load at the higher chord slenderness ratio than at the lower value. It can also be seen that lengthening of the imperfection along the chord does not have as significant an influence on the existing capacity as the actual presence of the imperfection itself. This is illustrated in Figure 5.29 where the results for the initial geometrically perfect full (i.e a zero imperfection) width joint are compared with those of the two imperfections (point and line length) described in 5.4.4.1 and 5.4.4.2.

The nature of actual imperfections in rolled products is difficult to determine and takes no regular format. Inherent in all the imperfections considered above is the fact that they are all perfectly symmetrical whereas this is unlikely to be the case in reality. Thus side sway of the complete joint has not been considered in this imperfection modelling due to the use of an existing symmetrical model. In order to do this, a half of the joint should be modelled with a consequent increase in cpu and model preperation time. Evidence that this mode of failure occurs

however could not be discerned in the experimental joints tested by Zhao (1992) although unsymmetrical imperfections are almost certainly likely to be present within the test specimen and in the fabrication of lattice girders.

5.6 Conclusions

1) The slenderness of the chord sidewall clearly has a direct and significant effect upon the elastic and ultimate behaviour for both β ratios as described below.

2) For β = 0.6 joints, design guidance and yield line theory generally give conservative predictions. These ultimate capacity predictions are below those of the finite element and experimental results by approximately 30% for planar joints for all slenderness ratios except 15.6. It can be seen that yield line theory gives conservative and rapid estimation of capacities for β = 0.6 joints..

3) Design capacities for full width joints (β = 1.0) understate the predicted finite element results by significant amounts regardless of actual slenderness.

4) The presence of the unloaded out-of-plane braces enhances the elastic stiffness and ultimate capacity of multiplanar joints by varying amounts according to the β ratio. This enhancement is greatest when the failure mode involves sidewall buckling (β = 1.0) where an average enhancement of 35% is observed over the range of slendernesses analysed. The existing IIW design recommendations (1989) makes no allowance for this. This is discussed in 6.6 where design rules for multiplanar effects are formulated for this joint configuration.

5) Geometrical imperfections in the sidewall can clearly have significant effects upon the joint capacity at higher β ratios, this being dependent upon the size of the imperfection and the slenderness of the chord sidewall. The longer the length of the imperfection the lower the peak load obtained and the higher the slenderness the larger the reduction in capacity from that of the geometrically perfect joint.

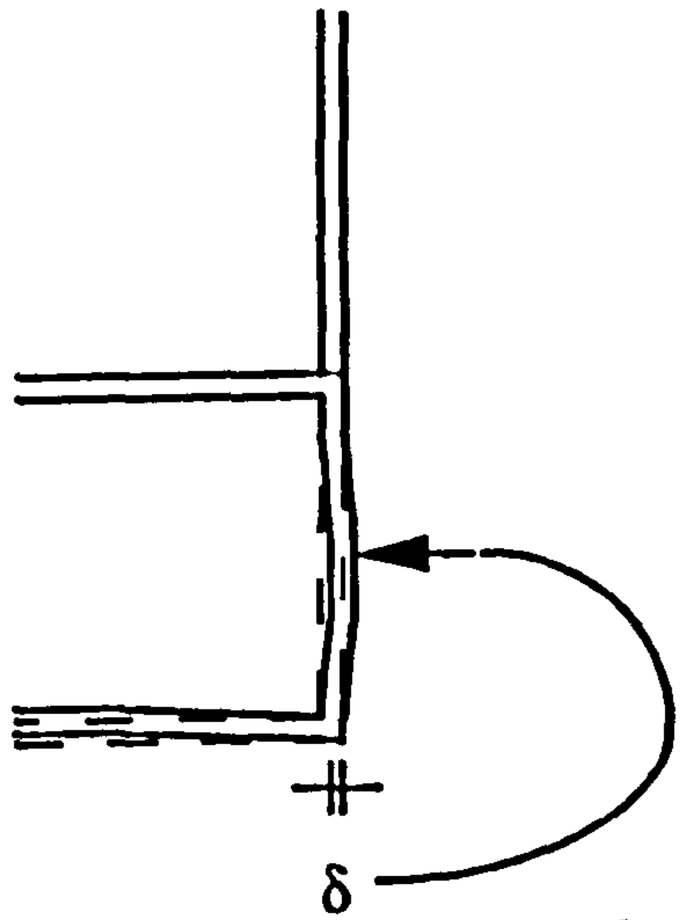

Figure 5.1 Chord Sidewall Buckling as a 'Strut'

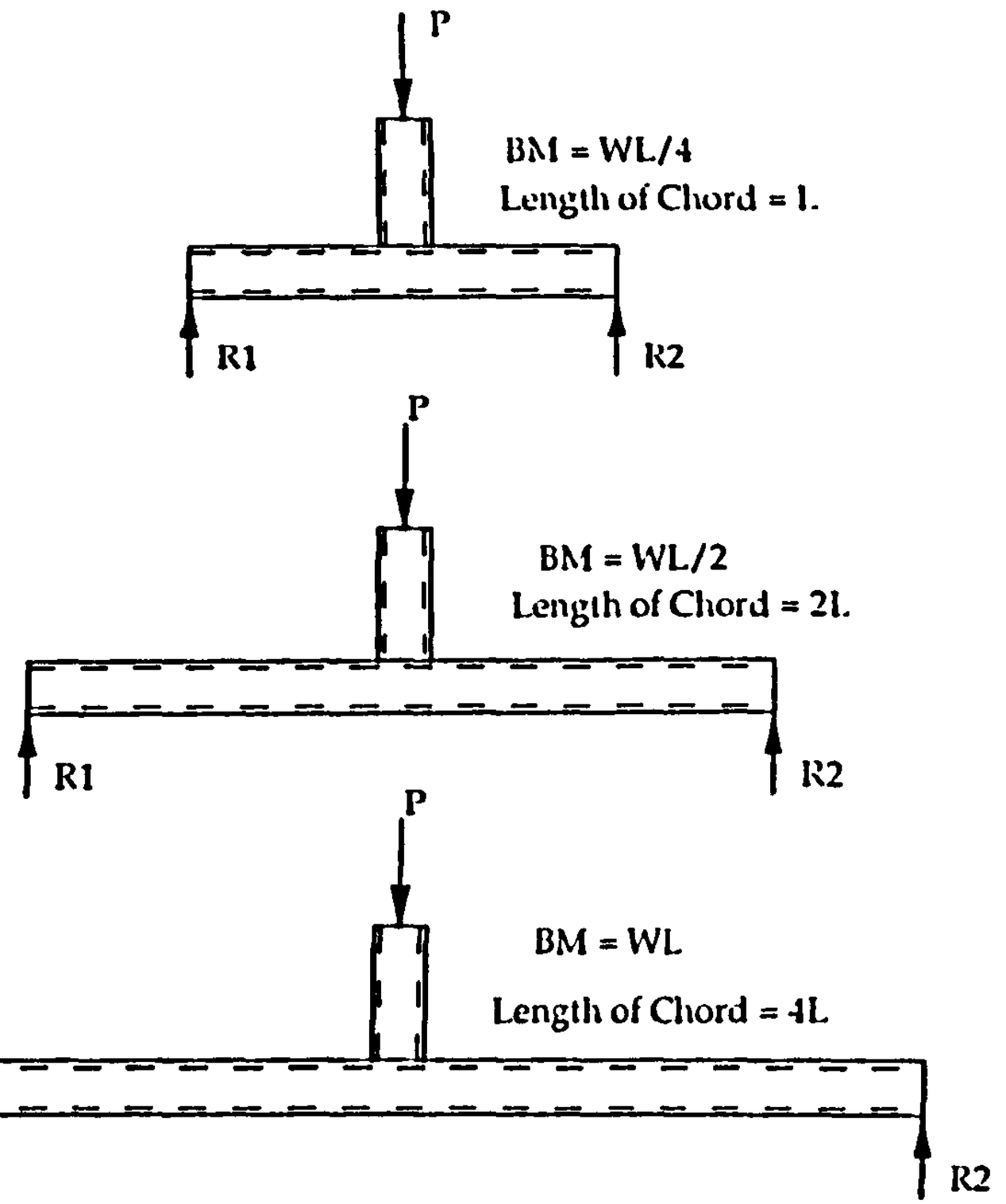

Figure 5.2 Chord Length Effects on the Moment Magnitude in T Joints

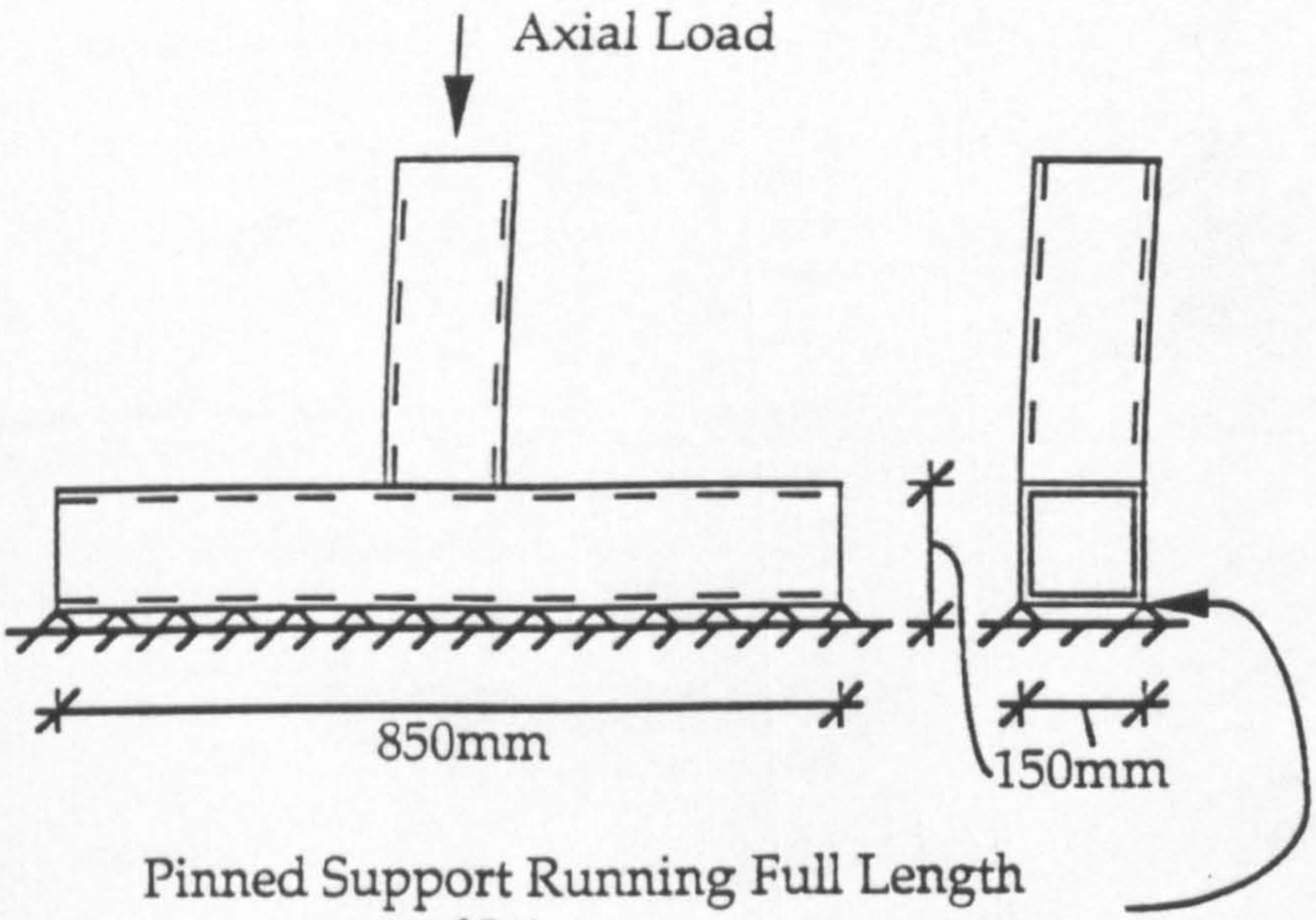

Figure 5.3 Method of Restraint for β = 1.0 T Joints
to ensure 'Joint' Failure

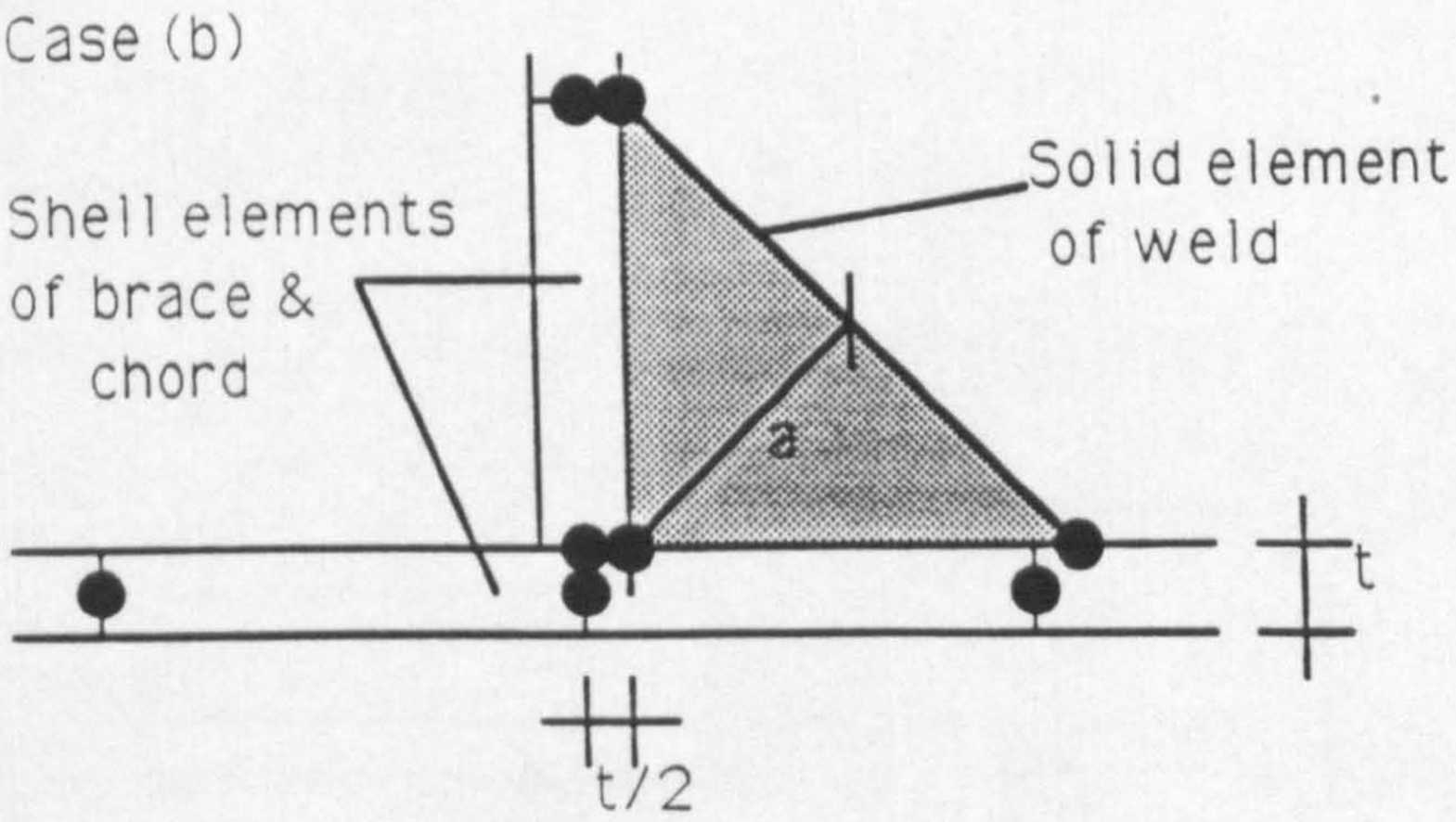

Figure 5.4 Basic Mesh Used in the Chord Length
Investigation for β = 0.6 and Detail of the
Fillet Weld Modelling.

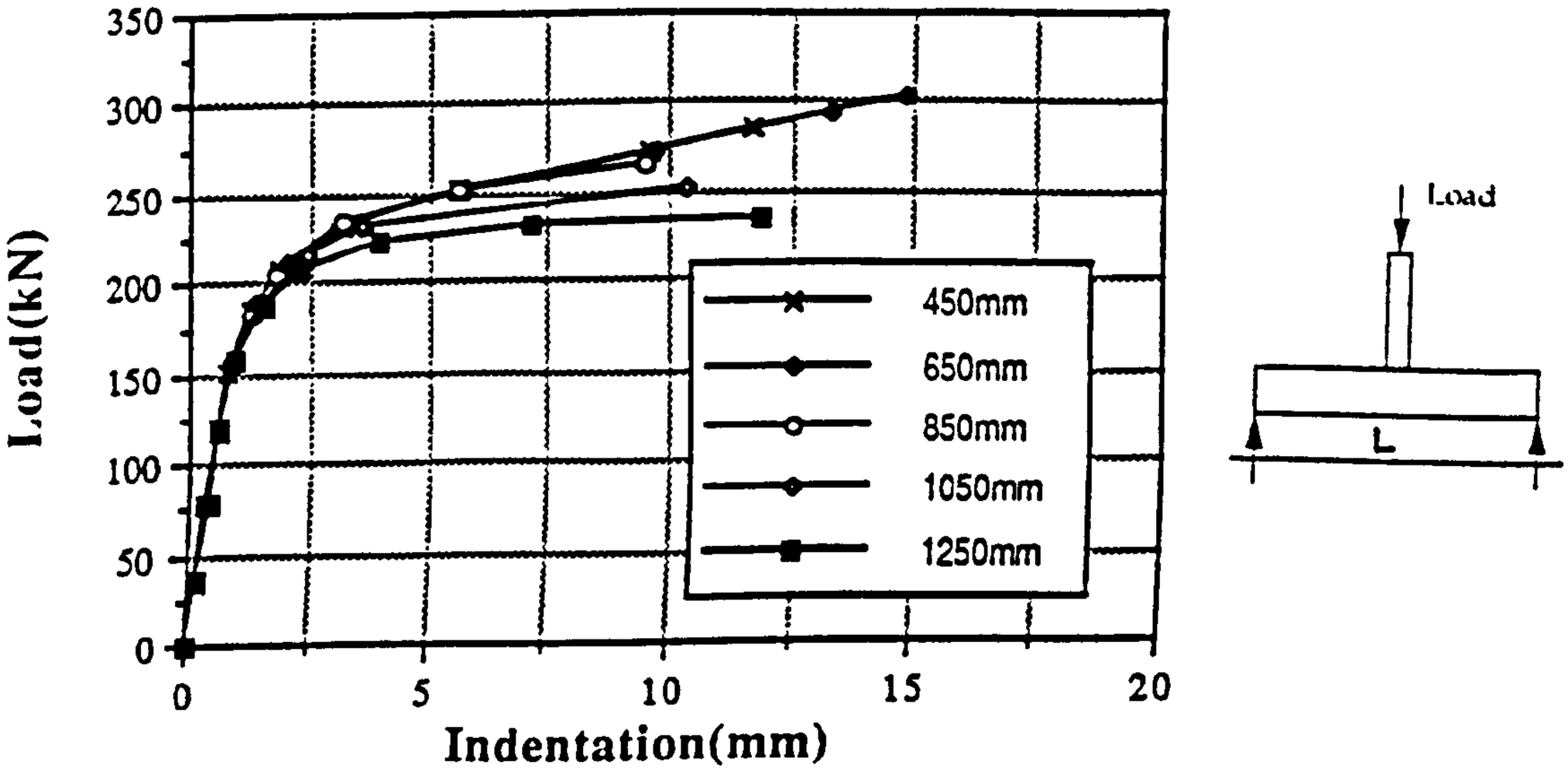

Figure 5.5 Effects of Chord Length on Multiplanar T Joint Capacity at $\beta = 0.6$. Slenderness = 23.8

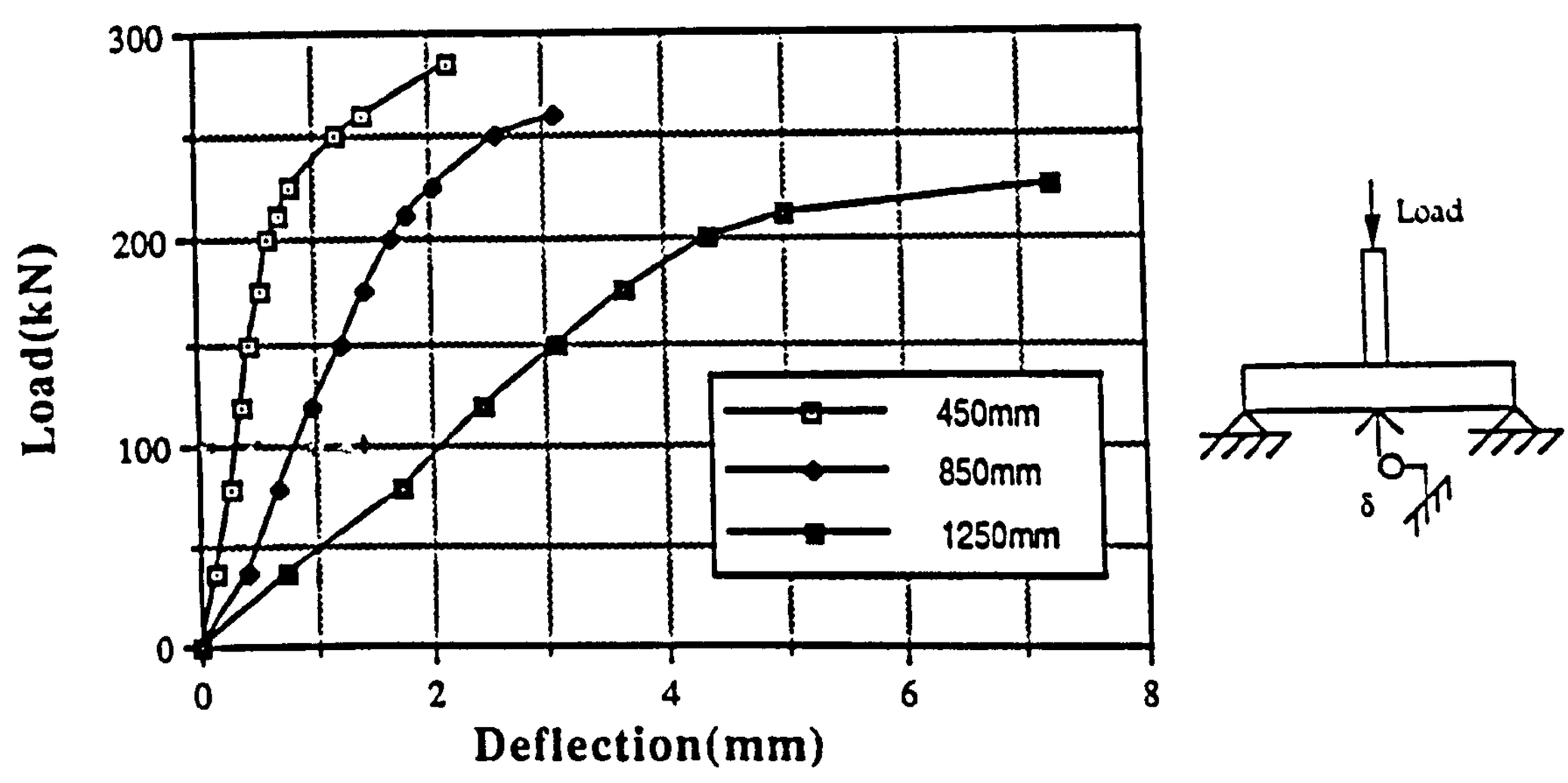

Figure 5.6 Chord Mid-Span Deflection against Load on $\beta = 0.6$ Multiplanar T Joints on chord underface edge.

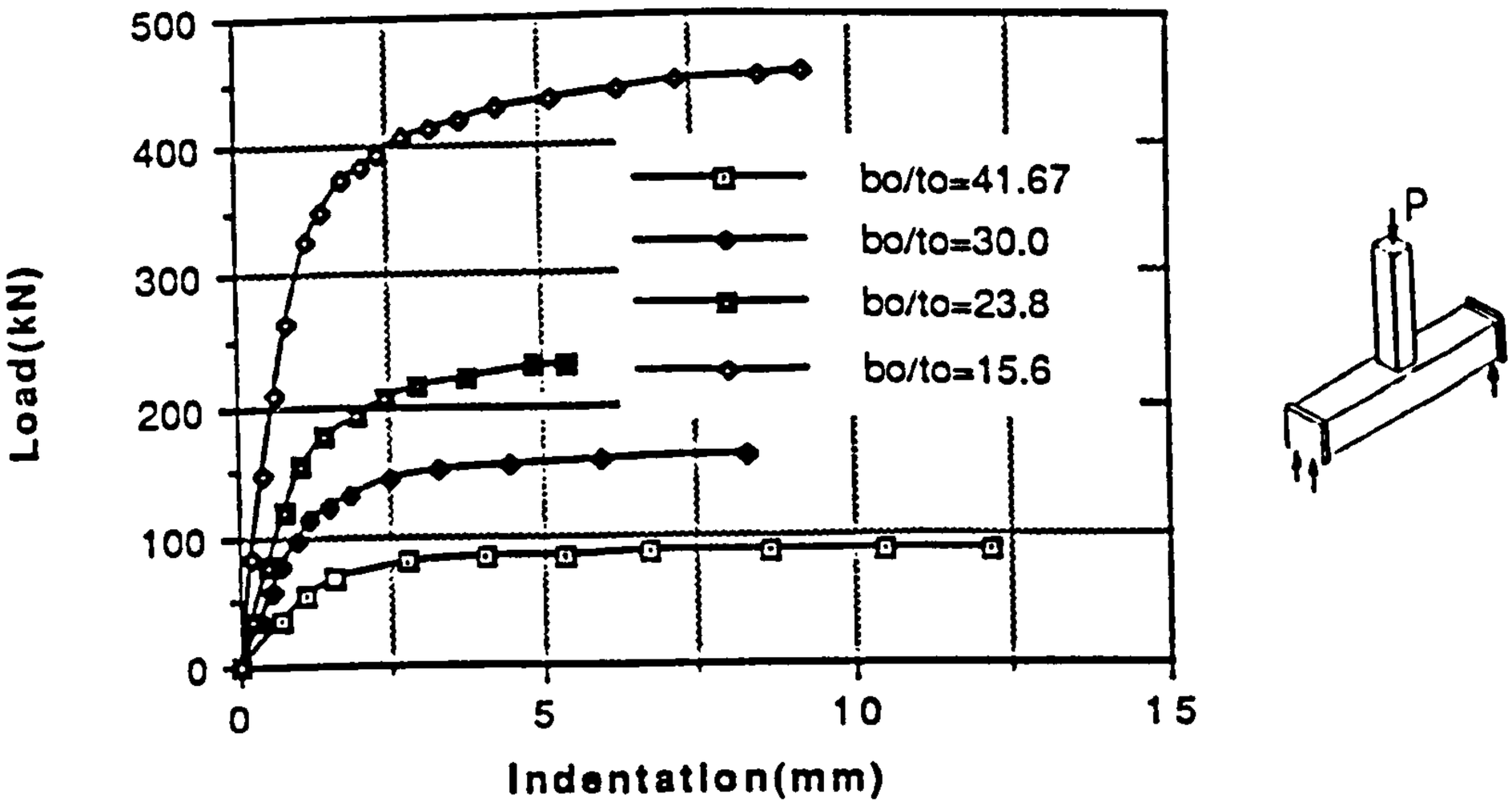

Figure 5.7 Load vs Indentation for β = 0.6 Planar Joints.
(Chord Length = 850mm)

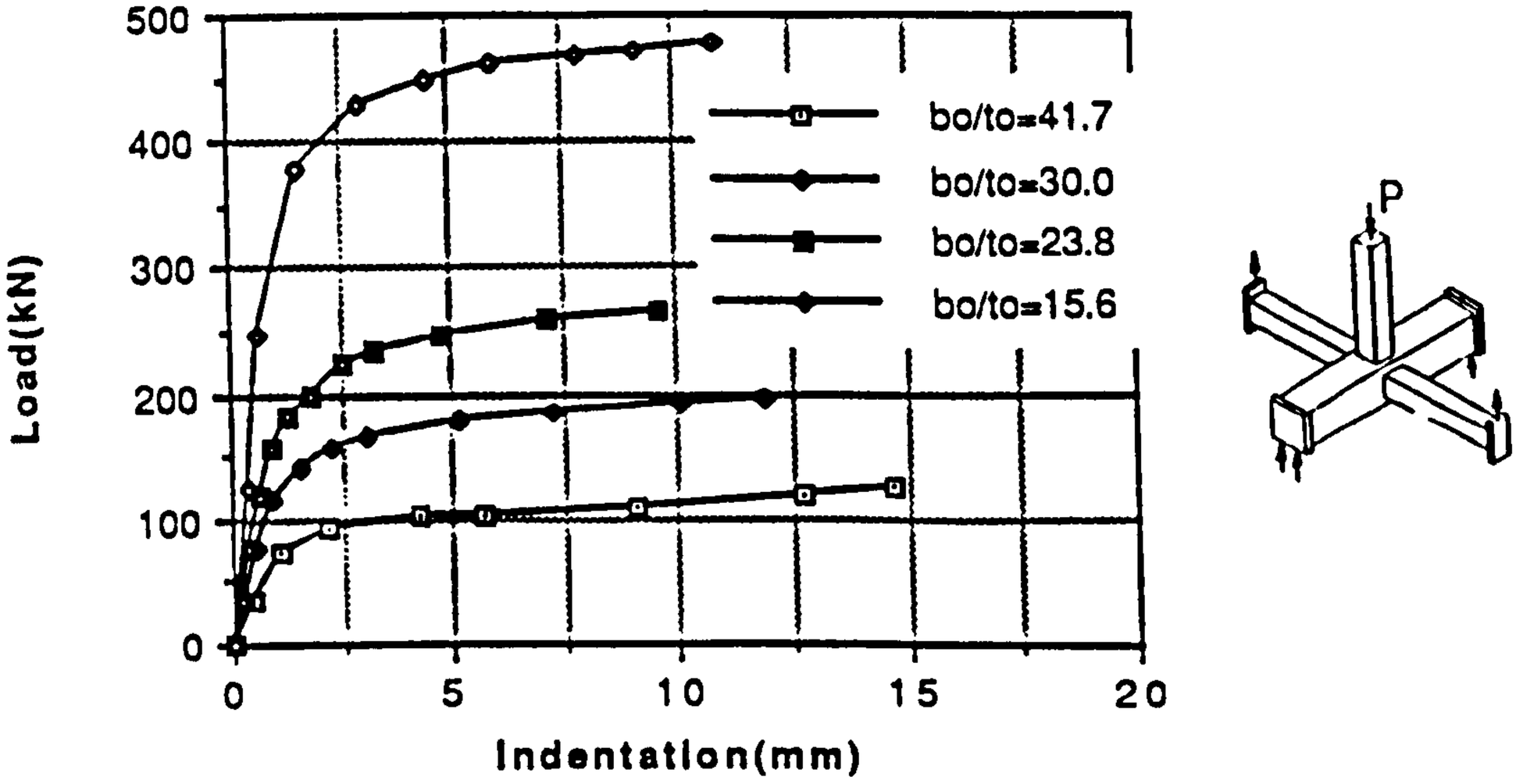

Figure 5.8 Load vs Indentation for β = 0.6 Multiplanar Joints
(Chord Length = 850mm)

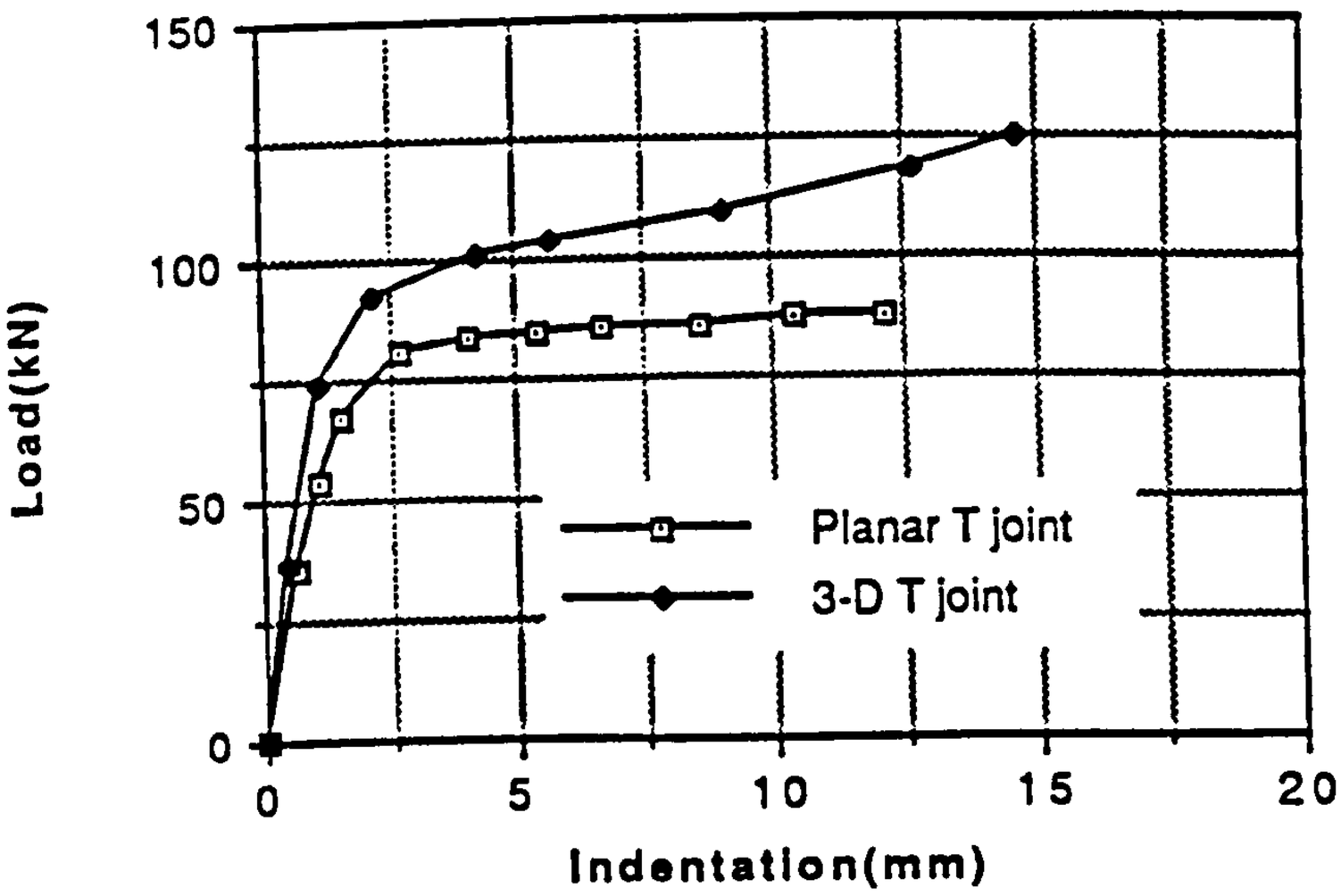

Figure 5.9 Comparison of Indentation for $\beta = 0.6$ Planar and Multiplanar Joints at $b_o/t_o = 41.7$

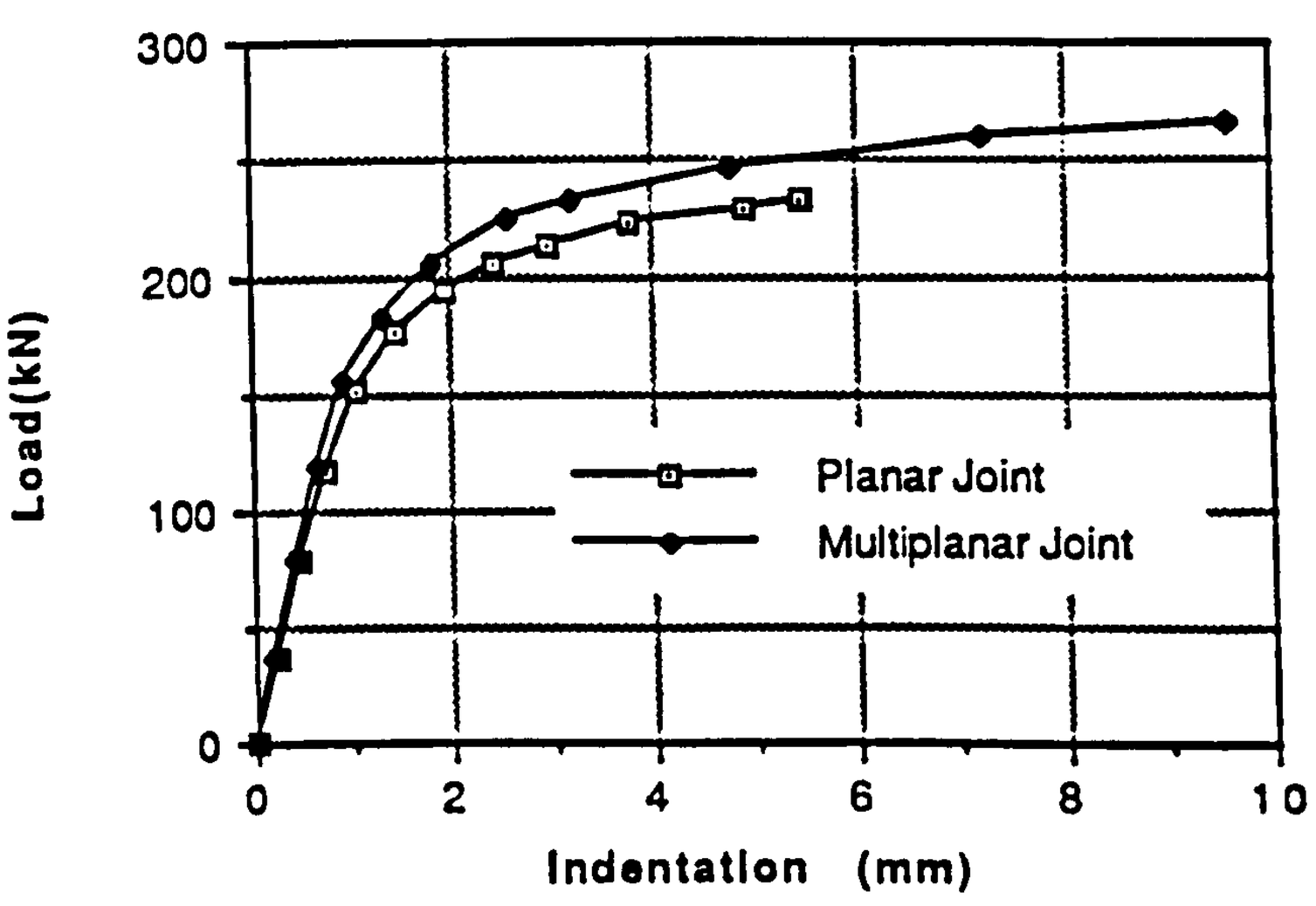

Figure 5.10 Comparison of Indentation for $\beta = 0.6$ Planar and Multiplanar Joints at $b_o/t_o = 23.8$

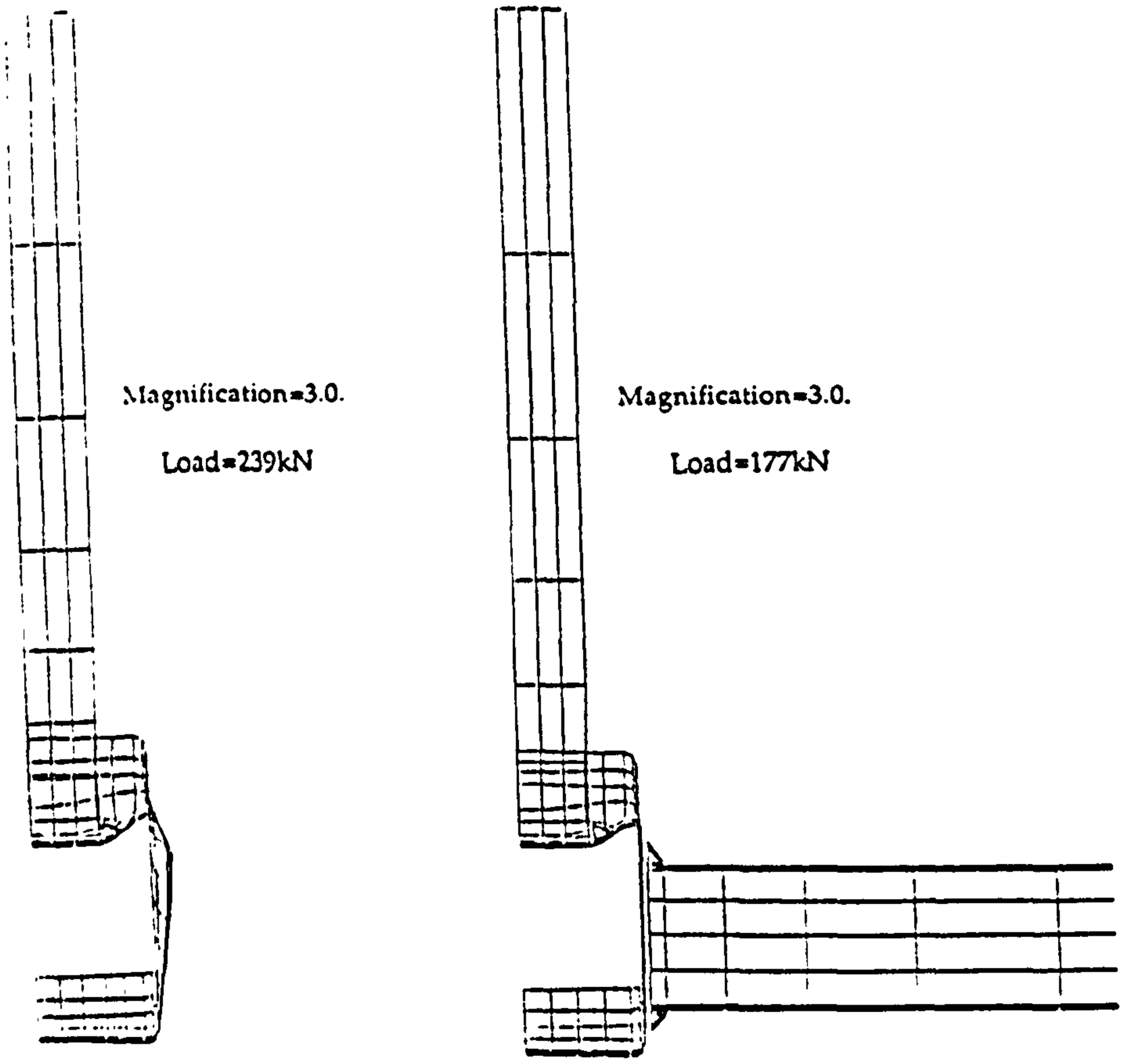

Figure 5.11 Displaced Shape Plots for β = 0.6 Planar and Multiplanar Joints.

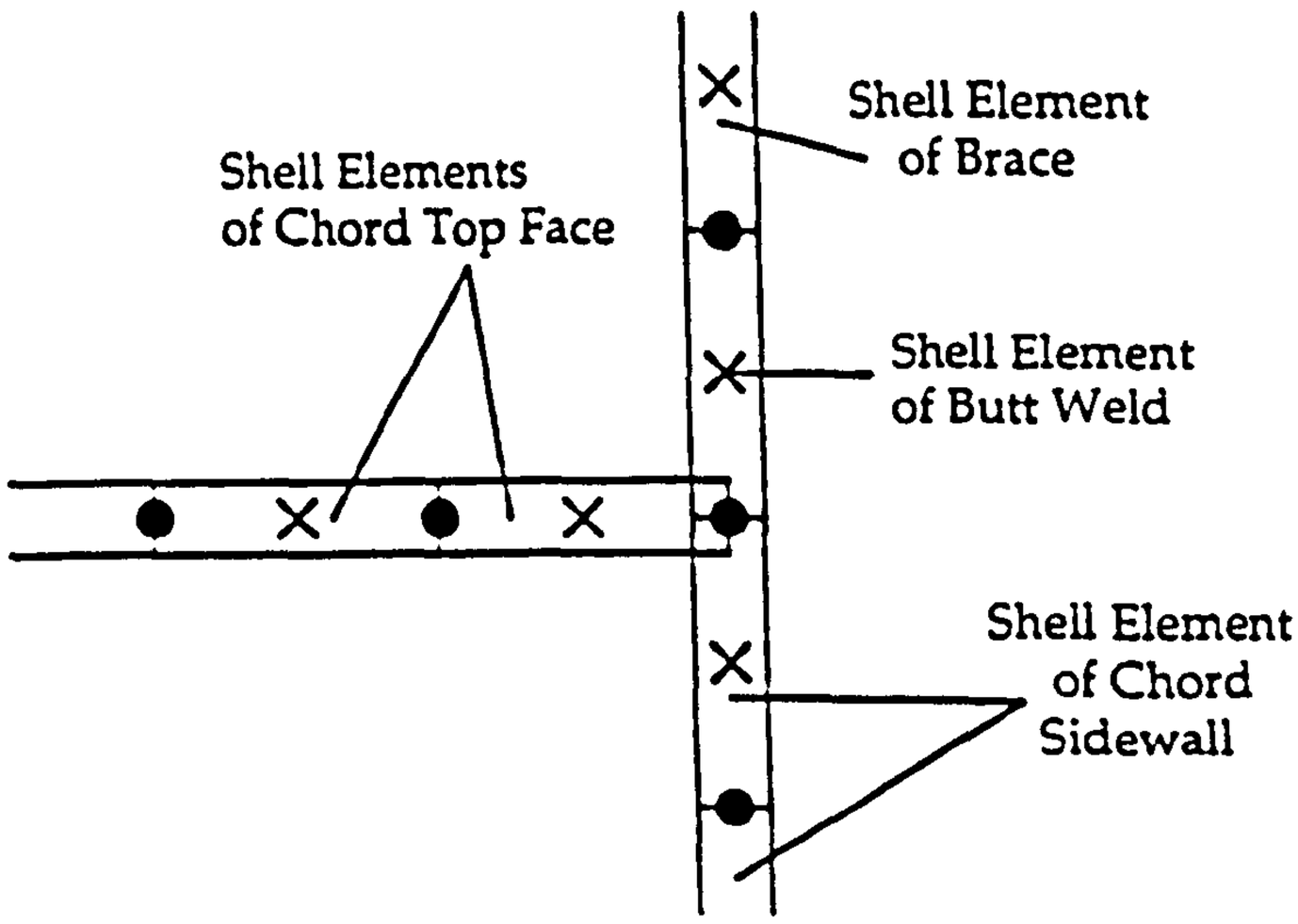

Figure 5.12 Method of Weld Modelling in β = 1.0 Joints

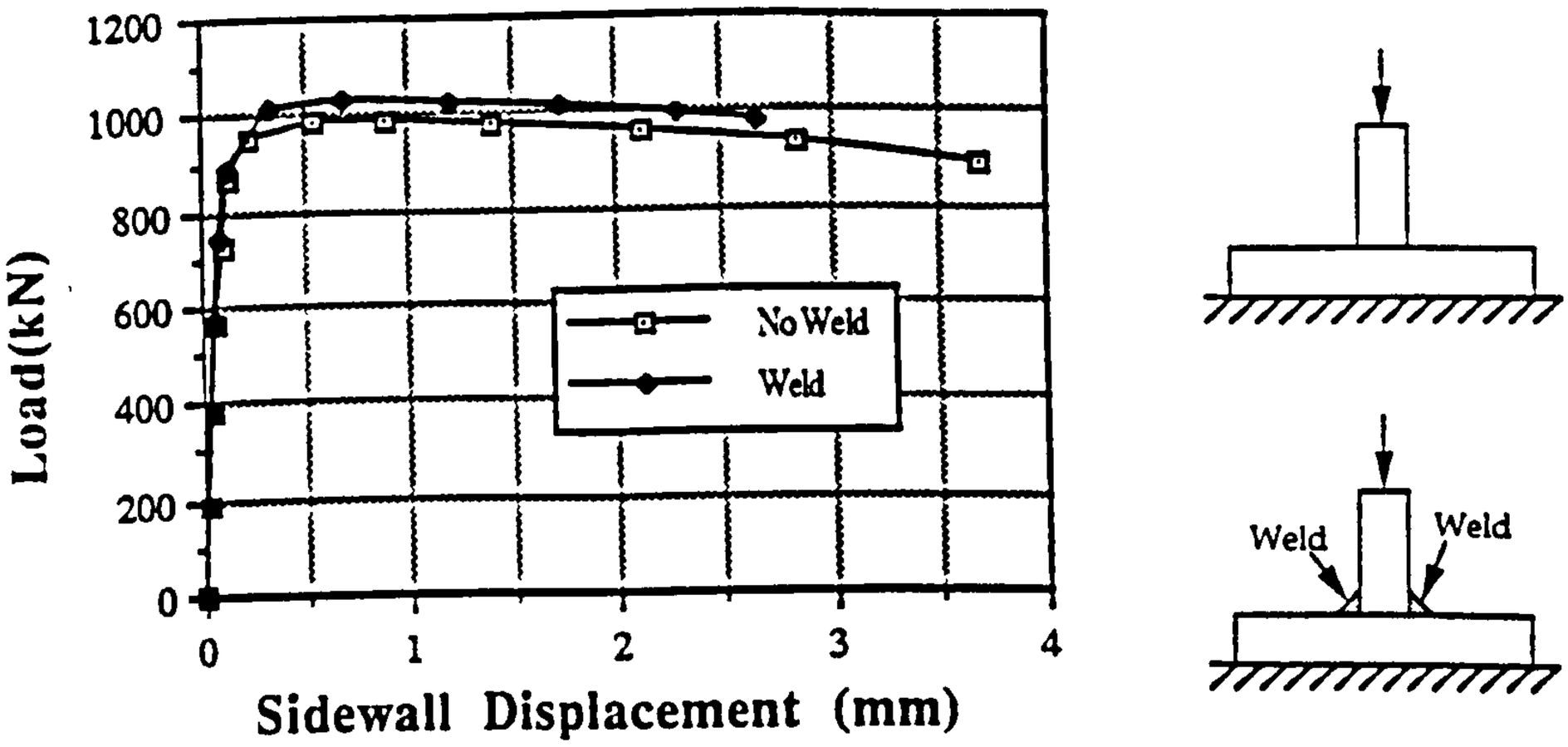

Figure 5.13 Effect of Inclusion of Chord Top Face Fillet Weld on Capacity and Sidewall Deformation

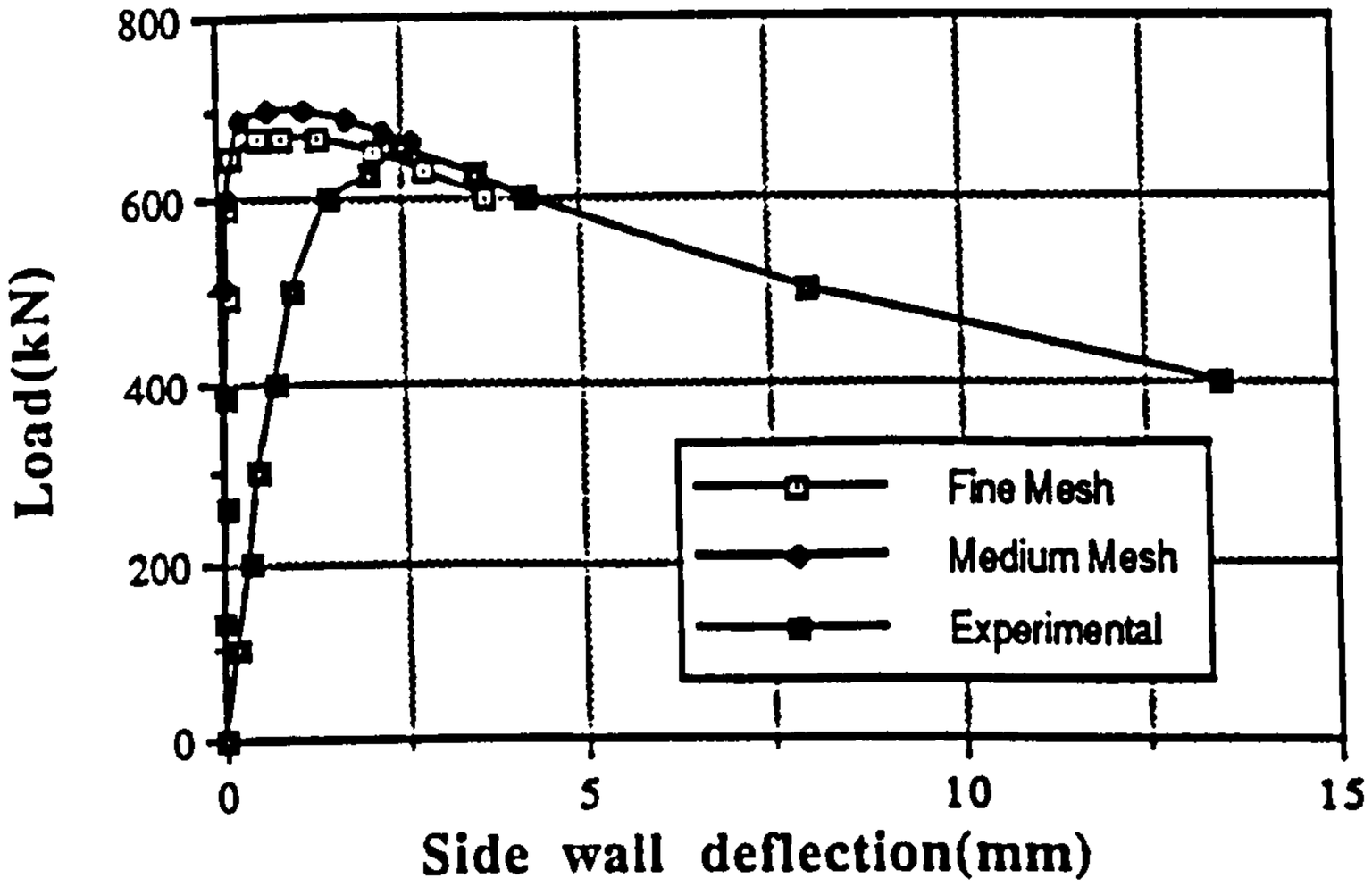

Figure 5.14 Comparison of FE Dense and Medium Meshes with Zhao's Experimental Results (1992)

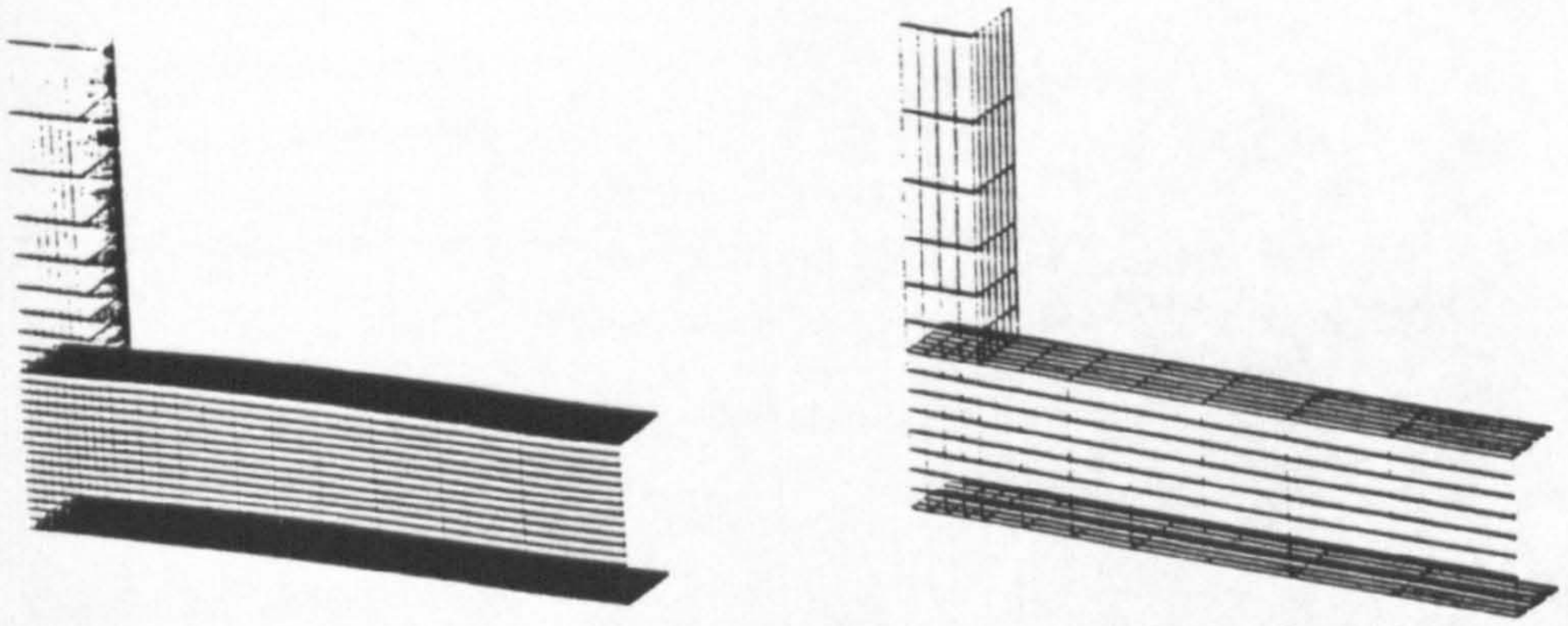

Figure 5.15 Meshes Used to Analyse the Zhao Experimental Specimen

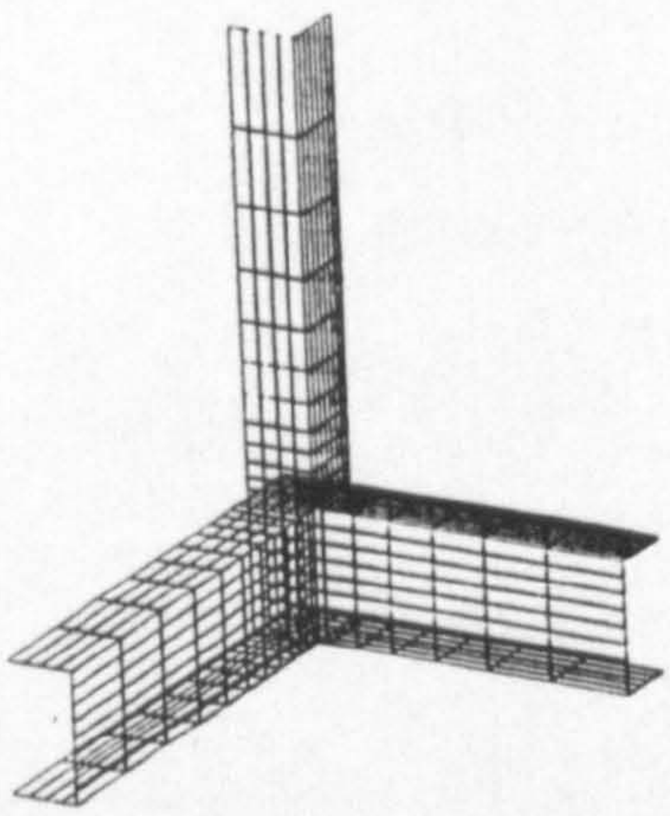

Figure 5.16 Mesh Used to Analyse the β = 1.0 Multiplanar Series in this Chapter

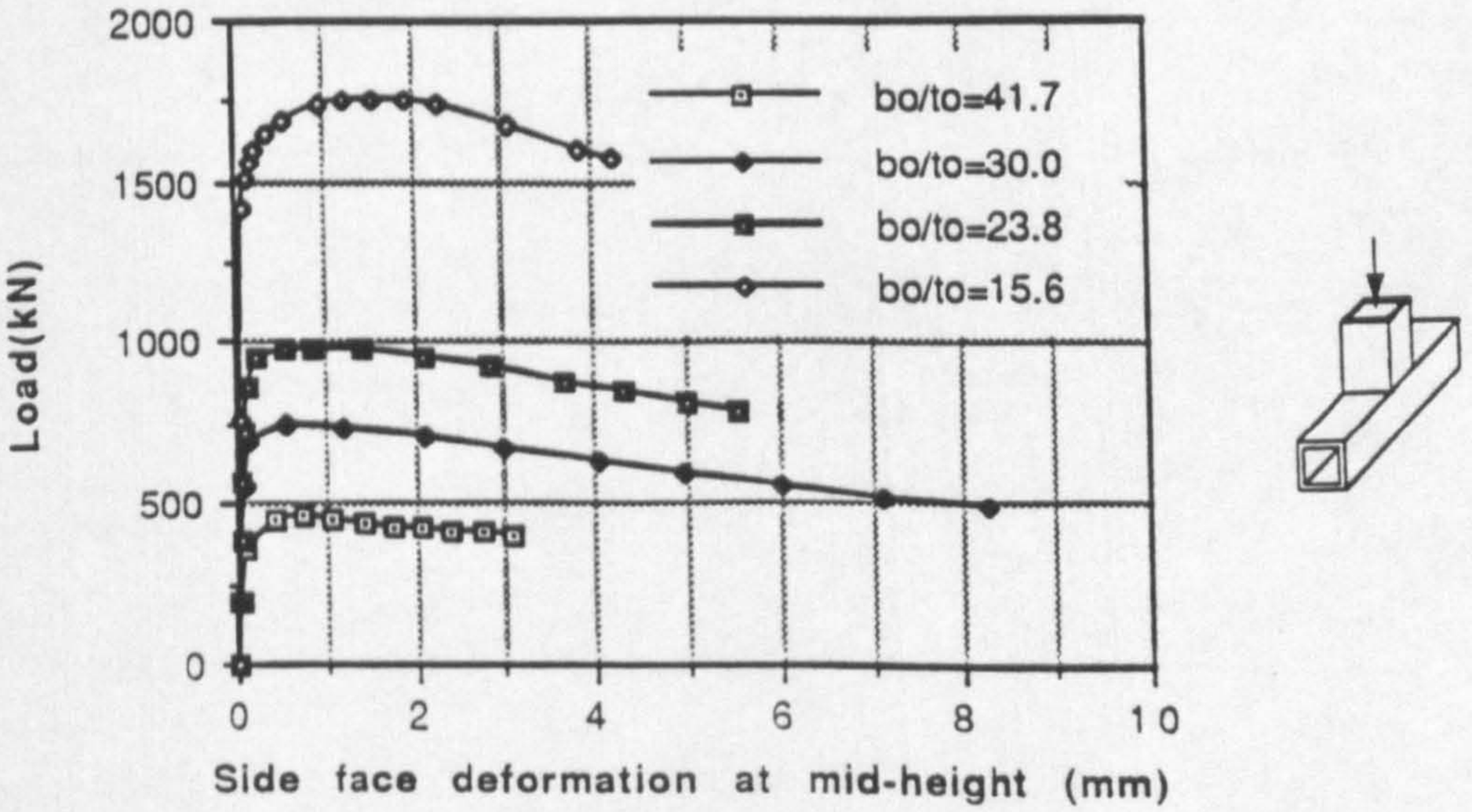

Figure 5.17 Load vs Chord Sidewall Deformation for β = 1.0 Planar Joints

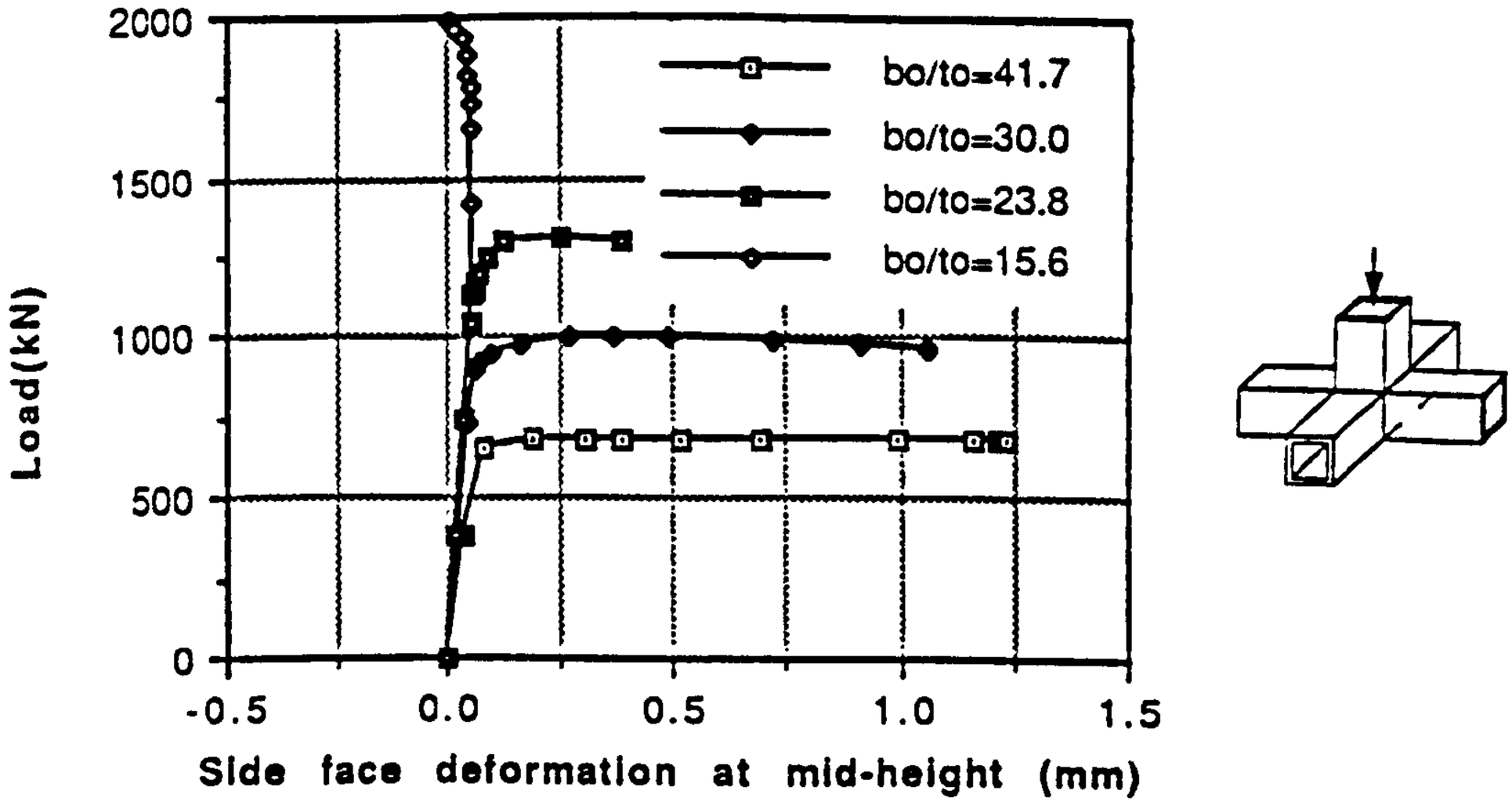

Figure 5.18 Load vs Chord Sidewall Deformation for $\beta = 1.0$ Multiplanar Joints

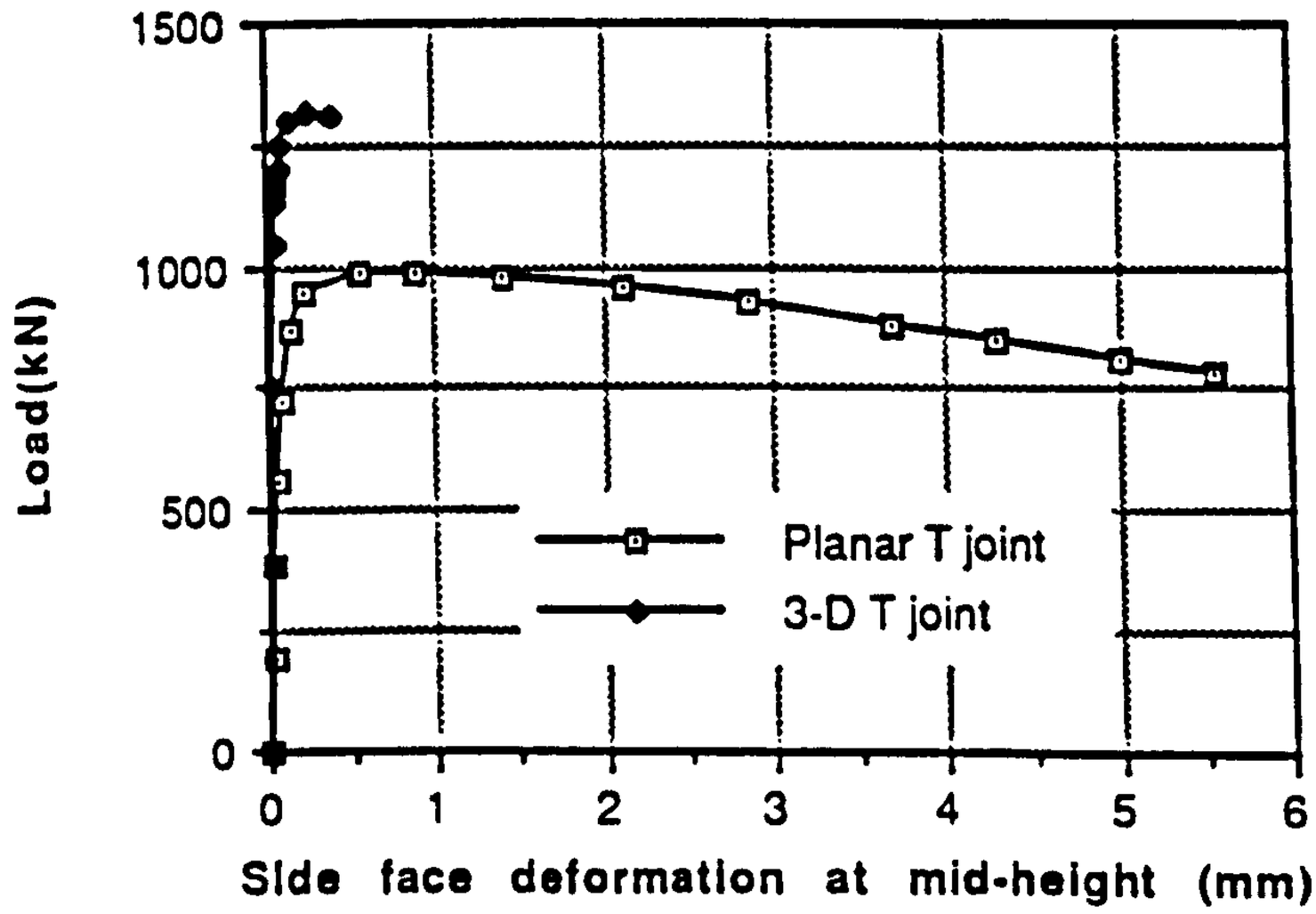

Figure 5.19 Comparison of Sidewall Deformation for $\beta = 1.0$ Planar and Multiplanar Joints at $b_o/t_o = 23.8$.

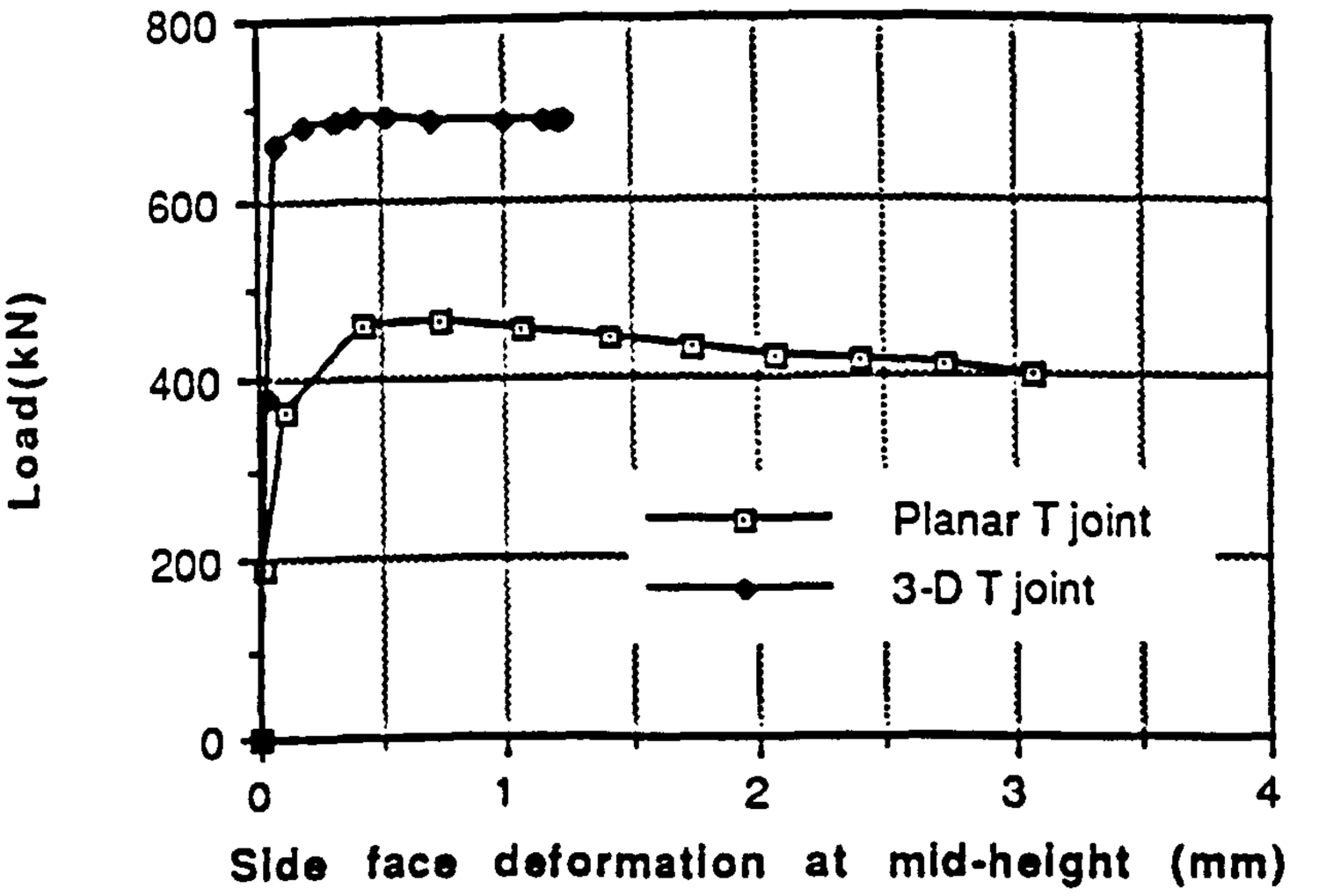

Figure 5.20 Comparison of Sidewall Deformation for $\beta = 1.0$ Planar and Multiplanar Joints at $b_o/t_o = 41.7$.

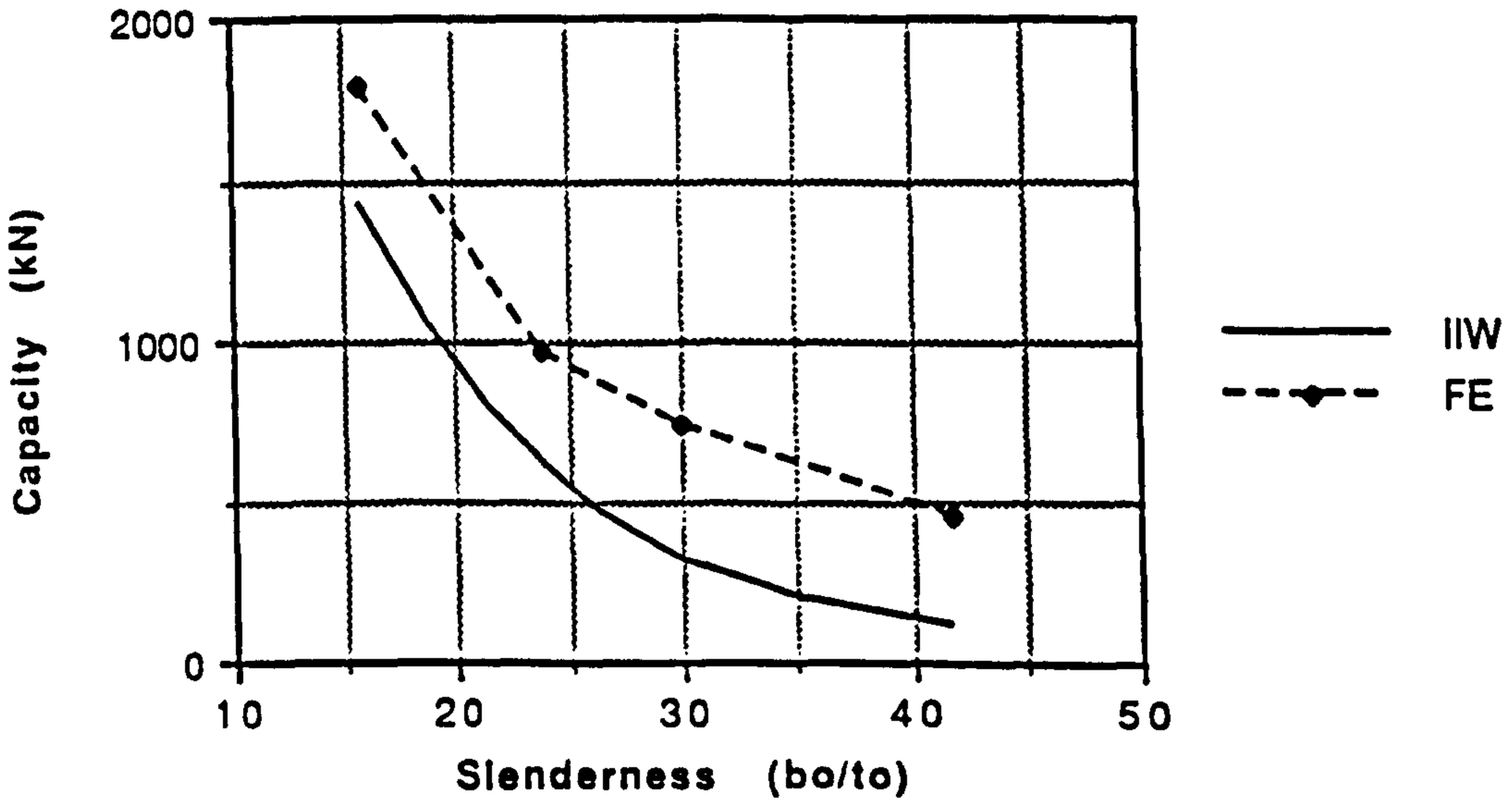

Figure 5.21 Comparisons of Planar FE $\beta = 1.0$ T Joints with IIW (1989) Joint Strength Prediction.

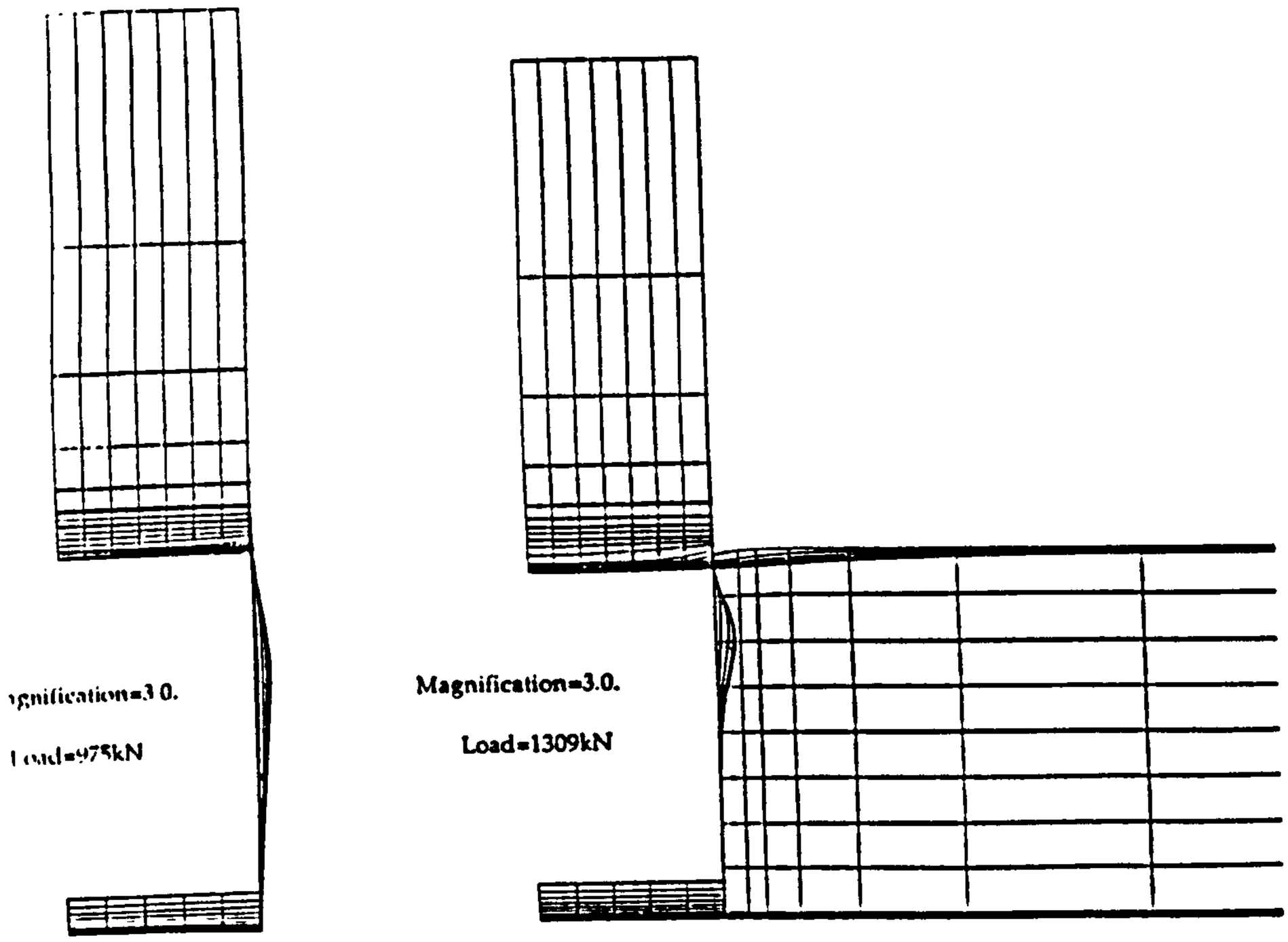

Figure 5.22 Displaced Shape Plots for β = 1.0 Planar and Multiplanar Joints

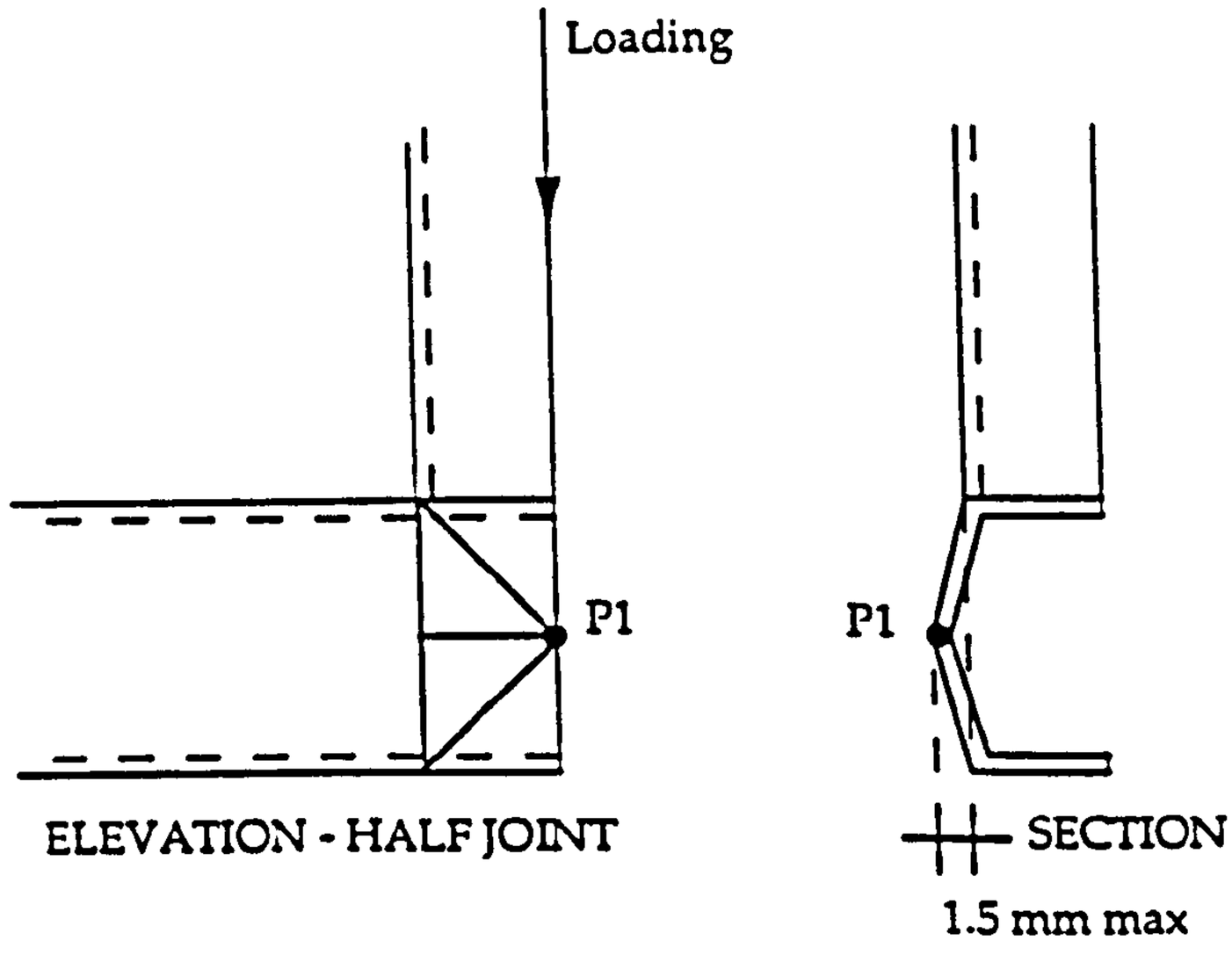

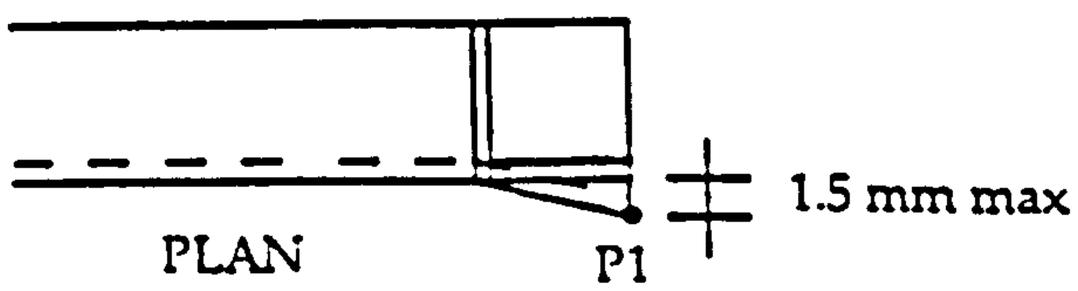

Figure 5.23 Initial Imperfection Installed on Chord Sidewall for β = 1.0 T Joints as Described in 5.4.4.1.

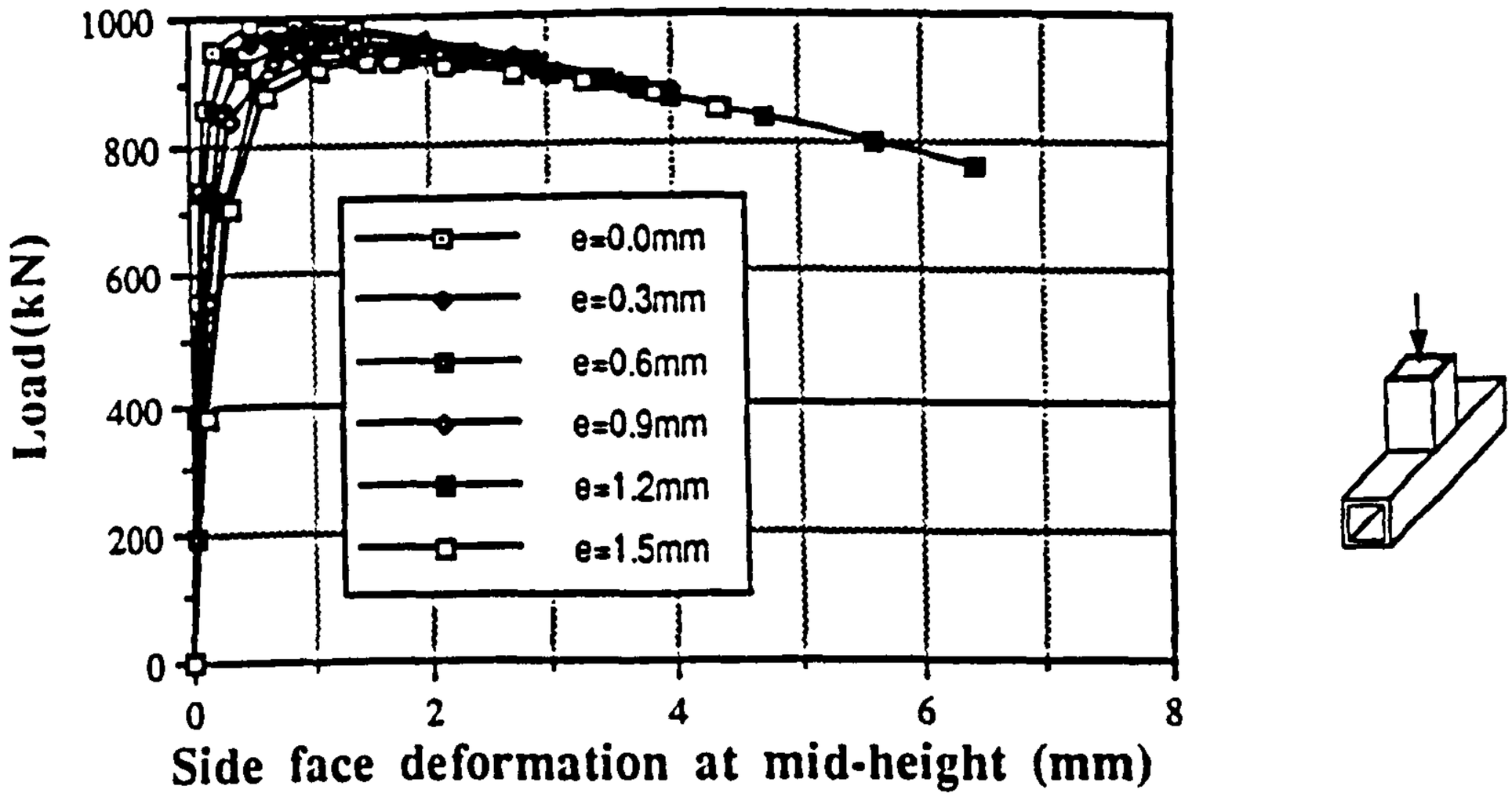

Figure 5.24 Load vs Sidewall Deformation Comparisons for Initial Imperfection at a Slenderness of 23.8

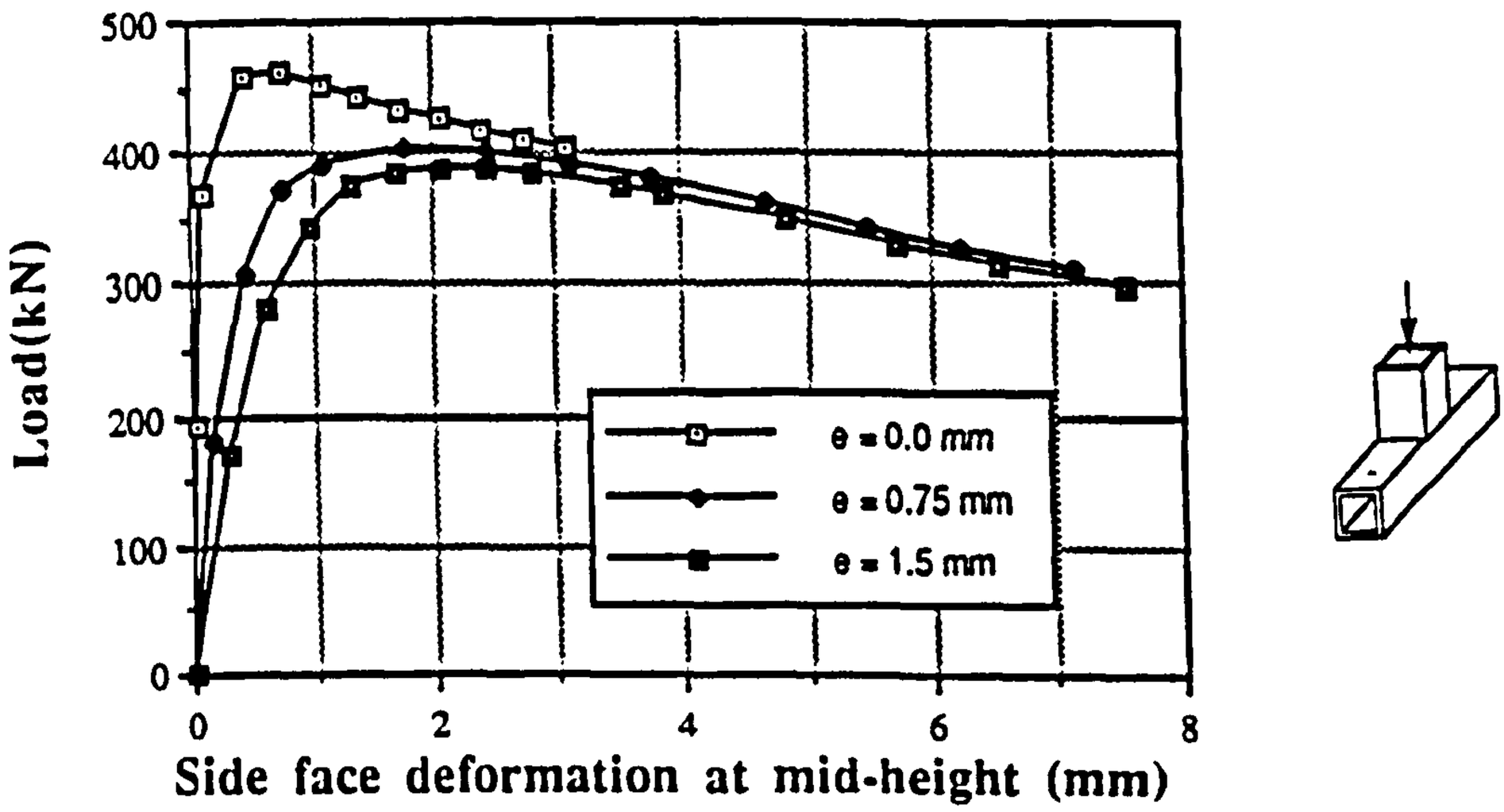

Figure 5.25 Load vs Sidewall Deformation Comparisons for Initial Imperfection at a Slenderness of 41.7

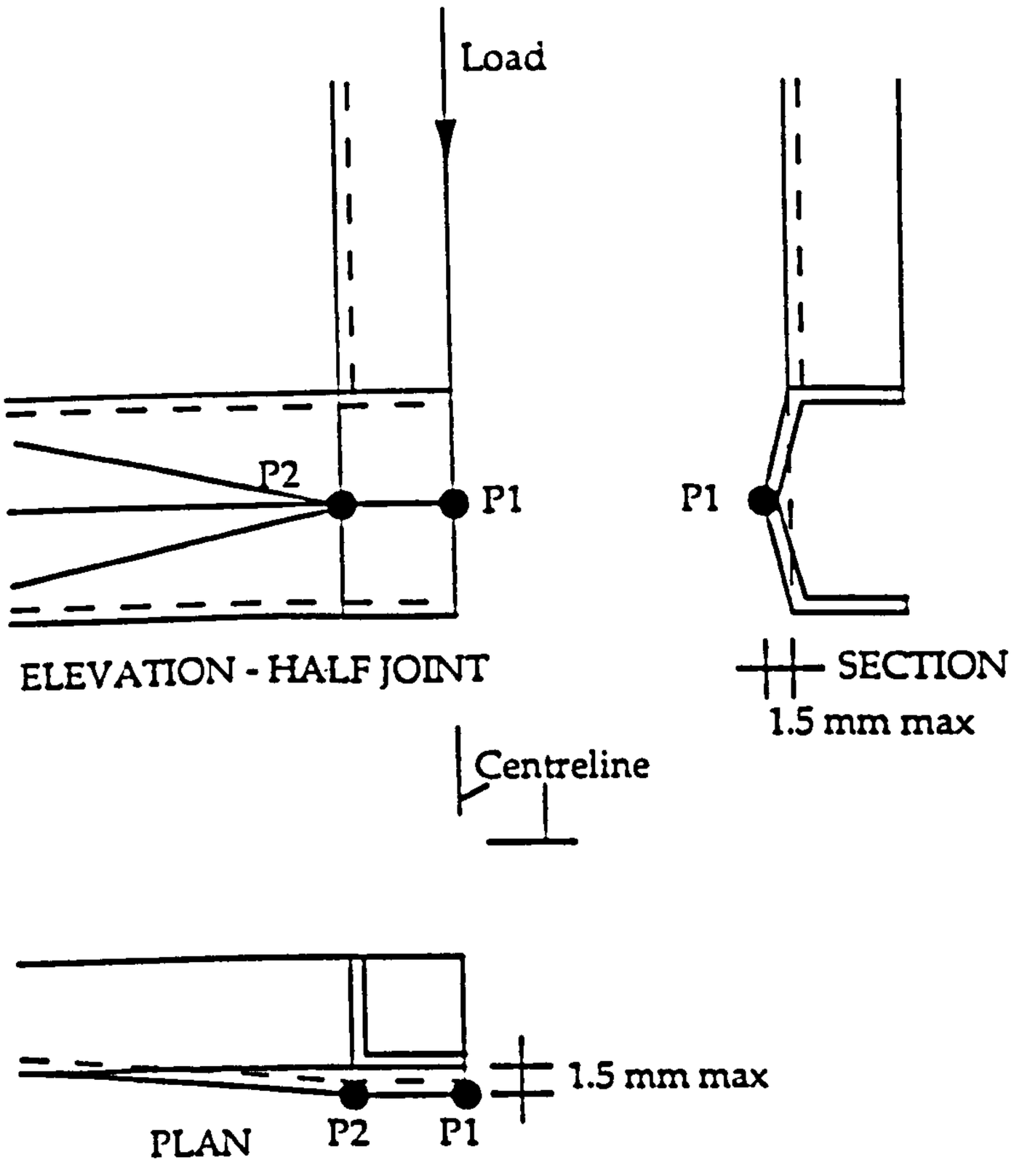

Figure 5.26 Second Imperfection Installed on Chord Sidewall for $\beta = 1.0$ T Joints as Described in 5.4.4.2.

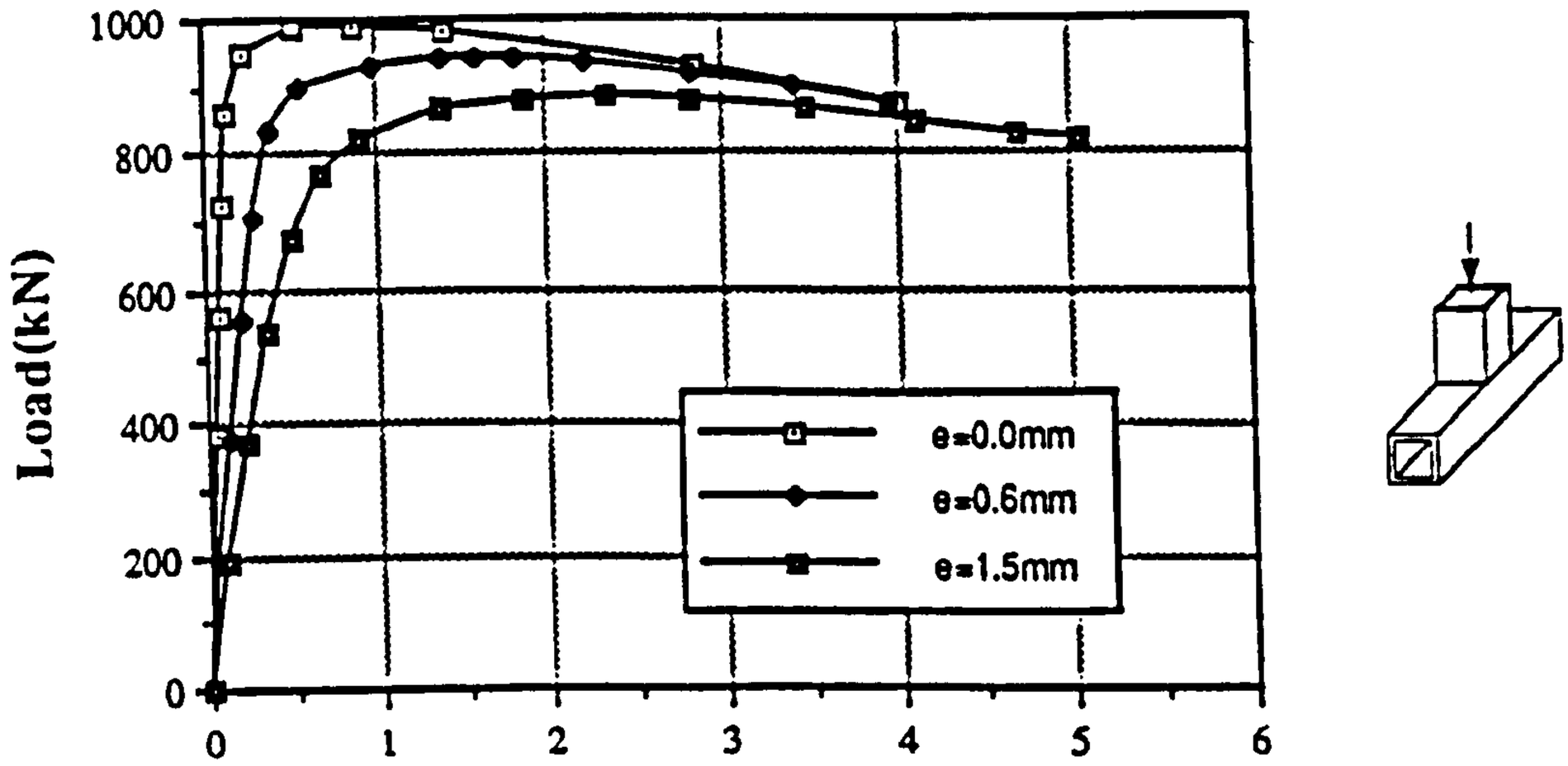

Figure 5.27 Load vs Sidewall Deformation Comparisons for Second Imperfection at a Slenderness of 23.8

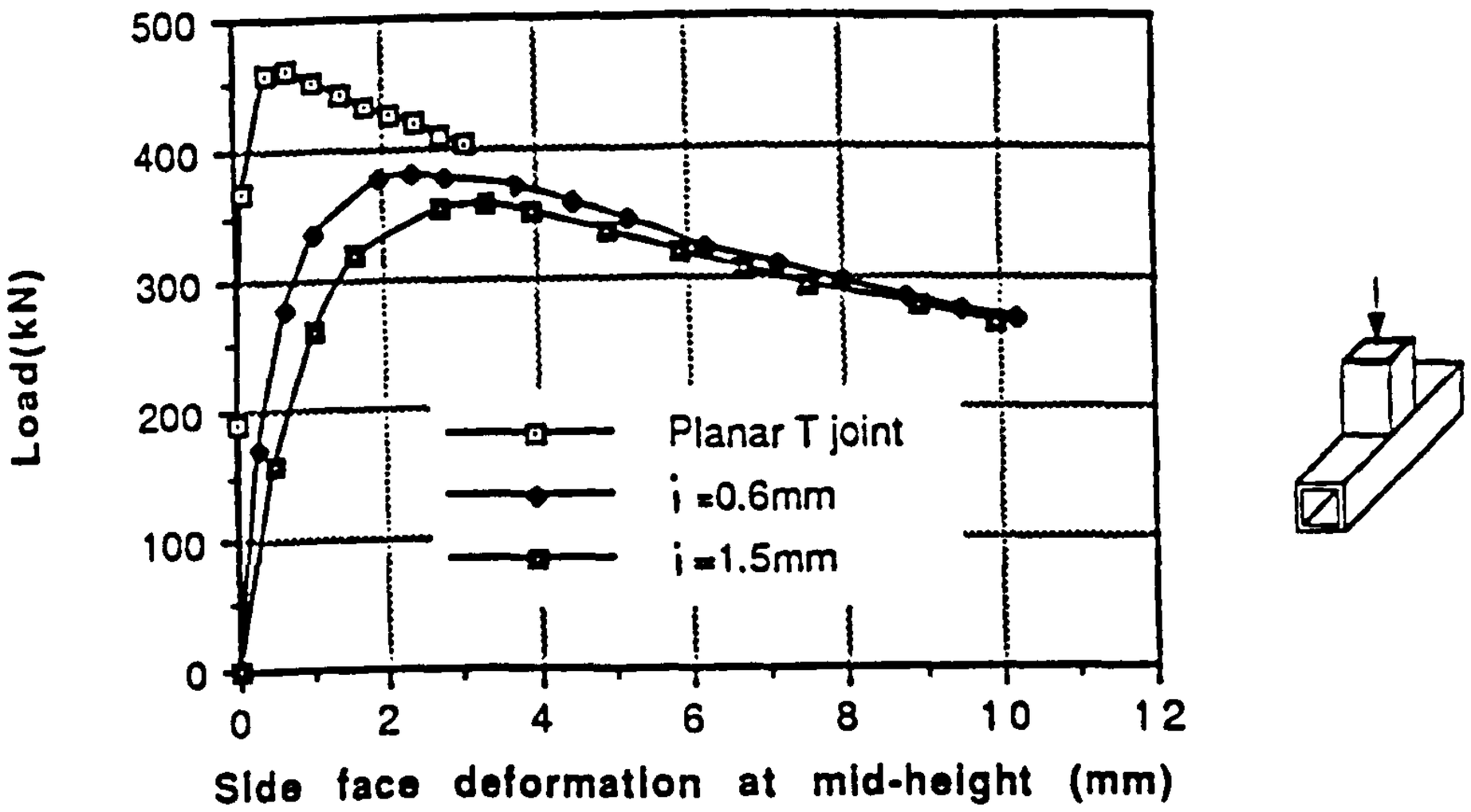

Figure 5.28 Load vs Sidewall Deformation Comparisons for Second Imperfection at a Slenderness of 41.7

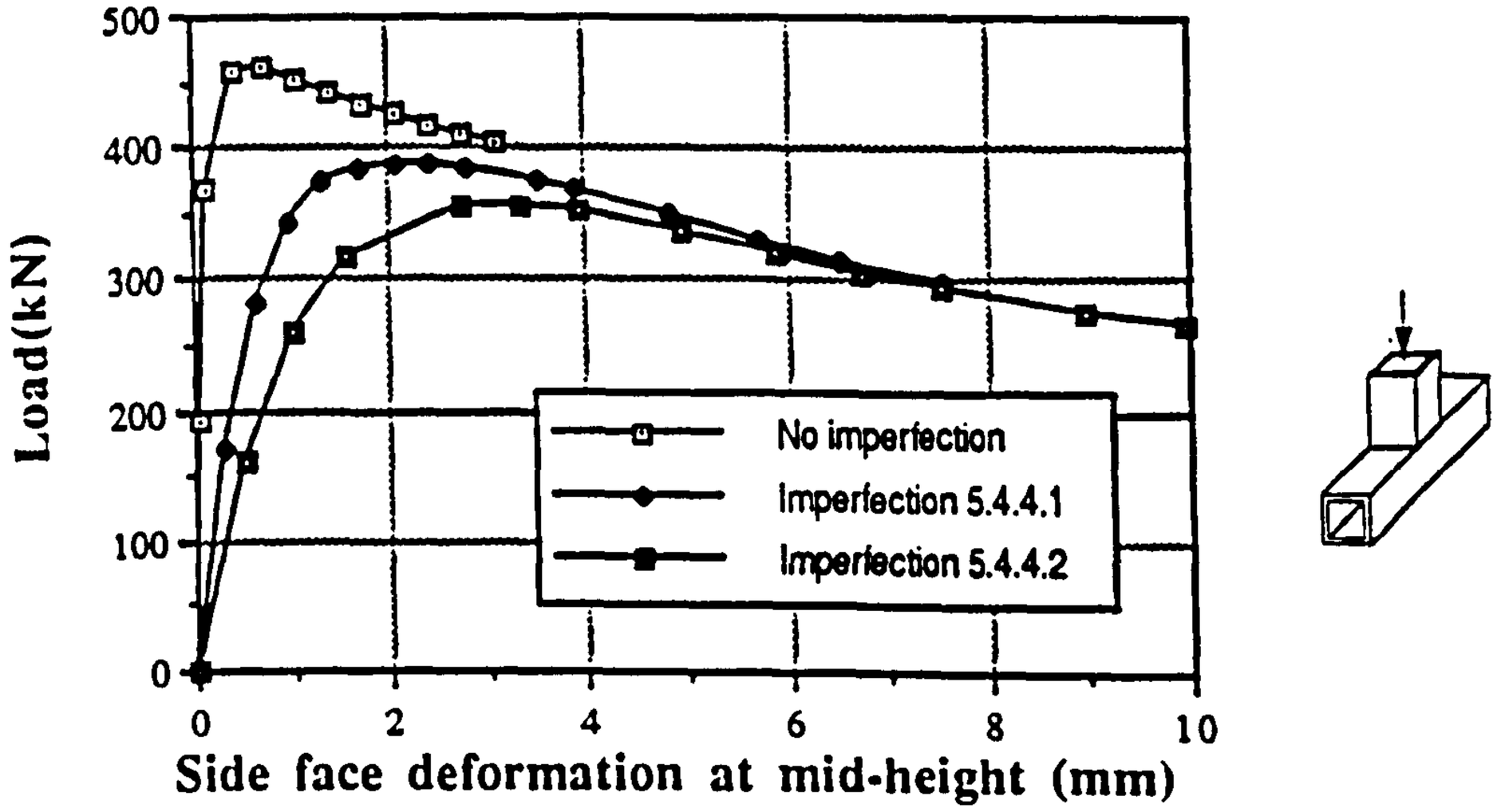

Figure 5.29 Comparisons of Initial and Second Imperfections on the Planar Joint at a slenderness of 41.7.

CHAPTER 6

RHS T-DT JOINTS: AN INTERACTION DIAGRAM AND THREE DIMENSIONAL EFFECTS.

6.1 Introduction

In this chapter a comprehensive investigation of the behaviour of axially loaded three dimensional RHS T-DT joints at three β ratios is carried out. Chord slenderness and length were examined in Chapter 5; the effects of the presence of out-of-plane braces, their method of restraint and the presence of axial loads of varying sense and magnitude in these braces has been investigated. To complete the picture a third β ratio of 0.25 (in addition to the existing ones of 0.6 and 1.0) is considered, enabling a more complete understanding of multiplanar joint behaviour across a range of β ratios to be established. Comparisons are also made between these FE predictions, yield line theories and the IIW (1989) design guidance for planar assessment.

Investigations by Vegte et al (1991) using the finite element approach have indicated the possibility of significant gains of stiffness and strength for both plane compressive axial loading of DT-DT joints in CHS. This has not been found to be so for the resistance capacity when using Rectangular Hollow Sections, either from the yield line analysis approach described by Davies and

Morita (1991) or indeed in the experimental work of Davies et al (1992), undertaken as part of a larger European program. One advantage of the FE approach is that once calibrated against experimental results, it can be easily adapted to examine the effects of different loading regimes, boundary conditions, material and geometric properties on the joint behaviour.

6.2 Finite Element Modelling of the $\beta = 0.6$ Joint Series

Using the existing multiplanar model from the analysis of the experimental results in Chapter 4 (four noded shells with eight noded offset solid weld), which calibrated well with the experimental results, two series of analyses on the $\beta = 0.6$ joints are described. The first constrained the out-of-plane (DT) braces to remain parallel during loading, the second allowing them freedom to rotate as detailed for the experimental programme. Both were carried out to illustrate some of the variations that may occur due to the frame environment. The basic test arrangement and loading mode for the joints is shown in detail in Chapters 3 and 4; however for completeness, Figure 6.1 shows the basic load and joint configuration and defines F_{ipb} and F_{opb}, the in-plane (T) and out-of-plane (DT) axial loads respectively.

6.2.1 Determination of Ultimate Capacities in the Joint Series

Failure of the compression loaded joints was determined as described earlier in section 3.3; however in order to complete a full interaction diagram of all axial load cases it is necessary to analyse some joints with tension loaded in-plane and out-of-plane. The

determination of failure of these joints is problematic, a typical static FE load vs out-pull of brace plot being shown in Figure 6.2. It can be seen that after initial plastification in the region (a) the FE load capacity still increases at an identifiable rate. Using the method described previously for compression joints, the intersection of the elastic part and the linear upper plastic region is used to define failure load. In reality failure will occur with the formation of cracks around the weld toe of the brace but this presents difficulty in the modelling. By its nature the formation of the crack will vary from specimen to specimen, its exact location depending on such things as residual stresses and initial material imperfections. Several researchers have modelled cracks using line spring elements in conjunction with solid elements (Tie-yun Chen 1992) but this still does not solve the problem of establishing the exact location where the crack begins to form. However the method of determining failure described above should give conservative results below those at which cracks would occur, especially as when compared to compression loaded joints that reach a plastic 'plateau' (i.e the capacity does not increase beyond a certain magnitude), the failure load will be slightly lower due to the slope of the upper portion (plastic plateau) of the load vs out-pull plot lowering the elastic-plastic intersection point, this being illustrated in Figure 6.2.

6.2.2. FE Analyses of the $\beta = 0.6$ Joint Series

Using ABAQUS the analyses described were undertaken under a comprehensive range of axial load combinations, these combinations and ultimate capacities being presented in Table 6.1 and Table 6.2 for the two different restraint conditions described in

section 4.2, along with some yield line results. The analyses used the mesh illustrated earlier in Figure 4.21. All ultimate capacities quoted on these two tables are those obtained using the elastic-plastic intersection technique described in 4.4.3. The series of ultimate capacities is then displayed in an interaction diagram in Figure 6.3. The effects of tension in one plane and compression in the other can clearly be seen. An interaction diagram of the yield line theories with no account taken of weld or corner radii in each case is given in Figure 6.4, derived from Davies and Morita (1991). Figure 6.5 shows Load vs indentation plots for the F_{ipb}-compressive F_{opb}-compressive loaded joints (top right quadrant of Figure 6.3) with free OPB (DT) braces, Figure 6.6 showing the same comparison for several of the joints with similar loading conditions and OPBs (DT) constrained to remain parallel. Figure 6.7 shows the load vs indentation plot for the F_{ipb}-compressive F_{opb}-tensile loaded joints (top left quadrant of Figure 6.3) with the OPBs (DT) free, Figure 6.8 showing the same comparison for those joints with OPBs restrained to remain parallel. Comparisons between restrained to remain parallel OPB joints and free to rotate OPB joints are made in Figures 6.9 and 6.10 for $F_{opb} = +/-0.56F_{ipb}$, displaced shape plots being shown for loading cases as indicated in Figures 6.11 and 6.12.

In-plane T Brace Loading	$\frac{F_{opb}}{F_{ipb}}$	FE (kN) Ult cap IP force	FE (kN) Ult cap OP force	Yield Line (kN) IP force	Yield Line (kN) OP force
1.0	0.0	230		155	
1.0	0.2	230		155	
1.0	0.4	235		155	
1.0	0.56	240		155	
1.0	0.8	245		155	
1.0	1.0	245		155	155
1.0	2.0	120	240	77.5	155
0.0	1.0		225		155
-1.0	1.0	165	165	119	119
-1.0	0.5	225	112.5	155	
-1.0	0.0	250		155	
-1.0	-0.5	250	125	155	
-1.0	-1.0	230	230	155	155
-1.0	-2.0	112.5	225	77.5	155
0.0	-1.0		190		155
1.0	-1.5	135	200	89.5	134
1.0	-1.0	162.5	162.5	119.4	119.4
1.0	-0.8	170	135	137.8	120.2
1.0	-0.56	192	108	155	
1.0	-0.4	220	87.5	155	
1.0	-0.2	222	40	155	

Table 6.1 Ultimate capacities for $\beta = 0.6$ joints with arms restrained horizontal and basic yield line theory. Compression +ive. $\frac{b_o}{t_o} = 23.8$.

Planar Joint Capacity = 195kN.

In-plane T Brace Loading	$\frac{F_{opb}}{F_{ipb}}$	FE Ult cap (kN) IP force	FE Ult cap (kN) OP force
1.0	0.0	212	
1.0	0.56	230	
1.0	0.8	230	182.5
1.0	1.0	190	190
1.0	1.0	100	200
0.0	2.0		200
-1.0	1.0	145	145
-1.0	0.5	190	95
-1.0	0.0	225	
-1.0	-1.0	240	240
-1.0	-2.0	125	250
0.0	-1.0		207
1.0	-2.0	105	210
1.0	-1.33	120	175
1.0	-1.0	150	150
1.0	-0.56	187.5	105

Table 6.2 Ultimate capacities for $\beta = 0.6$ joints with arms free.
Compression +ive $\frac{b_o}{t_o} = 23.8$. Planar Joint Capacity = 195kN.

6.3 Finite Element Modelling of the $\beta = 0.25$ Joint Series

Using the same chord dimensions and properties as for the $\beta = 0.6$ joints described in Table 3.1, a series of analyses were run on a β ratio of 0.25. β ratios less than 0.25 are rarely found in practical situations. The mesh used for the planar joint in this analysis series

is shown in Figure 6.13. As with the $\beta = 0.6$ joints, four noded shell elements were used in the brace and chord with six noded solid elements in the offset position for the weld. The lengths of the braces in both planes was reduced from 500mm to 250mm to avoid failure by member buckling of these ($b_i = 37.5$mm) as opposed to 'joint' failure. As for the $\beta = 0.6$ ratio joints, two sets of analyses were run, one involving out-of-plane braces restrained to stay parallel during the analysis and one in which the braces were free to rotate during the analysis. The results of this set of analyses are shown in Table 6.3 along with the analysis of a $\beta = 0.25$ planar T joint. In all analyses F_{ipb} was compressive, but F_{opb} had a variety of tension, compression and zero forces in the DT braces. Load vs indentation plots are shown in Figure 6.14 for the IPB, where

Model	Description	Out-of-plane braces held horizontal?	$\frac{F_{opb}}{F_{ipb}}$	IIW capacity (kN)	FE (kN)	$\frac{MP}{Planar}$
A	Planar	–	–	88.0	79.0	1.00
B	Multiplanar	Yes	0.0		79.0	1.00
C	Multiplanar	Yes	0.5T		71.0	0.90
D	Multiplanar	Yes	0.5C		80.0	1.01
E	Multiplanar	No	0.0		79.0	1.00
F	Multiplanar	No	0.5T		69.0	0.87
G	Multiplanar	No	0.5C		80.0	1.01
H	Multiplanar	No	1.0T		57.0	0.72

Table 6.3 Capacities for $\beta = 0.25$ ratio joints, in-plane load = 1.0 Compression =ive. $\frac{b_o}{t_o} = 23.8$.

indentation is as shown for the β = 0.6 joints in Figure 3.5. Displaced shape plots are shown in Figure 6.15 where the loading conditions are as labelled and an interaction diagram of the results in Table 6.3 shown in Figure 6.16.

6.4 FE Modelling of the β = 1.0 Joint Series

Using the model created in Chapter 5 for the chord wall slenderness investigation and no imperfections, four analyses on β = 1.0 joints at a slenderness ratio (b_o/t_o) of 23.8 were undertaken. The IPB was loaded in compression, one joint was planar, the other three having zero, tensile and compressive loads applied in the OPBs, these braces being left free to rotate. As described earlier eight noded shell elements were used for the brace and chord members in the analyses. Table 6.4 presents the results of these alongside the predicted planar capacity from the IIW recommendations. Displaced shape plots for the four joints are shown in Figures 6.17 and 6.18.

Model	Description	Load in out-of-plane braces	IIW capacity (kN)	FE peak (kN)
A	Planar	–	651.8	989.0
B	Multiplanar	0.0		1321.0
C	Multiplanar	0.5T		1259.0
D	Multiplanar	0.5C		1284.0

Table 6.4 Capacities for β = 1.0 ratio joints, in-plane load = 1.0 Compression. $\frac{b_o}{t_o} = 23.8$.

6.5 Discussion

6.5.1 $\beta = 0.6$ Joints

From Figure 6.3 it can be seen that for same sense F_{ipb} and F_{opb} loading no increase in capacity occurs compared with the $F_{opb} = 0$ multiplanar joint. Indeed it can be seen that some slight enhancement has taken place where compression of similar magnitudes is present in both planes. However where compression in one plane and tension in the other is present then the capacity can be significantly reduced. This is most marked when $|F_{opb}| > |0.5F_{ipb}|$, with lowered capacity below that of the planar T or DT joint (1.0). This clearly has implications for the design of such joints if they are designed on a plane by plane basis neglecting the multiplanar load effects. Restraining the arms to remain parallel during the loading process slightly enhances the strength except for the region where high tension exists in the OPBs, with tension or low compression present the IPB (T brace). The number of results in this region is low however and difficulties were encountered in the determination of tabled capacities under tensile loading as discussed in section 6.2.1. Results of the actual analyses, corresponding to points in Figure 6.3 are shown in Tables 6.1 and 6.2 alongside those of the basic yield line theory proposed by Davies et al (1992). The yield line theory is based upon the mechanisms shown in Figure 6.20 and the resultant equations shown below:-

$$P_y = \frac{f_y t_o^2}{(1-\beta)} \{ \frac{2h_i}{b_o} + 4(1-\beta)^{.5} \} \qquad [1]$$

$$\text{and} \quad P_y + 2P_x = \frac{4f_y t_o^2}{(1-\beta)} \{ \frac{h_i}{b_o} + (6(1-\beta))^{.5} \} \qquad [2]$$

Figure 6.4 displays an interaction diagram based upon this theory. β is assumed as 0.6 here although as discussed in Chapter 5 it may be adjusted to account for the effect of the weld and corner radii on the β ratio and the exact locations of the plastic hinges. The yield line theory in Figure 6.3 assumes that the out-of-plane braces remain parallel during the loading, this corresponding to one of the FE loading conditions examined here. Examination of both displaced shape plots and test specimens for the second loading condition (OPBs free to rotate) reveals that rotation of the out-of-plane arms was barely discernable.

Comparisons of the shape of the yield line theory diagram (Figure 6.4) and the numerically determined results (Figure 6.3) reveals that the shape remains similar confirming the reduction in capacity present where F_{opb} and F_{ipb} are of opposite sign. The rate of change in these regions however differs considerably. The finite element results indicate a roughly 45° fall in F_{ipb}/F_{opb} after F_{opb} reaches $-0.5F_{ipb}$, whereas the fall indicated by the yield line theory for the same case is much more rapid and occurs after F_{opb} reaches $-0.65F_{ipb}$. The difference between these sections of the interaction diagrams is likely to be caused by the gradual formation of the hinges that occurs in practice through the material thickness. The yield line theory assumes that rigid plasticity occurs immediately across the whole thickness of the chord material, whereas in reality this is not the case as the rectangular stress block for plastic hinges to occur builds up as the loading magnitude increases. The yield line theory also assumes that the hinge forms at a point whereas this is not the case in reality where, due to the spread of plasticity the actual position is much more difficult to establish. This is illustrated

in Figure 6.20. The yield line theory used here also takes no account of the corner radius influence on the location of the hinge or the small chord sidewall deformation which are both evident from the displaced shape plot of the planar joint in Figure 6.11(a).

The presence of compression in the free to rotate OPBs is illustrated in Figure 6.5 where the joint with $F_{opb} = 0$ is compared to a joint with $F_{opb} = 0.56F_{ipb}$. It can be seen that the presence of these compressive loads increases capacity by around 15kN in the plastic plateau region and they also considerably enhance the elastic stiffness. This is because during initial in-plane compression loading the tendency is for chord sidewalls to buckle outwards in the region below the brace in addition to the indentation of the in-plane (T) brace; therefore compressive loads in the out-of-plane braces in these regions will act to stabilise these sidewalls resulting in the increased stiffness and ultimate strength. Figure 6.6 illustrates the effect of F_{opb} being compressive where the out-of-plane braces are constrained to remain parallel during the analysis. The increasing elastic stiffness as F_{opb} increases from zero to being equal to F_{ipb} can clearly be seen. As F_{opb} increases, the ultimate load 'plateau' tends to be horizontal which therefore becomes equal to the failure load determined using the methods described in 4.4.3, indicating that the presence of the compressive loading in both planes has an effect mainly on the elastic behaviour of the joints.

The effects of varying amounts of tension in the out-of-plane braces is shown in Figure 6.7 (OPBs free to rotate) and Figure 6.8 (OPBs held parallel). It is clear that even modest values ($0.4F_{ipb}$) of tension in the out-of-plane braces reduce capacity. This can be explained in several ways. Firstly with the tendency for the chord sidewalls to buckle outwards under in-plane compression loading, the presence

of tension in the out-of-plane (DT) braces adding to this will cause increasing deformation of these sidewalls as opposed to the stabilising effect of compression discussed earlier. The reduction in capacity can also be explained by yield line theory where in the case of F_{opb} being tensile the top sidewall hinge (Figure 6.19) does not necessarily form, lowering the amount of work the applied forces need to do inflict a certain deflection under plasticity. Figures 6.9 and 6.10 compare the results between parallel held out-of-plane braced joints and free to rotate out-of-plane braced joints at a load ratio (F_{ipb}/F_{opb}) of 0.56. Differences between the two can be seen to be almost insignificant confirming the applicability of the yield line theory to the joints where arms are free to rotate in addition to the case where these braces are restrained horizontal.

6.5.2 $\beta = 0.25$ Joints

The results in Figure 6.14, Figure 6.16 and Table 6.3 for the $\beta = 0.25$ joints again illustrate the effect of loads of the opposite sense in the out-of-plane braces on the capacity of the joints. Here tension reduces the capacity of the multiplanar joints below that of the unloaded ($F_{opb} = 0$) out-of-plane multiplanar joint and the planar joint even where only a modest amount ($F_{opb} = -0.5F_{ipb}$) of tension was present in the out-of-plane braces. If design of such joints is based on a plane by plane assessment, this will be unconservative where loads of the opposite sense are present in the two loading planes. Addition of the unloaded out-of-plane braces offers no increase in strength over the original planar joint. The fact that the braces only cover 25% (the β ratio) of the chord sidewall gives a much reduced stiffening effect when compared to the larger braces

in the β = 0.6 joint series. When these braces are constrained to remain parallel it can be seen in Figures 6.14 and 6.16 that in the later loading stages (upwards of 100kN) a slight enhancement of strength over that of the equivalent free brace case can be observed. Compression in the OPBs under both restraint conditions can be seen to enhance strength slightly and also to significantly effect the stiffness. The IIW (1989) capacity predicts a strength of 88.0kN which when compared to the finite element results appears high. However it can be seen that in Figure 6.14 all the joints analysed exhibit considerable increases in capacity after plastification has occurred, indicating that all would achieve a capacity of 88.0kN. However although finite element results do not always predict results accurately, providing they achieve reasonable values, they are useful for examining trends and variations in parameters. As is illustrated here, although results fall some 10% low compared to the IIW capacity, which may be due to the way of determining failure, the effect on the capacity with regard to the addition of out-of-plane (DT) braces, method of restraint of these and loading of them can be investigated relatively.

6.5.3 β = 1.0 Joints

The β = 1.0 results series are shown in Table 6.4 along with displaced shape plots in Figures 6.17 and 6.18. These analyses were run with F_{ipb} compressive and out-of-plane braces (DT) free to rotate and it is evident from the displaced shape plots that the rotations are negligible, hence analyses with arms restrained parallel were not undertaken here. The loads in this case were peak loads achieved evaluated as stated in Chapter 5. It is clear here that

the addition of the out-of-plane (DT) braces has a very significant effect upon the ultimate capacity of the joints increasing the capacity by 33% over the planar joint. Reasons for this were given in the discussion in Chapter 5. Addition of loads to the out-of-plane (DT) braces however does not significantly effect results. This is because the DT braces are connected to the whole chord sidewall height. This ensures the out-of-plane brace connection to the main chord sidewall is restricted from pulling a portion of the chord sidewall outwards, the brace force effectively pulling on the whole chord member sideways. This does not give rise to the destabilising 'strut' effect on the sidewall evident in joints of β ratio 0.25 and 0.6 with loads in the out-of-plane (DT) braces. Of note is that tension and compression both lower the multiplanar capacity slightly when compared to the F_{opb} = 0 case, whereas at lower β ratios the compressive loading out-of-plane case enhances capacity slightly over the zero loaded case. The F_{opb} compression case alters the mode of sidewall buckling to in-punching of the chord sidewall as opposed to the normal mode of outward buckling evident in F_{opb} = 0, F_{opb} = tensile and planar joints, this normal mode being shown in Figure 6.18.

6.6 Conclusions

1.As the β ratio increases the enhancement effects of the out-of-plane braces increases from zero at a ratio of 0.25 to approximately 35% at a ratio of 1.0.

2.As the β ratio increases, the effect of the presence of loads in the out-of-plane braces becomes less significant and at a β ratio of 1.0 almost negligible.

3. For the β ratios of 0.25 and 0.6 the effect of tension in one plane and compression in the other is to reduce capacity at the more extreme cases below that of the planar joints. Where such joints are designed on a plane by plane basis as is the current practice, this has implications for design.

4. Design rules will be formulated for the joints discussed in this chapter. These will be published later , in a journal paper.

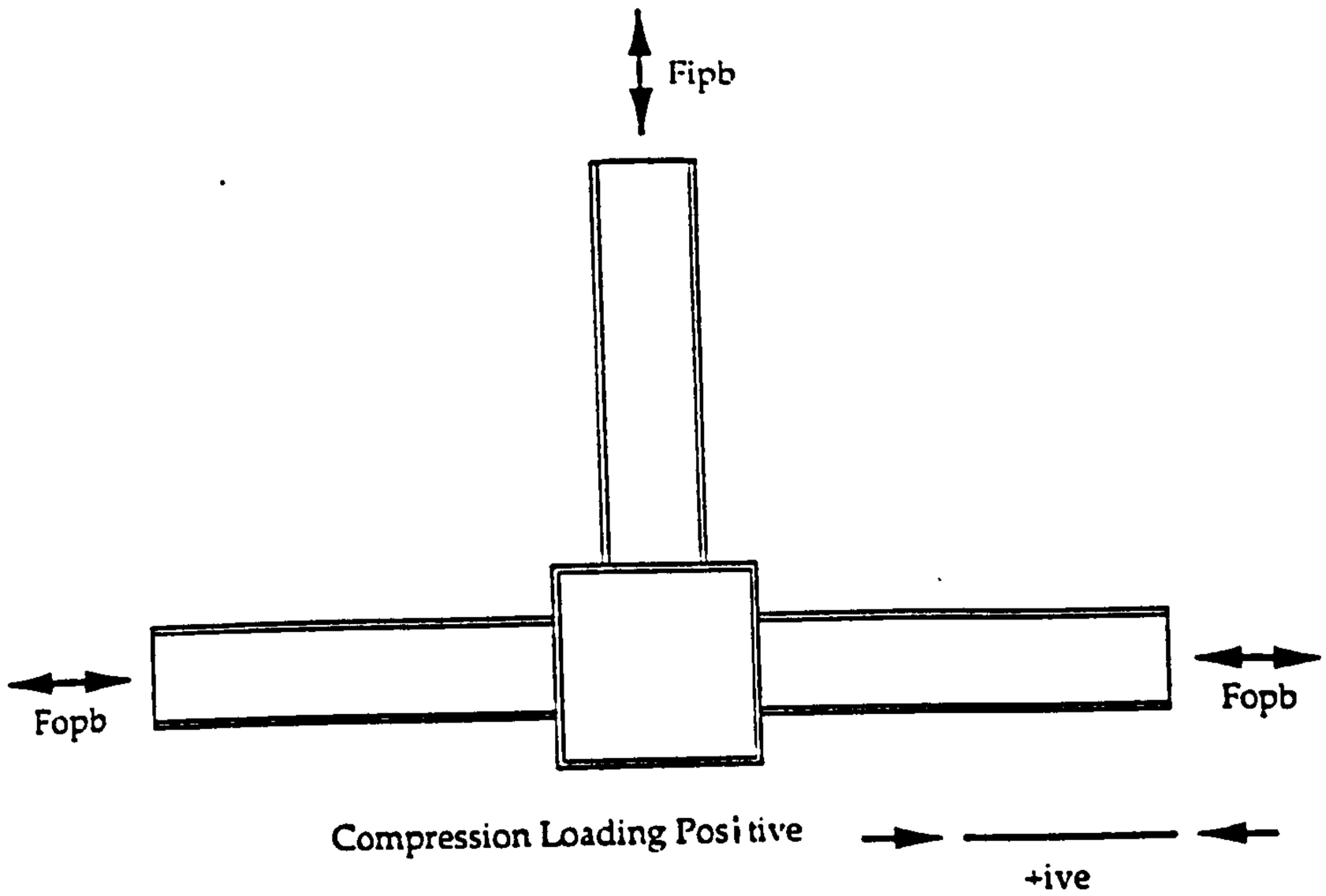

Figure 6.1 Basic Joint and Loading Configuration

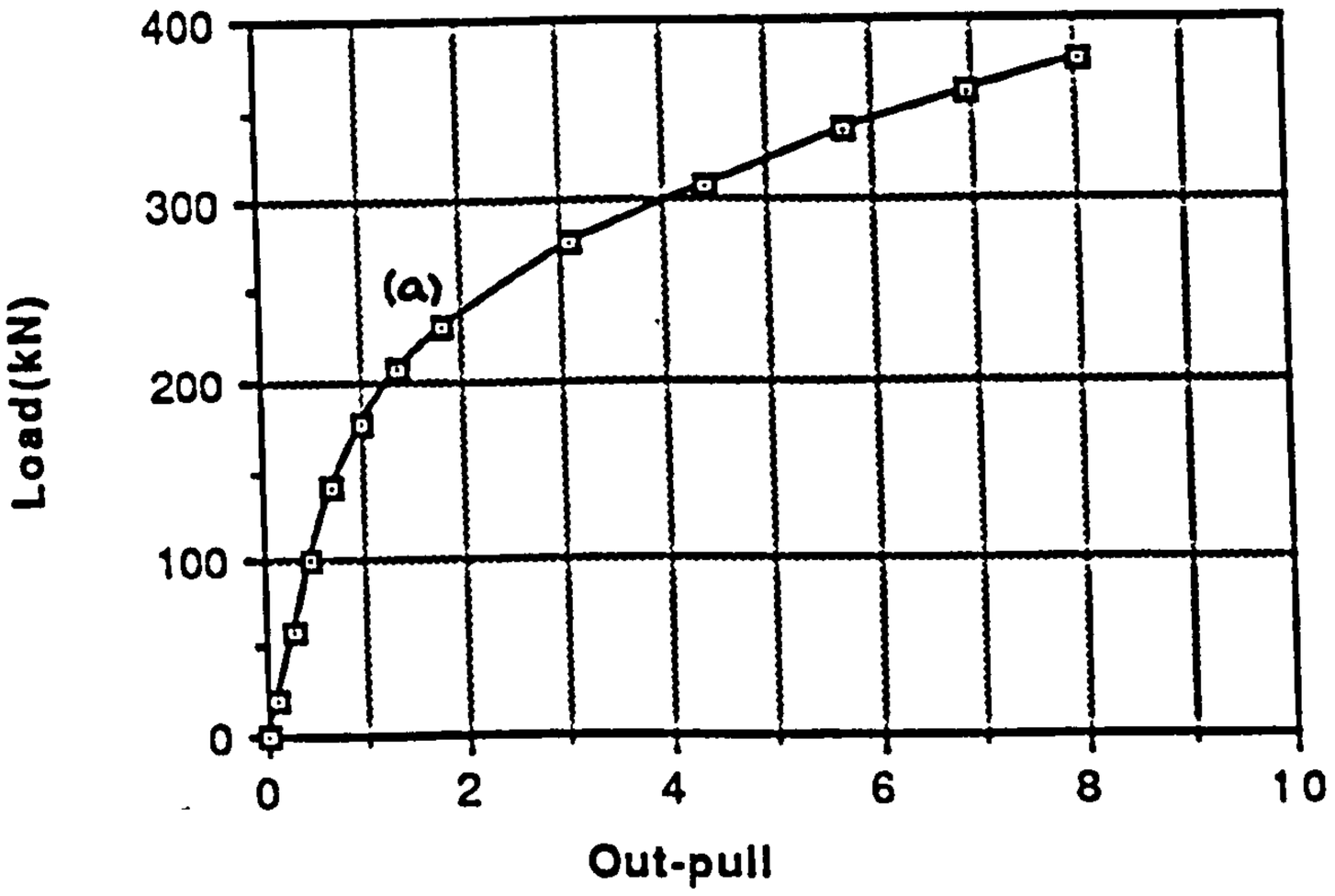

Figure 6.2 Determination of Ultimate Tensile Capacity

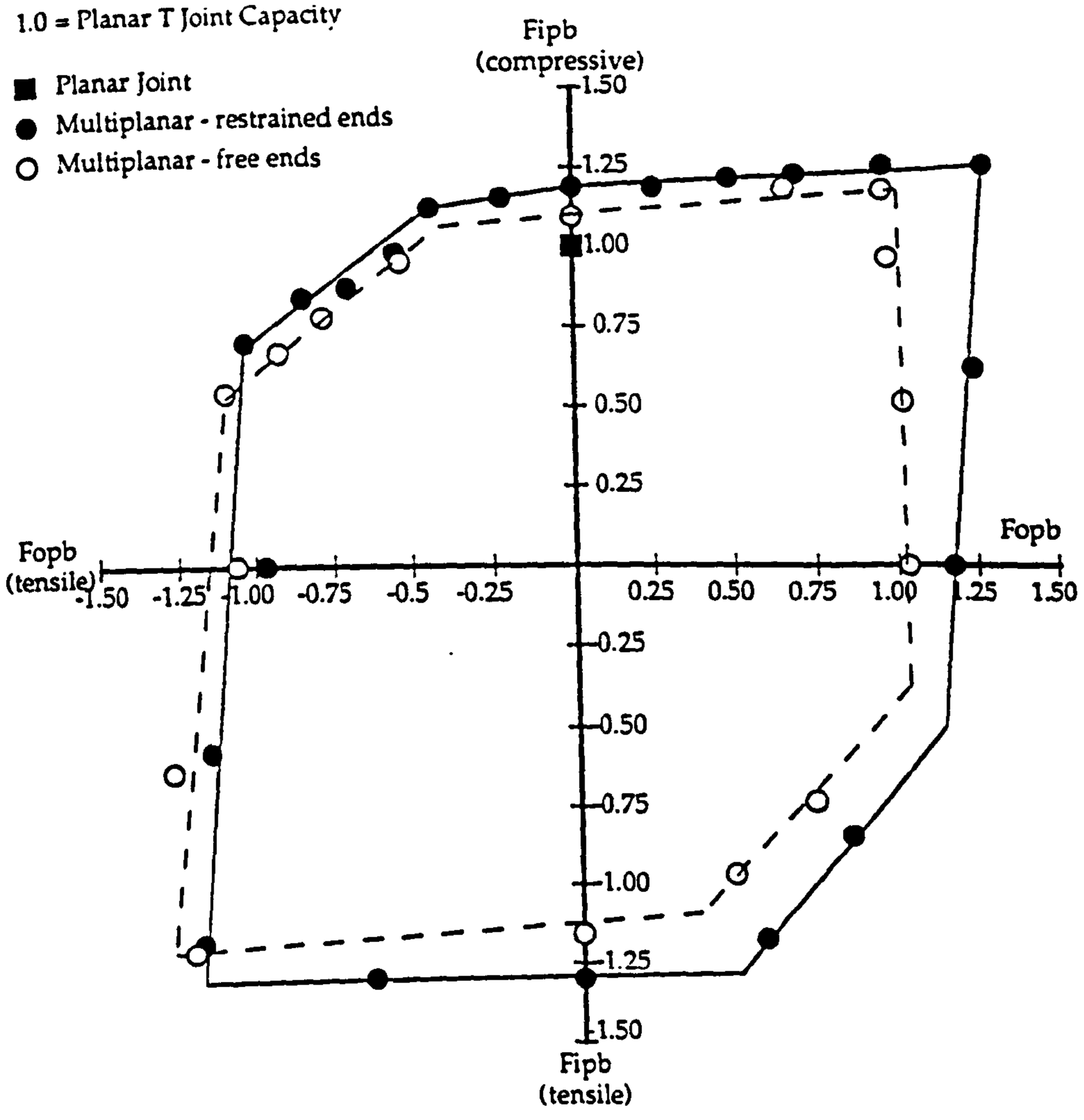

Figure 6.3 β = 0.6 Interaction Diagram (1.0 = Planar FE Capacity)

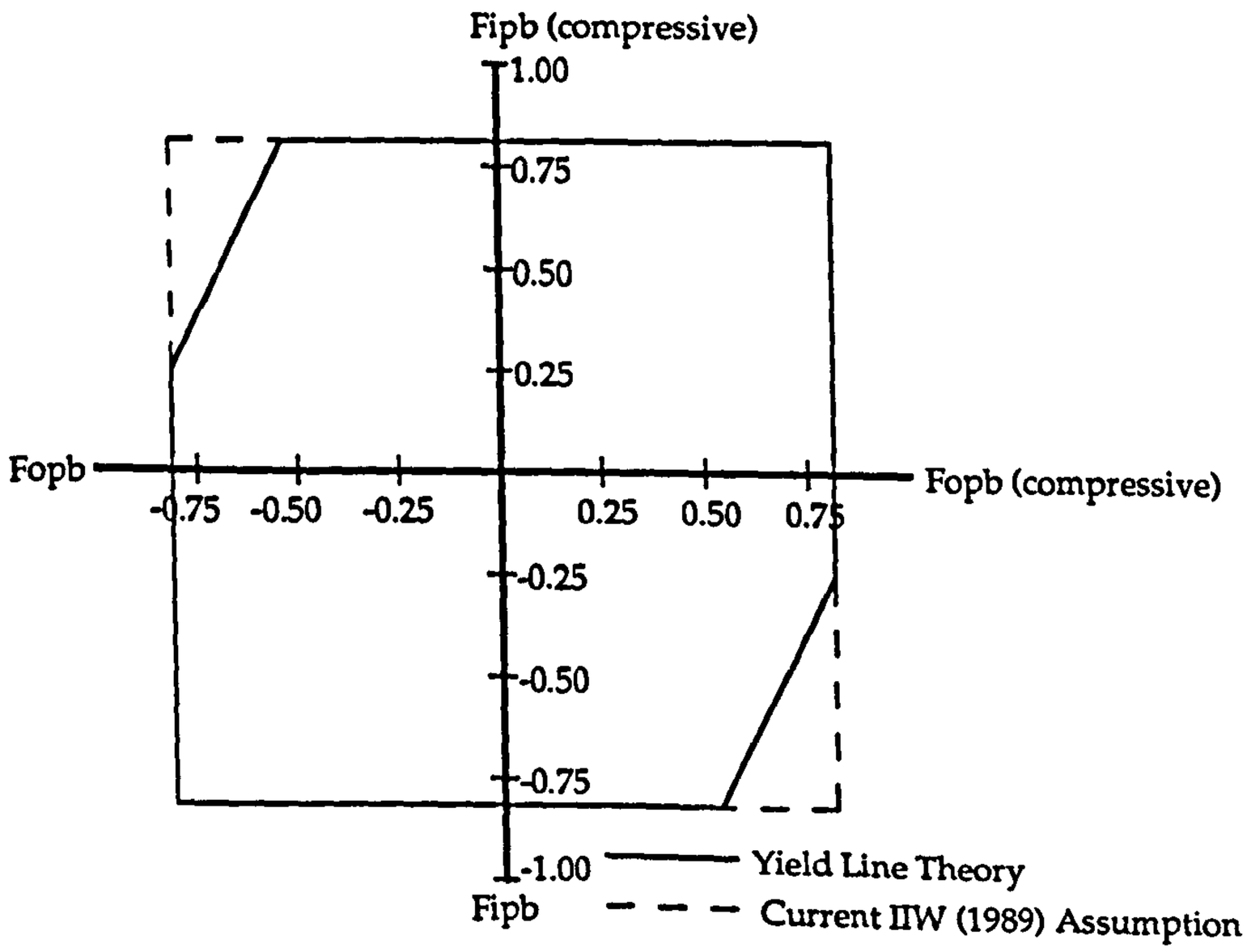

Figure 6.4 β = 0.6 Interaction Diagram - Yield Line Theory

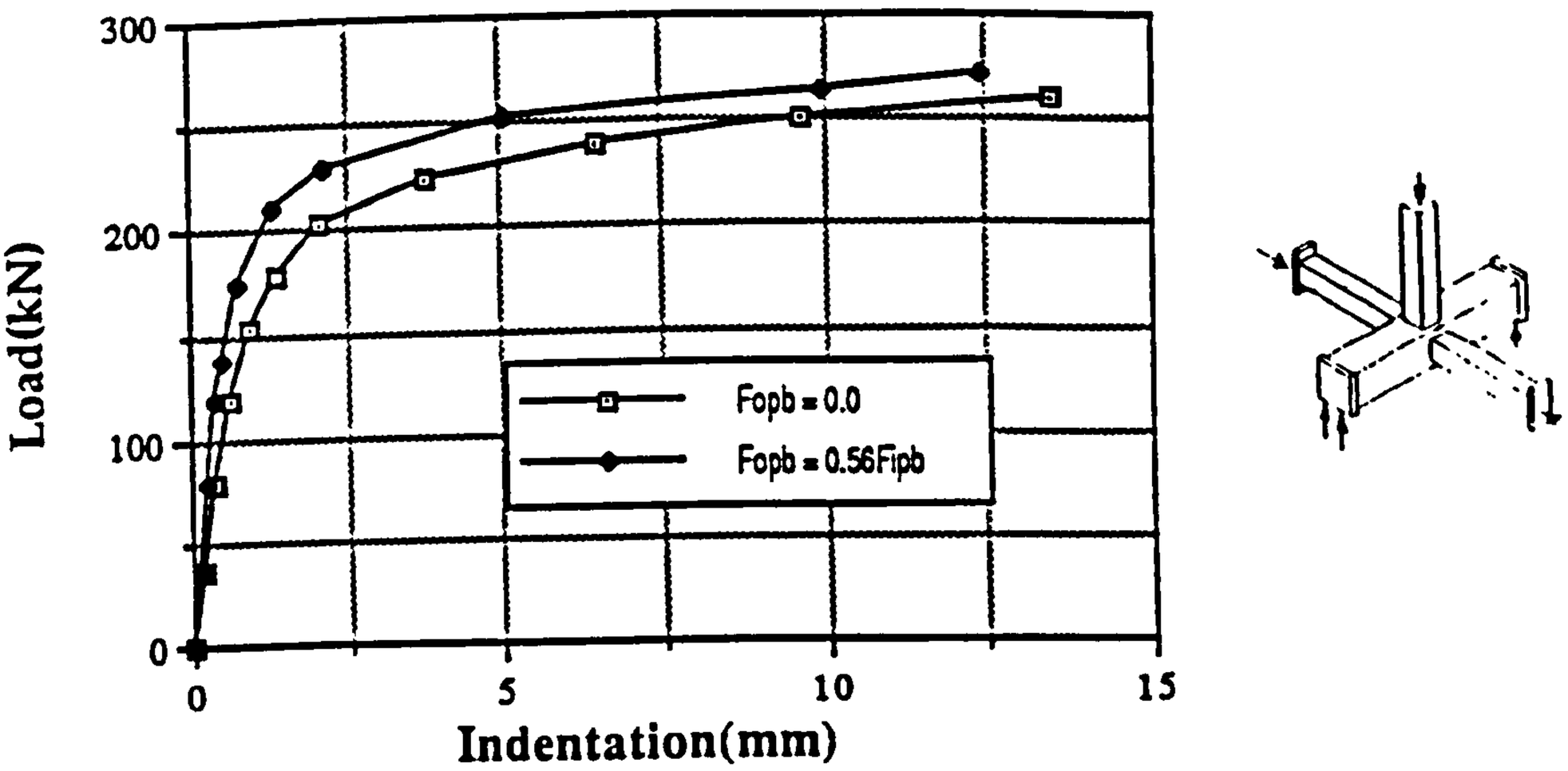

Figure 6.5 Effect of Fopb being Compressive on the $\beta = 0.6$ Multiplanar Joint

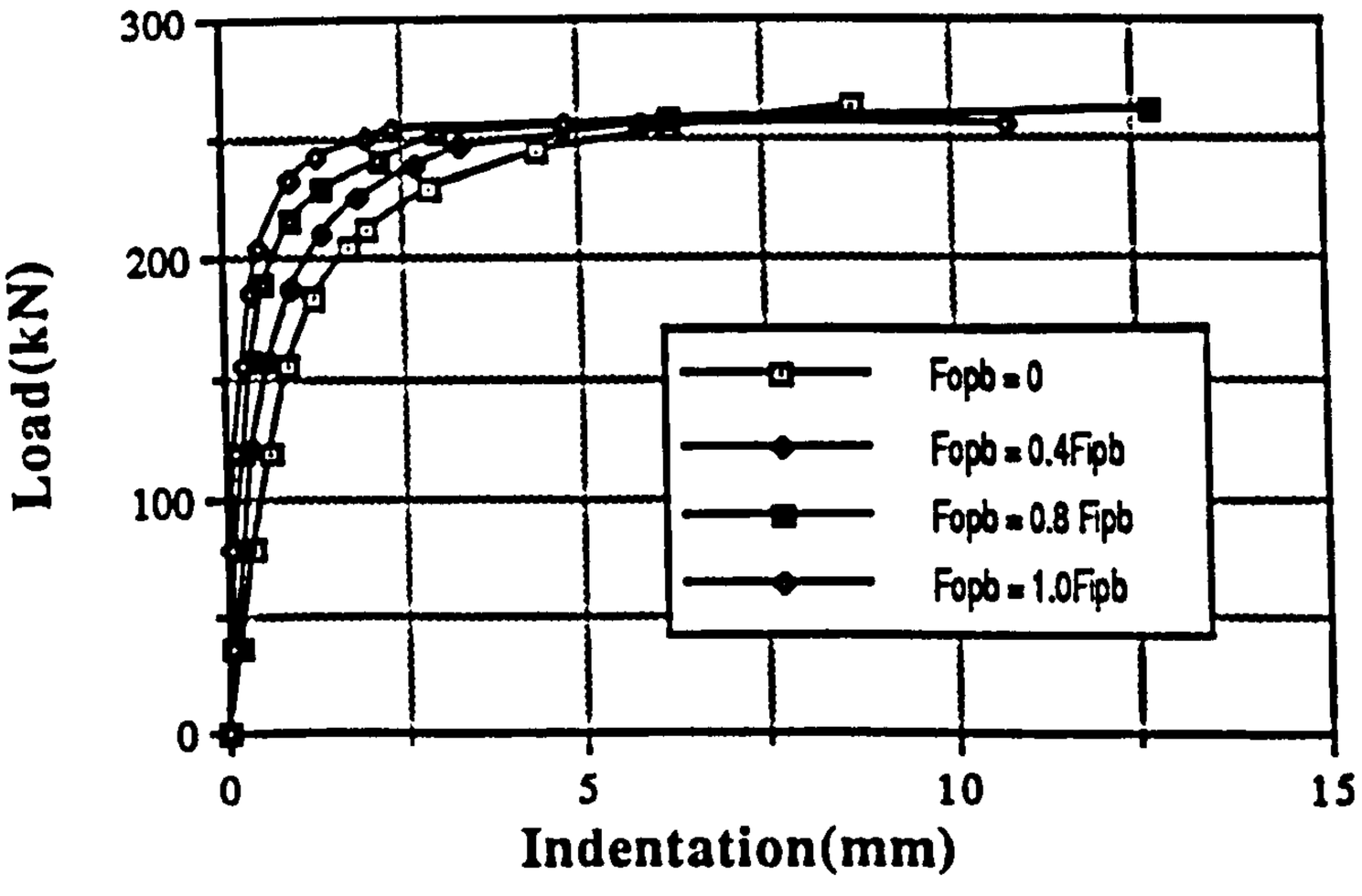

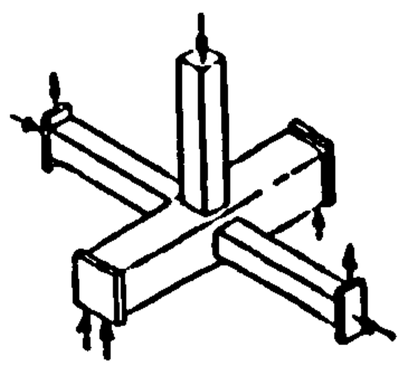

Figure 6.6 Load vs Indentation for F_{opb} $\beta = 0.6$ Compressive Series

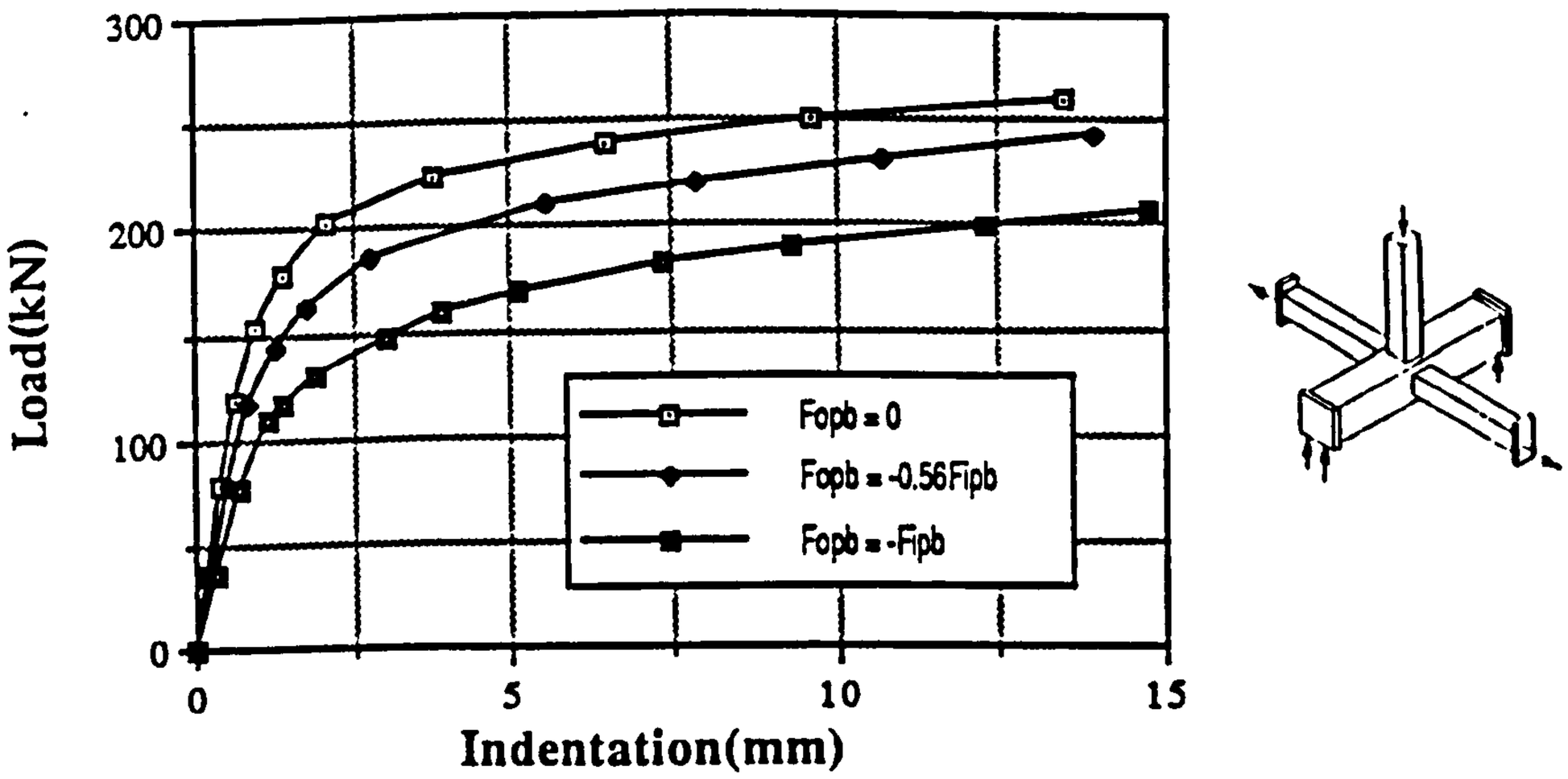

Figure 6.7 Effect of Fopb being Tensile on the $\beta = 0.6$ Multiplanar Joint

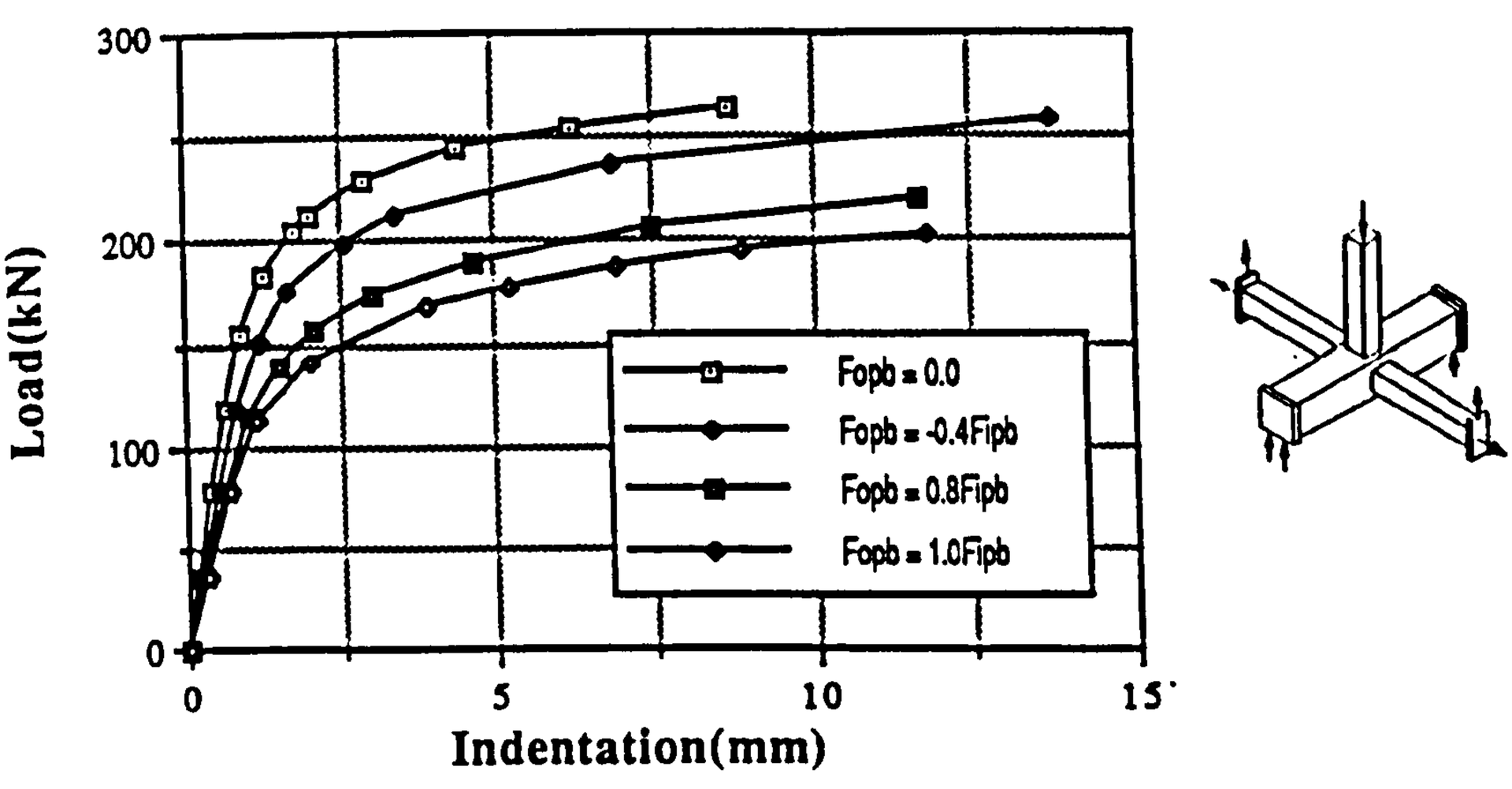

Figure 6.8 Load vs Indentation for F_{opb} Tensile $\beta = 0.6$ Series

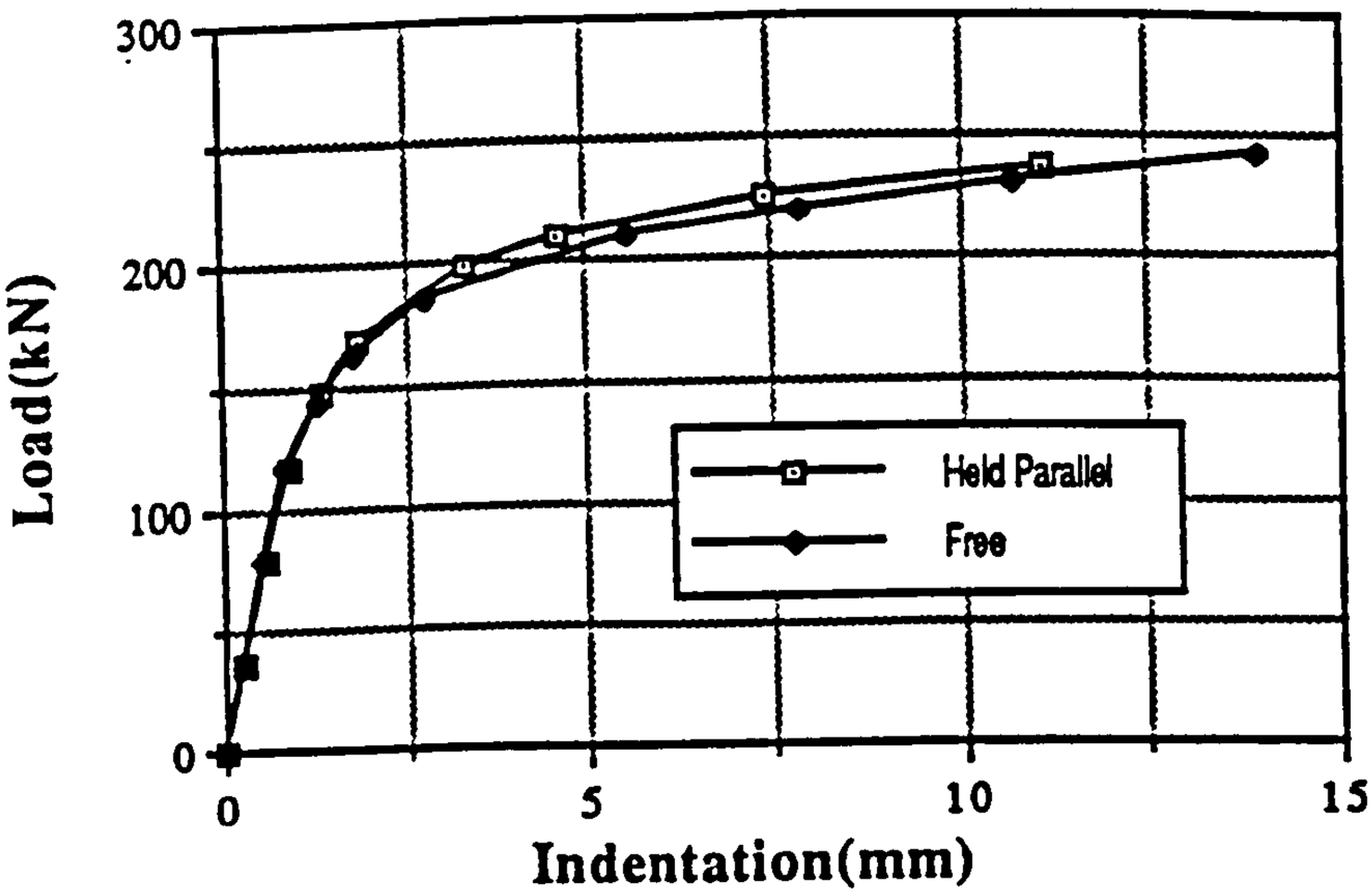

Figure 6.9 Comparison between Restraint Methods (F_{opb} tensile)

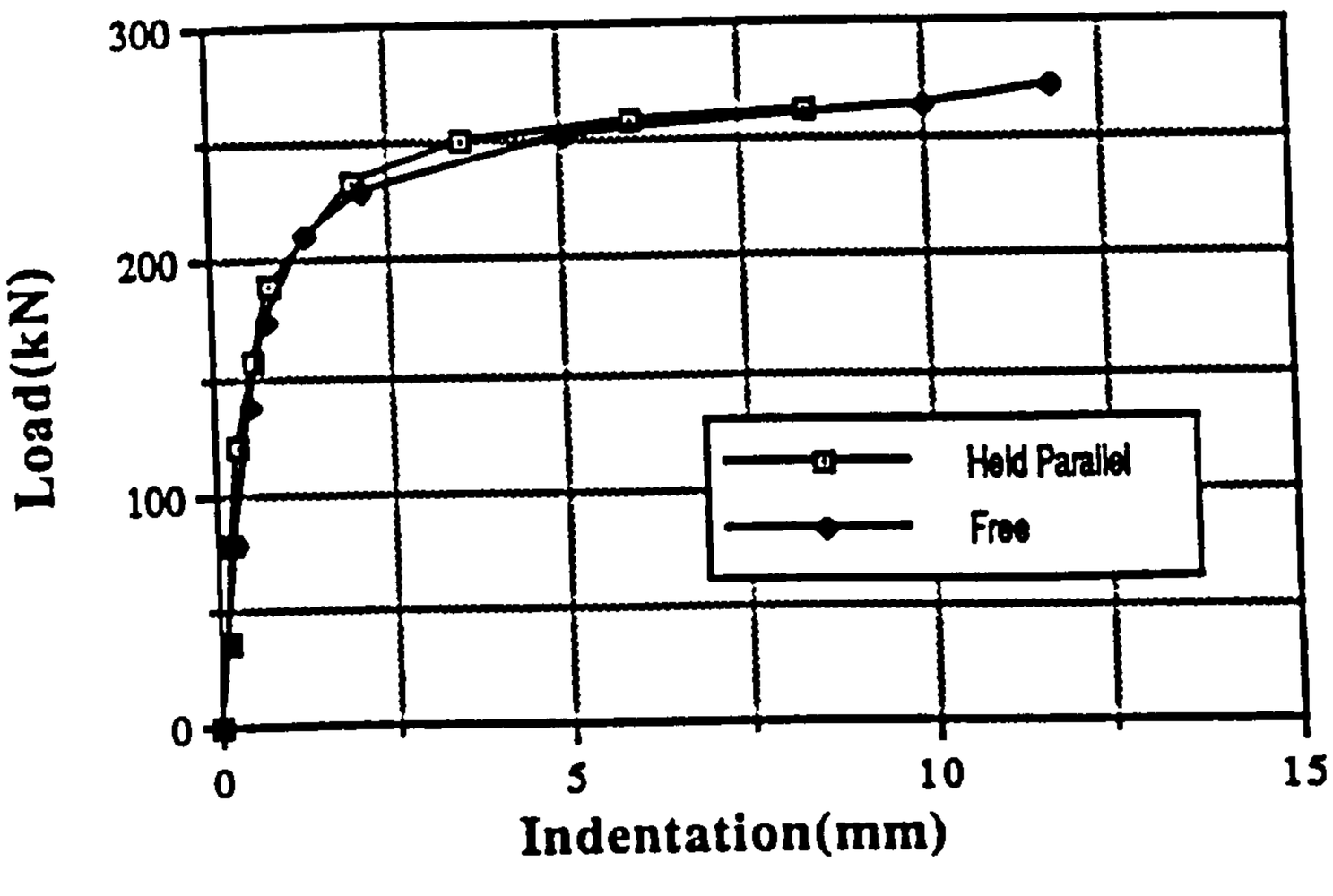

Figure 6.10 Comparison between Restraint Methods (F_{opb} compressive)

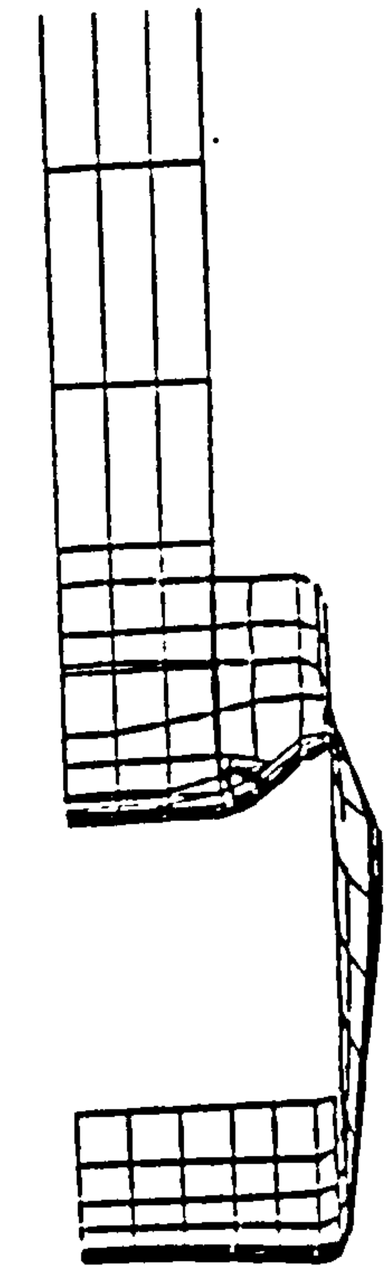

(a) Planar Joint

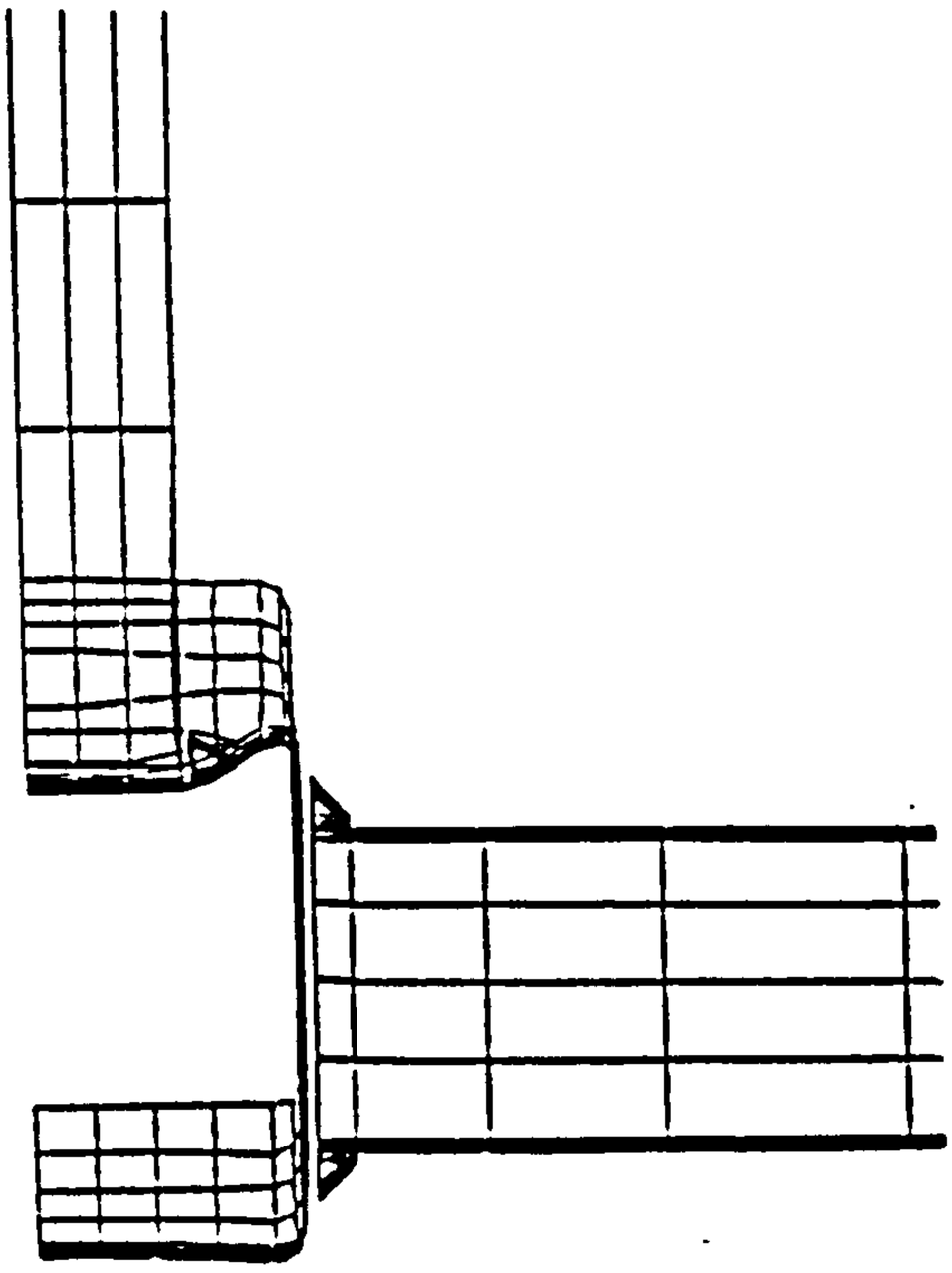

(b) Multiplanar Joint F_{opb} = 0.0, OPBs Held Parallel.

Figure 6.11 Displaced Shape Plots for Planar and F_{opb} = 0 Multiplanar Joints (β = 0.6)

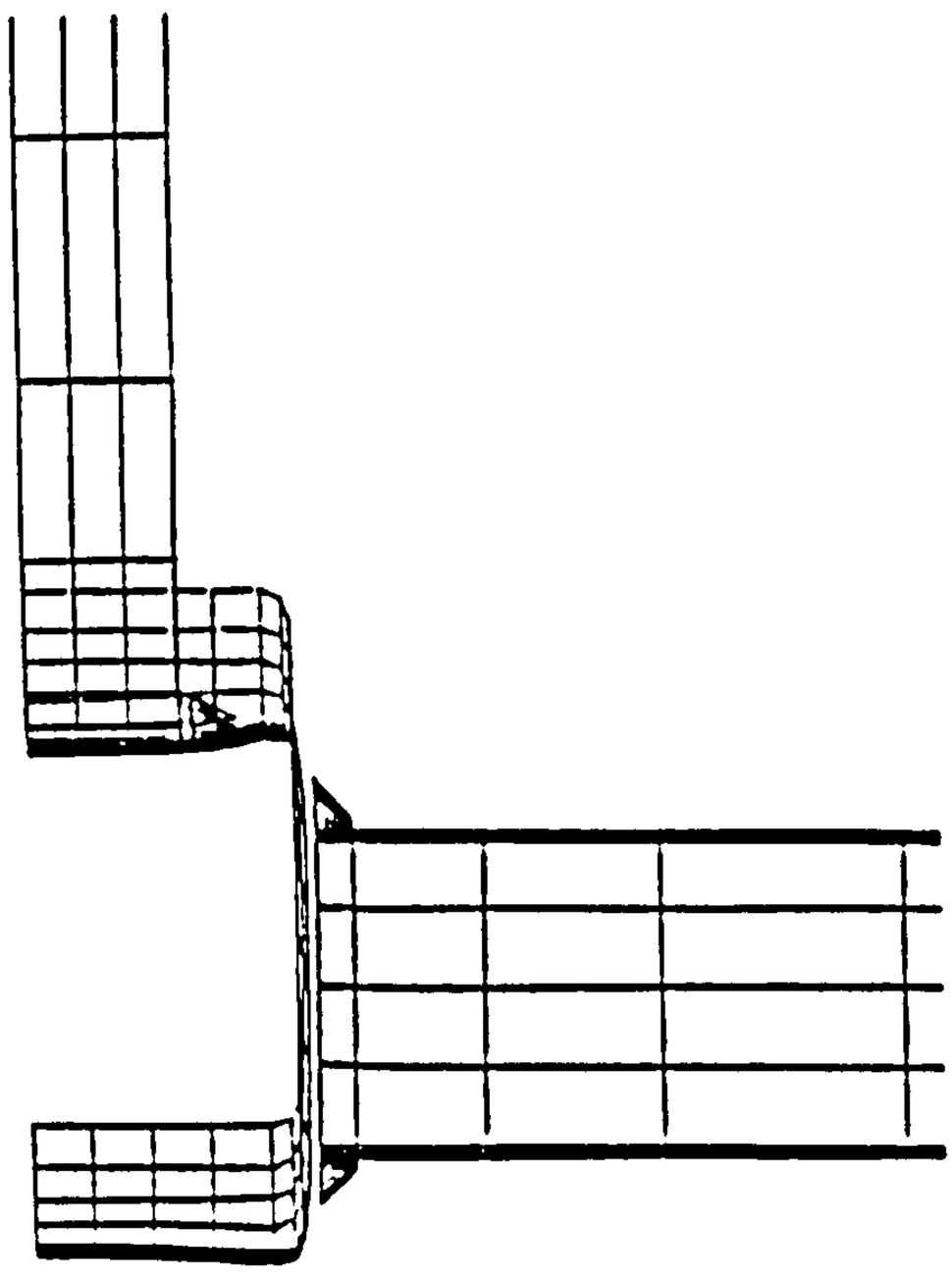

(a) Multiplanar Joint $F_{opb} = -0.56F_{ipb}$, OPBs Held Parallel.

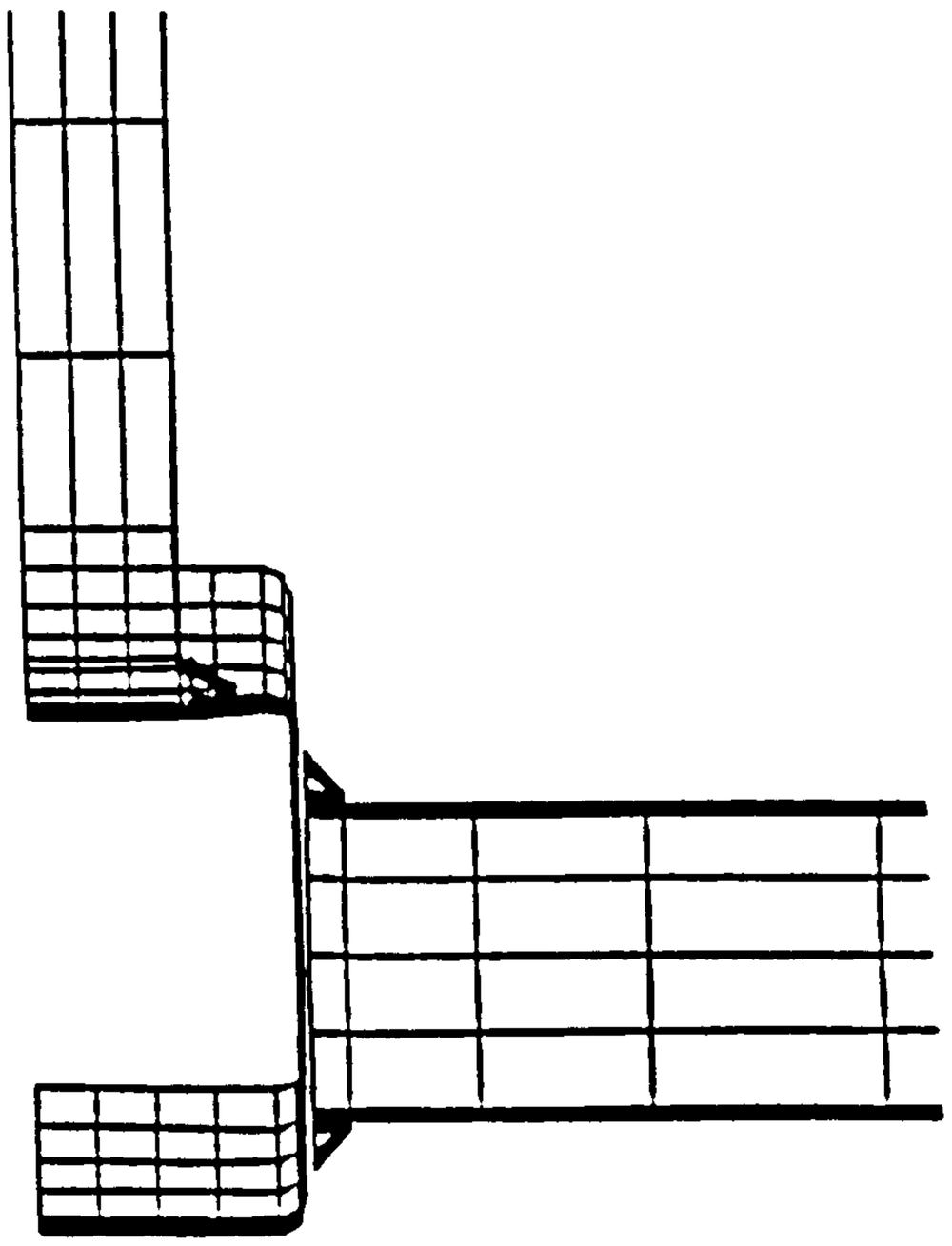

(b) Multiplanar Joint $F_{opb} = 0.56F_{ipb}$, OPBs Held Parallel.

Figure 6.12 Displaced Shape Plots for F_{opb} = +/-0.56F_{ipb} Multiplanar Joints (β = 0.6)

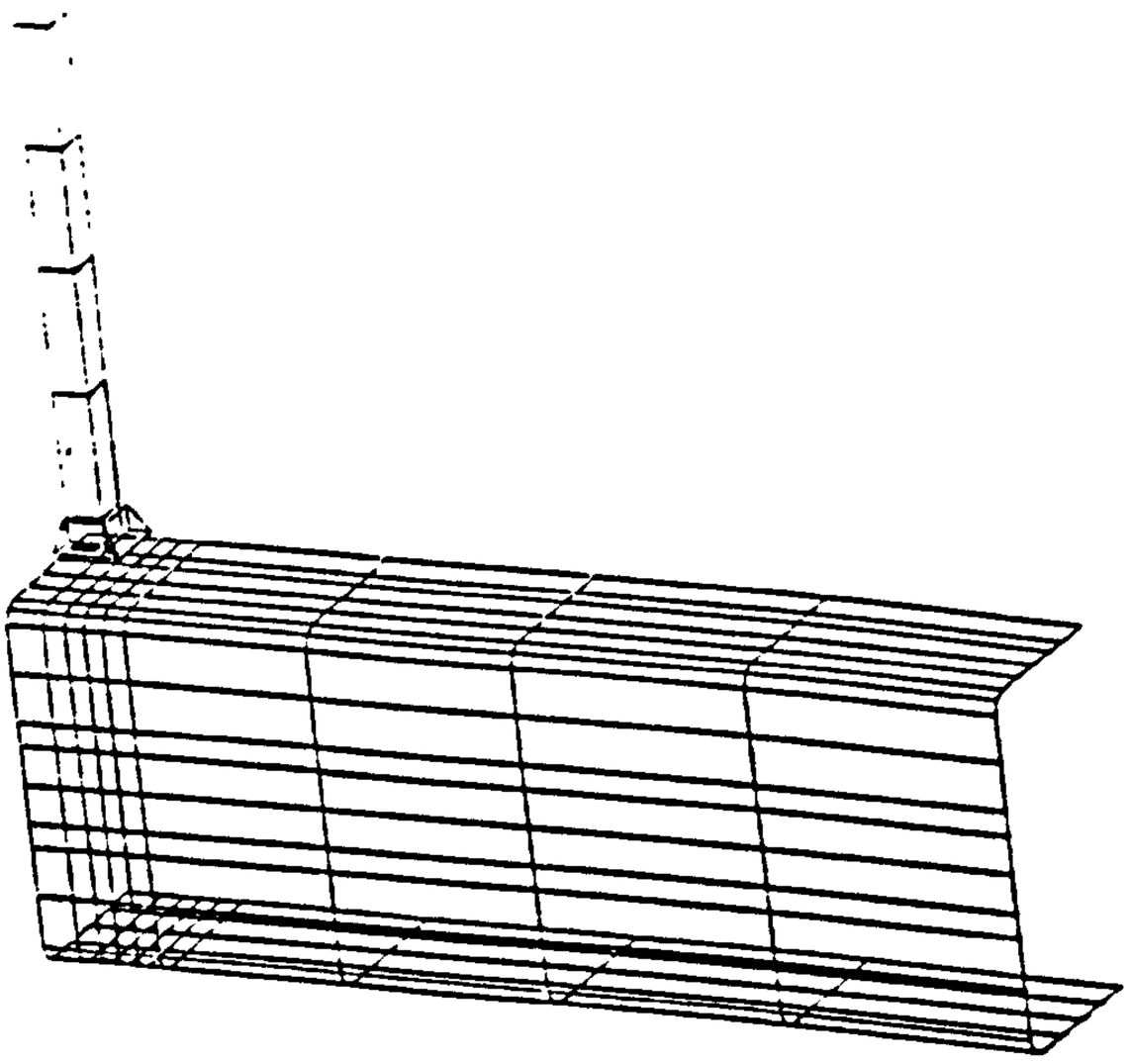

Figure 6.13 Mesh Used in $\beta = 0.25$ Analysis for Planar Joint

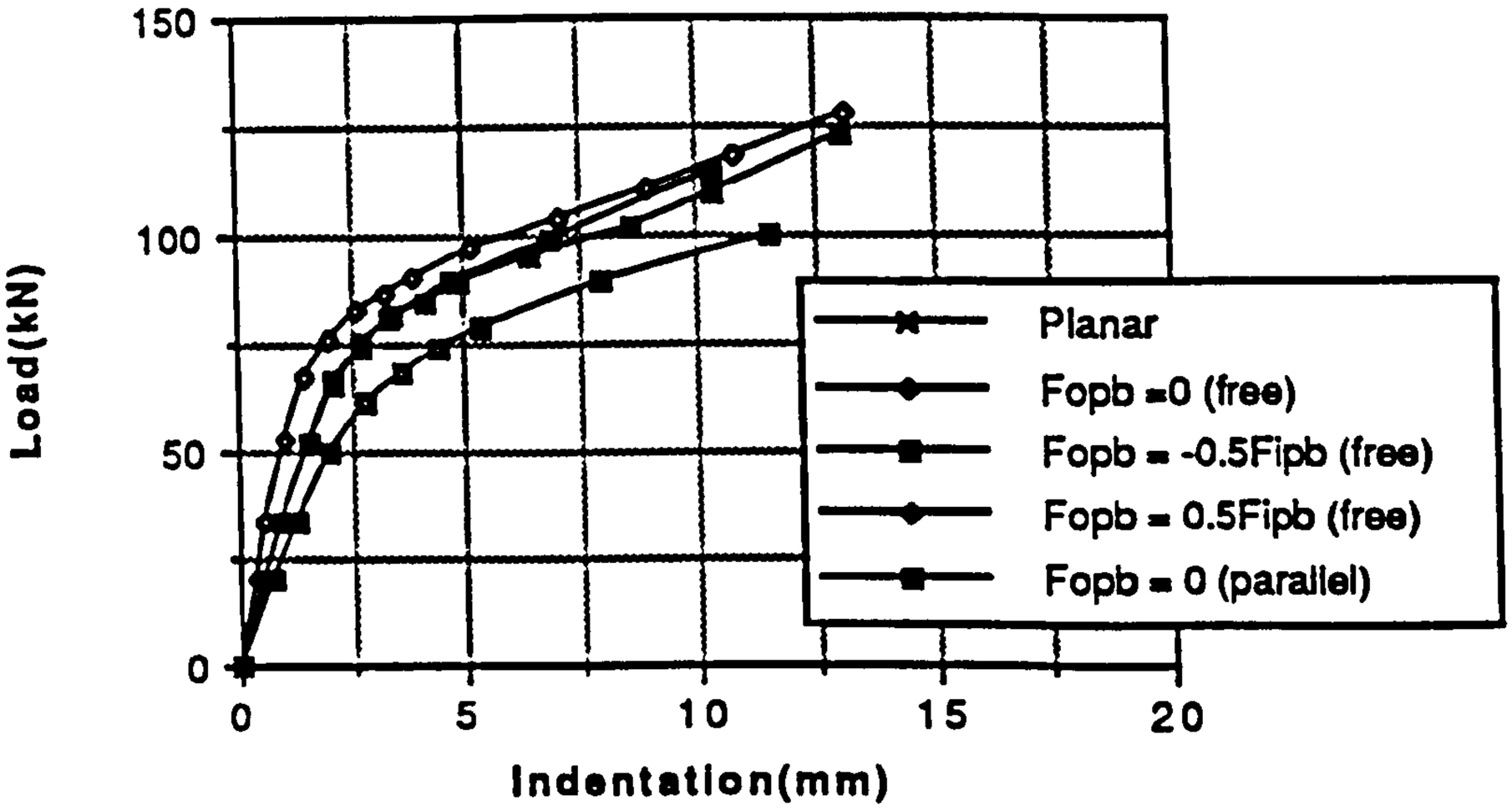

Figure 6.14 Load vs Indentation Plots for Several of the $\beta = 0.25$ Joints (Loading as Indicated).

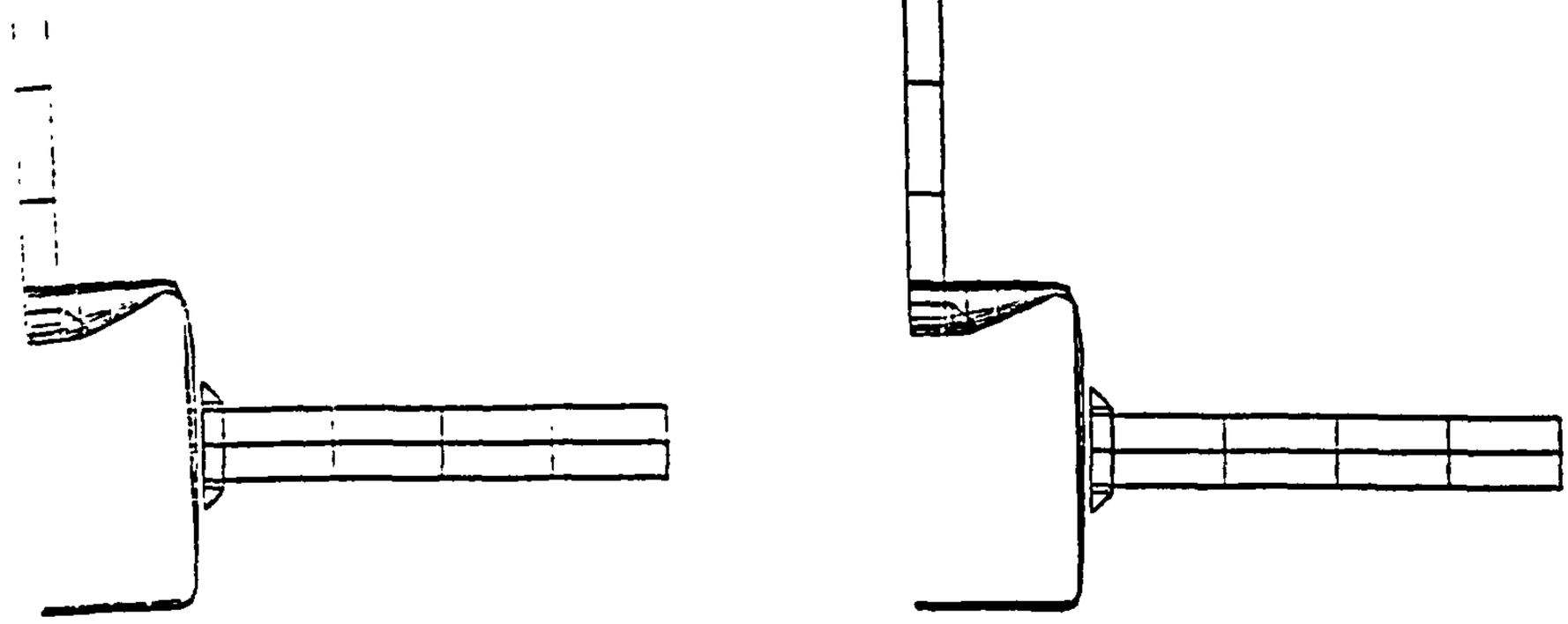

(a) Multiplanar Joint F_{opb} = 0.0,

OPBs Free to Rotate.

(b) Multiplanar Joint F_{opb} = 0.0,

OPBs Held Parallel.

Figure 6.15 Displaced Shapes for Two of the β = 0.25 Joints

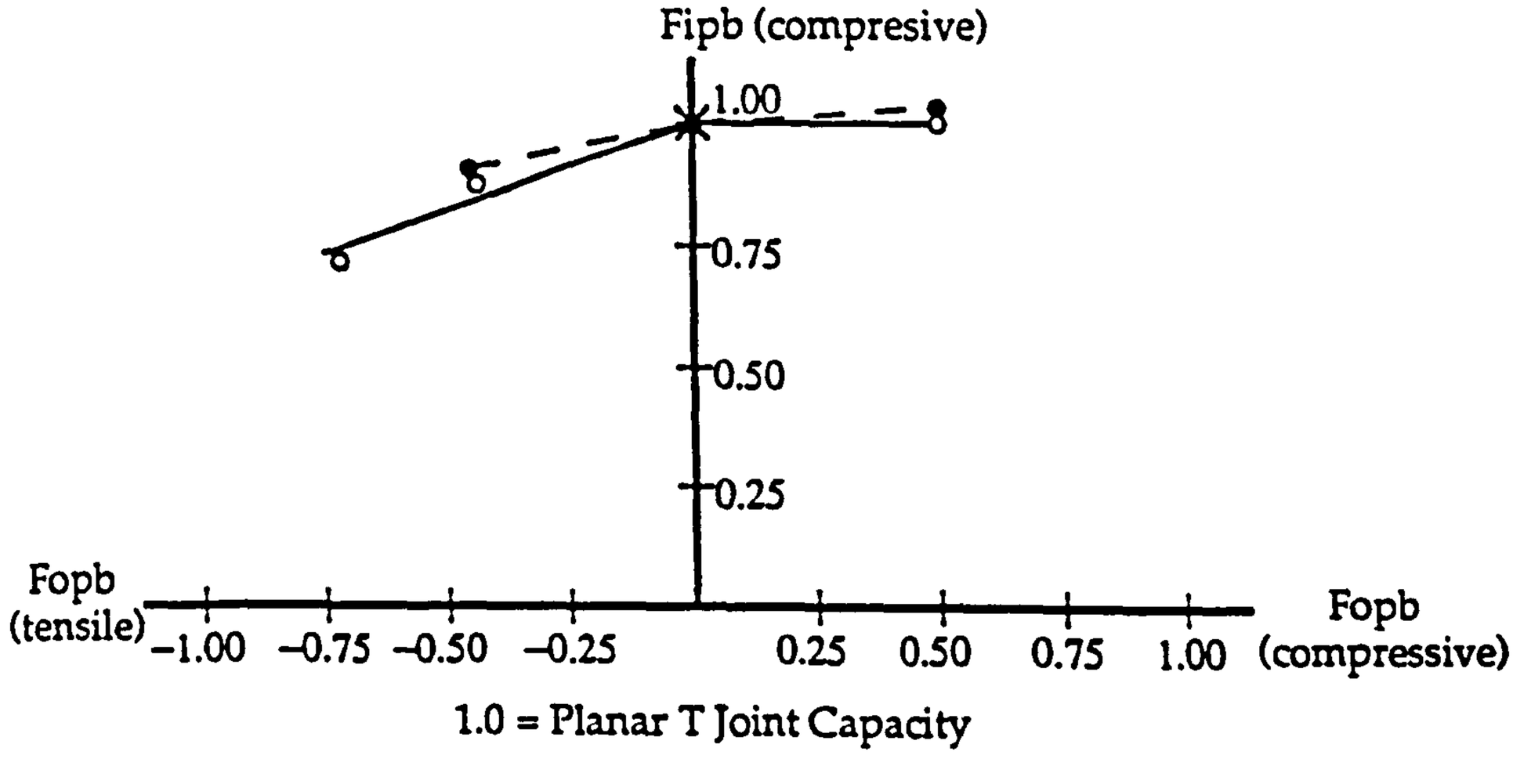

Figure 6.16 β = 0.25 Interaction Diagram (1.0 = Planar FE Capacity)

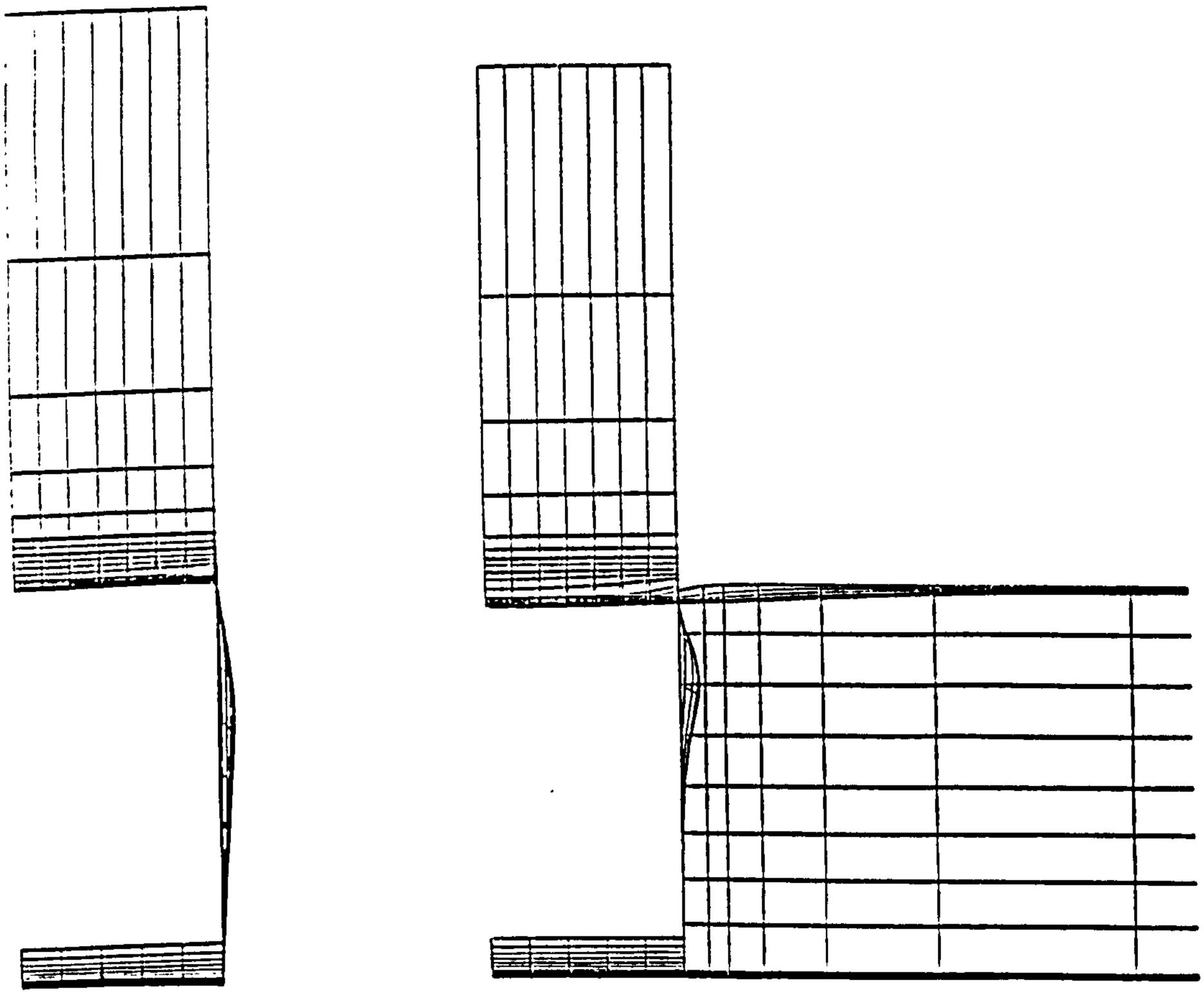

Figure 6.17 Displaced Shape Plots for Planar and F_{opb} = 0 Multiplanar Joints (β = 1.0)

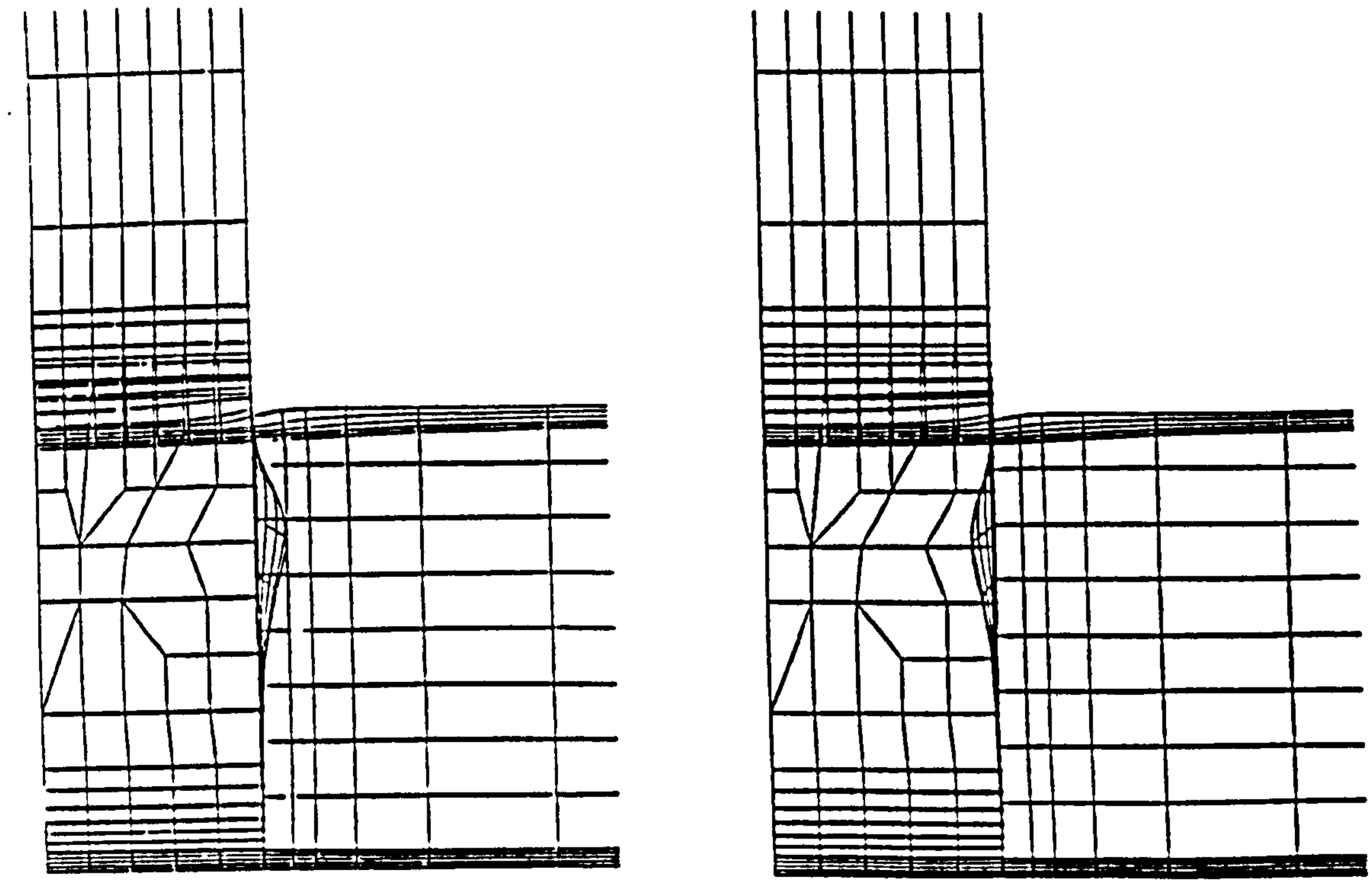

Figure 6.18 Displaced Shape Plots for F_{opb} = +/-0.5F_{ipb} Multiplanar Joints (β = 1.0)

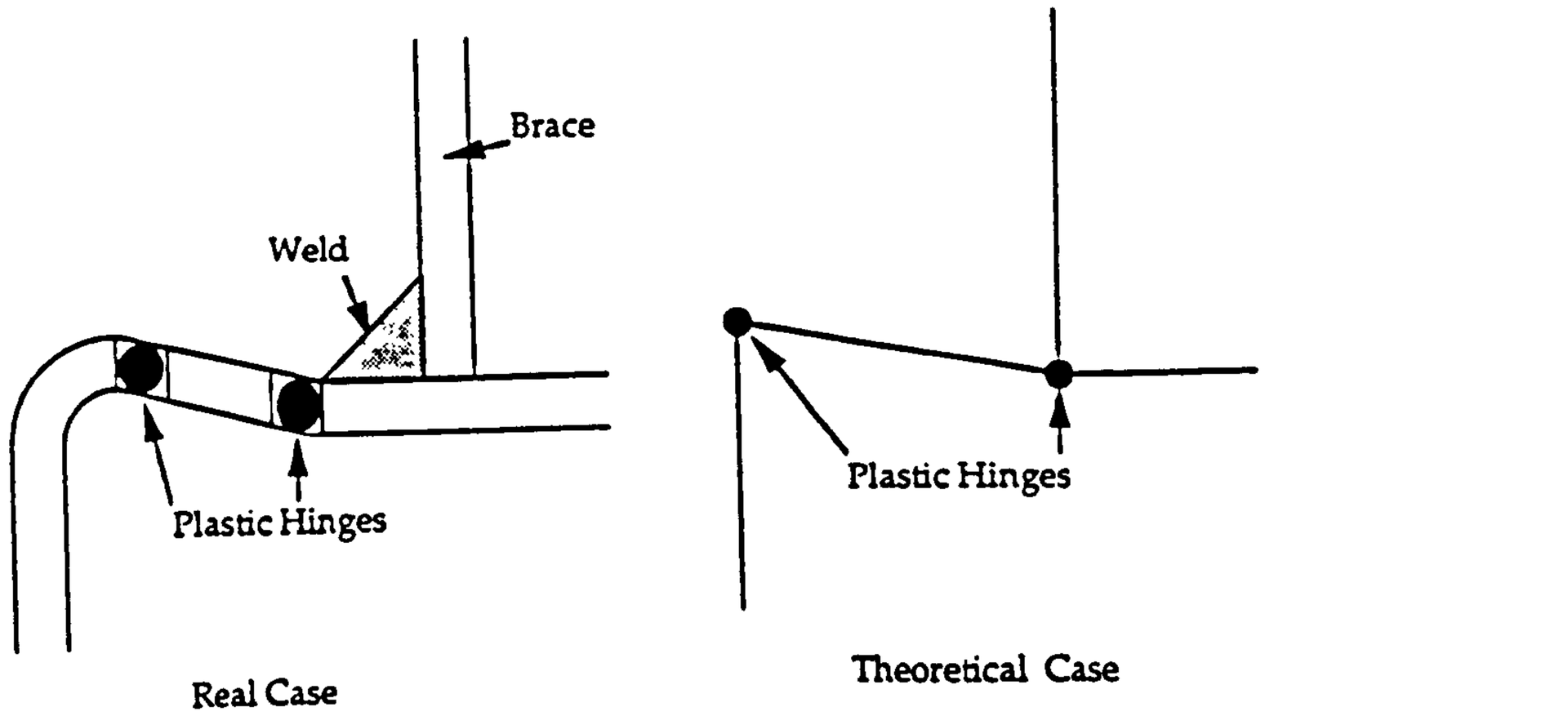

Figure 6.19 Yield Line Mechanisms

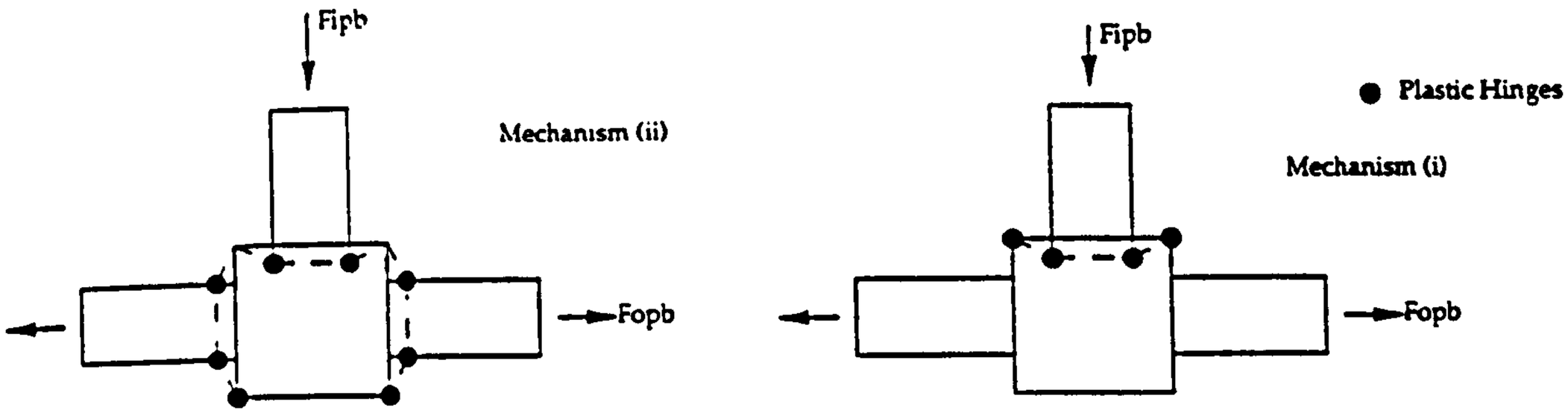

Figure 6.20 Differences between Idealised Yield Line Theory and Actual Hinge Formation in Reality

CHAPTER 7

MULTIPLANAR CHS T-DT JOINTS.

7.1 Introduction

As a comparison to the RHS T-DT joint strength interaction diagrams established in the previous chapter, an FE investigation using techniques developed in Chapter 3 was undertaken on CHS T-DT joints under axial loads to determine whether similar trends and behaviour would be observed. The work would also complement the work undertaken by Vegte et al (1991) on DT-DT CHS joints under axial loads and Paul et al (1991) on T-T joints under axial loads. Basic definitions of the joint configurations were given in Table 2.1 but the joints referred to in this chapter are shown again for clarity in Figure 7.1.

As mentioned earlier design of CHS multiplanar joints is traditionally based on a plane by plane basis. However as was shown by Vegte et al (1991) the presence of out-of-plane braces can enhance capacity and the presence of forces within these braces may further add to or reduce the capacity of the joint.

In this chapter non-linear FE analysis has been undertaken on T-DT joints at two different β ratios, 0.6 and 0.25 and $D/t_o = 23.8$. As with

the RHS joints in Chapter 6 various restraint conditions are considered on the out-of-plane braces (DT) to investigate the 'frame' effect on the capacity of the joint.

7.2 Joint Geometry and Load Effects β = 0.6 Joints

The general layout and dimensions of the β = 0.6 multiplanar joints are illustrated in Figure 7.2. These were chosen to correspond to those external dimensions of the RHS joints of β ratio 0.6 analysed in Chapters 4 and 6. The chord and brace FE model ends had 'stiff' diaphragm end plates attached through which the pinned supports and the axial loads could be applied to the braces. Restraint of the out-of-plane (DT) braces (OPBs) took one of two forms for the main analyses series. First the ends of the OPB's (DT) were completely free to rotate as the joint was loaded but any loads applied to them remaining parallel to their original line of action. The second restraint condition, as for the RHS joints in Chapter 4 was to constrain these braces to remain parallel as the joint was loaded, thus ensuring that the P-δ effect was substantially reduced. Further analyses for selected loading conditions under different boundary restraints were undertaken in Section 7.4.2 where it was felt that restraint conditions were having a significant effect on the behaviour and capacity of the joints.

7.3 Finite Element Modelling of the $\beta = 0.6$ Joint Series

7.3.1 Model Arrangement and Boundary Conditions

Using the symmetry of the joints only one quarter of the joint needed to be modelled. Restraint conditions similar to those illustrated in Figure 3.3 in Chapter 3 were applied to ensure these conditions were met. Due to the difficulties in generating the more irregular meshes and complex intersection geometry in circular members, a different method of mesh generation had to be found to that used for RHS. The mesh and geometry generating package FEMGEN (Femview Limited 1989) was used this being available by the kind permission of the Department of Mechanical Engineering at Nottingham University. Due to their quadratic shape formulation (i.e they can be initially curved on their boundaries), eight noded isoparametric thick shell elements (ABAQUS element S8R) were used for the brace and chord members, these being capable of modelling the curvature present in CHS. Material properties were taken as identical to those of the RHS multiplanar joints as shown in Table 3.1.

The initial mesh was graded according to experience gained in the modelling of the RHS joints earlier in Chapter 4. However by using supercomputing facilities at the Manchester Regional Computing Centre, a second 'finer' mesh was analysed. These two meshes are illustrated in Figure 7.3, the finer mesh containing 68% more elements than the less dense mesh used as the basis for the analysis. No weld modelling was undertaken in this mesh density investigation. The load vs IPB indentation plots for these two meshes are shown in Figure

7.4, no loading being applied to the OPBs during the convergence study. In-plane brace (T) indentation is measured as the change in length between a point at a height of 250mm (from the underside of the chord) on the brace and the central point on the underside of the chord. This is shown in Figure 7.2 as points p1 and p2. As can be seen the increasing of the number of elements by 68% does not effect the capacity or behaviour significantly establishing alongside the design code checks discussed in Section 7.3.3, that the medium mesh in Figure 7.3 is giving realistic ultimate capacity results and can be used in the main comparative analysis series.

7.3.2 Modelling of the Weld and Initial Boundary Condition Effects

As for the RHS joints (see Chapter 3) it was anticipated that non-inclusion of the weld in the FE modelling would give low capacities when compared to available experimental data. This was confirmed when the analysis of the planar T joint with simple supports on the chord ends gave an ultimate capacity of 206kN compared to the HSE (1990) design capacity of 212kN and mean of the test database of 276kN. Thus, as anticipated modelling of the weld is necessary to give realistic results. Initially as in the RHS modelling six noded solids were used (weld case (a) from Section 3.4.2.1), these having their nodes shared with the corner nodes of the eight noded shell elements of the brace and chord. The positions of these nodes were determined by the brace and chord geometry and the desire to maintain the weld throat thickness as 6.8mm (see Figure 3.6(a) in Chapter 3). This weld thickness was taken as the value from the RHS laboratory specimens described in

Chapter 3 whose brace and chord material thicknesses and external specimen dimensions were similar to those used here. Basic details of these weld dimensions are shown in Figure 7.5 at the crown and saddle locations. Vegte et al (1991) and de Koning et al (1992) have used eight noded shell elements in the modelling of the welds in CHS multiplanar connections but difficulties arise in choosing the appropriate element thickness and the need to avoid the possibility of their buckling. This approach was investigated here also on the planar joint, the assumed throat thickness (t_w) of 6.8mm being used as the thickness for these weld elements. A more thorough discussion of the advantages and disadvantages of the weld models was given in Chapter 3 (Section 3.5) and it is not felt necessary to repeat this here. Results of the three simply supported analyses on the planar T joint are shown in Figure 7.6.

7.3.3 Check of Meshes to HSE (1990) Guidance and Existing Databases

The multiplanar joint mesh used in the main series of analyses on the $\beta = 0.6$ joint series is shown in Figure 7.7, complete with the solid weld element model described in 7.3.2. Material properties were identical to the RHS in Chapter 4, having a yield strength of $420N/mm^2$ with an ultimate tensile strength of $540N/mm^2$. These properties were tabulated in Table 3.1 and shown in Figure 3.2. To establish whether this mesh was giving realistic results alternate braces and their welds were removed (OPBs removed to analyse as a T joint and the IPB removed to analyse as a DT joint) and the planar ultimate capacities obtained from these compared with the characteristic (design)

and mean values available in the HSE (1990), API (1991) and IIW (1989) design guides.

$$\text{HSE mean strength} = f_y t_o^2 (2.37 + 23.60\beta)\sqrt{Q_\beta'}\, K_a Q_g \quad \text{Eqn [7.1]}$$

$$\text{HSE characteristic} = f_y t_o^2 (1.82 + 18.17\beta)\sqrt{Q_\beta'}\, K_a Q_g \quad \text{Eqn [7.2]}$$

$$\text{API} = f_y t_o^2 (3.4 + 19\beta)\, Q_f \quad Q_f = 1.0 \text{ if no chord load} \quad \text{Eqn [7.3]}$$

$$\text{IIW} = p_y t_o^2 (2.8 + 14.2\beta^2)\gamma^{0.2} \quad \text{Eqn [7.4]}$$

where the symbols are as defined in the initial notation section.

The capacities obtained are tabulated alongside the design guidance in Table 7.1. FE capacities are determined as described earlier in Chapter 3, being peak load (if one reached) or the intersection of the elastic and plastic sections of the load vs indentation curves. The indentation for the DT joint was taken as that of the average displacement of two nodes, one on the topside and one on the lower side of the brace towards the centreline of the chord. These are shown as p3 and p4 in Figure 7.2.

all (kN)	Finite Element	HSE (mean) Eqn [7.1]	HSE (design) Eqn [7.2]	API (design) Eqn [7.3]	IIW Eqn [7.4]
T	251	276	212	248	216
DT	240	204	182	187	169

Table 7.1 Comparison of Planar FE Results with Code Capacities for the $\beta = 0.6$ Joints.

7.4 Analysis of the β = 0.6 Joint Series

7.4.1.The Main Multiplanar Analysis Series

Using the model illustrated in Figure 7.7 a comprehensive range of analyses under a combination of both in-plane and out-of-plane tensile and compressive axial loads was undertaken. These loads F_{ipb} and F_{opb} are illustrated in Figure 7.2. Two restraint conditions for the ends of the OPBs (DT) were studied, one where the DT braces were free to deflect and rotate at their ends and one where they were constrained to remain parallel during the analysis, these being described in Section 7.2. Using the methods for determining failure described in Section 7.3.3 an interaction diagram was established both of these restraint conditions under in-plane axial compression and a full range of tension and compression in the OPBs. The condition where the OPBs were free to rotate was then analysed under in-plane (T brace) tension also. These diagrams are shown in Figure 7.8, the other isolated analyses labelled on this being described later. Planar results are also plotted here for both the T and DT axial compression cases. Table 7.2 details the ultimate loads for all the loading combinations analysed alongside the details of their boundary conditions.

Joint Type	F_{ipb}	F_{opb}	Joint Capacity F_{ipb} (kN)	Joint Capacity F_{opb} (kN)	Brace of Failure	Boundary (DT braces) Peak or el-pl
Planar T	1.0 C		252	-	T	-
M-planar	1.0 C	0.5 C	298	149	T	Free - Peak
M-planar	1.0 C	1.0 C	184	184	DT	Free - Peak
M-planar	0.0	1.0 C	0	179	DT	Free - Peak
M-planar	0.5 T	1.0 C	-83	166	DT	Free - Peak
M-planar	1.0 T	1.0 C	-150	150	DT	Free - Peak
Planar DT	-	1.0 C	-	240	DT	-
M-planar	1.0 C	0	288	0	T	Free - Peak
M-planar	1.0 C	0.5 T	230	-115	T	Free - El-pl
M-planar	1.0 C	1.0 T	176	-176	DT	Free - El-pl
M-planar	0.5 C	1.0 T	117	-234	DT	Free - El-pl
M-planar	0.0	1.0 T	0	-275	DT	Free - El-pl
M-planar	1.0 T	1.0 T	-300	-300	DT	Free - Peak
M-planar	1.0 T	0.5 T	-275	-138	T	Free - El-pl
M-planar	1.0 T	0.5 C	-240	120	DT	Free - Peak
M-planar	1.0 C	1.0 C	300	300	DT	Parallel - Peak
M-planar	0.0	1.0C	0	300	DT	Parallel - Peak
M-planar	1.0 C	0.0	296	0	T	Parallel - Peak
M-planar	1.0 C	1.0 T	174	-174	T	Parallel - El-pl
M-planar	0.0	1.0 C	0	254	DT	Free * - Peak

Table 7.2 Joint series $\beta = 0.6$ for T-DT joints under combined axial loading. * Follower option applied.

Figure 7.9 shows the load vs IPB axial compression indentation for a series of joints under combined axial loading where the OPBs are free to rotate, together with the planar T joint. Figure 7.10 shows a similar plot for the cases where the out-of-plane (DT) braces are constrained to remain parallel. The indentation for the joint in Figure 7.10 where $F_{ipb} = F_{opb}$ is that of the OPBs (DT) which was established as described earlier in 7.3.3. Failure as a DT joint in compression becomes critical here where the compressive forces in the in-plane (T) and out-of-plane (DT) braces are equal, this being verified by all the design code recommendations as shown in Table 7.1. In Figure 7.11 the two analyses undertaken where $F_{ipb} = 0.0$ and F_{opb} is compressive, load vs indentation plots are compared with those of the planar DT joint analysed in Section 7.3.3. Displaced shape plots for the series of joints with free OPBs in Figure 7.9 are illustrated in Figure 7.12 at peak loads or in the initial stages of the plastic plateau.

7.4.2. Effect of OPB Boundary Conditions on Behaviour of T-DT Joints.

As can be seen in Figure 7.8, the restraint conditions applied to the OPBs of the T-DT joint can have a very significant effect on the capacity, for example the case where $F_{ipb} = 0.0$, F_{opb} is compressive and these braces are free to rotate having a capacity lower than that of the planar DT case (see also Figure 7.11). This will be discussed more fully later. It was however speculated that the rotation of these (DT) OPB's while their axial loads (F_{opb}) remained parallel may cause significant secondary moments in the braces thus reducing ultimate capacity. This is illustrated in Figure 7.13. As this would appear to cause large

differences in ultimate capacity (see Figure 7.11), several extra analyses were undertaken under varying boundary conditions. Firstly the analysis with the out-of-plane braces free to rotate was re-analysed (F_{ipb} = 0) under out-of-plane axial compression with the load *FOLLOWER option available in ABAQUS (1991) applied. This option ensures that the applied load rotates through the same angle as the node to which it is applied in the model, thus effectively eliminating secondary moments and ensuring the load remains axial. The load vs indentation results for this analysis are added to those of Figure 7.11 in Figure 7.14.

7.5 Analysis and Modelling of the β = 0.25 Joint Series

To investigate the effects of β ratio on the multiplanar capacity a second series of analyses were undertaken at a β ratio of 0.25, other dimensions being unchanged.

7.5.1 Modelling and Geometry of the β = 0.25 Joints

Apart from the bracing width (reduced to 37.5 mm from 90.0mm) all other dimensions remained the same as those of the β = 0.6 joint series. This layout is shown in Figure 7.15 alongside the loading modes F_{ipb} and F_{opb}. As with the β = 0.6 joints material properties were taken as those of the RHS joints and are detailed in Chapter 3, Table 3.1. FEMGEN (Femview Limited 1989) was again utilised to generate the models and the weld modelling was included directly as a solid weld as described in 7.3.2. Again the nodal points of the weld elements were

determined on the basis of maintaining the weld throat thickness to 6.8mm for reasons discussed earlier.

7.5.2 Basic Calibration to the Codes of Practice, $\beta = 0.25$

The OPBs (DT) and their welds were removed from the model to facilitate comparison as a planar T joint under axial compression with design guide predictions. In a similar fashion the in-plane (T) brace was removed and the analysis undertaken as an out-of-plane (DT) planar joint under axial compression (with the braces restrained to remain parallel because of the lack of mesh symmetry in this plane). The capacities were determined as for the $\beta = 0.6$ joints as either peak load (if one was reached) or the elastic - plastic intersection as described in Chapter 4. The results from these two analyses are shown in Table 7.3 alongside the various code provisions.

	FE (kN)	HSE (mean) Eqn [7.1]	HSE (design) Eqn [7.2]	API Eqn [7.3]	IIW Eqn [7.4]
T	128	138	106	136	101
DT	139	114	102	111	109

Table 7.3 Comparison of Planar FE Results with Code Capacities for the $\beta = 0.25$ Joints.

7.5.3 Analysis of the Multiplanar Joint Series

For the $\beta = 0.25$ joint series, analyses were undertaken for a range of in-plane (T) compression and out-of-plane (DT) tensile and compressive axial loads. As for the $\beta = 0.6$ ratio joints, two restraint conditions were considered, that where the OPBs were free to rotate and that where these braces were constrained to remain parallel during the analysis. The results of the series of loading conditions are shown in the interaction diagram in Figure 7.16. Comparisons of load vs indentation curves are shown in Figure 7.17 for the planar case and three cases under zero, tensile and compressive out-of-plane (DT) loads with free to rotate out-of-plane (DT) braces. The points of measurement of this indentation are shown as p1 and p2 in Figure 7.15. Figure 7.18 shows the nett in-punch of the out-of-plane braces (DT) for the planar DT calibration case and the two multiplanar restraint cases where $F_{ipb} = 0$ and F_{opb} is compressive. Displaced shape plots for the series of joints in Figure 7.16 are shown in Figure 7.19. The capacities of the whole set of joints in this analyses series are shown in Table 7.4 alongside their respective boundary conditions.

Joint Type	F_{ipb}	F_{opb}	Joint Capacity		Brace of Failure	Restraint to DT braces
			F_{ipb} (kN)	F_{opb} (kN)		
Planar T	1.0 C		128	-	T	-
M-planar	1.0 C	0.0	128	-	T	Free
M-planar	1.0 C	0.0	135	-	T	Parallel
M-planar	1.0 C	0.5 T	112	-56	T	Free
M-planar	1.0 C	0.5 T	118	-59	T	Parallel
M-planar	1.0 C	1.0 T	103	-103	DT	Free
M-planar	1.0 C	1.0 T	103	-103	DT	Parallel
M-planar	1.0 C	0.5 C	140	70	T	Free
M-planar	1.0 C	0.5 C	154	77	T	Parallel
M-planar	1.0 C	1.0 C	92	92	DT	Free
M-planar	1.0 C	1.0 C	154	154	DT	Parallel
M-planar	0.0	1.0 C	0	92	DT	Free
M-planar	0.0	1.0 C	0	140	DT	Parallel
Planar DT	-	1.0 C	-	140	DT	-

Table 7.4 $\beta = 0.25$ Joint Series Peak Capacities. * Follower option applied

7.6 Discussion

7.6.1 Check of the FE Model to Planar Design Guidance and Weld Considerations

As stated in Section 7.3.2 the initial planar $\beta = 0.6$ T analysis without a weld gave an ultimate capacity some 25% below that of the HSE (1990) design guidance prediction (Figure 7.6) and slightly below the characteristic prediction. As this joint model was simply supported (typical of many experimental specimens), it would be anticipated that the FE analysis capacity would be close to the mean of the experimental database if the modelling was giving realistic results. It was concluded that the absence of the weld was playing a major part in the capacity falling below the mean. This conclusion was supported by evidence from the earlier RHS study in Chapter 3 where it was shown that the presence of the weld had a significant effect on the β ratio and hence ultimate capacity. As can be seen in Figure 7.5 the inclusion of the weld as six noded solids with $t_w = 6.8$mm or as eight noded shells with $t_w = 6.8$mm enhances ultimate capacity to 9% below the HSE mean (Table 7.2) and above the characteristic/design capacities of all the codes indicating that the planar T joint model is giving a reasonable capacity prediction within the experimental scatter. The planar FE T joint capacity will be plotted amongst the HSE experimental dataset used to arrive at the HSE mean and characteristic later in Chapter 8. The analysis as a planar $\beta = 0.6$ DT joint with the solid weld model in place in compression can be seen from Table 7.1 to be 17% above that of the HSE mean, a similar trend being observed in Table 7.3 for the planar β

= 0.25 DT joint analysis. This may seem a little high and no reason could be traced for this. However the ultimate capacities of a $\beta = 0.6$ planar DT joint experimentally tested and numerically modelled by Paul et al (1990) were 430kN (experimental) and 447kN (FE) compared to an HSE (1990) mean prediction of 373kN, these being 15% and 20% greater than the HSE mean.

7.6.2. The Multiplanar Interaction Diagram for T-DT Joints, $\beta = 0.6$.

7.6.2.1.Out-of-plane (DT) Braces Free to Rotate

As can be seen in Figure 7.9, the addition of the OPBs to the planar T model adds to both elastic stiffness and ultimate capacity for the $\beta = 0.6$ joints. Addition of compressive forces to these braces has little effect on the ultimate capacity until the magnitude of these is enough to cause failure as a DT joint in the OPBs. This can be seen in the top right quadrant of the intersection diagram in Figure 7.8. These findings suggest that the increase observed in strength by compressive axial loading in both planes of DT-DT joints (some 200% where $F_{ipb} = F_{opb}$) by Paul et al (1990) does not occur in T-DT joints.

Addition of tensile forces to the OPBs (DT) while the IPB remains in compression can be seen in Figure 7.9 to reduce capacity below that of the multiplanar case where $F_{opb} = 0$. When these tensile forces reach 50% of the in-plane (T) compressive force (i.e $F_{opb} = -0.5F_{ipb}$) then capacity can be seen to fall below that of the planar T joint in the top left quadrant of the interaction diagram in Figure 7.8. Design only considered on a plane by plane basis will therefore be unconservative.

These tensile loads reduce the elastic stiffness of the joint by approximately 200% over the multiplanar $F_{opb} = 0$ case, as can be seen in Figure 7.9.

Where tension exists in the IPB (T) and the OPBs (DT), capacity in either plane is similar. Analyses were only undertaken with the out-of-plane (DT) braces free as the effect of any secondary moments induced in this loading mode is to stabilise and reduce the local deflection δ as shown in Figure 7.13. This occurs because the axial tensile loads in the OPBs act to maintain these braces parallel to the joint. In the lower right quadrant (F_{ipb} is tensile and F_{opb} is compressive) similar effects to those in the upper right quadrant can be observed. When the tensile force in the IPB (T) reaches 50% of the compressive force in the OPBs (i.e F_{ipb}=-0.5F_{opb}) ultimate capacity can be seen to fall below that of the multiplanar case where $F_{ipb} = 0$ and F_{opb} is compressive by 25% and below that of the planar DT joint by almost 50%. The realism of this restraint condition can be questioned in practice since 'in-frame' behaviour is unlikely to allow complete freedom of the DT braces. Thus secondary moment effects are likely to be much less severe; nevertheless a reduction in capacity below that of a corresponding compressive loaded planar DT joint is possible.

7.6.2.2. Out-of-plane Braces (DT) Constrained to Remain Parallel

Considering the second restraint case where the arms are constrained to remain parallel during the analysis it can be seen from Figures 7.8 and 7.10 that the 'welding in' of the DT braces increases capacity over the planar joint by around 20%. It can also be seen that

constraining these braces to remain parallel during the analysis enhances capacity over the case where they were free to rotate.

When tensile forces are added to the out-of-plane (DT) braces, similar effects to those observed for the joints with free OPBs can be seen; again where these tensile forces exceed 50% of the in-plane (T) compressive force, capacity can be seen to fall below that of the planar joint with consequent implications for design. It can be noted however that the reduction below the planar capacity for this loading case (where $F_{opb} = -F_{ipb}$) is similar to that observed by Paul et al (1990) for the DT-DT joint configuration at $\beta = 0.6$. These reductions are compared in Table 7.5.

Comparison of the Multiplanar Effects	$\frac{\text{Multiplanar}}{\text{Planar}}$	% Reduction of Planar Capacity
Paul (1990) Multiplanar DT-DT / Planar DT capacity	$\frac{10.08}{13.73}$	26.6%
Nottingham Multiplanar T-DT / Planar T capacity	$\frac{183}{250}$	26.8%

Table 7.5 Delft and Nottingham Multiplanar/Planar capacities ($\beta = 0.6$).
(Delft - Paul et al 1990)

When compressive forces occur in the out-of-plane (DT) braces similar effects are observed to the free out-of-plane brace cases up to a point (approximately $F_{opb} = 0.6F_{ipb}$) where compression failure as a DT joint occurs for the free out-of-plane brace cases, this particular failure case being aggravated by rotation of the out-of-plane braces and the

induced secondary moment effects of this, this being discussed in more detail in 7.6.2.3. However where the DT braces are constrained to remain parallel this rotation and hence P-δ cannot occur and the presence of the IPB (T) adds to the DT joint capacity. The implications of this will be discussed in more detail in the next section where the extra analyses on specific boundary conditions are considered alongside the planar DT joint.

7.6.2.3 Boundary Effects in the Compression-Compression (top right) Quadrant of Figure 7.8.

Considering the cases where $F_{ipb} = 0$ and F_{opb} is a compressive load it can be seen that a large variation in capacity occurs between the two restraint cases (179kN to 300kN) with the planar DT analysis having a capacity of 240kN lying approximately midway between these two. It can thus be seen that the addition of the unloaded in-plane T brace to the joint adds 25% to capacity when the DT braces are held parallel.

However when the IPB (T) brace is added to the planar compression loaded DT case and the DT braces are unrestrained, capacity reduces by 30%. From the displaced shape plots in Figure 7.12 (c) it can be seen that the out-of-plane (DT) braces are rotating considerably where compressive forces are present in them. In this analysis the OPB (DT) forces remain parallel to their initial direction and hence if rotation is significant then considerable secondary moments may develop, this Pδ effect being illustrated in Figure 7.13. The effect of these secondary moments was eliminated and

investigated using the axial load (*FOLLOWER) option described in Section 7.4.2. The effects of this are shown in Figure 7.14 alongside the other three analyses considered in this section. It can be seen that eliminating the secondary moment by maintaining the load as axial, while allowing the rotation of the out-of-plane (DT) braces gives an ultimate capacity slightly greater than that of the planar DT joint confirming the suspicion that the P-δ effect was influencing the capacity.

Where the out-of-plane (DT) braces were pinned at the ends to stop vertical deflection and the follower (axial load option) used, peak capacity was enhanced to 343.5kN for the same loading case (F_{opb} = $0.5F_{ipb}$). Again this analysis was undertaken to quantify the effects of extreme boundary conditions on capacity, this condition being unlikely to occur in practice.

7.6.3 Discussion Multiplanar Interaction Diagram β = 0.25 Joints.

The calibrations of the planar T and DT joints are shown in Table 7.3. As can be seen the T joint shows a similar pattern to that of the β = 0.6 equivalent in relation to the design codes, lying above all but the API (1991) design strengths and 9% below the mean strength on the HSE (1990) database. The capacity as a DT joint under axial compression can be seen to be 14% above that of the HSE mean. This observation is similar to that observed for the β = 0.6 planar joint and those of the Delft experiments and models discussed in Section 7.6.1.

The upper two quadrants of an interaction diagram are shown in Figure 7.16. Similar trends to the β = 0.6 joint series can be observed

regarding the two restraint conditions and trends between them. However, it can be seen in the right hand quadrant (F_{ipb} and F_{opb} both axially compressive) that an enhancement in strength above the F_{opb} = 0 case does occur where the out-of-plane braces (DT) are restrained to remain parallel. This can be seen in Figure 7.16 where when $F_{opb} > 0.5F_{ipb}$, capacity is increased over the F_{opb} = 0 case by 13% until failure as a DT joint occurs. Slight increases can be observed where the DT braces are free to rotate but these are not as significant as when those where the DT braces are restrained to remain parallel. Again similar trends can be observed where F_{ipb} = 0 and F_{opb} is compressive, secondary moments having a significant effect in lowering the capacity of the joint with DT braces free to rotate below that of the planar DT joint and corresponding multiplanar joint where the DT braces are restrained parallel.

The presence of tensile forces in the out-of-plane braces can be seen again to reduce capacity below that of the unloaded out-of-plane joints, reducing capacity by 20% in the worst case ($F_{opb} = -F_{ipb}$).

The major difference for β = 0.25 in Figure 7.16 when compared to Figure 7.8 for the β = 0.6 joints is the effect of 'welding in' unrestrained and unloaded out-of-plane (DT) braces onto the planar T joint. This can be seen to have little effect on the capacity whereas this was not the case for β = 0.6 joints.

7.7 Conclusions

1) For T-DT joints, the presence of out-of-plane braces and associated axial loads clearly has an impact on capacity. This is not as

marked as that observed by Paul et al (1990) on the DT-DT configuration.

2) It is shown that brace end boundary conditions can have a very significant effect on capacity where additional braces are added in an unsymmetrical manner.

3) The enhancement in strength through 'welding - in' of the out-of-plane braces is proportional to β ratio. For β = 0.25 the addition of out-of-plane braces (DT) to a planar T has no significant effect, whereas at a β ratio of 0.6 they enhance capacity by 12 -15 % depending on the method of restraint.

4) The effect of tension in one plane and compression in another can cause multiplanar capacity to fall below the corresponding planar capacity. This, where design is based on planar assumptions will clearly be unconservative.

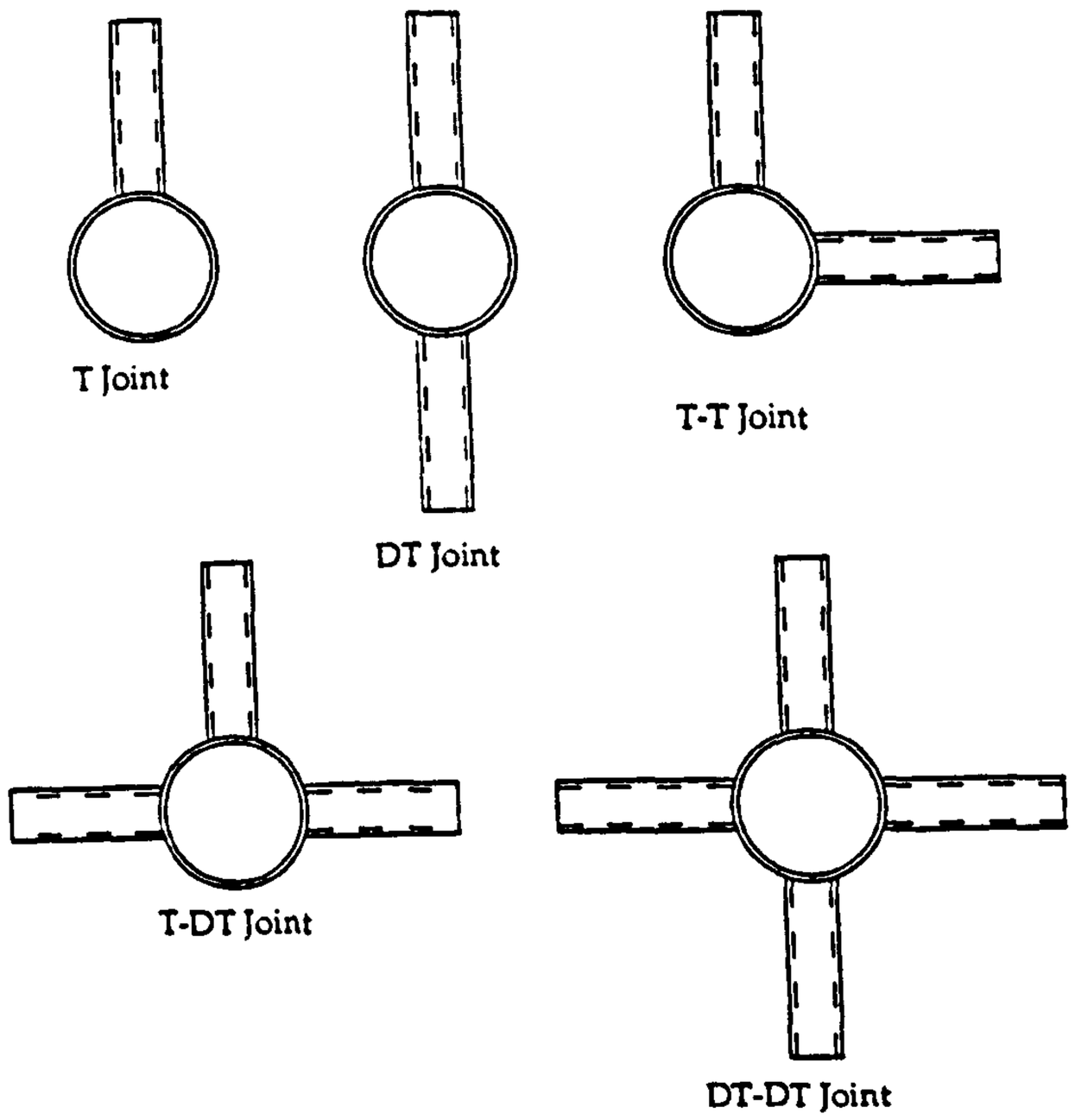

Figure 7.1 Joint Configurations and Definitions.

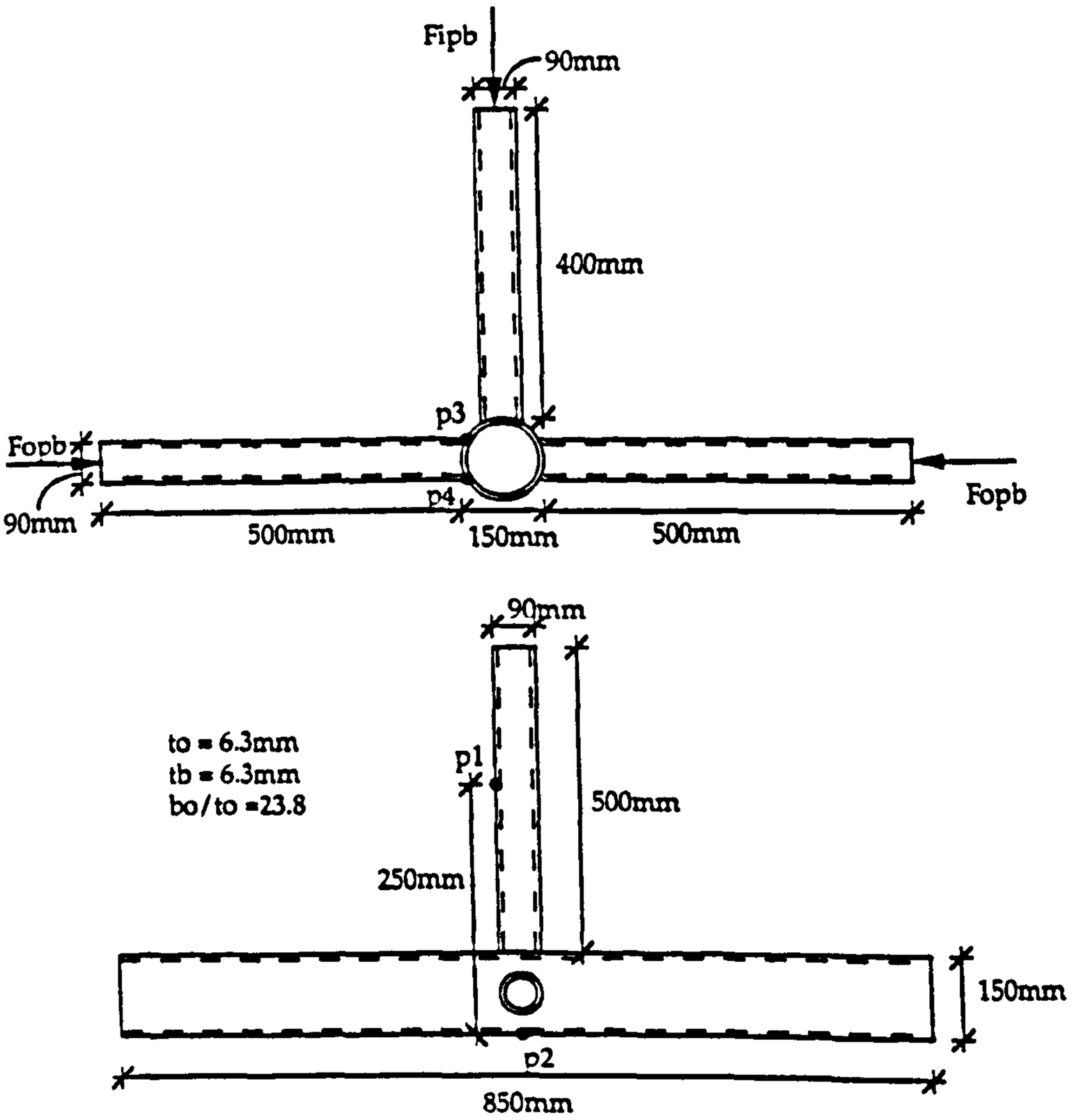

Figure 7.2 CHS D-DT Joint Geometry and General Layout $\beta = 0.6$

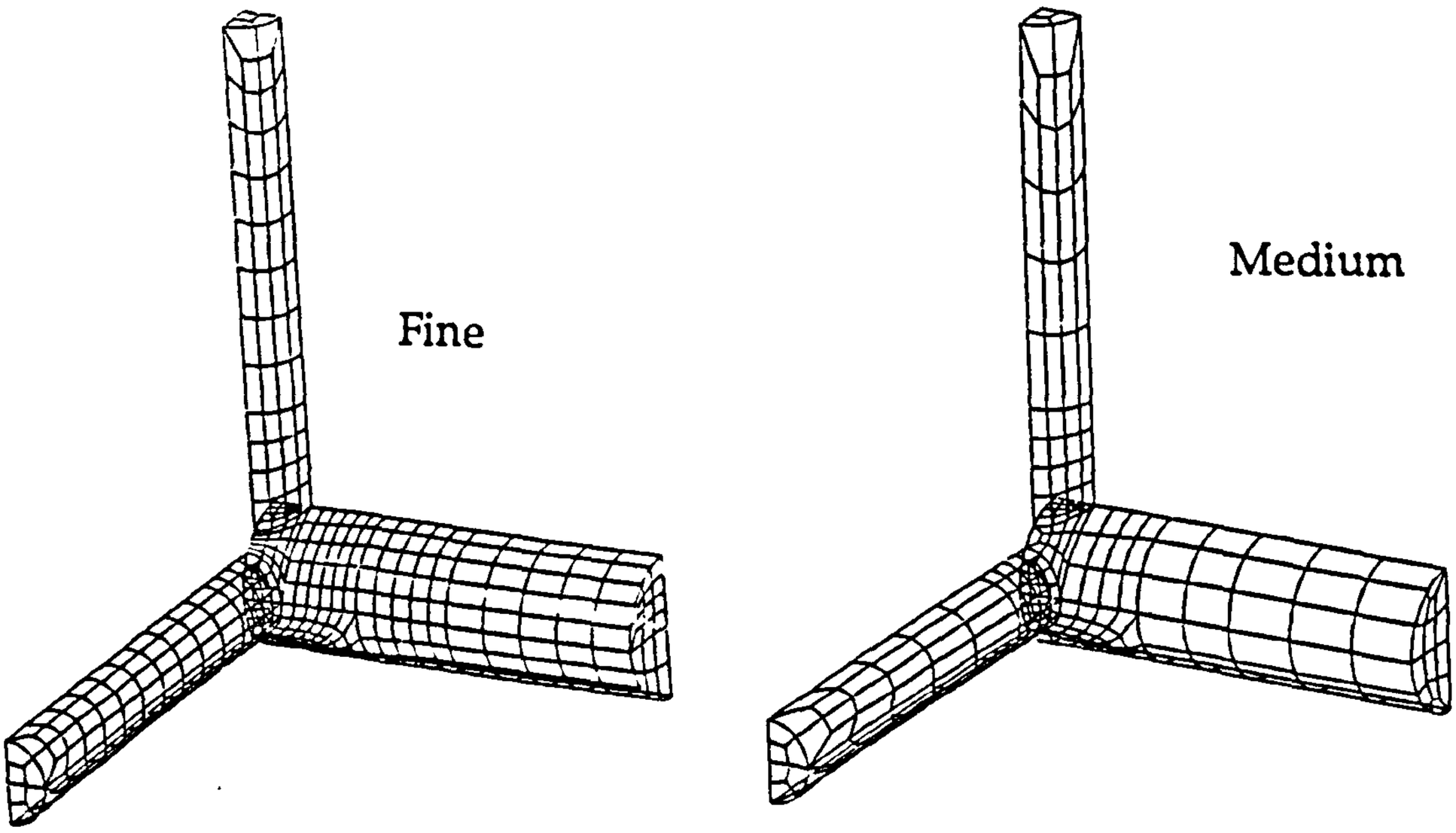

Figure 7.3 The Fine and Medium Meshes used in the Convergence Study

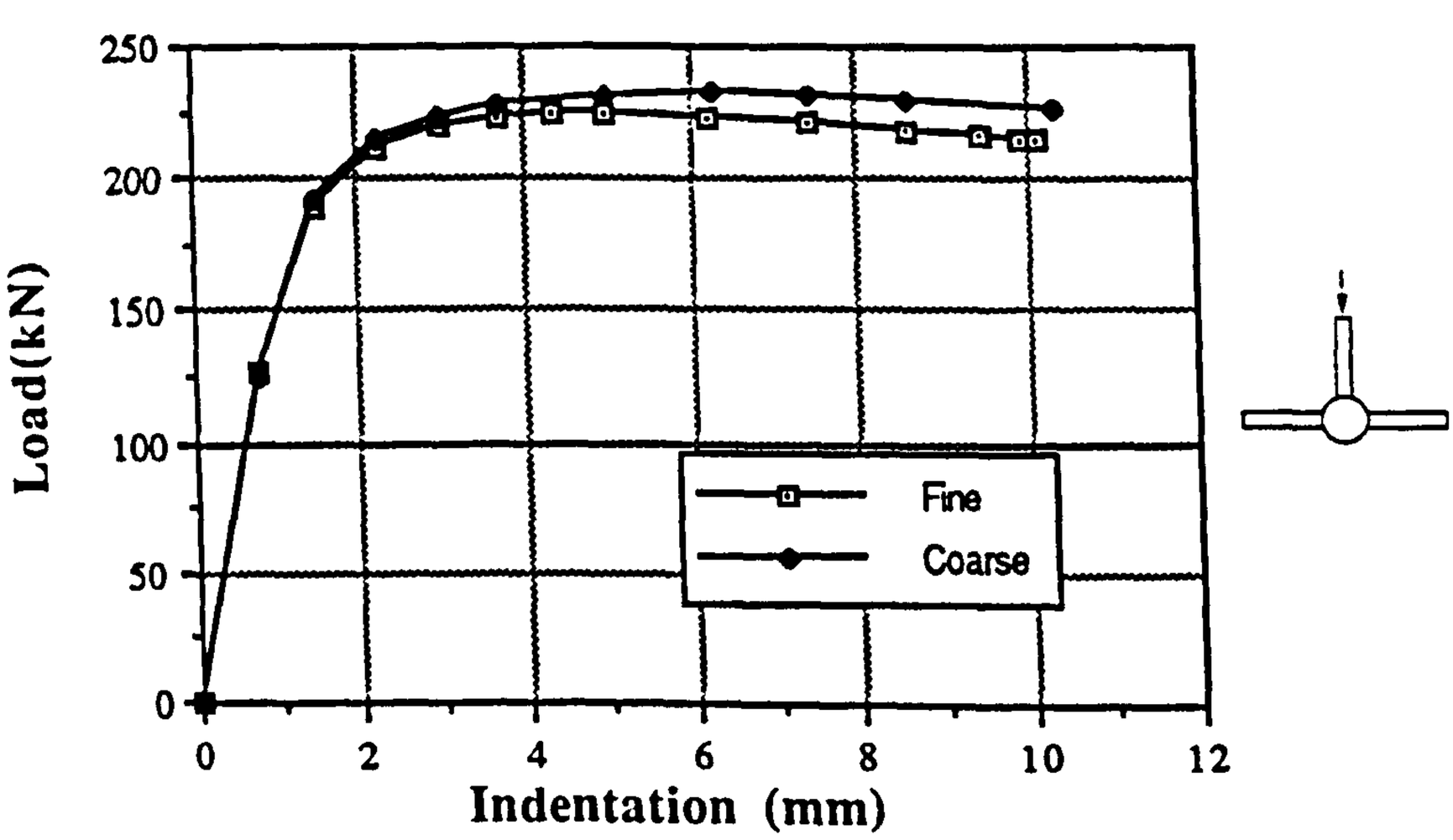

Figure 7.4 Mesh Convergence Load vs Indentation Plots

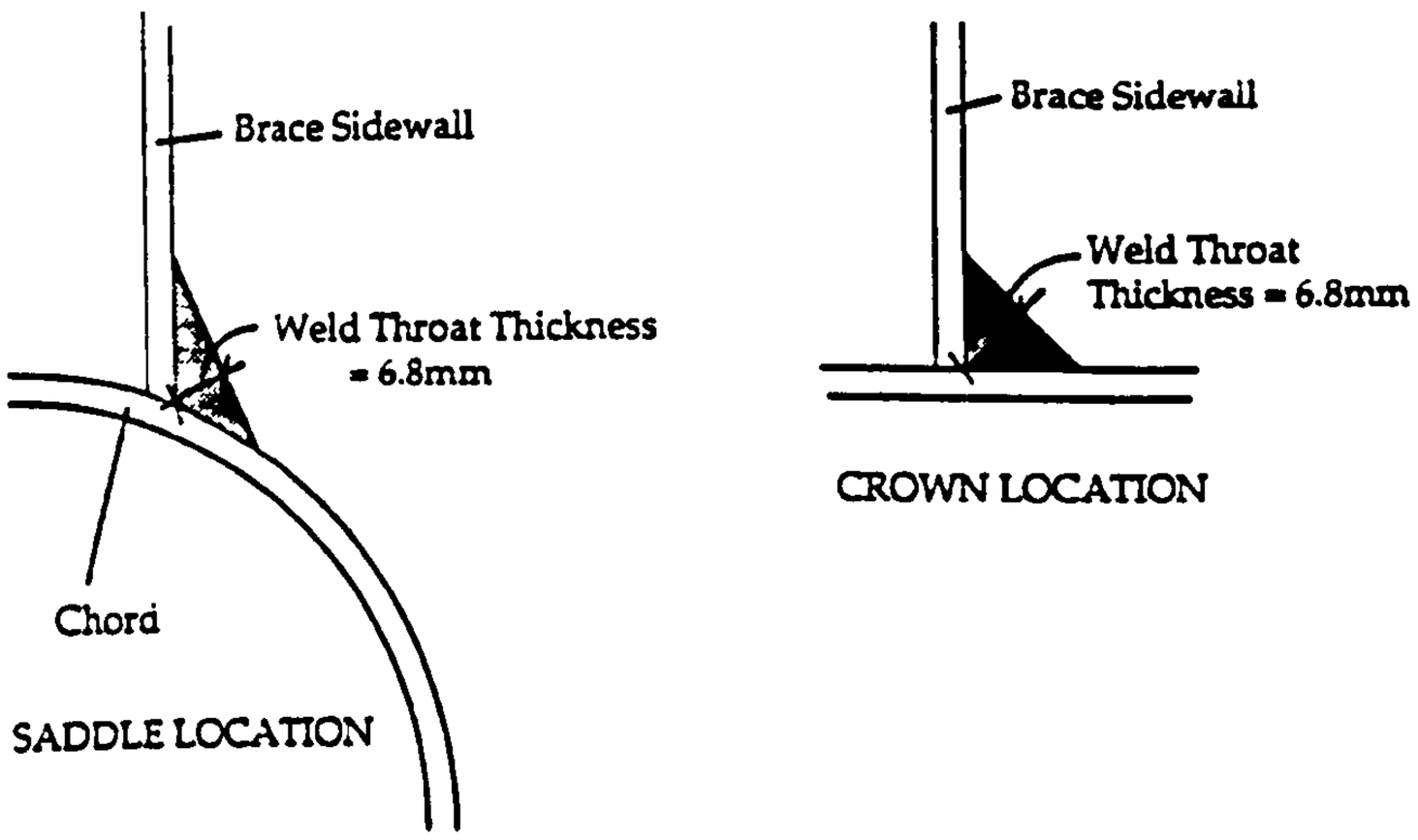

Figure 7.5 Detail of the Weld at Crown and Saddle Locations.

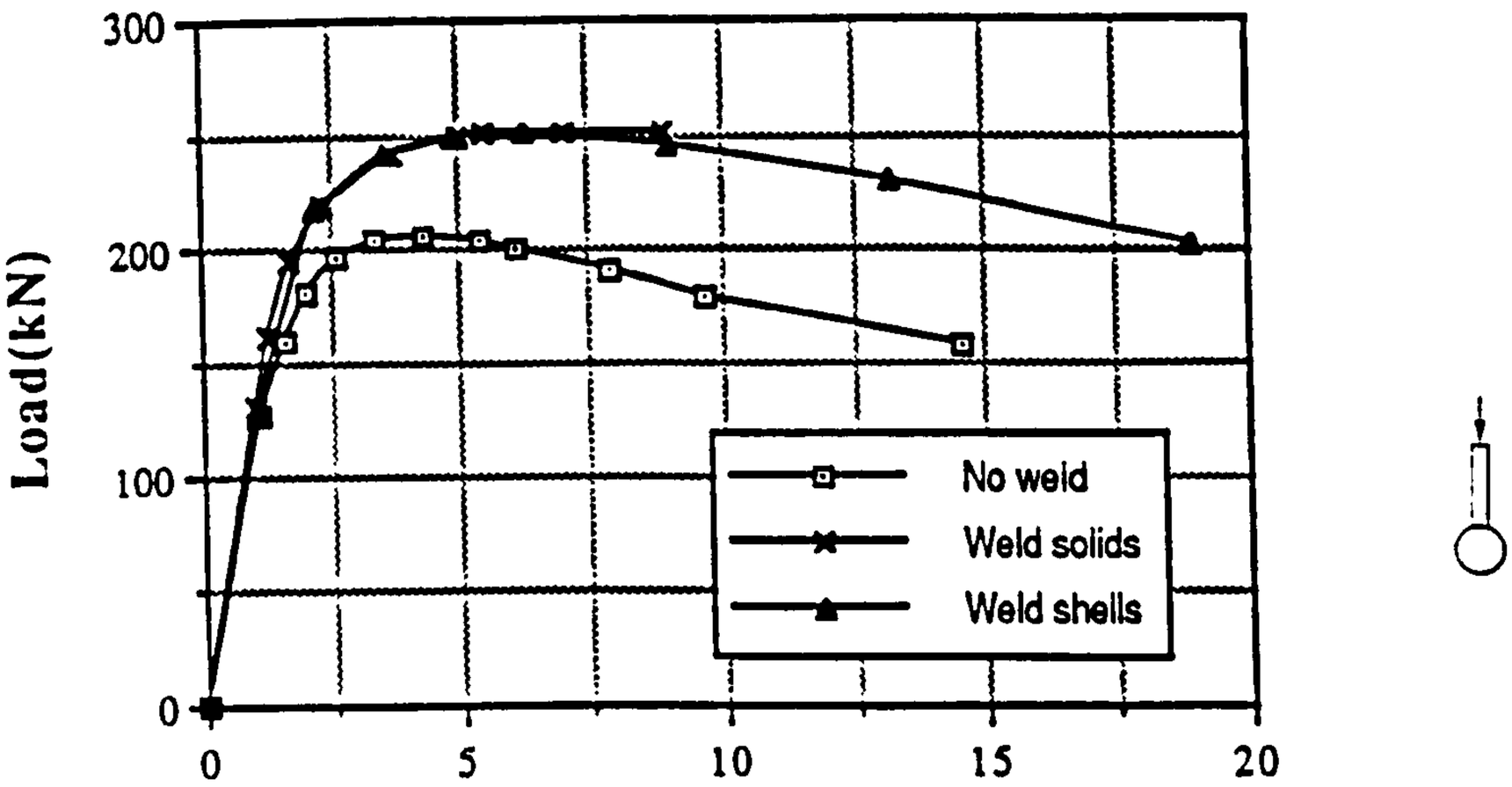

Figure 7.6 Load vs Indentation Plots for the Three Weld Cases Compared

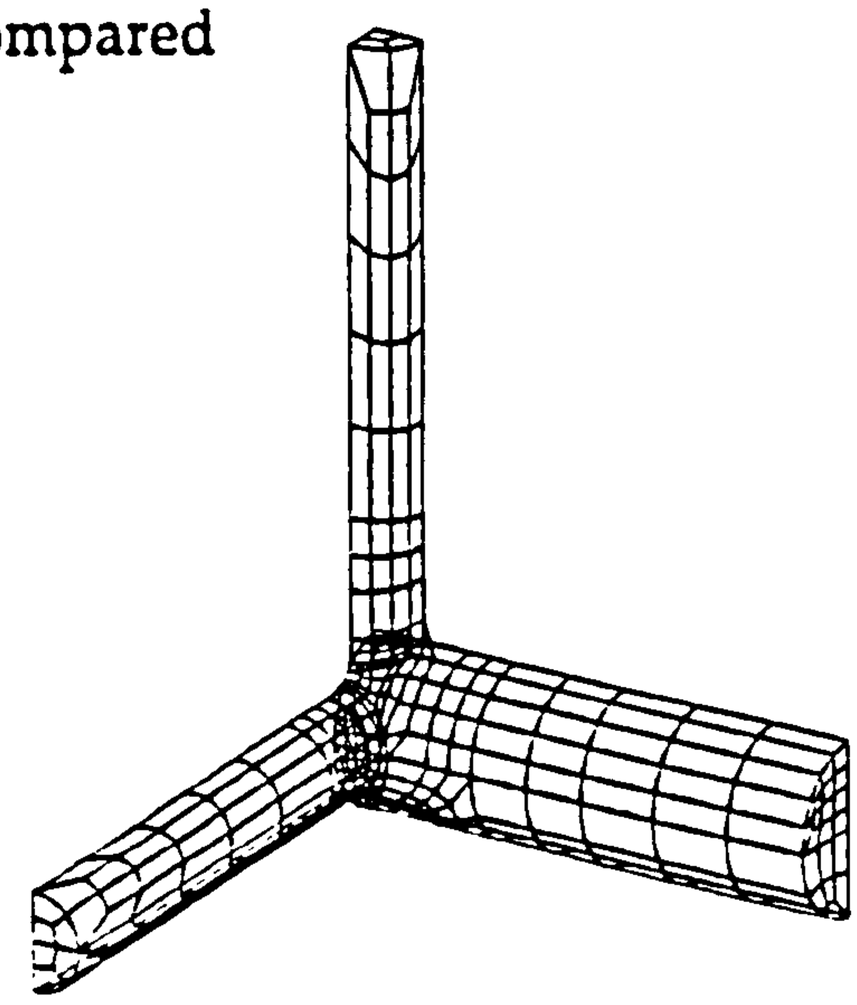

Figure 7.7 Mesh Used in Multiplanar Joint Analysis

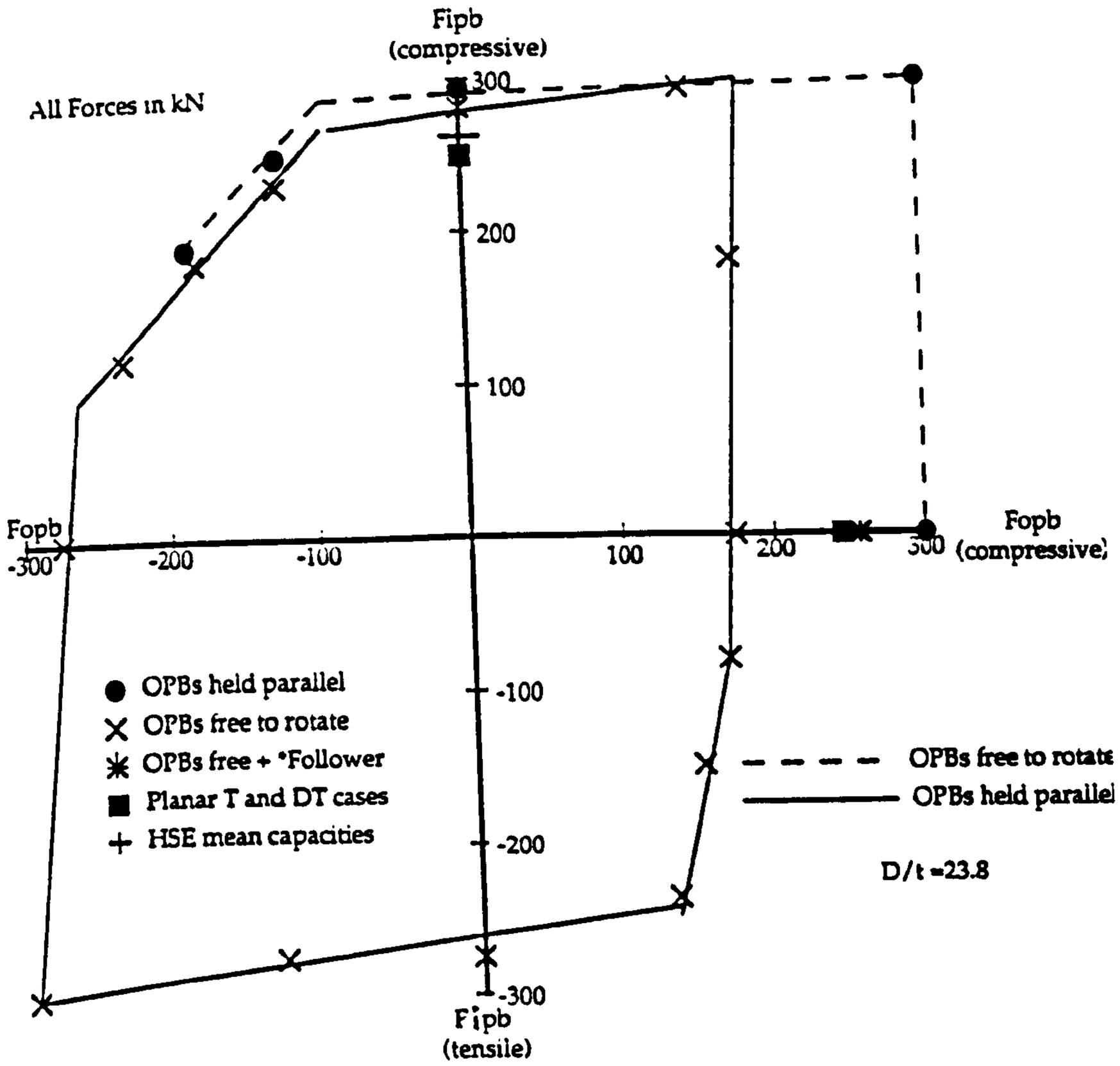

Figure 7.8 Interaction Diagram for β = 0.6 D-DT Joints

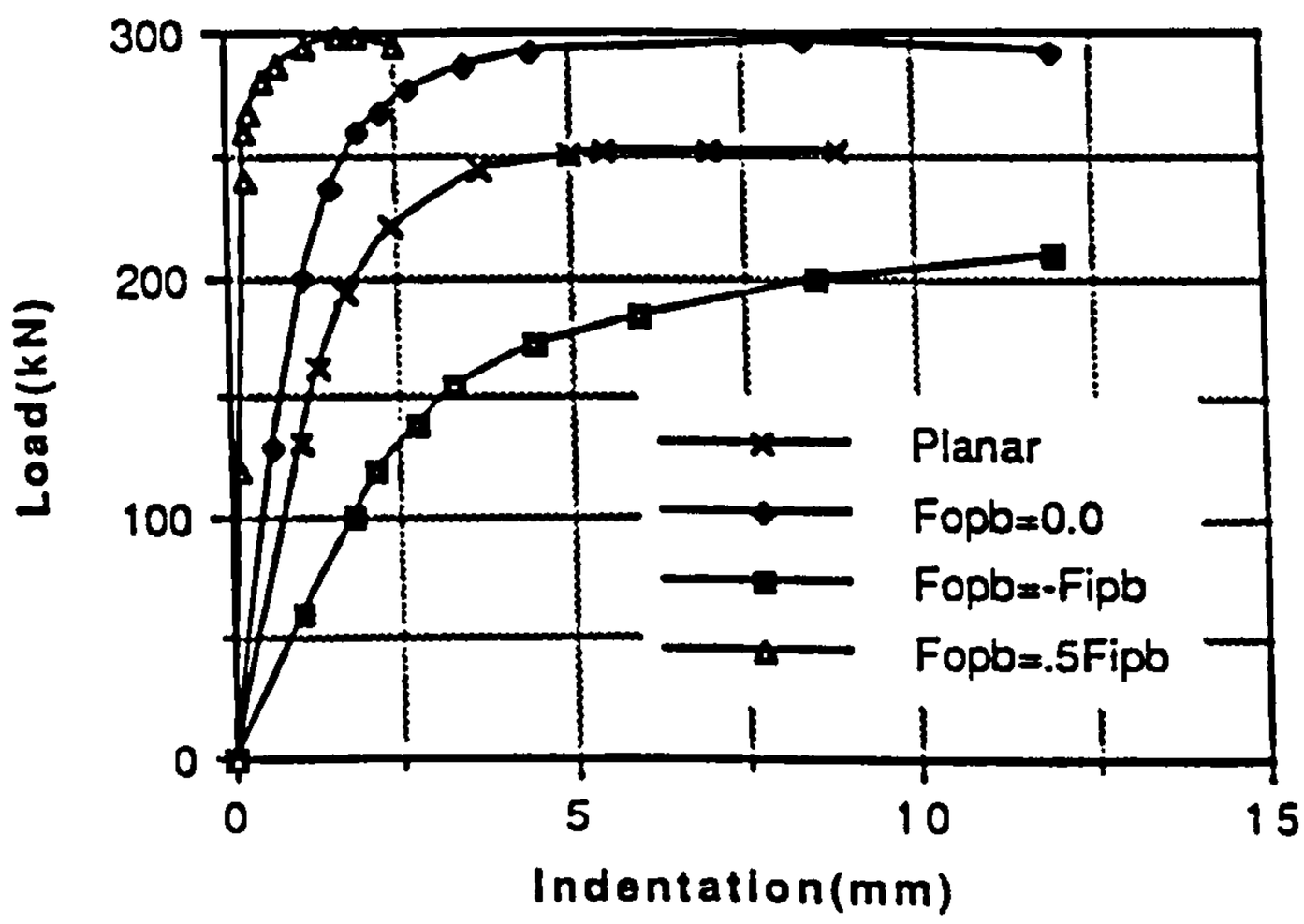

Figure 7.9 Load vs Indentation Plots for Planar Joint and Multiplanar Joints where OPB's (DT) are free to rotate, β = 0.6.

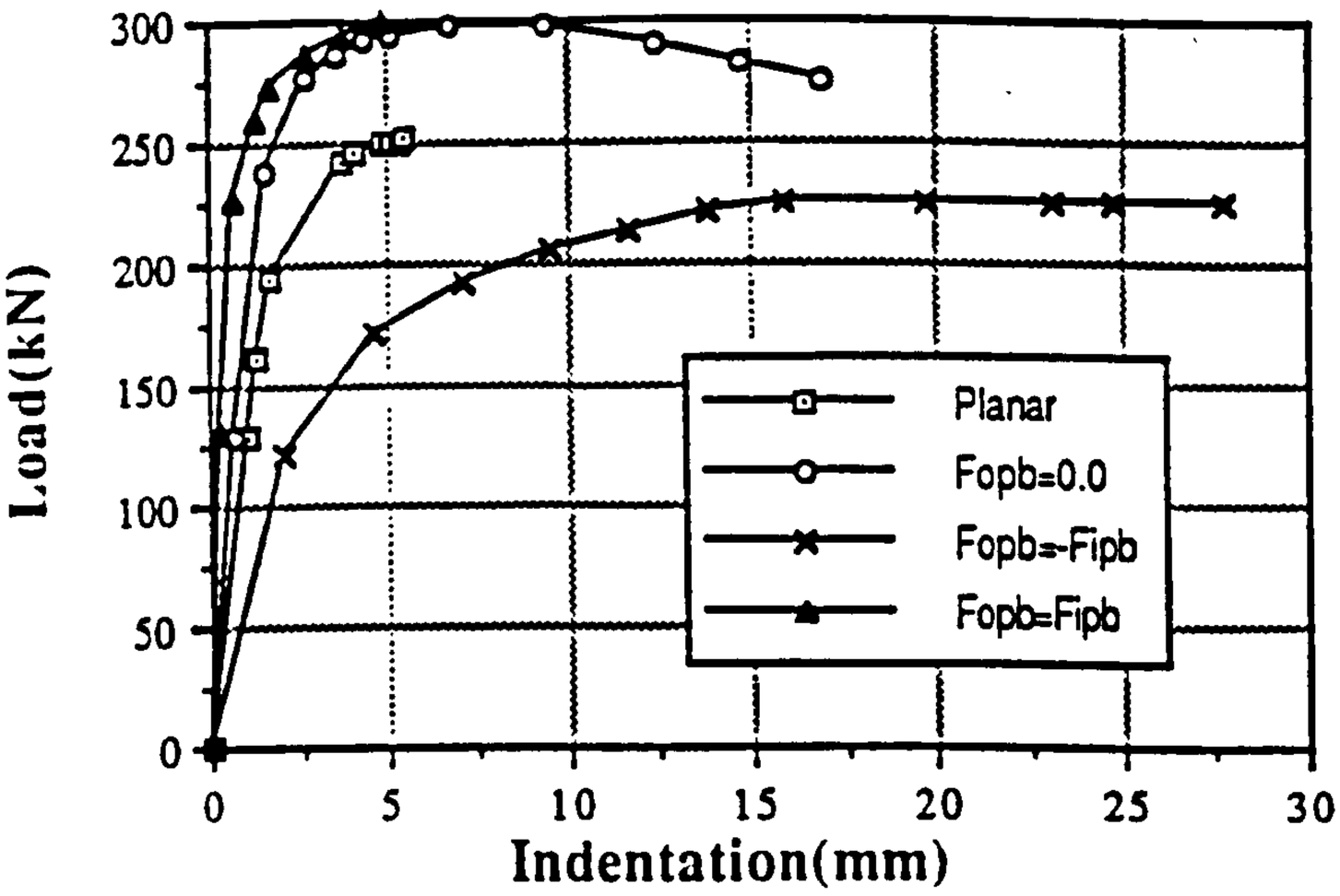

Figure 7.10 Load vs Indentation Plots for Planar Joint and Multiplanar Joints where OPB's (DT) are restrained parallel, $\beta = 0.6$.

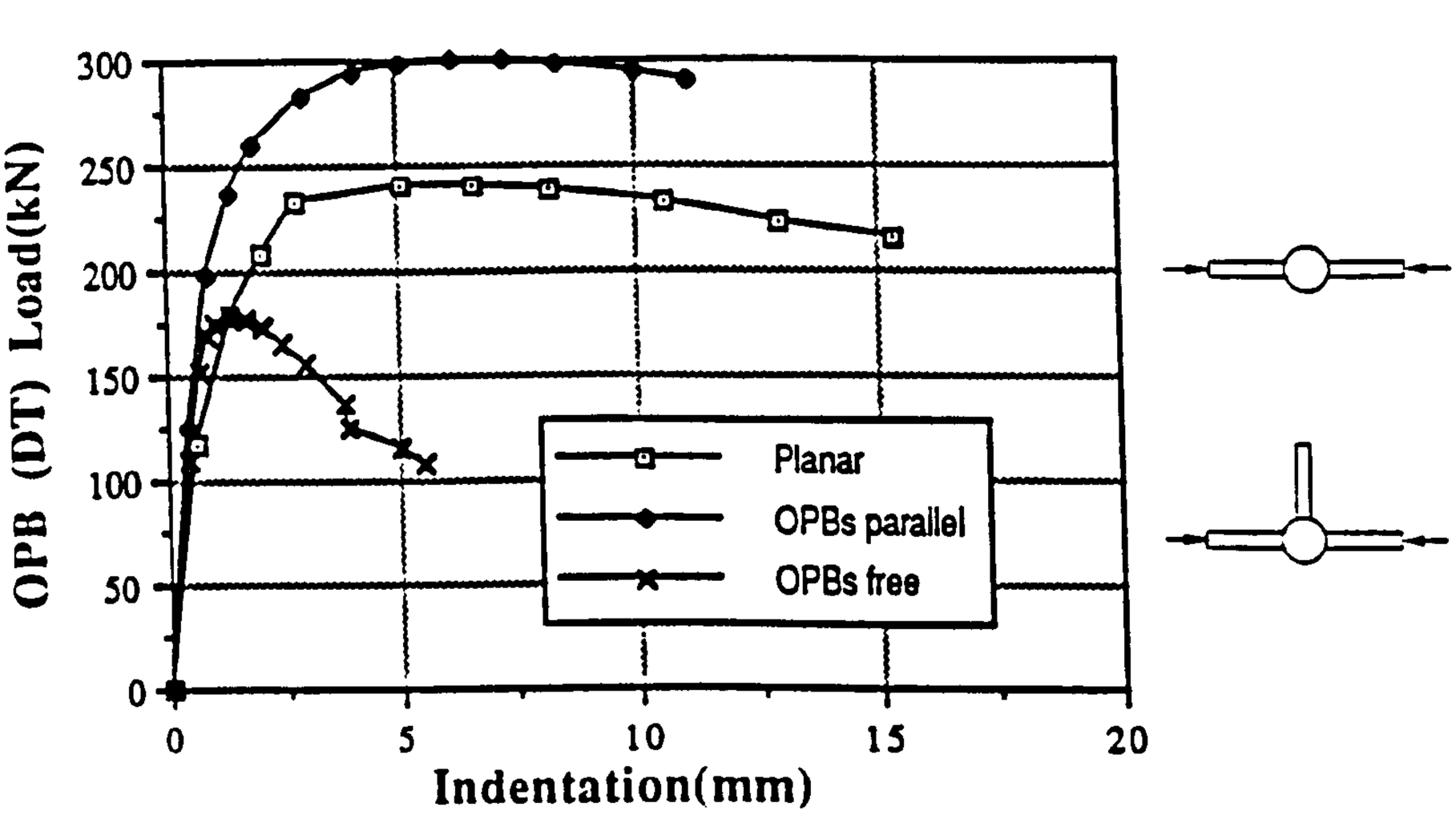

Figure 7.11 Load vs Indentation Plots for $F_{ipb} = 0$ and F_{opb} in compression $\beta = 0.6$

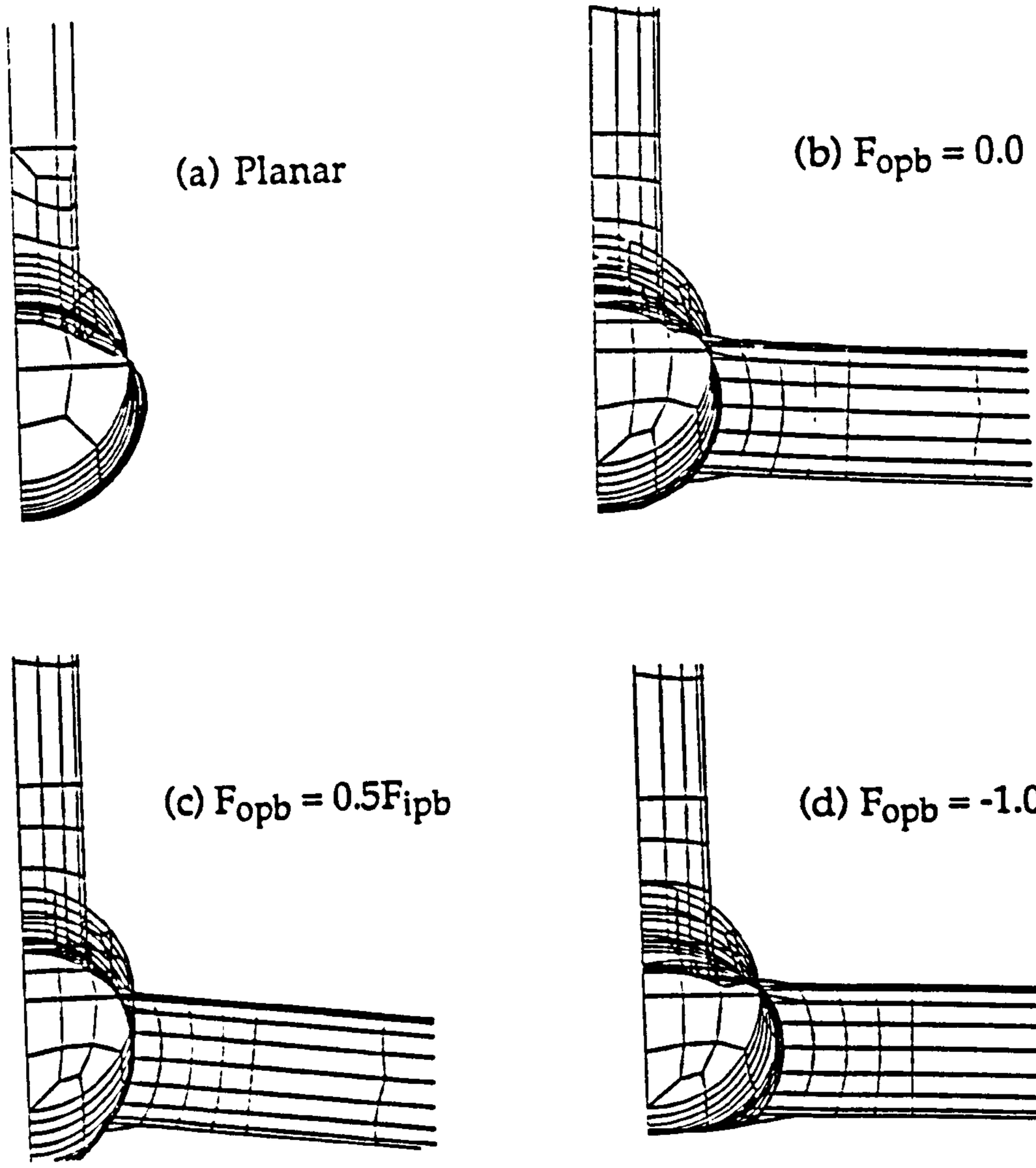

Figure 7.12 Displaced Shape Plots for β = 0.6 Joints with DT Braces Free to Rotate at or close to collapse, F_{ipb} is compressive.

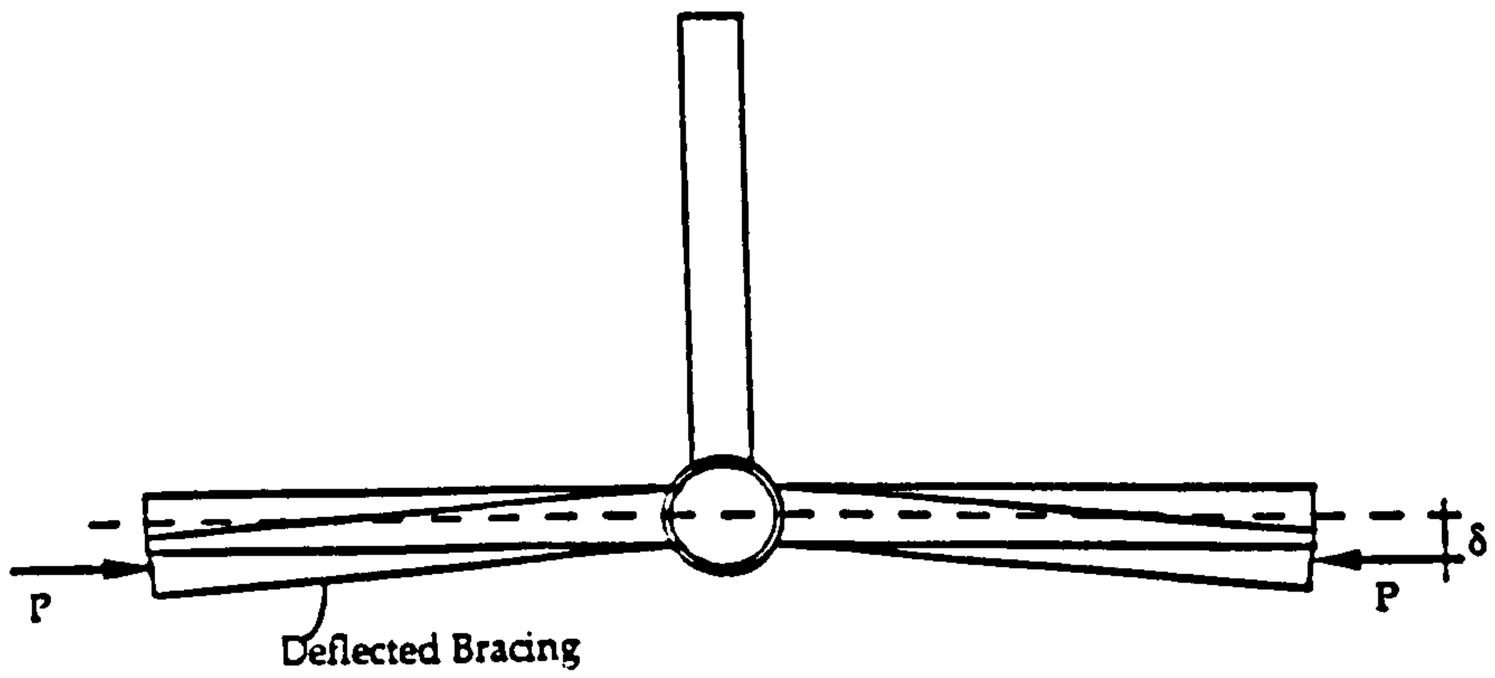

Figure 7.13 Illustration of Possible Secondary Moment Effects where DT Braces are Free to Rotate

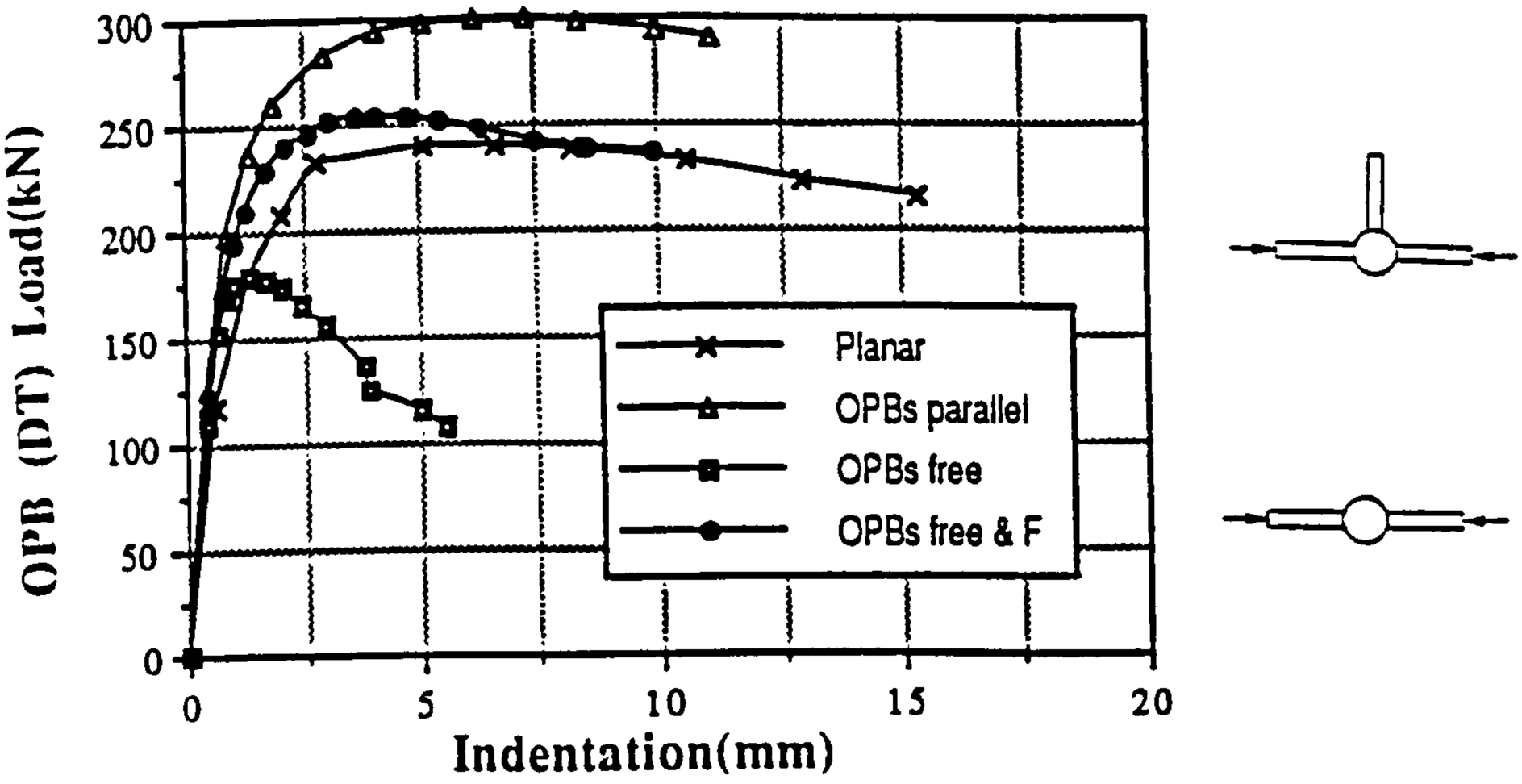

Figure 7.14 Load vs Indentation Plots for $F_{ipb} = 0$ and F_{opb} is compressive - effect of the *FOLLOWER parameter

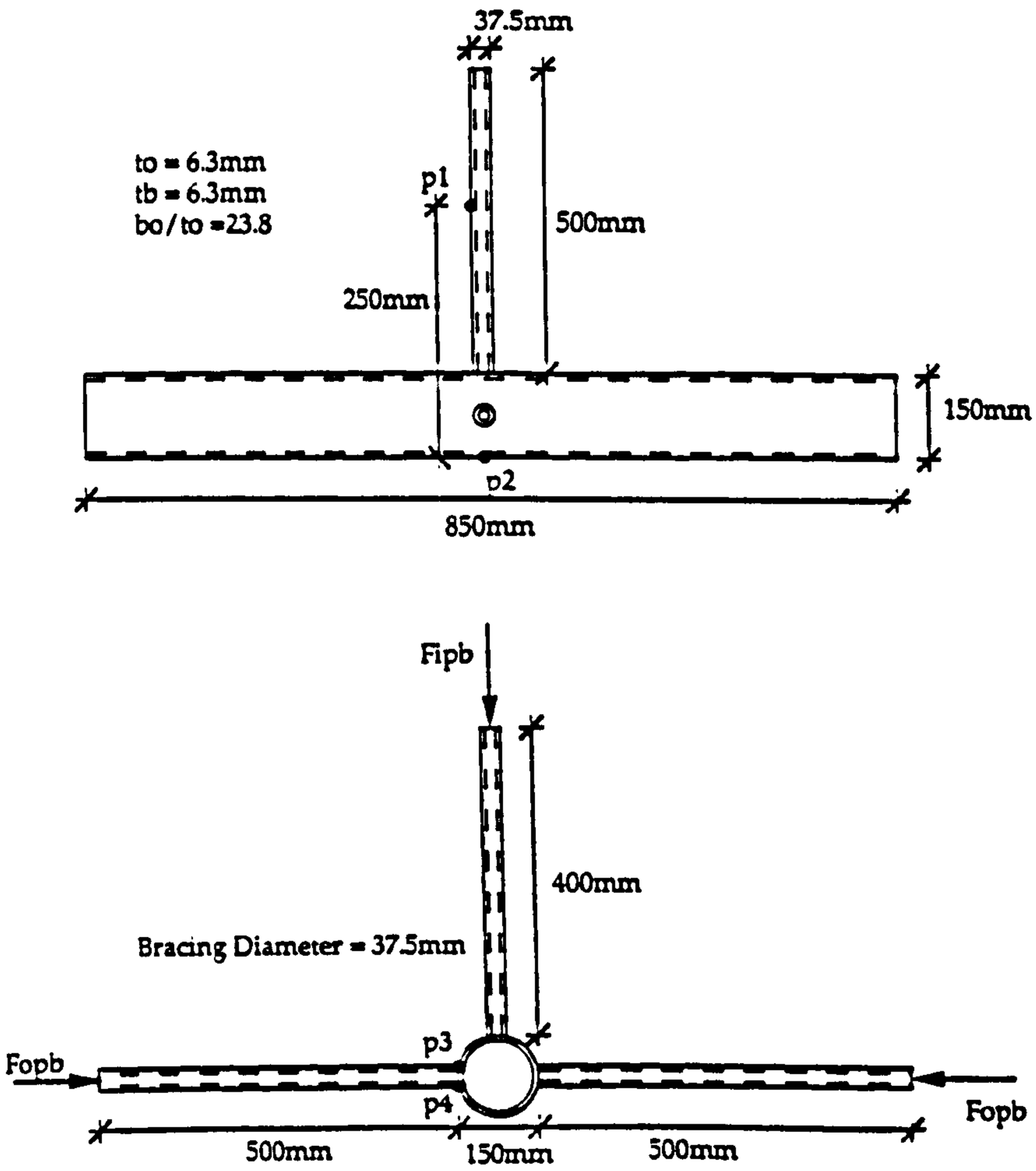

Figure 7.15 CHS D-DT Joint Geometry and General Layout $\beta = 0.25$

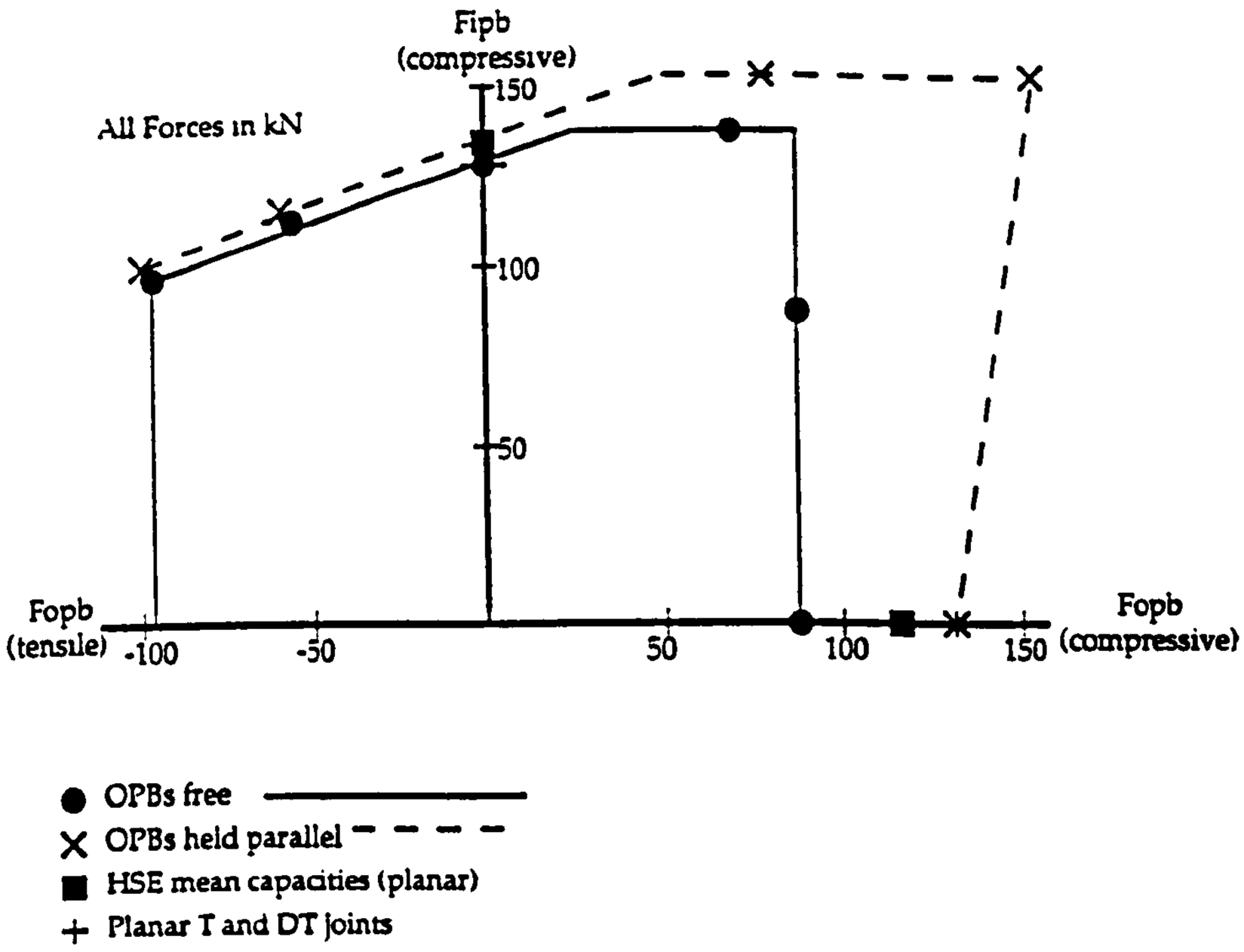

Figure 7.16 Interaction Diagram for β = 0.25 T -DT Joints

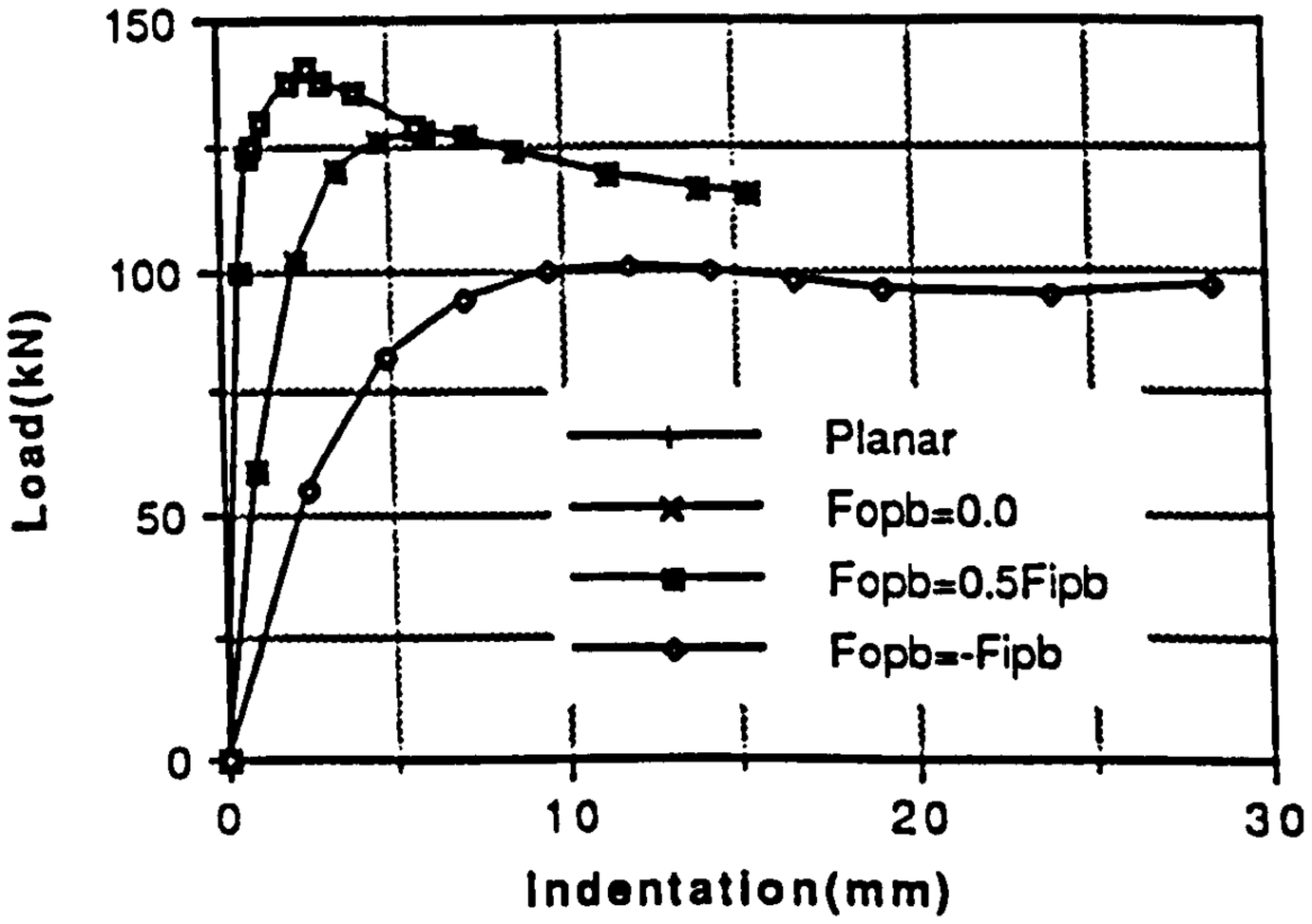

Figure 7.17 Load vs Indentation Plots for β = 0.25 Joints.
Planar and Multiplanar Joints where OPB's
(DT) are free to rotate

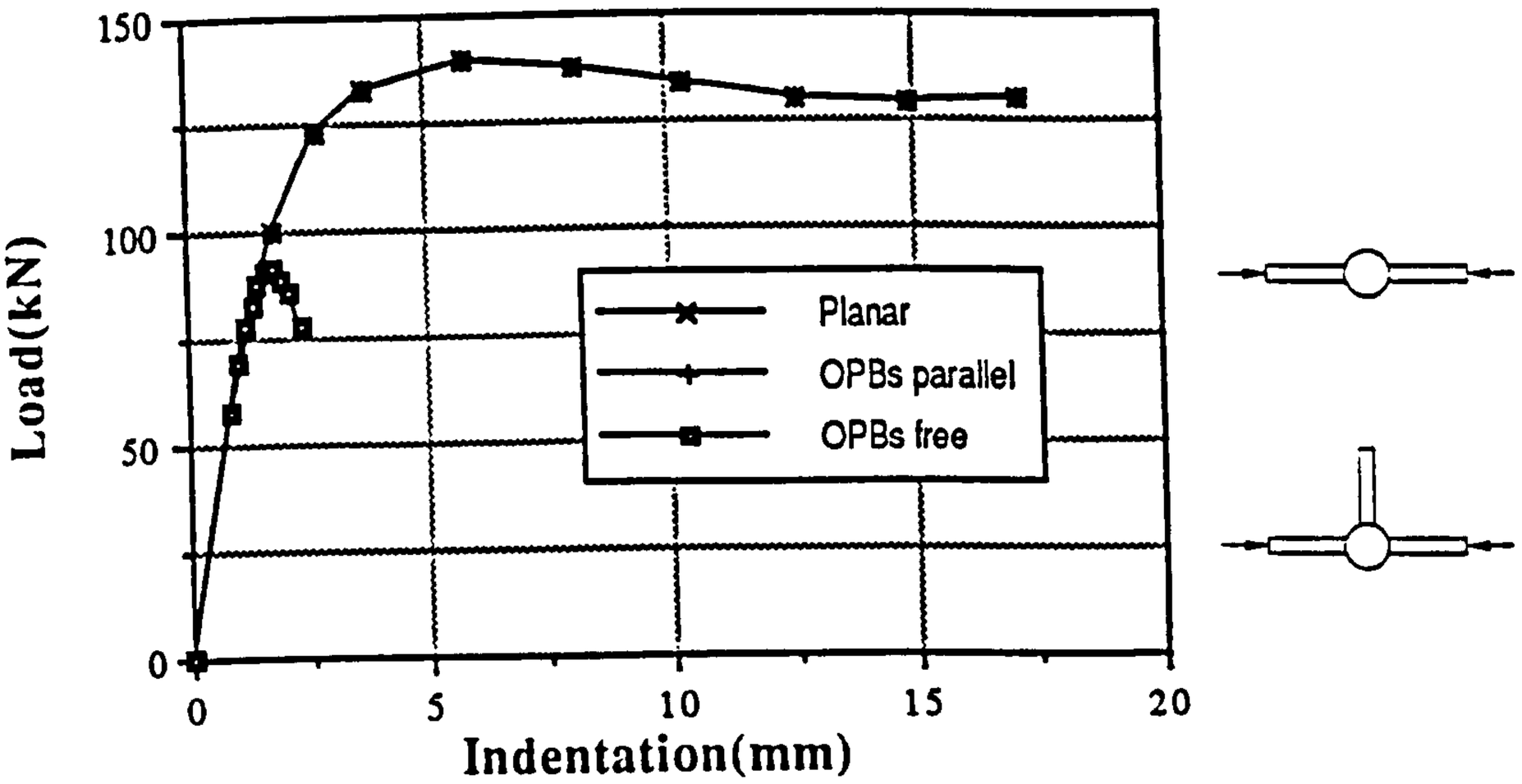

Figure 7.18 OPB (DT) Indentation for Planar DT and Multiplanar Joints where $F_{ipb} = 0$

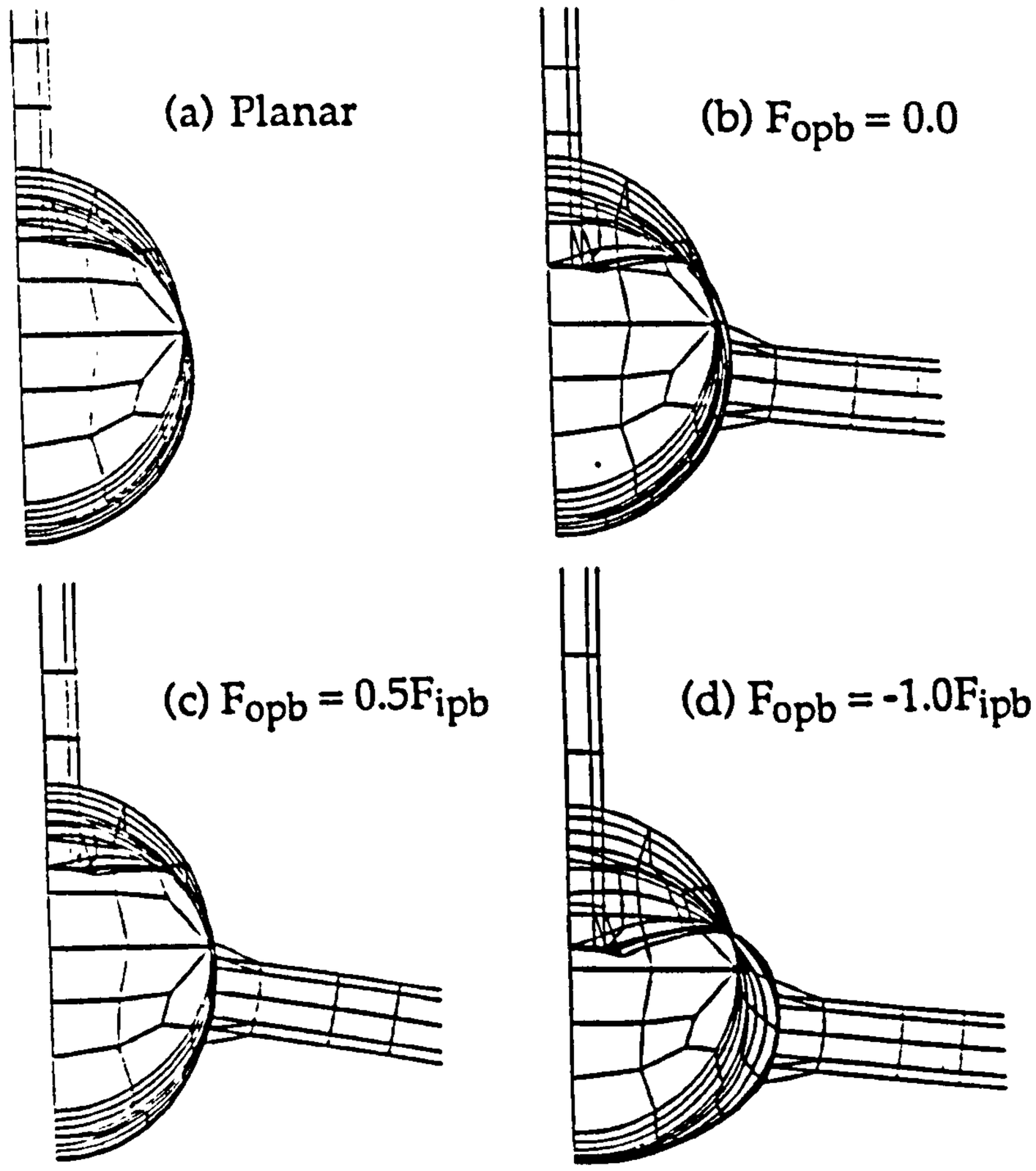

Figure 7.19 Displaced Shape Plots for $\beta = 0.25$ Joints where Braces are Free to Rotate, at or close to peak load, F_{ipb} is compressive.

CHAPTER 8

THE INFLUENCE OF BRACE ANGLE AND INTERSECTION LENGTH ON CHS T, X AND K JOINT CAPACITY

8.1 Introduction

This Chapter is concerned with a factor (K_a) established in the UK design guidance for offshore CHS construction that was causing discrepancies in the course of a large FE investigation for a North Sea operator. As such the aim of this chapter is to discuss the history of the adoption of the factor, a brief outline of the initial motivation for the analyses, details and results of the range of analyses undertaken and to discuss other work which supports the findings here with respect to that factor.

8.2 History of the Adoption of the Brace Projected Area Factor K_a

Two major codes are in use in offshore design guidance, those of the API (1991) and HSE (1990). Both are based on the statistical analysis of screened experimental test data to derive ultimate static strength equations for CHS joints. Both codes make certain assumptions and in the case of the HSE (1990) code there are two assumptions involving

the angle of intersection of the brace with the chord for T, Y, X, DT and K joints. The first of these is that the brace axial load is resolved into its component perpendicular to the chord for use in the ultimate static strength equation. This appears as a $\sin\theta$ term in the ultimate static strength equation. The second concerns the way in which the projected area of the brace footprint manifests itself on the joint capacity. As θ reduces, the length and hence projected area of intersection of the brace footprint increases, this being shown in Figure 8.1. The actual length is a complex function of the chord and brace diameters and the angle of intersection of the brace. BS 449 Part 2 (1969) gives the 'relative length' factor K_a' as :-

$$K_a' = x + y + 3\,(x^2 + y^2)^{1/2}$$

$$\text{where } x = \frac{1}{2\pi\sin\theta} \text{ and } y = \frac{3 - \beta^2}{3\pi(2 - \beta^2)}$$

This is simplified conservatively in the AWS (1990) as K_a where :-

$$K_a = \frac{(1 + \frac{1}{\sin\theta})}{2}$$

The HSE (1990) document describes the assumption of the validity of K_a, using it in the derivation of constants for the basic mean and characteristic strength formulae for CHS joints. Joint capacities of existing joints in the database where K_a has an effect (i.e where $\theta < 90^o$) are predicted by the strength formulae so derived against their actual experimental capacities. Details of this data will be discussed in Section 8.6.

The API (1991) code differs from the HSE code in its assumptions for brace angle treatment. As for the HSE (1990) document, the axial force in the brace is resolved into its perpendicular component for inclusion in the ultimate static strength equation. However, the API does not possess any factor relating to this 'projected area' of an inclined brace assumed in the HSE document, this being a major difference between the two codes. The two design formulae for the compressive strength equations in the API and HSE are shown below:-

$$(\text{HSE}) : P_u = f_y t_o^2 \, (1.82 + 18.17\beta) \sqrt{Q_\beta'} \frac{K_a Q_g}{\sin\theta} \qquad \text{[Eqn 8.1]}$$

where $Q_g = 1.0$ for T and Y joints and $Q_\beta' = 1.0$ for $\beta \leq 0.6$

$$(\text{API}) : P_u = f_y t_o^2 \, Q_f \frac{(3.4 + 19\beta)}{\sin\theta} \quad \text{where } Q_f = 1.0 \qquad \text{[Eqn 8.2]}$$

In Table 8.1 the non-dimensionalised capacities ($P_u \sin\theta / f_y t_o^2$) predicted by the two formulae are shown for a β ratio of 0.6 and different θ's.

θ	API $(3.4 + 19\beta)$	HSE $(1.82 + 18.17\beta)K_a$
90°	14.8	12.7
70°	14.8	13.1
45°	14.8	15.4
30°	14.8	19.0

Table 8.1 Effect of K_a on ultimate strength of T/Y joints for various brace angles θ.

Thus it can be seen that the inclusion of K_a can cause considerable divergence between the two predictions for lower θ values and have a significant effect on the calculated design capacity.

8.3 Original Motivation for the Analyses

As part of a re-analysis of a North Sea Jacket a complex nine braced multiplanar connection was found to be over-stressed under the most severe loading case according to the latest design codes available. Billington Osborne Moss Engineering Limited (BOMEL) were contracted by Amoco UK to undertake a large non-linear FE analysis of the joint in order to assess its ultimate capacity. To validate this complex model against existing codes and design guidance it was necessary to establish the most critical brace of the nine. Once the critical brace was identified, removal of seven or eight of the other braces from the model allows analysis of the critical brace as part of an axially loaded Y, X or gap K joint. This in turn establishes where the joint capacities obtained by FE modelling fall in relation to those obtained from the experimental database and design equations in the HSE document (1990). As the original FE Y joint had a low capacity when non-dimensionalised ($P\sin\theta / f_y t_o^2 K_a Q_g$) compared to the database the decision was taken to model a T joint of exactly the same dimensions to check the modelling. This would make comparison with the database easier as 39 of the 42 available T/Y tests were of the T configuration (i.e $\theta = 90^o$). The results of this T joint FE analysis were somewhat higher than the Y when non-dimensionalised and thus the suspected influence of K_a was investigated.

8.4 FE Modelling and Joint Properties T and Y Joints

8.4.1.FE Analysis Undertaken at BOMEL

The joint dimensions and material properties assumed in the analysis at BOMEL are shown in Figure 8.1 along with the loading mode. At first inspection, the dimensions may seem a little odd but these were the actual dimensions of the complex multiplanar joint under investigation, which were maintained for consistency. It should be noted here that the chord material is thickened in the joint region.

Models were established using the SDRC-IDEAS package (1991) and analysed on a Sun SparcII workstation using ABAQUS (1991). Three β ratios were analysed at a chord slenderness ratio (d_o/t_o) of 32.0:- 0.4, 0.667 and 0.9 to establish the effects of K_a over the whole range. The ratio of 0.667 was that of the original critical brace on the model. As for all analyses undertaken in this thesis so far, geometric and material non-linearity was used, peak loads being taken as the failure. $\theta = 46.1^o$ Y and T joints were analysed for the three β ratios, all chord ends being fully encastré, the brace ends remaining completely free. This again was to ensure compatibility with the original analysis of the complex multiplanar joint. No weld modelling was undertaken for these joints.

It is appreciated that at this α ($2L/d_o = 11.9$) short chord effects may enhance capacities of T and Y joints, especially where the chord ends are encastré restraints as here. The lack of weld modelling is likely to reduce capacity (for T and Y joints of β ratio = 0.6 approximately 20%) as was illustrated in Chapter 7, partly or perhaps fully offsetting the

'short chord' effect. There is no reason to suspect however, that these factors will effect the relative comparison between the T and Y joints and the effects of K_a. The effects of these encastré ends and the weld on the K_a comparison are investigated in 8.4.2. Load vs indentation plots for T/Y comparisons are less meaningful due to the different configurations than for the T-DT joints investigated in previous chapters so the ultimate capacities are presented in tabular form alongside HSE (1990) mean capacities in Table 8.2.

	Joint	HSE(mean) (kN)	FE (kN)	$\frac{FE}{HSE}$	$\frac{FE}{HSE}$ (no K_a)	$\frac{Y}{T}$
$\beta = 0.4$	T	2076.0	1717.6	0.827	0.827	
	Y	3439.8	2487.6	0.723	0.863	.874
$\beta = 0.667$	T	3202.0	3063.0	0.957	0.957	
	Y	5305.6	4179.8	0.788	0.941	.823
$\beta = 0.9$	T	4789.4	4430.8	0.925	0.925	
	Y	7935.7	5550.0	0.699	0.834	.755

Table 8.2 Comparisons of T and Y Joint analyses undertaken at BOMEL.

The data is then plotted as non-dimensionalised capacity vs β ratio alongside the HSE dataset on which the design capacity equation was based, in Figure 8.2. It can be seen that the Y joint strengths lie lower than the T joint data when K_a is included. Displaced shape plots for the six analyses undertaken are shown in Figures 8.3 to 8.8, these being taken at load increments just before the peak. Von Mises stress plots of the outer shell surfaces are shown for the $\beta = 0.4$ T and Y joints

in Figures 8.9 and 8.10 and for the $\beta = 0.9$ T and Y joints in Figure 8.11 and 8.12.

8.4.2 FE Analyses Undertaken at Nottingham

In order to establish more rigourously the validity of the results of the initial FE analyses undertaken at BOMEL, a further investigation was undertaken at Nottingham to establish the effects of different support conditions and the modelling of the weld on the differences between T and Y joints. A β ratio of 0.6 with a chord $d_o/t_o = 23.8$ and an α of 11.33 was used to enable the simply supported planar T joint analysis from the Chapter 7 to be used. FEMGEN (Femview Limited 1989) was used to establish the Y joint model, brace angle being 46.1^o,all other properties being the same as those of the planar T joint in Chapter 7. The two restraint conditions are shown in Figure 8.13, weld modelling being as described for the planar T joint (six noded solids) in Chapter 7. The non-dimensionalised peak capacities attained in each of these analyses, are given in Table 8.3. The results of the other analysis in Table 8.3 is for the free brace with the axially loaded (*FOLLOWER) option applied. As can be seen the three brace support conditions have little impact on the capacity of the Y joint as non-dimensionalised capacity varies only between 11.13 and 11.90.

Analysis	Non Dim Capacity $\frac{P_u \sin\theta}{f_y t_o^2 K_a}$	Remove K_a $\frac{P_u \sin\theta}{f_y t_o^2}$	$\frac{FE}{HSE\ mean}$
T	14.99	14.99	0.907
Y	11.13	13.28	0.804
Y + pin	11.90	14.20	0.859
Y + Follower	11.48	13.70	0.829

Table 8.3 Comparisons of Nottingham T and Y joint analysis with the HSE Guidance.

Load vs indentation comparisons for the three Y joint analyses are shown in Figure 8.14, a displaced shape plot for case A being shown in Figure 8.15. The combination of brace indentation and chord ovalisation in the failure can be seen. Indentation for the Y joints is taken as the change in distance between the central point on the end plate and a point on the chord mid-height which lies on the line of the brace central axis.

8.5 DT and X Joints

The K_a factor is also present in the HSE equation for X joints. In order to establish if K_a was valid for this joint type two FE analyses were undertaken. Firstly using the original geometry a 46.1° X joint analysis was undertaken, advantage being taken of the symmetry to model half of the joint. Secondly a DT (a 90° X joint) was modelled with all dimensions except θ remaining the same. Due to the slight variation in the chord length either side of the brace, symmetry only

allowed modelling of one quarter of the joint to be undertaken as opposed to the normal eighth for an axially loaded DT joint. Material and geometric properties were the same as those of the T/Y joints analysed in Section 8.4.1, chord ends being encastré, brace ends being free with compressive axial loading applied to these braces. The analyses again used geometric non-linearity, peak capacities of the DT and X joint analyses at a β ratio of 0.667 with d_o/t_o = 32.0 being shown in Table 8.4 and shown graphically in non-dimensionalised form alongside the HSE database in Figure 8.16. Displaced shape plots of the two joints are shown close to peak in Figures 8.17 and 8.18 while Figures 8.19 and 8.20 illustrate Von Mises stress plots for the outer shell surfaces of the joints.

	HSE (mean) - kN	FE (kN)	FE/HSE (mean)
DT	2363.4	2325.8	0.984
X	3916.1	3440.0	0.878

Table 8.4 Results of the DT and X joint analyses undertaken at BOMEL

8.6 Discussion

8.6.1 T and Y Joints

As can be seen from Table 8.2 and Figure 8.2 the ultimate capacities of the FE analysed Y joints lie below those of the HSE mean by an average of 26% while the T joints lie below by an average of 9%.

The FE Y joint data in Figure 8.2 is clearly falling outside the scatter of the database whereas the FE T joint data is giving good correlation. Further examination of the content of this database reveals that of the 42 points only three are actually Y joints (i.e $\theta < 90^o$), these all lying around a β ratio of 0.4. It can be seen in Figure 8.2 that two of these points lie below the mean line very close to the characteristic line, the ratios for these three joints when compared to the database mean being 0.86, 1.02 and 0.88 respectively, all having $\theta = 45^o$. A separate examination of the 18 experimental results in the corresponding T/Y tensile loaded database reveals again only two Y joints, both having an actual capacity to dataset mean ratio of 0.82, brace angle of 45^o and β ratios lower than 0.4. Thus it can be seen that data on which the validity of K_a was checked for Y joints was limited in both quantity and parameter range (β always less than 0.45) and that the tendency is for the actual Y joint experimental capacities that are available to be low when compared to the mean of the two axially loaded datasets as a whole. This difference has not been identified previously, partly due to a lack of experimental data (incomplete knowledge) but also due to the method of validating K_a in the HSE document.

As was stated earlier in Section 8.2 the initial assumption was that K_a is a valid parameter. It was then assumed to be a fundamental component in the establishment of design equations, its validity, where it had an influence on capacity (i.e where $\theta < 90^o$) being back checked by calculating capacities of these joints according to the derived formulae and comparing these predictions with the actual capacities from the database. The joints on which this was done contained the three compression loaded Y joints mentioned earlier and a set of 12 K

joints where the gap was large. The gap in K joints, where it is small ($g/D < 0.15$) has a very important effect on K joint capacity and thus only joints where the gap was sufficiently large enough to not be the dominant design strength factor were used to back check the validity of K_a. The HSE (1990) document establishes the fact that the formula including K_a predicts ultimate capacity to within a 3% average on the combined set of 15 joints, concluding that for the available data adoption of K_a appeared valid. However as discussed the volume of Y joint data was low (only 3 of the 15 points in the check data) and of these three Y joints, two had actual joint capacity to dataset mean ratios of 0.88 and 0.86.

Thus the FE analyses undertaken here over a wide β ratio, alongside nominally identical T joint specimens would appear in addition to the sparse available data indicate that K_a is not valid in the form given and its inclusion in the formula for T and Y joints is unconservative, where at a brace angle of 45º it can add up to 20% to the calculated capacity.

Further support to this conclusion is gained by an examination of nominally identical T and Y joints tested as part of the Joint Industry Static Strength Program. These are presented as β ratio against non-dimensional strength in Figure 8.21 alongside the existing HSE screened dataset, nominally identical T and Y specimens being indicated. The validity of these results has been cast into doubt due to concern over short chord effects enhancing capacity but, although these concerns would appear justified as all the results appear to be towards the high side of the database, there is no reason to suspect that the use of the data in a comparative T/Y sense is not valid.

Comparison of the simply supported cases A and B with the T joint with the inclusion of a weld model results in Table 8.4 also confirm that K_a is not a valid parameter. It also shows that the support conditions and inclusion of the weld are not having an influence on the T/Y strength ratio comparisons established in the earlier analyses. As can be seen the support of the brace end to be on a pin as opposed to being free enhances the capacity of the Y joint, this eliminating most of the secondary moment effects that occur when the loading point deflects off its axis. This was discussed more fully in Chapter 7.

Comparisons of T and Y joints at the same β ratios displaced shape plots (Figures 8.3 to 8.8) reveal that as expected both have similar failure modes with respect to indentation of the brace to the chord. However as the β ratio increases the tendency is for an increase in the deflection and global ovalisation of the chord to occur. This can be explained by the stress plots. As can be seen in Figures 8.9 and 8.10, for joints with $\beta = 0.4$ the tendency is for the yielding (red areas) to be localised around the footprint of the brace and the upper half of the chord area indicating that large strains and deformations are restricted to this region and the chord deformation is local 'in-punching' (as discussed for low β ratios in CHS in Chapter 1). Observing the Von Mises stress plots for the $\beta = 0.9$ T and Y joints (Figures 8.11 and 8.12) it can be seen that although similar yield patterns exist around the brace footprint to those at $\beta = 0.4$, yield also occurs on the underside of the chord (due to the chord beam failure expected at large β ratios and confirmed by the global chord 'beam' deflection in Figures 8.7 and 8.8). Considerable yield can also be seen to have taken place on the outer chord regions in both the T and Y joints at $\beta = 0.9$, this being caused by

the encastré end conditions and the reduction in chord material thickness described in Section 8.4.1, these boundary conditions being necessary to ensure compatibility with the original client's analysis. It may be said that this throws doubt on the validity of the actual magnitude of the capacities obtained in the FE analysis but there is no reason to suspect that the relative comparison between the T and Y joint capacities is not valid.

8.6.2 DT and X Joints

The FE results for the axially loaded X and DT ($\theta = 90$) joints are shown in Figure 8.16 and Table 8.5. It can be seen that the DT analysis gives very good correlation falling within 2% of the mean. The X however falls 13% below the mean after its non-dimensionalisation. Observation of the database reveals that all experimental tests under compression are DT joints; therefore no verification of K_a could be attempted for X joints due to the lack of experimental data available. The HSE (1990) document assumed that as its initial K_a check indicated K_a was valid for gap K and Y joints, then it was equally valid for X joints. This is backed up by the use of some JISSP data on three compression loaded X joints whose brace angles were at $\theta = 60^o$ ($2N^o$) and 75^o, no similar 90^o DT joint being undertaken in this program. It is perhaps unwise to base validation on these however due to the absence of a compatible DT (i.e $\theta = 90^o$) joint with which to compare these three X joints and the fact that all these three X joints had their β ratios equal to 1.0, where failure modes can significantly differ from those of

lower β ratio joints. Zettlemoyer (1988) discusses these points in some detail.

Comparing displaced shape plots for the DT and X joints (Figures 8.17 and 8.18) it can be seen that the mode of failure does not differ significantly, generally being associated with local chord deformation. Again the stress contour plots in Figures 8.19 and 8.20 can be seen to verify this yield occurring around the brace footprints and the chord mid-height confirming the combination of brace in-punch and chord ovalisation observed at this β ratio.

8.6.3 K Joint Implications

In the HSE back checking of the validation of K_a, twelve of the fifteen joints were of gap K configuration, the average capacity being predicted by the formula compared to each experimental result being within 3%. Removal of the Y joints whose capacities are overpredicted by the formula will further enhance this correlation suggesting that K_a's inclusion in the K joint capacity equation is not under conservative. However examination of the K joint database in the HSE document does reveal a large scatter of results and other factors such as the gap or restraint conditions may be affecting the capacity 'swamping' K_a effects.

8.7 Conclusions

1) The inclusion of K_a in the HSE design guidance was based on limited and incomplete information.

2) The analyses undertaken in this Chapter indicate that its inclusion in T/Y and DT/X joint axial capacity formula causes considerable divergence from the mean result and furthermore its inclusion is not conservative, causing capacity predictions for X and Y joints greater than available experimental and FE results indicate. Re-analysis of existing limited data would appear to confirm this.

3) A complete re-analysis of the HSE formulae is required since K_a was an implicit assumption from the beginning of the derivation. Care must be taken to ensure incomplete data and knowledge does not lead to unconservative assumptions being made in formulae derivation.

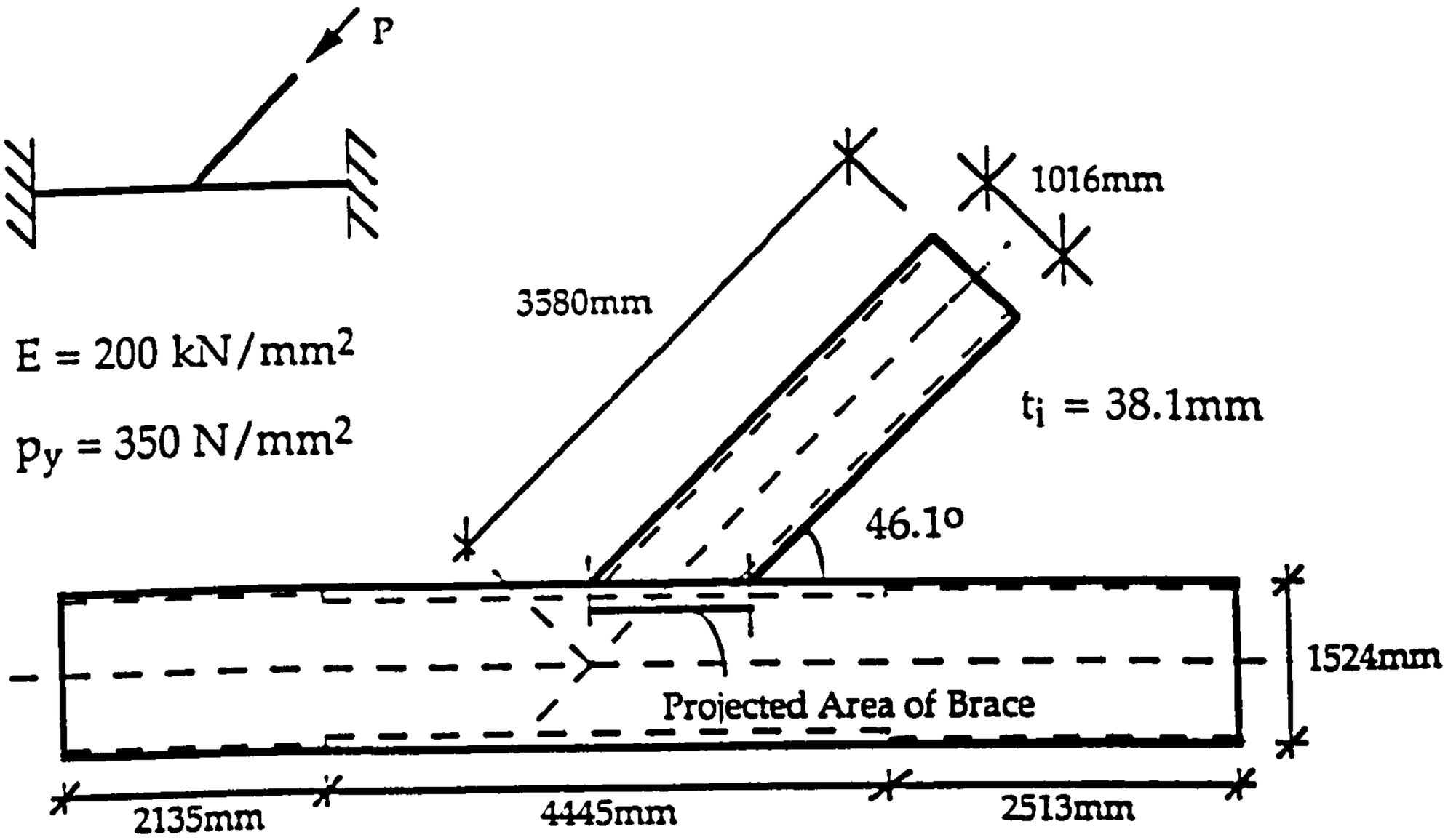

Figure 8.1 Y/T Joint Dimensions and Set up for Modelling

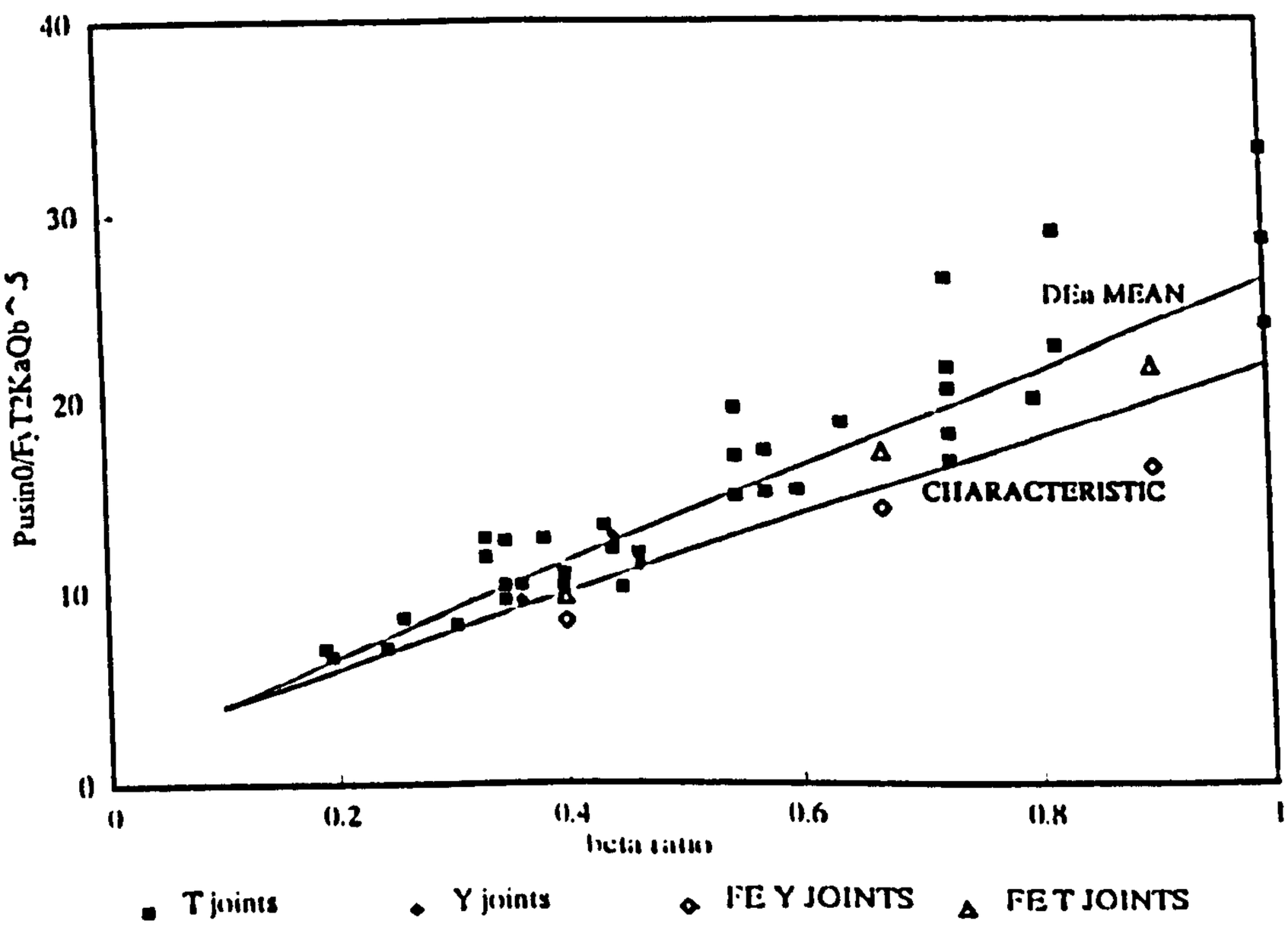

Figure 8.2 Non-Dimensionalised Capacity vs β Ratio
for T/Y Joints in HSE dataset and FE results.

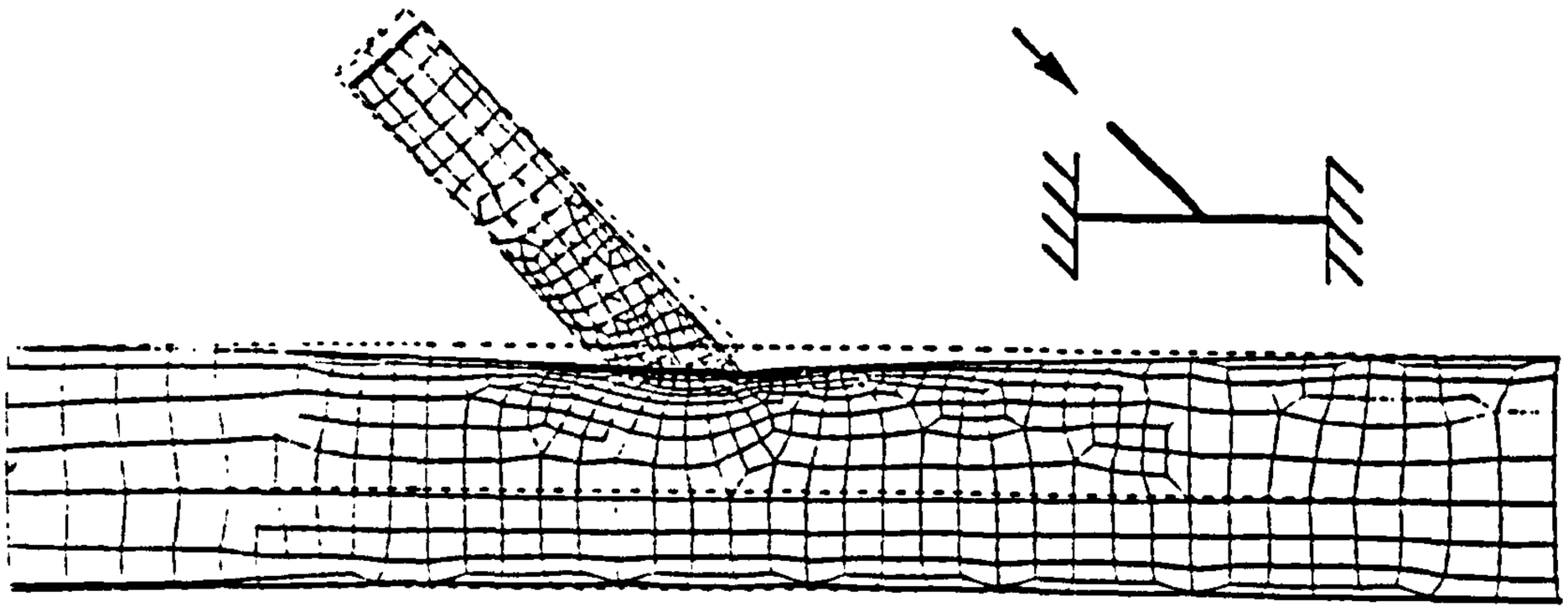

Figure 8.3 Displaced Shape Plot β = 0.4 Y Joint

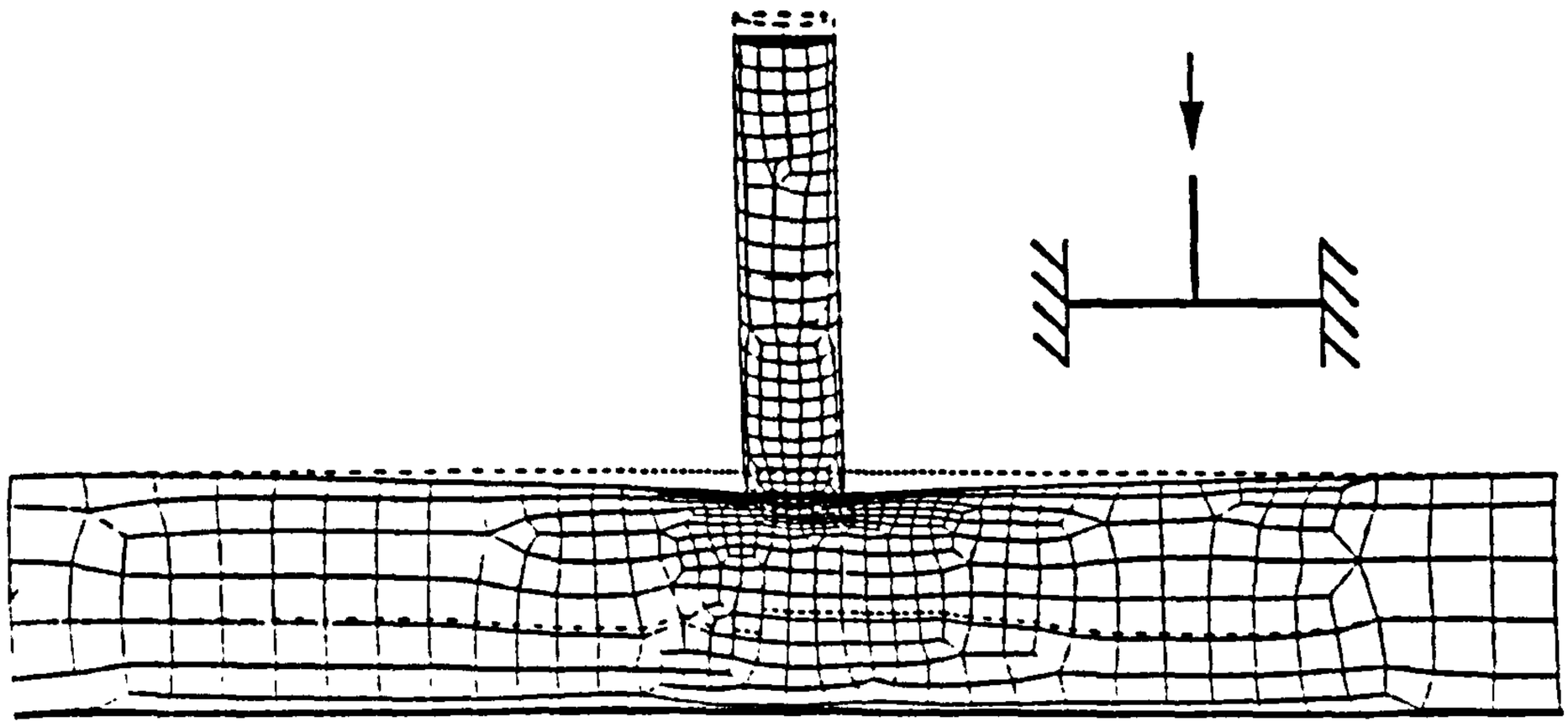

Figure 8.4 Displaced Shape Plot β = 0.4 T Joint

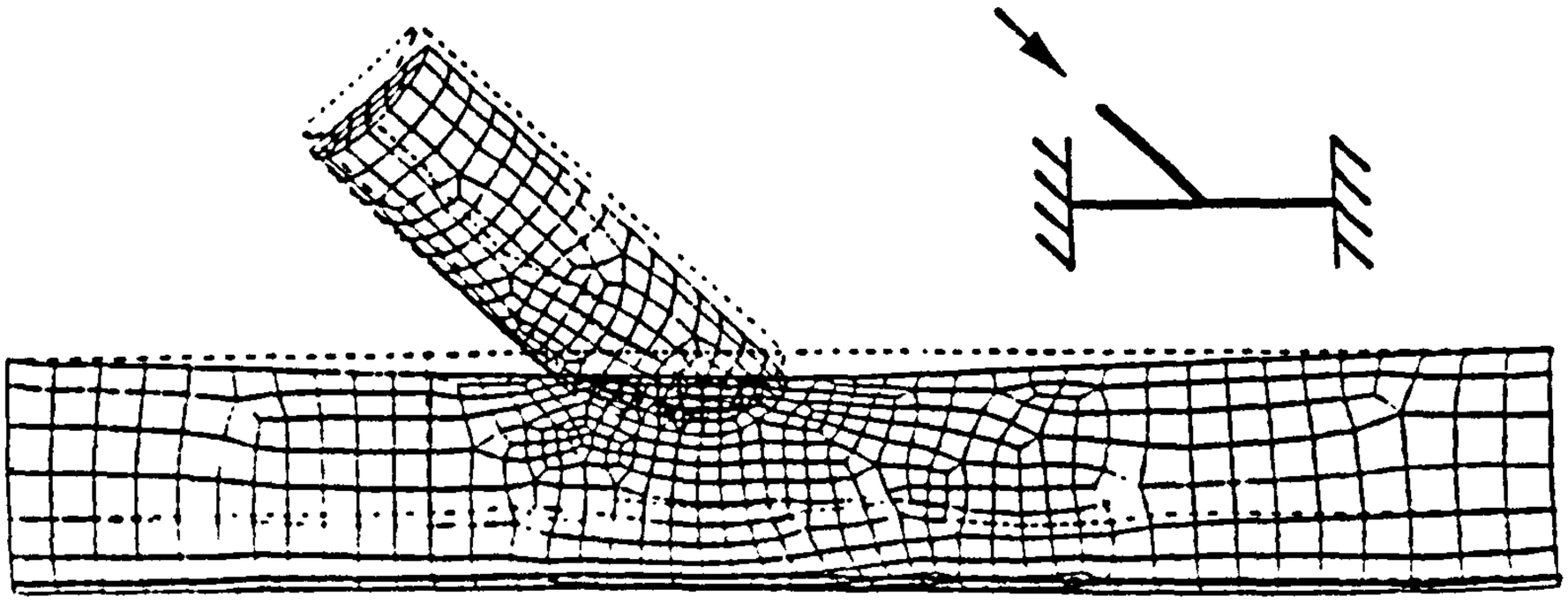

Figure 8.5 Displaced Shape Plot β = 0.667 Y Joint

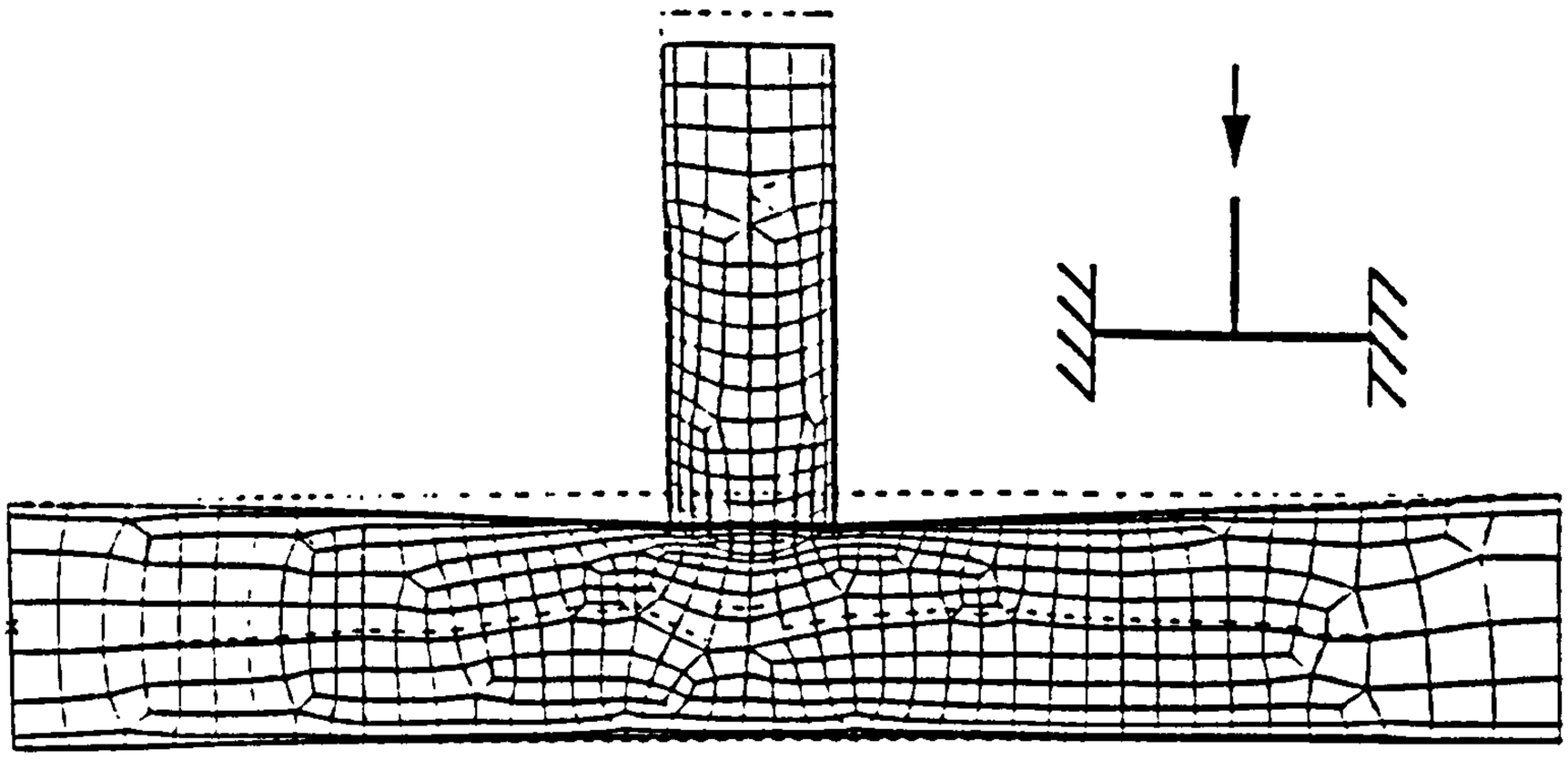

Figure 8.6 Displaced Shape Plot β = 0.667 T Joint

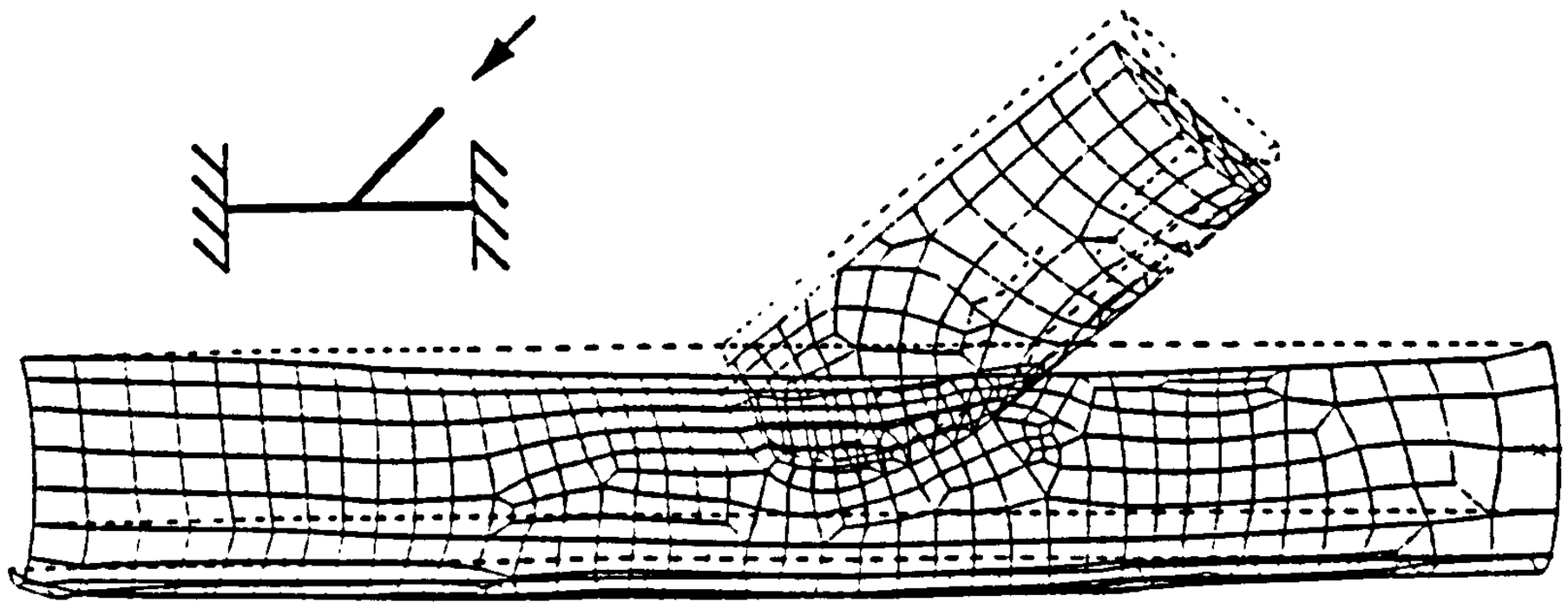

Figure 8.7 Displaced Shape Plot β = 0.9 Y Joint

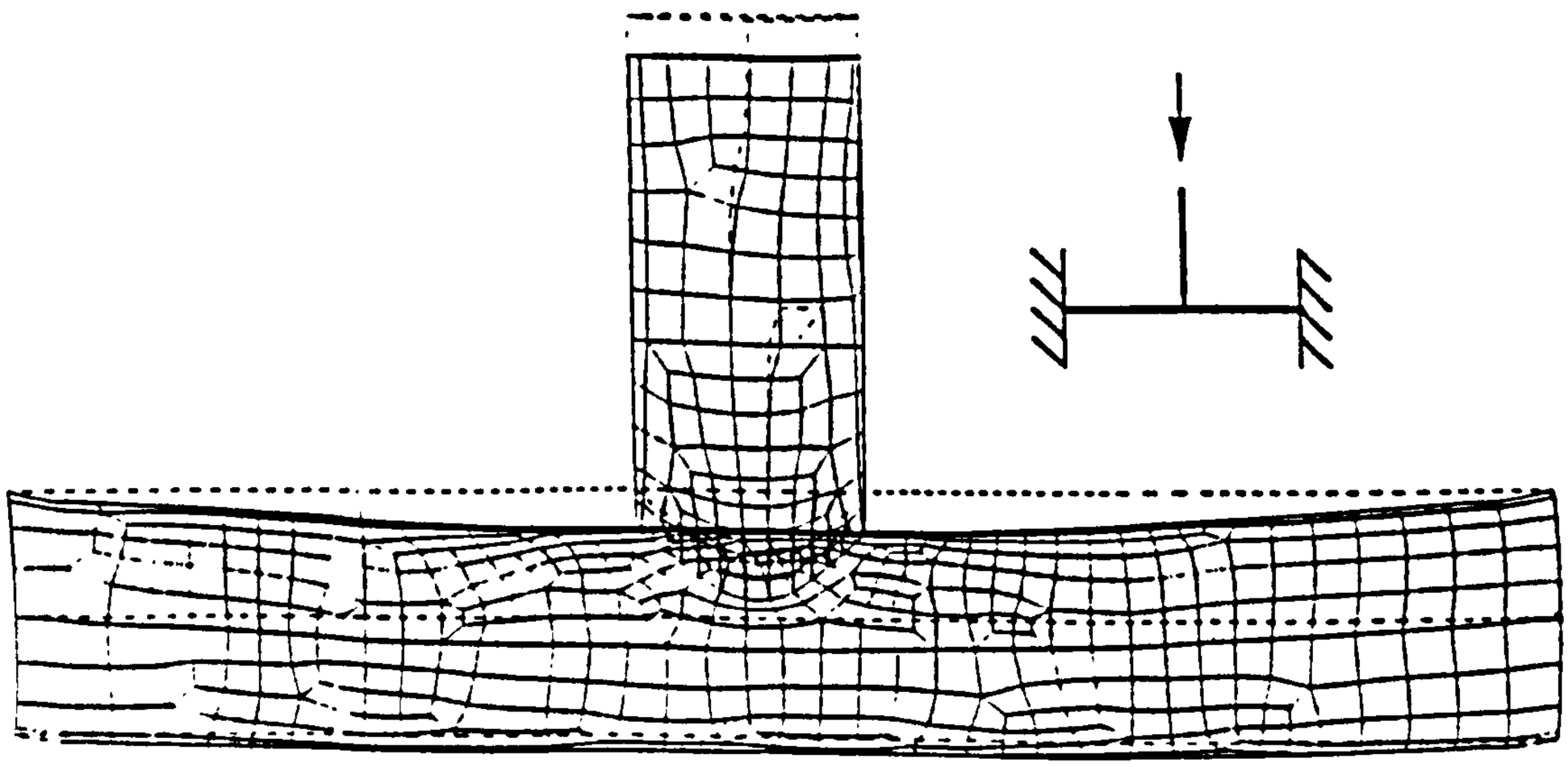

Figure 8.8 Displaced Shape Plot β = 0.9 T Joint

SDRC I-DEAS V1.i(s): FE_Modeling_&_Analysis 13-NOV-93 09:32:38

Database: none
View : No stored View
Task: Post Processing
Model: 1-FE MODEL1

Units : MM
Display : No stored Option
Model Bin: 1-MAIN
Associated Workset: 1-WORKING_SET1

ABAQUS 4-9-1 : *STATIC

LOAD SET: 1 TIMESTEP: 12 TIME: 0.2940918
FRAME OF REF: GLOBAL
STRESS - VON MISES MIN: 6033.48 MAX: 5.14E+05

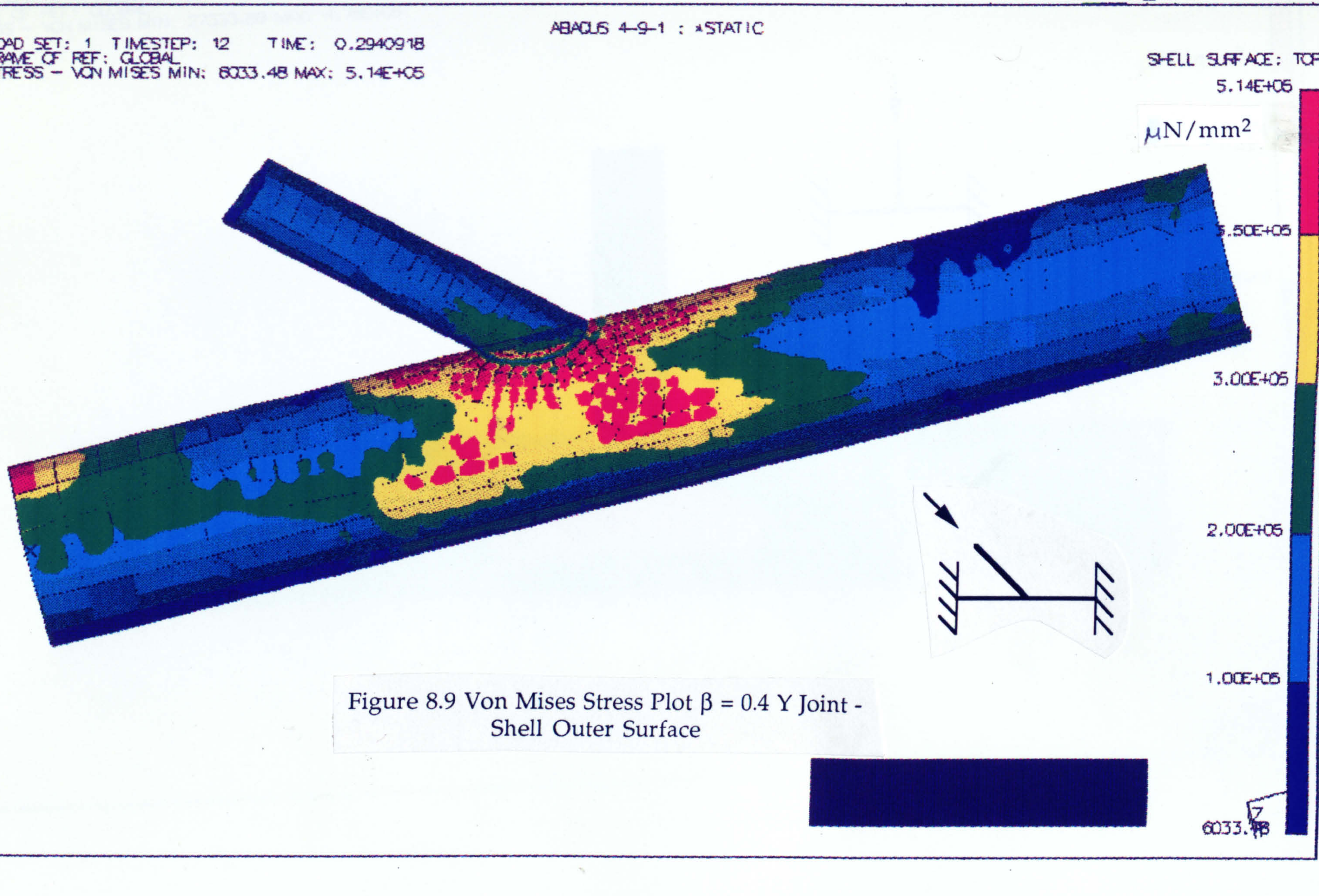

Figure 8.9 Von Mises Stress Plot β = 0.4 Y Joint - Shell Outer Surface

Some text bound close to the spine.

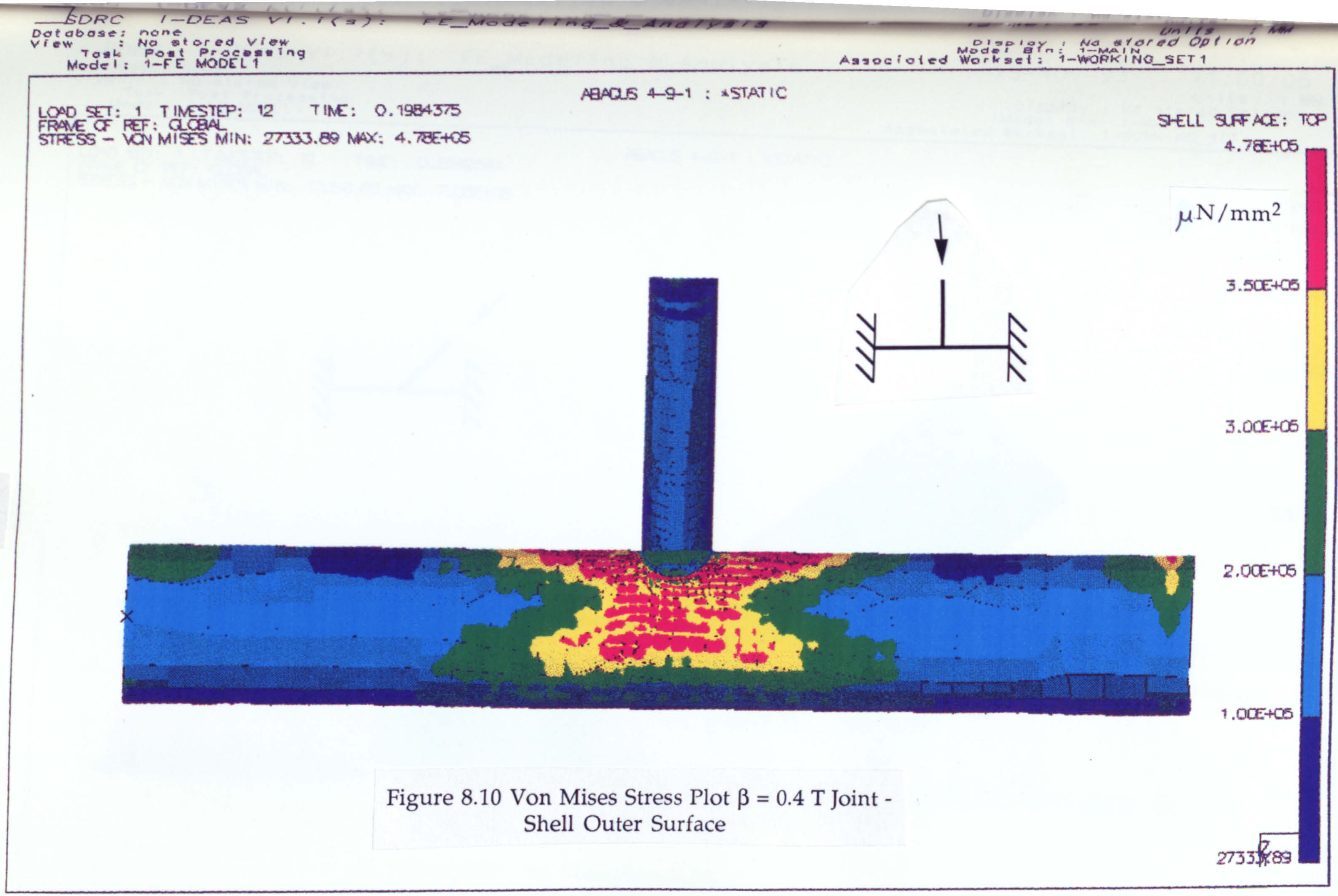

Figure 8.10 Von Mises Stress Plot β = 0.4 T Joint - Shell Outer Surface

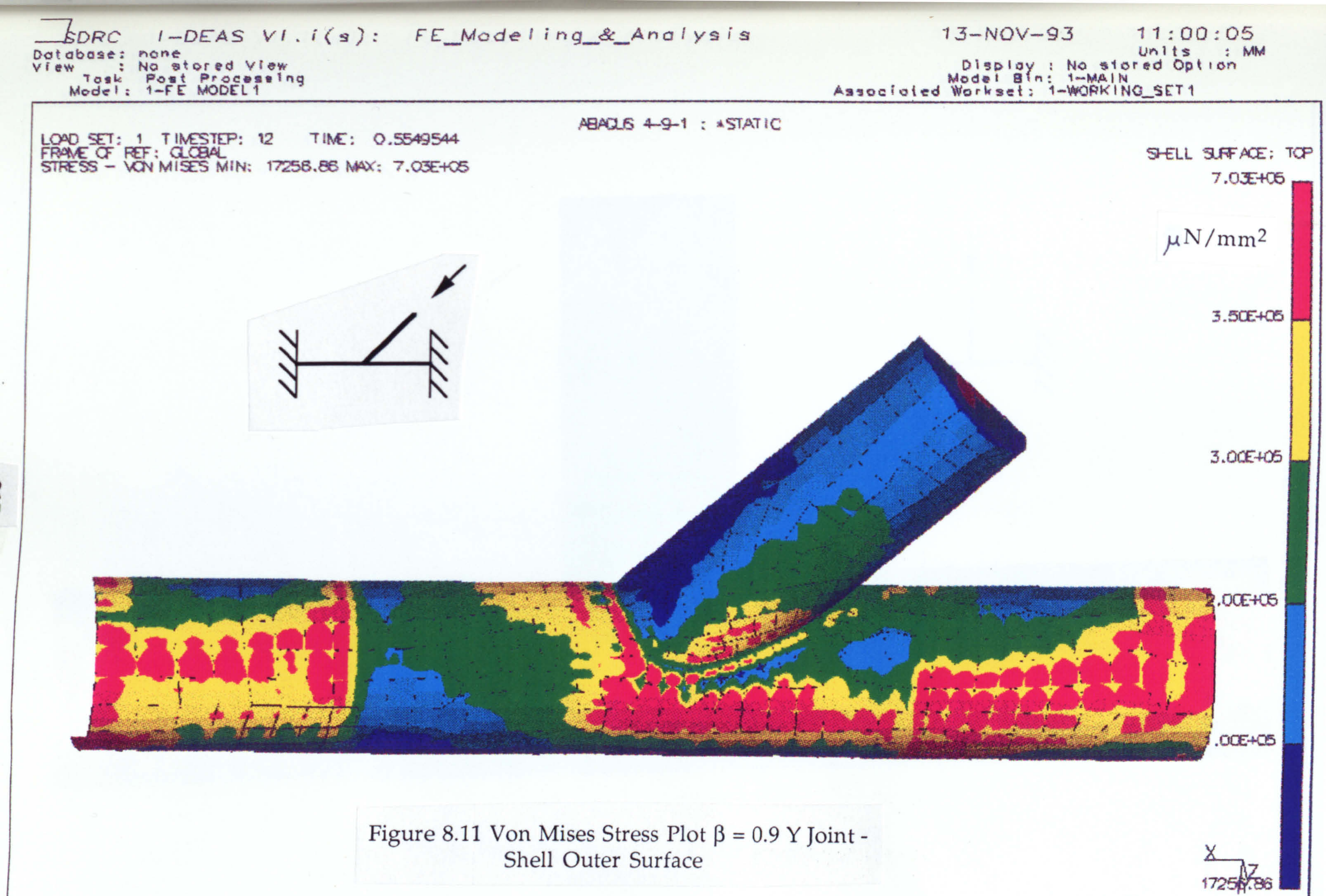

Figure 8.11 Von Mises Stress Plot β = 0.9 Y Joint - Shell Outer Surface

SDRC I-DEAS V1.i(s): FE_Modeling_&_Analysis 13-NOV-93 11:38:52
Units : MM
Database: none
View : No stored View
Task Post Processing
Model: 1-FE MODEL1
Display : No stored Option
Model Bin: 1-MAIN
Associated Workset: 1-WORKING_SET1

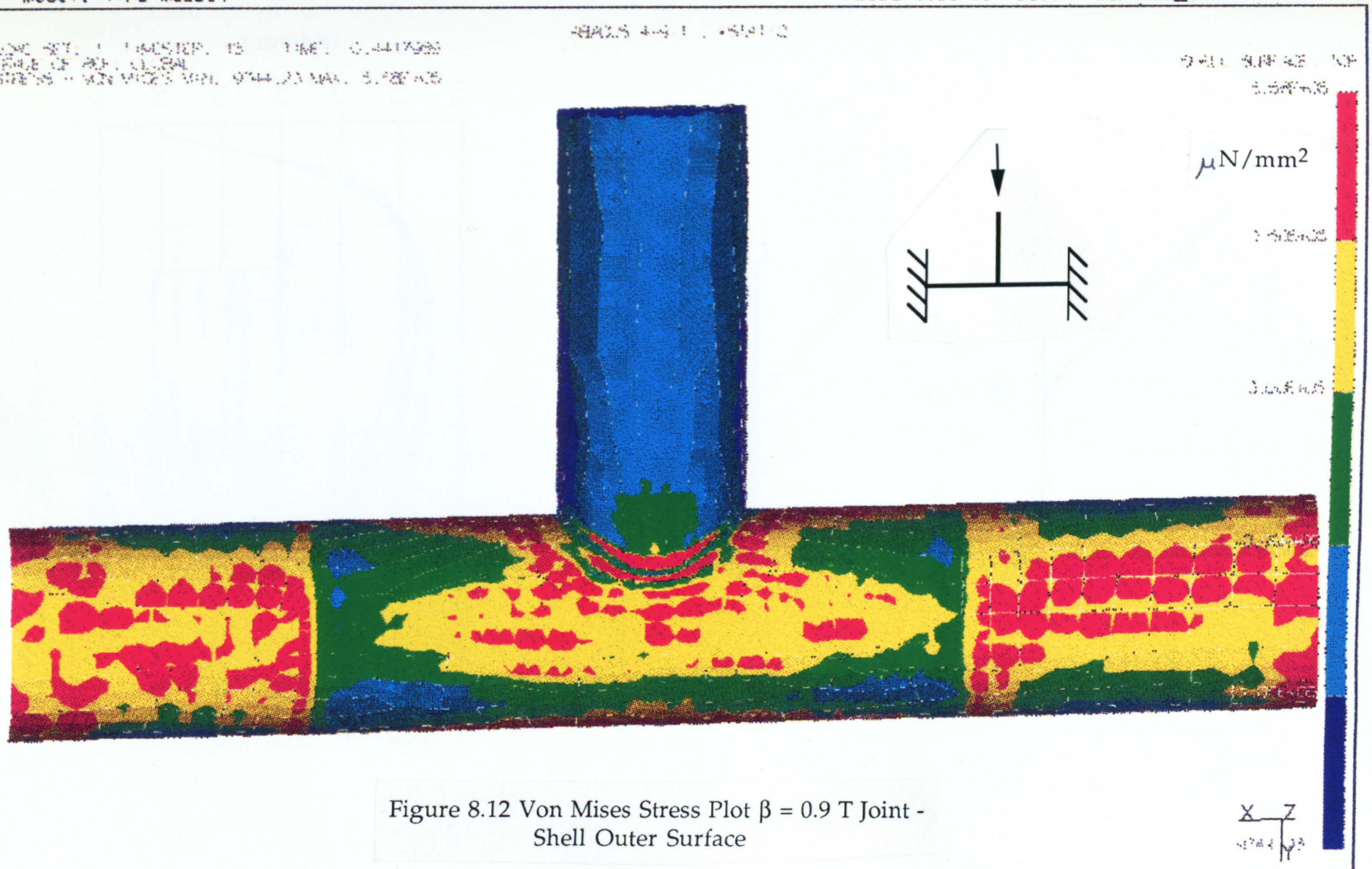

Figure 8.12 Von Mises Stress Plot β = 0.9 T Joint - Shell Outer Surface

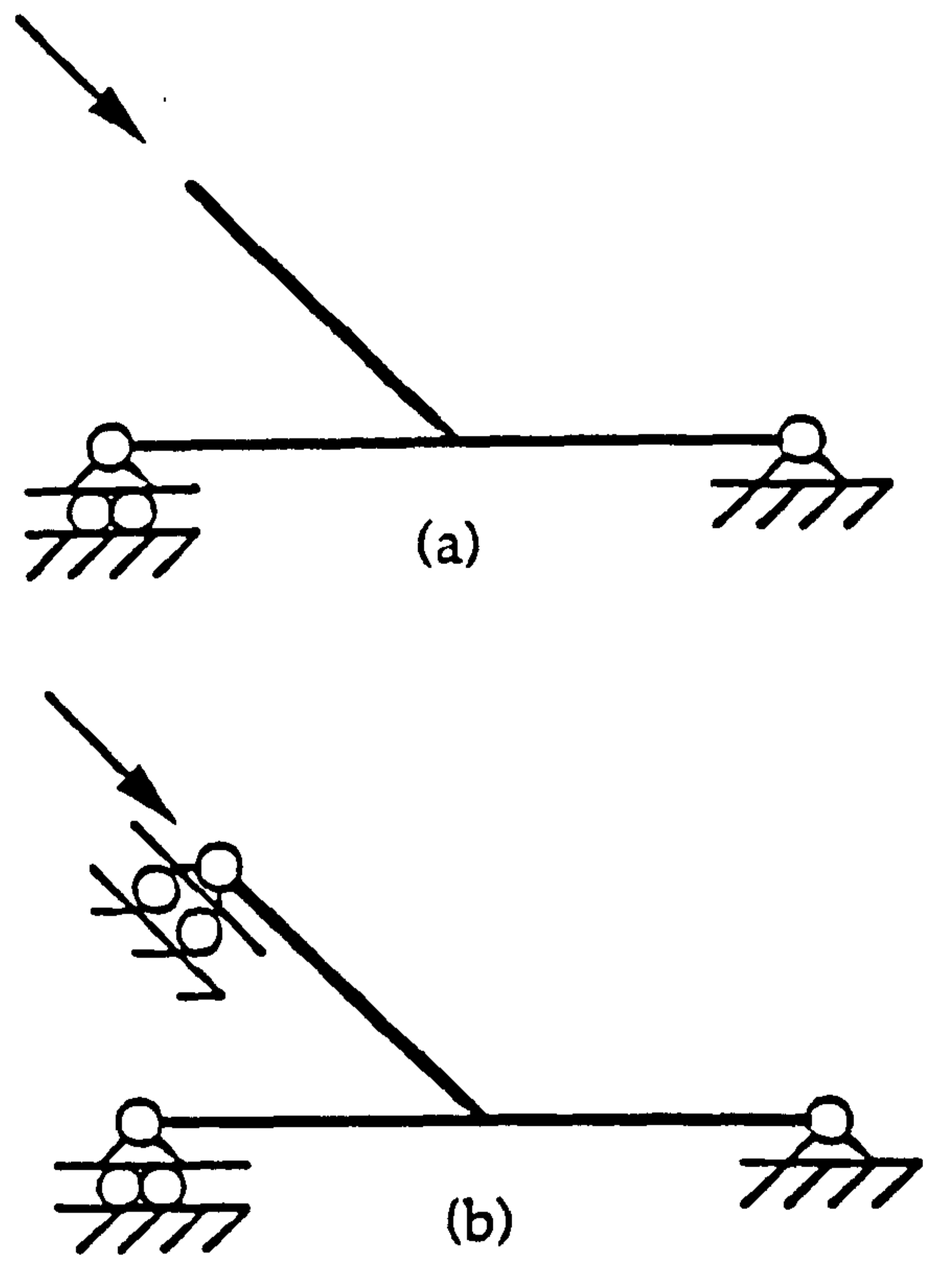

Figure 8.13 Y Joint Analyses undertaken at Nottingham Restraint Cases A and B.

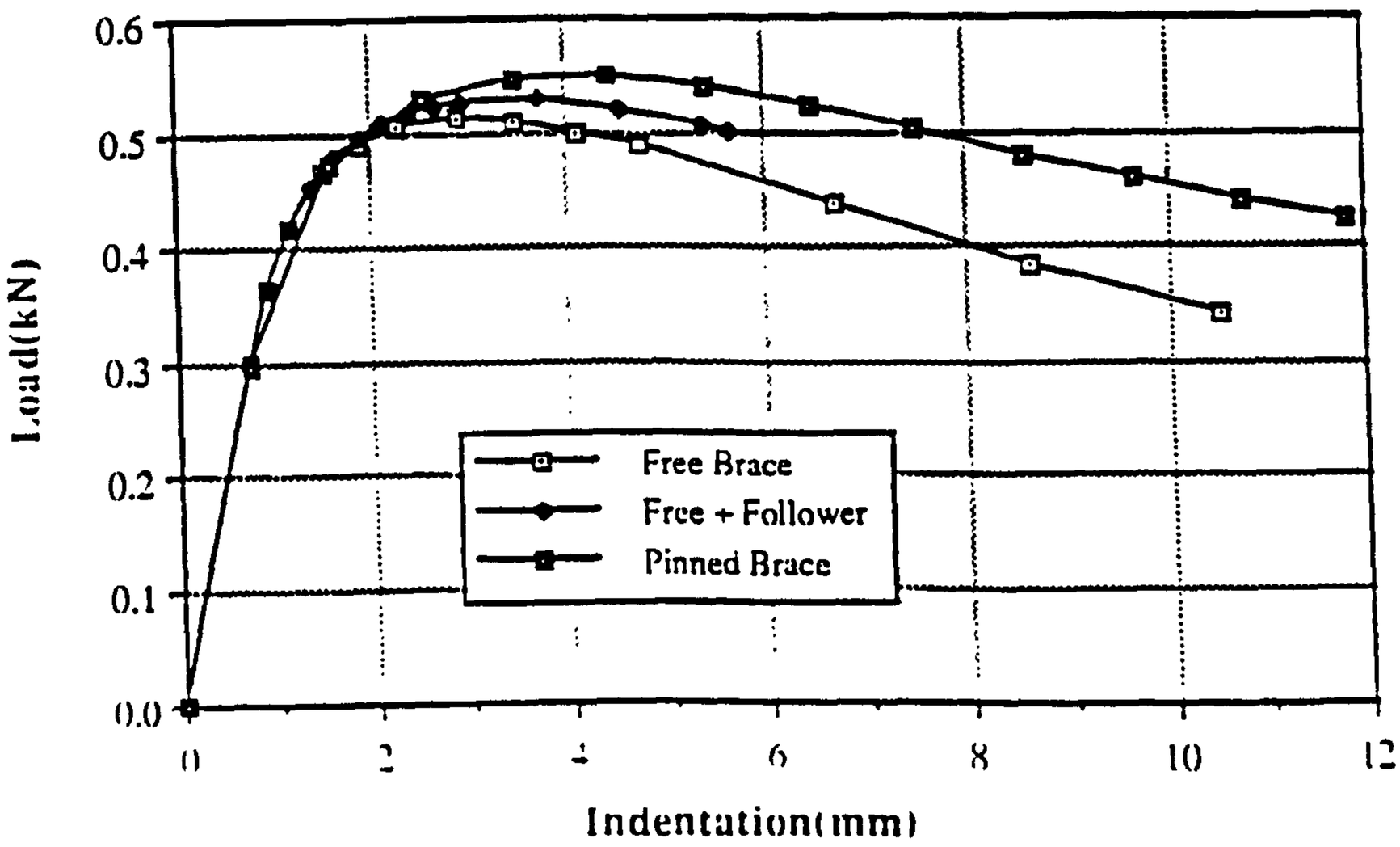

Figure 8.14 Load vs Indentation Plots for Y Joints Cases A and B

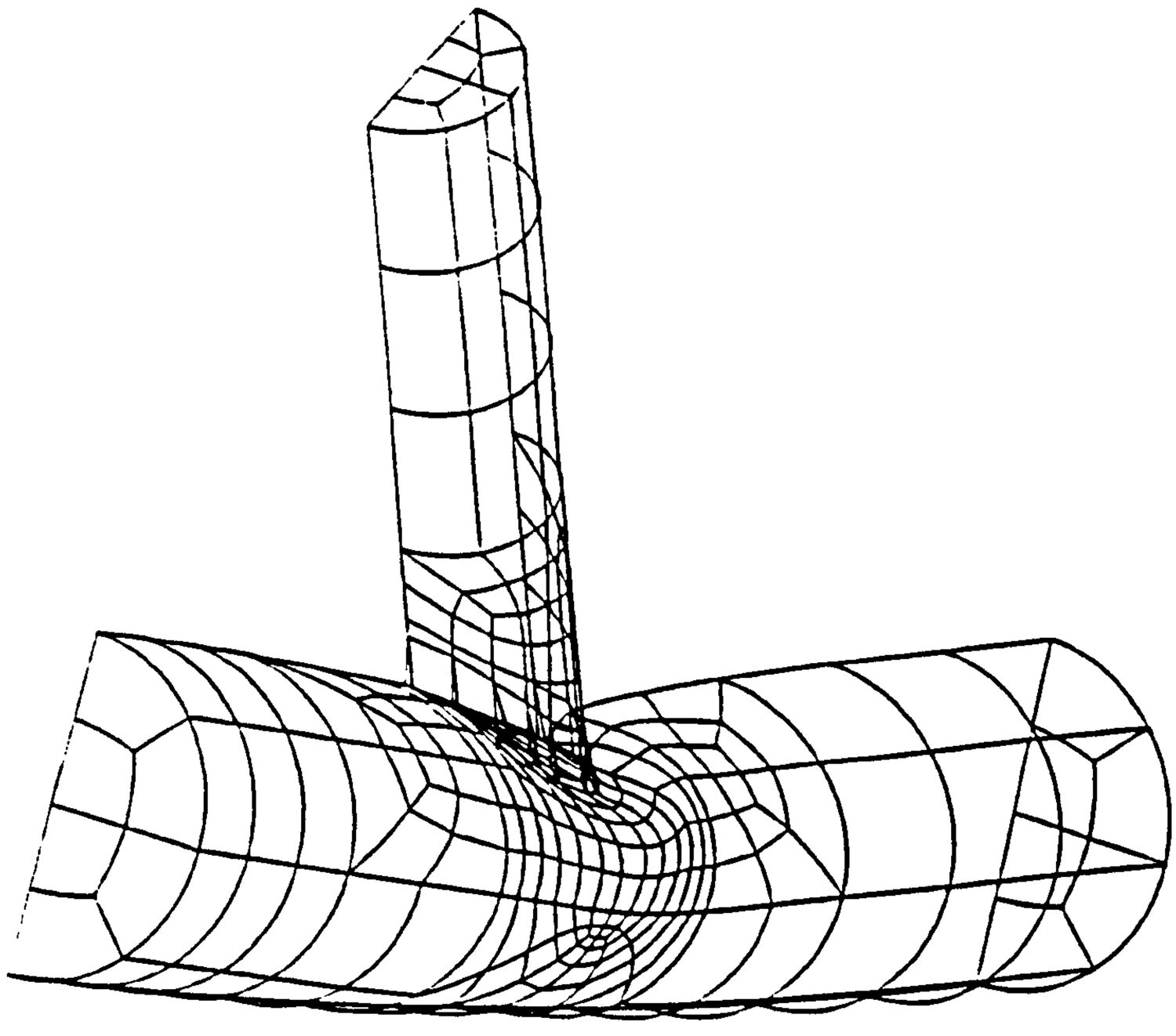

Figure 8.15 Displaced Shape for Restraint Case A

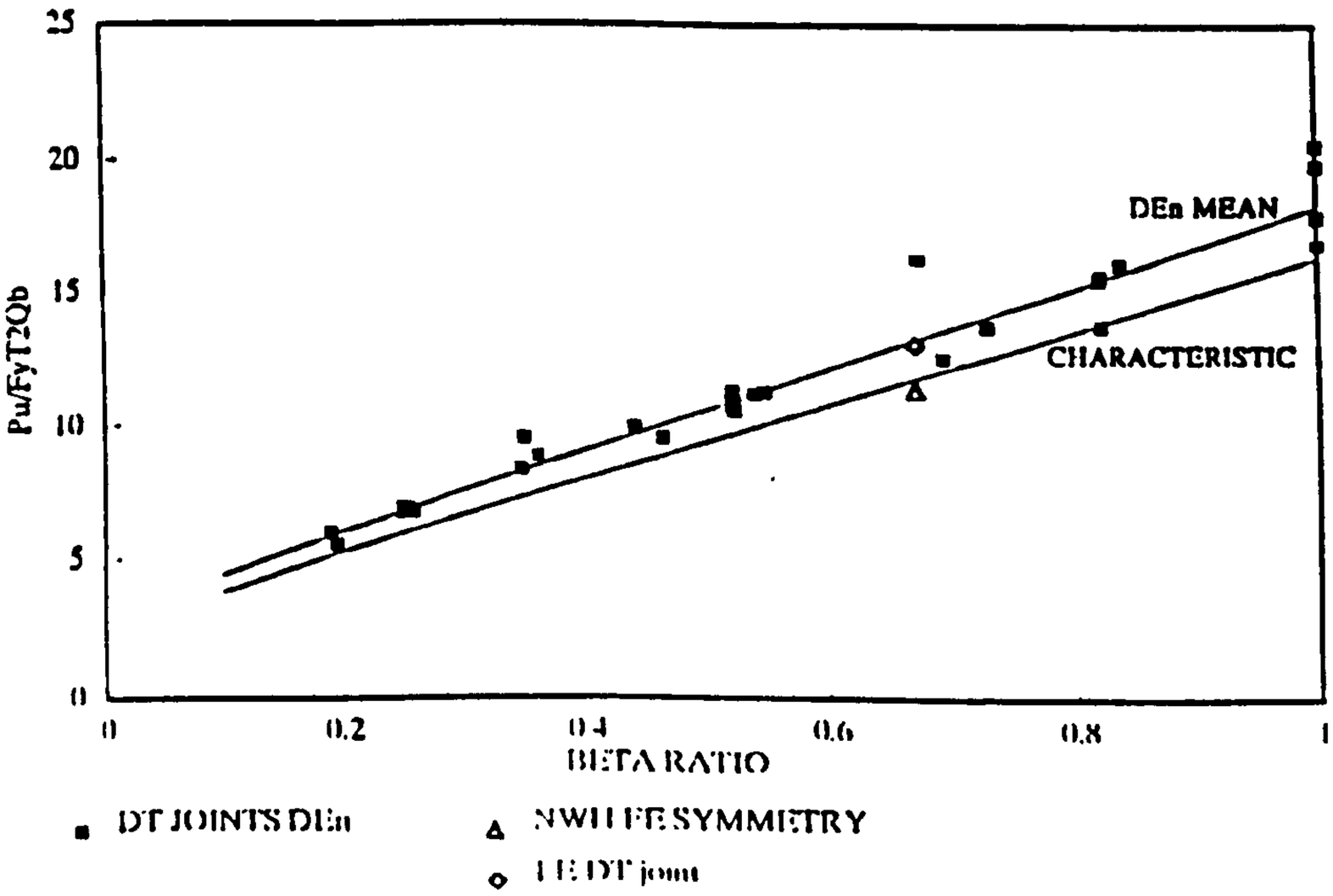

Figure 8.16 Non-Dimensionalised Capacity vs β Ratio for DT/X Joints in HSE dataset and FE results.

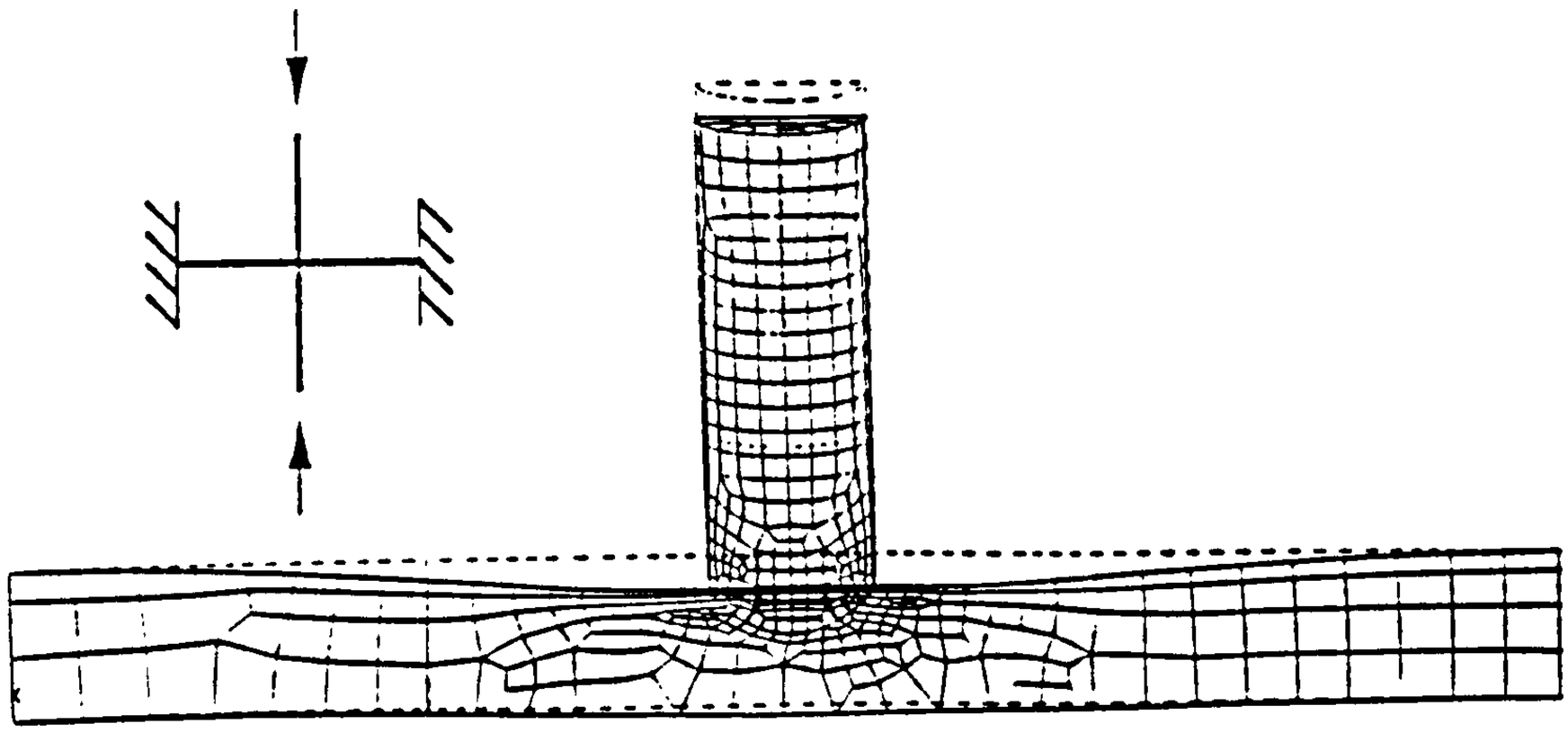

Figure 8.17 Displaced Shape Plot β = 0.667 DT Joint

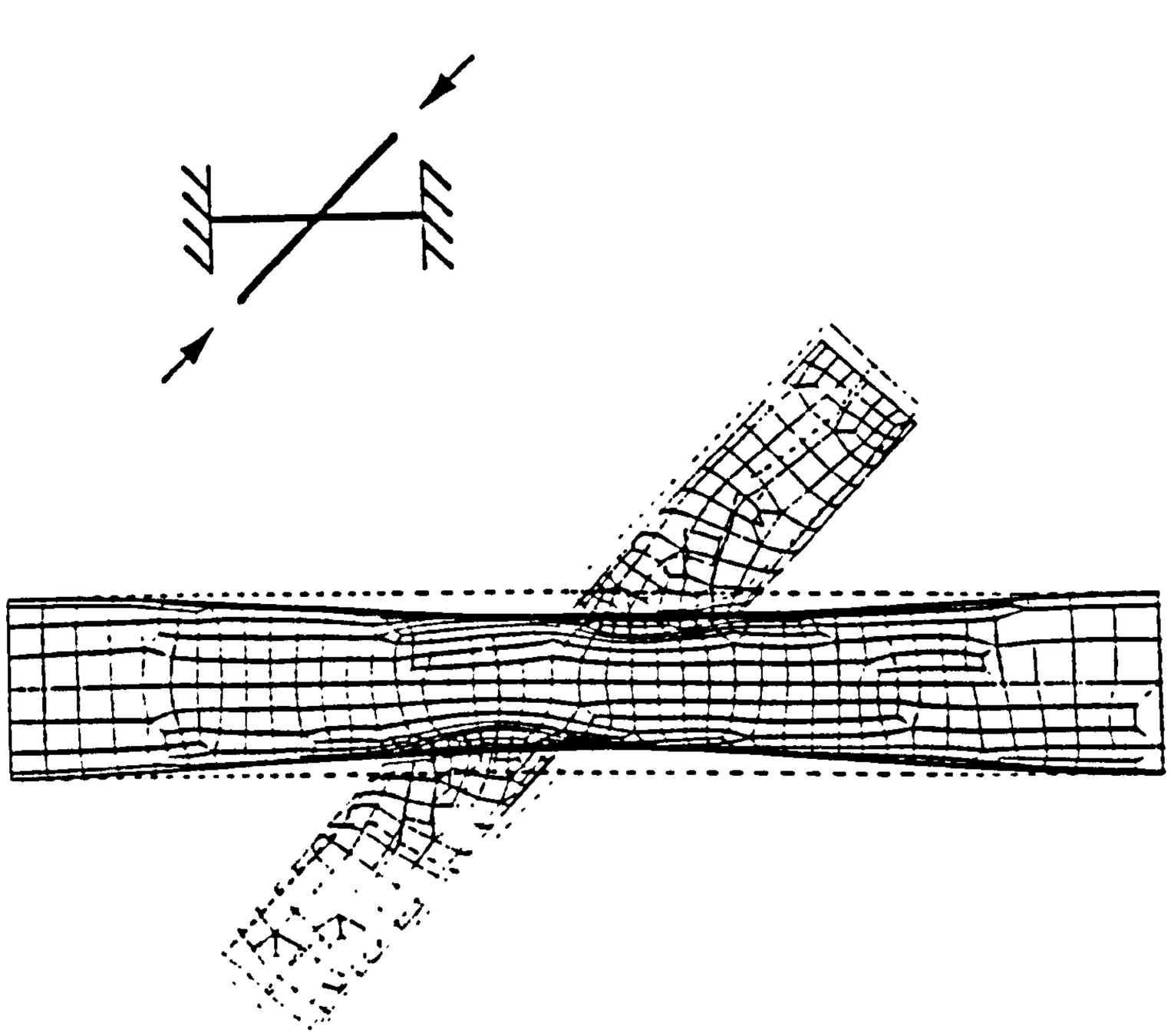

Figure 8.18 Displaced Shape Plot β = 0.667 X Joint

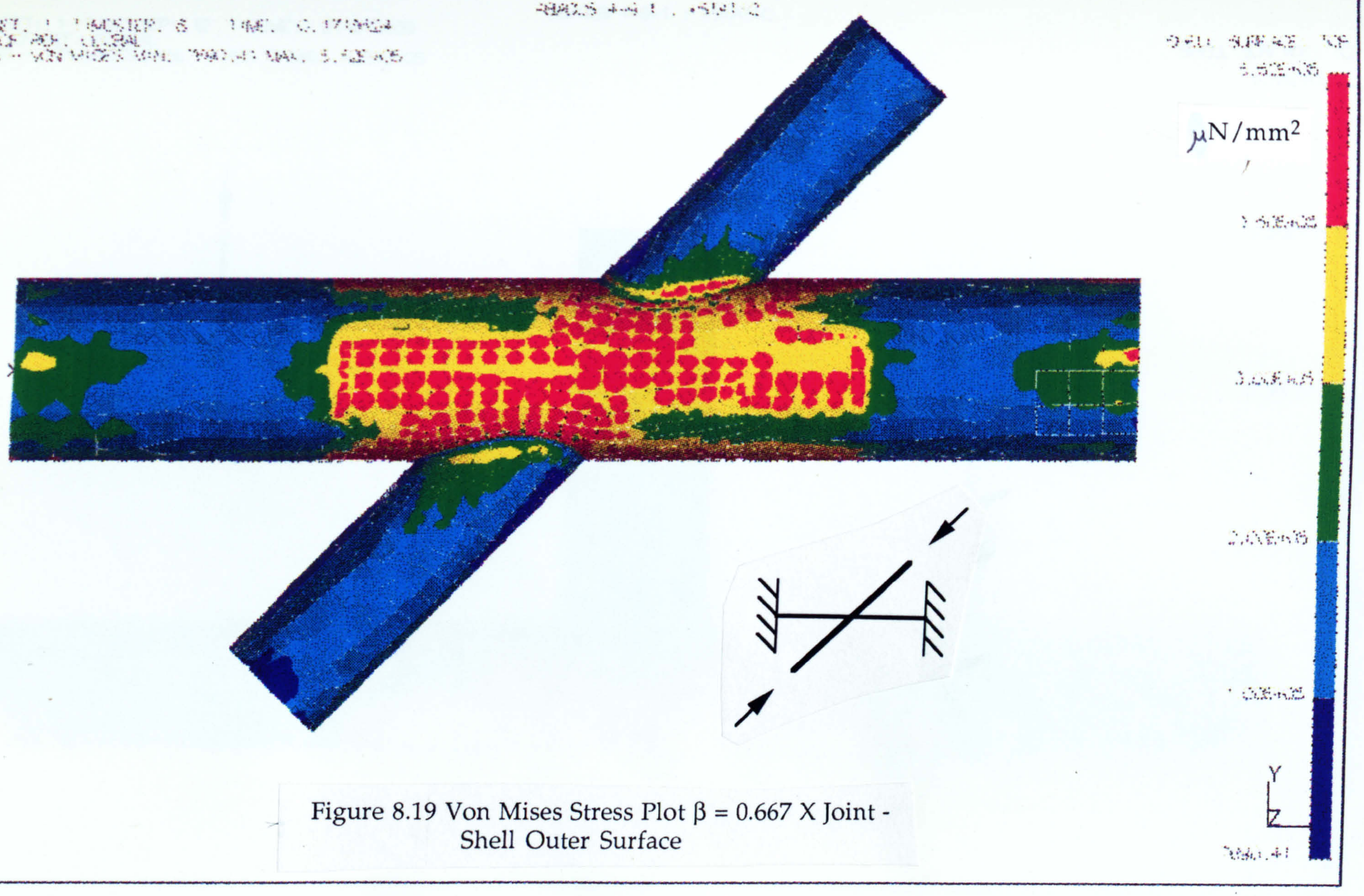

Figure 8.19 Von Mises Stress Plot β = 0.667 X Joint - Shell Outer Surface

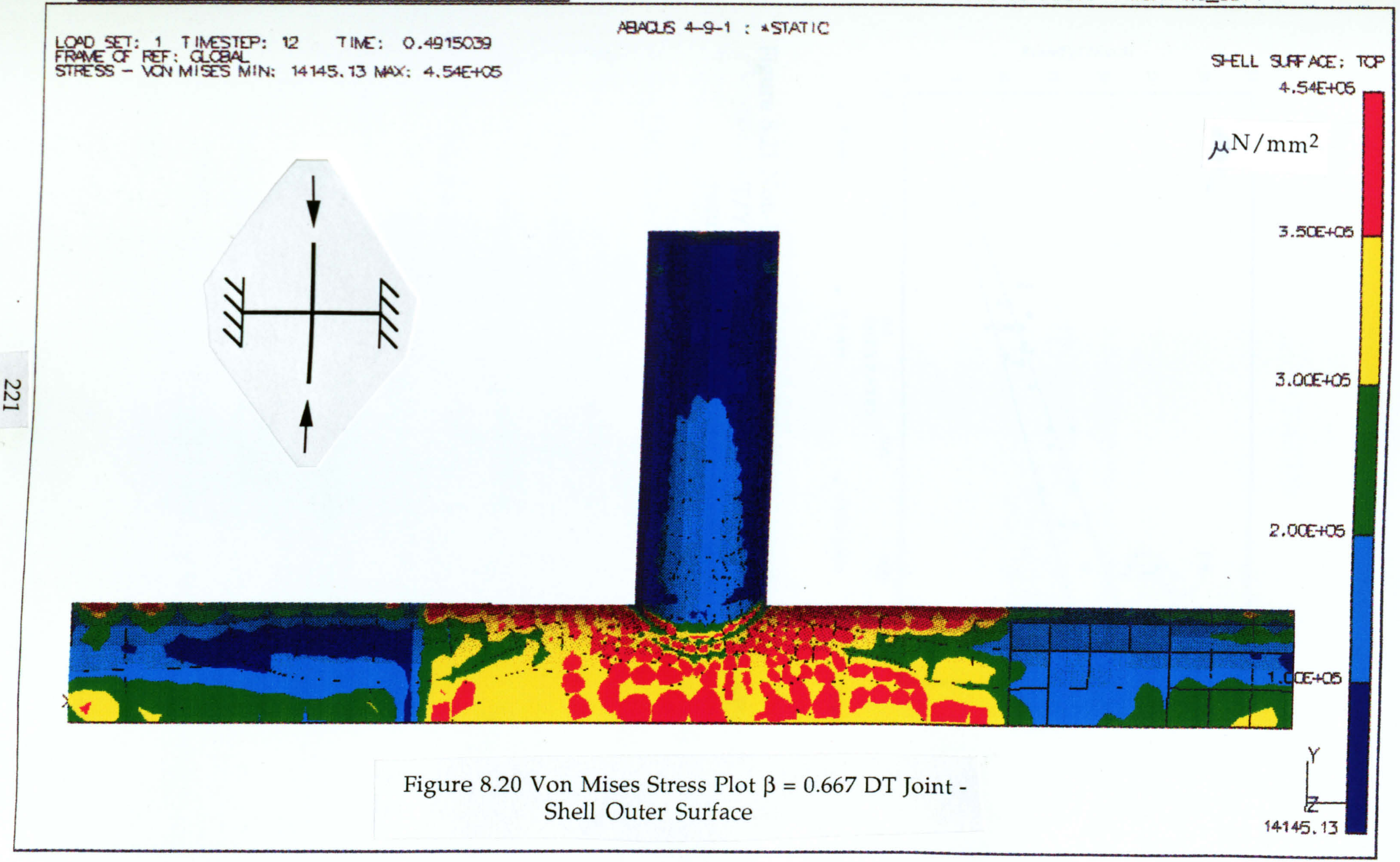

Figure 8.20 Von Mises Stress Plot β = 0.667 DT Joint - Shell Outer Surface

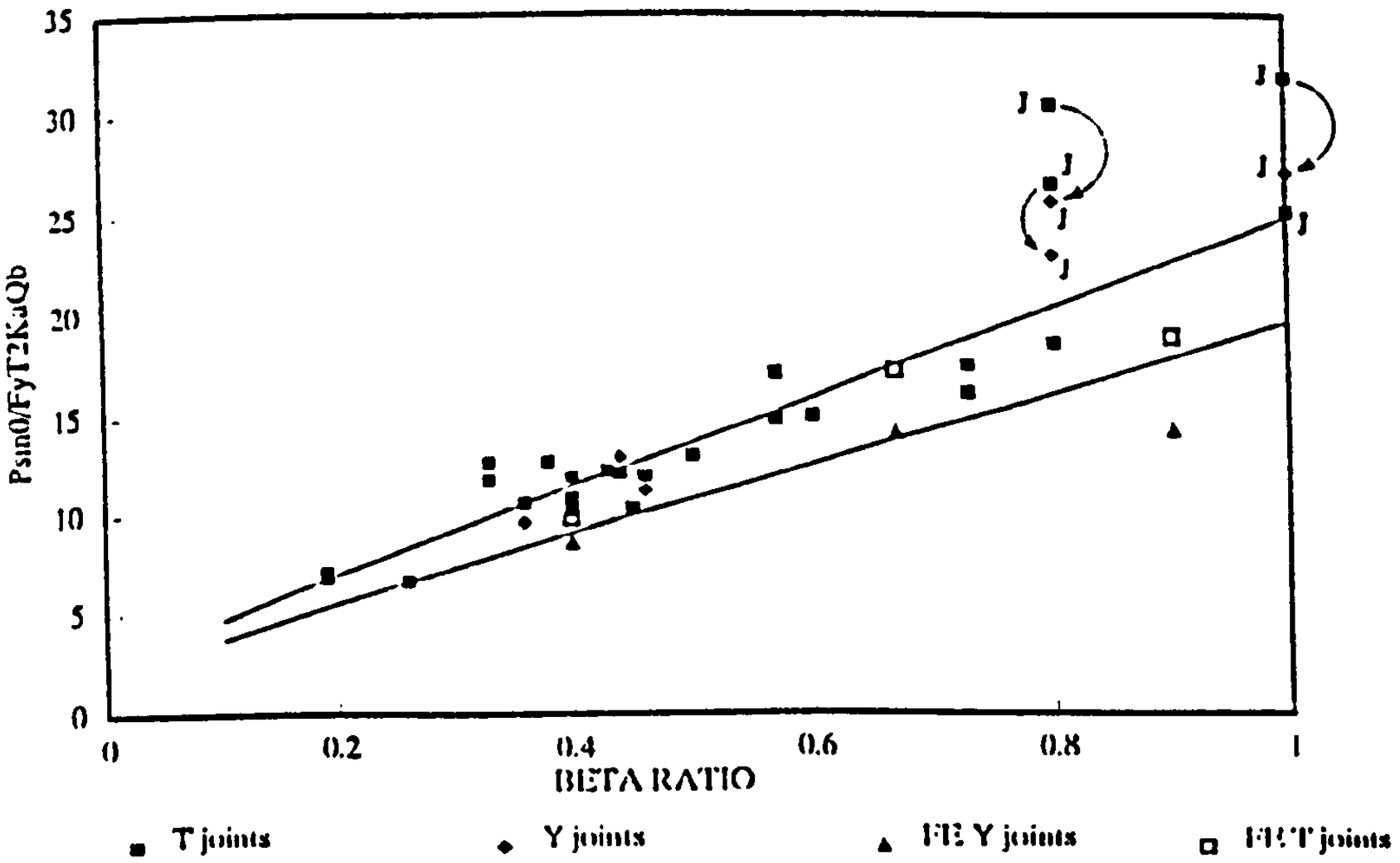

Figure 8.21 Non-Dimensionalised Capacity vs β Ratio for T/Y Joints in HSE dataset and JISSP 'short shord' results.

CHAPTER 9

INFLUENCE OF BRACE ANGLE AND INTERSECTION LENGTH ON RHS JOINT CAPACITY.

9.1 Introduction

Observation of the Packer et al (1992) design guidance on axially loaded single brace T and Y joints in RHS reveals two factors to account for the brace angle on the joint strength for both cases considered ($\beta < 0.85$ and $\beta = 1.00$). The two Packer formulae are as stated below:-

For $\beta < 0.85$

$$P_u = p_y t_o^2 \{ \frac{2h_1}{b_o \sin\theta} + 4\sqrt{1-\beta} \} \frac{1}{1-\beta} \frac{1}{\sin\theta} \qquad \text{Eqn 9.1}$$

For $\beta = 1.0$

$$P_u = f_k t_o [\frac{2h_1}{\sin\theta} + 10t_o] \frac{1}{\sin\theta} \qquad \text{Eqn 9.2}$$

where f_k is taken from BS5950 Table 27 (a)

both of these equations being relevant to failure in the chord.

Thus it can be seen that brace angle effects the joint capacity in two ways.

For both equations the load component is resolved to its value perpendicular to the chord, this being represented by the $1/\sin\theta$ term at the end of each equation.

For joints with $\beta < 0.85$ an additional term relates to the projected brace areas' effect on the capacity of the joint, similar to that for K_a in the HSE (1990) CHS formulation. This is based upon yield line theory. For joints with $\beta = 1.0$ the additional term manifests itself in two ways, the first being the projected length of the brace sidewall in contact with the chord sidewall, the other occurring in the slenderness derivation term f_k reflecting the change in buckling length of the chord sidewall due to the inclination of the load.

All experimental tests on joints in the literature were of $\theta = 90^o$ (i.e T joints). Therefore although yield line theory backed up the $\beta < 0.85$ joints with respect to the inclusion of the projected area term, no experimental evidence was available to verify this, hence the justification for this comparative FE study on RHS T and Y joints under axial load. Similarly no X joint data for which $\theta < 90^o$ (i.e DT) could be located where the β ratio was less than 1.0, this being briefly investigated later. Further justification for the study could be derived from the verification in the previous chapter of the apparent lack of validity of the K_a factor for CHS.

9.2 Yield Line Theory Verification for T and Y Joints

In Equation [9.1] the effective length term $2h_1/b_o\sin\theta$ appears to be justified being concerned with the lengthening of the hinge formed

by the brace sidewall. The effects of this on calculated capacity are shown in Table 9.1 for a $\beta = 0.6$ joint at various brace angles.

θ	$\frac{P_u \sin\theta (1 - \beta)}{f_y t_o^2}$ Eqn [9.1]	$\frac{Y}{T}$
30°	4.929	1.322
45°	4.226	1.133
70°	3.806	1.021
90°	3.729	1.000

Table 9.1 Variation of Packer et al (1992) Capacity with Brace Angle, θ for $\beta < 0.85$.

It can be noted here that this factor does not add as much to calculated capacity as that of K_a for CHS, this being due to the fact that the enhancement factor only effects two of the four brace edges in the RHS brace.

9.3 Finite Element Modelling

9.3.1 T and Y Joints

To make use of previously obtained T joint FE analyses results, the β ratios selected were $\beta = 0.25$, 0.6 and 1.0, Y joints constructed having brace angles of 45°. Basic dimensions of the Y ($\beta = 0.6$) joint are shown in Figure 9.1, all material properties being identical to those selected for the T joints modelled in Chapter 3, the material properties being shown in Table 3.1. All joints had a brace and chord thickness of

6.3mm. The weld in the $\beta = 0.25$ and 0.6 Y joints was modelled using the offset six noded solid model case (b) as described in Section 3.4.2.2. Weld modelling for the $\beta = 1.0$ Y joint was undertaken as discussed for the T ($\beta = 1.0$) joints in Chapter 5. For the Y ($\beta = 0.6$) joints several restraint conditions were investigated to establish whether supporting of the brace and the method of 'reacting out' the horizontal load component in the chord as tension or compression had any effect upon the ultimate capacity. $\beta = 1.0$ Y joint boundary restraint was undertaken as for the $\beta = 1.0$ T joints described in Chapter 5. As was stated in Chapter 8, load deformation plots are not so meaningful for T and Y comparisons as the points of measurement will be different, so the results for the joints are established in tabular format alongside the Packer et al (1992) design capacities in Table 9.2 ($\beta = 0.6$), Table 9.3 ($\beta = 0.25$) and Table 9.4 ($\beta = 1.0$). Failure capacity is determined as the elastic - plastic intersect or peak load as discussed in Chapter 3. Indication as to which was actually used to determine quoted failure capacities being given in the relevant tables. Load vs indentation plots for the four Y joint restraint cases in Figure 9.2 are shown in Figure 9.3. Displaced shape comparisons for T and Y $\beta = 0.6$ joints are shown in Figure 9.4, those for the $\beta = 0.25$ joints in Figure 9.5 and those for the $\beta = 1.0$ joints in Figure 9.6.

	FE (kN)	Packer (kN)	$\frac{FE}{Packer}$
T	190 (el-pl)	155	1.22
Y	295 (el-pl)	249	1.18

Table 9.2 T and Y Joint FE/Packer comparisons at $\beta = 0.6$. ($\frac{b_o}{t_o} = 23.8$)

	FE (kN)	Packer (kN)	$\frac{\text{FE}}{\text{Packer}}$
T	79 (el-pl)	88	0.90
Y	123 (peak)	131	0.94

Table 9.3 T and Y Joint FE/Packer comparisons at $\beta = 0.25$. ($\frac{b_o}{t_o} = 23.8$)

	FE (kN)	Packer (kN)	$\frac{\text{FE}}{\text{Packer}}$
T	990(peak)	655	1.51
Y	1309(peak)	920	1.42

Table 9.4 T and Y Joint FE/Packer comparisons at $\beta = 1.0$. ($\frac{b_o}{t_o} = 23.8$)

9.3.2 DT and X Joints

The Packer et al (1992) design capacity formulae for DT and X joints is the same as for T and Y joints reflecting the brace 'in-punch' deformation usually seen within these joints. Again the literature contains no evidence of experimental tests on X (i.e $\theta < 90^o$) joints with a β ratio of less than 1.0 being undertaken, hence the reason here for a brief comparison between a DT and a 45^o X joint at a β ratio of 0.6 to check the validity of the formula. Models were established using the techniques already described, advantage being taken of the symmetry to model half of the X joint and one eigth of the equivalent DT joint. The ultimate capacities obtained for these are compared to those of the Packer et al (1992) design formulae in Table 9.5, displaced shape plots being shown in Figure 9.7.

	FE (kN)	Packer (kN)	$\frac{\text{FE}}{\text{Packer}}$
DT	188.0	155.4	1.21
X	451.1	249.2	1.81

Table 9.5 DT and X Joint FE/Packer comparisons at $\beta = 0.6$. ($\frac{b_o}{t_o} = 23.8$)

9.4 Discussion

9.4.1 T and Y Joints

As can be seen in Table 9.2 at $\beta = 0.6$ the two FE results overpredict the design capacities by similar amounts, the T joint considered being calibrated against the original planar experimental test MPJT1 in Chapter 4. At this ratio both Y and T FE joint results overpredict Packer et al (1992) design capacities by around 20%, indicating that the inclusion of the brace face projection term $2b_1/b_o\sin\theta$ is valid for RHS Y joints at this β ratio. The differences in behaviour caused by reacting out the horizontal component of the brace load as tension or compression and the inclusion of a roller restraint on the brace can be seen to be almost negligible in Figure 9.3. Examination of the displaced shape plot in Figure 9.4 reveals that the failure mode of both the T and Y joints at $\beta = 0.6$ is mainly 'in-punch' of the brace into the chord top face. This confirms the validity of the yield line model for the Y joint discussed earlier where chord top face indentation was considered.

As can be seen from Table 9.3 both FE results underpredict IIW capacities by 6% (Y) and 10% (T), the T joint being that analysed earlier in Chapter 4. This would again indicate that the Packer et al (1992) design capacity is giving realistic predictions and the presence of the projected area term is valid. Problems were encountered on the Y analysis at this β ratio with the brace bending and buckling globally but these were resolved by including a second roller support half way up the brace to prevent this global buckling and ensure 'joint' as opposed to 'brace member' failure. It can be seen from Figure 9.5 that again the mode of failure was in-punching of the brace into the chord.

In Table 9.4 the capacities of the β =1.0 T and Y joints are compared to the Packer et al (1992) design capacities. It can be seen that again both FE models overpredict design capacity by the order of 40 to 50% indicating that the inclusion of the two terms relating to the projected area of the Y brace and the buckling length for Y joints are valid. Examination of the displaced shape plots in Figure 9.6 reveals that the failure modes for β = 1.0 Y and T joints are similar involving buckling our of the chord sidewall in the region immediately below the brace.

9.4.2 DT and X Joints

As can be seen in Table 9.5 both FE models overpredict the tabulated Packer et al (1992) capacities by 21% (DT) and 81% (X) respectively this indicating that both the terms included in the X joint formula to account for the angle of the brace are valid and are conservative. When the joint has an angle of 45° the FE capacity is

much larger than that of Packer. Where the angle is 90º the FE capacity can be seen to be 20% greater, the capacity here being similar to that of the equivalent T joint analysed in Chapter 4, this confirming the validity of the Packer (1992) assumption that DT and T capacities are predominantly similar in RHS. Observation of the displaced shape plots in Figure 9.7 confirms the mode of failure as in-punch of the braces into the chord for both DT and X joints at this β ratio.

9.5 Conclusions

1) The inclusion of a factor to account for the increase in strength created by the projected area of the brace onto the chord present in X and Y joints (i.e θ = 90º) appears valid for RHS, this not being the case for the CHS in Chapter 8.

2)Treatment of T and DT and X and Y joints with the same formula in the Packer et al (1992) design guidance appears to be valid.

3) Reacting out of the horizontal component of brace load in a Y joint as either tension or compression has no significant effects on joint capacity or behaviour.

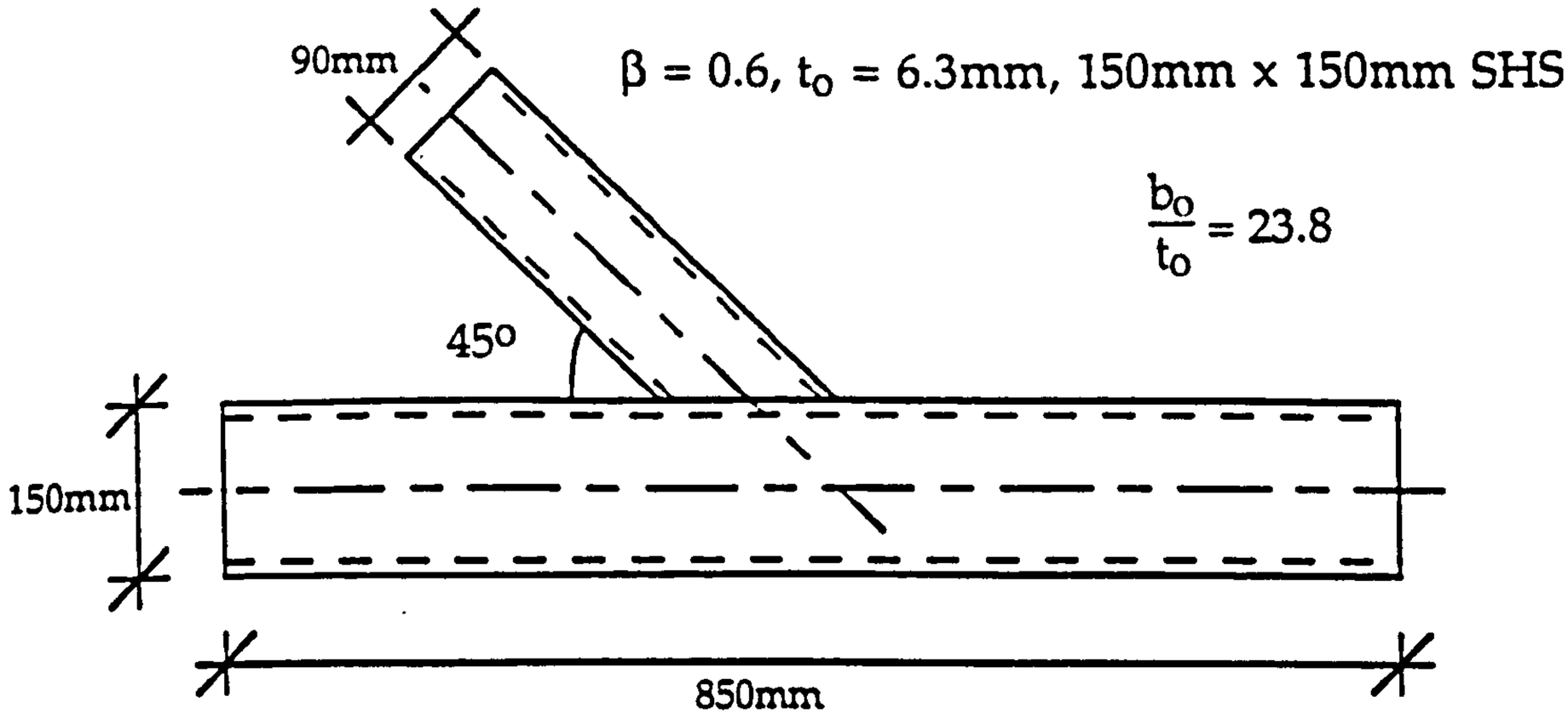

Figure 9.1 Dimensions for the β = 0.6 Y Joints.

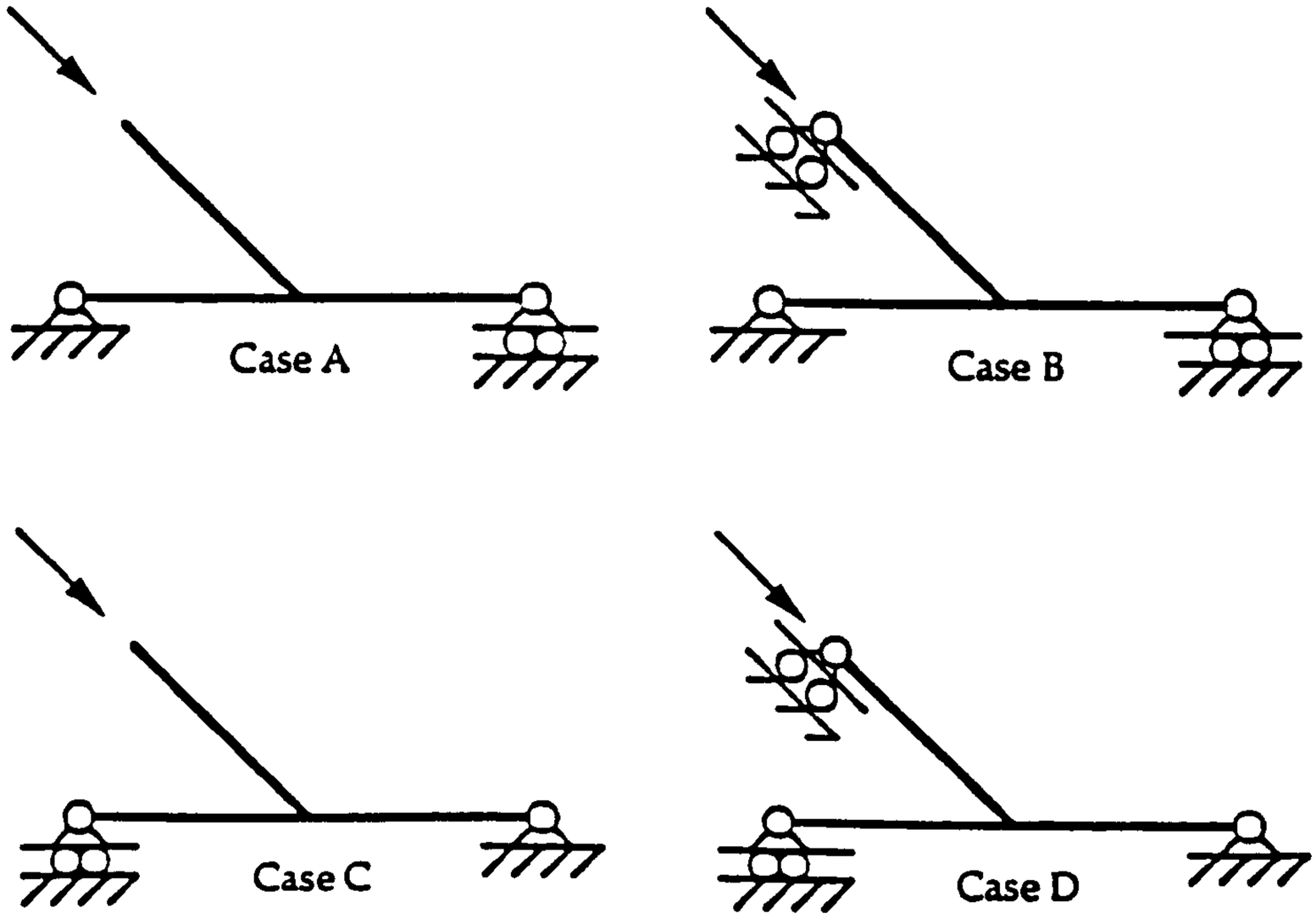

Figure 9.2 The Four Y Joint Boundary Cases.

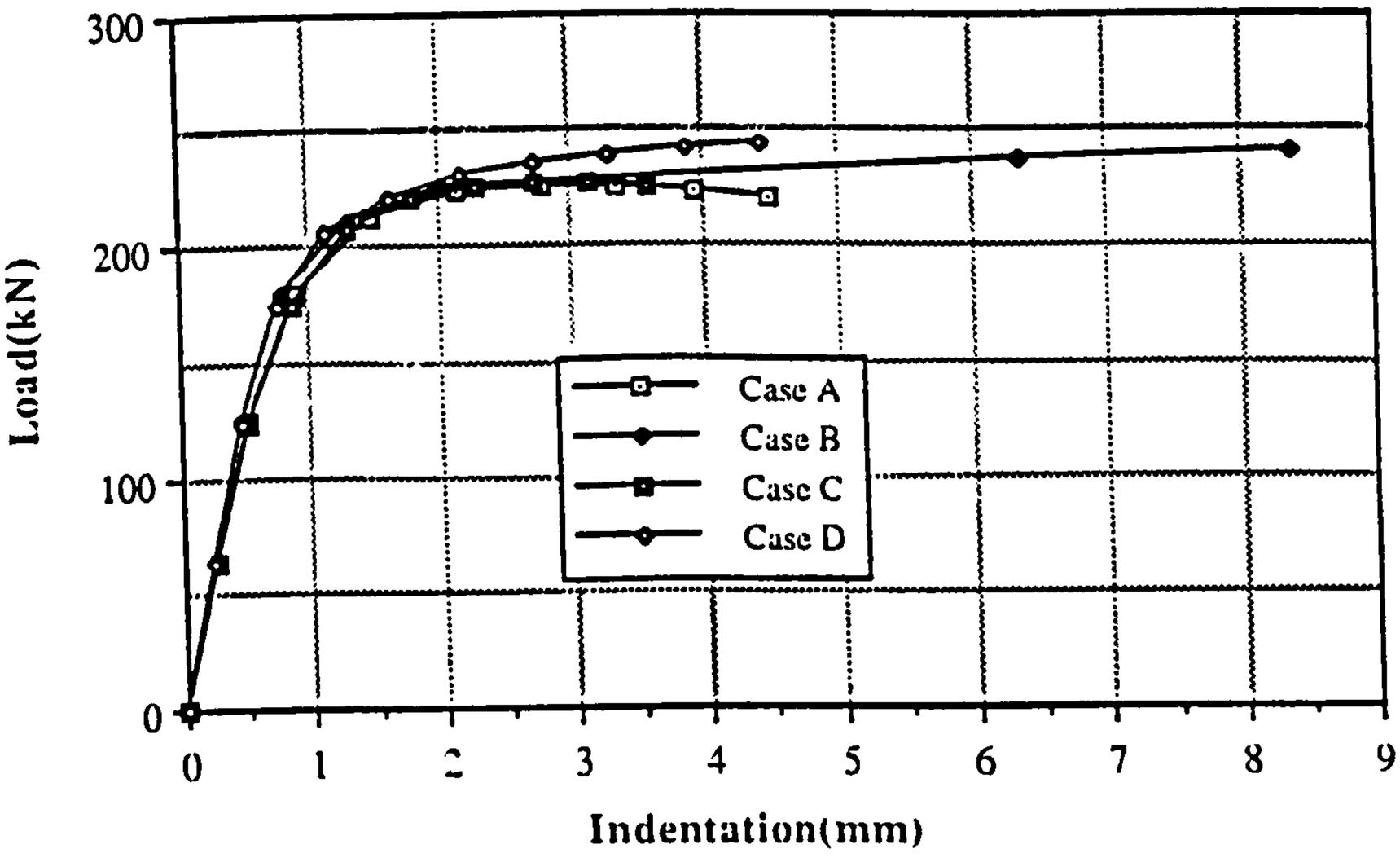

Figure 9.3 Load vs Indentation Plots for the Four Y Joint Boundary Cases.

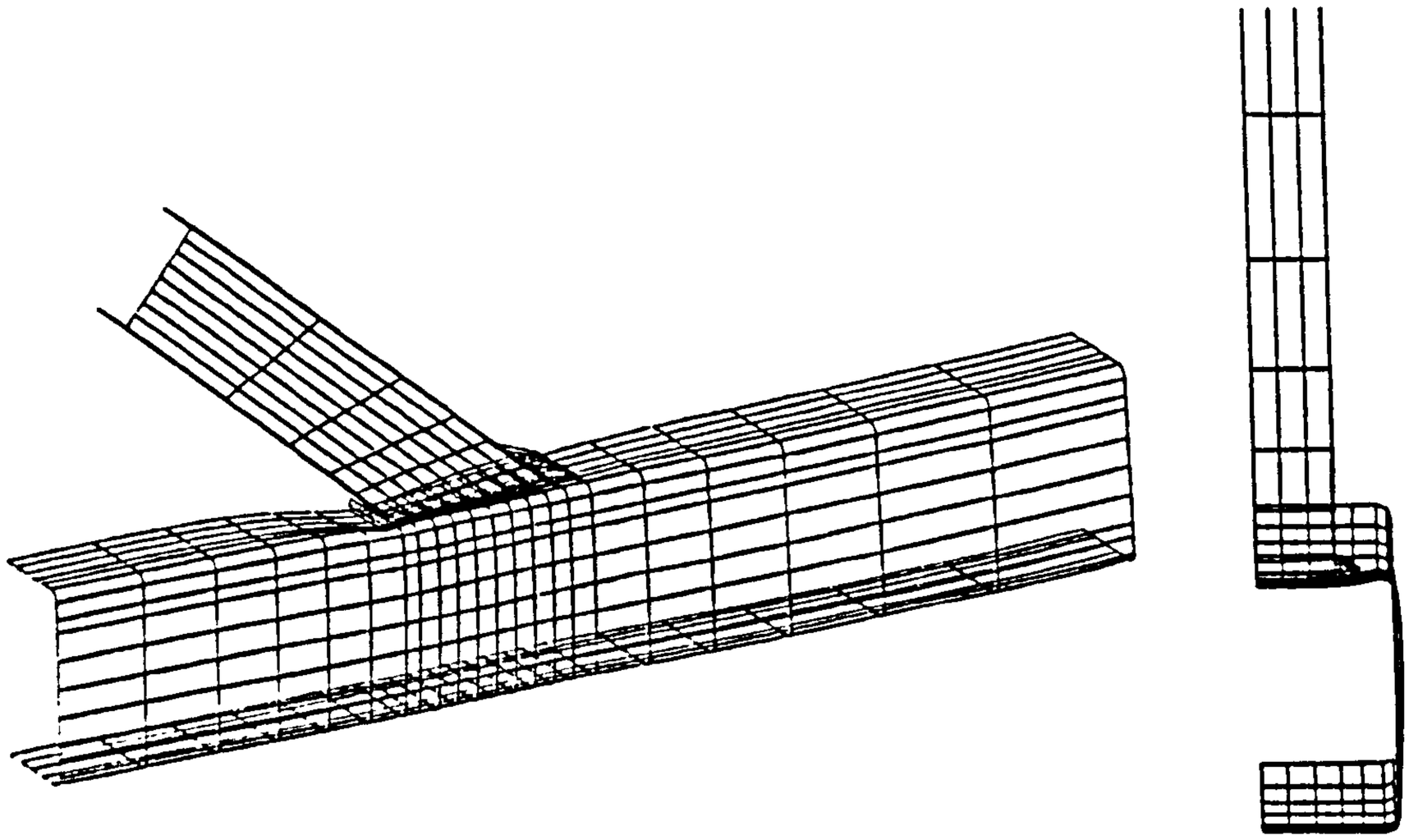

Figure 9.4 Displaced Shape Plots for T and Y Joints at $\beta = 0.6$.

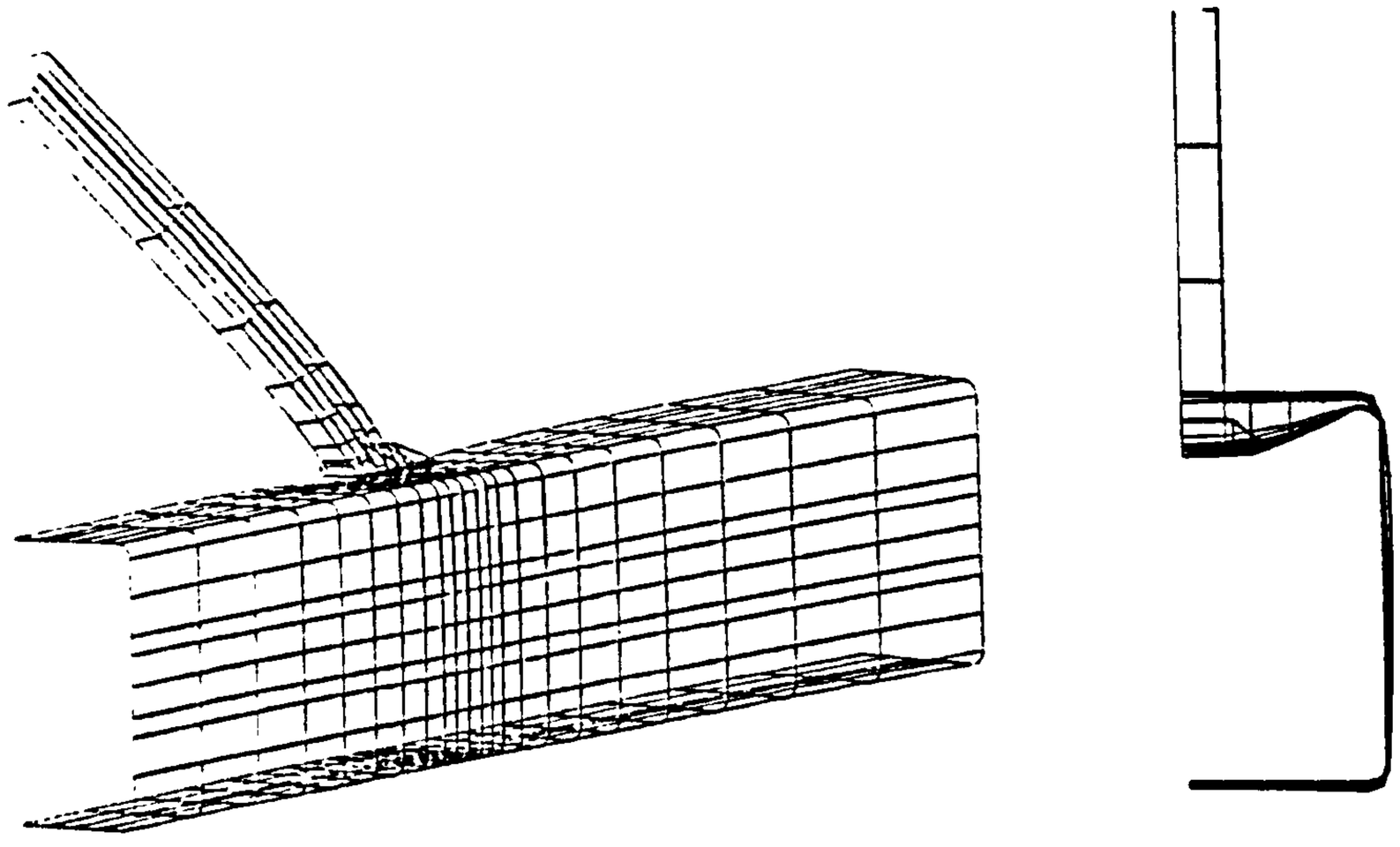

Figure 9.5 Displaced Shape Plots for T and Y Joints at β = 0.25.

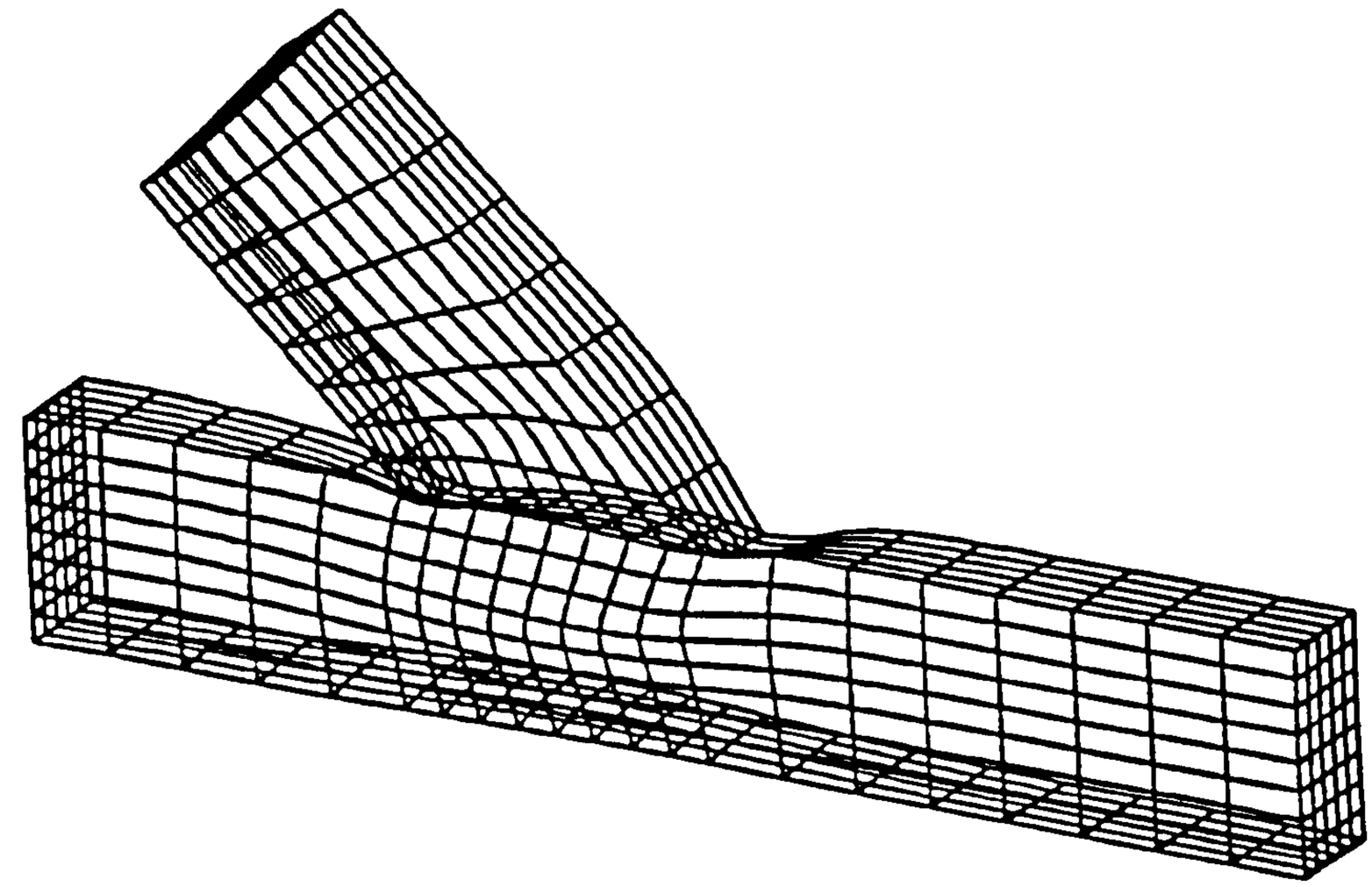

Figure 9.6 Displaced Shape Plots for Y Joints at β = 1.0.

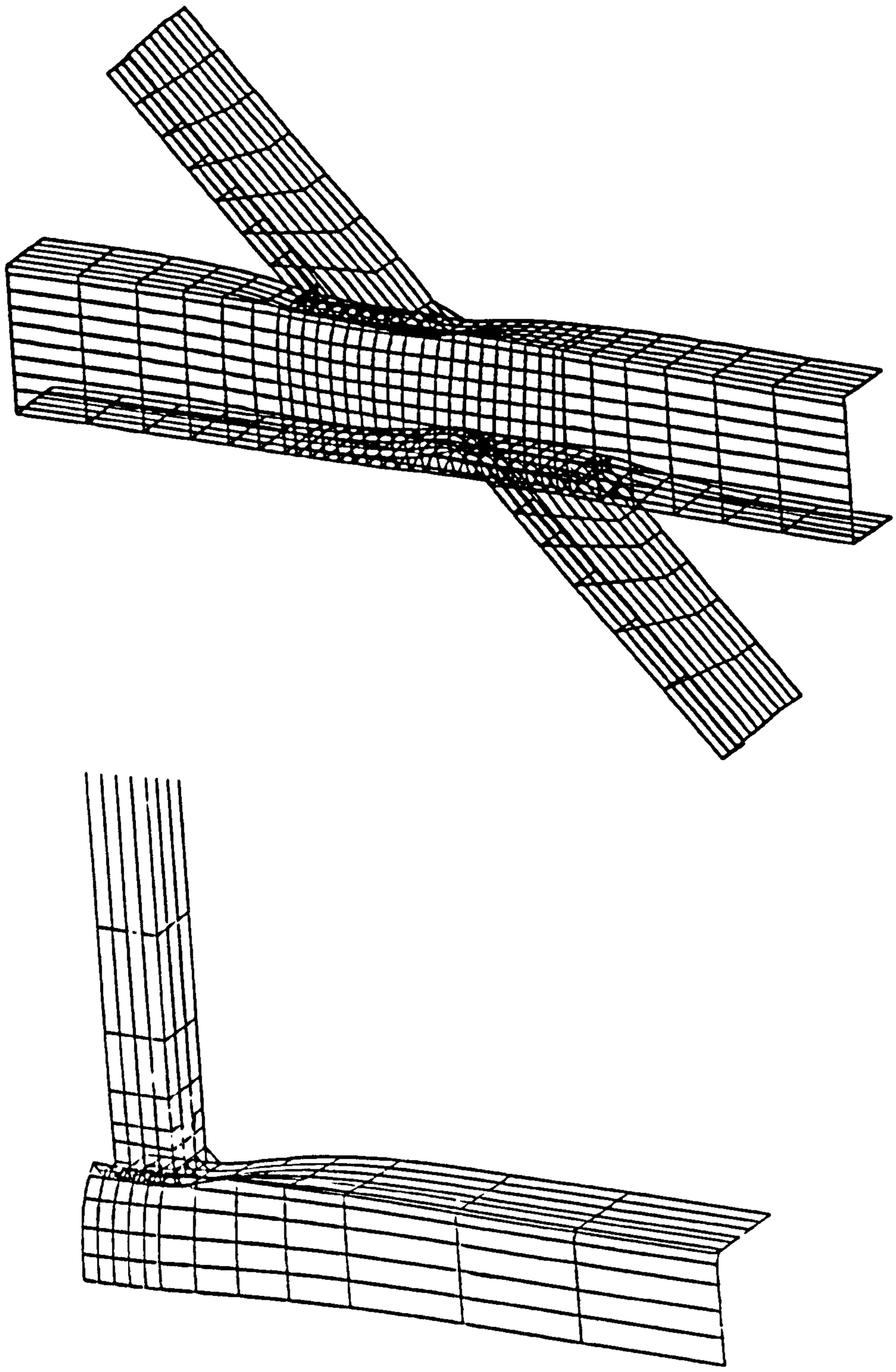

Figure 9.7 Displaced Shape Plots for DT and X Joints at $\beta = 0.6$.

CHAPTER 10

PARTIALLY OVERLAPPED RHS K JOINTS - BOUNDARY CONDITION EFFECTS

10.1 Introduction

It is accepted practice in girder and frame design to position bracing members so that their centre lines meet on the chord centreline, this being desirable to minimise the secondary bending moments induced in the braces and chord when axially loaded. In reality overall deflection, joint stiffness and local deflections can cause significant moments even where noding of the centrelines occurs. However CIDECT monograph 6 (1986) states that there is evidence that noding of the member centrelines reduces these secondary moment effects. In reality this noding can often only be achieved by partial overlapping of the braces as shown in Figure 10.1 compared with gap joints. Overlapping of braces often leads to an increase in strength, this being reflected in current IIW (1989) design guidance. This design guidance is developed largely from reviews of experimental programs on isolated joints (for Example Eastwood et al 1970) with some support from a series of full scale girder tests undertaken at the University of Nottingham (Dasgupta 1970), these being undertaken to verify whether

isolated test specimens were reasonably representative of 'in frame' behaviour. The object of the analyses in this chapter is to investigate the effect on ultimate capacity of a wide range of boundary conditions at two β ratios at θ = 60° in order to assess their effects and thus reasons for scatter in experimental data. Two β ratios are considered separately, 0.6 and 1.0 and for the purposes of avoiding primary moments due to the axial loading the brace centrelines node on the chord centreline as shown in Figure 10.1(a).

10.2 Modes of Failure of Overlap and Partial Overlap K Joints

The predominant mode of failure in overlap and partial overlap (where overlap > 25%) joints is local buckling of the compression brace adjacent to the connection with the tension brace (CIDECT monograph 1989), this mode being observed in the analyses described later. At smaller β ratios (i.e β < 0.4) and joints with a lower degree of overlap (where overlap < 25%) large deformation of the chord face beneath the heel of the compression brace has also been observed leading to failure. These are all shown in Figure 10.2. For β = 1.0, joint failure is often associated with chord top face deformation under the heel of the tension brace. Failure modes for overlapped and partially overlapped joints are often complex and many of those described briefly above are often found in combination as was the case for several of the analyses described in this Chapter. Further details of these modes of failure and the varying formats they can take are discussed by Bensalem (1989) and Coutie et al (1990).

10.3 Finite Element Modelling of K Joints

Due to their unsymmetrical nature, K joints require modelling of half of the joint when balanced axial loading is considered (i.e the resultant force perpendicular to the chord is zero). This necessitates a considerable amount of computing time and space to undertake the analyses and therefore all joints here and in Chapter 11 were analysed using ABAQUS on the SERC Fujitsu vpx mainframe at Manchester Computing Centre. Models were constructed at Nottingham directly as ABAQUS input decks, modelling techniques developed earlier in Chapter 3 being used throughout. Eight noded thick shell elements were used for the main brace and chord members and the end plates, six noded solids being used for the fillet welds. The weld modelling and attachment adopted is shown in Figure 10.3 alongside a typical mesh for the $\beta = 0.6$ joint corresponding to weld case (e) in 3.4.3.1. As can be seen the hidden weld is modelled using a shell element, the other welds using solids having common nodes with the corner nodes of the adjacent shell elements of the chord and bracing members. Chord, brace and weld material properties for all joints were taken as those in Table 3.1, but are repeated here for convenience in Table 10.1.

'Thick' end plates, as shown in the $\beta = 0.6$ mesh plot in Figure 10.3 were attached to the chord and brace ends to enable restraint conditions and axial loads to be applied at the centre points of these. Such end plates were assumed to be linear elastic in their behaviour (that is to say no plastic properties were given) and given a high E

	Chord	Brace
Thickness (mm)	6.3	6.3
External Dimensions (mm)	150 x 150	90 x 90
Yield Stress (N/mm^2)	420	420
Ultimate Stress (N/mm^2)	540	540

Table 10.1 Material Properties and Dimensions for K Joints.

value equal to 21,000 kN/mm^2 to ensure their deformation was negligible and that load transfer to the braces and chord was achieved.

10.4 Boundary Condition Study $\beta = 0.6$.

10.4.1 Boundary Condition Matrix

The matrix of boundary conditions investigated at $\beta = 0.6$ is shown in Figure 10.4 with defined 'normal' loading was compression in the through brace as shown. All other $\beta = 0.6$ joint dimensions are shown in Figure 10.5. All seven conditions were analysed twice, the repeated ones being with the loading reversed (i.e tension in the through brace). Analyses for cases f and g in Figure 10.4 were then re-analysed under the 'normal' condition with the *FOLLOWER option, described in 7.4.2 included for both braces. The *FOLLOWER option ensures that the load applied at any node rotates the same amount as that node during the analysis, effectively eliminating secondary moments except those caused by bending of the brace and local joint deflections.

10.4.2 Determination of Failure in K Joints

Modes of failure for RHS overlapped and partially overlapped K joints were discussed in Section 10.2, actual failure loads for these cases being determined as described in Section 3.3 and Figure 3.5. Most joint analyses reached peak load and this has been taken as failure; however where there was no peak the elastic-plastic intersection as described in Section 3.3 was established as the joint strength. Failure for K joints with $\beta = 0.6$ is commonly associated with an in-punching of the compression brace into the chord and this has been used to establish load vs indentation plots for the cases studied here. Indentation is taken as the change in distance between the point of application of the load and the point at mid-height on the chord sidewall that lies on the axis of the compression (and where e=0, by definition, the tension) brace. The location of this point is shown as 'P2' in Figure 10.6. A certain amount of this indentation will be axial shortening of the brace; however simple calculations according to $E = \sigma/\varepsilon$ reveal that at a brace load of 600kN this will be of the order of 0.5mm.

10.4.3 Analyses and Results for $\beta = 0.6$ Joints

Figures 10.7 (a) and (b) show the plots of brace load vs indentation for the series of joints a, f and g (Figure 10.4) where the chord is simply supported at both ends, Figure 10.8 showing the same again for the cases b, c, d, and i (Figure 10.4) where only one end of the chord is restrained. Figures 10.9 and 10.10 show the effects of adding the

*FOLLOWER (see Section 10.4) option to cases f and g under the 'normal' loading mode.

Displaced shape plots for the joints as labelled are shown in Figures 10.11 and 10.12. Table 10.2 presents the ultimate capacities of the joints in the matrix in Figure 10.4 alongside the Packer et al (1992) design strength. As the Packer et al (1992) formulae only give the strength for gap joints and joints with overlap > 25%, the capacity

Case	Compression in through bce (normal)	Tension in through bce (reversed)	Capacity (kN)	Packer capacity (kN)	$\frac{FE}{Packer}$
a	Yes		601.8	453.0	1.320
		Yes	645.5	453.0	1.420
b	Yes			453.0	
		Yes	351.2	453.0	0.775
c	Yes		644.1	453.0	1.422
		Yes	287.1	453.0	0.634
d	Yes		655.7	453.0	1.447
		Yes	647.0	453.0	1.428
f	Yes		268.1	453.0	0.592
		Yes	278.3	453.0	0.614
g	Yes		263.8	453.0	0.582
		Yes	278.3	453.0	0.614
i	Yes		603.3	453.0	1.332
		Yes	631.0	453.0	1.393

Table 10.2 Tabulated capacities of the $\beta = 0.6$ boundary condition matrix.

quoted in the table has been interpolated between these two formulae as the e = 0, β = 0.6 joint considered has an overlap of 20%. The reasons for adopting this in order to avoid moments induced due to noding eccentricity were discussed in Section 10.1.

10.5 K Joint Boundary Condition Study β = 1.0, θ = 60°.

The models for the noding K joints were set up using the same principles as for the β = 0.6 joints, brace angle again being 60°, joint dimensions being shown in Figure 10.13. Material thickness and other properties were kept the same as those in the β = 0.6 analysis series (Table 10.1) and the two boundary conditions used as shown in Figure 10.14. As can be seen fewer boundary conditions are considered here as it was anticipated that a substantial load transfer through the stable chord sidewalls would occur which would not exhibit the same flexibility and sensitivity to variations in support conditions. This is verified here in the small differences obtained with the results of the two cases which included and excluded brace rollers. With β = 0.6 joints this change in support condition caused considerable variation even after the addition of the *FOLLOWER option to reduce large deflection moments on the free braces of case (f). Due to the nature of the failure of full width K joints not being related to 'in-punch of the brace into the chord top face' ,indentation plots are not relevant. Hence the results are presented in terms of ultimate loads (peak) in Table 10.3 alongside the Packer et al design strength (1992). Two displaced shape plots for joint f one under normal and one under reverse loading are shown in Figures 10.15 (a) and (b) where the mode of failure can be

seen to be deformation of the chord top face under the heel of the tension brace although some small indentation of the compression brace does occur. Joints with boundary case (a) exhibited the same mode of failure.

Case	Compression in thru' brace	Tension in thru' brace	FE capacity (kN)	Packer capacity (kN)	Ratio
a	Yes		1103.6	988.9	1.12
		Yes	1129.3	988.9	1.14
f	Yes		988.9	988.9	1.00
		Yes	1117.0	988.9	1.13

Table 10.3 Tabulated capacities of the β = 1.0 boundary condition matrix. (Boundary conditions as shown in Figure 10.4. Brace squash load = 1520kN).

10.6 Discussion

10.6.1 β = 0.6 K Joints

It is clear from Figures 10.7 and 10.8 and Table 10.2 that boundary conditions have a significant effect on both the ultimate capacity and joint behaviour at this β ratio. Taking the cases where the chord is simply supported at both ends first (a, f and g) it can be seen that once supported the method of restraining the chord ends does not have much significance on the capacity (i.e whether fixed or pinned). This

can be observed for both loading modes for cases f and g in Figures 10.7(a) and (b). The joint capacities can be seen to be less than half of the Packer (1992) design capacity in Table 10.2 and the displaced shape plot (Figure 10.11) reveals the excessive rotation evident at the unrestrained compression brace end. This will induce a secondary moment in the brace significantly influencing capacity, as described for the CHS T-DT models in Section 7.4.2. In practice the braces of joints in lattice girders are unlikely to be free and thus it is likely that this boundary condition is unrealistic. The addition of rollers to restrict the lateral deflection of the brace ends along the original axis is then undertaken in case a. The effects of this can clearly be seen in Figure 10.7 (a) and Table 10.2. Here the capacity increases by 133% over that of case f when subject to compressive loading in the through brace. This condition is much more representative of frame or isolated test conditions found in practice and this is the basic restraint condition adopted for the investigations in Chapter 11. To reduce and quantify the effects of large brace deflections, cases f and g were re-analysed under compression in the through brace using the *FOLLOWER option detailed in section 7.4.2. The results of these are shown in Figure 10.9 and 10.10. It can be seen that the reduction in secondary moments caused by maintaining the load as axial has a significant impact on stiffness and on increasing the joint capacity, and also causes the behaviour to stabilise. It can be seen that of the four simply supported chord members, cases b and c give low results when reverse loading is applied (tension in the through brace). In these two cases the chord rotates considerably in-plane at the unsupported end as can be seen in Figure 10.12 (c). These cases are extreme compared to those that would be found in reality.

Examination of Table 10.2 reveals no particular trends in normal or reverse loading giving greater capacity. It is clear however that boundary conditions do have significant effects on ultimate capacities of $\beta < 1.0$ K joints. These are greater than those observed for the CHS gap K joints examined by Bolt et al (1992) where maximum differences were up to 10% for a similar boundary condition matrix to that used here. This is due to the much less stable chord top face deformation in the RHS members, whereas in CHS the loads are carried to the chord as a whole and the inherently more stable circular shape as opposed to the 'plate' type deformation in the RHS. Observation of the displaced shape plots in Figures 10.11 and 10.12 indicates that the failure is a combination of chord top face deformation and local compression brace buckling in all joints.

10.6.2 $\beta = 1.0$ K Joints

It can be seen from Table 10.3 that the addition of rollers to the braces (case a) has significantly less impact on the capacity than was the case for the $\beta = 0.6$ joints. This is to be expected as a substantial proportion of the loading is transferred from the brace through to the chord sidewall as well as the chord top face. The in-plane chord sidewalls are very stiff, this reducing deformations around the brace footprint and hence the effect of large deflection moments. Where the through brace is loaded in tension the addition of rollers to the braces has very little effect on capacity. It would appear from the results here that it is advantageous to load the through brace in tension. The mode of failure, as can be seen from Figures 10.15 (a) and (b), is

deformation of the chord top face under the heel of the tension brace, although some small local deformation of the compression brace adjacent to the tension brace can be observed.

10.7 Conclusions

1) Boundary conditions clearly have an impact on RHS joint behaviour, this being much more significant at lower β ratios.

2) Cases a, d and i are from the literature the most realistic conditions bearing most resemblance to those found in the isolated tests and 'in-frame' conditions.

3) It is difficult to conclude as to whether it is better to load the through brace in compression or tension here; this will discussed in more detail in Chapter 11, although of those boundary cases considered realistic (a, d, i at $\beta = 0.6$ and a and f at $\beta = 1.0$), loading of the through brace in tension is beneficial in four out of five cases.

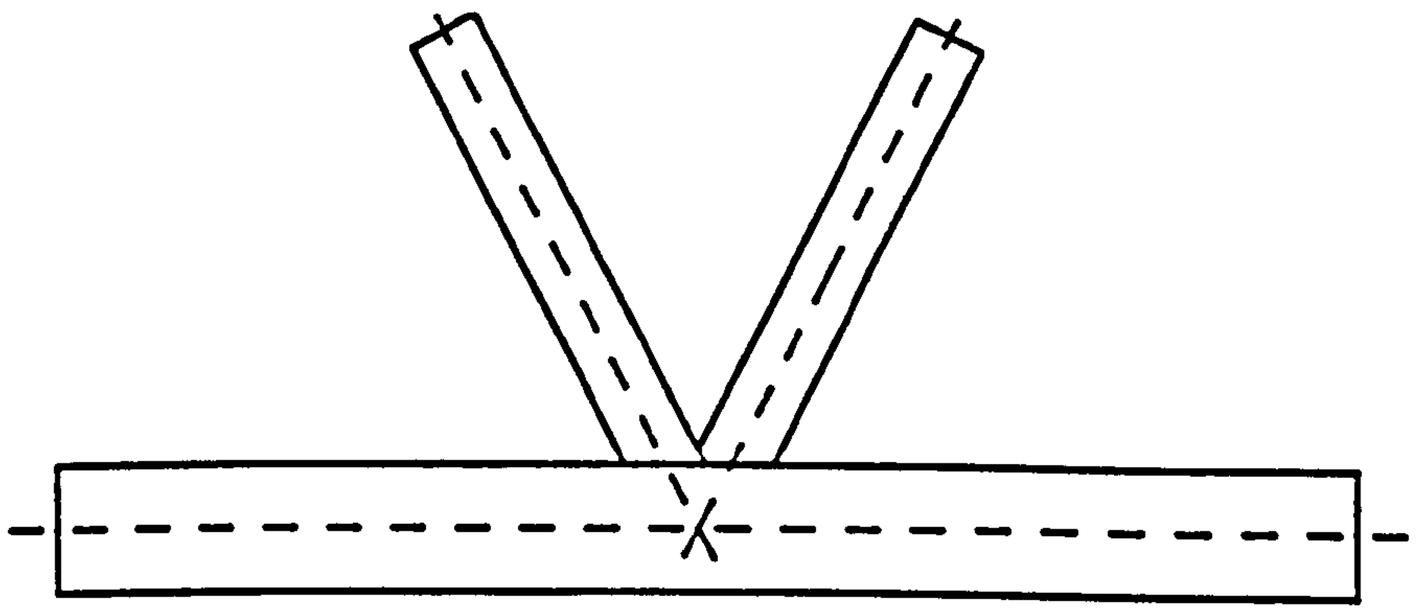

(a) Partial overlap K joint

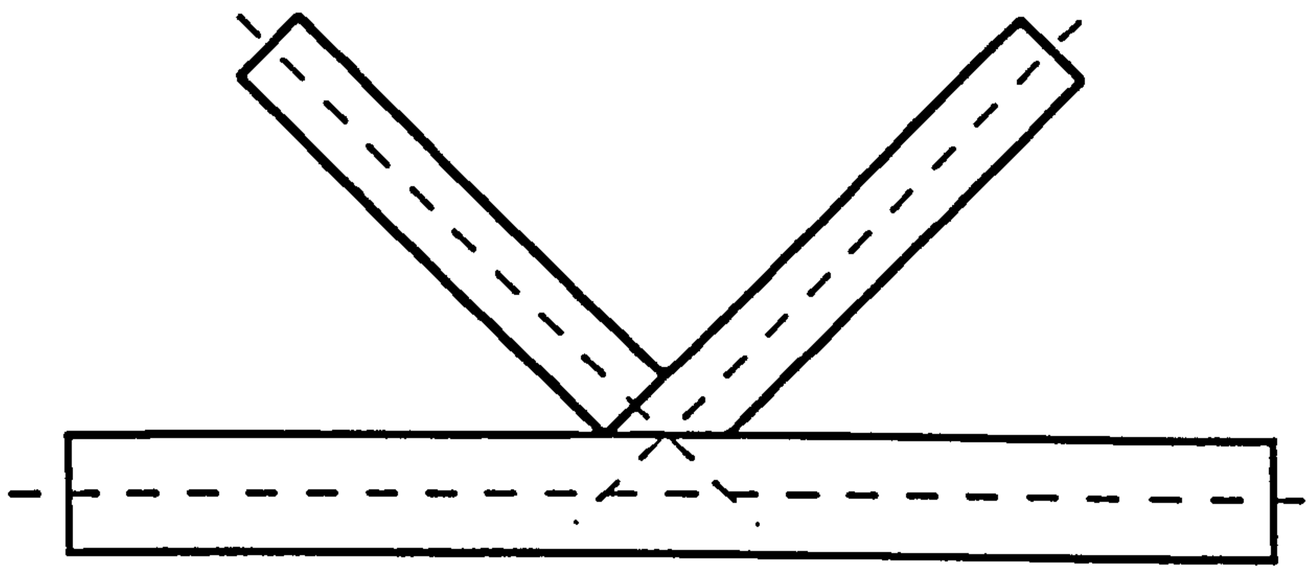

(b) Fully overlapped K joint

Figure 10.1 Partially Overlapped and Fully Overlapped K Joints.

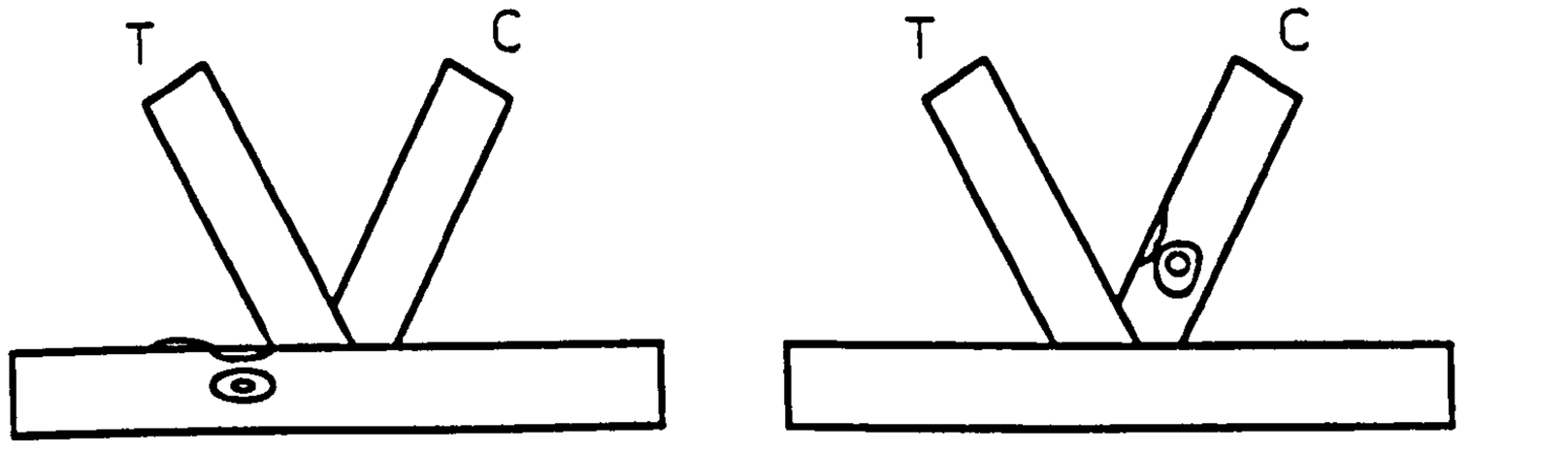

Chord top face deformation beneath tension brace

Local buckling of compression brace

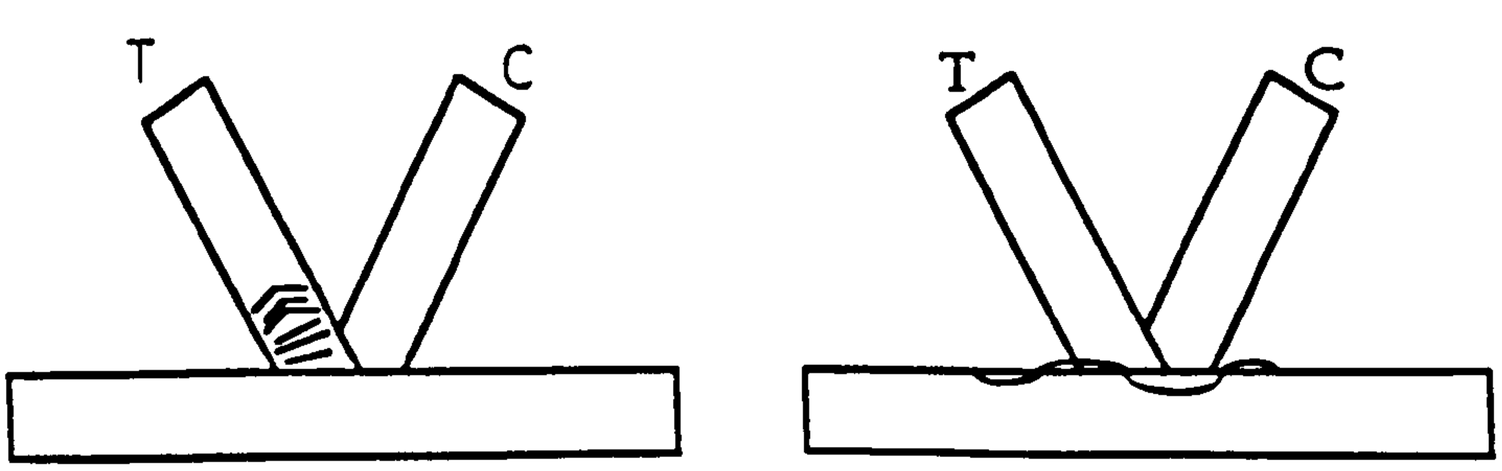

Yielding of tension brace in joint region

In-punching and out-pull of braces into chord top face

Figure 10.2 Common Modes of Failure in Overlapped Joints.

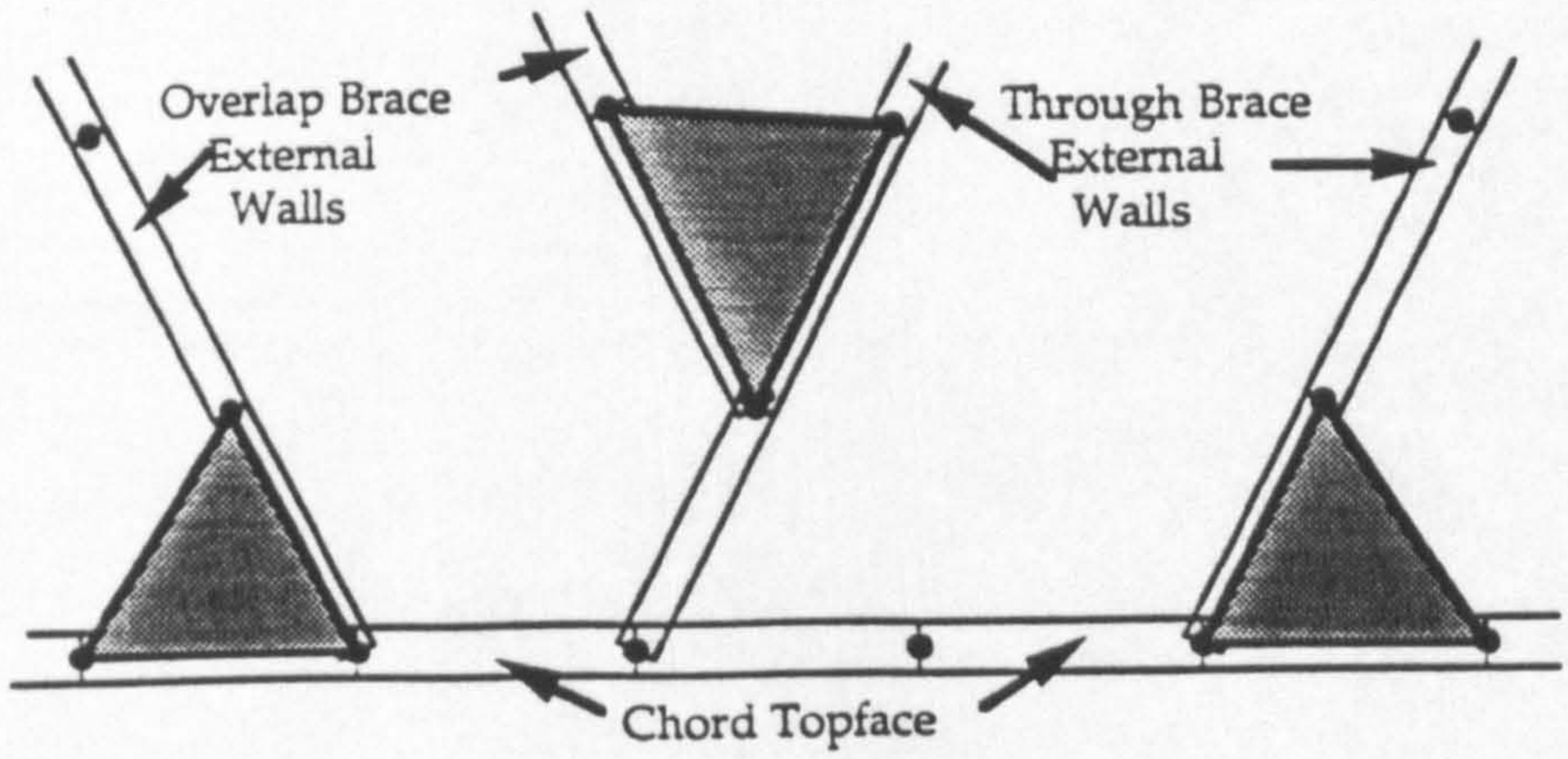

● Corner Nodes (Midside Nodes Omitted for Clarity)

E External (Visible) Fillet Welds

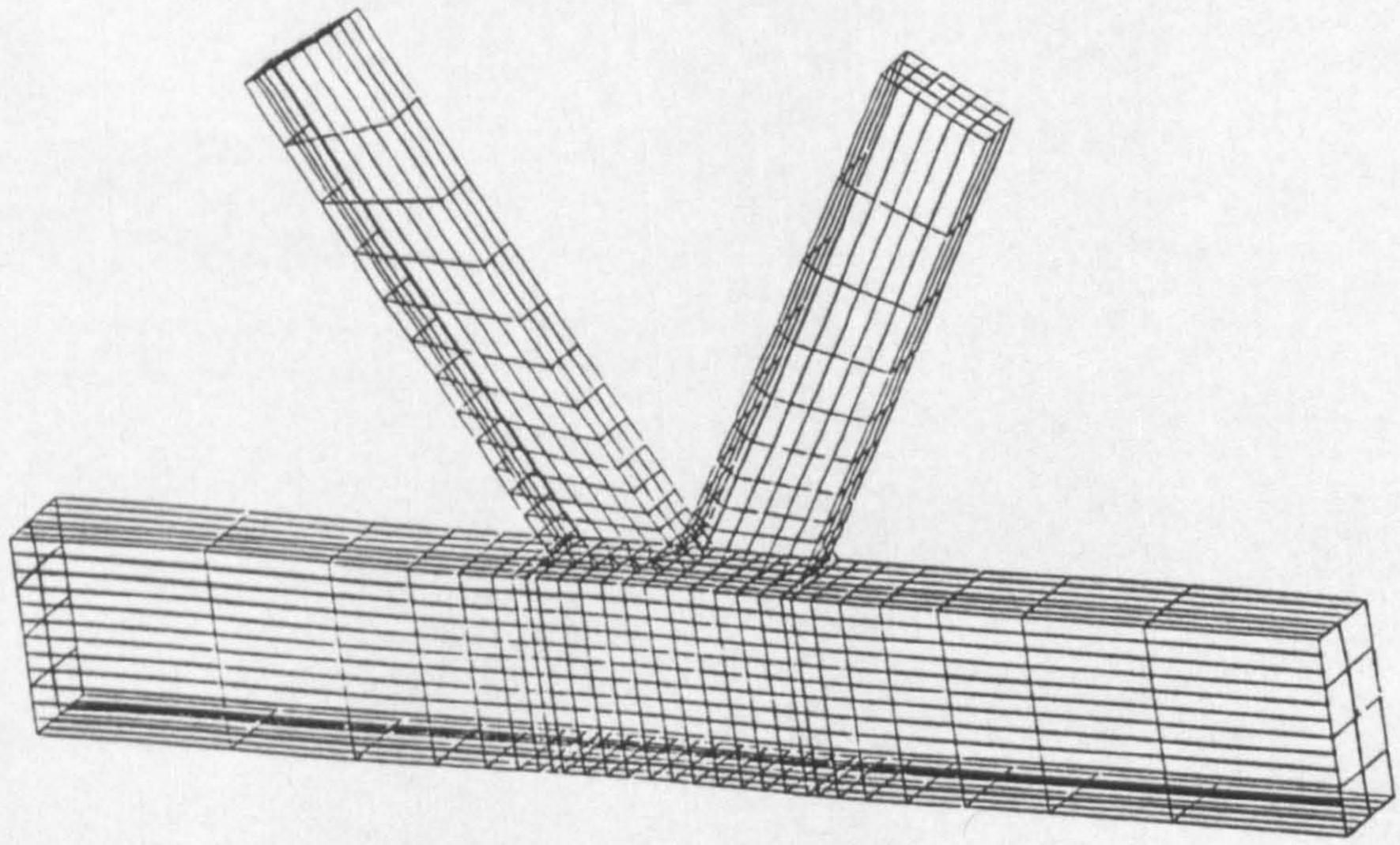

Figure 10.3 Detail of the Modelling of the Weld Region and $\beta = 0.6$ Mesh Plot.

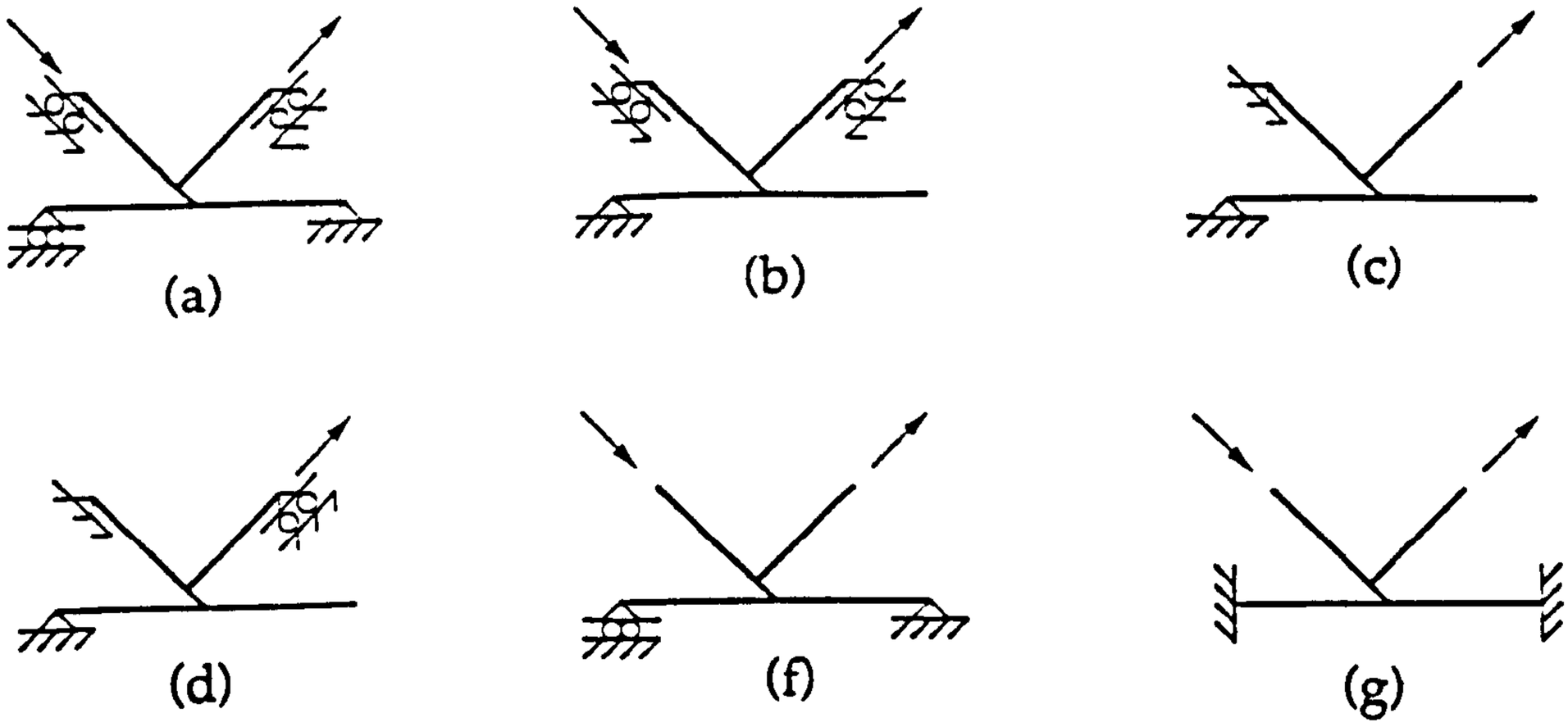

Figure 10.4 The Matrix of Boundary Conditions Investigated.

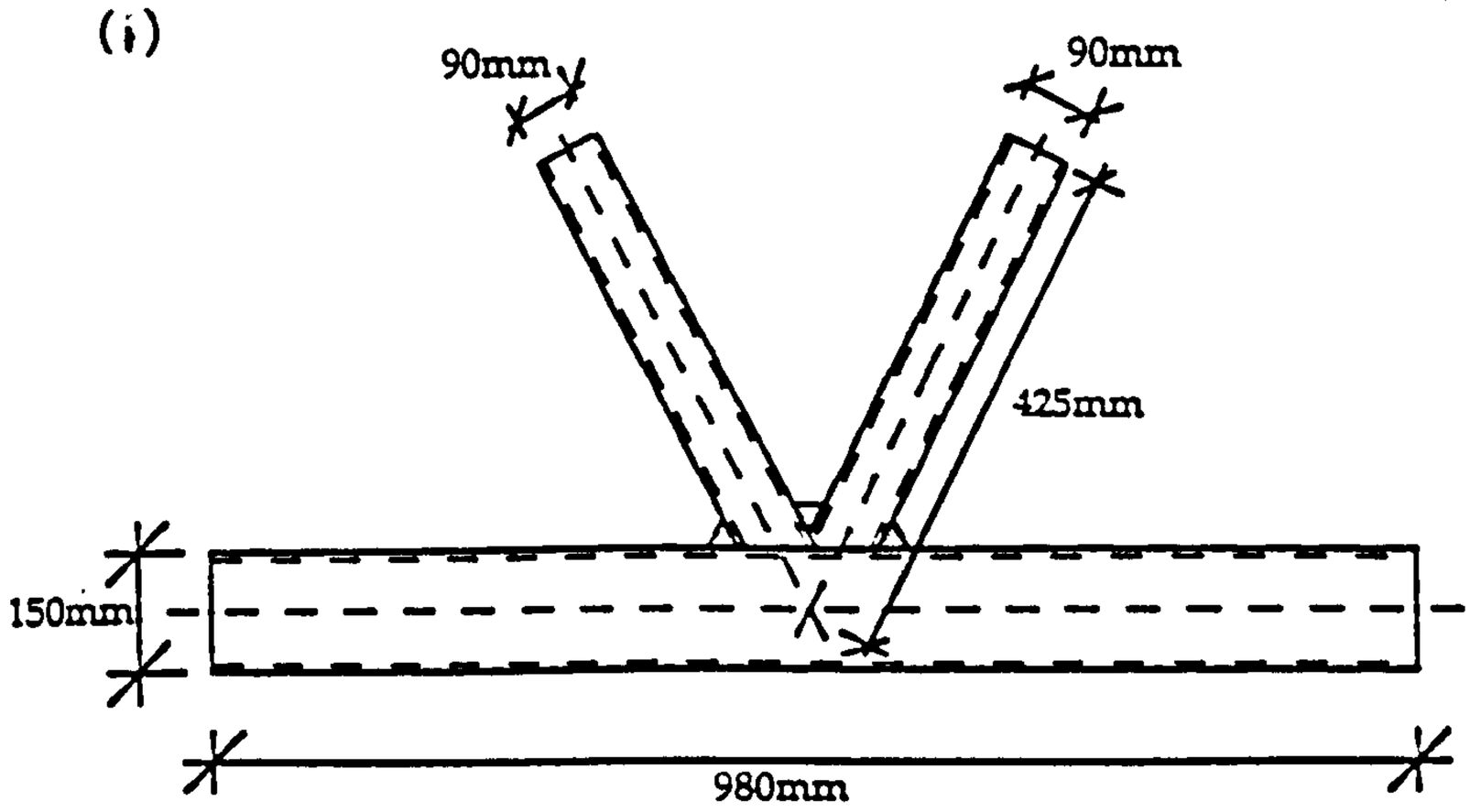

Figure 10.5 Dimensions of the Noding $\beta = 0.6$ 60° K Joint.

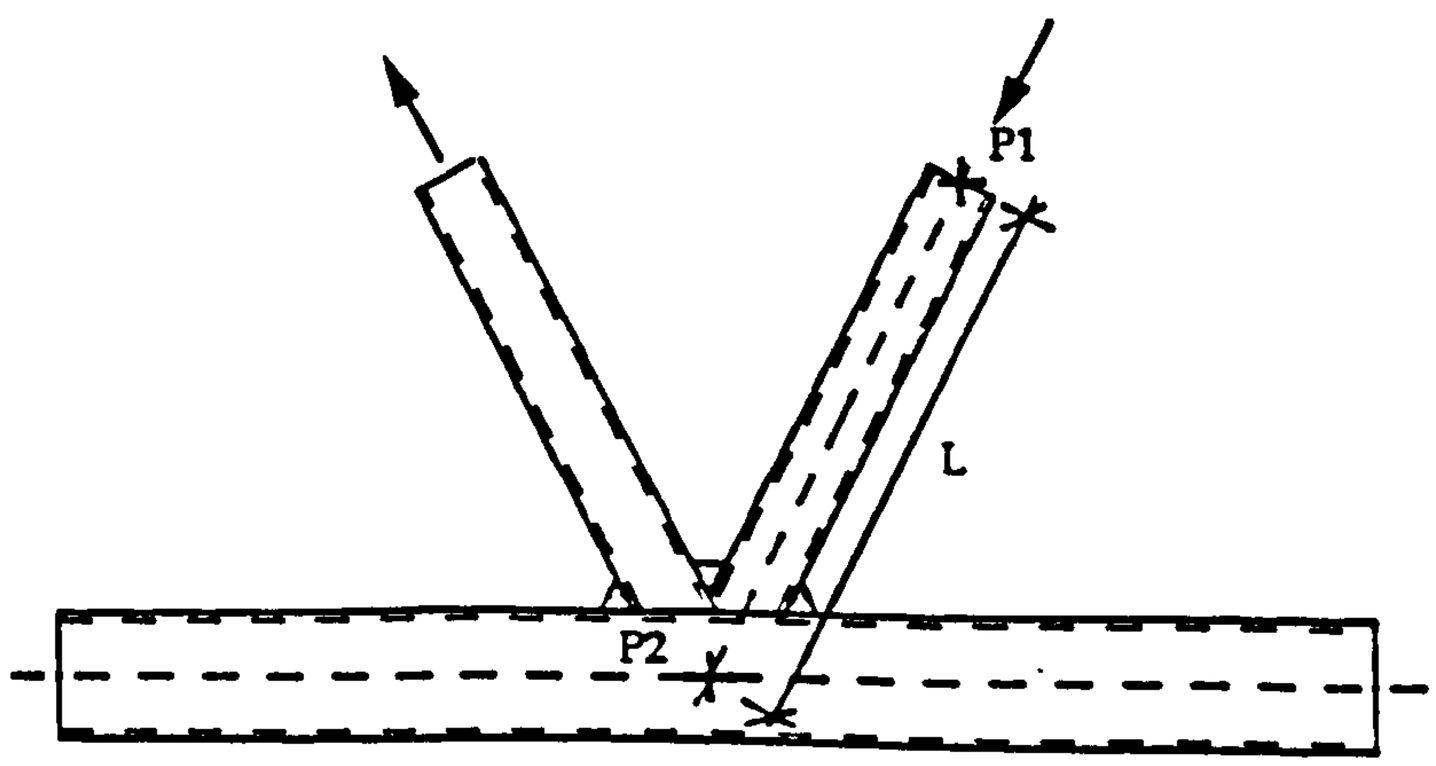

Figure 10.6 Method of Measuring the 'Indentation' of the Compression Loaded Brace.

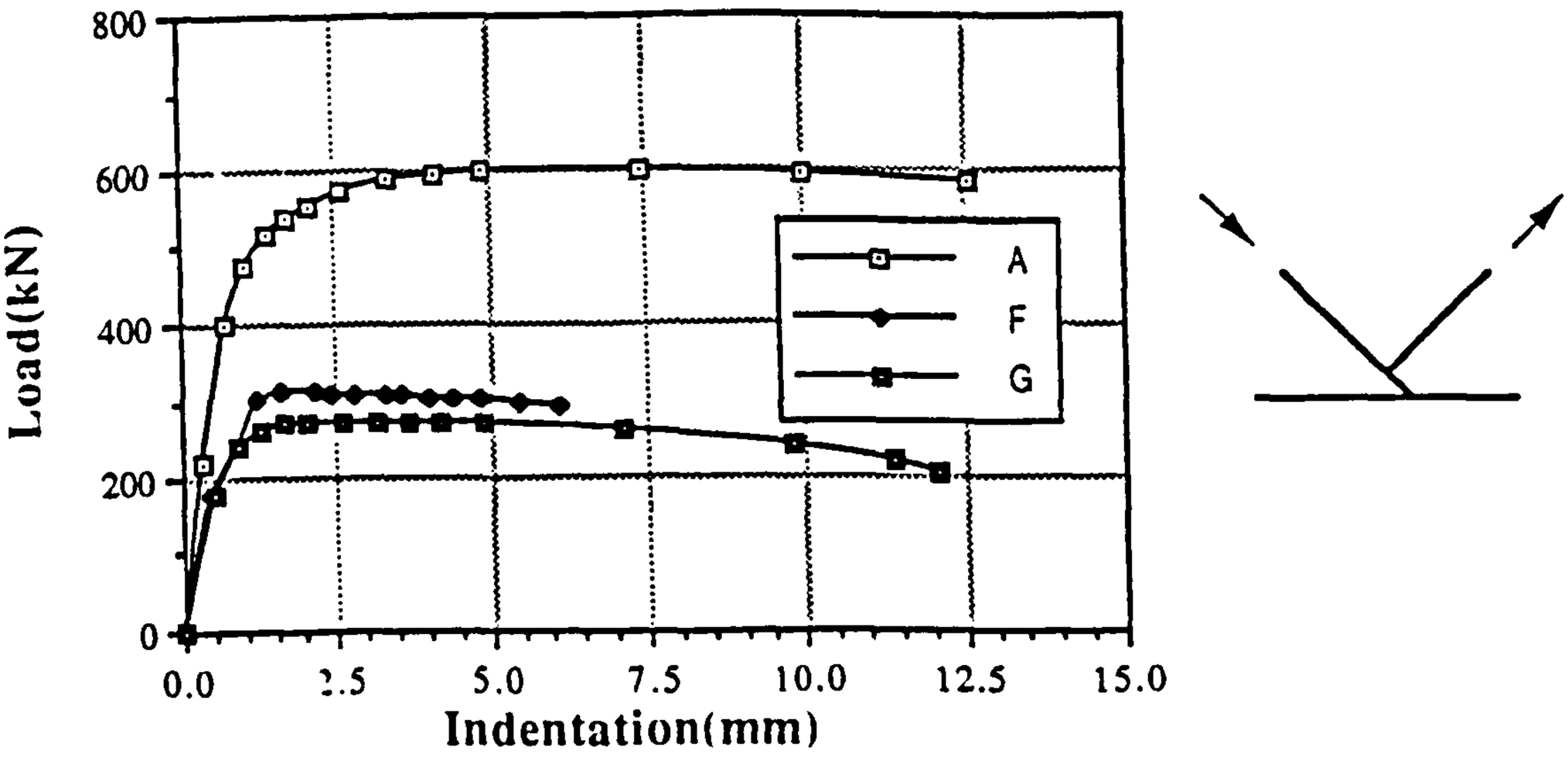

(a) Load vs Indentation Plots for Boundary Condition
Cases (a), (f) and (g) with Compression
Loading in the Through Brace.

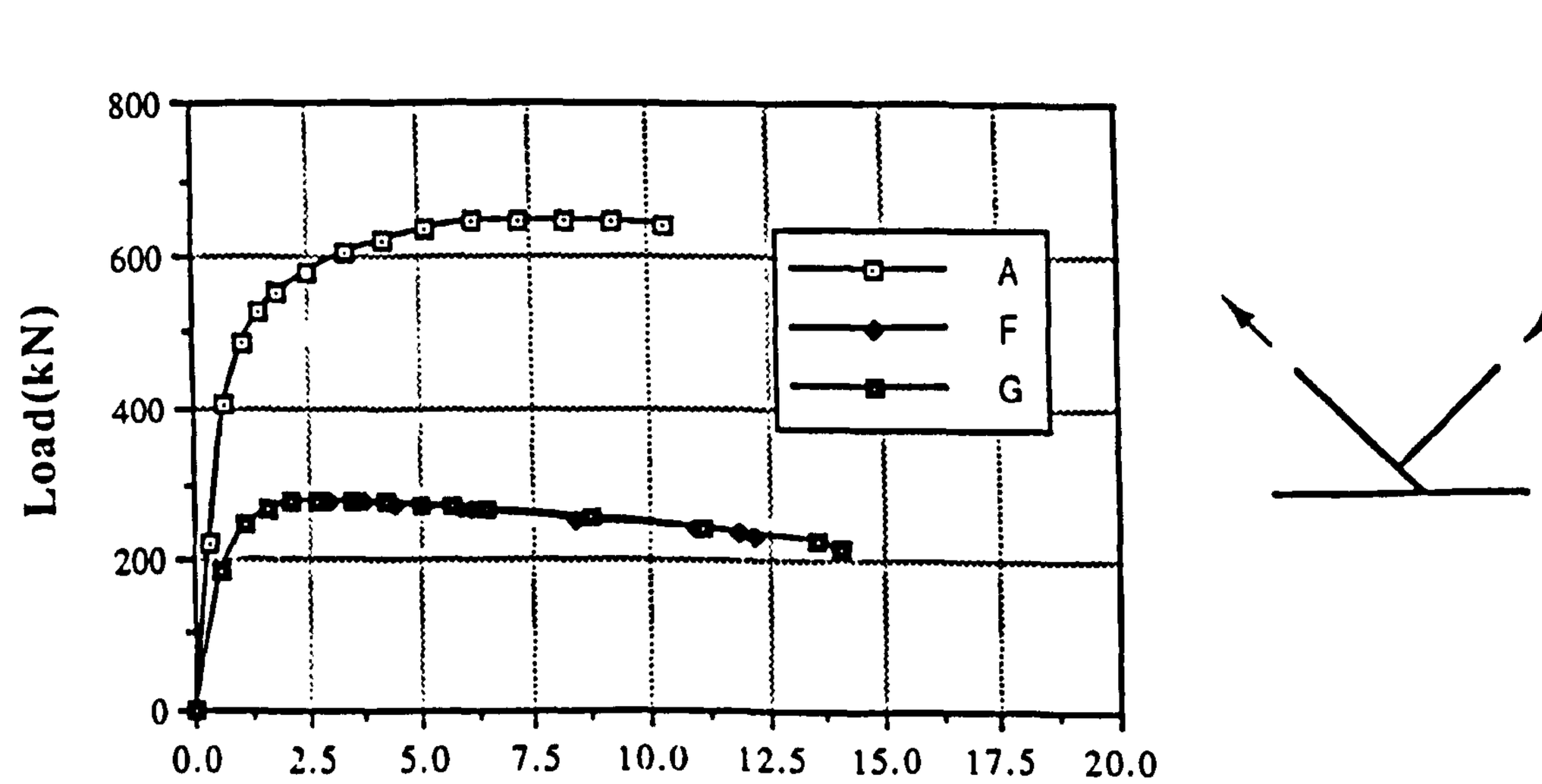

(b) Load vs Indentation Plots for Boundary Condition
Cases (a), (f) and (g) with Tension
Loading in the Through Brace.

Figure 10.7 Load vs Indentation Plots, $\beta = 0.6$,
$\theta = 60^{o}$ K Joints

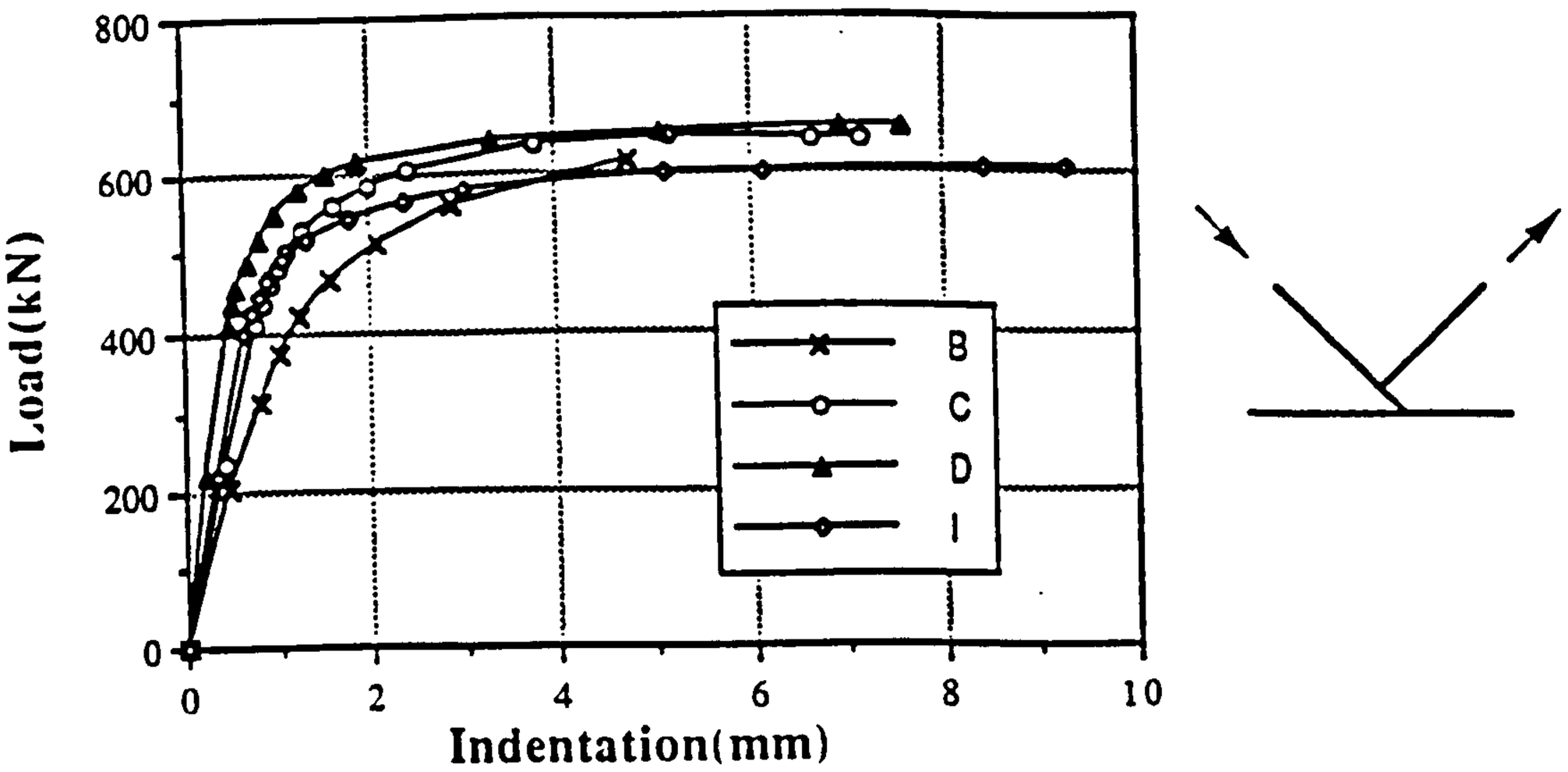

(a) Load vs Indentation Plots for Boundary Condition Cases (b), (c), (d) and (i) with Compression Loading in the Through Brace.

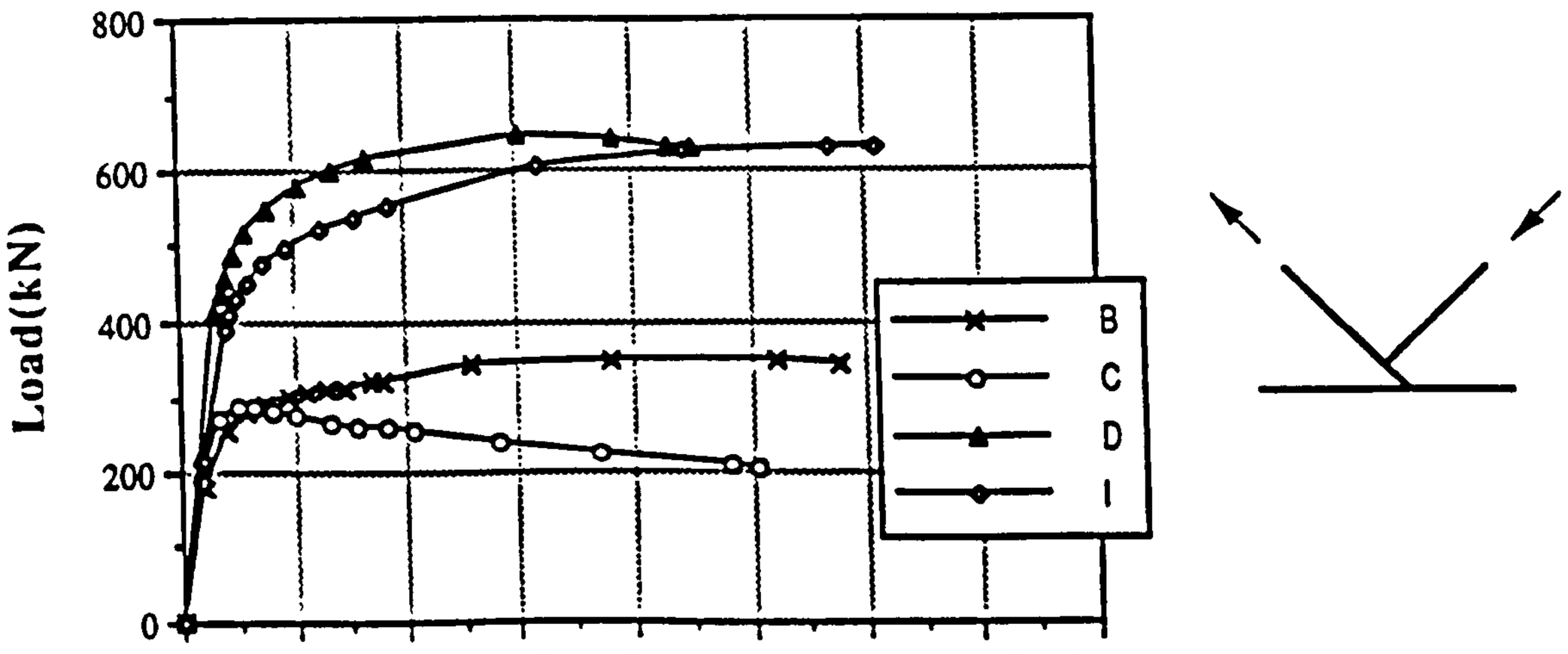

(b) Load vs Indentation Plots for Boundary Condition Cases (b), (c), (d) and (i) with Tension Loading in the Through Brace.

Figure 10.8 Load vs Indentation Plots, $\beta = 0.6$, $\theta = 60^{o}$ K Joints

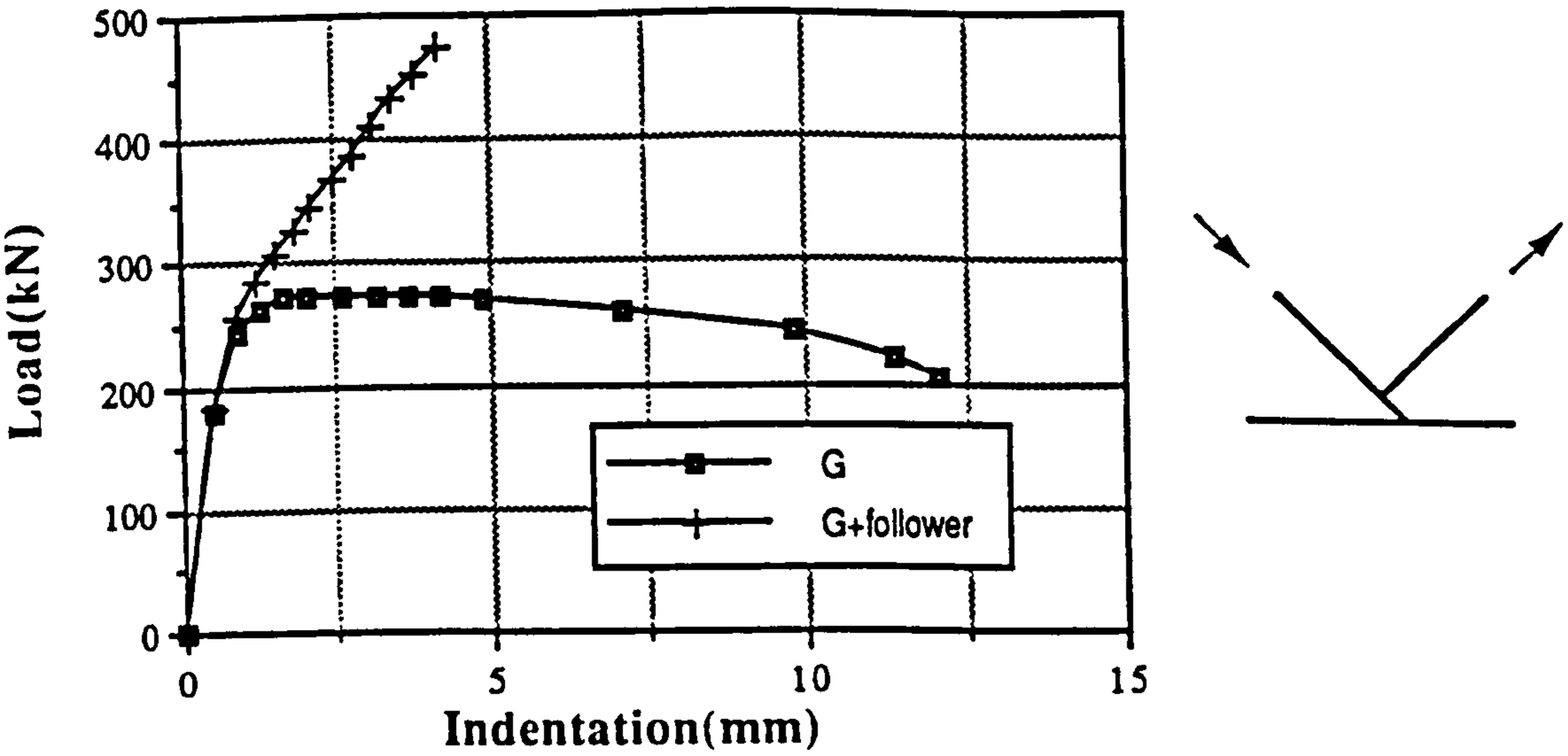

Figure 10.9 Load vs Indentation Plots for Boundary Case (g) and (g) with *FOLLOWER with Compression Loading in the Through Brace.

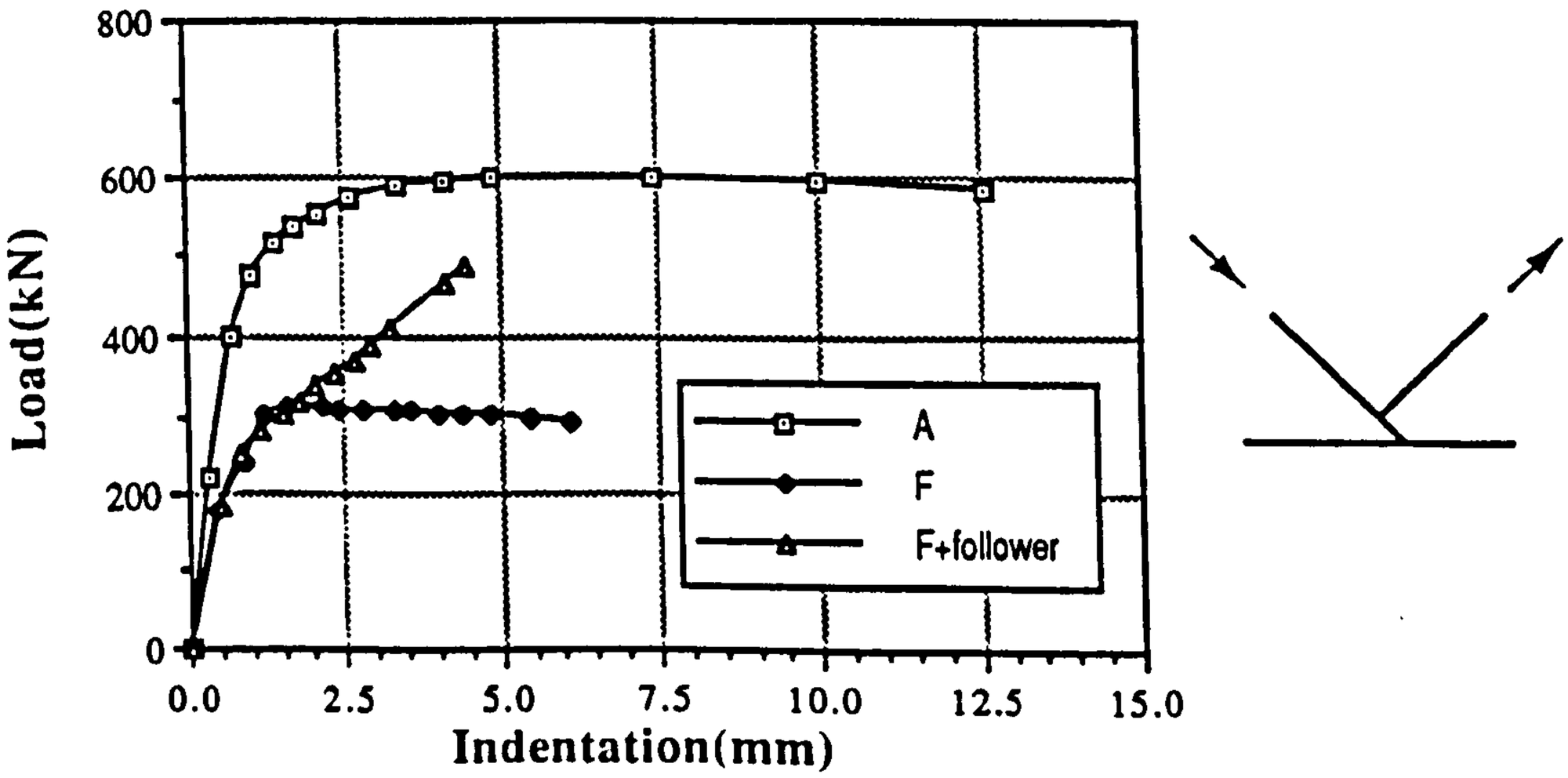

Figure 10.10 Load vs Indentation Plots for Boundary Cases (a), (g) and (g) with *FOLLOWER with Compression Loading in the Through Brace.

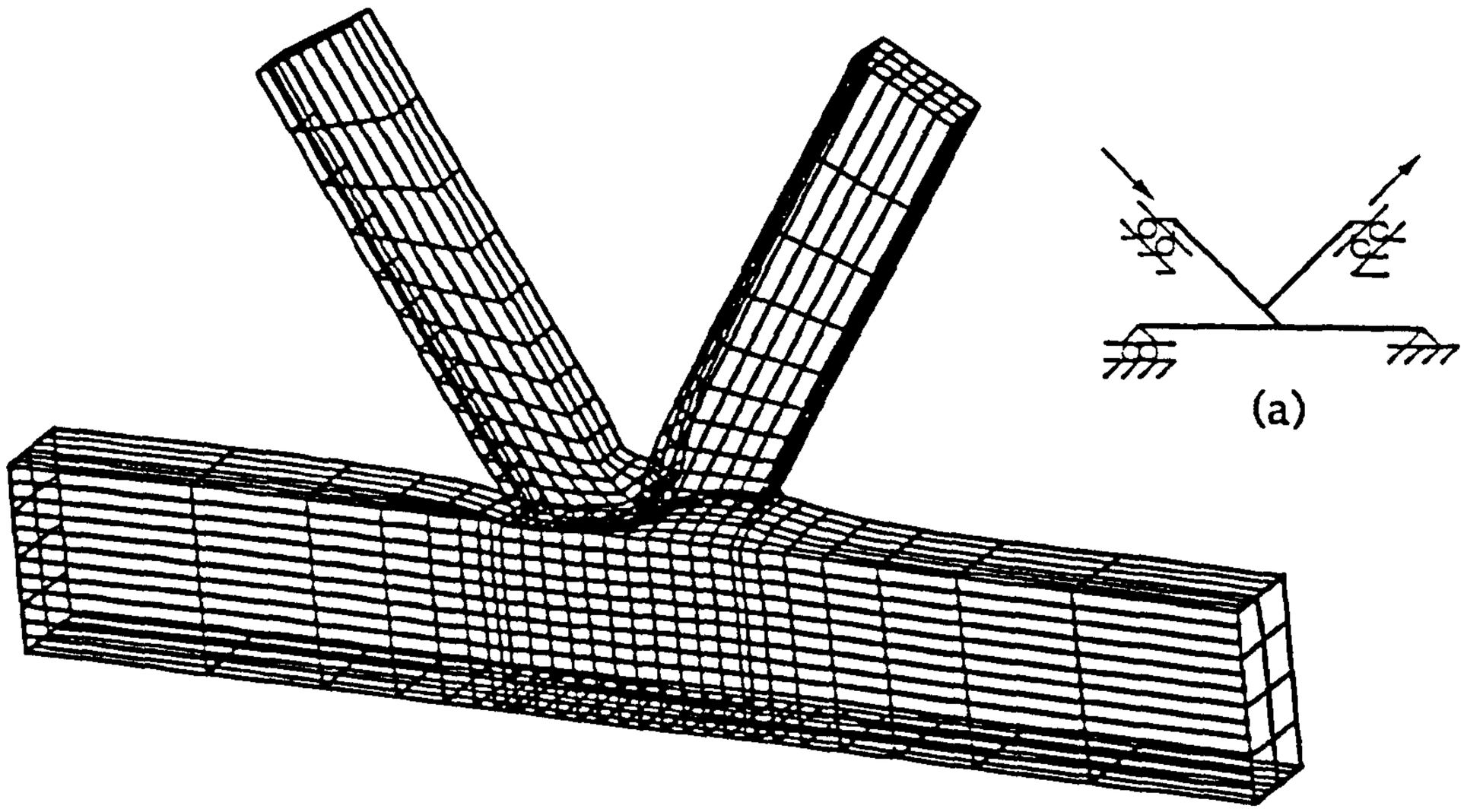

Figure 10.11(a) Displaced Shape Plot for Case (a) Under Compressive Loading in the Through Brace.

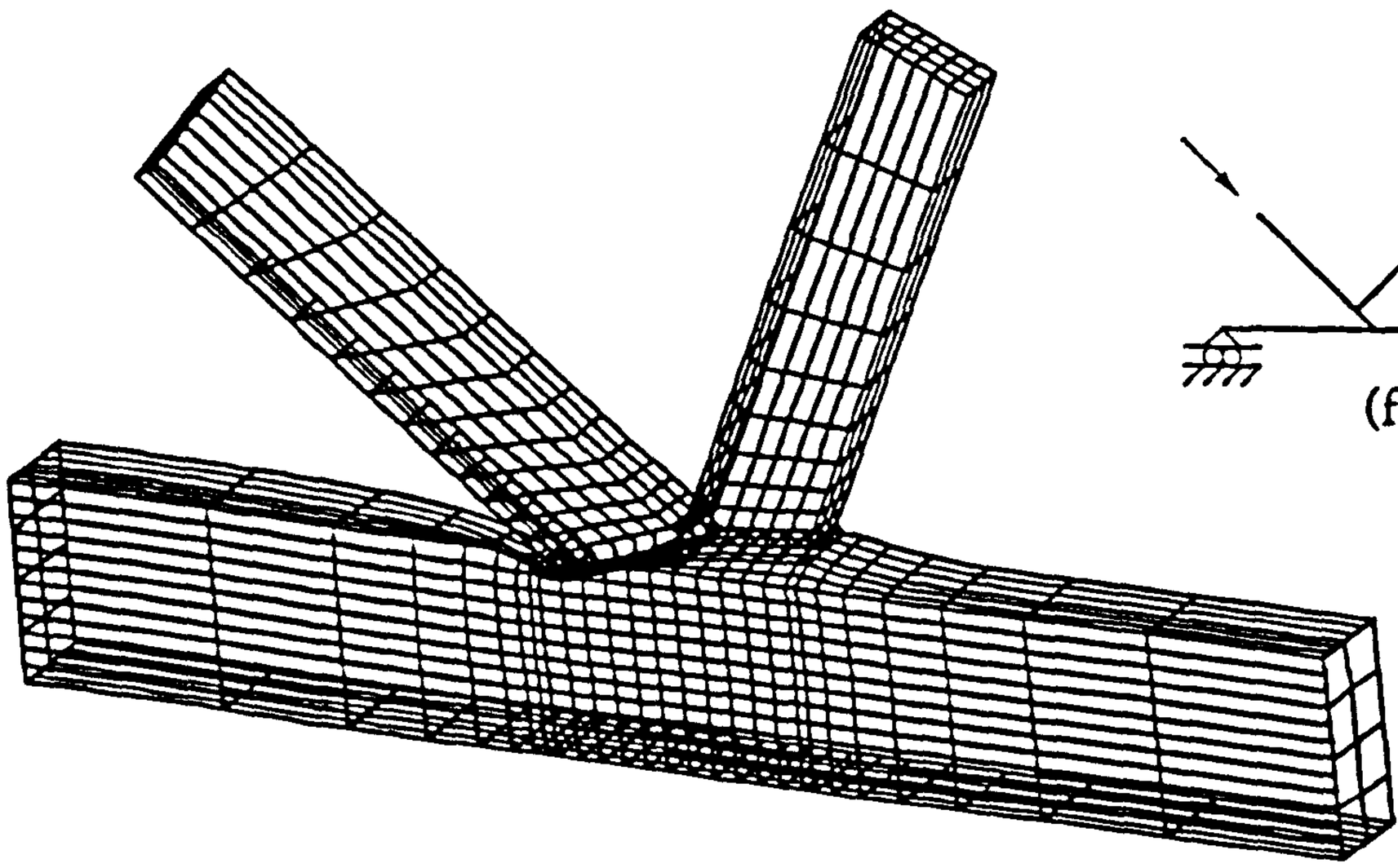

Figure 10.11(b) Displaced Shape Plot for Case (f) Under Compressive Loading in the Through Brace.

Figure 10.11 Displaced Shape Plots for Both Chord Ends Pinned $\beta = 0.6$.

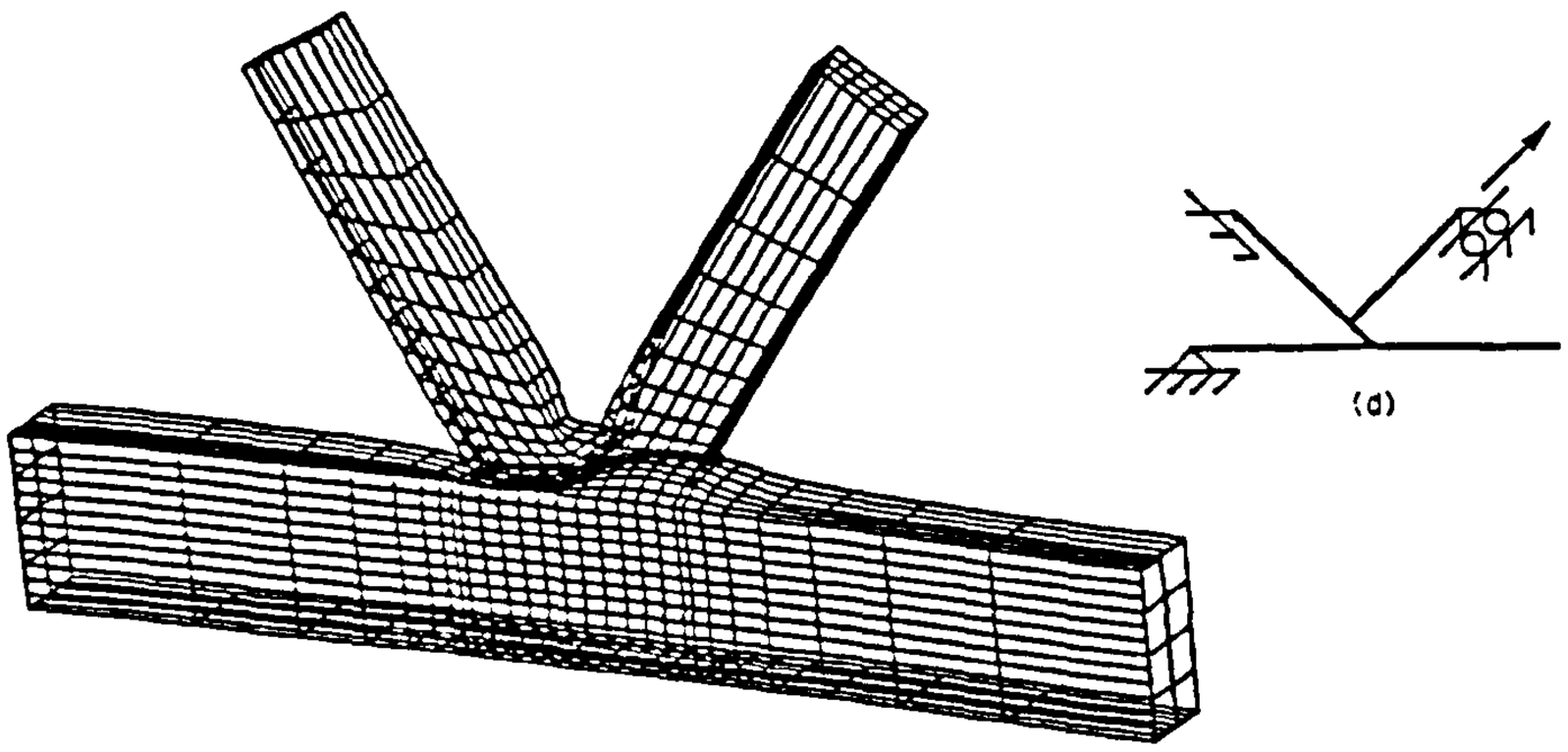

Figure 10.12(a) Displaced Shape Plot for Case (d) Under Compressive Loading in the Through Brace.

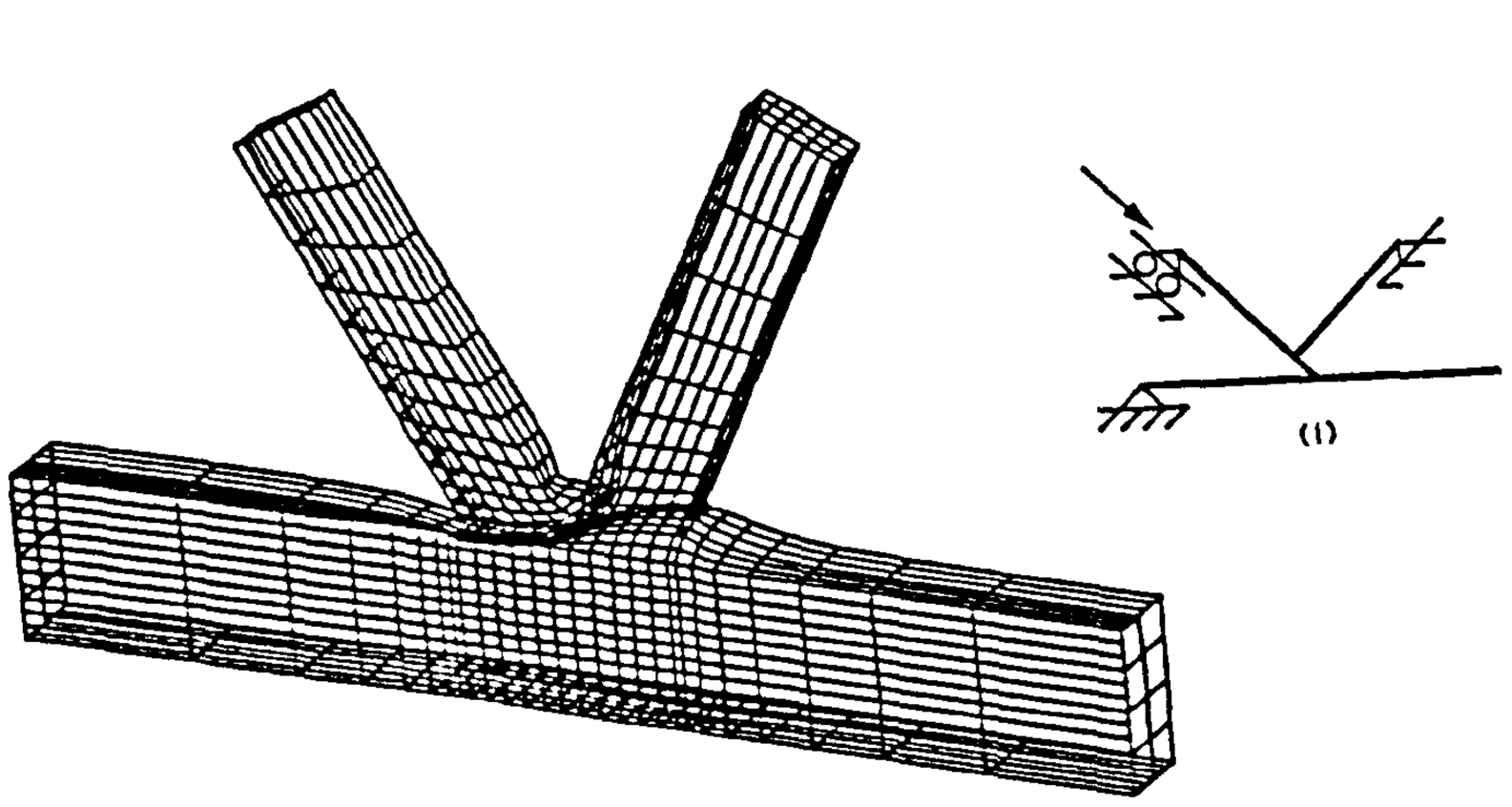

Figure 10.12(b) Displaced Shape Plot for Case (i) Under Compressive Loading in the Through Brace.

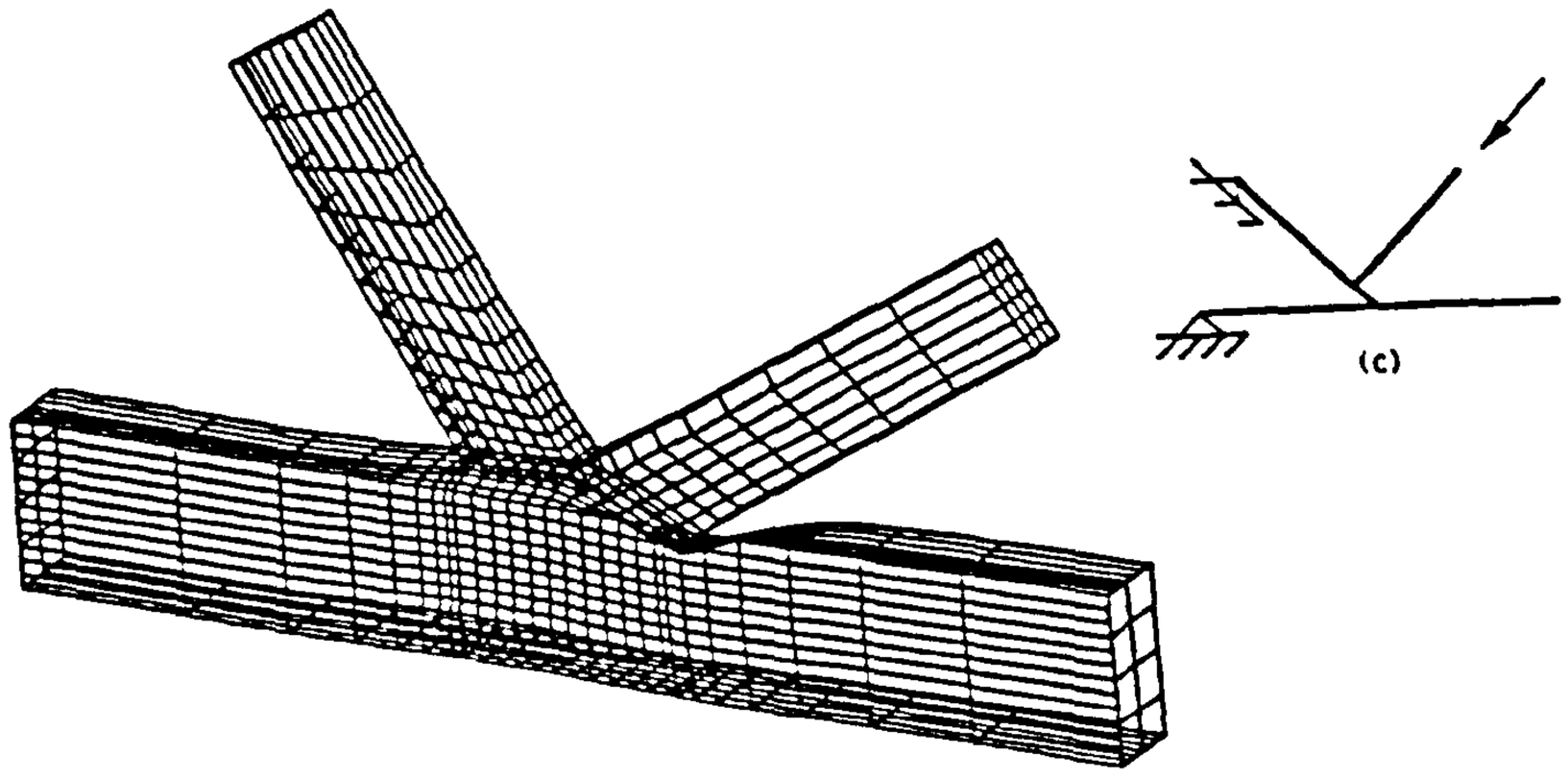

Figure 10.12(c) Displaced Shape Plot for Case (c) Under Tensile Loading in the Through Brace.

Figure 10.12 Displaced Shape Plots for Both Chord Ends Pinned $\beta = 0.6$.

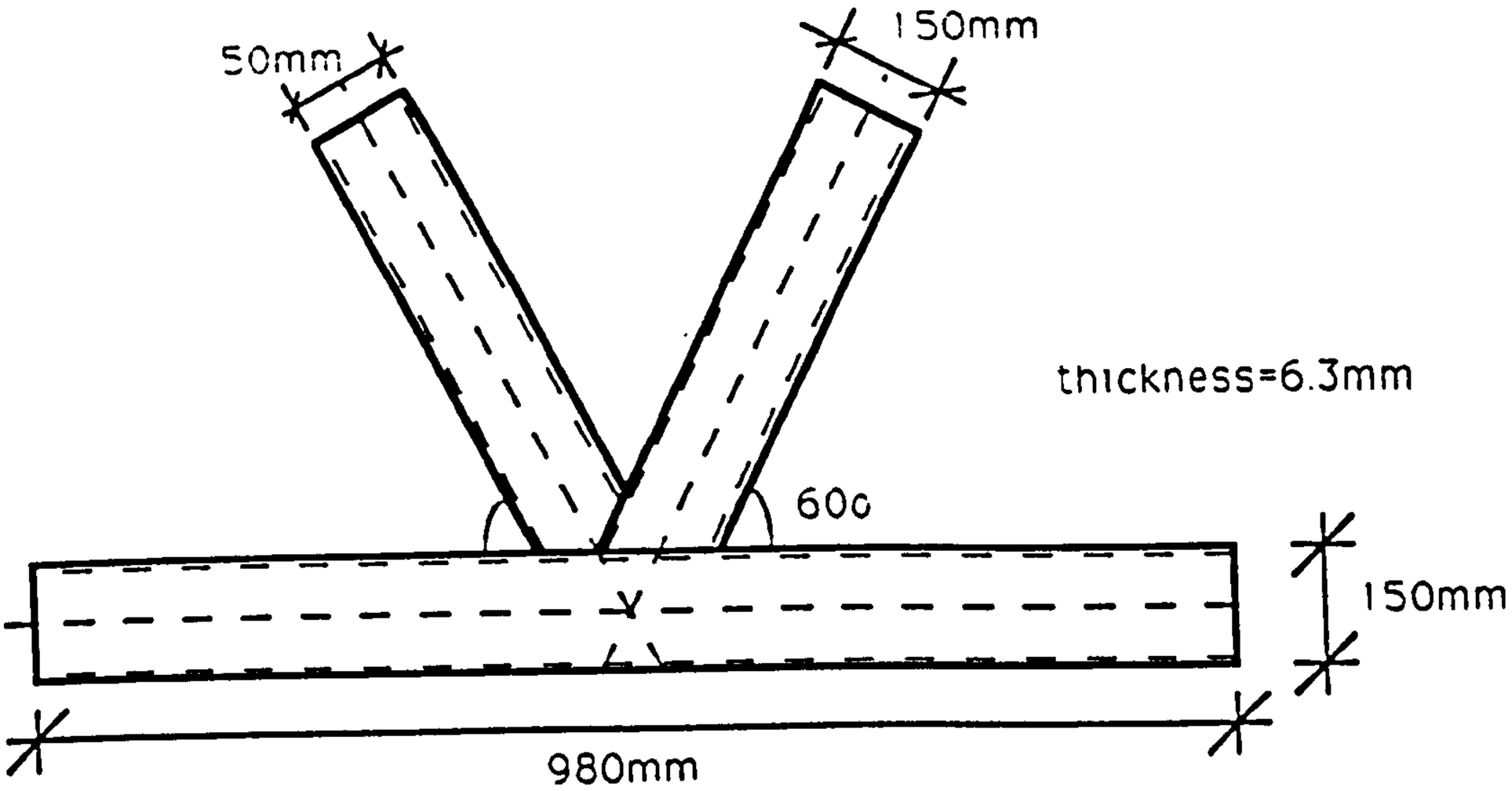

Figure 10.13 Dimensions of the Noding $\beta = 1.0$ 60° K Joint.

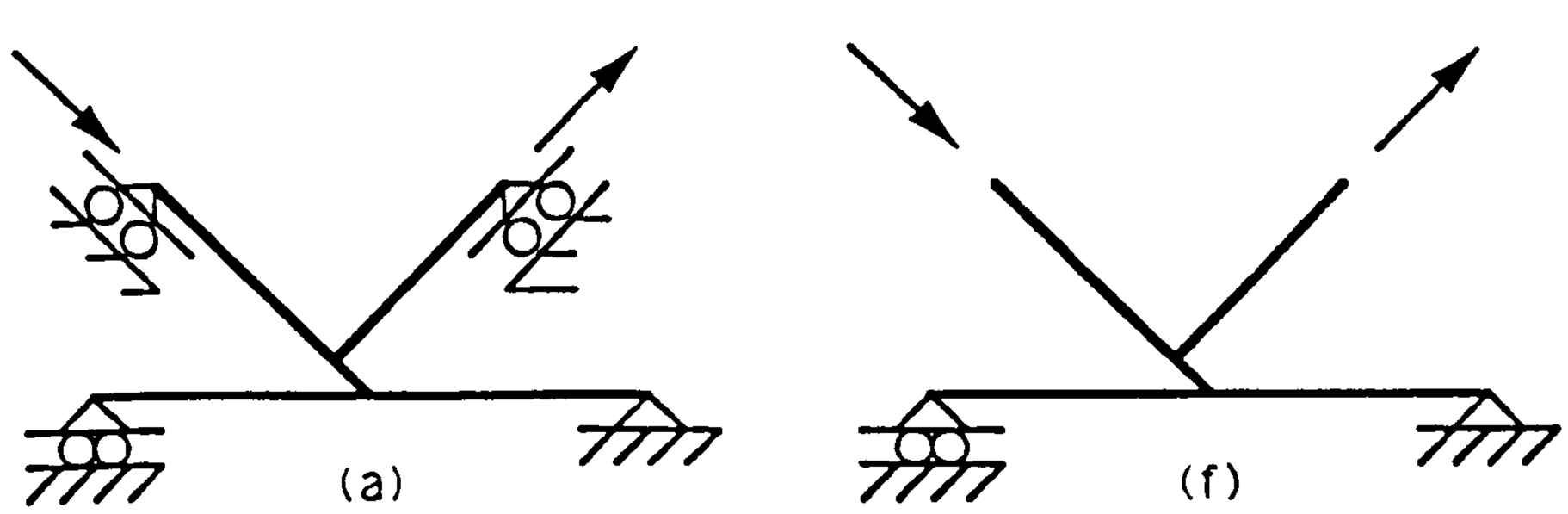

Figure 10.14 The Two Boundary Conditions Examined for $\beta = 1.0$ K Joints.

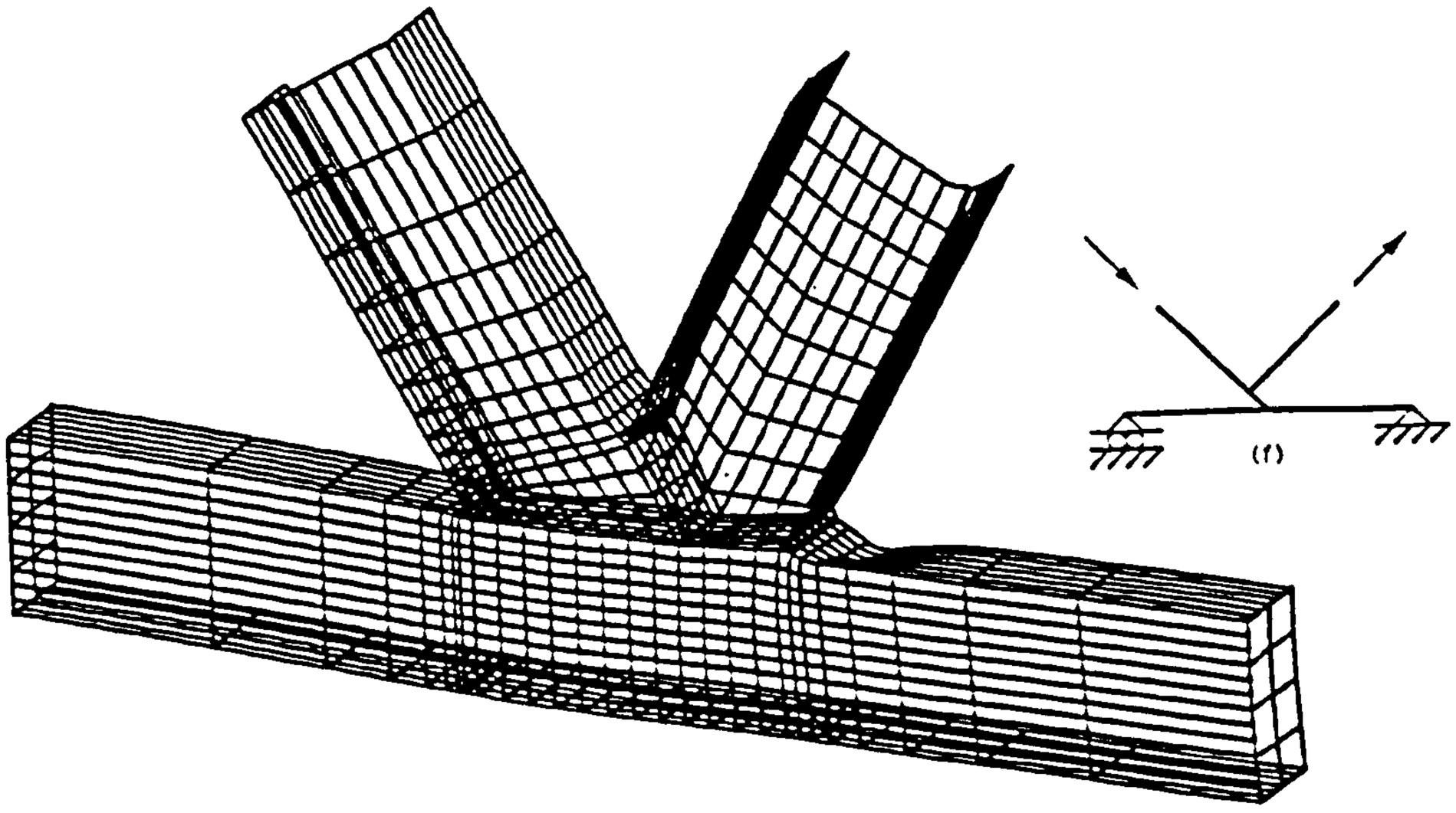

Figure 10.15(a) Displaced Shape Plot for Case (f) Under Compressive Loading in the Through Brace.

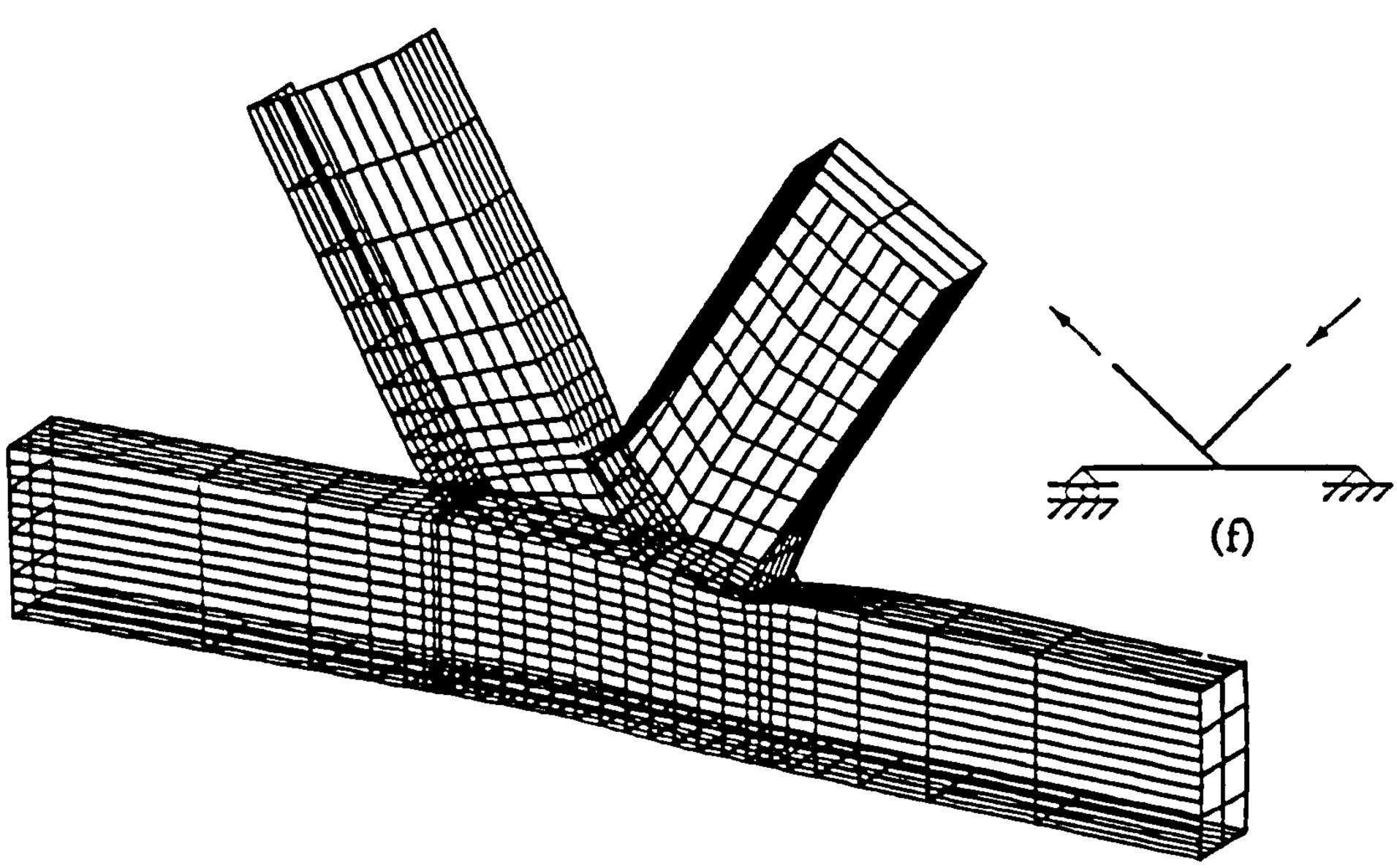

Figure 10.15(b) Displaced Shape Plot for Case (f) Under Tensile Loading in the Through Brace.

Figure 10.15 Displaced Shape Plots for Both Chord Ends Pinned $\beta = 1.0$.

CHAPTER 11

EFFECT OF HIDDEN WELD AND BRACE THICKNESS ON RHS PARTIAL OVERLAP K JOINT CAPACITY

11.1 Introduction

Traditionally lattice girders formed from open sections have been designed with noding of member centrelines at joints. This has been done to minimise joint eccentricity and associated bending moments due to the large axial forces, and consequently to simplify the design process. The same arguments have been adopted for girders in hollow section, although not always with the same conviction. Gap joints are usually the cheapest to fabricate, but can only occur with low angles and low width ratios in Warren type girders. For larger width ratios and particularly for Pratt type joints it is necessary to use partial or fully overlapped joints as shown in Figure 11.1. Unless both bracing members are mitered then the joint will be associated with some degree of non-symmetry so that the reversal of the directions of the bracing axial forces will have some effect on the joint stiffness and strength. The Finite Element method is used in this Chapter to investigate the extent of this effect on RHS joints.

An additional complicating factor is the way these joints are fabricated with the associated welding. Normally only the 'overlapping member' is mitered in a K joint, the 'overlapped' member being 'through' to the chord. It would appear sensible to weld the through member completely to the chord around the surface of contact. However the fabricating practice of assembling the whole girder by tack welding of the members together before the final welding is made prevents the toe of the weld of the through member being laid. Although the airtightness of the hollow sections is ensured by the external welds so that corrosion is controlled, the effect of leaving out the hidden weld on the stiffness and strength of the joint and its performance under reversed loading is difficult to estimate. The FE method is ideal for such an investigation. Preliminary work on CHS Warren joints has been carried out by Zettlemoyer et al (1991); however the effects for RHS joints, with their associated rectangularity and greater freedom of orientation make them potentially more significant.

The current recommendations for the design of partially overlapped joints in RHS included in EC3 (1992) are based on the earlier combined efforts of IIW and CIDECT. These were based on the statistical analysis of experimental tests (78 datapoints) discussed in CIDECT Monograph 6 (1986). It is worth noting that 55 of these datapoints were for N type joints, i.e where one angle is 90°. Definitive guidance is given by the IIW (1989) and published in a series of CIDECT design guides of which Packer et al (1992) is the most recent. The strength of these overlapped joints has been based on the 'effective width' concept for crosswalls and extended to all the walls, the effectiveness of each wall depending on the value of the overlap

defined by the ratio (q/h)sin θ, as defined in Figure 11.2. For an overlap between 50% and 80%, the value for design strength (Packer et al) is :-

$$P_i = p_y t_i \left[2h_i - 4t_i + b_e + b_{e(ov)}\right] \left\{\frac{1+\sin(\theta_1+\theta_2)}{2\sin(\theta_1+\theta_2)}\right\} \qquad \text{Eqn [11.1]}$$

where P_i is capacity of either of the braces.

and $b_e = \frac{10.0\, b_i}{(b_o/t_o)}$ and $b_{e(ov)} = \frac{10.0\, b_i}{(b_j/t_j)}$ for design.

where the symbols are as defined at the beginning of this thesis.

The FE study has considered a basic Warren joint where the width ratio is 0.6 and the chord and braces have slenderness ratios of 23.6 and 14.3 respectively. The corresponding limit on wall slenderness according to the IIW (1989) is 24.6 (b_o/t_o) for the yield value of 420 N/mm^2 chosen. Angles are varied from 30 to 60 degrees in the cases considered and for one case a full width joint (β = 1.0) is examined. The effect of excluding or including the hidden weld in these models is considered, together with that of reversing the end forces on the joint. In one case the effect of varying the thickness of the brace walls is also taken into account. The various modes of failure are described for each case.

11.2 Joints and Load Cases

11.2.1 Dimensions and Load Cases for Initial $\theta = 60^o$, $\beta = 0.6$ K Joints

The dimensions and material properties of the joint examined initially are shown in Figure 11.2 and Table 11.1.

	Overlapped Brace j (90 x 90 Square HS)	Overlapping Brace i (90 x 90 Square HS)	Chord (150 x 150 Square HS)
Angle	60^o	60^o	
Yield Stress (N/mm^2)	420	420	420
Tensile Strength (N/mm^2)	540	540	540
Thickness (mm)	6.3	6.3	6.3
Slenderness (b/t)	14.3	14.3	23.8
$\beta = 0.6$, e = -ho/4 = 37.5 mm, q = 57 mm, Ov = 58.8%			

Table 11.1 $\beta = 0.6$, 60^o K Joints Test Parameters and Material Properties.

Brace squash load = 885kN

With noding joints the brace overlap is 20% and falls outside the minimum 25% limit of the IIW (1989) recommendations. For this analysis series, an overlap of 58.8% is assumed based on an eccentricity of the centre lines of the brace members of $-h_o/4$ from the chord centreline, the joints investigated here being made eccentric to facilitate comparison with these recommendations. The restraint conditions

were as shown in Figure 11.3, case (i) and (ii), these corresponding to boundary condition (a) in Section 10.4.1. One chord end is supported at a pin, with rollers preventing normal displacement at all other support points, this being done to minimise any secondary moment effects due to the member ends deflecting perpendicular to their axis. Both loading modes illustrated are analysed to examine whether the presence or absence of the hidden weld has an effect on joint strength which due to lack of symmetry may depend on the direction of loading. In addition two further analyses were undertaken with this joint configuration using boundary cases (iii) and (iv) in Figure 11.3 to establish if the direction of the reaction in the chord (i.e tension or compression) was having an effect on joint capacity.

Following from the analyses on these joints at $\beta = 0.6$ and $\theta = 60^o$, further models were developed to undertake a series of joint analyses with $\beta = 1.0$ and $\theta = 60^o$ and $\beta = 0.6$ and $\theta = 30^o$ K joints to investigate the effects of brace angle and β ratio on the hidden weld effects.

11.2.2 Finite Element Modelling

Using the FE package ABAQUS (1991) a model of half of the joint was established, it only being possible to use the symmetry in one plane. Eight noded isoparametric thick shell elements (ABAQUS type S8R) with four integration points were used to model the main chord and brace members, six noded solids being used for the external fillet welds. Details of the modelling of the hidden weld are discussed later in 11.2.2. The mesh used for the $\beta = 0.6$, $\theta = 60^o$ K joints is shown in Figure 11.4, this having a total of approximately 1000 elements, the

grading being finer in the regions of high stress concentration around the brace to chord and brace to brace intersection. Both geometric and material non-linearity were used throughout, the properties being shown in Table 11.1. The material stress-strain curve used is shown in Figure 11.5. The joints were analysed on the Fujitsu vpx mainframe at Manchester Computing Centre. As can be seen in Figure 11.4, 'thick' end plates were included in the model and these were used to apply the axial loads through the pinned and roller restraints at the member ends. No corner radii modelling was undertaken on the chord due to difficulties experienced with the later ABAQUS Version 5.2 rejecting the curved corner radii elements as being too distorted.

11.2.3 Weld Modelling

All external fillet welds were modelled using six noded solid elements with nodes common with the corner points of the chord and brace shell elements. The layout of these external fillet weld elements is shown in Figure 11.6, common nodes between the weld and chord/brace elements being marked 'c'. The coordinates of the nodes 'c' in Figure 11.6 were determined by keeping the throat thickness at 6.8mm, this being selected as being typical from experimental specimens on RHS joints in Section 3.2 whose chord cross sectional properties and β ratios were the same as those of the chord here.

For the hidden weld however three different models were considered:-

Case A, the basic case was where the shell elements of the chord and brace were left intact sharing the intersection nodes and no

solid weld element was installed. This is illustrated in Figure 11.7(a) and was used throughout in Chapter 10. Although this simulates no physical case, it represents the current way such a connection would be modelled using the FE method with no allowance for the weld modelling, giving a useful 'benchmark' case. This case was considered for all four boundary condition cases in Figure 11.3.

Case B, the second case considered (in Figure 11.7 (b)), the hidden weld was included as a solid, this being identical to the external fillet welds.

In Case C (Figure 11.7 (c)(i)and c(ii)), no weld modelling was involved in this region and the physical separation of the shell elements of the chord and brace was undertaken, except for the node where they are attached to the chord sidewalls, this being labelled 'p' in Figure 11.7(c) (ii), which is the projection of this region.

11.3 Analyses and Results

11.3.1 Analyses of the Initial Warren K Joints, $\theta = 60^o$, $\beta = 0.6$ and Ov = 58.8%.

Six analyses (cases (i) and (ii) for each weld case) were undertaken and the capacities of each determined. The capacities are taken as peak loads and are tabulated alongside the Packer et al (1992) design capacity predictions in Table 11.2. Load vs compression brace indentation plots for the two series are shown in Figures 11.8 (compression in the

through brace) and 11.9 (compression in the overlap brace), indentation being measured as described in Section 10.4.2 and Figure 10.6. Displaced shape plots for the two joints of case B, boundary conditions (i) and (ii) being shown in Figures 11.10 and 11.11. An additional two analyses for weld case A were undertaken using boundary cases (iii) and (iv).

Weld Case	Comp (C) or Tension (T) in the thru'brace	FE capacity (kN)	Chord Reaction Tens (T) or Comp (C)	Packer design capacity(kN) Eqn [1]	$\frac{\text{FE}}{\text{Packer}}$
A - shells	C (Fig 11.8)	652.8	C (i)	728.6	0.90
"	T (Fig 11.9)	767.9	T (ii)	728.6	1.05
A - shells	C	657.1	T (iii)	728.6	0.90
"	T	763.8	C (iv)	728.6	1.05
B - solids	C (Fig 11.8)	655.7	C (i)	728.6	0.90
"	T (Fig 11.9)	805.8	T (ii)	728.6	1.11
C - gap	C (Fig 11.8)	645.5	C (i)	728.6	0.89
"	T (Fig 11.9)	706.7	T (ii)	728.6	0.97

Table 11.2 FE capacities for various hidden weld assumptions $\beta = 0.6$, $\theta = 60^{o}$ K Joints. Squash load of brace members = 885kN.

11.3.2 Analyses of the $\theta = 60^{o}$, $\beta = 1.0$ K Joints

A similar investigation has been undertaken on a full width K joint with the restraint condition shown in Figure 11.3 using the same

noding offset and three weld models described in Section 11.2.2. External dimensions of the joint are shown in Figure 11.12 and material properties in Table 11.3. Case A was analysed under all four loading and support conditions in order to establish under which regime the capacity was greatest, while the other two Cases (B and C) were analysed under tension in the through brace, compression in the overlapping brace under boundary case (ii). The loading mode where compression was applied in the through brace and tension in the overlapped brace can be seen in Figure 11.8 to not significantly effect capacity for these joints whether the hidden weld was present or not. Results for the $\beta = 1.0$ series of analyses in terms of peak loads are

	Overlapped Brace j (150 x 150 Square HS)	Overlapping Brace i (150 x150 Square HS)	Chord (150 x 150 Square HS)
Angle	60°	60°	
Yield Stress (N/mm^2)	420	420	420
Tensile Strength (N/mm^2)	540	540	540
Thickness (mm)	6.3	6.3	6.3
Slenderness (b/t)	23.8	23.8	23.8
$\beta = 1.0$, e = -ho/4 = 37.5 mm, q = 97 mm, Ov = 74.0%, Brace Squash Load = 1521kN			

Table 11.3 Test Parameters and Material Properties for the $\beta = 1.0$, 60° K Joints.

tabulated alongside the Packer et al (1992) design capacities in Table 11.4. As 'in-punch' of the braces into the chord , as discussed in Section 10.5 is not the predominant mode of failure for $\beta = 1.0$ joints, brace indentation plots were not produced, displaced shape plots for the two loading cases of weld case A are shown in Figures 11.13 (case (i) in Figure 11.3) and 11.14 (case (ii) in Figure 11.3).

Weld case	Compression in thru'	FE capacity (kN)	Packer capacity(kN) Eqn [11.1]	$\frac{\text{FE}}{\text{Packer}}$
A - shells	Y	1070.0	988.9	1.08
A - shells	N	1040.3	988.9	1.05
B - solids	N	1040.3	988.9	1.05
C - gap	N	1038.3	988.9	1.04

Table 11.4 FE capacities for $\beta = 1.0$, 60^o K Joints. Brace squash load = 1521kN.

11.3.3 Analyses of the $\theta = 30^o$, $\beta = 0.6$ K Joints. Ov = 56%.

So far the effect of the hidden weld has varied depending on the width ratio and the loading mode, and the effect of angle has not been considered. In order to quantify the effects more fully at the $\beta = 0.6$ ratio where the presence of the hidden weld appears to be significant under certain loading conditions, a series of analyses on $\theta = 30^o$, $\beta = 0.6$ K joints using the three weld models described in Section 11.2.2 was undertaken. For reasons discussed in 11.3.2 all three weld cases were

analysed under tension in the through brace with compression in the overlapping brace, while Case A was analysed additionally under the 'normal' (compression in the through brace) loading condition to establish which loading mode gave the greatest capacity. The overlap was maintained at 56% as was the case for the $\beta = 0.6$, 60^o joints resulting in an eccentricity from the chord centreline of $-0.36h_o$. Restraint conditions were case (iii) and (iv) in Figure 11.3, additional cases being analysed for weld Case A to establish if the direction of chord loading was having an influence on capacity, these being cases (i) and (ii) in Figure 11.3. External dimensions and material properties of the chord and brace were maintained as those of the earlier 60^o joints,

	Overlapped Brace j (90 x 90 Square HS)	Overlapping Brace i (90 x 90 Square HS)	Chord (150 x 150 Square HS)
Angle	30°	30°	
Yield Stress (N/mm^2)	420	420	420
Tensile Strength (N/mm^2)	540	540	540
Thickness (mm)	6.3	6.3	6.3
Slenderness (b/t)	14.3	14.3	23.8
$\beta = 0.6$, e = -ho/4 = 54 mm, q = 97.2 mm, Ov = 58.1% Brace Squash Load = 885kN			

Table 11.5 $\theta = 30^o$, $\beta = 0.6$ K Joint Test Parameters and Material Properties.

these being shown along with the eccentricity and a mesh plot in Figure 11.15 and Table 11.5. Results for the six analyses undertaken in terms of peak loads are shown in Table 11.6 alongside the Packer et al (1992) design capacities. Displaced shape plots for the two loading modes on case A, boundary conditions (iii) and (iv) being shown in Figures 11.16 and 11.17.

Weld case	Load in thru' brace (C or T)	Chord Load (C or T)	FE capacity (kN)	Packer capacity (kN)	$\frac{\text{FE}}{\text{Packer}}$
A - shells	C (iii)	T	826.2	728.6	1.13
A - shells	T (iv)	C	638.3	728.6	0.88
A - shells	C (i)	C	657.2	728.6	0.90
A - shells	T (ii)	T	869.9	728.6	1.19
B - solids	T (iv)	C	635.3	728.6	0.87
C - gap	T(iv)	C	633.8	728.6	0.87

Table 11.6 $\theta = 30^o$, $\beta = 0.6$ K Joint FE capacities. Brace squash load 885kN.

11.3.4 Effect of Brace Thickness on Ultimate Capacity

As stated in the introduction two analyses were undertaken on the $\beta = 0.6$, 60^o K joint with the brace material thickness (t_i and t_j) being varied from 9.6mm to 3.6mm. The IIW maximum limit on wall slenderness is limited to:- $1.1\sqrt{\frac{E}{p_y}}$. Loading was considered for compression in the through brace and tension in the overlapping brace, using weld Case A. The load vs indentation plot (measured as

described in Section 10.4.2) for these two analyses and the earlier Case A (t_i and t_j = 6.3mm) is shown in Figure 11.18, the peak capacities being shown in Table 11.7 alongside the Packer et al (1992) design predictions. Displaced shape plots to complement that in Figure 11.10 (t_i and t_j = 6.3mm) are shown in Figures 11.19 (t_i and t_j = 3.6mm) and 11.20 (t_i and t_j = 9.6mm). The different modes of failure evident from these will be discussed in Section 11.4.3. The boundary condition for the three analyses here was that of case (i) in Figure 11.3.

Weld case A t_o= 6.3mm all case (i)	FE capacity (kN)	Packer capacity (kN) Eqn [11.1]	$\frac{FE}{IIW}$	Brace Squash Load (kN)	$\frac{FE}{Squash}$	$\frac{Packer}{Squash}$
t_i=t_j = 3.6mm $\frac{b_i}{t_i}$ = 25.0	378.7	436.0	0.86	522	0.725	0.845
t_i=t_j = 6.3mm $\frac{b_i}{t_i}$ = 14.3	652.8	728.6	0.90	885	0.737	0.823
t_i=t_j = 9.6mm $\frac{b_i}{t_i}$ = 9.4	996.5	1139.5	0.87	1297	0.769	0.878

Table 11.7 FE peak loads for β = 0.6, 60° K Joints with varying brace thickness.

11.4 Discussion

The results are considered in three parts, the first dealing with the β = 0.6 joints analysed in Sections 11.3.1 and 11.3.3, the second dealing

with the β = 1.0 joints in Section 11.3.2 and the third section with the effect of brace thickness on joint capacity.

11.4.1 Hidden Weld Effects on β = 0.6 K Joints

It can be seen from Figure 11.8 that when the through brace is in compression then the presence of the hidden weld as a solid (Case B) over the gap case (Case C) has no significant effect on the capacity or behaviour of the joint, except to raise capacity a little in the elastic-plastic transition zone. This is shown in the ultimate capacities in Table 11.2 where joint peak capacities for compression in the through brace vary by only 1.6%. This effect is likely to be negligible in reality as when the gap (if the hidden weld is not included) closes under compression then the points of contact of the compression loaded through brace with the chord will be the same as those of the case where the hidden weld is included. The projected area of contact of the hidden weld would appear to have no influence on capacity under this loading condition. This is verified by the difference between Case A (where only shell elements are in contact with the chord in the hidden weld region) and Case B (where the area of contact in the hidden weld region is much increased with the addition of the solid element) being negligible. Figures 11.10 and 11.11 illustrate the failure of the joints under the two loading modes. As can be seen 'in-punching' of the compression brace into the chord occurs with significant chord top face deformation alongside local buckling of the compression brace (L6 type failure) around its intersection with the tension brace. This deformation also spreads to the other brace in this region. Significant

chord top face deformation can also be seen to occur under the heel of the tension brace.

Figure 11.9 shows the load vs indentation plots where the through brace is loaded in tension and these capacities are tabulated as peak loads in Table 11.2. As can be seen here the presence of the hidden weld would appear to have a significant effect on ultimate capacity. The inclusion of the weld as a solid element (case B) enhances capacity over that of the gap Case (C) by 14% from 706.7kN to 805.8kN, Case A lying between B and C. This can be explained with reference to the points and lines of contact of the tension loaded through brace with the chord top face. Where the hidden weld is not included (Case C in Figure 11.7(c)) and the brace is tension loaded then the gap will widen, therefore not at any time providing another face of load transfer between the brace and chord. Where a weld is included (Case B Fig 11.7(b)), then a substantial increase in the area of load transfer between this tension loaded brace and the chord top face occurs, this acting to reduce overall brace out-pull from the chord top face, thus stabilising this region a little. A typical displaced shape plot for this loading mode (Case A) was shown in Figure 11.11 and discussed earlier.

From Table 11.2 it can be seen that the reversal of the chord reaction component from compression to tension (boundary case (i) to (iii) or case (ii) to (iv)) has little effect on the ultimate capacity (approximately 1%); thus the direction of the chord reaction is having a negligible effect on joint capacity at this angle and β ratio.

Inclusion of the hidden weld is therefore beneficial from a strength point of view on this particular joint configuration, especially where the through brace is loaded in tension (the most efficient

loading mode). However inclusion will increase welding fabrication costs for square braces by around 11% (eight brace edges to weld as opposed to seven), the exact amount depending on the angle of inclination of the braces. Whether this expense is justified will depend on particular circumstances and if the enhancement in strength due to hidden weld inclusion is enough to counter the need to increase the bracing size or thickness and hence cost. In the case of a bracing size increase being necessary, inclusion of the hidden weld will almost certainly cost less, as a bracing size increase automatically implies an increase in the amount of external welding to be undertaken around such a brace.

Adjustment of the bracing angle to 30º, while maintaining the overlap percentage causes significantly different behaviour to occur. As can be seen from Table 11.6 the results for the analysis at a brace angle of 30º illustrate significantly different trends to those shown by the 60º joints.

It can be seen that reversing the load in the braces from compression to tension (cases (iii) to (ii) or (i) to (iv)) has little effect on the capacity. However the capacity is clearly influenced by the direction of the reaction force in the chord. Where this force is tensile the capacity of the joint is greater than when this force is compressive (case (iii) to (i) and (ii) to (iv)). Clearly for this angle of 30º, where failure is of the L7 type, that of chord yielding, buckling will occur where the chord reaction force is compressive. This is clear from the displaced shape plot for case (iv) in Figure 11.17. Where the reaction force within the chord is tensile however, membrane action occurs in the top face and a consequent increase in loading can occur. This is shown in Figure 11.16

for case (iii). A table of chord top face stresses for analysis case (i) is shown in Table 11.8. Elements 163 to 168 are those on the chord top face in the sixth row from the chord end plate at the through brace end. These stresses are taken at the peak load reached in the analyses and are direct stresses in the line of the chord on both the external face (face 1) and the internal face (face 2) of the elements.

Element	External Face 1 N/mm^2	Internal Face 2 N/mm^2
163	355	320
164	347	401
165	437	360
166	463	450
167	485	348
168	494	277

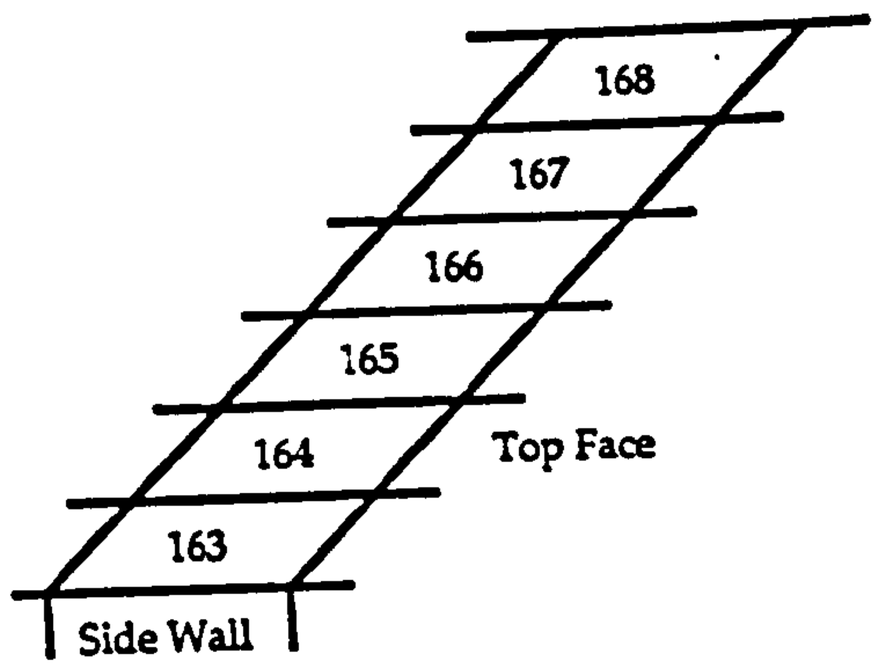

Table 11.8 Direct Stresses for Elements 163 to 168 (Chord Top Face).

It is clear from this that the stresses are reaching yield ($420N/mm^2$). Stress magnitudes above this are a result of the ABAQUS package interpolating these from the integration points of the elements to the nodes.

Where the through brace is loaded in tension in $\theta = 30^o$ joints, there is little difference between the ultimate capacities for the three weld cases, the effect of including the hidden weld on this brace angle thus being small. This can be explained by the mode of failure exhibited

by these joints. Figures 11.16 (compression in the through brace) and 11.17 (tension in the through brace) show the displaced shape plots for these joints (hidden weld Case A) at peak load. It can be seen that the main mode of failure here is concerned with both local and global chord bending. The bending is caused by the large noding eccentricity (-$0.36h_o$) due to the overlapping of the braces at such a shallow angle. The different sense of chord bending reflects yielding in tension (Figure 11.16), and yielding in compression (Figure 11.17) or local buckling (L7 type failure) in the chord next to the tension brace heel. This eccentricity causes the axial component of the brace loads to be offset in the chord, introducing a moment in the chord and hence member bending. A rapid evaluation of the chord top face stress according to :-

$$\text{Stress} = \frac{\text{axial load}}{\text{area}} + \frac{\text{moment}}{\text{elastic modulus}} \qquad \text{Eqn [11.2]}$$

where the chord elastic modulus, $Z = 165cm^3$ and area of chord= $3600mm^2$

the chord axial load is = 650 kN (= axial load in braces) x 2 x $\cos\theta$ and the chord moment = 650kN x 2 x $\cos\theta$ x $0.36h_o/2$.

gives a chord top face stress of $460N/mm^2$ this being greater than the yield strength of $420N/mm^2$ indicating that the chord material will have yielded or buckled on the top face, confirming the observation that chord global failure is occurring in this instance rather than the brace failure associated with Equation 11.1.

From load vs indentation plots derived (using points on the chord mid-height on the brace centrelines and points on the brace as per the method described in Section 10.4.2) the indentations were

always found to be small, this confirming that local in-punch of the braces into the chord top face was not a major mode of failure in this joint configuration. The effect of the increase in contact area provided to the tension loaded through brace by the inclusion of the hidden weld does not have a significant impact on the ultimate capacity of 30°, $\beta = 0.6$ K joints. This is because failure occurs mainly in the chord due to bending as opposed to brace in-punch and out-pull observed in the previous 60°, $\beta = 0.6$ K joints. This chord deformation occurs in regions well away from the hidden weld, hence minimising its effect on capacity.

Figure 11.21 shows the peak capacities for the four boundary cases for $\beta = 0.6$ at both brace angles, 30° and 60° alongside the Packer (1992) formulae. The FE and code capacities are presented as ratios with respect to the brace squash load.

From this diagram it is apparent that both the direction of the chord reaction and the load in the brace can effect joint capacity and behaviour, their effect being dependent on brace angle. Where $\theta = 30°$, the direction of chord load is clearly the major influence on capacity and when $\theta = 60°$ the direction of the brace load is the main influence. When the through brace is loaded in tension, capacity is raised above the corresponding compression loaded case.

11.4.2 Hidden Weld Effects for the $\beta = 1.0$, 60° K Joint Series

The results for the series of analyses undertaken on this joint series are tabulated in terms of peak capacities in Table 11.4, since

indentation plots are not relevant here as the major mode of failure is local chord buckling L7 which is shown in Figures 11.13 and 11.14. Deformation of the chord top face is restricted however for these full width joints, by the load transfer directly into the 'stiff' chord sidewalls.

With reference to Table 11.4, it can be seen that it is slightly beneficial to load the through brace in compression, this giving an ultimate capacity some 3% higher (weld Case A, boundary case (i)). However, the differences in the results of tension or compression in the through brace can be seen to be small regardless of whether the chord reaction force is tensile (case(ii)) or compressive (case(i)). The three analyses with tension in the through brace indicate that the inclusion of the hidden weld has no effect on ultimate capacity. This is likely to be explained by the mode of failure. As the chord sidewalls provide two strips of load transfer between the braces and chord for the axial load and are very stiff in the loading plain, they act to stabilise the deformation of the chord top face which occurs at lower β ratios. The inclusion of the hidden weld has little effect on enhancing the strength in this region or that of the region under the heel of the tension brace where deformations are largest, due to its physical remoteness from these; hence the lack of influence observed on capacity.

11.4.3 Effect of Brace Thickness on Capacity

The three load vs indentation results obtained from an investigation of the effects of brace thickness are shown in Figure 11.18 and tabulated in terms of ultimate capacities in Table 11.7. All three analyses contained weld case A for the hidden weld and all were loaded

in compression in the through brace. It can be seen that increasing the brace thickness by 75% and 167% (from 3.6mm) increases capacity by 36% and 107% respectively. As can be seen from the indentation plot all joints experience an 'in-punching' of the brace into the chord type failure but observation of the displaced shape plots in Figures 11.10 (t_i and t_j = 6.3mm), 11.19 (t_i and t_j = 3.6mm) and 11.20 (t_i and t_j = 9.6mm) reveals that differences are caused in modes of failure by the brace thickness. At t_j = 3.6mm (Figure 11.19) the main mode of failure is seen to be local buckling of the compression brace in the region of its connection with the tension brace. Some deformation of the chord top face can also be observed. As the braces are thickened (Figure 11.10) to 6.3mm the chord top face deformations increase in significance compared to the local buckling of the brace to brace intersection. At a brace thickness of 9.6mm (Figure 11.20) the predominant mode of failure can be seen to be chord top face buckling beneath the heel of the tension brace although some deformation in the region of the compression brace - tension brace intersection can still be observed. The capacities are tabulated next to those of the Packer et al (1992) predictions in Table 11.7. It can be seen that the Packer formulae would appear to account for the effect of brace thickness in a similar manner to that of the FE analyses. The ratios of the Packer prediction and FE capacities to those of the brace squash loads (yield strength/gross cross-sectional area) are shown graphically in Figure 11.22 for the three different brace thicknesses studied here. It can be seen that the two sets of results appear to follow similar trends over the limited parameter range studied here. However, given the wide differences in behaviour of K joints observed due to the hidden weld effects caused by changes

in θ and the β ratio it is difficult to make predictions as to the effect of brace thickness without a study over a much wider range of β ratios and brace angles. In the absence of this it is difficult to draw conclusions here except that the formulae appears 'on the whole' to agree with the FE in its treatment of brace thickness.

11.5 Conclusions

1) The hidden weld can, depending on configuration and loading mode have a significant effect on joint capacity where β ratios are less than one. These circumstances would appear to be where the brace angle is steep (i.e 60° as opposed to 30°) and the through brace is loaded in tension. No effect due to the hidden weld was observed at a brace angle of 30° while an increase in ultimate strength of 12% was observed for a joint with a brace angle of 60°. The effect of the size of the overlap on the hidden weld was not investigated here, although this too may have an influence on the effect of the hidden weld.

2) The mode of failure appears to determine whether the hidden weld has an effect. Where the predominant mode of failure is in-punch or out-pull of the braces into the chord top face (as where β = 0.6 and θ = 60°) then the presence of the hidden weld would appear to have a significant impact. Where other failure modes are predominant (i.e chord top face deformation under the heel of the tension brace or chord bending) the hidden weld impact appears to be much less.

3) Whether to place the hidden weld will depend on the economics. If the hidden weld can increase the joint capacity enough to

negate the need to increase bracing size or thickness and presuming its cost is cheaper then its inclusion will be worthwhile.

4) As recognised in the Packer et al (1992) formulae brace thickness has an influence on joint capacity and failure modes. Without a more extensive study over wider parameter ranges this cannot be quantified further here, suffice to say that the Finite Element study results would appear to agree with the general trend of the IIW formula.

5) Loading of the through brace in tension or compression can be beneficial or not. From the results here and those in Chapter 10 it would appear that this depends on both β ratios, support conditions and brace angle. It would appear that for $\theta = 60^o$ joints with a β ratio less than 1.0 it is beneficial to load the through brace in tension but where the angle is shallower (30^o) then chord failure predominates therefore ovewhelming the brace loading mode effects.

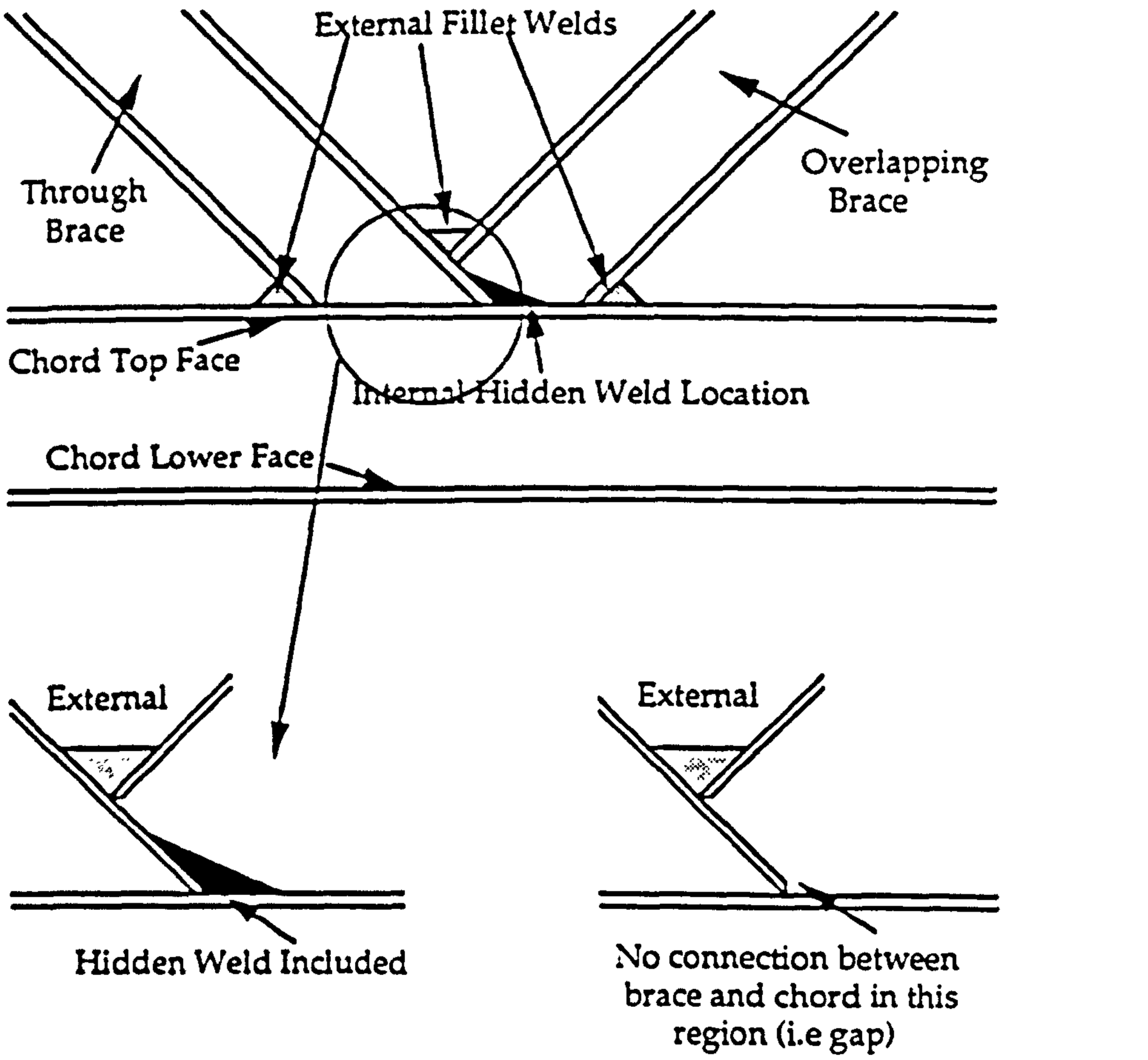

Figure 11.1 The Hidden Weld in Partial Overlap K Joints.

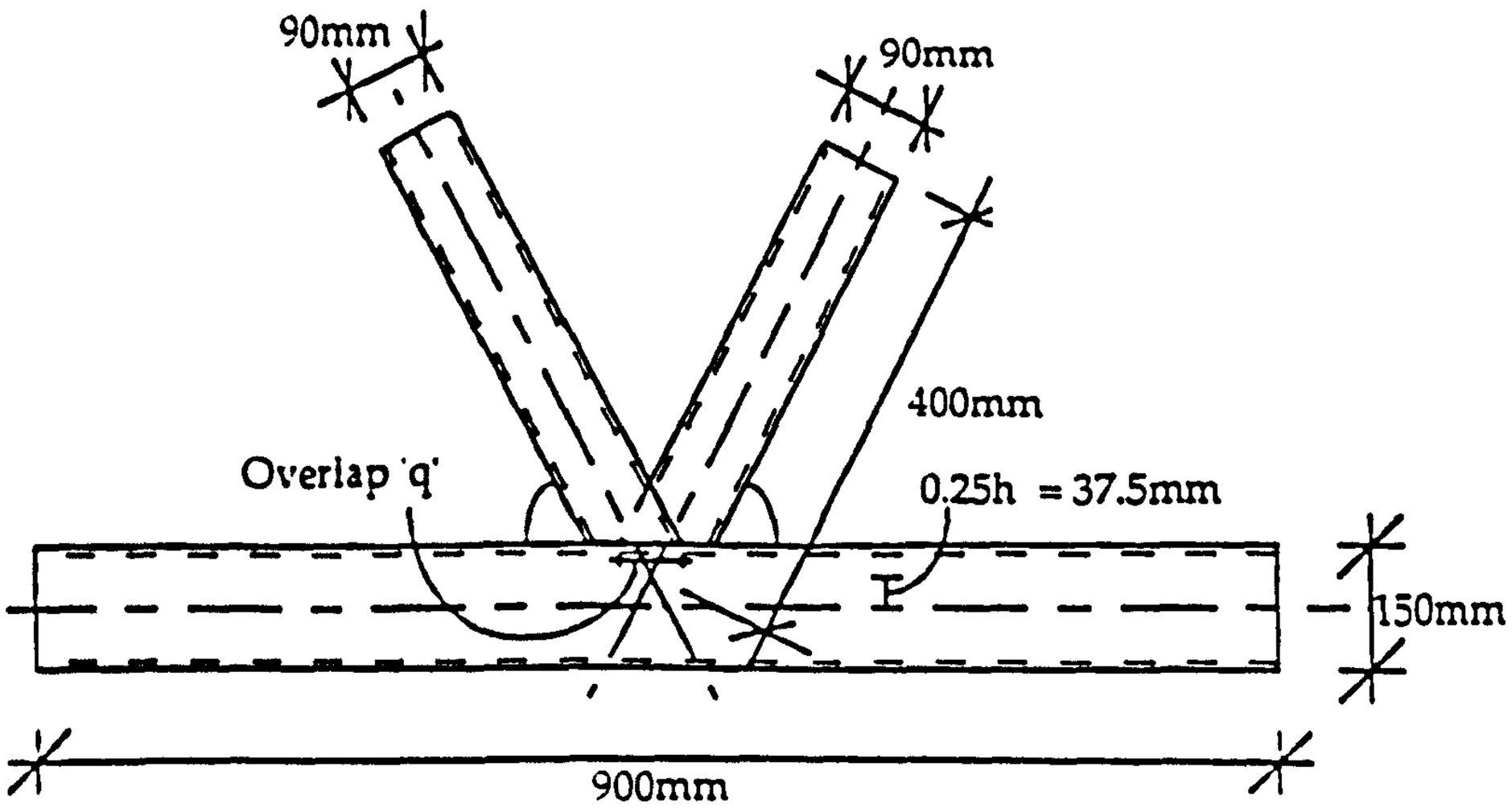

Figure 11.2 Dimensions of the $\beta = 0.6$ 60° K Joint.

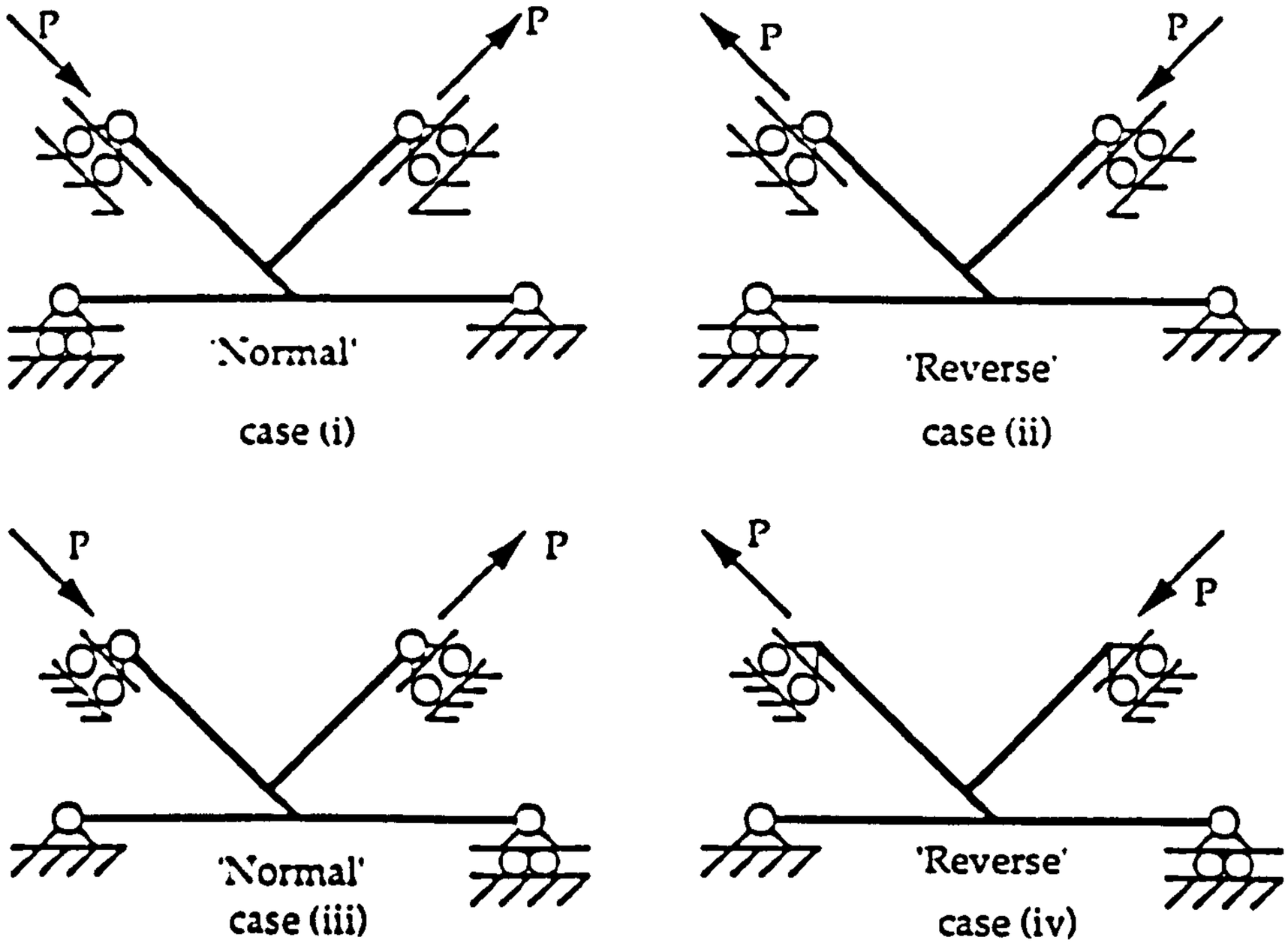

Figure 11.3 Loading and Support Conditions for the Joints.

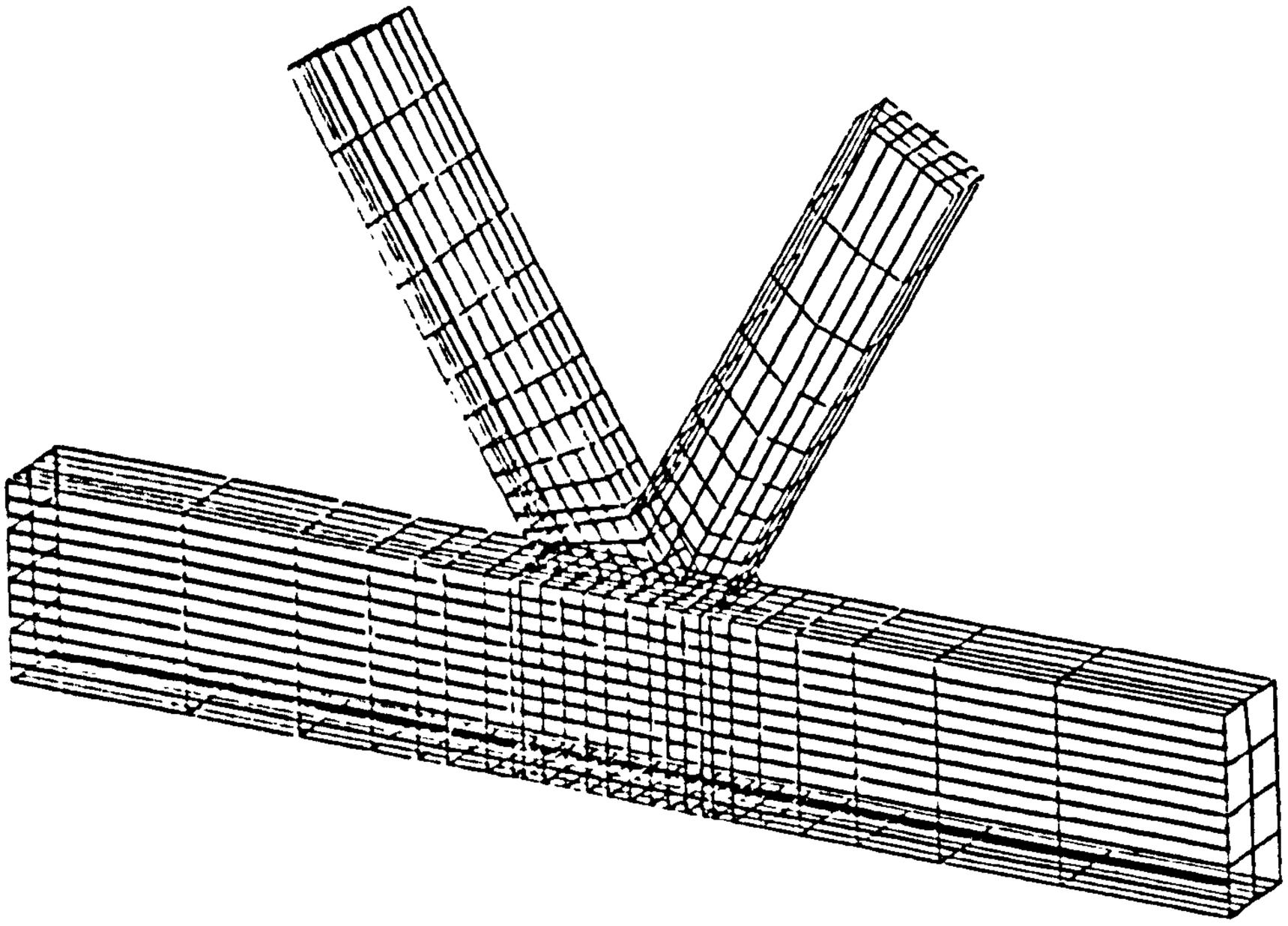

Figure 11.4 Mesh Plot for the $\beta = 0.6$ 60° K Joint.

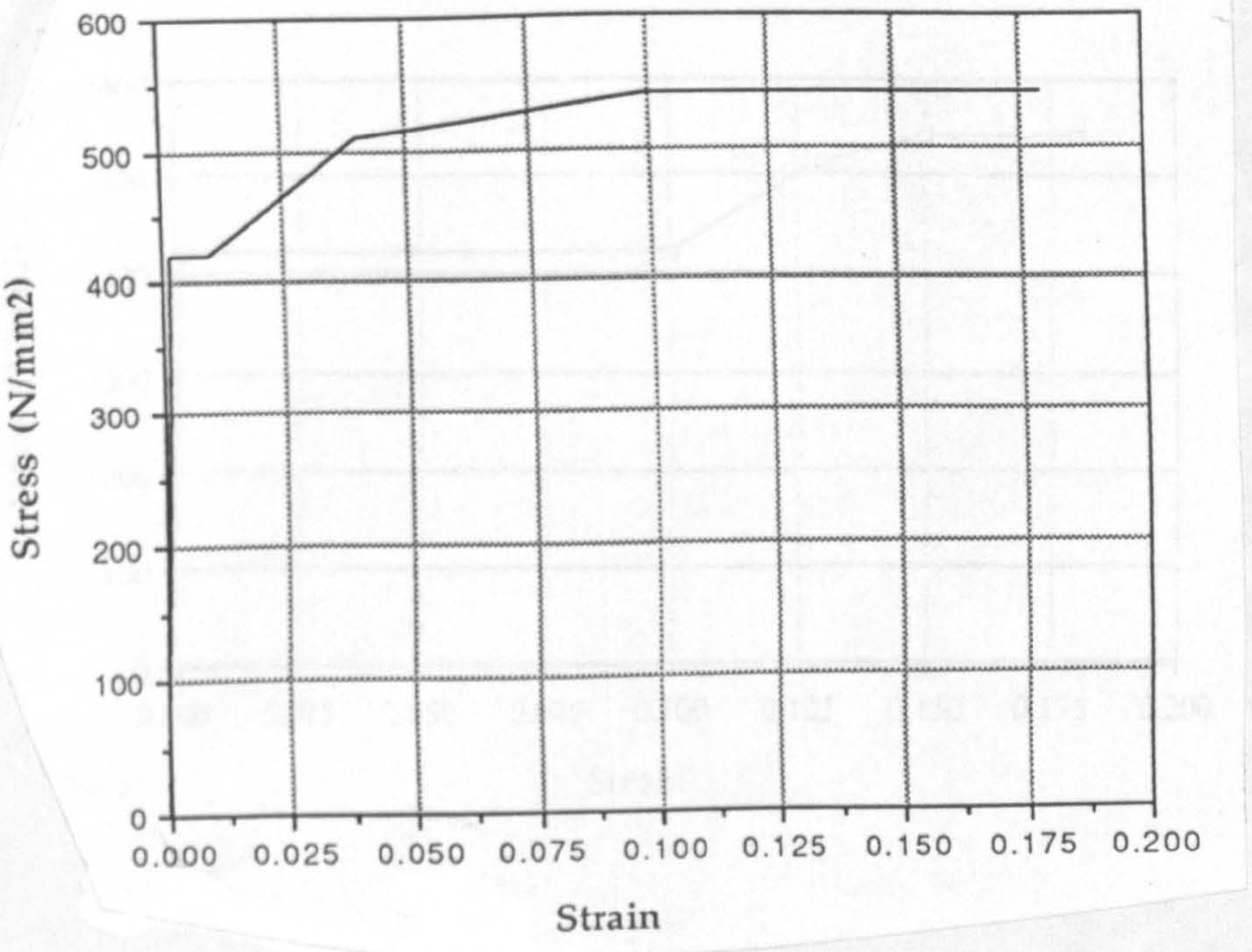

Figure 11.5 The Material Stress - Strain Relationship for all Joints.

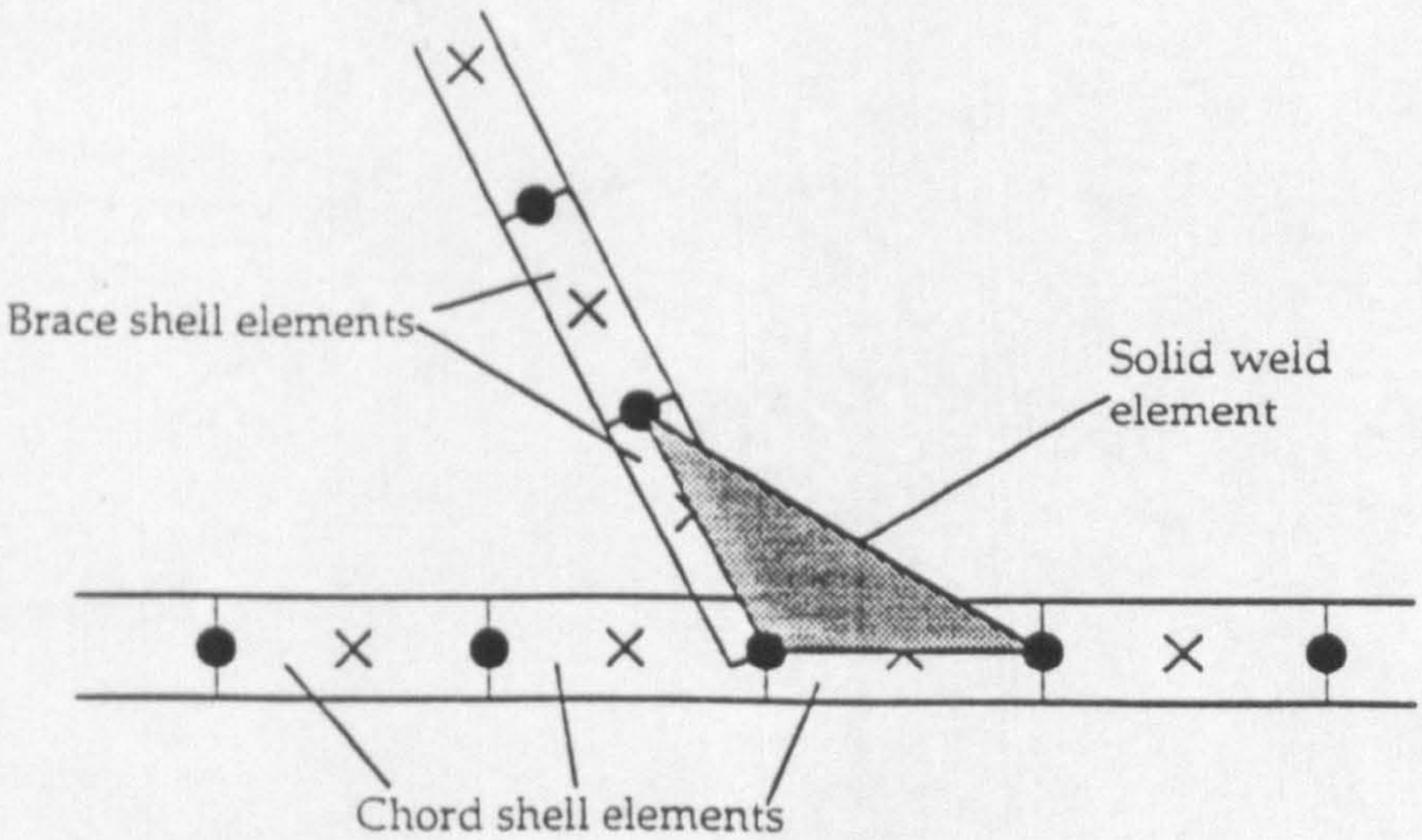

Figure 11.6 External (visible) Fillet Weld Modelling Details.

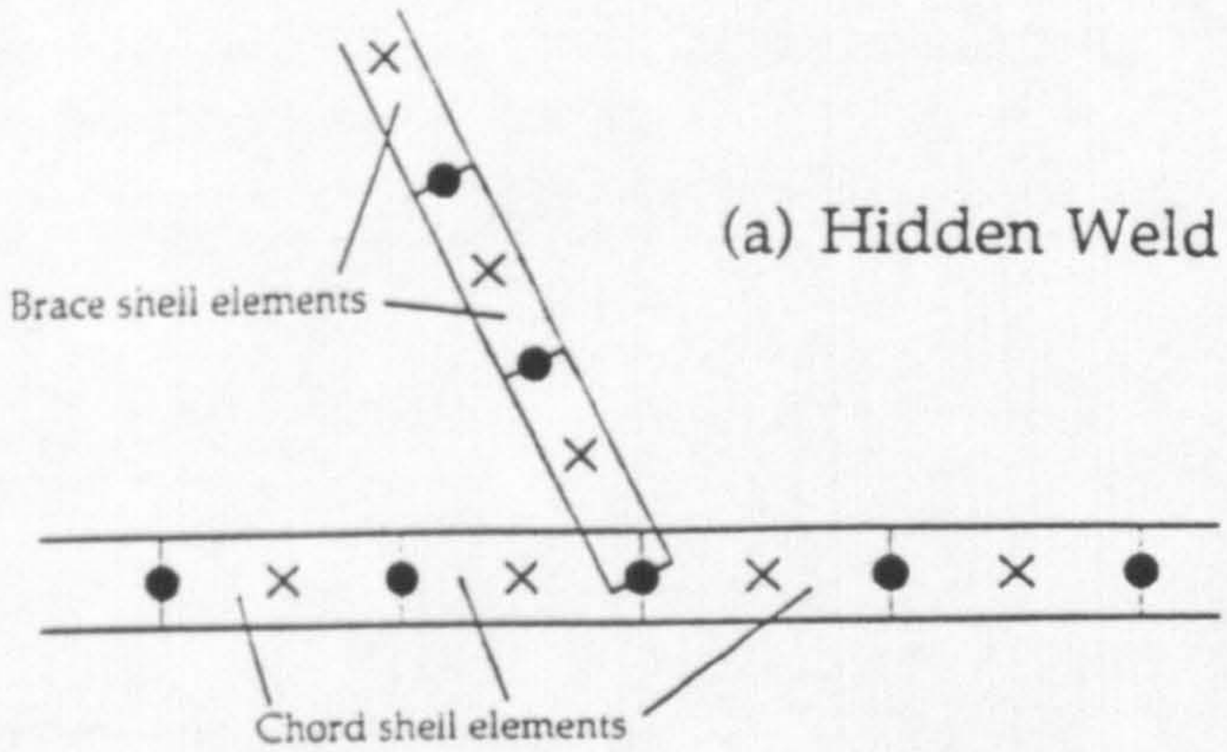

(a) Hidden Weld Case A Detail - Shell

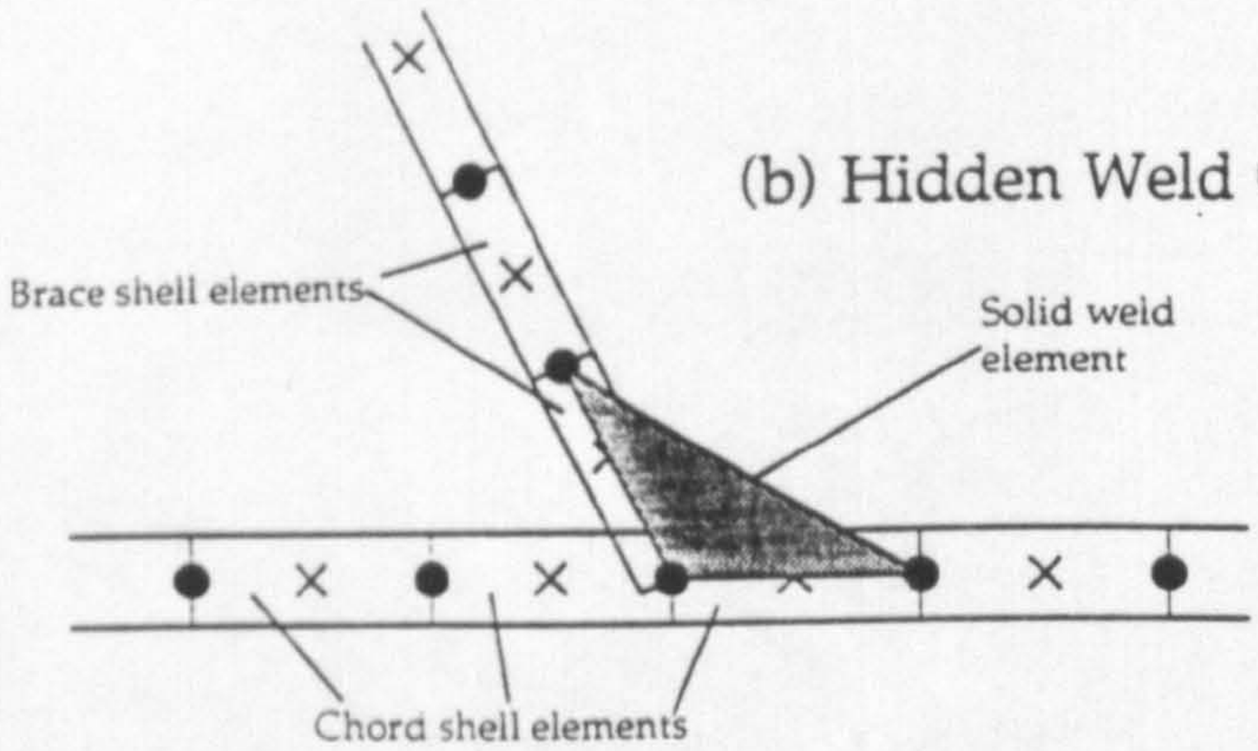

(b) Hidden Weld Case B Detail - Solid

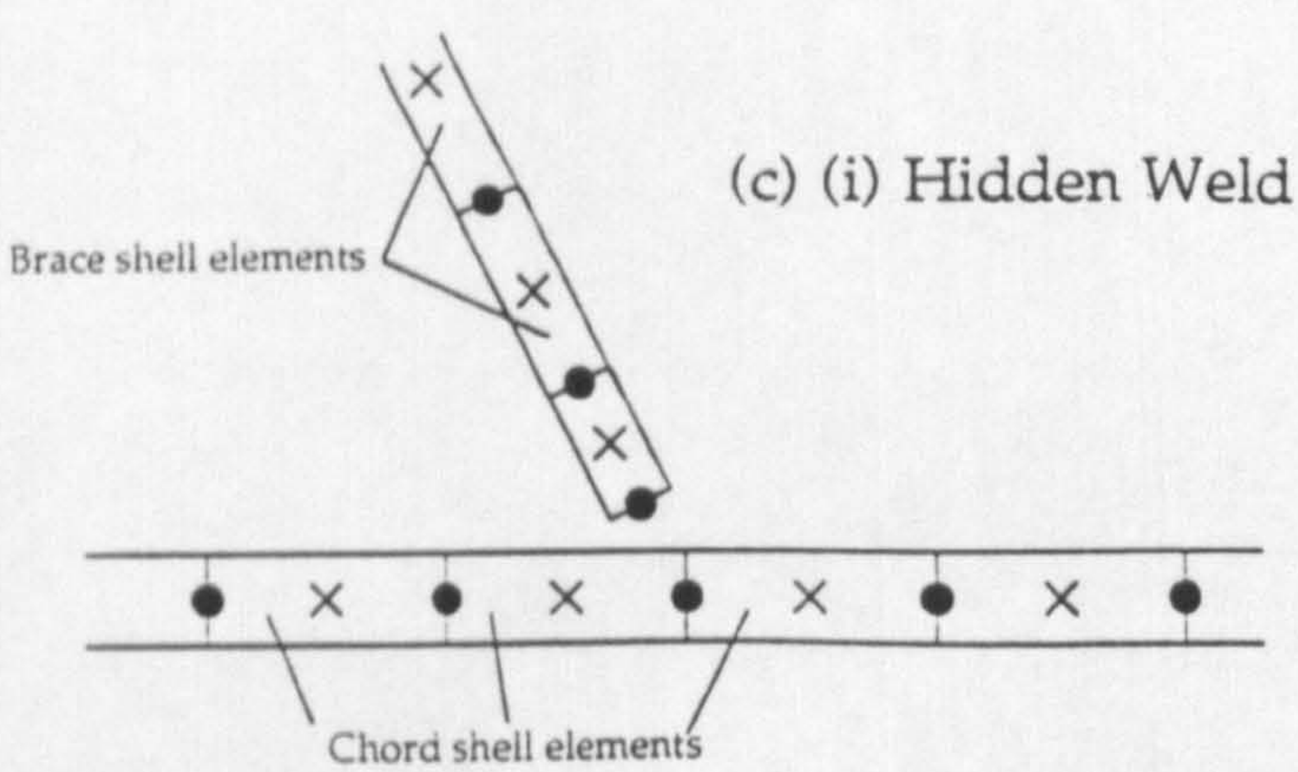

(c) (i) Hidden Weld Case C Detail - Gap

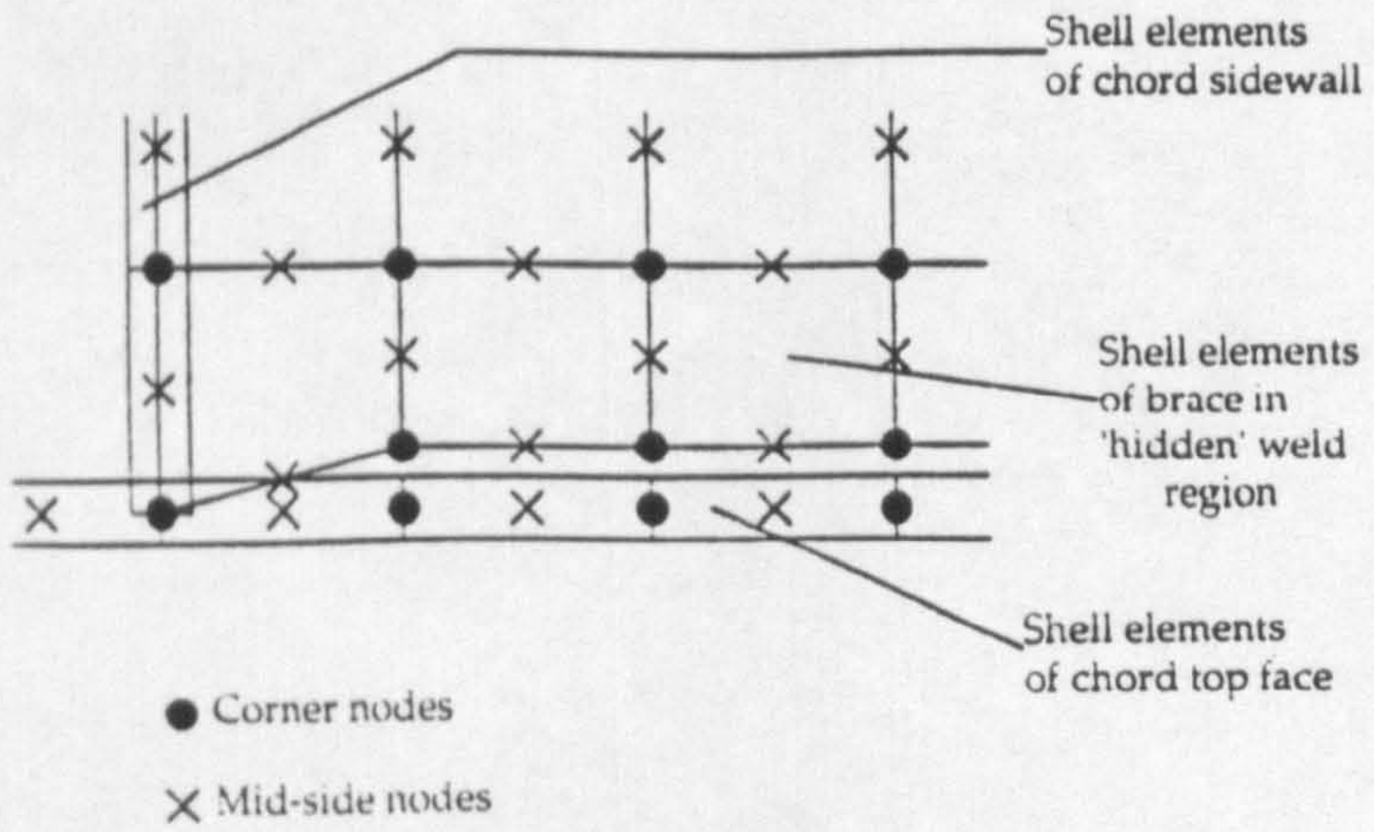

(c) (ii) End Projection of Hidden Weld Case C Showing Gap Region (see Figure 11.6(c)).

Figure 11.7 The Three Hidden Weld Cases.

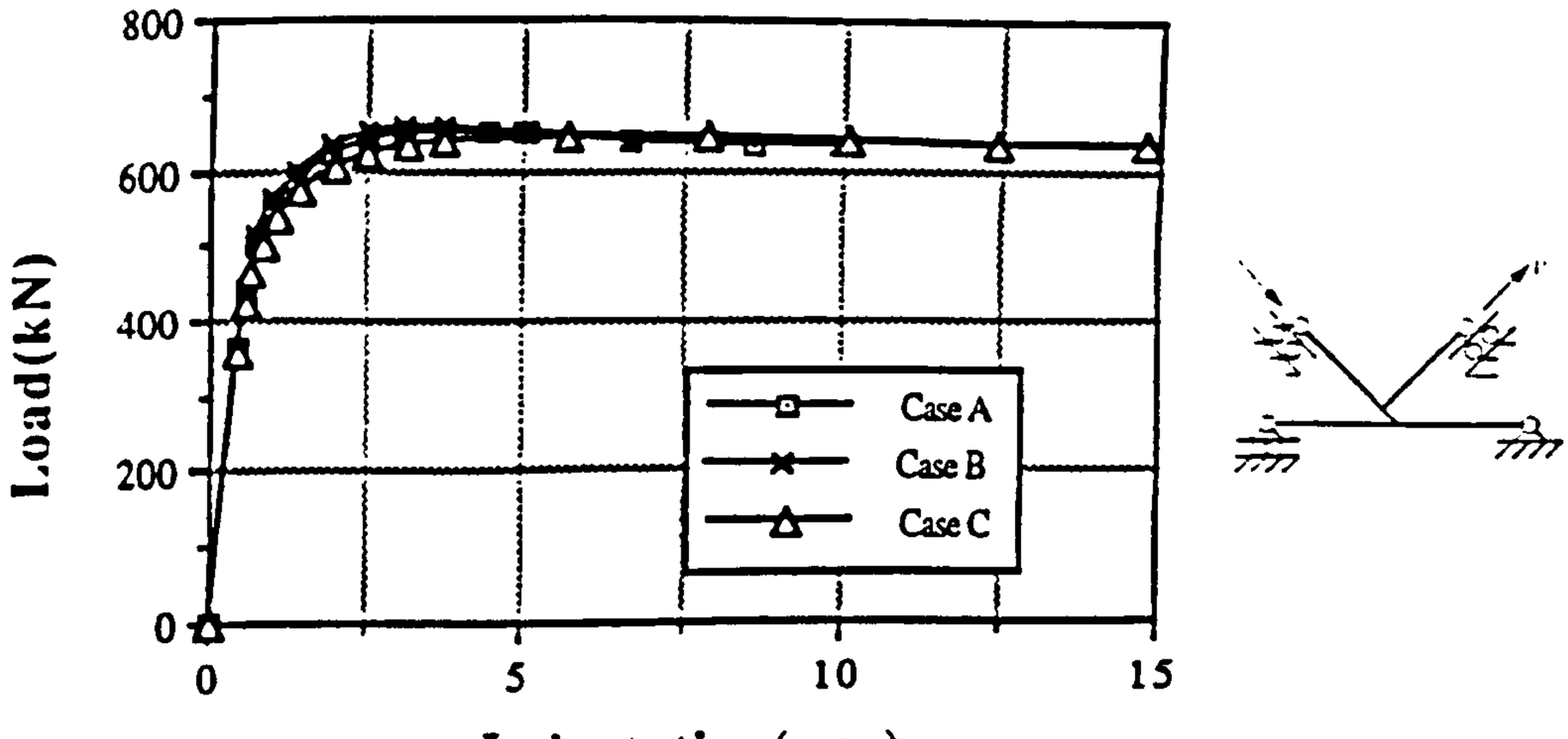

Figure 11.8 Load vs Indentation Plots for Joint Weld Cases A, B and C Where the Through Brace is Loaded in Compression. $\beta = 0.6$, $\theta = 60^{o}$.

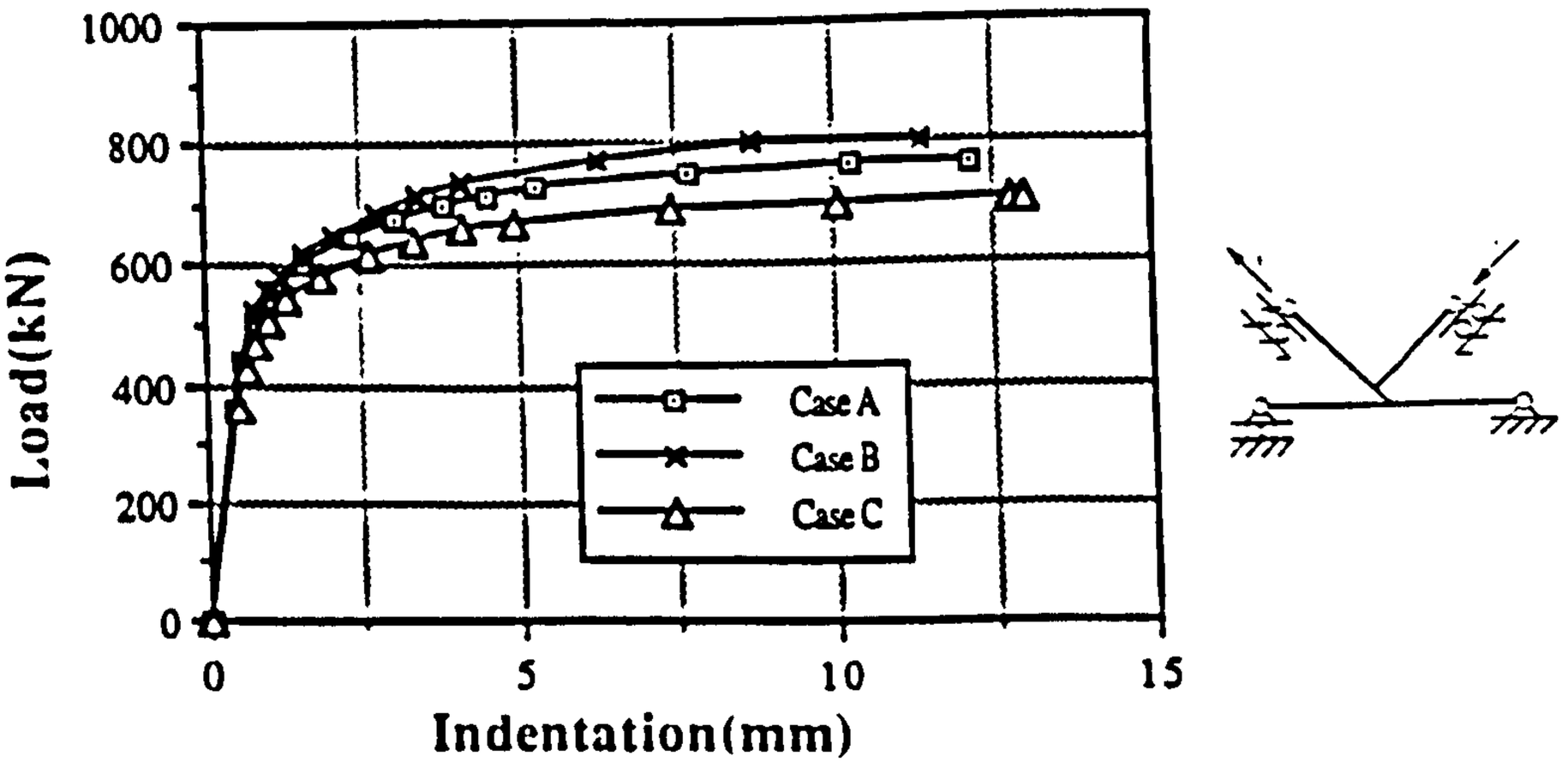

Figure 11.9 Load vs Indentation Plots for Joint Weld Cases A, B and C Where the Through Brace is Loaded in Tension. $\beta = 0.6$, $\theta = 60^{o}$.

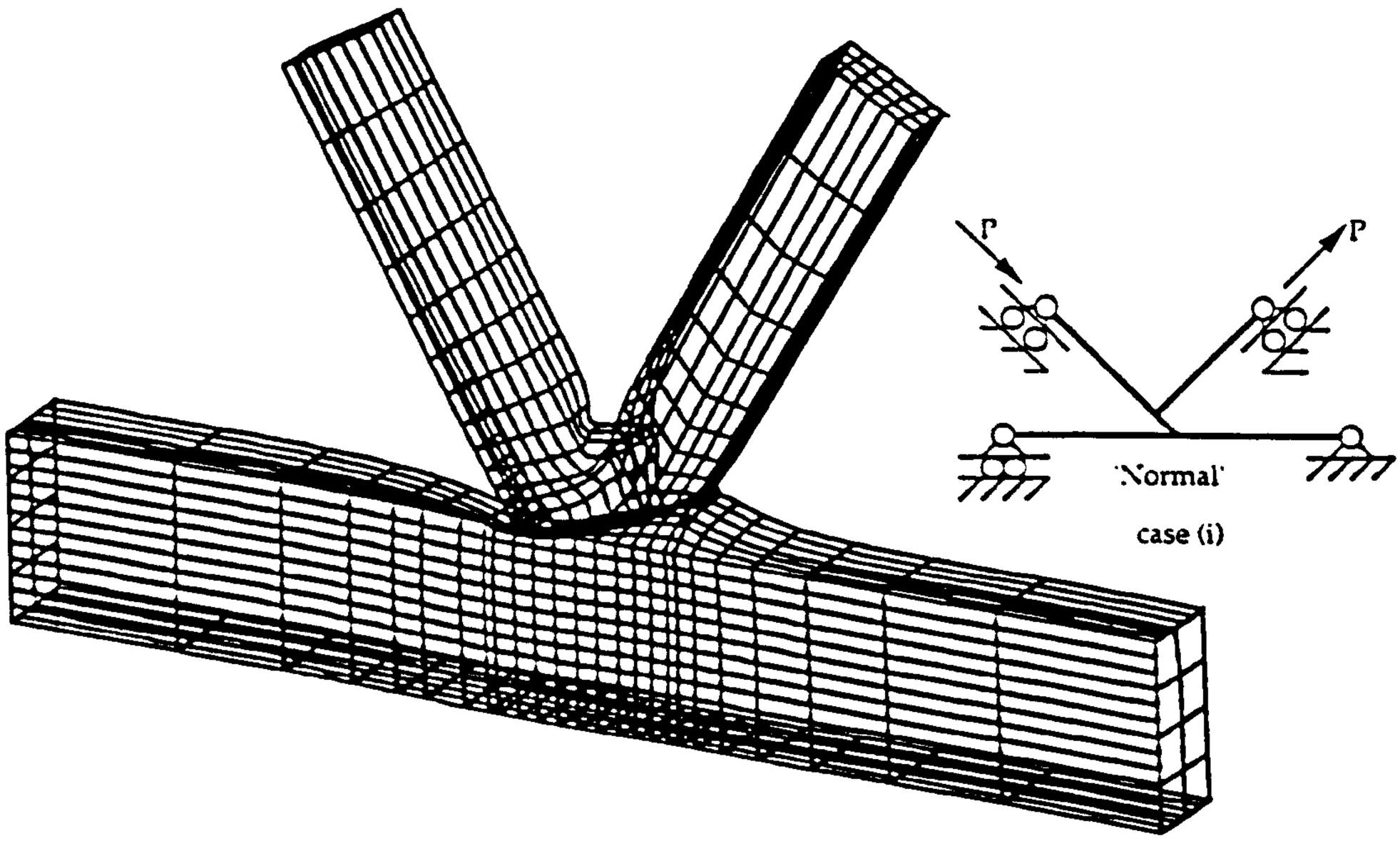

Figure 11.10 Displaced Shape Plot for β = 0.6 60° K Joint where Through Brace is Loaded in Compression.

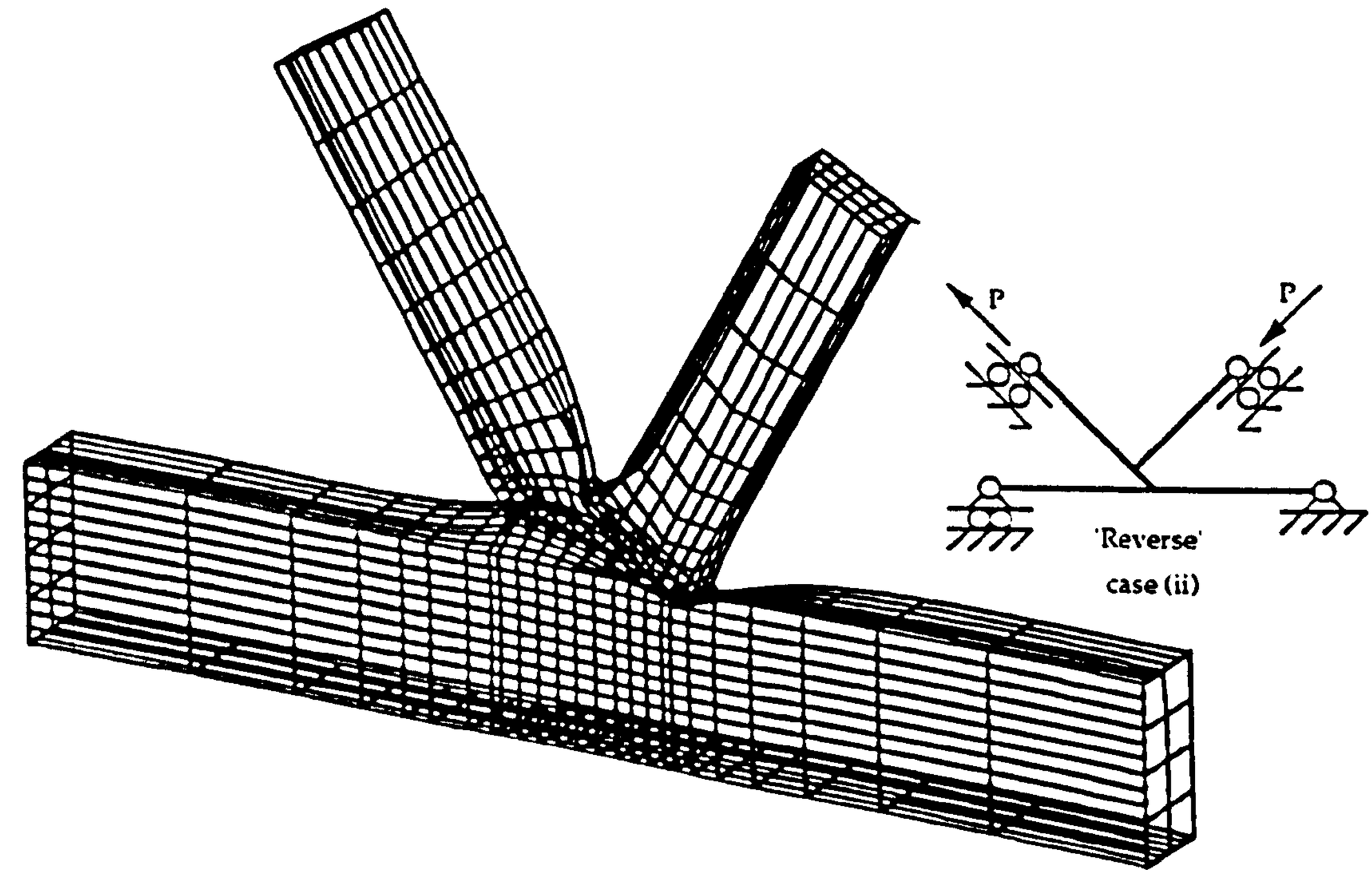

Figure 11.11 Displaced Shape Plot for β = 0.6 60° K Joint where Through Brace is Loaded in Tension.

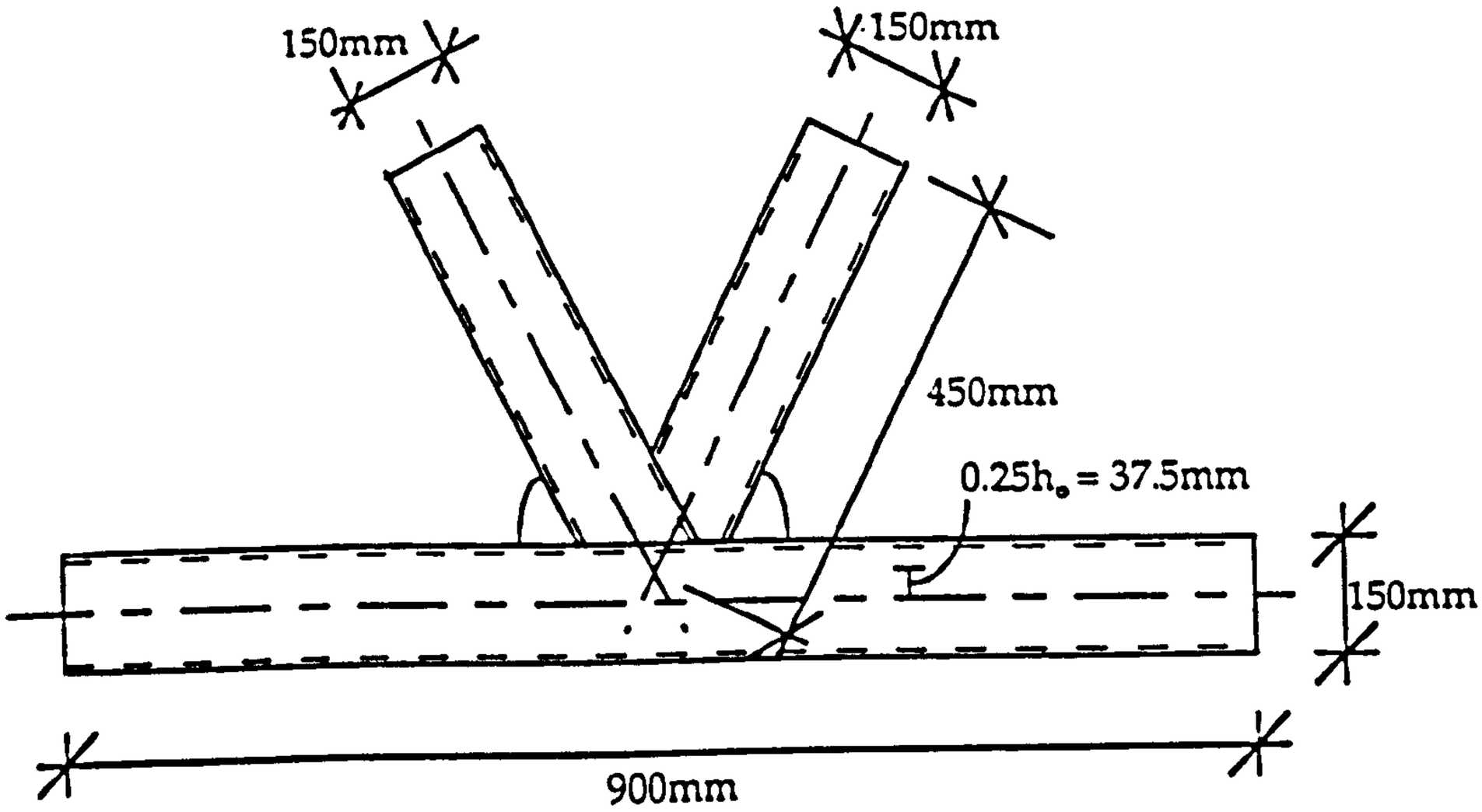

Figure 11.12 Dimensions of the β = 1.0 60° K Joint.

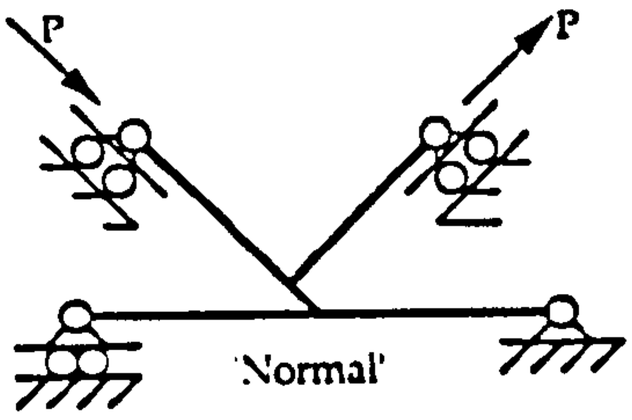

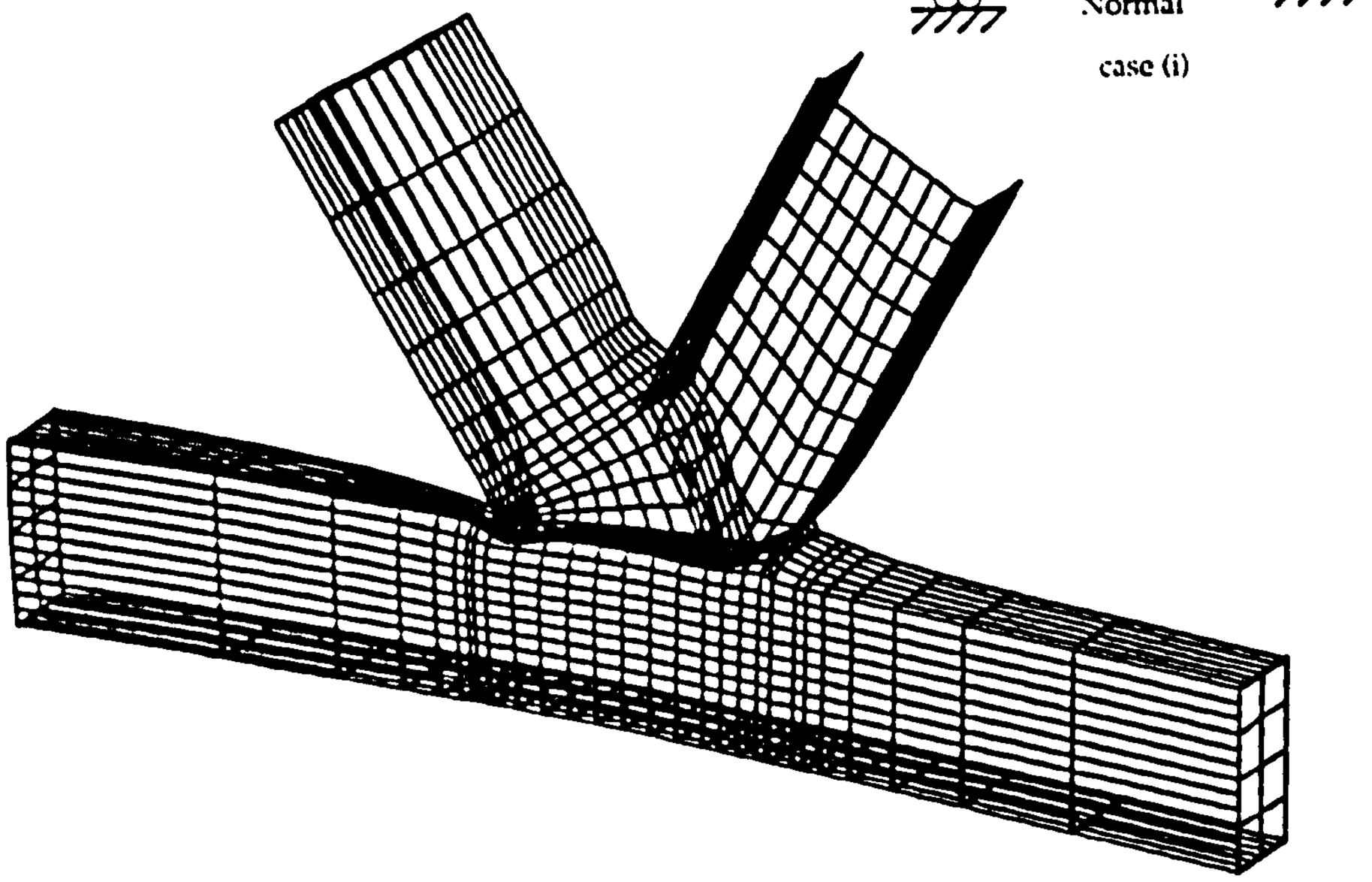

Figure 11.13 Displaced Shape Plot for β = 1.0 60° K Joint where Brace is Loaded in Compression.

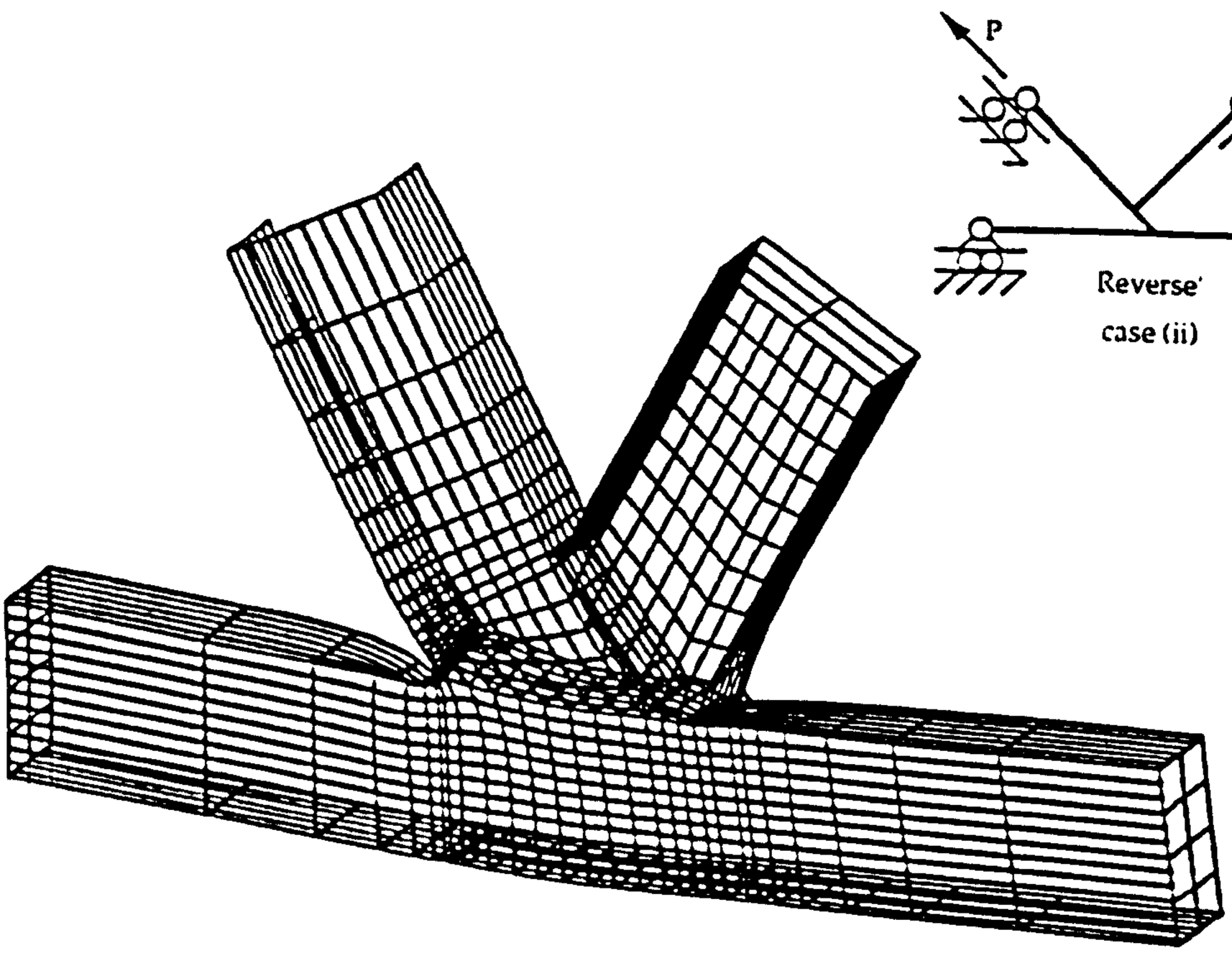

Figure 11.14 Displaced Shape Plot for β = 1.0 60° K Joint where Through Brace is Loaded in Tension.

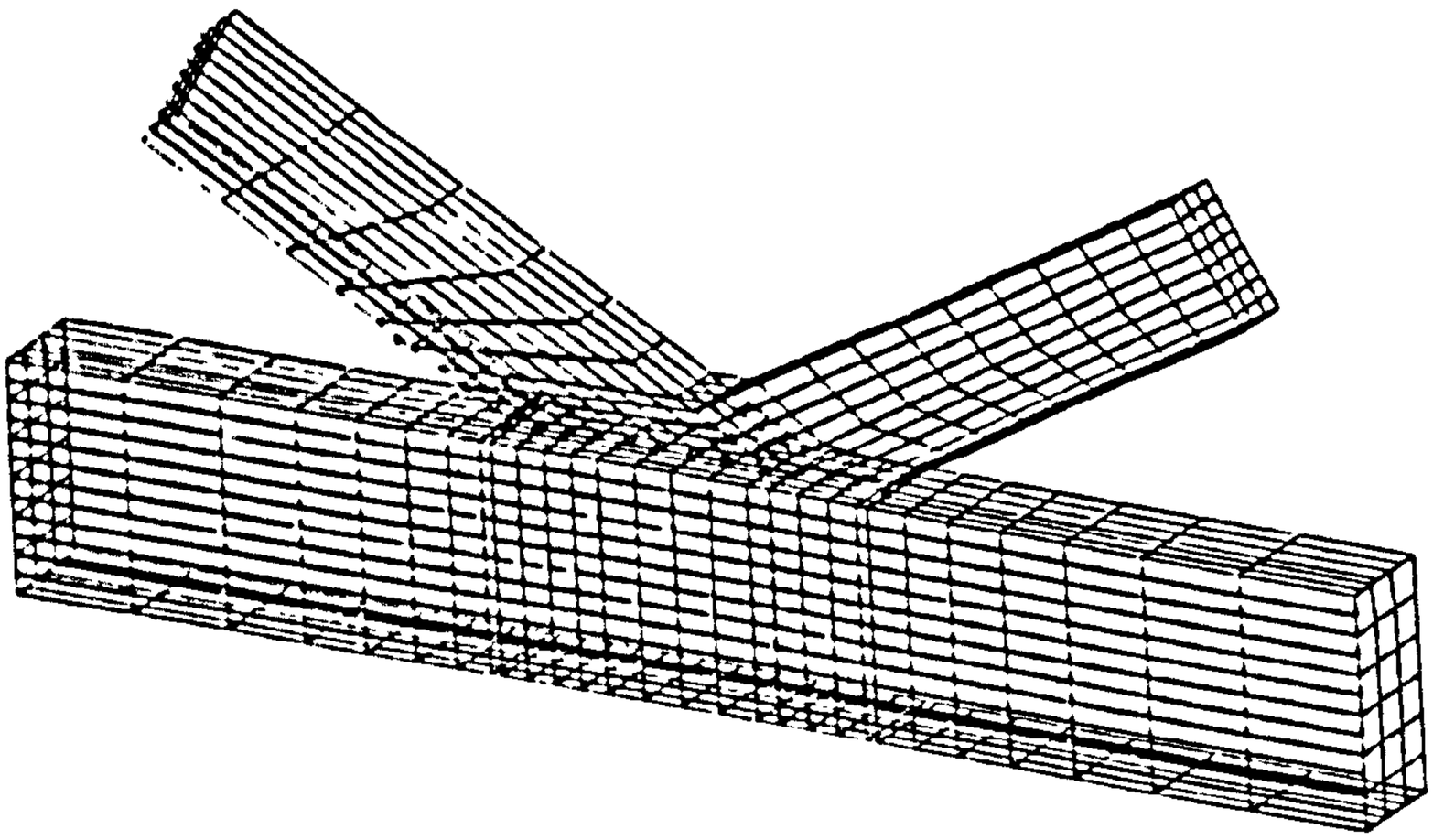

Figure 11.15 Dimensions of the β = 0.6 30° K Joint.

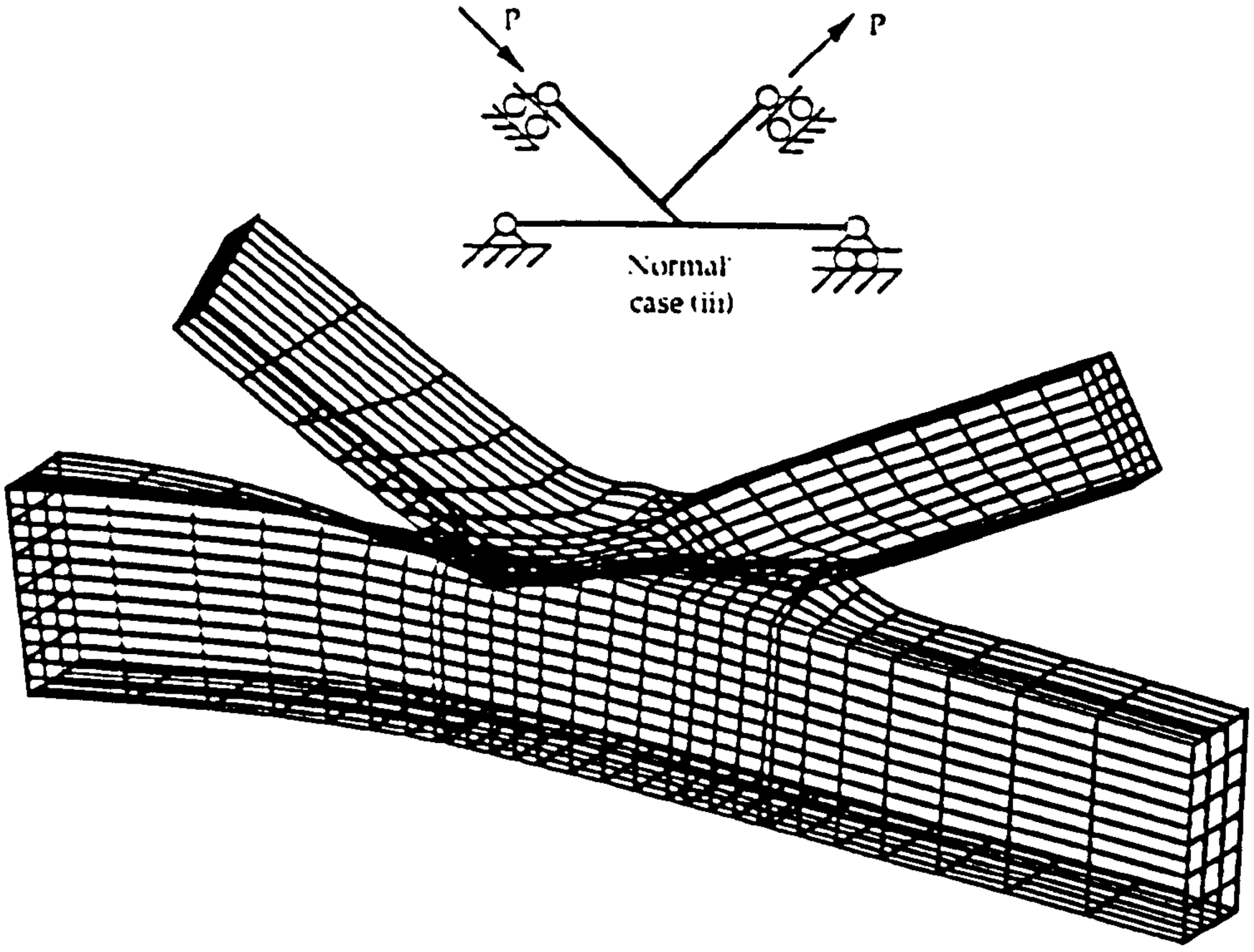

Figure 11.16 Displaced Shape Plot for β = 0.6 30° K Joint where Through Brace is Loaded in Compression.

Figure 11.17 Displaced Shape Plot for β = 0.6 30° K Joint where Through Brace is Loaded in Tension.

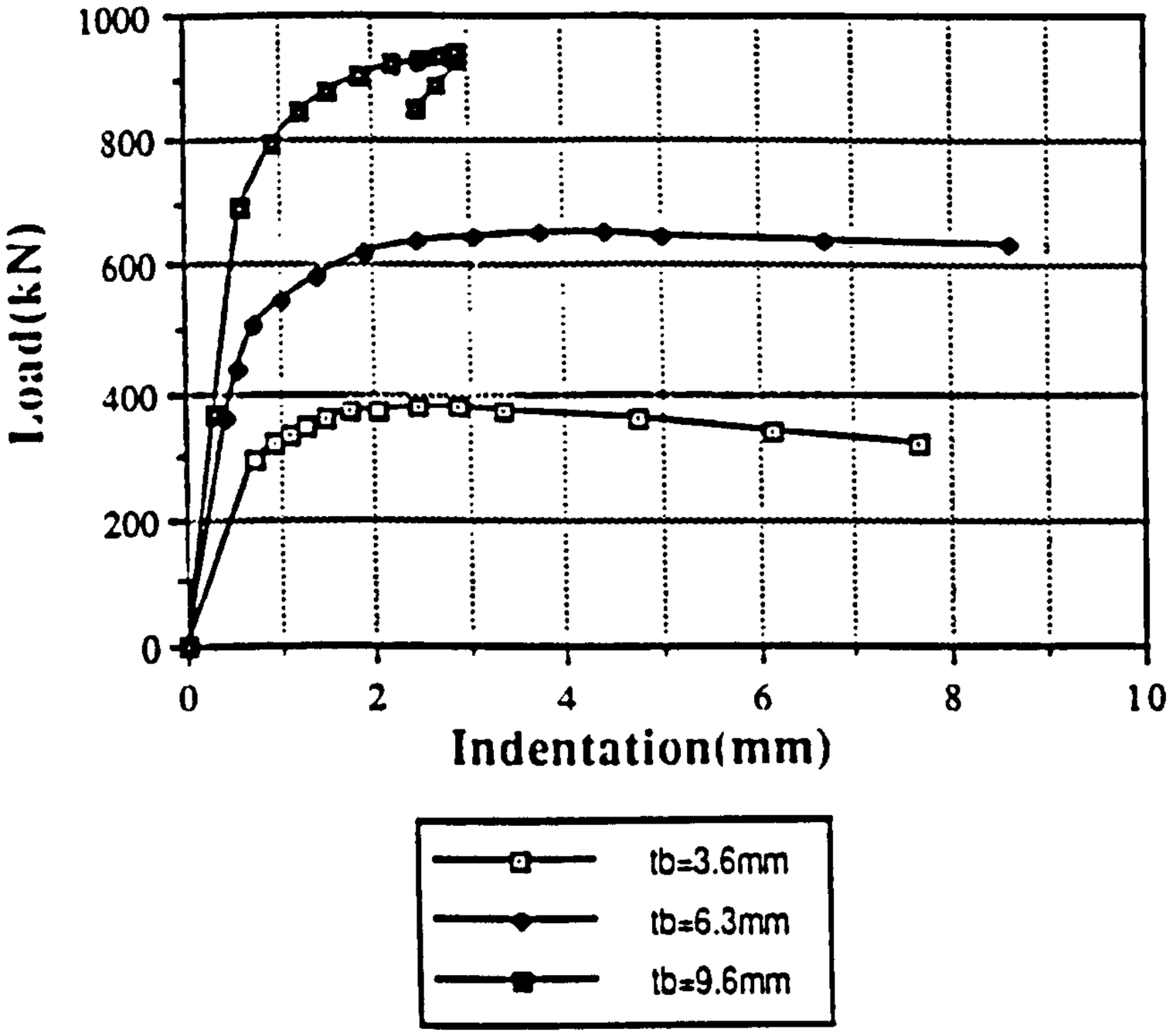

Figure 11.18 Load vs Indentation Plot for Variations on Brace Thickness for $\beta = 0.6$, $\theta = 60^{o}$ K Joints.
(tb = thickness of both braces).

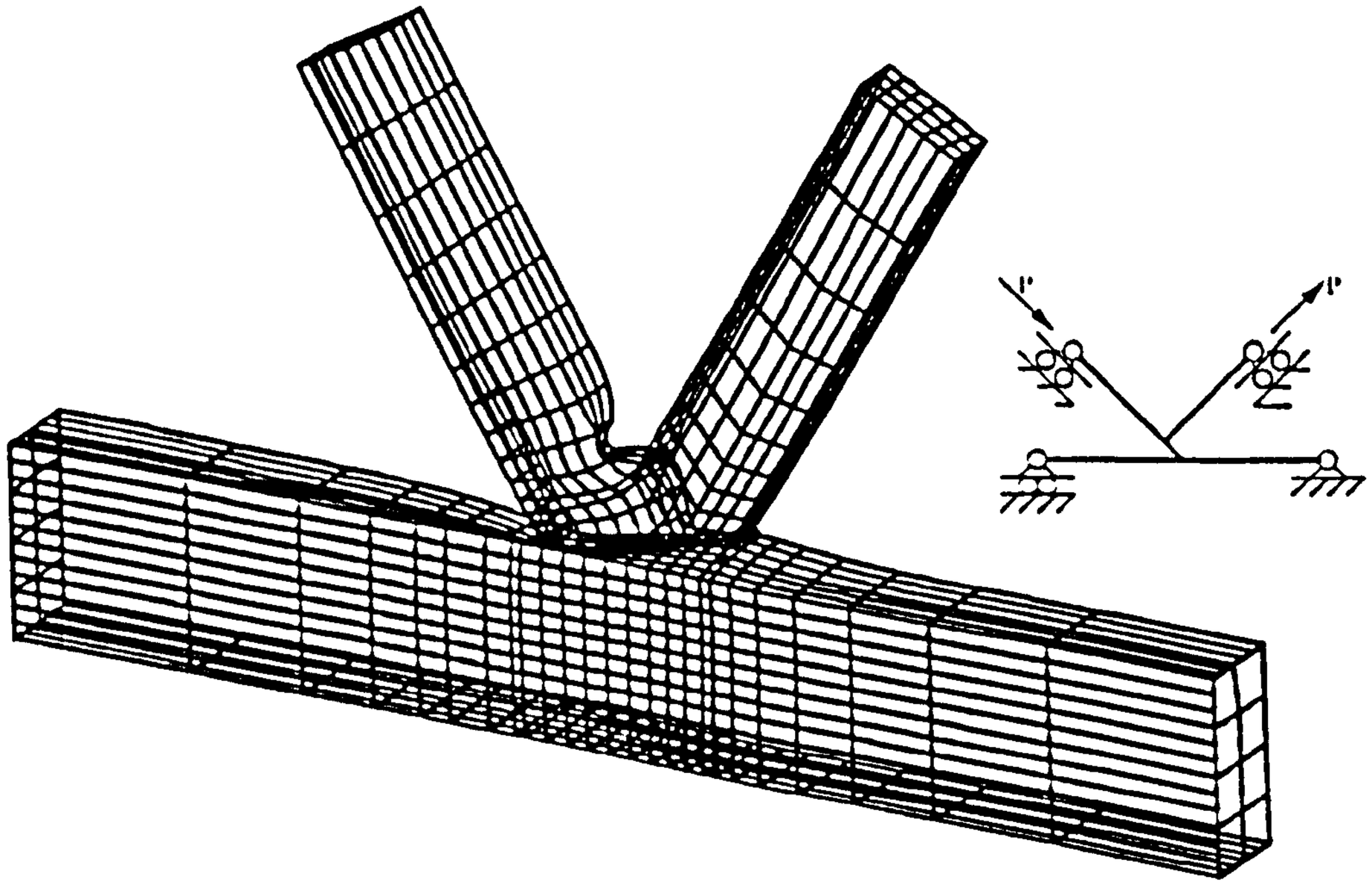

Figure 11.19 Displaced Shape Plot for $\beta = 0.6$, $\theta = 60^{o}$ K Joint where Through Brace is Loaded in Compression.
Brace thickness = 3.6mm.

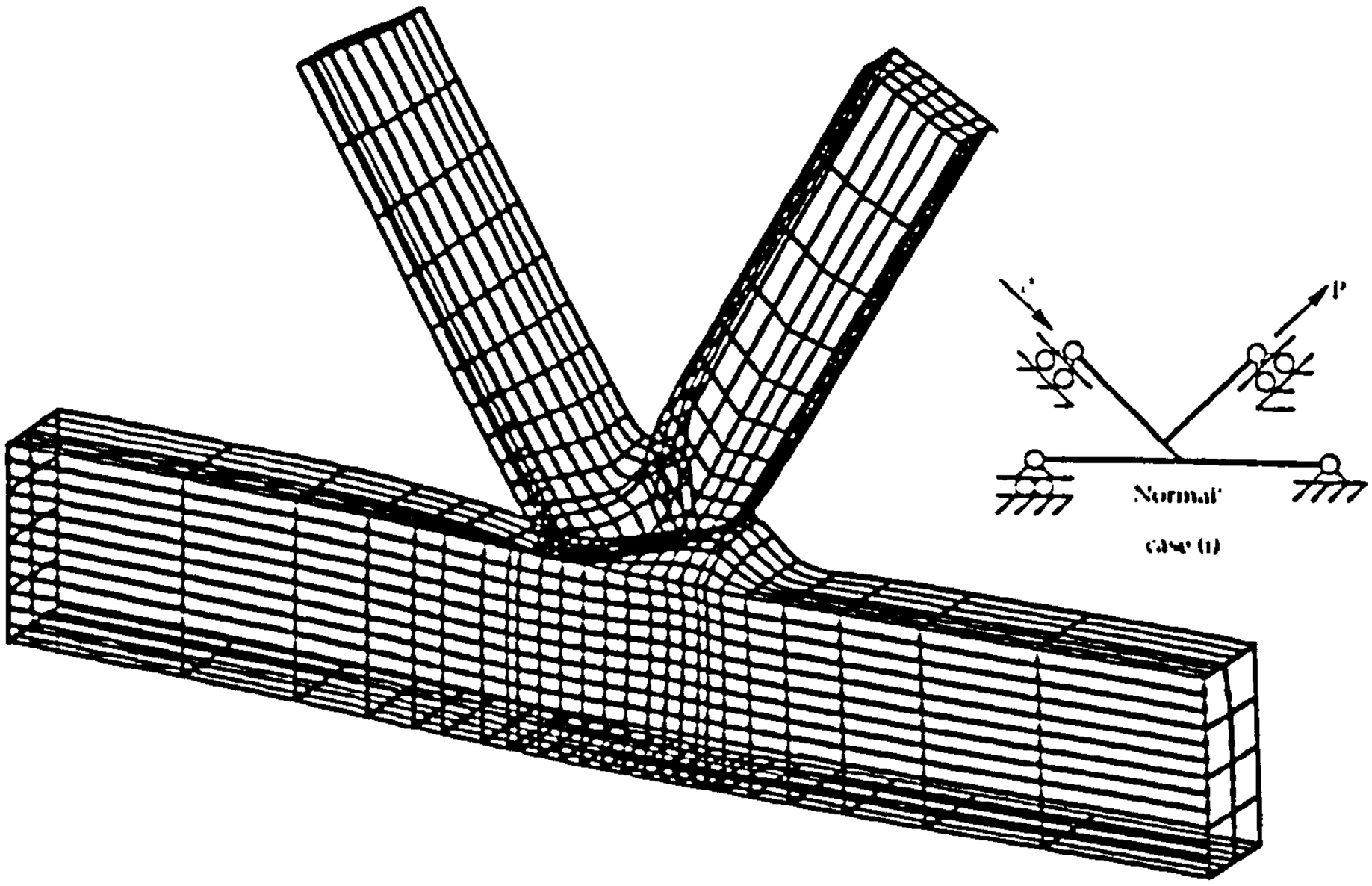

Figure 11.20 Displaced Shape Plot for $\beta = 0.6$, $\theta = 60^{o}$ K Joint where Through Brace is Loaded in Compression. Brace thickness = 9.6mm.

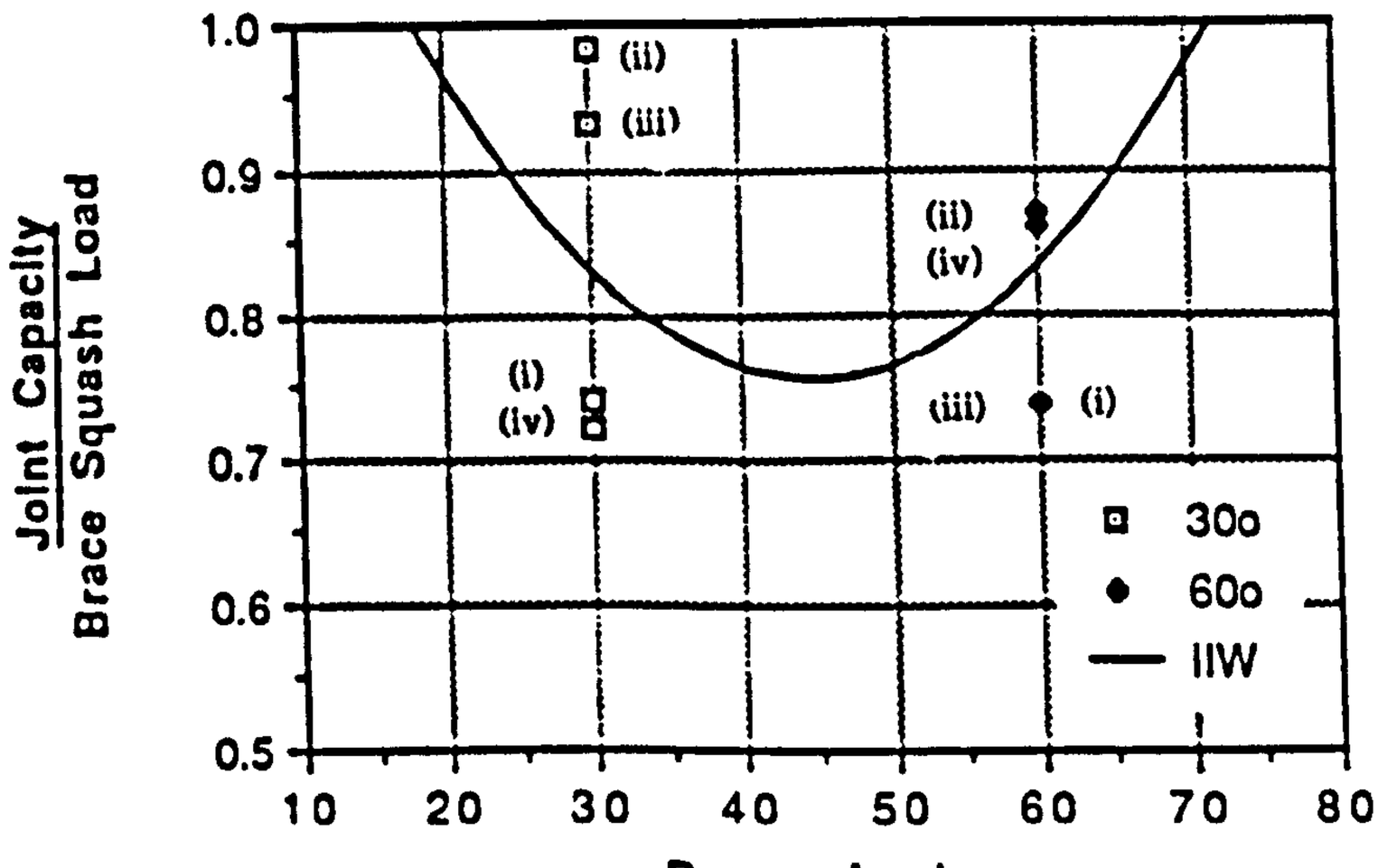

Figure 11.21 Brace Angles vs Joint Capacity/Brace Squash Load for FE, $\beta = 0.6$ K Joints and the IIW Formulae Prediction.

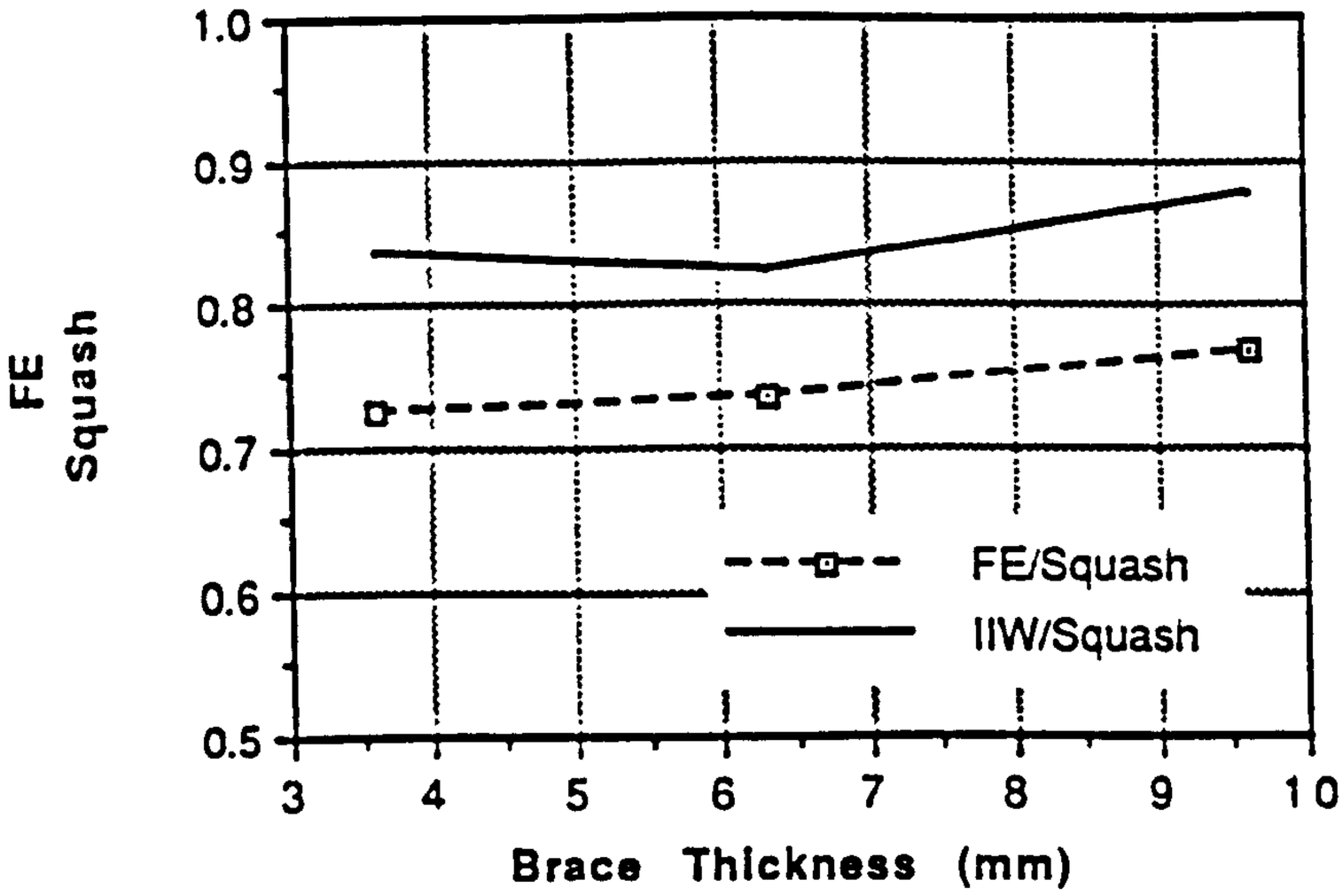

Figure 11.22 Comparison of the FE and IIW Predictions for Varying Brace Thicknesses on $\beta = 0.6$, 60° K Joints.

CHAPTER 12

CONCLUSIONS AND RECOMMENDATIONS FOR FURTHER WORK

12.1 Introduction

In this thesis non-linear geometric and material FE analyses have been carried out on a variety of tubular joint problems in both CHS and RHS. Motivation for these analyses has come from a variety of sources. The multiplanar RHS T-DT joint analyses were undertaken to provide additional information to an ECSC funded project already underway. The CHS T-DT multiplanar analyses were undertaken to supplement this and the work carried out by other researchers on CHS T-T and DT-DT joints. Motivation for the two sets of CHS Y and T joint comparison analyses was gained from initial findings while undertaking work at BOMEL for a North sea operator. Finally the K joint work was influenced by CIDECT/IIW interest in the hidden weld effects in RHS partial overlap K joints.

12.2 Conclusions

Specific conclusions were drawn for each topic at the end of the appropriate chapter, the aim of this chapter being to summarise the main conclusions on the joints studied and the use of the FE

method in simulating joint behaviour with or without the support of experimental results.

1) The FE method is now a valuable tool for investigating the ultimate static strength of welded tubular connections. Parameter changes (γ, β etc) can be rapidly and economically quantified. In addition, where the FE results can be calibrated against experimental results for particular joints, changing such items as the geometric and material properties and boundary conditions and loading mode can generate additional results which can be used alongside experimental ones in the development of databases and joint design guidance.

2) In the absence of experimental results, FE analyses have been compared to design code predictions which have themselves been derived from experimental test databases. This however requires an awareness of how the codes were derived and the margin by which the code prediction falls below the mean of the database used in its derivation. For this, access to the datasets used in the code derivation is extremely valuable (as discussed in Chapter 8 when using the HSE code).

3) Even if direct comparison with experimentally derived design guides or test results cannot be made, the FE method can be used to investigate the trends introduced by parameter changes as opposed to the absolute values of actual capacity changes. This was illustrated in the imperfection investigation in Chapter 5, where an experimental investigation into such imperfections would be impossible to perform.

4) Mesh convergence studies undertaken on both the RHS and CHS T-DT configurations indicate that the medium meshes illustrated in Chapters 4 and 7 are suitable for analysing the joints

with a view to establishing sufficiently accurately ultimate capacities of joints. However as was demonstrated in Chapter 4 in regions where the strain gradients are 'steep' then considerable refinement is necessary to measure FE strains with similar accuracy to the experimentally measured values. This ability must be offset against the extra computing time required to analyse more refined meshes. The magnitude of these strains is more likely to be of interest in Stress Concentration Factor determination and the much finer mesh necessary for this can be offset against the savings in cpu time obtained by undertaking a linear elastic analysis only for SCF evaluation.

5) The inclusion of modelling of the fillet welds for all but high β ratio joints is essential if the FE model is not to significantly underpredict the ultimate capacities. This has been illustrated for both CHS and RHS joints in this thesis.

6) For fillet weld modelling in RHS joints a six noded solid weld element, (offset from the main chord and brace elements by half the wall thickness and with weld nodes connected to adjacent chord and brace nodes (see Section 3.4.2.2)) gave the best correlation of Finite Element to experimental correlation for a planar joint. Such a model also gave very satisfactory calibration with six experimental results undertaken on multiplanar RHS T-DT joints. For CHS fillet weld modelling both six noded solids and eight noded shell elements gave equivalent results on an axially loaded planar T joint. Both gave capacities 25% greater than the equivalent no weld included case and both were close to the mean of the experimental database. Difficulties with the curvature and complex geometry of the brace chord intersection in CHS make modelling of the weld much more difficult than with the RHS case. For the

multi-planar T-DT CHS investigations in this thesis, the solid weld model was selected as this avoided the possibility of problems with the weld element buckling, the possibility of an air gap and what throat thickness to make the weld element should it be a shell. This was discussed in Section 7.3.

7) It was found that for RHS joints the addition of DT braces to a planar T joint could add significantly to joint capacity. This increase was found to be greatest for $\beta = 1.0$ while at $\beta = 0.25$ no increase was observed. The presence of loads of the same sense in the DT braces as those in the T brace has little influence on capacity at all β ratios. However where the loads are of opposite sense in the DT braces (i.e tension in one plane and compression in the other) reductions in capacity below the corresponding planar joints can occur in certain circumstances. These effects depend on β ratio. Where the $\beta = 1.0$ the reductions are negligible but where $\beta = 0.6$ or 0.25 capacity can fall below that of the planar joints. Thus when design is based on a plane by plane analysis the design of such joints may become unconservative and hence there is a need to reflect this in the design codes.

8) For CHS joints conclusions on multiplanar effects in T-DT joints similar to those above can be drawn for the $\beta = 0.25$ and 0.6 joints investigated. However, there is one important difference due to the P-δ effect when the DT braces are loaded in compression. This is discussed in detail in Chapter 7. It can be stated that the boundary conditions or 'frame' effects can have a much more significant effect on joint capacity with CHS rather than RHS members. Under certain extreme conditions (i.e no load in the T brace, compressive load in the DT braces and these DT brace free to rotate) the capacity for the multiplanar T-DT joint can fall below that of the

corresponding (compressive loaded DT) planar joint. When design is based on a plane by plane assessment, this is again unconservative and needs to be recognised in the codes of practice. The results of this investigation indicate that when compression is applied to both planes (T and DT) the very significant increase in strength observed by Vegte et al (1991) on the DT-DT joint configuration does <u>not</u> occur for the T-DT joints studied here.

9) A re-examination of the inclusion of the brace projected area term, K_a (where brace angle <90°) causing an increase in predicted capacity in a major CHS design guide has been carried out indicating that the term is not justified, and furthermore its inclusion is unconservative for Y and X joints. This has been backed up by a re-appraisal of other relevant information available.

10) Similar studies on RHS however have found that the inclusion of an equivalent factor based on similar assumptions about the effect of brace projected area in design codes to be valid for axially loaded RHS Y and X joints.

11) The effects of the hidden weld in partial overlap RHS K joints have been investigated. It has been demonstrated that under certain conditions and configurations the presence or absence of this hidden weld may have a significant effect on the joint capacity. These conditions arise where the β ratio is lower than 1.0, the bracing angle is steep (i.e 60° as opposed to 30°) and the 'through' brace, (at whose toe the hidden weld or gap is located) is loaded in tension. The increase in strength observed here for a $\theta = 60°$, $\beta = 0.6$ K joint was 12% above that of the corresponding gap case. There are no recommendations relating to this in the codes currently.

12) A brief study on the influence of brace thickness on partial overlap K joint capacity has been undertaken. The findings

generally agree with those predicted in the IIW design guidance but a more thorough study covering different brace angles and β ratios is required to draw more complete conclusions.

13) Limitations of the FE method currently include the difficulty in observing failures induced by cracking (especially in tensile loading situations). Although there are currently some attempts to model such cracks using line spring elements as discussed in Chapter 4, there are difficulties in predicting where exactly the crack will begin.

12.3 Recommendations for Further Work

1) There is a clear need for new work to be undertaken on multiplanar connections in both CHS and RHS. This work should cover the effects of moment loading (both in-plane and out-of-plane moments) on joint configurations already studied in this thesis and those studied by others. Most work on multiplanar connections so far has been on axial loading effects. Further multiplanar joint configurations need to be examined to enable a more comprehensive picture to be drawn up. Configurations such as X-X are common offshore and have not yet received any attention. This is also true for planar X (i.e $\theta < 90^o$) joints in the HSE datasets as discussed in Chapter 8. There is also a need to study configurations already examined in the literature over different β ratios as this had a significant impact on the effects of multiplanar joint behaviour in this thesis. Such work should involve physical testing if substantial differences are expected but there is no reason why non-linear FE analyses calibrated to existing planar design guides and tests cannot

be used for initial investigations and to identify areas in need of attention as within this thesis in Chapter 7.

2) For the T-DT joints considered here, the effect of chord slenderness should be investigated (in this thesis it is mainly kept constant at 23.8) to see if this has an influence on the trends caused by multiplanar brace and load addition. Brief investigation in Chapter 5 suggests that as b_o/t_o increases the increase in capacity caused by addition of multiplanar (DT) braces to a planar T joint becomes more significant for RHS. The FE approach is ideal for examining the effects of parameter changes as once developed a model can be rapidly re-analysed for a different slenderness, material properties and loading/boundary conditions by altering minimal amounts of data in the FE input deck.

3) The studies here suggest there is a need to re-examine the assumption of the validity of K_a the brace effective area term for CHS in the HSE design guidance, particularly for Y and X joints. This is supported by a re-examination of existing data.

4) The differences in hidden weld effect caused by the variation of the yield stress of the material need to be considered as this could have a significant impact on the buckling and failure in the brace-brace intersection region which may cause the hidden weld to have a negligible effect at lower yield stresses than those considered here in the $\beta = 0.6$, $\theta = 60^o$ K joint.

5) Additional work needs to be undertaken on the significance of the hidden weld in RHS K joints. The work should focus on different angles (i.e N type joints $45^o/90^o$ and $45^o/45^o$ K joints), β ratios and different overlap percentage ranges in addition to further parameter studies involving chord and brace slendernesses on the joint configurations analysed within this thesis. Again the FE

approach is ideal to study a wide range of parameters such as these to build a comprehensive picture of their effects.

5) The presence of the hidden weld in partial overlap CHS K joints should be investigated. Although it is current practice to avoid partial overlap joints in construction many existing structures have partial overlap joints in them and knowledge of the hidden weld and its effect on capacity is important when such structures are re-analysed or re-appraised.

6) A more comprehensive study containing several β ratios and brace angles is required before the trends in the strength predicted by the IIW RHS partial overlap K joint formulae for differing brace thicknesses can be checked or validated here.

7) A similar study on the brace thickness effects in overlapped and partially overlapped CHS K joints should be undertaken and the influence of tension loading in the through brace considered. The data on which the HSE guidance was developed contains only sixteen data points, all having the through brace loaded in compression and a limited range of β ratios ($0.41 < \beta < 0.68$).

REFERENCES

ABAQUS user manual, Version 4.9, Hibbit, Karlsson and Sorenson. 35 Angel Street, Providence, Rhode Island 02906, USA (1991).

ANSYS user manual rev 5.0, Swanson Analysis Systems Inc, PO Box 65 Johnson Road, Houston, PA 15342-0065 Ph (412) 746 - 3304, USA.

API (American Petroleum Institute). 'Recommended Practice for Planning, designing and constructing fixed offshore platforms'. API RP2A, 19th Edition (1991).

AWS (American Welding Society) Structural Welding Code - Steel, AWS D1.1-90, American Welding Society, Miami (1988).

Bensalem.K. 'Behaviour of fully Overlapped Rectangular Hollow Section Joints in Isolated Tests'. MPhil thesis. University of Nottingham (1989).

Bhuyan.G.S, Munaswamy.K and Arockiasamy.M. 'Through Thickness and Surface Stress Distribution of Welded Tubular T Joints using the FE Method'. Canadian Journal of Civil Engineering, Vol 13 (1986).

Billington Osborne Moss Engineering Limited (BOMEL). 'Joint Industry Tubular Frames Project'. (confidential to participants until 1995).

Bolt.H.M and Lalani.M. 'Strength of Mutliplanar Joints on Offshore Platforms'. Proceedings of the Third International Symposium on Tubular Structures, Lappeenranta, Finland (1990).

Bolt.H.M, Seyed-Kebari.H and Ward.J.K. 'The Influence of Chord Length and Boundary Conditions on K Joint Capacity'. Proceedings of the 2nd International Offshore and Polar Engineering Conference, San Francisco, USA (1992).

BOMEL. 'Joint Industry Tubular Frames Project'. Phases I and II, BOMEL, Maidenhead, UK (on-going and confidential to participants until 1995).

BOMEL. 'Design and Reassessment of Tubular Joints for Offshore Structures'. Chapter 4: SCFs and Local Joint Flexibility. Report C6060R08.01.Rev a (1993). Confidential.

British Standards Institution, BS5950. 'Structural Steelwork in Building Part 1. Code of Practice for Design in Simple and Continuous Construction: Hot Rolled Sections'. British Standards Institution (1990).

British Standards Institution BS639. 'British Standard Specification for Covered Carbon and Carbon Manganese Steel Electrodes for Manual Metal-arc Welding'. BSI (1986).

British Standards Institution BS449. 'Specification for the Use of Structural Steel in Building'. BSI (1969).

BS (British Steel) General Steels. ' Hot Finished Structural Hollow Sections- Sizes, Properties and Technical Data". BS Welded Tubes General Steels (1992).

CIDECT Monograph 6. 'The Strength and behaviour of statically loaded welded connections in Structural Hollow Sections'. Comité International pour le Développment et l'étude de la Construction Tubulaire (1986).

Coutie.M.G, Davies.G, Philiastides.A, Roodbaraky.K and Yeomans.N. 'Fully overlapped RHS Joints - Isolated Joints and Trusses'. Proceedings of the Third International Symposium, Lappeenranta, Finland (1990).

Coutie.M.G and Davies.G. 'Tubular Structures V' Proceedings of the Fifth International Symposium. E & FN Spon (1993).

Dasgupta.A. 'Behaviour of Joints in Tubular Trusses'. PhD thesis. Department Of Civil Engineering, Nottingham University, U.K (1970).

Davies.G, Coutie.M.G and Bettison.M. 'The Behaviour of Three Dimensional Rectangular Hollow Section T Joints Under Axial Branch Loads'. Proceedings of the Fifth International Symposium, Nottingham, U.K (1993).

Davies.G and Crockett.P. 'An Interaction Diagram for Three Dimensional T Joints in Rectangular Hollow Sections Under In-Plane and Out-of-Plane Axial Loads'. Proceedings of the Fifth International Symposium, Nottingham, U.K (1993).

Davies.G, Coutie.M.G and Bettison.M. 'Three Dimensional RHS Tee Joints Under Axial Branch Loads'. Proceedings of the 3rd Pacific Structural Steel Conference, Tokyo (1992).

Davies.G, Coutie.M.G and Bettison.M. 'The Static Strength of Multiplanar Hollow Section Joints - Tee Joints'. Technical Report No.2. Nottingham University Report No SR91051. February 1992.

Davies.G, Coutie.M.G and Bettison.M. 'The Static Strength of Multiplanar Hollow Section Joints - Tee Joints'. Technical Report No.3. Nottingham University Report No SR92035. July 1992.

Davies.G and Morita.K. 'Three Dimensional Cross Joints under Combined Axial Branch Loading' Proceedings of the Fourth International Symposium, Delft, Netherlands (1991).

Davies.G and Roper.C.G. 'Gap Joints with Tubular Members - A Yield Line Approach'. Building Science Vol 10 pp 199-205, Pergamon Press (1975).

de Koning.C.H.M, Liu.D.K, Puthli.R.S and Wardenier.J. 'Static Behaviour of Multiplanar Connections in Rectangular Hollow Sections'. Stevin report 6.92.28/A1/11.08. Delft University/TNO (1992).

Eastwood.W, Osgerby.C, Wood.A.A and Mee.B.L. 'An investigation into the behaviour of the strength of ordinary and stiffened joints in tubular plane frameworks'. Department of Civil and Structural Engineering, Sheffield University. Report to CIDECT (1970).

Eastwood.W, Osgerby.C, Wood.A.A and Mee.B.L. 'An experimental investigation of joints in rectangular hollow section'. Department of Civil and Structural Engineering, Sheffield University. Report to CIDECT (1970).

Eastwood.W, Osgerby.C, Wood.A.A and Blockley.D.I. 'An Experimental investigation into the behaviour of joints between structural hollow section'. Department of Civil and Structural Engineering, Sheffield University. Report to CIDECT (1967).

Eurocode No 3 'Design of Steel Structures' (Annex K). (1992).

Efthymiou.M. 'Development of SCF Formulae and Generalised Influence Functions for use in Fatigue Analysis'. Offshore Tubular Joints Conference, Egham, Surrey, UK (1988).

Femview Limited 'FEMGEN/FEMVIEW user's manual'. (1989).

Healy.B.E and Zettlemoyer.N. 'In-Plane Bending Strength of Tubular Joints'. Proceedings of the Fifth International Symposium, Nottingham, U.K (1993).

HSE (Health and Safety Executive). 'Background to New Static Strength Guidance for Tubular Steel Offshore Structures'. Offshore Technology Report OTH 89 308 (1990).

International Institue of Welding. 'Welding of Tubular Structures'. Proceedings of the Second International Conference, Boston, USA (1984).

IIW (International Institute of Welding). Minutes of the Meeting on 28/08/93 at Nottingham. Document XV-E-93-199 (1993).

IIW (International Institute of Welding). 'Design Recommendations for Hollow Section Joints - Predominantly Statically Loaded'. Document XV-701-89 2nd edition (1989)

JSSC (Japanese Society of Steel Construction). 'Study of tubular joints used in marine structures (in Japanese)'. Society of Steel Construction in Japan (1972).

Johnston.L.P. 'The Welded Tubular Joint Problem in Offshore Structures'. Shell EPR Publication 326. Ist University of Texas Conference on Drilling and Rock Mechanics, Austin, Texas (1963).

Kanatani.H. 'Experimental Study on Welded Tubular Connections No 12. Memoirs of the Faculty of Engineering, Kobe University (1966).

de Koning.C.H.M, Liu.D.K, Puthli.R.S and Wardenier.J. 'Static Behaviour of Multiplanar Connections in Rectangular Hollow Sections'. Stevin report 6.92.28/A1/11.08. Delft University/TNO (1992).

de Koning.C.H.M, Liu.D.K, Puthli.R.S and Wardenier.J. 'Static Behaviour of Multiplanar Welded Joints in Circular Hollow Sections'. Stevin report 26.6.90.13/A1/11.03. Delft University/TNO (1991).

Kurobane.Y et al. 'Ultimate Strength Formulae for Simple Tubular Joints'. Kumamoto University, Japan (1976).

Makino.Y, Kurobane.Y and Oochi.K. 'Ultimate Strength of Tubular Double K Joints'. Welding of Tubular Steel Structures, IIW, Permagon Press (1984).

Marshall.P.W. 'Design of Welded Tubular Connections - basis and use of AWS code provisions'. (1992).

Mouty.J and Rondal.J. Study of the Behaviour under Static Loads of Welded Triangular and Rectangular Lattice Girders made with Circular Hollow Sections. CIDECT Report 5AS-92/1.

O'Connor.M. 'Static strength of Multiplanar K Joints in Rectangular Hollow Section'. Proceedings of the Fifth International Symposium, Nottingham, U.K (1993).

Paul.J.C, Ueno.T, Makino.Y and Kurobane.Y. 'Ultimate Behaviour of Multiplanar Double K Joints of Circular Hollow Section Members'. Proceedings of the Second International Offshore and Polar Engineering Conference, San Francisco, USA (1992),

Niemi.E and Makelainen.P. 'Tubular Structures' Proceedings of the Third International Symposium. Elsevier Applied Science (1990).

Packer.J.A, Wardenier.J, Kurobane.Y, Dutta.D and Yeomans.N. 'Design Guide for Rectangular Hollow Section (RHS) Joints under predominantly Static Loading'. Comité International pour le Développment et l'étude de la Construction Tubulaire (1992).

Paul.J.C, Ueno.T and Kurobane.Y. 'The Ultimate Behaviour of Circular Multiplanar T-T Joints'. Proceedings of the Fourth International Symposium, Delft, Netherlands (1991).

Paul.J.C, van der Valk.C.A.C and Wardenier.J. 'The Static Strength of Circular Multiplanar X Joints'. Proceedings of the Third International Symposium on Tubular Structures, Lappeenranta, Finland (1990).

Reimer.R.B, Litton.R.W and Babcock.J.H. 'Finite Element Analysis of Complex Welded Tubular Joints'. Paper 11th Annual Offshore Technology Conference (OTH), Houston, Texas, USA (1979).

Rockey.K.C, Evans.H.R, Griffiths.D.W and Nethercot.D.A. 'The Finite Element Method - A basic introduction for engineers'.2nd edition. (1983).

SDRC. 'IDEAS-FEM Finite element modelling user's guide'.(1990).

Smedley.P.A and Fisher.P.J. 'SCFs for Simple Tubular Joints'. Proceedings of the 1st International Offshore and Polar Engineering Conference, Edinburgh, UK (1991).

Stasa.F.L. 'Applied Finite Element Analysis for Engineers'. (1985).

Tie-yun Chen and Xiao-bo Yu. 'Stress Intensity Functions of Surface Cracks in Welded Tubular T-Joints'. Proceedings of the 2nd International Offshore and Polar Engineering Conference, SanFrancisco, USA (1992).

Vegte van der.G.J, de Koning.C.H.M, Puthli.R.S and Wardenier.J. 'Static Behaviour of Multiplanar Welded Joints in Circular Hollow Sections'. Stevin report 26.6.90.13/A1/11.03. Delft University/TNO (1991).

Ward.J.K and Izzudin.B. 'Ultimate Limit State of Tubular Framed Structures'. Offshore Tubular Joints Conference, UEG/SCI, Surrey, UK (1986)

Wardenier.J, Kurobane.Y, Packer.J.A, Dutta.D and Yeomans.N. 'Design Guide for Circular Hollow Section (CHS) Joints under predominantly Static Loading'. Comité International pour le Développment et l'étude de la Construction Tubulaire (1991).

Wardenier.J and Panjeh Shahi.E. 'Tubular Structures' Proceedings of the Fourth International Symposium. Delft University Press (1991).

Wilmhurst.S.R and Lee.M.M.K. 'Non-linear FEM Study of Ultimate Strength of Tubular Multiplanar Double K Joints'. Proceedings of the 12th International Conference on Offshore Mechanics and Arctic Engineering, Glasgow, U.K (1993).

Yeomans.N. 'Rectangular Hollow Section Double K Joints - Experimental Tests and Analysis'. Proceedings of the Fifth International Symposium, Nottingham, U.K (1993).

Yeomans.N. 'An Overview of CIDECT Research on Tubular Structural Joints'. Proceedings of the Fourth International Symposium, Delft, Netherlands (1991).

Yu.Y, Liu.D.K, Puthli.R.S and Wardenier.J. 'Numerical Investigation of the Static Strength of Multiplanar Welded Hollow Section Joints in R.H.S'. Stevin report 6.92.37/11.08. Delft University/TNO (1993).

Yura.J.A, Zettlemoyer.N and Edwards.I.F. 'Ultimate Capacity Equations for Tubular Joints'. Offshore Technology Proceedings, Vol 1, No 3690 (1980).

Zhao.X.L. 'The Behaviour of Cold Formed Rectangular Hollow Section Beams Under Combined Actions'. PhD thesis, School of Civil and Mining Engineering, University of Sydney (1992).

Zettlemoyer.N. 'Developments in Ultimate Strength Technology for Simple Tubular Joints'. Offshore Tubular Joints Conference, CIRIA-UEG, Surrey, UK (1988).

Zienkiewicz.O.C. 'The Finite Element Method'.3rd edition. (1977).